Universidade do Minho
Escola de Engenharia

Bernardo Rodrigues de Sousa Ribeiro

Thermodynamic optimisation of spark ignition engines under part load conditions

Dezembro de 2006

Universidade do Minho
Escola de Engenharia

Bernardo Rodrigues de Sousa Ribeiro

Thermodynamic optimisation of spark ignition engines under part load conditions

Tese de Doutoramento
Engenharia Mecânica / Máquinas Térmicas e de Fluidos

Trabalho efectuado sob a orientação de
Professor Doutor Jorge José Gomes Martins

Dezembro de 2006

To my grandmother
and my parents

Acknowledgements

The author wishes to thank the following persons for their support during all the work herein described:

Jorge Martins, PhD
Heitor Almeida, PhD
Júlio Caldas
Ricardo Macedo
Eurico Seabra, PhD
Eduardo Ferreira
Eduardo Pereira
Nico Jansens
Hans Verraes
Nikit Kothary
Michal Zajicek
Emin
João Vale
Ivan Abreu

The author also wishes to thank:

Albra – Industrias de Alumínio Lda.
Cenfim – Centro de Formação para a Industria Metalomecânica - Trofa

The author thanks the FCT (in the scope of QCA III) for the financial support given for his research activities:
SFRH / BD / 11194 / 2002.
FCT/FEDER POCI/ENR/59168/2004.

Thermodynamic optimisation of spark ignition engines under part load conditions

Abstract

The rational use of fossil fuels, the minimisation of noxious emissions and the reduction of green house gases emissions are the targets of internal combustion engines research and development activities. Several technological developments have been proposed to reduce the fuel consumption from engines. The integration of variable valve timing (VVT) systems, the use of direct injection and lean burn are the most common technologies proposed by engine manufacturers and research centres to attain these goals, in parallel with exhaust gases purification systems.
Car engines are used at part load conditions most of the time and spark ignition engines have reduced thermal efficiency when working under these conditions. This is caused mainly by the use of a throttle valve to control the engine load and a consequent reduction of effective compression ratio. Thus transportation fuel consumption can be reduced if the performance of engines at part load is improved.
A theoretical analysis has been developed for different internal combustion engine cycles using classical thermodynamics. The objective is to evaluate the behaviour of each cycle in terms of thermal efficiency throughout the load range of the engine. Both spark ignition and compression ignition engine cycles have been analysed. Miller cycle (over-expanded cycle), Diesel and dual cycles proved to bring improvements in relation to a conventional (Otto) spark ignition engine at part load operation. Supercharged cycles were also analysed, revealing that compression ignition engines can also be improved with it, while spark ignition engines lose efficiency with supercharging.
A computer model that simulates spark ignition engines at steady-state conditions was developed and later calibrated with data from engine tests. This computer model was implemented in Matlab – Simulink. It includes sub-models for temperature and pressure calculation, gas properties calculation, combustion, heat transfer, mass exchange and friction. The model was extended to calculate the entropy generated during the engine cycle. Simulations revealed an improvement in terms of fuel consumption with the use of over-expansion and an even higher improvement when over-expansion is combined with compression ratio adjustment. At the same time, the amount of entropy generated reduces when over-expansion combined with compression ratio variation is used.
Bench tests have been performed to obtain experimental data to corroborate the theoretical results. A single cylinder DI Diesel engine was tested and modified to work as a spark ignition. This allowed direct comparison between compression ignition and spark ignition engines. Different camshafts were used to perform different intake valve closure timings (to model VVT) and different pistons were used to perform different compression ratios (to model variable compression ratio - VCR). In the spark ignition version, the engine was tested as Otto, Miller (using different camshafts) and as Miller VCR (using different camshafts and different pistons) configurations.

Optimização Termodinâmica de Motores de Combustão Interna de Ignição Comandada a Carga Parcial

Resumo

O objectivo das actividades de investigação e desenvolvimento em motores de combustão interna são a utilização racional dos combustíveis fósseis, minimização da emissão de gases tóxicos e redução da emissão de gases de efeito de estufa. Vários desenvolvimentos tecnológicos têm sido propostos para a redução do consumo de combustível em motores. A integração sistemas de variação da abertura de válvulas (VVT), a utilização de injecção directa e queima pobre são as soluções mais comuns propostas pelos fabricantes de motores e centros de investigação para atingir aqueles objectivos, paralelamente com os sistemas de tratamento de gases de escape.

Os motores de automóveis, na maior parte do tempo, são usados em condições de carga parcial e nestas condições têm um rendimento térmico baixo. Isto é causado principalmente pela utilização da válvula de borboleta para o controlo da carga do motor e uma consequente redução da taxa de compressão efectiva. Assim, o consumo de combustível em transportes pode ser reduzido se o desempenho dos motores em condições de carga parcial for melhorado.

Neste trabalho foi desenvolvida uma análise teórica, a diferentes ciclos de motores de combustão interna usando a termodinâmica clássica. O objectivo é avaliar o comportamento de cada ciclo em termos de rendimento térmico ao longo da gama de carga do motor. Foram analisados quer motores de ignição comandada, quer motores de ignição por compressão. Provou-se que o ciclo Miller (ciclo sobre-expandido), o Diesel e o dual conduzem a melhorias em relação ao ciclo convencional de ignição comandada (Otto) em condições de operação a carga parcial. Foram também analisados ciclos sobrealimentados, revelando-se que os ciclos de ignição por compressão beneficiam com a utilização desta técnica, enquanto que os ciclos de ignição comandada têm o seu rendimento reduzido com a utilização da sobrealimentação.

Foi desenvolvido um modelo computacional para simulação de motores de ignição comandada em regime estacionário, sendo posteriormente calibrado com os dados resultantes de ensaios de motores. Este modelo foi implementado em Matlab – Simulink. Inclui sub-modelos para o cálculo de temperatura e pressão, cálculo das propriedades dos gases, combustão, transferência de calor, transferência de massa e atrito. Este modelo foi alargado para o cálculo da entropia gerada durante o ciclo do motor. As simulações revelaram uma melhoria em termos de consumo com a utilização de sobre-expansão e uma melhoria ainda superior quando é combinada a sobre-expansão e a optimização da taxa de compressão. Ao mesmo tempo, a quantidade de entropia gerada reduz-se quando é utilizada a sobre-expansão combinada com a variação da taxa de compressão.

Foram executados testes em banco para a obtenção de dados experimentais que corroborem os resultados teóricos. Foi testado um motor Diesel de injecção directa monocilíndrico que posteriormente foi modificado para trabalhar como motor de ignição comandada. Isto permitiu a comparação directa entre motores de ignição comandada e motores de ignição por compressão. Foram utilizadas várias árvores de cames para executar diferentes tempos de fecho da válvula de admissão (VVT) e vários pistões para executar diferentes taxas de compressão (variação da taxa de compressão - VCR). O motor, na versão de ignição comandada, foi testado como Otto, Miller (utilizando diferentes árvores de cames) e como Miller VCR (utilizando diferentes árvores de cames e diferentes pistões).

Table of contents

List of Figures

List of Tables

Symbols

a	Crank radius
	Acceleration
A	Area
B	Bore
C_D	Discharge coefficient
c_p	Specific heat at constant pressure
C_{tre}	Transmission efficiency coefficient
c_v	Specific heat at constant volume
D	Diameter
F	Force
g	Gravity acceleration (9.8 ms^{-2})
h	Specific enthalpy
k	Specific heat ratio
l	Connecting rod length
m	Mass
$\dot{m}$	Mass rate
M	Mach number
	Molar mass
N	Crank Speed
p	Pressure
	piston
P	Power
Q	Heat
$\dot{Q}$	Heat rate
r	Radius
R	Gas constant
S	Entropy
	Speed
	Stroke
$\dot{S}$	Entropy rate
t	time
T	Temperature
	Torque
u	Specific internal energy
U	Internal Energy
v	Velocity
V	Volume
W	Work
$\dot{W}$	Work rate
x	Mass fraction
α	Heat transfer coefficient
β	Supercharge ratio
	Intake pressure ratio
ΔV	Volume difference
ε	Compression ratio
γ	Specific heat ratio
λ	Relative air/fuel ratio
μ	Viscosity
η	Efficiency
θ	Crank Angle
ρ	Density

σ	Expansion ratio
τ	Temperature ratio

Subscripts

a	Air
atm	Atmospheric
b	Burned
	Bearing
c	Combustion
	Combustion chamber
C	Compressor
cw	Cylinder wall
cyl	Cylinder
conv	Convection
d	Dual
	Displaced
	Downstream
D	Diesel
F	Fuel
g	Geometric
gas	Gas
gen	Generated
H	Higher
i	indicated
in	Introduced
	Into
IVC	Intake valve closure
L	Lower
lim	Limit
LHV	Lower heating value
max	Maximum
opt	Optimum
out	Out
p	Constant pressure
	Products
r	Reactants
R	Released
	Reference
rad	Radiation
S	Stoichiometric
Sc	Supercharge
T	Turbine
	Total
TDC	Top Dead Centre
tr	Trapped
	Transfer
trbch	Turbocharger
u	Upstream
v	Constant volume
	Valve
w	Wall
0	Reference value

Abbreviations

ABDC	After Bottom Dead Centre
A/F	Air/Fuel ratio
ATDC	After Top Dead Centre
BBDC	Before Bottom Dead Centre
BDC	Bottom Dead Centre
bmep	Break Mean Effective Pressure
bsfc	Break Specific Fuel Consumption
BTDC	Before Top Dead Centre
CA	Crank Angle
CI	Compression Ignition
CR	Compression Ratio
CVT	Continuous Variable Trasmission
DI	Direct Injection
DOHC	Double Over-Head Camshafts
EGM	Entropy Generation Minimization
EGR	Exhaust Gas Recycle
EIVC	Early Intake Valve Closure
EVC	Exhaust Valve Closure
EVO	Exhaust Valve Opening
fmep	Friction Mean Effective Pressure
imep	Indicated Mean Effective Pressure
isfc	Indicated Specific Fuel Consumption
IVC	Intake Valve Closure
IVO	Intake Valve Opening
LIVC	Late Intake Valve Closure
MBT	Maximum Break Torque
NA	Naturally Aspirated
NEDC	New European Driving Cycle
Nu	Nusselt Number
pmep	Pumping Mean Effective Pressure
Re	Reynolds Number
sfc	Specific Fuel Consumption
SI	Spark Ignition
TDC	Top Dead Centre
TWC	Three Way Catalyst
VCR	Variable Compression Ratio
VVA	Variable Valve Actuation
VVT	Variable Valve Timing
WOT	Wide Open Throttle

1 - Introduction

1 INTRODUCTION

1.1 Use of energy and the environment

During the last decades and especially after the first oil crisis in the 70's, public has been aware of matters such as energy savings and environment protection [1]. Both reasons walk hand to hand once it is known that almost all energy resources that the so-called civilized society is using for their living are not endless and produce environment problems. Among the energy resources, oil is the most problematic.

One of the most oil consumer sectors is transportation. Final energy consumption in the EU-25 increased by about 8 % over the period 1990 to 2002 and transport has been the fastest-growing sector since 1990, now being the largest consumer of final energy [2].

During the last decades and especially in recent years (since 2004) the almost constant rise of oil prices lead to several questions on the rational use of energy. From July 2004 to July 2006, the oil price raised from around 38$ a barrel to near 75$, which means that it almost doubled. Before the beginning of this period and for years the oil price was oscillating between the 20$ and 30$ per barrel.

Another fact that must be added to this discussion is the application of more and more restrictive legislation limiting the pollutants emissions, namely green house gases (GHG). These are directly connected with the amount of energy (fuel) consumed, and again the need for more energy efficient devices. Legislation limiting the GHG emissions can be a consequence of international agreements (e.g. Kyoto protocol) or as an initiative of governments or other institutions that regulate the energetic, environmental or industrial sector.

All countries that signed the Kyoto protocol are enforced to reduce their overall emissions of such gases by at least 5 % below 1990 levels during the commitment period 2008 to 2012 [3].

In different globe regions several regulations have been adopted to limit the gaseous pollutants, from fuel combustion devices and specifically from internal combustion engines on automotive applications. In the United States, Corporate Average Fuel Economy (CAFE) is the required average fuel economy for a vehicle manufacturer's entire fleet of passenger cars and light trucks for each year model [4].

The EU's aim is to reach an average CO_2 emission figure of 120 g/km for all new passenger cars marketed in the Union, by 2010 at the latest. Commitments have been

concluded with the European (European Automobile Manufacturers' Association - ACEA), the Japanese (Japan Automobile Manufacturers' Association - JAMA) and Korean (Korean Automobile Manufacturers' Association - KAMA) automobile industries. All three Commitments are equivalent of having a CO_2 emission objective of 140 gCO_2/km (to be achieved by 2009 by JAMA and KAMA and by 2008 by ACEA). In other words the fleet of new passenger cars put on the market in 2008/2009 will consume on average about 5.8 L petrol/100 km or 5.25 L diesel/100 km. [5]

Alternatives exist to the use of the internal combustion engines in transport applications. At the beginning of the XX century the electric vehicle was preferable for its silent operation, comfort and reliability. However due to the evolution of the internal combustion engines, the electric vehicle was withdrawn from the market, except in some specific applications. Recently, almost all automakers presented a version of a hybrid vehicle. It uses an internal combustion engine, usually of a smaller size (downsized) than an equivalent vehicle using just a combustion engine, and an electric motor. The transmission can be either in parallel (both electric motor and combustion engine power the vehicle) or series (combustion engine is connected to a generator, which charges batteries and feeds the electric motor). Usually, for fuel consumption improvement, the combustion engine used in hybrid vehicles is an over-expanded engine named Miller cycle engine. The load range at which the engine is used is limited which means that it can be easily optimised to those conditions. In fact, fuel consumption is significantly reduced. However, the production of such vehicles as well as its state of the art are not good enough to answer the market demands. The improvement of the existing internal combustion engines is still a significant alternative to solve the energetic and environment problems arising from transportation demands.

1.2 The part load problem

From the application of internal combustion engines for electricity production to the automotive applications, engines are used in a wide variety of functions. This variable application of engines has different requirements. An engine for electricity production works at a constant speed and load, whether a car engine works under very different speed and load conditions, using almost all its operation range. In the first case the engine may be designed to have its optimum working point (maximum power or

minimum consumption) at the demanded conditions. In the second case the establishment of the optimum working conditions is a matter of compromise trying to define a point or a range most frequently used.

In compression ignition engines the load is controlled by the amount of fuel injected in each engine cycle. The result is increasing engine efficiency as the load reduces, due to the combustion method used. In the case of spark ignition engines a throttle valve, upstream of the intake valve, controls engine load. This throttle valve creates a pressure reduction at the intake manifold, reducing the amount of air induced in each engine cycle and also the amount of fuel, considering stoichiometric working conditions. As a consequence of the intake manifold pressure reduction, when the engine load is reduced, the effective compression of the engine is also reduced. Lower peak temperature and peak pressure are present during the combustion process, thus reducing the relation between the amount of fuel burned and the amount of work delivered by the engine (engine thermal efficiency).

1.3 Progress

Thermodynamic optimisation is, literally, the search for the best thermodynamic performance subject to present-day constraints [6]. To improve the efficiency of internal combustion engines the thermodynamic analysis should include the second law. In this scope, the use of internal combustion engines is analysed focusing on the consequences to the universe, whether by destructing availability (exergy) or by entropy generation. These two kinds of analysis are very similar. From their result it is possible to define strategies that minimize the impact of the working engine on the environment, reduce energy degradation and save natural resources and money. The objective is always to get the same performance with the lowest “price”. Or, with the same “price” improve its performance. In the specific field of internal combustion engines, several works have been presented on the availability destruction during engine operation [7,8,9,10,11,12,13,14,15,16].

From a physics perspective, the use of energy has been treated under several manners. Effort has been made on the determination, for each type of thermal engine, of the optimum (most efficient) working point. And for the determination of this optimum

point several criteria have been applied, such as the maximum power conditions, maximum power density or the establishment of an ecological criterion.

In the specific case of internal combustion engines, the most common method for the analysis of the engine operation is the exergy destruction method. Considering the energy potential of the fuel introduced in the engine, the losses are evaluated for each irreversibility source in the engine.

The typical application where internal combustion engines are used at part load is the automotive. For this case several improvements (or improvement systems) have been introduced in engines so that “several optimum points” could be achievable in the same engine. Such systems are Variable Valve Timing (VVT) [17,18,19,20,21], Variable Compression Ratio (VCR) [22,23,24,25,26], Variable Displacement [27,28], Charge Stratification [29,30,31], or Variable Turbulence Generation [32,33].

1.4 Proposed strategy

Throughout the present work one solution is proposed for the reduction of the consumption impact on spark ignition engines at part load operation, which is the combination of the over-expansion principle together with the adjustment of the compression ratio. Over-expansion is achieved by the use of different intake valve closure timings and compression ratio variation is achieved by the use of pistons with different size combustion chambers.

For low engine speed, if maximum volumetric efficiency is achieved with intake valve closure around BDC, any change (advance or delay) of the intake valve closure time reduces the amount of mass trapped within the cylinder, thus controlling engine load. As the exhaust valve timing is fixed, expansion becomes longer than the compression, i.e. the engine works under over-expansion conditions. This also produces a reduction of the effective compression ratio, resulting in thermodynamic losses during the combustion process. Compression shall be adjusted for pre-knock conditions or maximum torque. The objective is to always reach the best efficient combustion conditions, independently of the load level demanded, thus improving the thermodynamic performance of the engine, namely at part load operation.

A detailed overview is presented of several technologies, which somehow help to reduce the fuel consumption under part load conditions, used either in research and development activities or already on production.

The thermodynamic improvement proposed above is analysed on a theoretical basis, with the objective of evaluating its preliminary improvement potential. Results are compared with similar analysis made to other engine cycles (stratified charge, compression ignition, supercharge). Comparison is made always using the load criterion.

The same analysis is made using a computer model capable of simulating spark ignition engines, simulating working conditions as close as possible to the reality. In this case the potential improvement results are refined and predictions are closer to reality. The entropy generation criterion was used to evaluate the thermodynamic processes that take place during the engine cycle and establish an optimisation priority. Acting on just two or three processes is possible to reduce the entropy generated significantly, thus improving thermodynamic performance.

The confirmation of the effectiveness of the proposed strategy was made through engine tests, revealing the effective improvement brought by the referred optimisation strategy. The same engine was tested in a compression ignition configuration and in a spark ignition configuration. In the spark ignition tests, the engine was tested working as an Otto cycle engine. Different camshafts were manufactured with modified intake cam profiles so that different intake valve closure timings were used. Using this method the engine was tested as a Miller engine. Finally, different pistons with different sized combustion chambers and consequently different compression ratios were used to obtain optimised combinations of intake valve timings and compression ratios for best working conditions.

1.5 References

1 Ealey, L. A., Mercer, G. A., *Tomorrow's cars, today's engines*, Mckinsey Quarterly, Number 3, 2002.

2 *The European Environment, State and Outlook 2005*, European Environment Agency, 2005.

3 *Kyoto Protocol to the United Nations Framework Convention on Climate Change*, United Nations, 1998.

4 http://www.epa.gov/ - 25/09/06 23:45.

5 http://ec.europa.eu/environment/co2/co2_home.htm - 27/09/06 23:00.

6 Bejan, A., Mamut, E. (eds.), *Thermodynamic Optimization of Complex Energy Systems*, 45-60, Kluwer Academic Publishers, 1999.

7 Shapiro, H. N., Gerpen, J. V., *Two Zone Combustion Models for Second Law Analysis of Internal Combustion Engines*, SAE 890823, 1989.

8 Bozza, Fabio, et. al., *Second Law Analysis of Turbocharged Engine Operation*, SAE 910418, 1991.

9 Caton, Jerald A., *A Cycle Simulation Including the Second Law of Thermodynamics for a Spark-Ignition Engine: Implications of the Use of Multiple-Zones for Combustion*, SAE 2002-01-0007, 2002.

10 Caton, Jerald A., *A Review of Investigations Using the Second Law of Thermodynamics to Study Internal Combustion Engines*, SAE 2000-01-1081, 2000.

11 Lipkea, William H., DeJoode, Arnold D., *A Comparison of the Performance of Two Direct Injection Diesel Engines From a Second Law Perspective*, SAE 890824, 1889.

12 Anderson, Michael K., et. al., *First and Second Law Analyses of a Naturally-Aspirated, Miller Cycle, SI Engine with Late Intake Valve Closure*, SAE 980889, 1998.

13 Caton, J., *Operating Characteristics of a Spark Ignition Engine Using the Second Law of Thermodynamics: Effects of Speed and Load*, SAE 2000-01-0952, 2000.

14 Caton, J., *On the destruction of availability (exergy) due to combustion processes – with specific application to internal-combustion engines*, Energy 25 (2000), 1097-1117.

15 Caton, J., *Use of a Cycle Simulation Incorporating the Second Law of Thermodynamics: Results for Spark-Ignition Engines Using Oxygen Enriched Combustion Air*, SAE 2005-01-1130, 2005.

16 Farrell J. T., Stevens, J. G., Weissman, W., *A Second Law Analysis of High Efficiency Low Emission Gasoline Engine Concepts*, SAE 2006-01-0491, 2006.

17 Hannibal, W., Flierl, R., Stiegler, L., Meyer, R., *Overview of Current Continuously Variable Valve Lift Systems for Four-Stroke Spark-Ignition Engines and the Criteria for their Design Ratings*, SAE 2004-01-1263, 2004.

18 Leone, T. G., Christenson, E. J., Stein, R. A., *Comparison of Variable Camshaft Timing Strategies at Part Load*, SAE 960584, 1996.

19 Stone, Richard, Kwan, Eric, *Variable Valve Actuation Mechanisms and the Potential for their Application*, SAE 890673, 1989.

20 Dresner, T., Barkan, P., *A Review and Classification of Variable Valve Timing Mechanisms*, SAE 890674, 1989.

21 Ahmad, T., Theobald, M. A., *A Survey of Variable-Valve-Actuation Technology*, SAE 891674, 1989.

22 Kajiwara, Kenichi, *A Variable-Radius/Length Engine*, SAE 920453, 1992.

23 Schwaderlapp, M., Habermann, K., Yapici, K.I., *Variable Compression Ratio – A Design Solution for Fuel Economy Concepts*, SAE 2002-01-1103, 2002.

24 Drangel, H., Olofsson, E., Reinmann, R., *The Variable Compression (SVC) and the Combustion Control (SCC) – Two Ways to Improve Fuel Economy and Still Comply with World-Wide Emission Requirements*, SAE 2002-01-0996, 2002.

25 Wong, V. W., Stewart, M., Lundholm, G., Hoglund, A., *Increased Power Density via Variable Compression/Displacement and Turbocharging Using the Alvar-Cycle Engine*, SAE 981027, 1998.

26 Moteki, K., Aoyama, S., Ushijima, K., et al., *A Study of a Variable Compression Ratio System with a Multi-Link Mechanism*, SAE 2003-01-0921, 2003.

27 Albertson, W., et al., *Displacement on Demand for Improved Fuel Economy without Compromising Performance in GM's High Value Engines*, Powertrain International, Vol. 7, Num. 1, Winter 2004.

28 Jost, K., *Mercedes-Benz launches cylinder cutout*, Automotive Engineering International, January 1999, pp.38-39.

29 Kettner, M., Fischer, J., Nauwerck, A., Tribulowski, J., Spicher, U., Velji, A., Kuhnert, D, Latsch, R., *The BPI Flame Jet Concept to Improve the Inflammation of Lean Burn Mixtures in Spark Ignited Engines*, SAE 2004-01-0035, 2004.

30 Kettner, M., Rothe, M., Velji, A., Spicher, U., Kuhnert, D, Latsch, R., *A New Flame Jet Concept to Improve the Inflammation of Lean Burn Mixtures in SI Engines*, SAE 2005-01-3688, 2005.

31 AEI August 2005, pp.38-9.

32 Olofsson, E., Alvestig, P., Bergsten, L., Ekenberg, M., Gawell, A., Larsén, A., Reinmann, R., *A High Dilution Stoichiometric Combustion Concept Using a Wide Variable Spark Gap and In-Cylinder Air Injection in Order to Meet Future CO_2 Requirements and World Wide Emission Regulations*, SAE 2001-01-0246, 2001.

33 Hirooka, H., Mori, S., Shimizu, R., *Effects of High Turbulence Flow on Knock Characteristics*, SAE 2004-01-0977, 2004.

2 – State of the Art

2 STATE OF THE ART

2.1 Introduction

To optimise future engine performance, advanced technologies will focus on "variable everything". Adding "on-demand" and "variable controls" to almost any system can improve fuel economy and lower parasitic losses [1].

This has been the aim of the engine research and development in recent years. The use of technologies such as Variable Compression Ratio, Variable Valve Timing or Charge Stratification are the testimonial of the general tendency to create and design engines that work under different conditions depending on the demand, with constant improvement of fuel consumption. The conventional engine where everything is fixed and where the change on the engine is made only by the throttle position, is being more and more replaced by engines that can change the amount of fuel per cycle or the spark timing (the most basic engine variation) up to the change in the valve event duration and even the engine effective displacement. As engines in automotive applications are supposed to be operated at several conditions of load and speed, a constant configuration engine is a very limiting constraint, forcing designers to assume compromise solutions for the engine configuration and working conditions. This usually also results in poor engine fuel economy. However, the variation of engine parameters, allows for the use of the same engine over a wider range of working conditions in the best performance regime. The objective is always the decrease of fuel consumption and thus the thermodynamic improvement.

The sources of inefficiencies or losses in the spark ignition internal combustion engines are presented in Table 2-1, where several technical solutions are related to minimize those losses. The table also shows the way those technologies can improve engine performance by reduction of the referred losses.

The improvement potential of such techniques by their own is significant, but the combination of several of these variable techniques allows even higher improvements in spark ignition engine performance. A numerical study [2] presents results such as:

- The use of variable valve timing and lift without any throttle lead to an improvement in terms of fuel economy that can go up to 5%.
- The increase of compression ratio for part load operation allows a fuel economy improvement of up to 7%.

- The use of lean mixtures lead to an improvement in terms of fuel economy that goes up to 17% at part load conditions.
- The combined effect of all the technologies referred in the study is said to improve fuel economy in 24%, which is very close to the actual part load Diesel engine fuel consumption.

Table 2-1 – Reduction of different losses for improved fuel economy.

	VCR	VVA	Turbocharging	Water Injection	Over-Expansion	Stratified Charge	Downsizing	Turbulence Generation	Variable Displacement
Pumping		✓	✓		✓		✓		✓
Friction							✓		✓
Exhaust to Ambient	✓	✓	✓	✓	✓	✓	✓		
Crevice Effects and Leakage	✓					✓	✓		✓
Incomplete Combustion	✓			✓		✓		✓	✓
Exhaust Blow Down	✓	✓	✓		✓	✓			✓
Heat Transfer				✓	✓	✓	✓	✓	✓

This project studies the potential benefits of two emerging technologies used simultaneously: VVT and VCR. Therefore an extended view of the existing systems that allow for a thermodynamic improvement of engines is presented. In the following sections an analysis will be made on these technologies, focusing on the achievements reached in the past years in terms of engine thermal efficiency and other performance measures.

2.2 Variable Compression Ratio (VCR)

The possibility of spark ignition engine compression ratio variation has direct influence in the performance of the engine in terms of specific fuel consumption. In fact the theoretical engine thermal efficiency is given by:

$$\eta = 1 - \frac{1}{\varepsilon^{\gamma-1}} \tag{2.1}$$

Once the gas characteristics (γ) are basically constant for every spark ignition engine, the main variable that controls the efficiency of the engine is compression ratio (ε). However, the possibility of changing this parameter is limited, as the knock limit of the fuel imposes an upper barrier for the compression ratio. At first glance, the change of the fuel is the first variable that may allow a significant increase of the compression ratio.

Although an increase of heat transfer happens with the increase of the compression ratio, it was shown [3] that the increase in efficiency due to compression ratio increase is due to the thermodynamic effect of having a larger volume expansion ratio.

Compression may be changed in an engine as a result of changes in work conditions like load decrease by throttling, which allows the compression to be increased. Also if altitude conditions are changed, an adjustment of the compression ratio may contribute to an increase of power output as well as increase of engine efficiency.

Engine compression ratio of reciprocating internal combustion engines can be adjusted by different design of several components of the engine. An analysis of the several ways of performing this adjustment was presented [4,5] for each engine component. These methods of performing VCR are summarized in Figure 2-1. The comparative evaluation of these concepts is made in Table 2-2.

All the compression ratio adjustment systems are reviewed with more detail in the following sections.

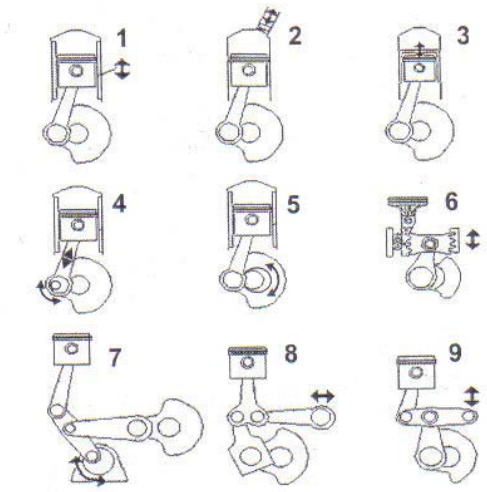

1: moveable cylinder block
2: changing head design
3: changing piston geometry
4: eccentric con rod bearing / con rod length
5: eccentric crank shaft bearing
6: force transmission by rack gear
7-9: second adjustable pivot point for con rod

Figure 2-1 – Variants of Variable Compression Ratio [5].

Table 2-2 – Comparison of VCR concepts [5].

Concept	Combustion chamber geometry	Force requirement adjusting unit	Design efforts	Additional forces of inertia	Controllability
Variable combustion chamber volume auxiliary piston	--	+	+	++	+
Piston with adjustable compression height	○	Self reg ++	+	-	○
Movable cylinder head, cylinder barrel	○	--	--	++	○
Two-piece pivoted connecting rod	○	○	-	--	+
Crankshaft positioning	○	+	+	++	+

++	Excellent
+	Good
○	Satisfactory
-	Disadvantageous
--	Insufficient

2.2.1 Moving cylinder block

This engine is able to change its compression ratio by moving the upper part of the cylinder block. The compression ratio of the Saab Variable Compression (SVC) [6, 7] engine is continually adjusted to the optimum value for the prevailing conditions.

The mono-head can be inclined up to four degrees (Figure 2-2) to achieve optimum compression, which means that the engine always works at its most efficient level. The engine is able to vary the compression ratio from 8:1 up to 14:1, depending on the engine load. SVC engine concept has been implemented in a 5 cylinder, 1.6 litre supercharged unit producing 225 bhp and delivering 305 Nm of torque. This concept enables fuel consumption to be radically cut (reduction of 30%) without impairing engine performance. This engine is as fuel efficient under normal conditions as a conventional 1.6 litre engine, but can deliver the power of a 3-litre engine whenever the need arises. The emissions of carbon dioxide are reduced proportionately to the fuel consumption, while the CO, HC and NOx emissions will enable the SVC engine to meet all the current and proposed future legal requirements.

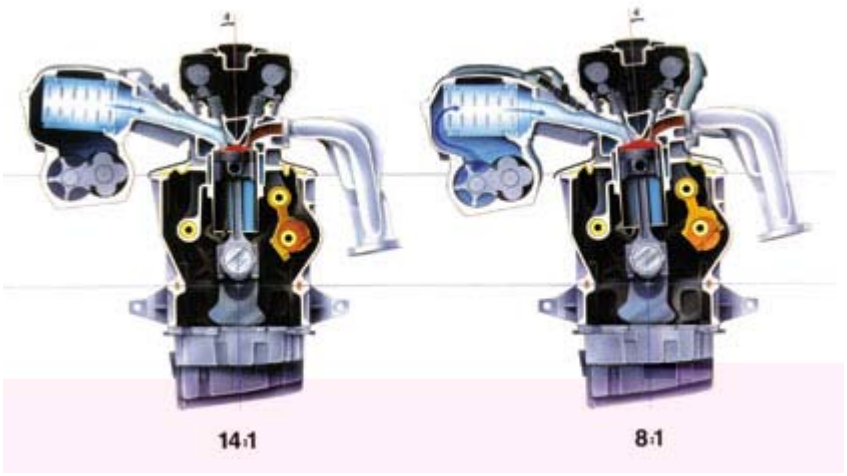

Figure 2-2 - Saab SVC engine in extreme positions.

This engine is also able to run using a variety of fuels, since its compression ratio may be adjusted to the fuel being used.

2.2.2 Combustion chamber volume variation

2.2.2.1 Ford type

This VCR system, patented by James Clarke and Rodney Tabaczynski from Ford [8] may be used either in compression ignition and in spark ignition engines and allows for a continuous compression ratio variation within a certain range.

The combustion chamber volume variation is achieved through the ascending and descending movement of a plunger, which is actuated using a cam positioned by a step motor. The motor is operated by a controller which defines the motor position using a variety of inputs from a plurality of sensors which may include, for example, throttle position, engine speed, intake manifold pressure, exhaust gas temperature, exhaust gas pressure, exhaust gas oxygen, air/fuel ratio, spark timing, engine knock, cylinder pressure or other parameters.

The plunger is moved back within a bore to the point where it defines a cylindrical recess (40 in Figure 2-3), which is in fact a supplemental combustion chamber volume. The position of the plunger is established based on the engine running conditions given from the parameters measured through the sensors.

If the controller determines that the engine is either knocking excessively or running at high loads which could generate knock at a level necessitating of the clearance volume beyond the first predetermined compression ratio range, the plunger will be moved back to a point such that the added clearance volume will be the cylindrical volume (40) plus the volume of a chamber (30) fixing the compression ratio at its lowest value.

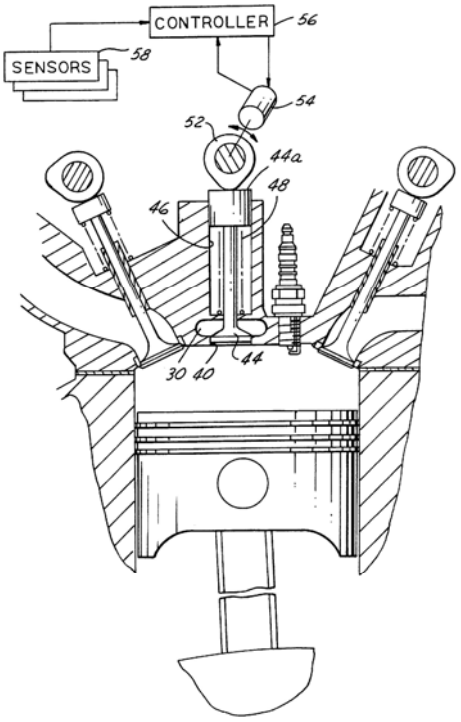

30 – Supplemental clearance volume
40 – Cylindrical recess
44 – Plunger
46 – Bore
48 – Plunger spring
52 – Cam
54 – Step motor
56 – Motor controller
58 – Engine parameters sensors

Figure 2-3 - Ford VCR system thorough combustion chamber volume variation [8].

2.2.2.2 Volvo/Alvar type

This VCR system presented by Volvo [9] has a complementary capability of varying the engine displacement. Variable geometry is achieved by a secondary piston reciprocating in an auxiliary chamber in the engine head (Figure 2-4). The intake, compression, expansion and exhaust characteristics can be controlled by adjusting the phase difference between the primary and secondary pistons. Since the total swept volume (primary plus secondary) depends on the phase difference of the pistons, the total engine displacement can also be varied.

A small crank and piston mechanism, which varies the volume of each combustion chamber, is mounted in the cylinder head. This mechanism utilises a secondary piston, for each cylinder of the engine, connected to a secondary crankshaft, which is driven at

half speed from the main crankshaft. A phase shifting mechanism between the crankshafts enables variation of the compression ratio.

When working at low load the secondary piston is at its lowest position when the primary piston is at TDC, thus maximum compression is achieved during the combustion event.

At full engine load the secondary piston is at its highest position when the primary piston is at its TDC, thus lowest compression is achieved during the combustion event, reducing the probability of engine knock.

Alvar engine is capable of operating at much higher boost levels, when compared to a conventional engine before knock onset. This is due to the capability of the engine to selectively vary the compression ratio according to engine load and intake boost.

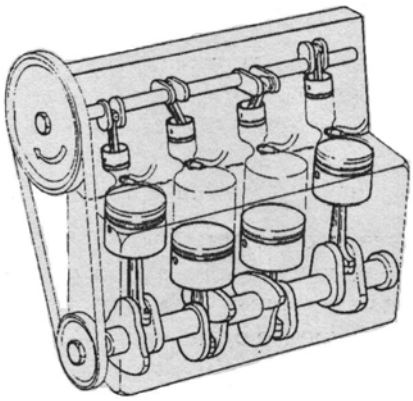

Figure 2-4 - The Volvo/Alvar VCR engine.

2.2.2.3 Riley Engine

This engine [10] is a conventional 4-stroke or 2-stroke internal combustion engine, which has an auxiliary chamber connected to the combustion chamber (Figure 2-5), where a secondary piston (8 in Figure 2-5) slides increasing or decreasing the combustion chamber volume and hence the geometric compression ratio of the engine. An adjustable rod (10) actuates the secondary piston. A spring (17) connects the rod to the piston so that a small relative movement is allowed between them. The chamber between the piston and the auxiliary cylinder is filled with an incompressible hydraulic fluid, which accomplishes two functions: absorption of forces transmitted from the combustion chamber pressure (so that the adjustable rod is not damaged) and cooling of the piston that contacts with the burned gases of the combustion chamber.

The engine has also delayed intake valve closure timing and thus a lengthened expansion stroke, increasing the thermal efficiency of the engine.

The same variable combustion chamber volume device can be used with 2-stroke internal combustion engines. In this case an additional rotary valve is used to control the amount of air-fuel mixture trapped in the cylinder. The valve is opened during the compression realising the air from the cylinder back to the intake manifold.

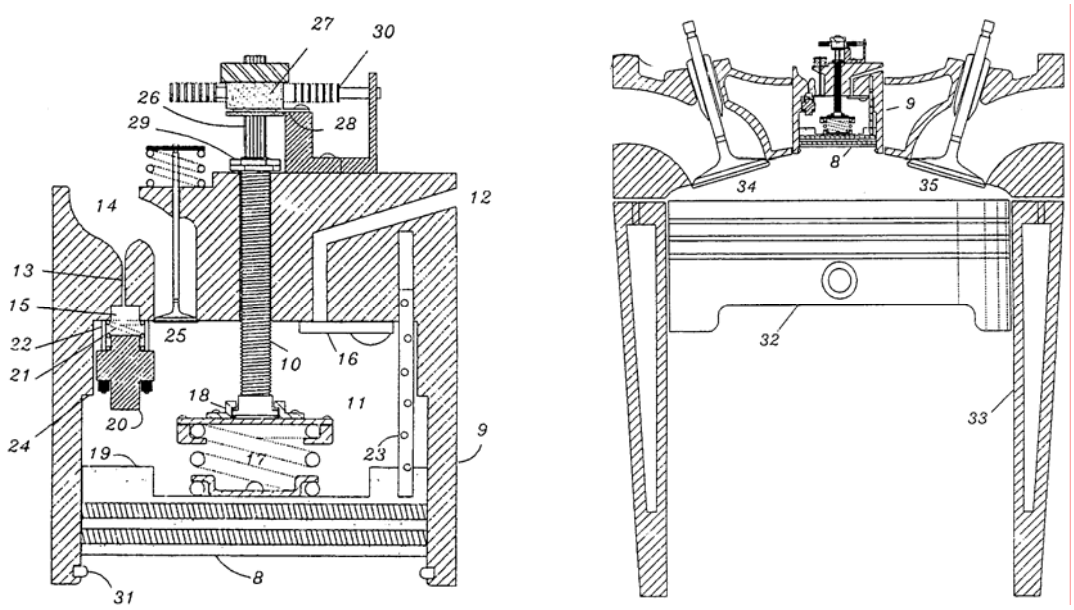

Figure 2-5 – The Riley engine.

2.2.3 Piston with adjustable compression height (Ford) [11]

The VCR piston from Ford (Figure 2-6) is an assembly of two parts: a trunk portion with a bore for receiving the piston pin and a crown portion slidably mounted upon the trunk portion. The piston rings are mounted in the piston crown portion. Between the trunk portion and the crown portion is placed a resilient element that tends to separate both portions.

During the lower pressure part of the cycle (intake stroke), the volume of the cylinder will be lower, because the crown portion will be at its upper position, and the amount of fuel trapped will be lower. The resilient element will be compressed during the high pressure part of the cycle (combustion and expansion stroke) and the volume of the cylinder or the expansion performed during the cycle will be higher.

The resilient element may comprise a conical, or Belleville washer extending between an interior surface of the crown and the upper surface of the trunk portion. Alternatively the resilient element may comprise an annular spring, or a combination of an annular spring and a pneumatic spring positioned between the crown position and the trunk position. The pneumatic spring may be supplanted by a plastic foam spring.

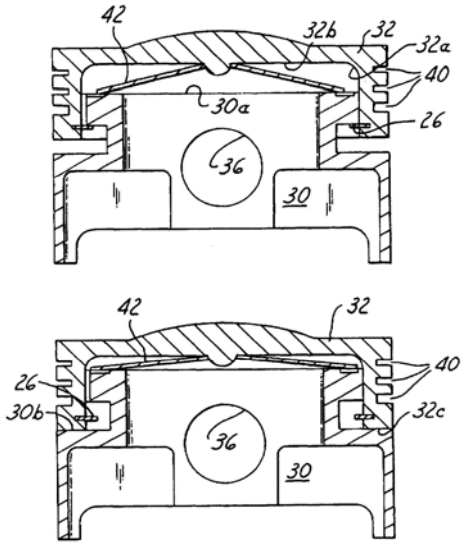

26 – Snap ring
30 – Trunk portion
32 – Crown portion
36 – Piston pin bore
40 – Piston rings groves
42 – Belville washer

Figure 2-6 - The Ford VCR piston in the fully extended and fully retracted positions [11]

2.2.4 Eccentric Crankshaft Bearing

A VCR system was developed by FEV [5] in which the variation of the combustion chamber volume is achieved by the change of the centre of the crankshaft. The crankshaft turns in eccentric bearings. As these eccentric bearings are rotated the vertical position of the crankshaft bearings is changed and thus the position of the top and bottom dead centre are shifted (Figure 2-7). The eccentric positioning of the crankshaft axis has to be compensated at timing and flywheel drive in order to achieve a concentric rotation. This requirement implies the introduction of a variable offset coupling.

Despite the increase of moving parts and connections the friction mean effective pressure of this engine is very close, and some times lower, than a conventional engine in the market.

A Romanian patent [12] describes a VCR system in which the bearings of the crankshaft journals are fitted in bores, which rotate eccentrically, leading to a variation of the dead centres and thus a compression ratio variation.

The system is controlled by a worm gear (1) (Figure 2-8), that drives a lever shaft, which, with lever (2), causes some eccentrically bored bushes (4, 5) fitted to a bearing (7) to rotate. A step-by-step electrical motor based on load and speed sensors actuates the worm gear. Depending on the direction of rotation of shaft 1, the compression ratio increases or decreases.

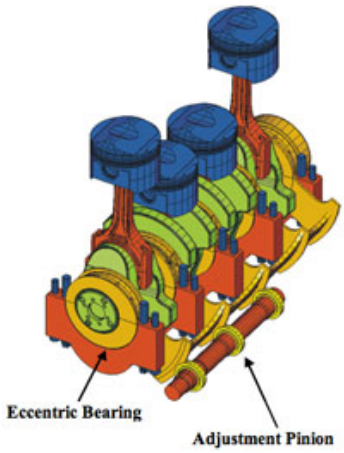

Figure 2-7 – FEV VCR system.

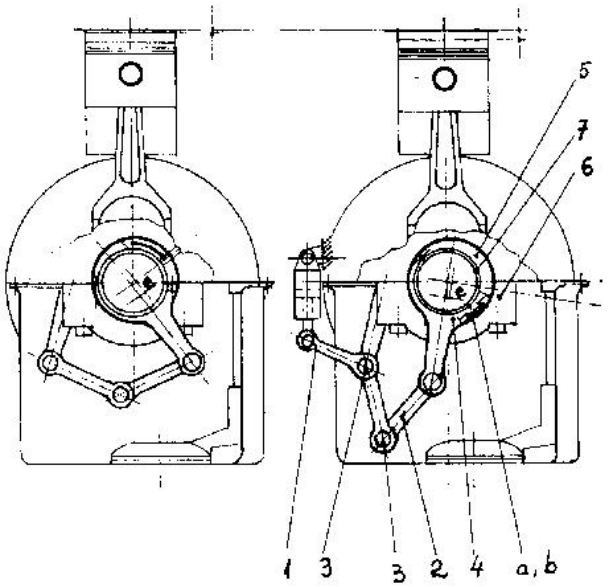

Figure 2-8 – Displaced Crankshaft Journals System.

2.2.4.1 Variable-Radius/Length (V-L/R) Engine [4]

This engine is equipped with an eccentric between the crankpin and the connecting rod big end (Figure 2-9). This eccentric rotates with respect to the crankpin. On the outside of the eccentric exists an external gear. An internal gear inscribed in the eccentric gear is installed in the crankcase. A worm gear commands the position of the internal gear and

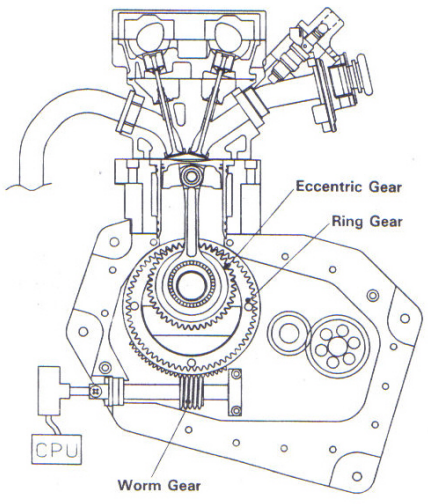

Figure 2-9 – The V-L/R Engine Structure.

regulates the compression ratio of the engine. In this engine the position of the BDC is constant but the position of the TDC is different from the combustion TDC and the overlap TDC, being higher in the latter. The compression ratio of the engine can varied from 8.5:1 up to 14:1. However friction losses are referred to increase.
The increase of the eccentric size is shown to be an effective factor on engine performance improvement. Compared to the standard engine, the V-R/L engine shows a 7% increase in output torque. This is due to the increased volumetric efficiency, that is, the effect of a larger TDC top clearance volume and an increased expansion stroke.

2.2.4.2 Hipocycloidal engine - The GoEngine

An engine of hypocycloidal motion is presented by Bert de Gooijer [13]. The GoEngine is said to be the only VCR engine with a true 720 degree cycle, which features an over-expanded engine cycle, different TDC positions within one cycle, a variable inlet volume and an important reduction in piston skirt friction. This engine is able to have an over-expansion from 125% up to 200% and a VCR from 6 to 15. This leads to a big reduction in fuel consumption (40% less) and increased power output (10% more). The basic concept beside this engine is the use of the maximum pressure after combustion as total as possible, for an expansion longer than the compression.

Figure 2-10 - The GoEngine structure. It can be seen the inner gear connected to the crankshaft.

The hypocycloidal engine is made of a fixed gear with teeth on the internal circumference, and this engages the external teeth of a gear wheel of 2/3 the diameter. The centre of this inner gear is connected to the crankshaft (Figure 2-10). The actual crankpin is offset from the centre of the internal gear by 1/3 of the length of the primary crank link. The extra eccentric between the crankshaft and the big end of each connecting rod, which follows the eccentric and not the crankpin as in a conventional engine. This mechanism makes that both TDC positions of the piston are the same but not the BDC. The piston position at the end of the expansion is lower than the position of the piston at the end of intake stroke.
The engine is also able to vary continuously the TDC while the engine is running. This can be made by rotating the ring-gear slightly in either directions.

2.2.5 Adjustable pivot point for connecting rod

2.2.5.1 Mayflower [14]

In this system, compression ratio adjusts according to engine speed and load, which means that the engine will run with optimal combustion pressures at all times. This VCR system allows a supercharger or a turbocharger to be used without compromising low engine speed performance. This means that the size of the engine can be reduced with no loss of performance.

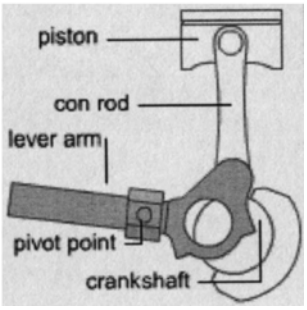

Figure 2-11 - The Mayflower engine concept.

In the Mayflower e3 engine, a pivoted lever arm is introduced between the crankshaft and the con-rod (Figure 2-11). This gives a more elliptical path to the con-rod big end, which changes the piston motion. Mayflower claims as benefits of the VCR system:

- Combustion improvement. The piston is slowed momentarily just after ignition and this allows the flame to spread faster. The fuel burns more completely which generates more power and reduces unburnt fuel emissions.
- Air intake and efficiency improvement. The more elliptical path of the con-rod big end means the intake and expansion strokes become longer.
- Friction reduction. The piston and con-rod are aligned in a torque-producing angle (and are not vertically aligned as a conventional engine) when combustion occurs around top dead centre.

The pivot point can be moved vertically and horizontally to vary the lever arm geometry while the engine is running. This has the effect of changing the compression ratio and/or the capacity of the engine. This also gives the engine a variable geometry that can adapt intelligently to power demands.

2.2.5.2 Nissan

Nissan patented [15] a different mechanism of VCR, also using a modification of the link between the crankshaft and the connecting rod. The system (Figure 2-12) comprises an upper link, connecting the piston to a lower link, rotatably connected to a crankpin of

the crankshaft. The lower link is also connected to a control link. This one is connected in the opposite side to the engine body, although being able to move in relation to it. By means of the control link, the degree of freedom of the lower link is properly restricted. The lower end of the control link is rockabilly supported by means of an eccentric cam, which is fixed to a control shaft, actuated by a compression-ratio control actuator. By rotary motion of the control shaft and cam, the centre (the pivot axis) of oscillating motion control link is shifted or displaced relative to the engine body. As a consequence, the TDC position of the piston, that is, the compression ratio of the engine can be varied.

It was shown [16,17] that engine friction attributable to piston side-thrust can be reduced through an upright orientation of the upper link in the expansion strokes. Later [18] it was shown that piston motion near TDC is slower than at near BDC, the first half of the expansion stroke in the VCR engine being 14% longer in terms of crank angle than in a conventional engine. This allowed for an improvement in combustion stability. A maximum fuel consumption reduction of 13% was achieved with a compression ratio of 14.3:1.

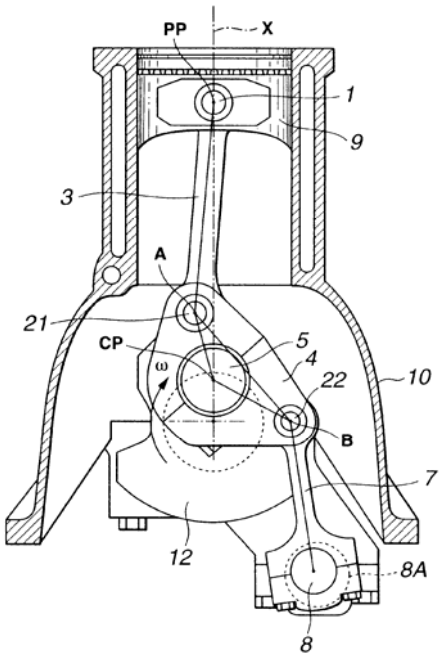

1 – Piston pin
3 – Upper link
4 – Lower link
5 – Crankpin
7 – Control link
8 – Cam
8A – Control shaft
9 – Piston
10 – Engine block
12 – Crankshaft
21 – Connecting pin
22 – Connecting pin

Figure 2-12 - VCR mechanism patented by Nissan. The piston is at the TDC.

2.2.5.3 Peugeot

The French OEM Peugeot detains a patent [19] of a system to be applied in internal combustion engines that is able of varying the compression ratio and the swept volume. The system, presented in Figure 2-13, is composed of two con rods. The piston rod (or also called slave con rod) is connected to a main con rod that turns with the crankshaft. The main con rod is also connected with a rocker arm associated with a control device of the position of the rocker arm. The main con rod has a long arm (connected to the rocker arm) and a small arm (connected to the piston rod).

The position of the control device, and as a consequence of the rocker arm, determines the position of the piston TDC, which in turn determines the piston stroke and the BDC, or the displacement and the compression ratio.

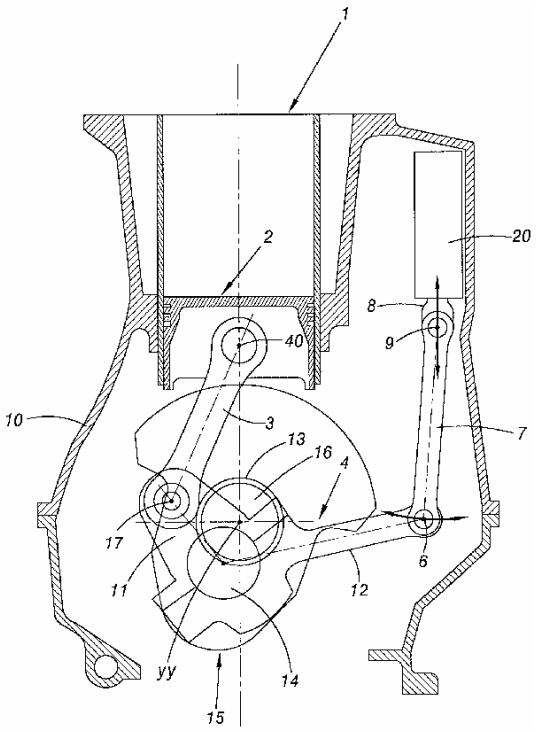

1 – Cylinder
2 – Piston
3 – Piston rod (slave)
4 – Main con rod
6 – Connecting point of the main con rod and the rocker arm
7 – Rocker arm
8 – Control device
9 – Connecting point of the control device and the rocker arm
10 – Engine block
11 – Small arm of the main con rod
12 – Long arm of the main con rod
14 – Crank
15 – Crankshaft
16 – Crankshaft journal
17 – Connecting point of the main con rod and the piston rod
20 – Actuator

Figure 2-13 - The VCR system from Peugeot.

The authors of this system suggest as main advantages:

- Important potential gains in consumption, through:
  - Efficiency improvement at part load when rising the compression ratio and lowering the displacement;

  - Possible increase of the supercharge ratio without knocking, due to a reduction of the compression ratio;
  - After-expansion management over a great using range;
  - Particularly combustion modes: auto-ignition, poor homogeneous mixture, significant EGR.
- Possible variation of displacement of more than 25 % for a compression ratio variation of 100 %;
- Simple technology for the several components of the system;
- System compact and with low mass.

2.3 Variable Valve Actuation

Variable valve actuation (VVA) systems are devices that give the ability of engines to have different valve events in terms of timing (variable valve timing - VVT), phasing and lift. At the same time, VVA may also give engines the ability to vary the valve opening area.
The different variable valve event systems, are compared in Table 2-3 [20]:

Table 2-3 – Potential improvements and rating of VVA systems.

Function	Improvement			Effort	Rating
	Consumption	Emissions	Mep		
Continuous cam phasing	+	++	++	-	3
Variable opening period	+	O	++	---	4
Variable valve lift with cam phasing	++	+++	+++	--	1
Contin. variable lift with cam phasing	+++	+++	+++	----	2
Lost motion	++	O	++	---	3
Electromagnetic valve operation	+++	++++	++	----	2

The continuous variable lift with cam phasing and the electromagnetic valve operation are the most promising, but at the same time require the greater effort for research and development and production.

An increasing interest on VVA systems can be assessed by the number of patent applications made in this area (Figure 2-14). It reveals the great interest that automobile companies have in the development and production of such systems. The decrease in the number of patents in recent years does not mean a reduction of innovative work but is caused by the fact that some patents were not disclosed at the time of the study.

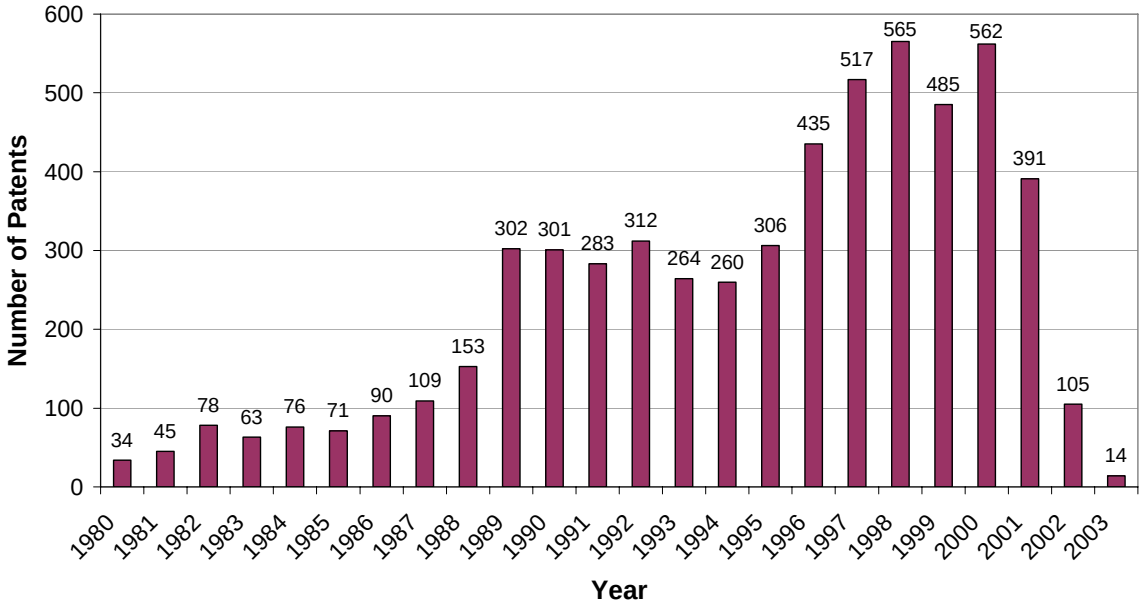

Figure 2-14 - Number of patent applications relating to variable valve control systems [21].

2.3.1 Effects of valve timing and lift

Valve actuation variation allows, depending on the valve actuation system configuration, the variation of the following variables:

- Valve opening and closing instants
- Valve lift
- Valve velocity

By changing these variables several effects may be achieved in engine performance. For a VVA system to be efficient it is required that the frictional losses, introduced by the system, be small in order to yield efficiency gains.

2.3.1.1 Variable Intake Timing

The change of the intake valve closure timing can be used to control the engine load. The throttle valve at the intake manifold entrance creates the pumping loss that reduces useful work. If the throttle valve is kept fully open the change of the intake valve closure timing (advancing or delaying) controls the amount of mixture inducted in the cylinder. With this technique the pumping work is reduced, with an associated fuel efficiency improvement. It was reported [28] that the early valve closure allows lighter loads, than it is possible with late intake valve closure. When using late intake valve closure a problem may appear at very low loads because ignition may happen before intake valve is closed [29]. Using this method to control engine load, the response of the engine to accelerations is improved, as there is no delay associated to the filling of the intake manifold.

To achieve good cycle efficiency the fuel must be burned at a high rate and next to the top dead centre. The burning rate is heavily dependent on the turbulence of the mixture inside the cylinder. At low engine speed the turbulence generated during intake is very reduced. This can be overcame by delaying the intake valve opening time so that it takes place at the instant when the piston has its higher speed, already during the descending stroke. This increases the air velocity entering the cylinder and the internal turbulence.

Engines with a conventional valvetrain produce a torque curve with a distinct peak value near the middle range of engine speed, as a result of the compromise design of the cams shape, to produce its maximum torque at the middle engine speeds. A flatter torque curve can be produced with intake valve timing adjustment. At the high speeds the valve closure is varied to take the advantage of the ram effects. At low engine speeds, the valve closing delay must be avoided to obtain maximum effective compression ratios. This effect can also be used during the whole engine operating range, leading to an engine with variable compression ratio and with fixed expansion stroke, with advantages in terms of fuel efficiency.

Late intake valve closing made at low engine speed causes some of the fresh charge to be pushed back into the intake port during the first part of the compression stroke. To maintain a given load a higher manifold absolute pressure is required, and intake stroke pumping work is reduced. However, this also brings a reduction of the effective compression ratio, with a consequent reduction of the engine performance.

2.3.1.2 Variable Exhaust Timing

The possibility of changing the opening of the exhaust valve can be used to optimise the expansion ratio at low engine speeds. As there is more time for blow-down, the opening event may be delayed. This leads to an improvement in fuel efficiency, specially at low loads and a general torque improvement. However, space availability between the valve and the piston to avoid interference limits this procedure [23].
The exhaust valve closure timing can also be used to control the amount of exhaust gas recirculated, eliminating the need for external equipment to promote exhaust gas recirculation. Early or late exhaust valve closure may retain, or suck back from the exhaust manifold, respectively, a greater quantity of burned gas inside the cylinder. This method is complementary of the load control by the intake valve closure timing.

2.3.1.3 Variable Valve Lift

Changing the valve lift as function of speed allows for some energy savings in the valvetrain motion. At lower speeds, the valve stroke can be reduced, saving energy, with thermal efficiency improvement. Also at low speeds, if the lift is reduced, the air speed crossing the valve is higher, increasing turbulence and improving burning conditions due to better mixture formation. However, an optimum operating point must always be found between mixture formation and minimization of pumping losses.
Another method to control air motion within the cylinder can be achieved in two intake valve engines by lifting unequally both valves. In this case air flows into the cylinder in two unequal streams, which, when mixed, can provide a variety of in-cylinder flow patterns.
Exhaust valve lift reduction may also be used to throttle the exhaust flow, retaining in the cylinder the last portion of the exhaust charge that contains the highest concentration of unburned hydrocarbons, which are then burned in the following cycle.

2.3.1.4 Valve Overlap

One of the variables controlled by valve actuating mechanisms is valve overlap, the period when both (intake and exhaust) valves are opened, affecting emissions, full load performance and idle behaviour.

The correct adjustment of the exhaust valve closure and intake valve opening (valve overlap) for minimum residual gas inside the cylinder, contributes to better idle stability. The amount of exhaust gas inside the cylinder may be controlled and reduced during idle operation. Moreover, at part load operation and if overlap is shifted to the intake stroke, the amount of residual gas in the cylinder will be higher, reducing the produced NO_x. Two other effects are also achieved: the reduction of unburned hydrocarbons, which are the last part of the exhaust flow living the cylinder are drawn-back before exhaust valve closure; and the reduction of the pumping work during intake [22]. However, too large valve overlaps lead to higher HC emissions due to the large amount of residuals retained in the cylinder which slows down the combustion and leads to combustion instability [23].
Valve overlap adjustment with valve lift variation, allows for a lower idle speed thus achieving a significant reduction in fuel consumption.

2.3.1.5 Valve Velocity

In engines with conventional valvetrains, the lifting velocity of the valve is related to the crankshaft speed, making the valve move faster only when the engine speed is higher. The change (increase) of the lifting velocity of the valve allows for the rise and descent period occupying a shorter time in the entire valve event. The shape of the lift curve plotted against crank angle becomes rectangular like at low speeds and trapezoidal at high speeds. This represents an increase of the valve area, which is a significant factor in the increase of the engine volumetric efficiency and higher torque.

2.3.1.6 Valve Deactivation

Valve deactivation allows the insulation of one or more cylinders of the engine, forcing the remaining cylinders to operate at a higher load so that the engine can have the same torque output. When working at a higher load, the fuel consumption is reduced. This technique is mostly known as Variable Displacement and will be treated with more detail below. When working at idle conditions, valve deactivation can be used to insulate one or more cylinders increasing the load on the active cylinders so that the specific consumption on those cylinders could be reduced [24].
At part load, cylinder deactivation improves fuel consumption by [25]:

- Reducing pumping losses: Pumping losses in the deactivated cylinders are completely eliminated. The active cylinders work at a higher load, also decreasing the pumping losses of those cylinders.
- Improving combustion: The active cylinders work at higher load, so at higher effective compression ratios, due to the increase of the manifold absolute pressure, thus improving the combustion efficiency.
- Reducing mechanical losses: Mechanical losses in the valve train are reduced due to a reduction of forces (thus friction) in the valve train contacts, once valves are not compressed to open.

By using valve deactivation different air motion patterns inside the cylinder can be achieved. In engines with two inlet valves the deactivation of one of the valves favours a swirl air motion pattern, while the operation of the two valves favours a tumble motion pattern. This effect can even be more pronounced if valve deactivation is used simultaneously with late intake valve opening. In this case the air flow rate at the opening of the intake valve is higher, increasing the turbulence inside the engine cylinder [26].

For several reasons misfire may occur during engine operation. Without burning, an amount of unburned hydrocarbons passes to the exhaust system and catalytic converter, where it may burn, and this can be very damaging. Using valve deactivation the cylinder where misfire has occurred can be kept close in order to perform combustion in a subsequent cycle.

Another benefit of valve deactivation is the reduction of the cranking torque. Deactivating some cylinders (open valves, inactive fuel injectors), will substantially reduce the power requirement for an electric starter and, possibly, allow to combine a starter and an alternator into one reversible electrical machine.

2.3.2 Systems classification

Throughout the literature on internal combustion engines, three articles were found as being of the most interest for an introduction and some detailed description about variable valve timing systems.

A taxonomy for classification of VVT systems has been proposed [27] which is shown in Figure 2-15. A different approach is proposed [28] which is presented as a table on Figure 2-16 with 15 concepts for valve actuation mechanisms, presenting limitations,

approximate ranges of duration and advance that can be achieved and best features. In the third study [29] of different variable valve actuation mechanisms, various systems are divided through categories that comprise:

- Passive devices
- Fixed-Lift, Two-Position Phase Shifters
- Fixed-Lift, Continuously Variable Phase Shifters: Unmodified Lift Curve
- Fixed-Lift, Continuously Variable Phase Shifters: Modified Lift Curve
- Variable Lift, Duration and Phasing

In terms of systems capabilities, another comparative scheme is proposed [30]. Based on the division proposed above, it adds the potentialities and limitations of the several system types in terms of control parameters.

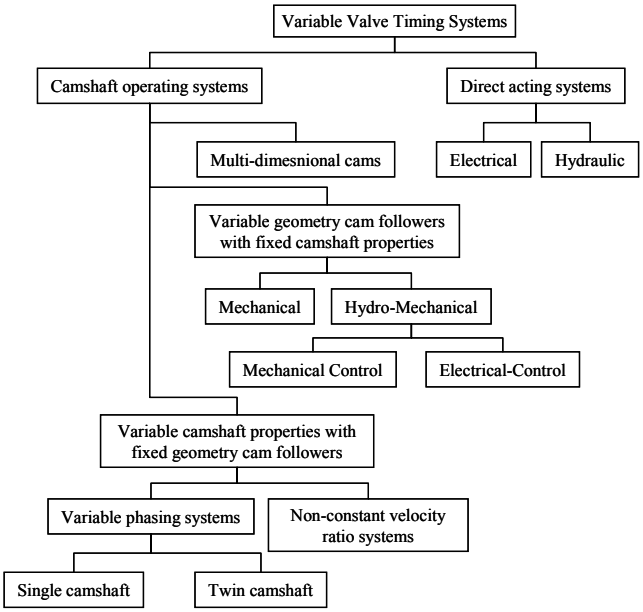

Figure 2-15 - Taxonomy of VVT systems [27].

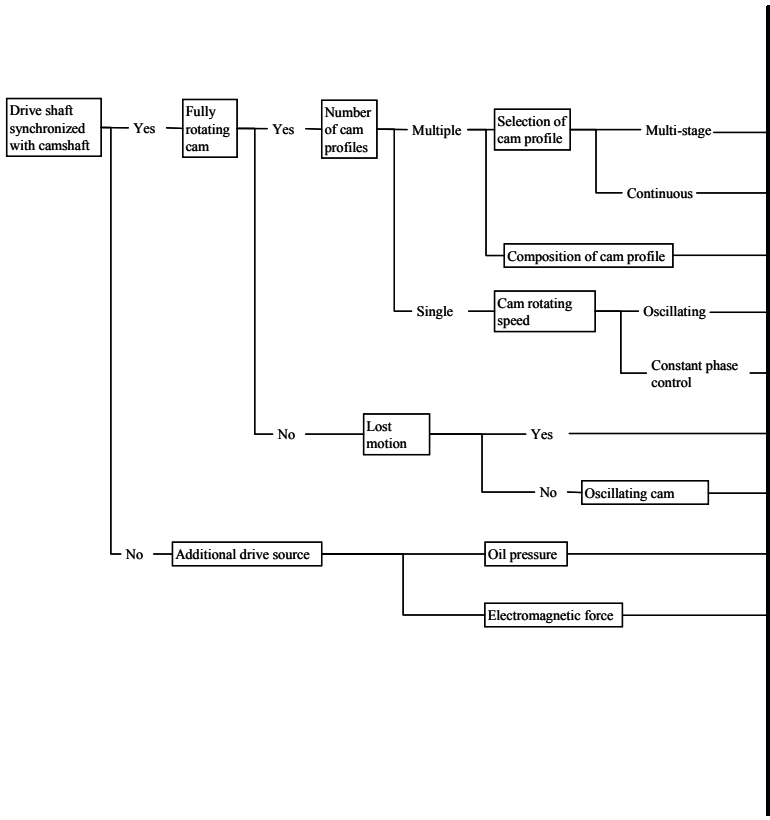

Example of study	Selectable stages	Control		
		Event angle	Lift	Phase
VVL	2 or 3 stages	●	●	(●)
3D Cam	Continuous	●	●	(●)
Prism cam	Continuous	●	●	(●)
VVE	Continuous	●	-	(●)
VTC	Continuous	-	-	●
HVT	Continuous	●	●	(●)
VEL	Continuous	●	●	(●)
HEV	Continuous	●	●	●
EMV	Continuous	●	-	●

VVL – Variable Valve Lift
VVE – Variable Valve Event & Timing
VTC – Variable Timing Control
HVT – Hydraulic Variable Valve Train
VEL – Variable Event angle & Lift
EHV – Electro Hydraulic Valve
EMV – Electro Magnetic Valve
(●) - Restricted

Figure 2-16 – VVT systems classification and functioning range [30].

2.3.3 Variable Valve Timing Systems

In the following sections a brief description is made of some variable valve timing systems. As long as it is available, some information is given about the benefits achieved with each system.

2.3.3.1 Variable cam phasing

A strategy of variation of the valve events is by phase-shifting the camshaft in relation to the crankshaft. This technique was evaluated for engine operation at part load [23,31,32]. The Dual Equal strategy involves phase-shifting the intake and exhaust events equally. This phasing shift is normally performed with the use of a phaser in each camshaft [23].

The effect of the valve event variation was explained previously, but this strategy adds another effect, the overlap shift, specially delayed overlap. Valve overlap happening

during the downward movement of the piston leads to an amount of exhaust gases being drawn back from the exhaust manifold into the cylinder. Three results are expected:

- NOx reduction because of the increased internal residual;
- Unburned HC reduction because these are the last part of the exhaust and thus the first to be drawn back into the cylinder;
- Intake stroke pumping work is reduced due to the need of higher manifold absolute pressure as a consequence of the increased internal residual, to maintain a given load. Also, the exhaust gases drawn back into the cylinder are at exhaust backpressure, which corresponds to higher cylinder pressure.

Retarding cam events can affect the in-cylinder air-fuel mixing, and a reduction of CO emissions may be reached, due mainly to:

- Increase of the inflow velocity into the cylinder due to the increase of the piston velocity in relation to the intake valve lift, caused by the delay in the opening of the intake valve. This higher velocity of air leads to better mixing with fuel;
- The previous effect can be even more intensified if valve mask is used to induce air turbulence, swirl or tumble. The resulting turbulence will be more intense and mixing will be more effective;
- The increase of the internal residual at high temperatures promotes fuel vaporization in the cylinder and so better air-fuel mixing.

It has been shown [23] that for constant values of intake valve opening, the retard of the exhaust influences fuel economy in three ways:

- Exhaust back pressure is near atmospheric and during the intake stroke the exhaust valve is opened reducing the pumping losses. However as the speed increases exhaust cam retard must be reduced because of the effects of the late blow-down on pumping loss become significant;
- Increased expansion due to retard exhaust valve opening;
- The residual gas fraction is increased, reducing the temperature of the burned gas and the heat loss to the combustion chamber walls.

Intake cam timing affects consumption through pumping loss and compression ratio variation. Retarding intake valve closure leads to more push back of the charge into the intake manifold, and at the same time the effective compression ratio is reduced with a consequent reduction of thermal efficiency happens.

The overall cam phasing strategy can be represented graphically as shown in Figure 2-17, where cam timing requirements for several working conditions are represented. The black square represents the working area for the cam phasers to change cam timing.

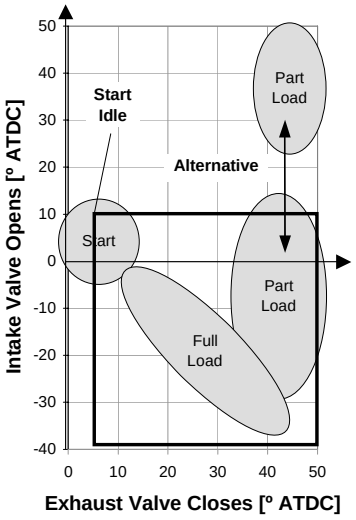

Figure 2-17 – Cam phasing strategy for Twin VCT [23].

Another example of variable phasing is performed in a DOHC engine with a fixed belt extender, which is converted into a variable working position belt extender [33] (Figure 2-18). By changing the belt extender working position, two different intake valve timing may be achieved. The exhaust camshaft is connected to the driving gear, while the intake camshaft is connected to the driven gear. Hence the exhaust valve timing is kept constant and only the intake valve timing is changed. When the belt extender moves in one direction or the other, the belt length between one gear and the other is changed and so is the intake cam timing. Under full load condition, more than 11% torque increase was obtained at low-speed and more than 7% torque increase at high-speed. The benefit of intake valve closure timing on engine power output mainly occurs at heavy load, such as the load rate greater than 60%, especially over 80%. Fuel economy improvement was achieved in most of the speed range, especially at high speed. The CO emission was reduced significantly and the HC emission was reduced only at high speed. However NO_x emission increased by more than two folds of the baseline level.

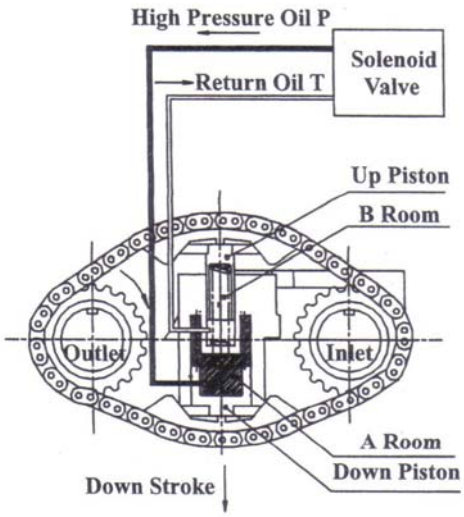

Figure 2-18 – Variable working position belt extender.

2.3.3.2 Valve timing by cam follower

The following VVT systems are characterized by changing the valve timing by offsetting the lift curve. By reducing the valve lift, the opening and closing time is changed. When the valve lift is reduced, the opening is delayed and the closing is advanced. The modification is made usually at the cam follower or rocker arm, by mechanical means or by the introduction of an hydraulic device in between.

Valve Lift and Timing Control

A system was presented [34] where the modification of the valve motion is commanded by the rocker arm positioning mechanism. The variation of the cam timing is made around the maximum lift timing, which is always fixed. The system is shown in Figure 2-19. The system has a rocker arm with a curved back surface, a lever that supports and runs along the back surface of the rocker arm, a hydraulic lash adjuster that supports the end of the lever and a control cam that varies the slant of the lever. The rocker shaft is able to move vertically thanks to the fork that extends downward from the lever. When the control cam pushes the lever down, the system commands the valve for maximum lift (left side of Figure 2-19). As the control cam is rotated upward (right side of Figure 2-19), the lever also moves upward and the motion transmission between the cam and the valve is reduced and consequently the lift is reduced. Results of the performance of this system showed a torque improvement at low and medium speeds and a maximum power output of 7%. As valve lift is reduced fuel consumption is also reduced and an improvement of 11% was achieved.

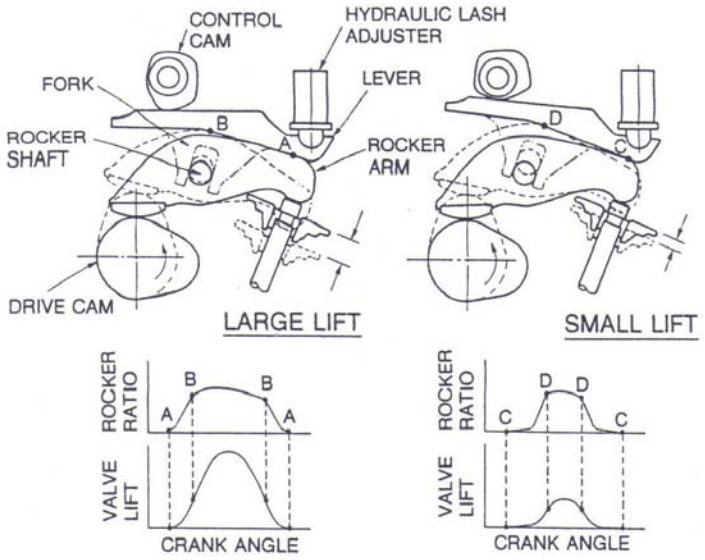

Figure 2-19 – Valve Lift and Timing Control (VLTC).

Hydraulic Systems

Some hydraulic systems for valve command appeared [35,36,37]. which also include a camshaft and are able to make variations of the intake valve closure timing (early), and reducing the valve lift.

These systems include the camshaft and a modified linkage between the camshaft and the valve. One of the examples presented in the literature [37] includes two pistons positioned in the same axis (Figure 2-20), one connected to the camshaft and other connected to the valve. Between the two pistons exists a chamber with pressurized oil. When the lifting movement of the cam starts the first piston compresses the oil and it returns back to the tank through a discharge nozzle, until that nozzle is closed by the first piston and the oil pressure inside the cylinder starts to increase forcing the secondary piston to move and the valve to open. The head of the first piston has a spiralled canal, which allows different instants for the pressure in the chamber to rise as this first piston is rotated.

Specific consumption improvements were reported at low speed and low and medium load, as a consequence of the reduction of gas exchange losses but also due to the positive combustion effects arising from reduced residual content of the charge. At full load, improvements in output torque were also reported. However at medium and higher speeds as well as low loads the poorer mixture formation offsets the gains in brake

specific fuel consumption derived from the reduced throttling losses. Despite this, the tests made over a series of engine operating points demonstrated that these VVA systems are generally beneficial [35]. The reported results on these engines demonstrate improvements in terms of torque [36,37].

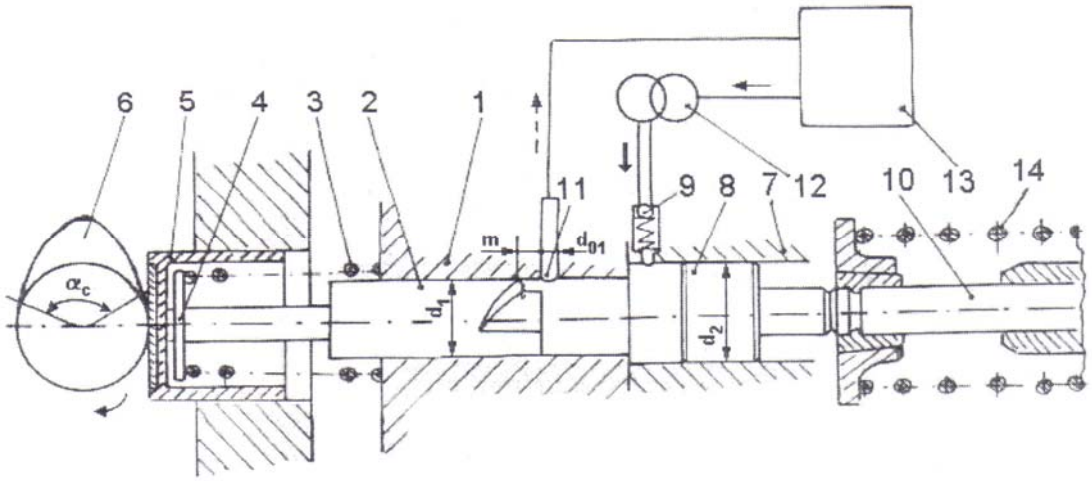

1 – Cylinder
2 – Delivery Piston
3 – Spring of the Delivery Piston
4 – Disc
5 – Tappet
6 – Camshaft
7 – Actuation Cylinder
8 – Actuation Piston
9 – Supplying Valve
10 – Engine Valve
11 – Discharge Nozzle
12 – Supplying Pump
13 – Oil Tank
14 – Spring of the Engine Valve

Figure 2-20 – Variable Valve Timing system [37]

Subaru

Subaru presented its ZE30-R flat 6-cylinder engine, an upgraded version of the ZE30. One of the major new features of this version is AVCS (Active Valve Control System), which includes variable direct valve lift. This provides the ZE30-R with an output of 184 kW, which is close to the 191 kW of the 2-liter flat four turbo engine. The latest electronic technology of variable direct valve lift adjusts the valve lift in accordance with the driving situation. At low engine speeds, the valve lift is different for the two intake valves, thus providing swirl to achieve a better air/fuel mixture [38].

2.3.3.3 Valve timing via phase and lift

The following VVT systems can change both lift and cam phase.

VARIOCAM Plus

The VarioCam Plus system [20] uses two types of valve variation. Valve lift variation and valve phasing variation. The valve variation is not continuous and the possible lift curves are shown in Figure 2-21. Long valve lift is used to get the maximum torque over the complete engine speed range. For reduced torque at speeds up to 50% of the engine range the short valve lift is used.

To achieve two valve lift modes, two sliding tappets are located one inside the other and arranged in such a way that each tappet is controlled by a valve lift curve of its own (Figure 2-22). This configuration allows either short valve lift or long valve lift. The short valve lift is determined by the inner tappet with its integrated hydraulic valve play compensation element. The two tappets move independently and the inner one commands the valve, while the outer tappet is not linked to the valve. The movement of the outer tappet relative to the inner one corresponds to the differential between the two lift curves. For long valve lift, the outer tappet is connected to the inner tappet via a spring-loaded locking plunger. There is no lift differential between the two tappets and the movement of the outer tappet commands the valve.

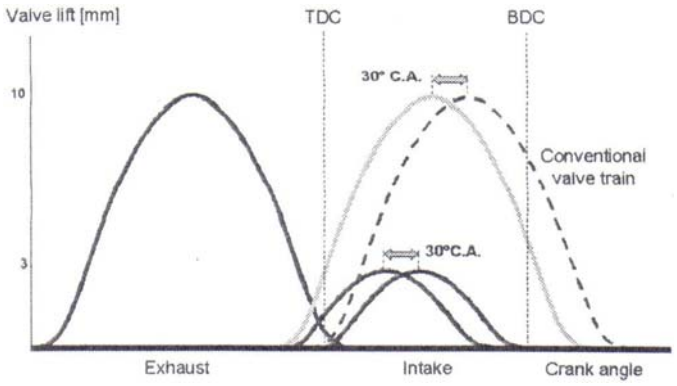

Figure 2-21 – Lift profiles produced by the VarioCam Plus.

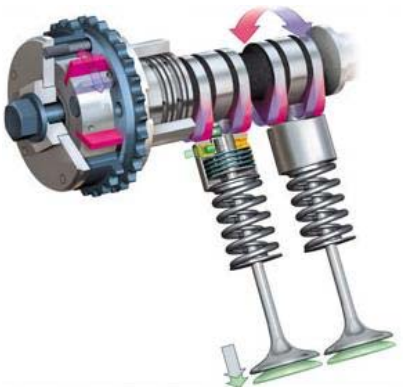

Figure 2-22 – The VarioCam Plus.

For valve timing variation, a geared camshaft adjuster with 30º CA variation was incorporated. The system includes an axial plunger, which is submitted to oil pressure via a switch valve. The plunger moves the outside stator relative to the inner rotor.

Using the short lift curves, the fuel saving at idle is up to 13% and an improvement of 45% in HC emissions. At part load operation fuel economy is improved on 3.3%.

VALVETRONIC

BMW was the first company to present an engine in production that is fully controlled by intake valve timing avoiding throttle [39]. This management system is patented and called Valvetronic [40]. The system is reported to reduce fuel economy by 10% and reduce emissions accordingly.

The system is composed by the so called double-VANOS, which is a cam-phaser system applied to both overhead camshafts and a intake valve lift variation device. This adjustment is accomplished by a lever between the camshaft (Figure 2-23) and two intake valves on each cylinder, the distance between the lever and the camshaft being infinitely adjustable by an additional, electrically controlled, eccentric shaft. Depending on its position, the lever can "transform" the cam lobes to provide higher or lower valve lift.

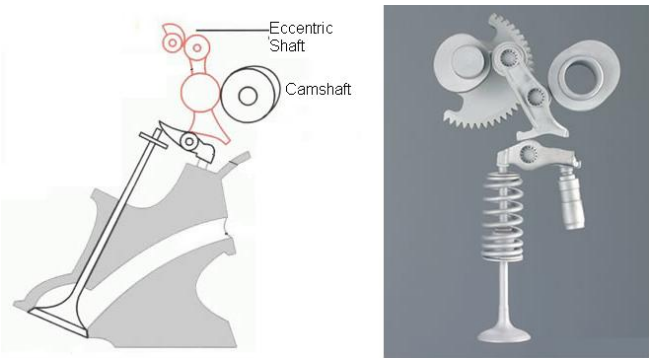

Figure 2-23 – BMW Valvetronic system.

Nissan Variable Valve Event and Lift

The Nissan Variable Valve Event and Lift (VEL) system [30,41] enables continuous control of both valve events, opening duration and valve lifts, from the lowest lift or deactivation state to a long event and high lift state. Figure 2-24 presents the VEL operation.

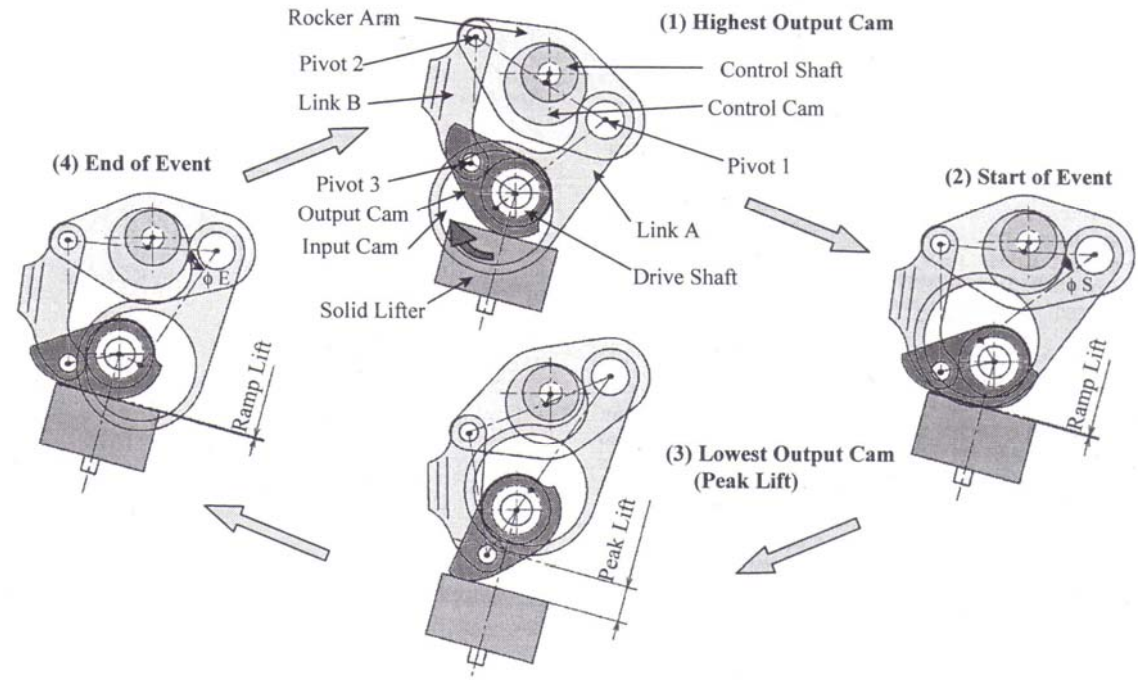

Figure 2-24 – Nissan VEL system.

A drive shaft, driven by the crankshaft, rotates at half the speed of the crankshaft. The axis of the drive shaft is located in a position equivalent to that of the conventional camshaft. An input cam (drive cam) is mounted in the drive shaft. A transmission mechanism made up of the input cam, link A, the rocker arm, and link B, converts the rotational movement of the drive shaft into an oscillating movement of opening and closure of the valve. An electrical actuator controls the position of the control shaft, allowing for the variation of valve event and lift. The control shaft has an eccentric control cam, inserted into the fulcrum cylinder of the rocker arm, so as to change the state of the transmission mechanism and the output cam and in turn, the valve event and lift. The axis cylinder of the large end of link A is supported on the outer periphery of the eccentric input cam. The smaller end of link A is connected to the rocker arm (pivot 1). Consequently, as the input cam rotates, it moves link A up and down, oscillating the rocker arm around the fulcrum cylinder. The other end of the rocker arm (pivot 2) fits at the end of link B. The up and down movement of link B can change with the rocker ratio change. The other end of link B is connected to the output cam through pivot 3. The up and down movement of link B makes the output cam to rotate around drive shaft axis, acting the valve lifter and thus moving the valve. Valve lift and event duration are controlled by adjusting the phase angle of the control shaft.

Engine tests showed a fuel consumption reduction of 9%. This is attributed both to the effect of reduced friction resulting from small valve lift and reduced pumping loss due to optimised valve overlap. Small valve lift worked to reduce exhaust emissions and to raise the exhaust temperature at a cold engine start to the same extent as a swirl control valve. This is thought to be largely due to a reduction of residual gas, improvement of the effective compression ratio and promotion of fuel atomisation.

VTEC

Intelligent VTEC technology (i-VTEC) (Figure 2-25), from Honda, is employed in engines (1.8-L) to vary intake charge volume. The engine has four valves and SOHC, which carries five sets of roller-rocker arms and cams for each cylinder. The fixed timing/lift cams operate intake valve No. 2 and exhaust valves. Intake valve No. 1 is operated by the familiar VTEC phasing/lift switching mechanism, with high-output (HO) and fuel-economy (FE) cam profiles.

The FE cam, engaged during part-load operations such as steady cruising below usually 3500 rpm, delays No. 1 intake valve's closing timing by 63º vs. the HO cam (94º ABDC vs. 31º ABDC). In this mode, the engine operates in the over-expansion cycle, which Honda prefers to describe as "variable intake volume control of the fuel-air mixture". In the over-expanded cycle, part of the charge is pushed back through the still-open valve to the intake port in what is normally the compression stroke, and allows for a wider throttle valve opening, thus reducing pumping loss by as much as 16 %.

In smaller engines (1.3-L) with two valves per cylinder the three stage i-VTEC is employed with three electronically controlled hydraulic pathways to couple and decouple five rocker arm/cam assemblies per cylinder, providing three stages of valve control: 1) normal intake and exhaust valve timing/lift, 2) high-output intake cam profile, and 3) cylinder deactivation by closing all valves by what Honda calls Variable Cylinder Management (VCM) during deceleration and breaking. [42]

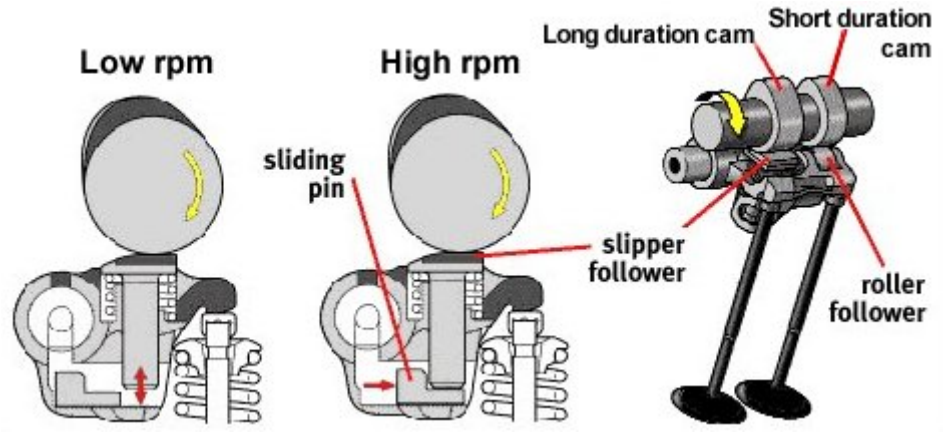

Figure 2-25 – Honda VTEC system.

Taylor Engineering

In 2004 Taylor Engineering presented its TE 401 model for lift/duration subassembly that provides variable valve timing. This system can be used in engines with two, three and four valves per cylinder. It accepts control and status outputs from a vehicle onboard computer and applies control signals sequentially to each valve, positioning them to within ± 0.005 in (0.13 mm) [43].

2.3.3.4 Fully Variable Valve Trains

Valve trains capable of variation of the valve lift, valve timing and valve phasing are called fully variable. An overview of continuous variable valve actuation systems has been presented [21] containing systems examples from automobile manufacturers.
These are called direct acting systems as opposed to others that use at least one camshaft and a set of connections link the camshaft to the valve. The direct acting systems can be implemented whether electrically or hydraulically or by using a mix of both technologies, replacing the conventional valve train, composed of camshaft, cam followers, pushrods, rocker arms, springs. These can be considered the most flexible systems, allowing a full and continuous control of valve timing, phasing and lift.
This type of valve actuation allows for a reduction in the engine weight and height and offer a continuously variable and independent control of all aspects of valve motion. Some engines have been presented [44] without camshaft allowing a great range of valve motion variation.

This valvetrain type can provide new working regimes to engines so that fuel consumption may be reduced, torque increased or power increase. More than the cycle improvements presented above, which may be achieved by variable valve actuating systems, the camless engine may provide other cycle modifications.
In a conventional engine, the firing order is a fixed parameter and is set for reducing the engine vibration, which may not be ideal for all speed/load operating range. With a valvetrain with camshaft, the order of valve opening and closure is also constant. Camless engines, as the valve actuating mechanism is independent for all valves allow for the change in the opening and closure order as well as for a change in the cylinder firing order.
The camless engine can deactivate valves and cylinders for significant short periods as one cycle. This variable activation frequency [44] in engines, as for the variable displacement engine (because cylinders are insulated for one cycle), is of special interest in part-load operation. When operating at part-load, the engine has one or more cylinders deactivated and as the deactivation is made in all cylinders in different cycles, the cooling effect of the deactivated cylinder is avoided, as well as the hydrocarbon emissions during reactivation. During part load or idle operation the engine imep can be increased to reduce throttling in the active cylinders and the possibility of changing the firing order allows for the engine operation with the same torque and speed.
The camless engine can even go further by switching the engine working cycle from four to two stroke [44, 45], just by doubling the valve actuation and injector frequency.

A system presented [46] comprehends a dc electric motor that is attached to a cylindrical cam. A reciprocating assembly, with roller followers, is attached to the engine poppet valve in each engine cylinder. The motor controls the valve motion to allow for active actuation of the valve. This provides full flexibility. In simple terms, as the motor-rotor rotates the cylindrical cam rotates with it. This rotation will then be converted to a reciprocating motion through the roller followers assembly, which is attached to the valve.

Lotus AVT

Lotus engineering called Active Valve Train (AVT) to its Fully Variable Valve Train (FVVT). The use of electro-hydraulic valve actuation technology enables the camshaft

to be replaced by lighter and more compact hardware. This enables virtually infinite manipulation of the timing, duration and extent of lift for each valve.

The main benefits presented for this system are [47]:

- Reduced emissions and fuel consumption
- Increased torque (up to 10%) and power output potential
- Reduction of engine-out nitrogen oxides (NOx) emissions up to 98% through Controlled Auto Ignition
- No need for engine oil in engine head
- Independent control of each cylinder (allows for the downsizing of the starter and battery)

A later study using again this system [48] refers the possibility of using this valve actuation system to avoid variable geometry intake manifolds, through the change of the firing order of the engine cylinders.

In electromagnetic systems for valve command, an assembly of coils and springs is used to move the valve. An example of an electromagnetic system was presented [49], comprehending two springs, two coils and a magnet. In the valve closed position, spring A is compressed and spring B is released (Figure 2-26). The radially poled permanent magnet holds the valve in position by creating the necessary latching magnetic force on the plunger in airgap A. The magnet's hold is released by exciting the coils to reduce the magnetic flux in the airgap, and the springs then provide motive force. As the valve reaches the other end of its travel, the permanent magnet latches the compressed spring and holds the valve.

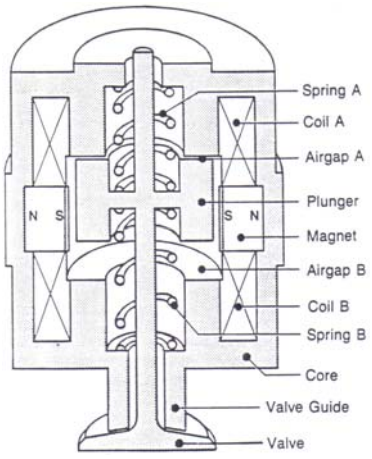

Figure 2-26 – Electromagnetic system for valve command.

In this engine two turbulence effects were generated and studied: squish and quiescent. Two load control strategies were used: throttle with and without EGR and EIVC with and without EGR. In each engine turbulence configuration the use of EIVC without EGR is always preferable. EIVC has always a better performance in relation to the throttling load control method. Also a reduction of NO_x emissions was reported.

Daimler Chrysler

The fully variable valve for single overhead camshafts from Daimler Chrysler only adds to the conventional valvetrain one moving part [50]. The pivot shaft position determines the maximum valve lift. Mechanical lash is incorporated between the rocker arm and valve cap, and may be varied over the range of movement of the pivot shaft. The combination of lash variation and reduced rocker ratio allows the duration of valve events to be varied while maintaining suitable opening and closing velocities. This results in lost motion, allowing the valve events to occur on the flanks of the cam, shortening duration. A single actuator moves the pivot shaft through its range of motion. As it was presented this system allows only valve lift reduction, with intake valve closure made earlier.
After tests on a conventional engine and a VVA engine, it was concluded that at maximum lift the VVA system had the same levels of friction as a conventional engine. In terms of performance a reduction of torque was recorded. At part load the indicated mean effective pressure was higher in the VVA engine. This was reflected in a reduction of the indicated specific fuel consumption.

2.3.4 Displacement on demand/cylinder deactivation

When an engine operates at low torques a solution to improve engine efficiency and consumption is the deactivation of one or several cylinders of the engine in order to reduce the total displacement of the engine. This system called “displacement on demand” is a particular and simple case of VVT use. This is simply the closure of both the intake and exhaust valves, closing the cylinder. One example is the Cadillac engine in 1981 [28]. In these engines the number of cylinders for which the valves were disabled was varied as a function of the engine operating parameters to vary the effective engine displacement, thereby improving engine efficiency. Mitsubishi

introduced a 1.6 litre 4-cylinder engine with a hydro-mechanical valve deactivation system in 1992 (MIVEC-system), with 2 cylinders being cut-off between idle and 3400 rpm. This system allows a reliable switching within two engine cycles, by using an additional oil pump [51]. Also Mercedes-Benz used this technique calling it cylinder cut-out [51,52]. The resulting improvement in fuel consumption of the 5L V8 engine is 6.5% in the New European Driving Cycle.

Other cylinder deactivation systems [51] report engine thermodynamic improvements such as a 20% saving in fuel consumption at low load, when a four cylinder is deactivated to work only with two cylinders.

GM presented a system performing displacement on demand [53]. The technology deactivates every other cylinder in the firing order (two on each bank of the V-8 and one entire bank of the V-6), by automatically sequentially closing both exhaust and intake valves, and turning off the fuel injectors. When load demand is increased, the system automatically and seamlessly reactivates the deactivated cylinders. These cylinders are reactivated in a fraction of a second, making the transition imperceptible to the driver.

A solenoid valve per cylinder controls the oil flow to the cylinder to be deactivated. When the proper conditions for Displacement on Demand operation are met, the Engine Control Module (ECM) sends a signal to each of the control valves based on the engine's position relative to the valve events for each cylinder being deactivated. When the control valves are opened, oil flows through the engine block down to special Displacement on Demand lifters (Figure 2-27). The oil pressure acts on upon a latching mechanism within the lifter via a port on the side of the lifter. The latching mechanism moves, allowing lost motion within the lifter, thereby disabling the valve line.

Conversely, when conditions warrant a return to V-8 mode operation, the ECM shuts off the current flow to the control valves. The valves then close and the pressure in the control port is exhausted. A spring-loaded mechanism in the lifter then returns to the reengaged position, resulting in reactivation of the valve line. Both the deactivation and reactivation events occur within a window of less than 20 milliseconds for an individual lifter, on the camshaft lobe base circle, from the time the ECM command is given.

Cylinder deactivation is only allowed in higher gears (third and fourth) to provide the maximum fuel economy benefit without introducing torque disturbances and launch variation in the low gears.

After long deactivation times, reactivated cylinders without fuel compensation will/can exhibit partial combustion resulting in low engine torque, causing a noticeable vehicle disturbance.

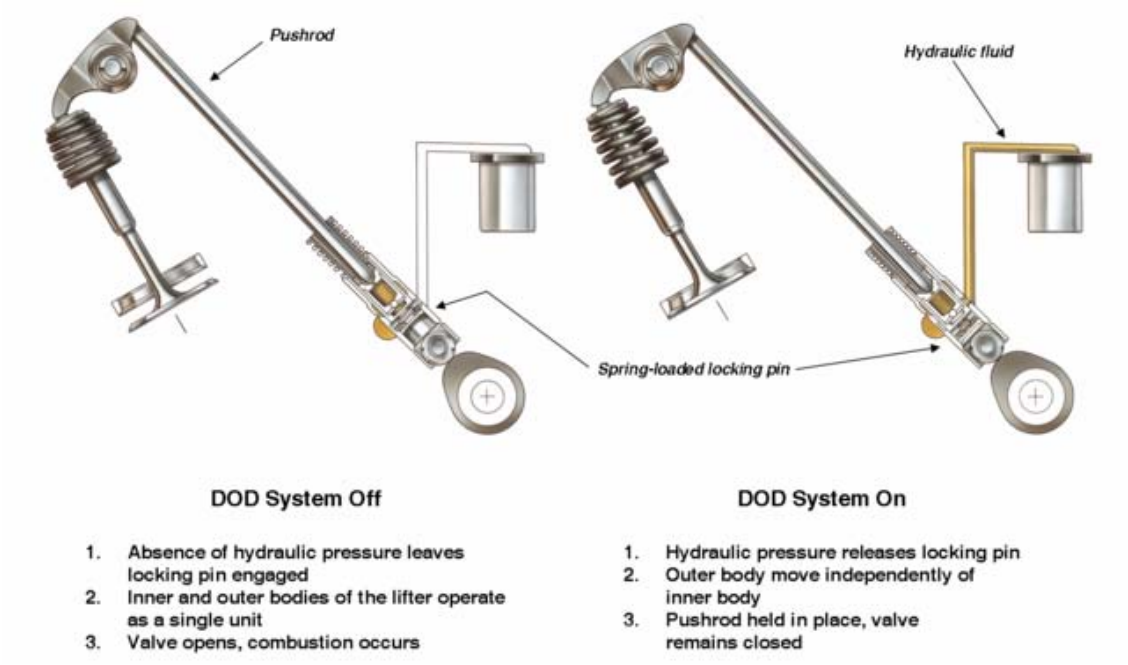

Figure 2-27 – Displacement on Demand from GM.

Through modelling and simulation of a Federal Test Procedure (FTP) test, the vehicle spent 75% of the miles and 59% of the time in V-4 mode.
GM has demonstrated that Displacement on Demand, improving fuel economy by 6-8%, can be cost effectively implemented on GM's high value engines while maintaining or improving vehicle performance, emissions and the drive quality.

Split Engine

Another method for performing the variable displacement engine was presented [54], consisting in the splitting of the engine in two modules, which may have or may not have the same displacement. It operates with the first module during typical driving and activates the secondary module to assist with high-power driving. The two crankshafts of the engine are connected and disconnected through a one-way clutch, capable of achieving a correct relative phase of the engine modules. In the split engine the benefits are due to the reduction of pumping losses, but also due to the reduction of friction

losses, once half of the engine is stopped. Fuel economy is said to improve about 30 %, depending on the driving pattern.

2.3.5 Load Control

Load control in throttleless engines through the control of the intake valve closure timing (mainly early intake valve closure) was proposed in several studies [35,36,55]. However this method showed some disadvantages specially at low loads and medium and high speeds due to poor mixture formation. At these conditions:

1. The open duration of the intake valve is very short, while the period between valve closure and combustion is very long, this results in charge turbulence reduction.
2. The manifold pressure is high (near atmospheric pressure) and the difference between the cylinder and the manifold at TDC is lower, leading to lower backflow of residual gases.
3. The temperature at BDC is low due to the adiabatic process after intake valve closure, which corresponds also to a reduced effective compression ratio.

The combination of all these factors explains the reduction of combustion efficiency, by the initial kernel cooling down (3), the slower flame propagation speed (1 and 3), and the presence of non uniform residual gas (1 and 2). The load control system has to obtain the optimum working conditions that reduces the pumping work and at the same time creates enough turbulence at the intake valve gap for acceptable mixture formation. A load control strategy was proposed recently [56] using late exhaust valve closure and early intake valve closure timing. Starting from the full load condition, the first step is to increase the exhaust valve closure delay to reduce engine output torque. In fact during intake stroke some exhaust gas enters through the opened exhaust valve increasing the exhaust gas recirculation quantity and thus reducing the fresh mixture mass charge and consequently the output torque. This condition can be increased up to the point when combustion stability starts to deteriorate. From this state forward, load is reduced by reduction of fresh mixture trapped in the engine, advancing the closure timing of the intake valve. At the same time it is necessary to reduce the exhaust valve closure delay in order to maintain the maximum allowable percent of EGR. This strategy has better results than just increasing the advance of the intake valve closure timing.

2.4 Turbocharging

Turbocharging technology is used widely in Diesel engines improvement in terms of fuel consumption and engine output. However on the spark ignition engines field, the use of these systems has not proven yet to be a real improvement for fuel consumption reduction. Since it is desirable to maintain the same full load torque characteristics of an original larger engine in a downsized engine, the intake air must be compressed, usually by a turbocharger. In this case the fuel savings are lost due to the reduction of the compression ratio, which is necessary to avoid engine knock at full load. FEV used a traditional turbocharge scheme in a downsized engine, but when working at low speeds in order to avoid the rapid descent of the engine torque (below the torque obtained from a larger engine), the turbocharge system was complemented by a roots compressor driven by the crankshaft or electrically driven. The result of simulations performed using booth concepts shown a better engine low-end torque. The next stage of this study by FEV is to complete the supercharging with variable compression ratio [57].

When the downsize design concept is used for spark ignition engine/car design, the improvement can be achieved. This is because a smaller engine runs at more optimum conditions while the turbocharger "steps in" to provide additional air/torque/power normally achieved by a larger engine [58]. To improve fuel economy several combinations of turbocharging and other technologies or engine configurations are possible [59]:

- Lean Boost Direct Injection with lean operation at full-load to control octane requirement while maintaining a high compression ratio
- EGR boost with cooled EGR dilution rather than excess air to control octane requirement
- Miller cycle concept, where valve timing strategies are employed to reduce the effective compression ratio at high load
- Dual injection strategies to control octane requirement

Another technology combination gets together turbocharging, gasoline direct injection, downsizing and variable valve timing [60]. At lower loads charge stratification can be used until 7 bar imep, at the same time compression variation is achieved by late intake

valve closure. At higher loads turbocharging is the method to improve volumetric efficiency.

One of the disadvantages of the turbocharging technology is the time lag for the turbo to be effective or during the low speed torque or transient operation. Several engineering solutions are being proposed:

- Turbocharger with electrically-driven supercharger
- Electrically assisted turbocharger:

  e-Turbo is a Honeywelll's technology that assembles an electric motor generator on the same shaft as the turbocharger. When the vehicle/engine demands more torque and turbo needs some help, the electrical motor "steps in" to provide extra air/torque. When there is too much exhaust energy, it generates electricity to store in batteries. This synergy with hybrid philosophy offers the opportunity to further downsize the engine while at the same time reducing the capacity or weight of batteries needed [58].
- Variable geometry compressors and turbines

For fuel consumption and power improvement, Subaru introduces in its competition turbo engines an afterburner technology in the exhaust system at the entry of the turbocharger. Secondary air, a part of the pressurized air from the turbocharger, is injected into the afterburner chamber and reacts with the unburned exhaust gas, increasing exhaust pressure and temperature. This allows a full usage of fuel in reach mixtures and at the same time reduces the turbo lag delay [61].

Combining lean-burn direct injection gasoline and pressurized air holds great promise for improving thermal efficiency of gasoline engines [61]. An engine that has this technology implemented is reported to have fuel economy benefits of more than 20% when compared to a NA engine [59].

With boosted engines water injection is used to reduce cylinder charge temperature and allow higher compression ratios without knock onset. Subaru introduced water injection in World Rally Championship engines. The system has been very effective in precluding harmful knocking and improvement of combustion, allowing an 11:1 compression ratio for highly boosted engine [61].

2.5 Stratified charge/Lean burn

The use of lean mixture in automotive applications is reported to the mid 80's, when reductions of 7% in fuel consumption were achieved when compared to stoichiometric engines [68]. In the case of lean burning engines the leanness of the mixture is limited by the combustion stability so that the engine operation conditions are assured.

Charge stratification comprehends a non-homogeneous mixture in the cylinder, the zone near the spark plug being richer than the rest of the cylinder charge. This burning method is only applicable in direct injection gasoline engines, with precise electronically controlled mixture. Using the appropriate airflow in the combustion chamber (tumble) and late injection timing, it is possible to obtain relatively rich mixture near spark plug with overall lean mixture at low load engine running. Honda extended the K20B engine's air/fuel ratio to as lean as 65:1 during its stratified charge operation [61]. Using early injection (during intake) with homogeneous near stoichiometric mixture at middle and full load operation, it is possible to keep all good advantages of conventional spark ignition engines, i.e. higher specific output. This technology can be used to control load without throttling, just by controlling the amount of fuel injected. Thus when operating at part load, the engine becomes more efficient in thermodynamic terms than the convention throttled engine with port injection.

Several improvements have been proposed and studied around these engines in past years. Variables that mainly influence the performance and optimisation of stratified charge engines are injection conditions (pressure, spray shape, number of injector holes), piston head shape and air motion within the cylinder.

The design process of a small engine working on stratified conditions is described in [62]. Direction and spray shape were considered as key elements for combustion efficiency improvement and wall wetting reduction. At part-load operation the fuel plume target should be matched to the piston in such a way that containment within the bowl is ensured, so that fuel economy benefits are reached. In fact, the volume of the piston bowl is the key for ensuring sufficient mixing at higher loads of the part-load operation. Swirl motion at part-load is primarily related to bulk transport rather than enhanced mixing. Reverse tumble is specially important in lifting the mixture towards the spark gap.

The improvement of charge stratification can also be made by timed EGR supply [63]. If EGR is introduced during the first part of intake it occupies the lower part of the

cylinder volume leaving the upper space for the stratified fuel mixture. Combustion duration reduction was achieved with benefits in terms of fuel consumption. Benefits in terms of engine emissions were also achieved, but these are due to cylinder charge composition difference rather than stratification.

To optimise mixture preparation high pressure injection was proposed [64]. It was observed that droplet velocity does not increase in the same dimension as fuel pressure. However with the increase of the fuel pressure the droplet diameter was reduced shortening the evaporation time. Ignition time can than be adjusted for optimal thermodynamic conditions.

Another method proposes the use of high pressure (higher than 30 Mpa) single-fluid fuel injector to induce a circulatory flow motion inside the piston bowl for forming the stratified mixture [65]. This method allowed the application of heavy EGR keeping stable combustion conditions reducing significantly at the same time the NO_x level. The circulatory flow movement in the bowl promotes fuel evaporation avoid wall wetting.

When fuel is injected a charge cooling happens due to fuel evaporation. This fact allows an even higher compression ratio of the engine with a consequent increase of the thermal efficiency, specially at part-load operation. Experiments were made to test this variation [66]. Increase in thermal efficiency and pumping losses are reported. However, with the increase of the compression ratio, an increase of unburned HC is reported, due to crevice loading, reducing combustion efficiency. Despite this, an increase in thermal efficiency is obtained. The rate of improvement is about 2.6% per compression ratio unit and increases with the load due to sensitivity to combustion efficiency. This compression ratio adjustment allowed an increase of 3 to 5 percentage points referring to PFI (meaning a 11% to 22% efficiency increase).

In DISI engines the NOx emissions are a relevant item, since the conventional three way catalyst (TWC) can not be used, once the burned mixture is not stoichiometric but lean. In these working conditions the NO_x storage catalyst is generally used due to its superior potential over other available lean operating catalysts. However these are not so durable or efficient as TWC [67]. However if the air fuel ratio is increased to higher values, the amount of NO_x produced during the combustion is reduced, thus avoiding the use of catalysts.

A Bowl-Prechamber-Ignition (BPI) concept was presented [68,69], to ignite premixed lean mixtures in DISI engines. It is characterised by a combination of a prechamber spark plug and a piston bowl (Figure 2-28). An important feature of the concept is its

dual injection strategy. A pre-injection in the inlet stroke produces a homogeneous lean mixture with an air fuel ratio of λ=1.5 to λ=1.7. A second injection with a small quantity of fuel is directed towards the piston bowl during the compression stroke. The enriched air fuel mixture of the piston bowl is transported into the prechamber by the pressure difference between main combustion chamber and prechamber. After ignition of the mixture strong flame jets penetrate the main combustion chamber and initiate the main combustion process. With this engine, improvements were obtained in terms of fuel consumption, NO emissions and unburned HC, relatively to homogeneous charge engine. At part load operation a significant improvement of the inflammation of lean mixtures is achieved. Combining lean burn and EGR a positive influence is achieved in the trade-off between NO and HC emissions or fuel consumption.

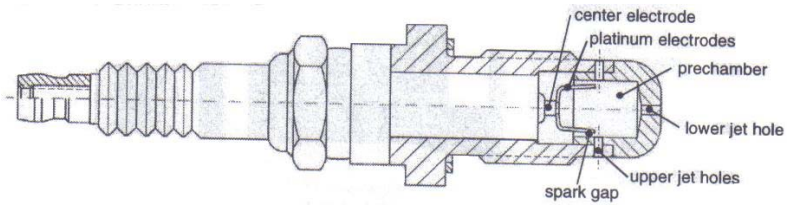

Figure 2-28 – BPI concept.

2.6 Engine Downsizing

The downsizing technique aims at the reduction of engine size in order to improve fuel consumption, although keeping the same or near the same engine performance. Reduction of displacement shifts the part load operating points to higher specific loads, which are more efficient due to the reduction in pumping losses and increase of effective compression ratios. The reduction of engine displacement also reduces friction mean effective pressure.

To improve the effectiveness of the downsizing concept, the use of direct injection technology is important. Fuel injection allows for an increase of the compression ratio of 1 – 1.5 compared with an equivalent port-injected engine, as a result of charge cooling.

Recently the opposite concept, upsizing, was presented [70]. In the downsizing concept displacement is reduced and load increased, keeping the friction on the same values. In

the upsizing concept the displacement is increased and engine speed is reduced so that friction mean effective pressure is also reduced. Some modifications need to be implemented. An helical intake port and twin spark plug need to be adopted so that combustion efficiency is maintained, despite the engine speed reduction. This concept is referred to contribute to fuel economy in 30%.

2.7 Variable Stroke Engine (VSE) [71]

The VSE is an engine capable of displacement variation, keeping though the compression ratio. Several mechanisms are proposed to perform this engine concept [72, 73, 74]. Recently [71] the use of such mechanisms (by stroke variation) was proposed to control the engine load, eliminating the use of throttling. In that case the pumping losses are constant because the engine operates always at WOT, throughout the whole load range. Reductions in NO emissions (33%) and improvements in brake specific fuel consumption (21%) at the typical road loads are referred. However the engine has some limitations, such as the need of an extra throttle valve for the low load operation, engine braking and idling. In terms of combustion, the use of short strokes leads to less inner cylinder turbulence, which added to the geometrical proportions of the combustion chamber cause slow burning rates.

2.8 Over-expansion

An over-expanded engine may be defined as an engine that has an expansion stroke longer than the compression stroke. Figure 2-29 presents the theoretical Miller cycle p-V diagram. As it can be seen, the compression does not begin at BDC (point 5), as in the Otto cycle, thus being shorter than the engine stroke. Expansion is made the same way as in the Otto cycle, using all the stroke length. This effect can be achieved through several technological arrangements, described below.

In the literature an over-expansion engine is often referred as an Atkinson cycle engine. The Atkinson cycle was invented by James Atkinson (1846-1914) and is characterised by a different length between the intake/compression and expansion/exhaust strokes. This was reached with a different arrangement of the traditional crankshaft/connecting

rod configuration. The over-expansion thus obtained was complete and the exhaust gases are at atmospheric pressure at the exhaust valve opening [75].

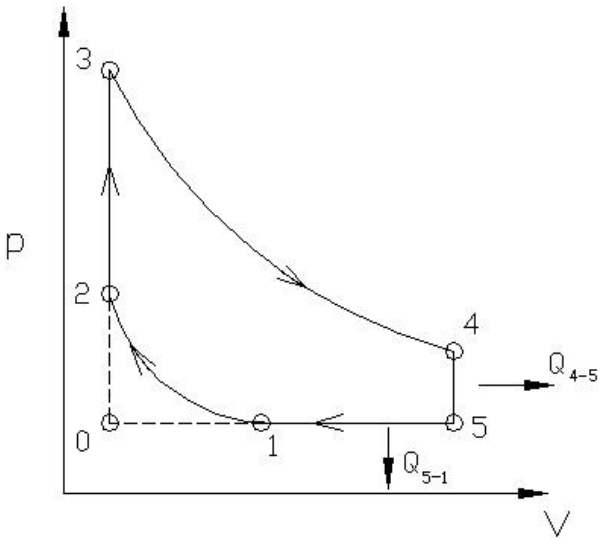

Figure 2-29 – Theoretical Miller cycle (p-V diagram).

In the case of the Miller cycle, invented by Ralph Miller, the conventional crankshaft/connecting rod configuration is used but the over-expansion exists due to a different timing of the intake valve. The intake valve is kept open during more time, leading to some of the inducted mixture being blown-back to the intake manifold. The principle is to use high geometric compression ratio, typically around 14:1, giving good part-load economy, and to control knock by reducing the effective in-cylinder compression ratio by late intake valve closing. As this reduces volumetric efficiency, higher boost pressures are required to achieve the same bmep. However, as more of the compression is done in the external compressor and an intercooler can be used, the in-cylinder charge temperature at ignition will be lower than for a conventional boosted engine, even with the same trapped mass. This will not require a fuel with so high octane index [59].

Miller cycle engines were produced by Mazda in the 1980s. They had a fixed late intake valve closure and were supercharged. In 1993, Mazda introduced in the market a supercharged Miller cycle gasoline engine as an answer to the requirement of CO_2 emissions reduction [76]. To improve thermal efficiency the Miller cycle with supercharging is proposed. This technology combination allows an engine downsize with the implications in terms of reduction in friction losses due to the reduction of

engine displacement. The improvement of break specific fuel consumption may be achieved by the reduction of cooling loss, exhaust energy loss and friction loss, as shown in Figure 2-30.

The Miller cycle engine with high compression ratio shows almost the same antiknocking performance as a conventional supercharged engine with low compression ratio. In terms of valve timing, it was shown that the late intake valve closure has a better effect on decreasing mixture temperature compared with early intake valve closure. In the latter case, during the compression stroke after intake valve closure, the mixture warms up due to heat transfer from engine walls. This engine was compared with an equivalent DI Diesel engine and it was shown that the Miller supercharged engine has the potential to exhibit higher thermal efficiency, provided lean-burn is incorporated into it [76].

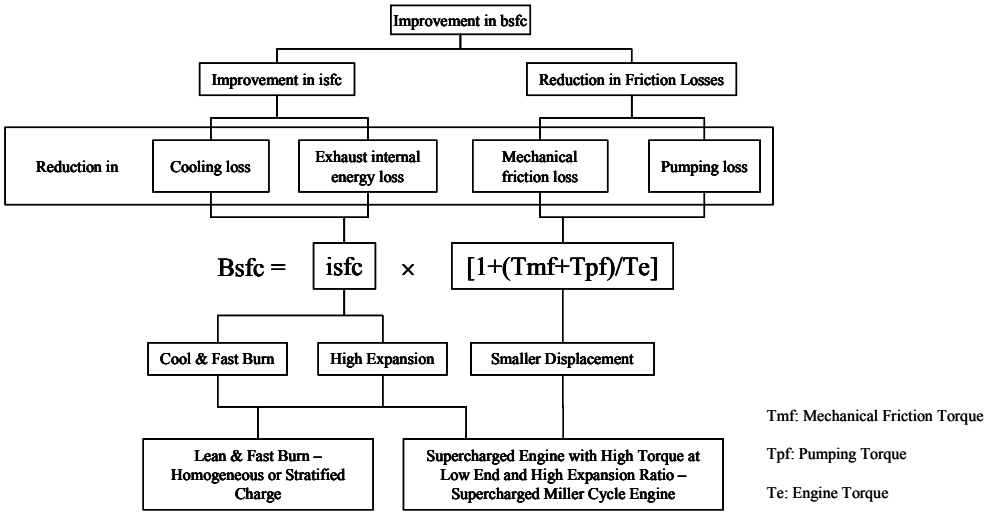

Figure 2-30 – Schematic diagram of improving Fuel Economy [76].

A paper from the same company [77] refers a numerical study of a Miller cycle supercharged engine. Using a theoretical calculation method it is shown that the Miller cycle engine with supercharging and an efficient intercooling device is able to increase imep satisfactorily.

Toyota introduced in the market, its car model Prius, fitted with the Toyota Hibrid System, which uses an internal combustion engine and an electric motor linked by a planetary gear system [78]. The internal combustion engine has a displacement of 1497 cc, with a geometric compression ratio of 13.5:1, but the effective compression ratio is limited to the range of 4.8:1 to 9.3:1 by using variable valve timing to time the intake

valve closing between 80º and 120º after bottom dead centre. In order to minimize friction losses the engine speed was lowered. In this engine the fuel consumption was reduced to a level of 230 g/kWh. In this engine the VVT system is also used to reduce engine vibration during starting and stop. At these situations, the valve closure delay is maximum at 120º ATDC so that the volume of intake air can be reduced, reducing the vibrations during compression and expansion.

Another method for realizing over-expansion is by crankshaft offset. This consists in deviating the axis of the crankshaft in relation to the axis of the cylinder (Figure 2-31). By doing this, the piston motion is modified and the cycle strokes duration is changed, depending on the side to which the crankshaft is offset. Advantages of this configuration modification are: slower piston speed at TDC, making the combustion close to constant volume; friction reduction by changing the connecting rod to cylinder centreline relationship, such that a straighter rod angle is achieved during the early parts of the expansion stroke, thus to reducing piston side forces when cylinder pressure is highest. For this, the crankshaft needs to be offset towards the major thrust side. However, the friction forces during the compression stroke increase for the same reason, but results have shown that the decrease during expansion was greater than the increase during compression resulting in a net friction reduction [79]. A recent study [80], however, reports that at part load no differences exist between the conventional configuration engine and the crankshaft offset configuration. In terms of combustion, it is important to refer that although combustion is made almost at constant volume conditions, the cylinder remains longer at high temperature during combustion, which leads to an increase of the heat losses during the combustion and during the beginning of expansion [81].

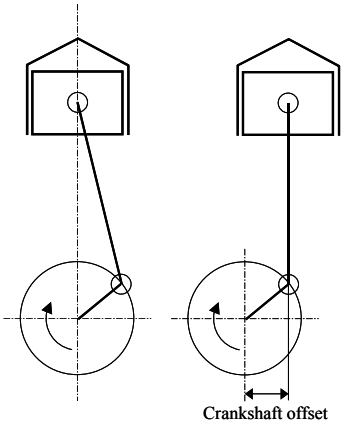

Figure 2-31 – Crankshaft offset.

Another example of Miller cycled engine was tested and presented [82]. In this engine, named as an Extended Expansion Engine (EEE), both late intake valve closure and clearance volume were changed in order to get different relations for expansion (from 1:1 to 2.27:1) and compression (from 6:1 to 8:1). Improvement is registered in terms of break thermal efficiency, which can go, depending on the load level, up to 19% when compared to a conventional engine. It was suggested that this engine modification has

the potential for thermal efficiency improvement in internal combustion engines, especially when used in automotive applications. Table 2-4 shows the results of the investigation presented and these are compared to the performance results of a standard spark ignition engine.

Table 2-4 – Engine specifications and performance of the Extended Expansion Engine (EEE) [82].

	Standard Engine	Modified Versions			
		Version I	Version II	Version III	Version IV
IVO BTDC	4.50	4.50	4.50	4.50	4.50
IVC ABDC	35.00	115.00	107.00	113.00	137.00
ER/CR	1.00	1.27	1.50	1.72	2.27
Vol. Efficiency %	98.00	72.60	62.00	52.00	40.00
Max. Brake Power (kW)	5.56	4.45	3.65	2.91	1.85
Percent of Max. Power Output of Std. Engine	100.00	80.00	65.65	52.34	33.30
Max. Break Thermal Effic.	31.32	31.50	32.28	29.51	23.10
B.Th.Eff. of Std Engine at Corresponding Power Output	31.32	30.00	27.20	25.00	20.00
Percentage Improvement	0.00	5.92	17.20	19.00	17.95

Kentfield [83] presented an extended expansion engine using a different linkage between the piston to the crankshaft (Figure 2-32). There is also the possibility of adjusting the compression ratio with engine running, keeping the compression ratio value for several expansion conditions. A maximum expansion ratio of 2.5:1 is attainable with this system and the compression ratio can be adjusted from 7.5:1 up to 10:1.

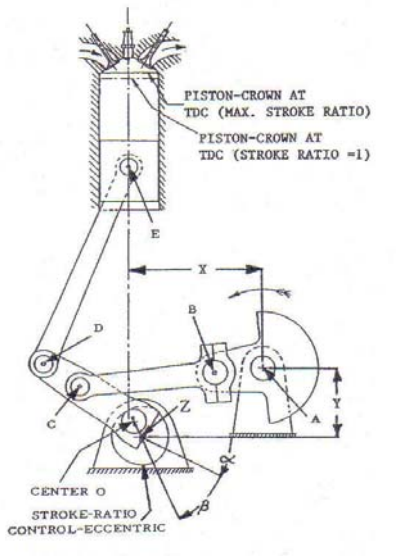

Figure 2-32 – Arrangement of a four-stroke Variable Expansion Ratio Engine.

The reduction of specific fuel consumption with this system is in the region of 20% over the range from 14% to about 40% of full load. The fuel economy can be improved even more, to about 24%, when the compression ratio is adjusted.

Notwithstanding the complexity of this design, it is claimed that the losses due to friction are lower than in conventional engines. These losses, determined by monitoring tests are referred as 90 % in terms of fmep in relation to an equivalent conventional configuration engine [84].

Figure 2-33 shows the predicted performance of the over-expanded engine (S.I.) compared to the performance resulting from tests made in a Miller cycle (with constant stroke and VVT) and an IDI, both from Mazda and a conventional Otto cycle engine. It can be seen that the variable expansion engine shows the best performance.

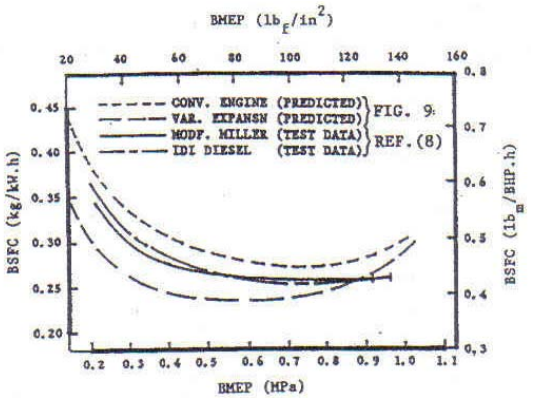

Figure 2-33 – Experimentally obtained performances of a Mazda modified-Miller-Cycle Spark-Ignition Engine and a Mazda IDI Diesel Engine.

This engine was also studied in terms of turbulence generation [85]. The squish turbulence generation mechanism is not available during all the load range of the engine, because of the cycle modification, and new methods of turbulence generation are proposed focusing specially in the air injection at the end of induction.

Another method of changing the expansion relation was suggested by the use of a rotary valve for intake control [86]. The engine has a geometrical compression relation of 14:1, which effectively can be varied and controlled by the rotary valve. The variation of the opening and closing timing of the rotary valve controls the load of the engine and the effective compression ratio. Remarkable reduction on throttling losses is reported using this engine configuration. However the use of throttling is unavoidable at idle conditions. When compared to an equivalent engine with a compression ratio of 9.5:1 the improvement in terms of break specific fuel consumption was between 15% and 20% at loads above 33%. These results are better than the fuel consumption characteristic of general IDI diesel engines of similar size. The naturally aspirated version of this engine has a mileage improvement prediction of no more than 10%. More improvement would be expected if supercharging was used.

A second engine with rotary valve for load control at the intake was presented [87]. In this case the expansion ratio was extended from the original 8.4 to 11:1 in a 2.6 litre

spark ignition engine. It is referred that this engine realizes the similar characteristics of both fuel consumption and power output of a 3 litre IDI Diesel engine. Again the use of the Miller cycle and the use of the rotary valve at the intake reduce the volumetric efficiency with engine speed increase. In terms of fuel consumption the break specific fuel consumption curve of the Miller cycle and the Diesel are very close to one another, the Miller engine being lower at lower loads and the Diesel lower at the high loads. The output of the Miller engine is better in terms of torque and power at the higher speeds (higher than 3000 rpm). If the Miller engine is compared to the Diesel engine the amount of emissions of the second one is lower. However, the use of the three-way catalyst allows for a reduction of the amount of emissions from the Miller engine.

The Miller engine was also applied to stationary engines. In this case the engine works always at the same conditions, which allows the use of the maximum efficiency conditions as the specification for the engine design. Variables such as effective compression ratio, expansion ratio, speed, ignition timing are optimised. Gas engines with power output ranging from 280 to 1115 kW were proposed for commercialisation, using the Miller cycle and turbocharging [88]. These engines have an expansion ratio of 15 and an effective compression ratio of 11, working with lean-mixtures at speeds from 1200 to 1800 rpm. From tests and using the turbocharger, the efficiency of these engines could go up to 42.2%.

Finally the “High Efficiency Hybrid Cycle” engine (HEHC) borrows elements from Otto, Diesel, Atkinson and Rankine cycles. It is a rotary engine with some particular features. Air is compressed and introduced in a separate combustion chamber where fuel is injected and combustion proceeds in truly isochoric conditions. After the combustion is complete the burned gases expand to an expansion chamber, which has an expansion ratio higher than the compression ratio of the compression chamber. HEHC engine is said to offer nearly 35% improvement in efficiency over Otto and Diesel engines [89].

2.9 Turbulence Generation

Combustion efficiency is ruled among other factors by gas motion within the engine cylinder. This factor has a main influence in flame speed (or combustion duration), in mixing of fuel and air and in heat transfer. The basic methods for turbulence generation

in spark ignition internal combustion engines are attained during induction or during compression [75]. During induction, the generated turbulence may be swirl or tumble, depending on the flow pattern, and during compression the effect is mainly squish.

Swirl may be generated in twin inlet valve engines, by deactivating one of the intake valves or intake passage during induction (port de-activation throttles [90]).

Swirl is referred to have a relatively little contribution to the kinetic energy available for turbulence, in contrast to the Diesel engines [85]. In tests made in over-expanded spark ignition engines, high swirl ratios were rejected [88]. The use of high swirl ratios increased heat release rate during combustion, reducing the combustion period, which causes the knock onset to be easily achieved. Meantime the heat transfer ratio increases with a reduction in the thermal efficiency of the engine. However there are benefits in the reduction of HC emissions, due to more complete combustion.

Turbulence may be generated by the use of turbulator vanes in the intake duct upstream of the inlet valve [85]. However this method has not so much success due to reduction in volumetric efficiency caused by pressure loss during intake.

Another technique for turbulence increasing is by injecting pressurized air or recirculated burned gases, during intake or compression. This turbulence improvement can go up to three times of the kinetic energy input due to squish [85]. However the complexity of the engines also increases. As seen in another study [91], the use of direct high pressure air injection was used to improve burn rate in the later stages of the combustion period and improvement in knock characteristics. As a result, the output torque is increased 10% at the low and medium engine speed conditions.

Saab proposed the Saab Control System (SCC) [67, 92], which introduces the air injection as a method for turbulence induction within cylinder mixture. It uses a spark plug injector that performs both functions, spark plug and air injector. It injects a small amount of air during compression. This system allows that turbulence is independent from engine speed. Intake ports may then be designed for optimum WOT conditions, once high burning rate is assured by the additional turbulence generation at low loads and idle speed.

2.10 Summary

Several technologies to improve fuel consumption on spark ignitions engines at part load conditions were analysed. From these technologies special focus will be given to the Miller cycle (over-expansion) and VCR. Each of these methods by itself or by combination of the two will be evaluated to predict its thermodynamic improvement potential.

2.11 References

1 Mark Perlick, Automotive Engineering International, August 2005, p. 75.

2 Tomić, M., Petrović, S., *Spark Ignition Engine Part Load Fuel Economy Improvement: Numerical Consideration*, FME Transactions (2003) 31, 21-26.

3 Ayala, F. A., Gerty, M. D., Heywood, J. B., *Effects of Combustion Phasing, Relative Air-Fuel Ratio, Compression Ratio, and Load on SI Engine Efficiency*, SAE 2006-01-0229, 2006.

4 Kajiwara, Kenichi, *A Variable-Radius/Length Engine*, SAE 920453, 1992.

5 Schwaderlapp, M., Habermann, K., Yapici, K.I., *Variable Compression Ratio – A Design Solution for Fuel Economy Concepts*, SAE 2002-01-1103, 2002.

6 Klein, m., Eriksson, L., Nilsson, Y., *Compression Estimation from Simulated and Measured Cylinder Pressure*, SAE 2002-01-0843, 2002.

7 Drangel, H., Olofsson, E., Reinmann, R., *The Variable Compression (SVC) and the Combustion Control (SCC) – Two Ways to Improve Fuel Economy and Still Comply with World-Wide Emission Requirements*, SAE 2002-01-0996, 2002.

8 Clarke, et al., *Internal combustion engine with adjustable compression ratio and knock control*, US Patent 6,135,086, 2000.

9 Wong, V. W., Stewart, M., Lundholm, G., Hoglund, A., *Increased Power Density via Variable Compression/Displacement and Turbocharging Using the Alvar-Cycle Engine*, SAE 981027, 1998.

10 Riley, M., *Internal Combustion Engine with Variable Combustion Chambers and Increased Expansion Cycle*, US Patent 5,341,771, 1994.

11 Brevick, *Variable compression ratio piston*, US Patent 5,755,192, 1998.

12 Rapan, G., Rapan, I., *Variable compression ratio engine*, Romanian Patent RO115662B, 2000.

13 www.gomecsys.com

14 www.mayflower-e3.com

15 Moteki, et al., *Variable compression ratio mechanism of reciprocating internal combustion engine*, US Patent 6,505,582, 2003.

16 Moteki, K., Aoyama, S., Ushijima, K., et al., *A Study of a Variable Compression Ratio System with a Multi-Link Mechanism*, SAE 2003-01-0921, 2003.

17 Takahashi, N., Aoyama, S., Moteki, K., et al., *A Study Concerning the Noise and Vibration Characteristics of an Engine with Multi-Link Variable Compression Ratio Mechanism*, SAE 2005-01-1134, 2005.

18 Hiyoshi, R., Aoyama, S., Takemura, S., Ushijima, K., Sugiyama, T., *A Study of a Multiple-Link Variable Compression Ratio System for Improving Engine Performance*, SAE 2006-01-0616, 2006.

19 Beroff, J., *Moteur A Combustion Interne, A Rapport Volumetrique et a Cylindree Variables*, French Patent FR 2 807 105, 2000.

20 Brüstle, C., Schwarzenthal, D., *VarioCam Plus – A Highlight of the Porsche 911 Turbo Engine*, SAE 2001-01-0245, 2001.

21 Hannibal, W., Flierl, R., Stiegler, L., Meyer, R., *Overview of Current Continuously Variable Valve Lift Systems for Four-Stroke Spark-Ignition Engines and the Criteria for their Design Ratings*, SAE 2004-01-1263, 2004.

22 Leone, T. G., Christenson, E. J., Stein, R. A., *Comparison of Variable Camshaft Timing Strategies at Part Load*, SAE 960584, 1996.

23 Kramer, U., Philips, P., *Phasing Strategy for an Engine with Twin Variable Cam Timing*, SAE 2002-01-1101, 2002.

24 Bozza, F., Gimelli, A., Senatore, A., Caraceni, A., *A Theoretical Comparison of Various VVA Systems for Performance and Emission Improvements of SI-Engines*, SAE 2001-01-0670, 2001.

25 Kreuter, P., et. Al., *Meta – CVD System An Electro-Mechanical Cylinder and Valve Deactivation System*, SAE 2001-01-0240, 2001.

26 Johansson, B., Söderberg, F., *The Effect of Valve Strategy on In-Cylinder Flow and Combustion*, SAE 960582, 1996.

27 Stone, Richard, Kwan, Eric, *Variable Valve Actuation Mechanisms and the Potential for their Application*, SAE 890673, 1989.

28 Dresner, T., Barkan, P., *A Review and Classification of Variable Valve Timing Mechanisms*, SAE 890674, 1989.

29 Ahmad, T., Theobald, M. A., *A Survey of Variable-Valve-Actuation Technology*, SAE 891674, 1989.

30 Takemura, S., et. al., *A Study of a Continuous Variable Valve Event and Lift (VEL) System*, SAE 2001-01-0243, 2001.

31 Stein, R.A., Galietti, K.M., Leone, T.G., *Dual Equal VCT – A Variable Camshaft Timing Strategy for Improved Fuel Economy and Emissions*, SAE 950975, 1995.

32 Fu, H., Chen, X., Mustafa, E., Trigui, N., Richardson, S., Shilling, I., *Analytical Investigation of Cam Strategies for SI Engine Part Load Operation*, SAE 2004-01-0997, 2004.

33 Li, L., Tao, J., Wang, Y., Su, Y., Xiao, M., *Effects of Intake Valve Timing on Gasoline Engine Performance and Emissions*, SAE 2001-01-3564, 2001.

34 Hara, S., Kumagai, K., Matsumoto, Y., *Application of a Valve Lift and Timing Control System to an Automotive Engine*, SAE 890681, 1989.

35 Lenz, H. P., Geringer, B., Smetana, G., Dachs, A., *Initial Test Results of an Electro-Hydraulic Variable-Valve Actuation System on a Firing Engine*, SAE 890678, 1989.

36 Urata, Y., Umiyama, H., Shimizu, K., Fujiyoshi, Y., Sono, H., Fukuo, K., *A Study of Vehicle Equipped with Non-Throttling S.I. Engine with Early Intake Valve Closing Mechanism*, SAE 930829, 1993.

37 Negurescu, N., Pana, C., Popa, M. G., Racovitza, A., *Variable Valve – Control Systems for Spark Ignition Engine*, SAE 2001-01-0671, 2001.

38 AutoTechnology, Oktober 2003, p.18

39 Automotive Engineering International, January 2002, p.32.

40 Flierl, R., Kluting, M., *The Third Generation of Valvetrains – New Fully Variable Valvetrains for Throttle-Free Load Control*, SAE 2000-01-1227, 2000.

41 Nakamura, M., *A Continuous Variable Valve Event and Lift Control Device (VEL) for Automotive Engines*, SAE 2001-01-0244, 2001.

42 Automotive Engineering International, October 2005, pp. 20-2.

43 Automotive Engineering International, March 2004, p.80.

44 Schechter, M. M., Levin, M. B., *Camless Engine*, SAE 960581, 1996.

45 *Ricardo Quarterly Review*, Q1, 2005, p. 24.

46 Henry, R. R., *Single-Cylinder Engine Tests of a Motor-Driven, Variable-Valve Actuator*, SAE 2001-01-0241, 2001.

47 Auto Technology, Oktober 2003, p32-33

48 Turner, J., Bassett, M., Pearson, R., Pitcher, G., Douglas K., *New Operating Strategies Afforded by Fully Variable Valve Trains*, SAE 2004-01-1386, 2004.

49 Theobald, M.A., Laquesne, B., Henry, R., *Control of Engine Load via Electromagnetic Valve Actuators*, SAE 940816, 1994.

50 Riley, M.B., Fiddes, D., *Fully Variable Valve for SOHC Engines*, Autotechnology December 2005, pp. 52-55.

51 Kreuter, P., et. Al., *Meta – CVD System An Electro-Mechanical Cylinder and Valve Deactivation System*, SAE 2001-01-0240, 2001.

52 Jost, K., *Mercedes-Benz launches cylinder cutout*, Automotive Engineering International, January 1999, pp.38-39.

53 Albertson, W., et al., *Displacement on Demand for Improved Fuel Economy without Compromising Performance in GM's High Value Engines*, Powertrain International, Vol. 7, Num. 1, Winter 2004.

54 Ross, M., López, A. J., , Walker, F. H., *High Fuel Economy Enabled by the Split Engine*, ICEF2005-1324, Proceedings of ICEF2005, ASME.

55 Hara, S., Nakajima, Y., Nagumo, S., *Effects of Intake-Valve Closing Timing on Spark-Ignition Engine Combustion*, SAE Transactions, Vol. 94, Section1, pp. 1396-1405, 1985.

56 Moro, D., Ponti, F., Serra, G., *Thermodynamic Analysis of Variable Valve Timing Influence on SI Engine Efficiency*, SAE 2001-01-0667, 2001.

57 Auto Technology, February 2004, pp 48-51.

58 AEI September 2005, pp. 86-7.

59 Lake, T., Stokes, J., Murphy, R., Osborne, R., Schamel, A., *Turbocharging Concepts for Downsized DI Gasoline Engines*, SAE 2004-01-0036, 2004.

60 Wirth, M., Mayerhofer, U., Piock, W. F., Fraidl, G. K., *Turbocharging the DI Gasoline Engine*, SAE 2000-01-0251, 2000.

61 AEI August 2005, pp.38-9.

62 Lippert, A., El Tahry, S., Huebler, M., Parrish S., Inoue, H., Noyori, T., Nakama, K., Abe, T., *Development and Optimization of a Small-Displacement Spark-Ignition Direct-Injection Engine – Stratified Operation*, SAE 2004-01-0033, 2004.

63 Woo, Y., Yeom, K., Bae, C., Oh, S., Kang, K., *Effects of Stratified EGR on the Perfoemance of a Liquid Phase LPG Injection Engine*, SAE 2004-01-0982, 2004.

64 Nauwerck, A., Pfeil, J., Velji, A., Spicher, U., Richter, B., *A Basic Experimental Study of Gasoline Direct Injection at Significantly High Injection Pressures*, SAE 2005-01-0098, 2005.

65 Hiraya, K., Hotta, I., Takahashi, E., Tsuchida, H., Urushihara, T., *A Study of a DISI Engine with a Centrally Located High-pressure Fuel Injector*, SAE 2004-01-2944, 2004.

66 Muñoz, R., Han, Z., VanDerWege, B., Yi, J. *Effect of Compression Ratio on Stratified-Charge Direct-Injection Gasoline Combustion*, SAE 2005-01-100, 2005.

67 Drangel, H., Olofsson, E., Reinmann, R., *The Variable Compression (SVC) and the Combustion Control (SCC) – Two Ways to Improve Fuel Economy and Still Comply with World-Wide Emission Requirements*, SAE 2002-01-0996, 2002.

68 Kettner, M., Fischer, J., Nauwerck, A., Tribulowski, J., Spicher, U., Velji, A., Kuhnert, D, Latsch, R., *The BPI Flame Jet Concept to Improve the Inflammation of Lean Burn Mixtures in Spark Ignited Engines*, SAE 2004-01-0035, 2004.

69 Kettner, M., Rothe, M., Velji, A., Spicher, U., Kuhnert, D, Latsch, R., *A New Flame Jet Concept to Improve the Inflammation of Lean Burn Mixtures in SI Engines*, SAE 2005-01-3688, 2005.

70 Suzuki, M., Ando, R., Ishibashi, Y., Paradoxical Approach to Improve Fuel Economy for Small Practical Motorcycles, SAE 2004-01-0989, 2004.

71 Alsterfalk, M., Filipi, Z. S., Assanis, D. N., *The Potential of the Variable Stroke Spark-Ignition Engine*, SAE 970067, 1997.

72 Pierce, J., *Variable Stroke Mechanisms*, US Patent 1,112,832, 1914.

73 Biermann, A. E., *Variable Stroke Piston Engines*, US Patent 2,909,163, 1959.

74 Welsh, H. W., Riley, C. T., *The Variable Displacement Engine: An Advanced Concept Power Plant*, SAE 710830, 1971.

75 Heywood, J. B., *Internal Combustion Engine Fundamentals*, McGraw-Hill, 1988.

76 Hitomi, M., Sasaki, J., Hatamura, K., Yano, Y., *Mechanism of Improving Fuel Efficiency by Miller Cycle and Its Future Prospect*, SAE 950974, 1995.

77 Hatamura, K., Hayakawa, M., Goto, T., Hitomi, M., *A study of the improvement effect of Miller-cycle on mean effective pressure limit for high-pressure supercharged gasoline engines*, JSAE Review 18 (1997), 101-106.

78 Hirose, K., Ueda, T., Takaoka, T., Kobayashi, Y., *The high-expansion-ratio gasoline engine for the hybrid passenger car*, JSAE Review 20 (1999), 13-21.

79 Wakabayashi, R., Takiguchi, M., Shimada, T., Mizuno, Y., Yamauchi, T., *The Effects of Crank Ratio and Crankshaft Offset on Piston Friction Losses*, SAE 2003-01-0983, 2003.

80 Shin, S., Cusenza, A., Shi, F., *Offset Crankshaft Effects on SI Engine Combustion and Friction Performance*, SAE 2004-01-0606, 2004.

81 Suzuki, M., Iijima, S., Moriyoshi, Y., Sano,M., *A Trial of Improving Thermal Efficiency by Active Piston Control – Speed Control Effect of Combustion Chamber Volume Variation on Thermal Efficiency*, SAE 2004-32-0080, JSAE 20044367, 2004.

82 Nagesh, M. S., Govinda Mallan, K. R., Gopalakrishnan, K. V., *Experimental Investigation on Extended Expansion Engine (EEE)*, SAE 920452, 1992.

83 Kentfield, J. A. C., *Extended, and Variable, Stroke Reciprocating Internal Combustion Engines*, SAE 2002-01-1941, 2002.

84 Kentfield, J.A.C., Fernandes, L.C.V., *Friction Losses of a Novel Prototype Variable Expansion-Ratio, Spark Ignition, Four-Stroke Engine*, SAE 972659, 1997.

85 Kentfield, J. A. C., *Air-Injection, and Other, Combustion-Turbulence Generators for Extended Expansion-Stroke Spark-Ignition Engines*, SAE 961679, 1996.

86 Ichimaru, K., Sakai, H., Kansaka, H., *A Rotary Valve Controlled High Expansion Ratio Gasoline Engine*, SAE 940815, 1994.

87 Ueda, N., Sakai, H., Iso, N., Sasaki, J., *A Naturally Aspirated Miller Cycle Gasoline Engine – Its Capability of Emission, Power and Fuel Economy*, SAE 960589, 1996.

88 Fukuzawa, Y., Shimoda, H., Kakuhama, Y., Endo, H., Tanaka, K., *Development of High Efficiency Miller Cycle Gas Engine*, Mitsubishi Technical Review, vol. 38, No. 3 (Oct. 2001).

89 Shkolnik, N., Shkolnik A. C., *High Efficiency Hybrid Cycle Engine*, ICEF2005-1221, Proceedings of ICEF2005, ASME.

90 Baker, T.G., Nightingale, C. J. E., *Port Throttling and Port De-activation Applied to a 4-Valve SI Engine*, SAE 960587, 1996.

91 Hirooka, H., Mori, S., Shimizu, R., *Effects of High Turbulence Flow on Knock Characteristics*, SAE 2004-01-0977, 2004.

92 Olofsson, E., Alvestig, P., Bergsten, L., Ekenberg, M., Gawell, A., Larsén, A., Reinmann, R., *A High Dilution Stoichiometric Combustion Concept Using a Wide Variable Spark Gap and In-Cylinder Air Injection in Order to Meet Future CO_2 Requirements and World Wide Emission Regulations*, SAE 2001-01-0246, 2001.

3 - Theoretical analysis of engine cycles

3 THEORETICAL ANALYSIS OF ENGINE CYCLES

3.1 Introduction

In the thermodynamic optimization of internal combustion engines the first step must always be the identification of the causes of efficiency losses during the working process. In this chapter an analysis is made to several engine cycles using classical thermodynamics. Cycles are considered closed, where heat is supplied to simulate combustion and cooling substitutes the exhaust and intake processes. The cycles analysed are the so called ideal cycles, because some other real phenomena such as heat losses to the surroundings, friction, mass flow phenomena, etc are not considered.
In each cycle the objective is always to evaluate the thermal efficiency of the cycle, which can be defined as:

$$\eta_{thermal} = \frac{W_{output}}{Q_{sup\ plied}} \tag{3.1}$$

The analysis of thermal engine cycles from a theoretical point of view will be made starting from the naturally aspirated engines and then supercharged cycles. The natural aspirated spark ignition engine cycles analysed are: Otto, Otto DI, Otto VCR, Miller and Miller VCR. Diesel and dual cycles (compression ignition) are also analysed and all these cycles are compared in terms of thermal efficiency at the low load region. Supercharged Otto, Miller and dual cycles are analysed as well and compared using the same criterion. Supercharging is used as a technique for enthalpy recovery from exhaust gases, thus being a potential method for thermodynamic improvement of internal combustion engines.
The objective is to understand the thermodynamical performance of each cycle through the load range.

3.2 Naturally Aspirated Engine Cycles

3.2.1 Otto Cycle at part load

When working at idle or at light loads conventional spark ignition engines, usually lower the intake pressure of the air to reduce load. When engines work under the Otto cycle this pressure reduction on the engine charge may be obtained by throttling, keeping the mixture at stoichiometric conditions, so that the three-way catalytic converter may work at optimal conditions. This will lead to a reduction on the intake pressure, the engine working as an air pump during the intake stroke. The reduction of the intake pressure leads to a reduction of the mass of air and fuel (assuming a stoichiometric mixture) trapped in the cylinder. In the p-V diagram of this cycle (Figure 3-1), the pumping work (negative, because this work spend by the engine that represents no output shaftwork) is represented by the area defined by 1'-6-7-1-1' (or 5-6-7-1-5), while the positive work is 5-1'-2-3-4-5 (or 1-2-3-4-1).

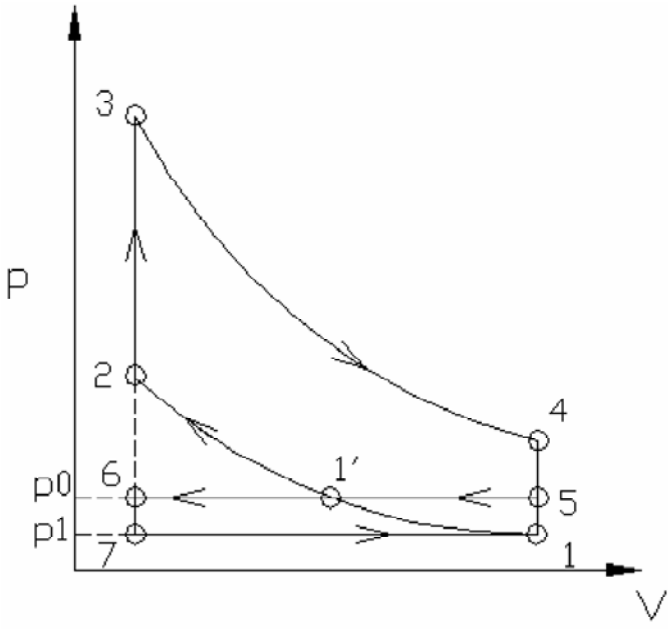

Figure 3-1 - p-V diagram of the Otto cycle at part load.

Considering the work involved in this cycle:

$$W = W_{1'2} + W_{34} + W_{51'} + W_{1'6} + W_{71} + W_{11'} \tag{3.2}$$

All the terms are throughoutly analysed in Annex A. The thermal efficiency as defined in (3.1) is calculated as:

$$\eta_O = \frac{W}{Q_H} = \frac{p_1 \cdot V_1 \cdot \frac{B}{\varepsilon^{\gamma-1}}\left(\varepsilon^{\gamma-1} - 1\right) - p_1 \cdot V_1 \cdot \left(\frac{1}{\beta} - 1\right)\frac{\varepsilon - 1}{\varepsilon}}{\frac{m}{1 + A/F} \cdot Q_{LHV}} \tag{3.3}$$

where:

$\beta = \frac{p_1}{p_0}$ is the ratio between the atmospheric pressure and the intake pressure

$B = \frac{\frac{1}{1 + A/F} \cdot Q_{LHV}}{R \cdot T_1}$ is a constant (considering that the mixture is always stoichiometric)

$\varepsilon = \frac{V_1}{V_2}$ is the compression ratio

Efficiency may also be written as:

$$\eta_O = \frac{\frac{B}{\varepsilon^{\gamma-1}}\left(\varepsilon^{\gamma-1} - 1\right) - \left(\frac{1}{\beta} - 1\right)\frac{\varepsilon - 1}{\varepsilon}}{B} \tag{3.4}$$

Knowing that the maximum work produced by the Otto cycle is for the wide open throttle (WOT) operation:

$W_{max} = W$ when $p_1 = p_0$ or $\beta = 1$

comes:

$$\frac{W}{W_{max}} = \frac{p_1 \cdot V_1 \cdot \frac{B}{\varepsilon^{\gamma-1}} \cdot \left(\varepsilon^{\gamma-1} - 1\right) - p_1 \cdot V_1 \cdot \left(\frac{1}{\beta} - 1\right) \cdot \frac{\varepsilon - 1}{\varepsilon}}{p_0 \cdot V_1 \cdot \frac{B}{\varepsilon^{\gamma-1}} \cdot \left(\varepsilon^{\gamma-1} - 1\right)} \tag{3.5}$$

An equation can be presented that gives the load for the Otto cycle as a function of the pressure ratio (β):

$$\frac{W}{W_{max}} = \beta\left[1 - \frac{\left(\frac{1}{\beta} - 1\right)\cdot\frac{(\varepsilon - 1)}{\varepsilon}}{\frac{B\cdot\left(\varepsilon^{\gamma-1} - 1\right)}{\varepsilon^{\gamma-1}}}\right] \tag{3.6}$$

The values of efficiency of this cycle are plotted against β and against load on Figure 3-2 and Figure 3-3 respectively, for an engine with $\varepsilon = 12$.

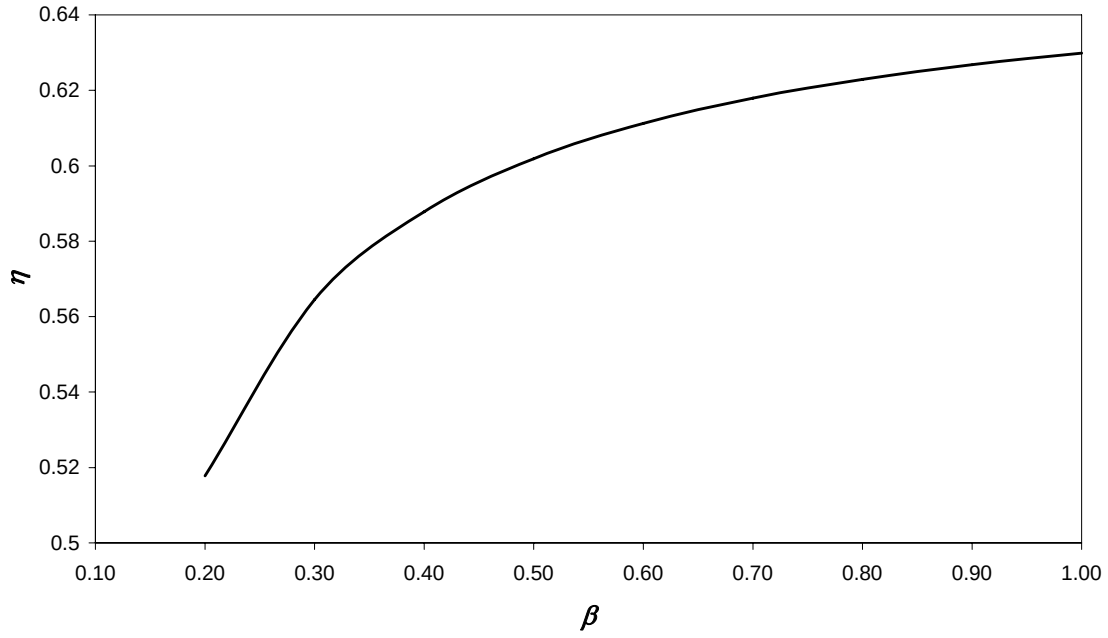

Figure 3-2 – Thermal efficiency of Otto cycle at part load as a function of pressure ratio.

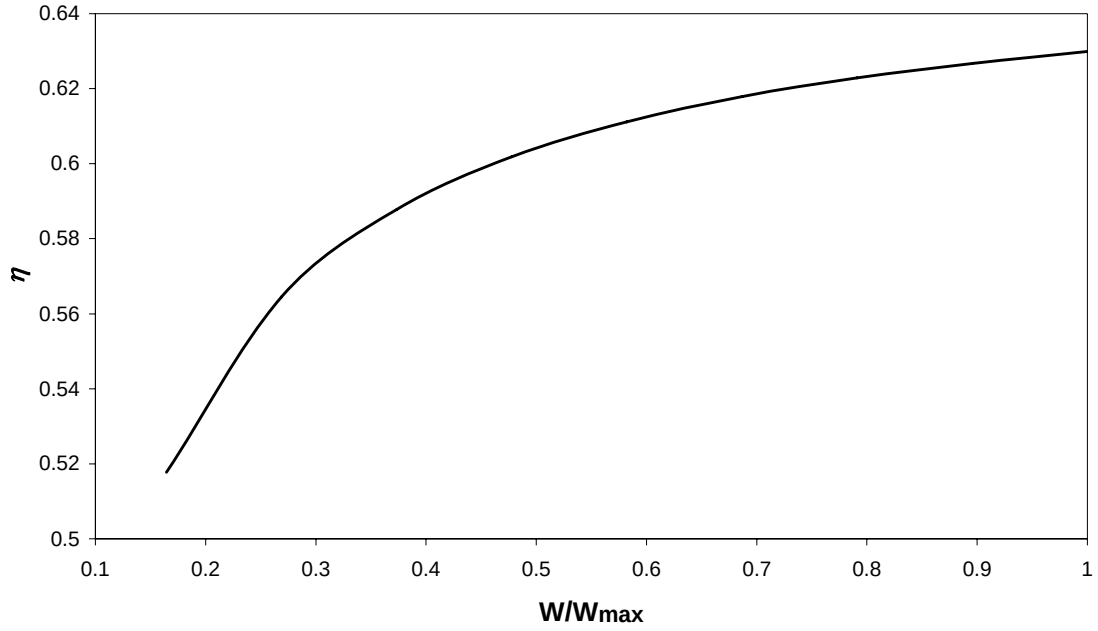

Figure 3-3 – Thermal efficiency of Otto cycle at part load as a function of load.

3.2.2 Otto cycle with direct injection (stratified charge) at part load

In the previous cycle an amount of work was spent in pumping the mixture so that the intake quantity would be lower than the cylinder capacity at atmospheric conditions. In order to eliminate this work, the direct injection system can be used together with the concept of charge stratification. In this case the quantity of intake air will remain the same (the cylinder volume) but the amount of injected fuel will be lowered with the required load, thus using lean mixtures (or using stoichiometric mixture and a large value for EGR). As a consequence, the pressure and temperature at the end of combustion will also be lower. The reduction of load in this cycle can be seen in the p-V diagram (Figure 3-4), as a lower dashed line between points 3' (end of combustion) and 4' (end of expansion).

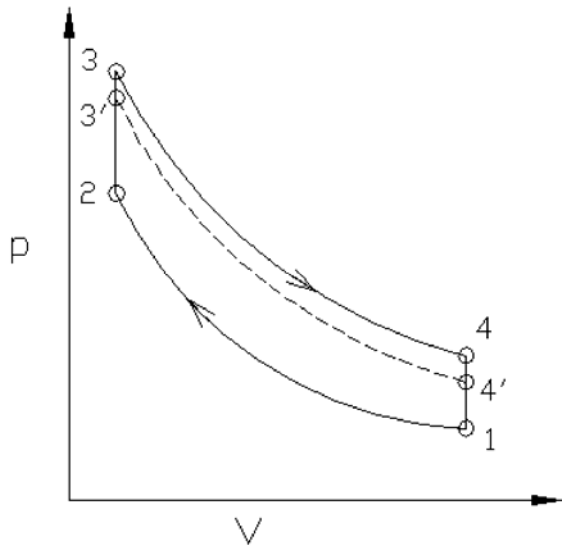

Figure 3-4 - p-V diagram for the Otto cycle with direct injection.

The efficiency of this cycle is analysed in annex A and can be written as:

$$\eta_{OD} = 1 - \frac{\frac{1}{\varepsilon^{\gamma-1}} \cdot \left[1 + \frac{(\gamma-1)\cdot C}{\varepsilon^{\gamma-1}} \cdot \frac{1}{1 + \frac{\left(A/F\right)_S}{\Phi}} \right] - \frac{1}{\varepsilon^{\gamma-1}}}{\frac{(\gamma-1)\cdot C}{\varepsilon^{\gamma-1}} \cdot \frac{1}{1 + \frac{\left(A/F\right)_S}{\Phi}}} = 1 - \frac{1}{\varepsilon^{\gamma-1}} \qquad (3.7)$$

where :

$C = \frac{Q_{LHV}}{R \cdot T_1}$ is a constant

$\varepsilon = \frac{V_1}{V_2}$ is the compression ratio

Φ is the fuel/air equivalent ratio, defined as the relation of the stoichiometric mixture and the effective intake mixture:

$$\Phi = \frac{\left(A/F\right)_S}{A/F} = \frac{F/A}{\left(F/A\right)_S} \qquad (3.8)$$

As can be seen from (3.7), the efficiency of this cycle is not dependent on the fuel/air equivalent ratio. This means that the Otto direct injection cycle does not depend on load, but only compression ratio.

3.2.3 Otto Variable Compression Ratio engine

The Otto engine with Variable Compression Ratio (VCR) is already implemented [1] and adjusts the compression ratio of the engine to the load conditions at each condition. The relation between these two variables is based on the knock onset condition. Theoretically knock onset may be considered to happen at the end of combustion (point 3 in Figure 3-1), which is the point of maximum temperature in the cycle and thus of maximum pressure because ideal gases are considered. Increasing the intake pressure ratio (β), defined as the ratio between the intake pressure (p_1) and the atmospheric pressure, and keeping temperature (and pressure) level of points 2 and 3, as high as possible, the compression ratio will have to be adjusted (reduced) to prevent knock onset. Considering the conditions of knock as a compression ratio of 12 (ε_{limit}) at full load ($p_1 = p_{atm}$), and based on Figure 3-1, comes:

$$p_{2limit} = p_1 \left(\frac{V_1}{V_2} \right)^{\gamma} = p_{atm} \varepsilon_{limit}^{\gamma} \tag{3.9}$$

Considering now the points from the cycle presented in Figure 3-1, comes:

$$p_1 = \frac{p_{2limit}}{\varepsilon^{\gamma}} \tag{3.10}$$

From this equation and the definition of β, this can be expressed as:

$$\beta = \frac{p_1}{p_0} = \frac{p_{2limit}}{p_{atm} \varepsilon^{\gamma}} = \left(\frac{\varepsilon_{limit}}{\varepsilon} \right)^{\gamma} \tag{3.11}$$

This relation is plotted for several values of the compression ratio (ε) in Figure 3-5, considering that ε_{limit} is 12.

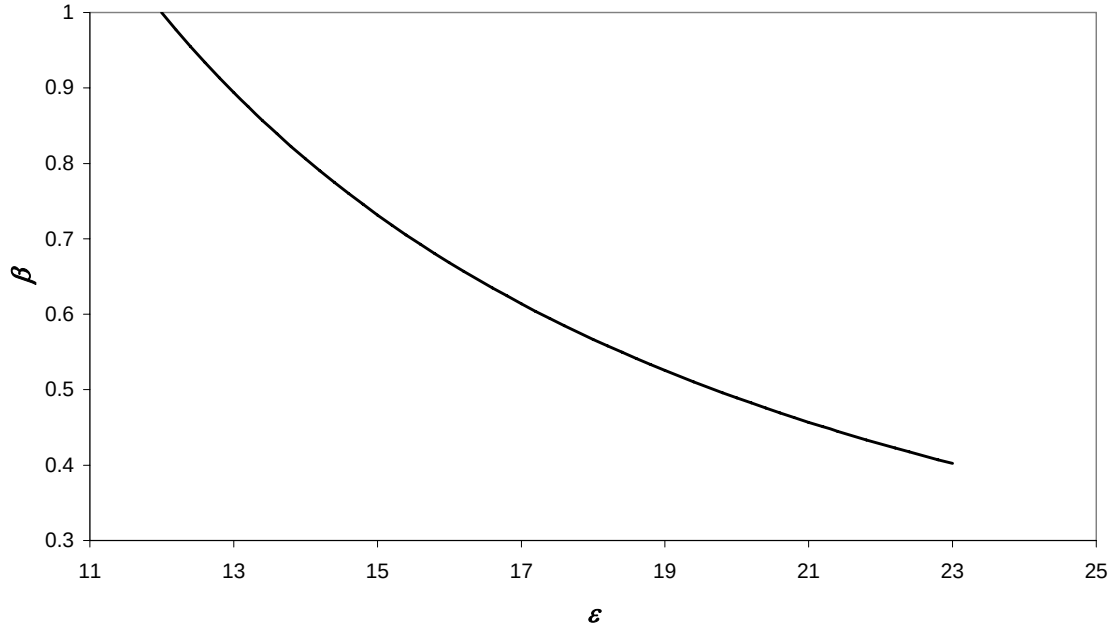

Figure 3-5 - Maximum values of the part load ratio (β) as the effective compression ratio (ε) increases.

Looking to this relation in the *p*-*V* diagram, the pressure at the end of compression is the same and the volume at the end of compression reduces as the load decreases (Figure 3-6).

The efficiency of an Otto cycle working at part load is given above (3.4) [2]. The variation of β is shown to decrease the thermal efficiency of the engine with the reduction of the load. In that case it is also considered that the compression ratio is constant. If that process would be described as isentropic a different behavior of the efficiency would be obtained for different throttling conditions. Also if the compression ratio could be adjusted to the intake pressure in order to get the same pressure (p_{2limit}) at the end of compression defined by equation (3.9), the following modifications must be done in (3.4):

$$\eta_O = 1 - \left(\frac{\beta^{\frac{1}{\gamma}}}{\varepsilon_{limit}} \right)^{\gamma-1} - \frac{\left(\frac{1}{\beta} - 1 \right) \left(1 - \frac{\beta^{\frac{1}{\gamma}}}{\varepsilon_{limit}} \right)}{B} \tag{3.12}$$

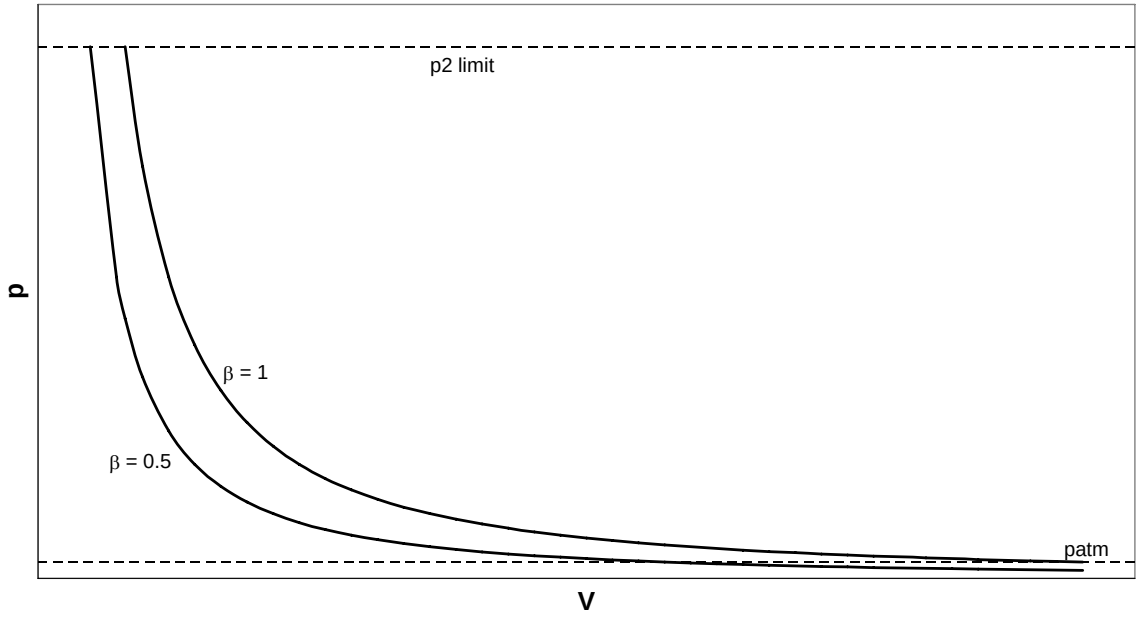

Figure 3-6 – *p-V* diagram for two compressions at different loads and VCR.

Again, if the load is considered as W/W_{max}, the substitution of (3.9) can be made in expression (3.6), which comes:

$$\frac{W}{W_{max}} = \beta\left[1 - \frac{\left(\frac{1}{\beta} - 1\right)\cdot\left(1 - \frac{\beta^{\frac{1}{\gamma}}}{\varepsilon_{limit}}\right)}{B\cdot\left[1 - \left(\frac{\beta^{\frac{1}{\gamma}}}{\varepsilon_{limit}}\right)^{\gamma-1}\right]}\right] \tag{3.13}$$

The efficiency of an engine working under these conditions is plotted in Figure 3-7 and Figure 3-8 as function of the intake pressure ratio and load respectively.

Comparing these values with the results presented in [2] for SI engines at part load condition, it can be seen that the efficiency can be improved as the compression ratio is adjusted to the knock conditions. The maximum value for the efficiency can reach 68.7% if the throttling is considered isentropic, being 12% better than the part load Otto cycle without adjustment of the compression ratio. As the pressure at the intake is reduced, the improvement of efficiency between fixed compression and variable compression cycles is always increasing.

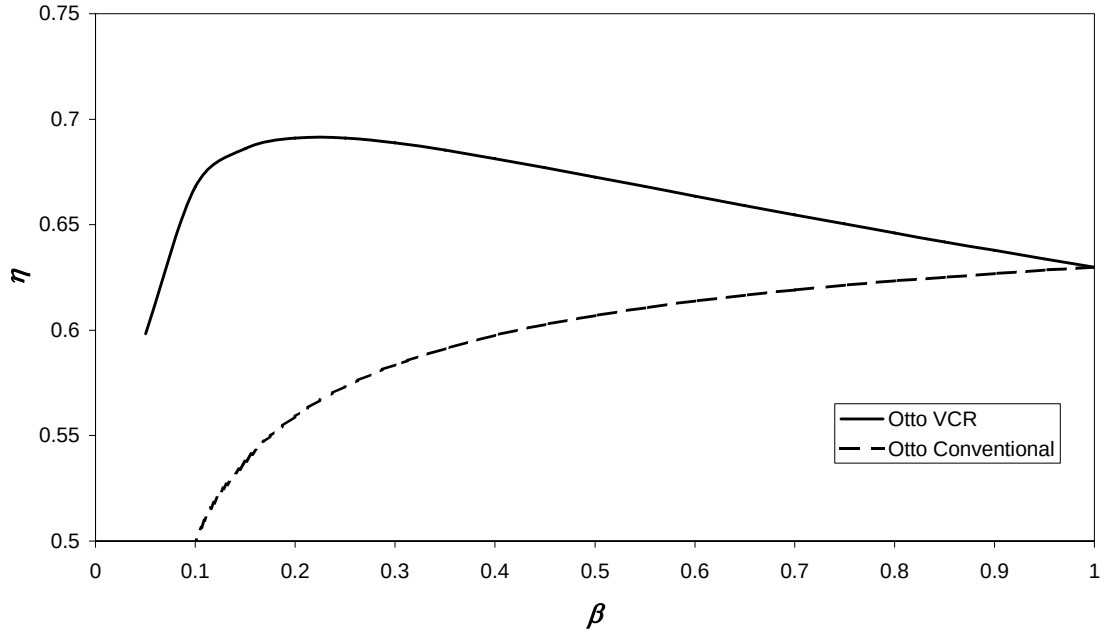

Figure 3-7 – Efficiency of the Otto cycle working under part load conditions with and without compression ratio adjustment for the knocking conditions.

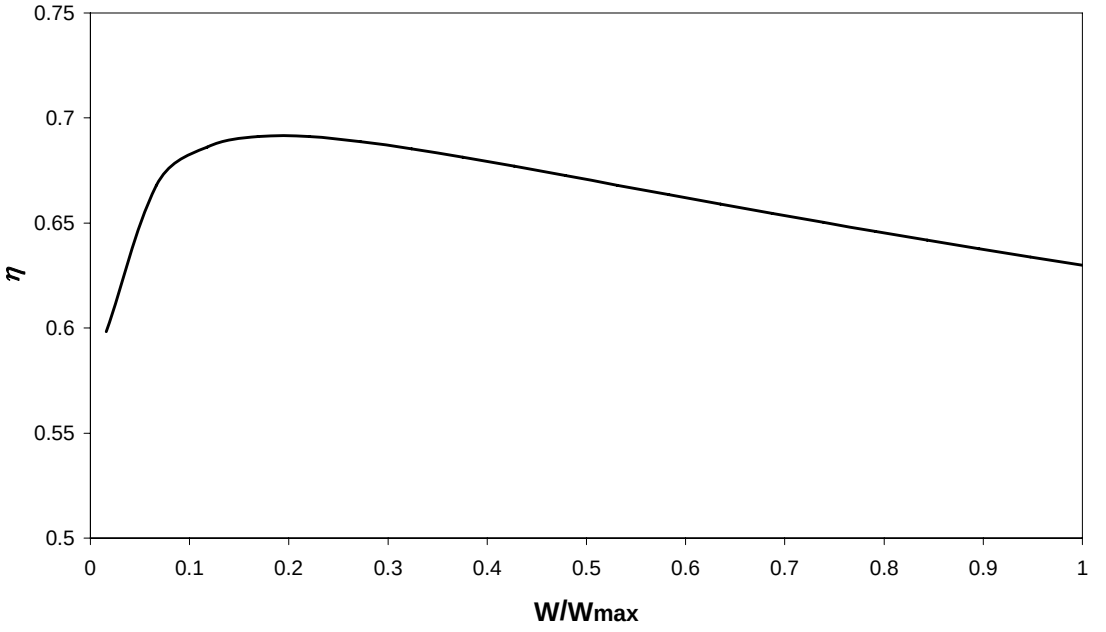

Figure 3-8 – Efficiency of the Otto cycle working under part load conditions with compression ratio adjustment for the knocking conditions as a function of load.

3.2.4 Miller Cycle

In conventional configuration reciprocating engines the Miller cycle is achieved by using Variable Valve Timing (VVT) technology. The difference between the effective compression and expansion results in over-expansion. By changing the intake valve event, the amount of mass trapped in the cylinder at each cycle can be reduced. In a conventional internal combustion engine (e.g. Otto engine - Figure 3-1) with a fixed geometry, the compression ratio was defined in (A.3d). Hereafter this geometric compression ratio is named as ε_g. When studying the Miller cycle, due to the cycle operation (effective admission is shorter than the piston stroke), we must consider another compression ratio that is the effective compression ratio (here named trapped - ε_{tr}). This is defined in the same manner described in (A.3d), but instead of considering the V_{BDC}, the cylinder volume at beginning of compression (where the pressure is still atmospheric, i.e. the moment when the intake valve closes) is considered instead:

$$\varepsilon_{tr} = \frac{V_{IVC}}{V_{TDC}} = \frac{V_1}{V_2} \tag{3.14}$$

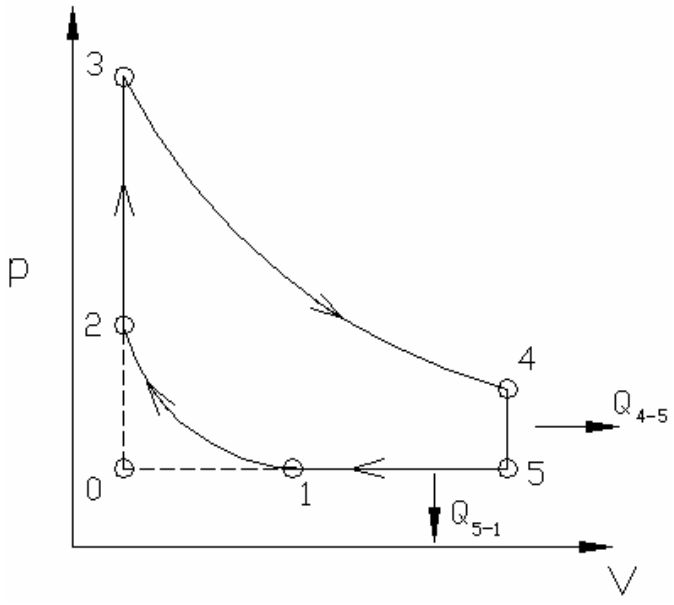

Figure 3-9 – p-V diagram of a Miller cycle.

In this kind of cycle the ratio between expansion and compression (expansion-compression ratio - σ) must be considered, which is a characteristic parameter of the Miller cycle:

$$\sigma = \frac{V_{BDC}}{V_{IVC}} = \frac{V_5}{V_1} \tag{3.15}$$

From the parameters defined in (A.3d) and (3.14) comes:

$$\sigma = \frac{\varepsilon_g}{\varepsilon_{tr}} \tag{3.16}$$

This means that σ also shows the relation between geometric compression ratio and the trapped compression ratio. In the Otto cycle the value of this parameter is one, since that theoretically expansion equals compression.

Following the cycle presented in Figure 3-9, compression occurs from 1 to 2, and the combustion until 3. Expansion is performed from 3 to 4, which correspond to the total length of the piston stroke from TDC to BDC. In 4 the exhaust valve is opened starting the exhaust. At TDC the exhaust valve is closed and the intake valve is opened, and so it remains during the descent of the piston from TDC to BDC and for part of the upward stoke, closing again only at point 1. In the theoretical study this is considered a closed cycle (constant mass, like Otto or Diesel cycles) that loses heat in processes 4-5 and 5-1, the processes 1-0 and 0-1 not being considered as they are reversed.

To the thermal efficiency study of the Miller cycle, it will be necessary to deduce expressions to calculate temperatures in the different points of the cycle. These points and processes are those represented in the diagram of Figure 3-9.

Thermal efficiency for the Miller cycle as explained in Annex A can be written as:

$$\eta_{MG} = 1 - \frac{1}{\varepsilon_g^{\gamma-1}} - \frac{\sigma^{\gamma}(\gamma-1) - \gamma \cdot \sigma^{\gamma-1} + 1}{(\gamma-1) \cdot \sigma^{\gamma-1} \cdot B} \tag{3.17}$$

where B is defined as: $B = \dfrac{m \cdot Q_{LHV}}{p_1 \cdot \Delta V \cdot \left(1 + A/F\right)}$

It is possible to represent graphically the thermal efficiency of Miller cycle as a function of σ, for several geometric compression ratios (ε_g) using this expression. This diagram is shown in Figure 3-10.

In this case engine efficiency values are calculated keeping the geometric compression ratio constant at typical values used in spark ignition engines. This implies that when raising the value of σ, the pressure at the end of compression decreases once the trapped compression ratio (which is the real compression ratio of the mixture contained in the cylinder) is reduced for the same geometric compression ratio. In this figure it is possible to observe that the maximum efficiency is obtained with $\sigma = 1$, that is the Otto cycle at WOT. Simultaneously it is possible to observe that efficiency also increases when the geometric compression ratio increases. This is due to the corresponding raise of pressure (and temperature) obtained at the end of the compression stroke. Dashed lines represent the cases when the pressure at the end of the expansion stroke is lower than the atmospheric pressure.

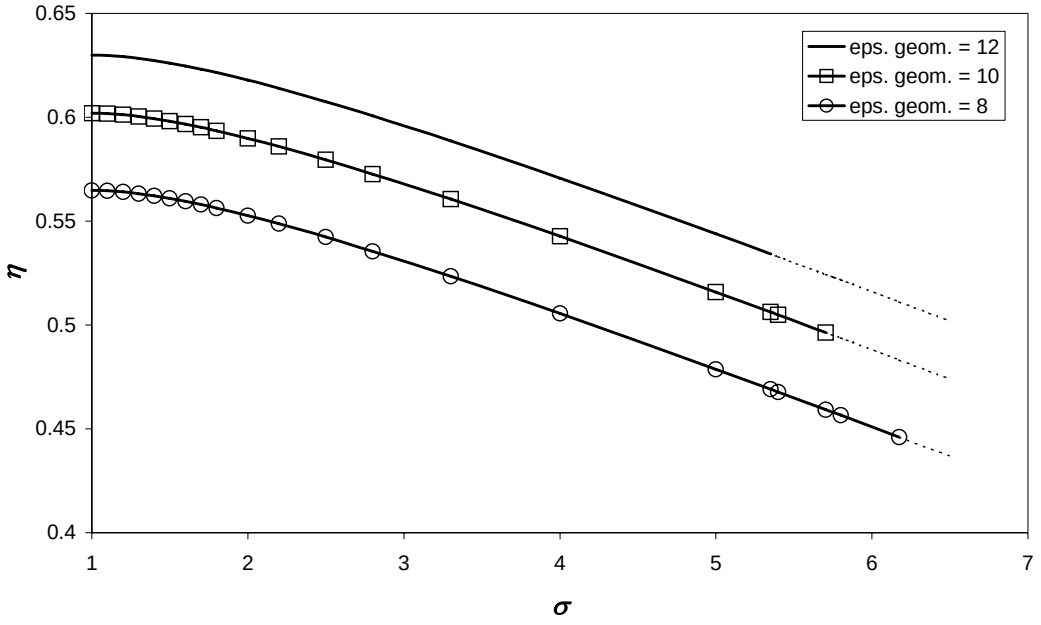

Figure 3-10 - Thermal efficiency as a function of σ for different geometric compression ratios.

3.2.5 Miller Variable Compression Ratio (VCR)

Now considering that instead of keeping the geometric compression ratio constant, we keep the trapped compression ratio and the engine displacement constant, expression (3.17) may be written using expression (3.16) (substituting ε_g by $\varepsilon_{tr} \cdot \sigma$):

$$\eta_{MT} = 1 - \frac{1}{\varepsilon_{tr}^{\gamma-1} \cdot \sigma^{\gamma-1}} - \frac{\sigma^{\gamma}(\gamma-1) - \gamma \cdot \sigma^{\gamma-1} + 1}{(\gamma-1) \cdot \sigma^{\gamma-1} \cdot B} \tag{3.18}$$

A graphical representation of this expression is shown in Figure 3-11.

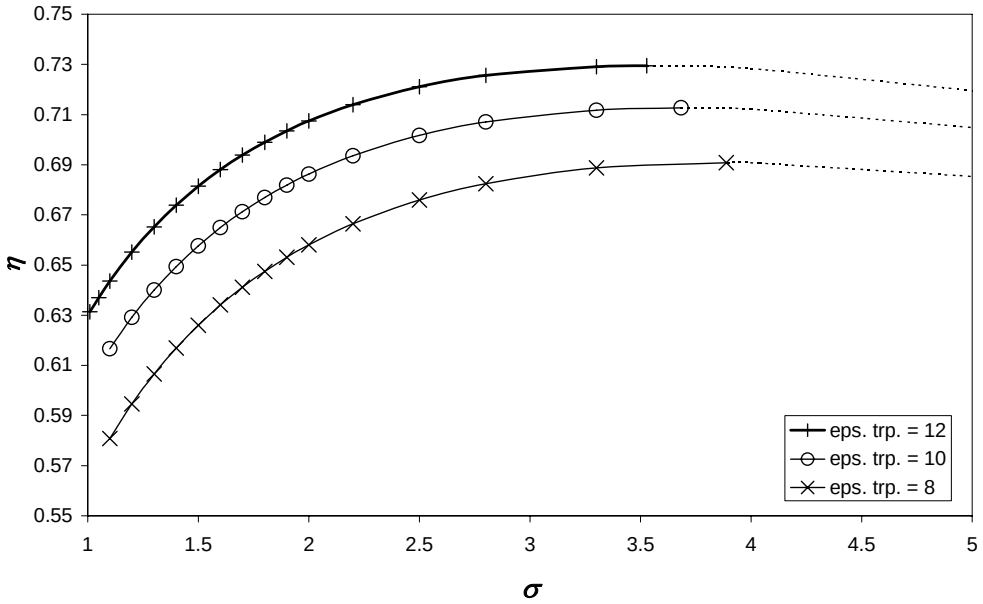

Figure 3-11 - Thermal efficiency as a function of σ for different trapped compression ratios.

It is clear from Figure 3-11 that efficiency increases when comparing the Miller cycle with the Otto cycle ($\sigma = 1$). As the engine displacement is kept constant, the increase of σ implies a reduction of the combustion chamber volume (point 2 of the *p*-*V* diagram in Figure 3-9)

To use the Miller cycle full potential, it shall be necessary to know the maximum value of σ which occurs when, at the end of expansion, the pressure equals the admission pressure. At such point, the engine efficiency is maximum and corresponds to the Atkinson cycle, in which the expansion is extended to its maximum. In Figure 3-11 the transition from continuous to dashed lines represents this point of maximum efficiency.

So it is necessary to determine the volume where the pressure at 4 equals the pressure at 1. Using the isentropic expressions for ideal gas:

$$p_4 = p_3 \left(\frac{V_3}{V_4} \right)^{\gamma} = p_3 \left(\frac{1}{\varepsilon_g} \right)^{\gamma} \tag{3.19}$$

Using expressions (A.29) and (3.14) successively comes:

$$p_4 = p_3\left(\frac{1}{\varepsilon_g}\right)^{\gamma} = p_2\left[1+\frac{(\gamma-1)\cdot B}{\varepsilon_{tr}^{\gamma-1}}\right]\cdot\left(\frac{1}{\varepsilon_g}\right)^{\gamma} = p_1\left(\frac{1}{\sigma}\right)^{\gamma}\cdot\left[1+\frac{(\gamma-1)\cdot B\cdot\sigma^{\gamma-1}}{\varepsilon_g^{\gamma-1}}\right] = \\ = p_1\cdot\frac{1}{\sigma^{\gamma}}\left[1+\frac{(\gamma-1)\cdot B}{\varepsilon_{tr}^{\gamma-1}}\right] \tag{3.20}$$

In Figure 3-12 is represented (3.20) with p_4/p_1 function of σ.

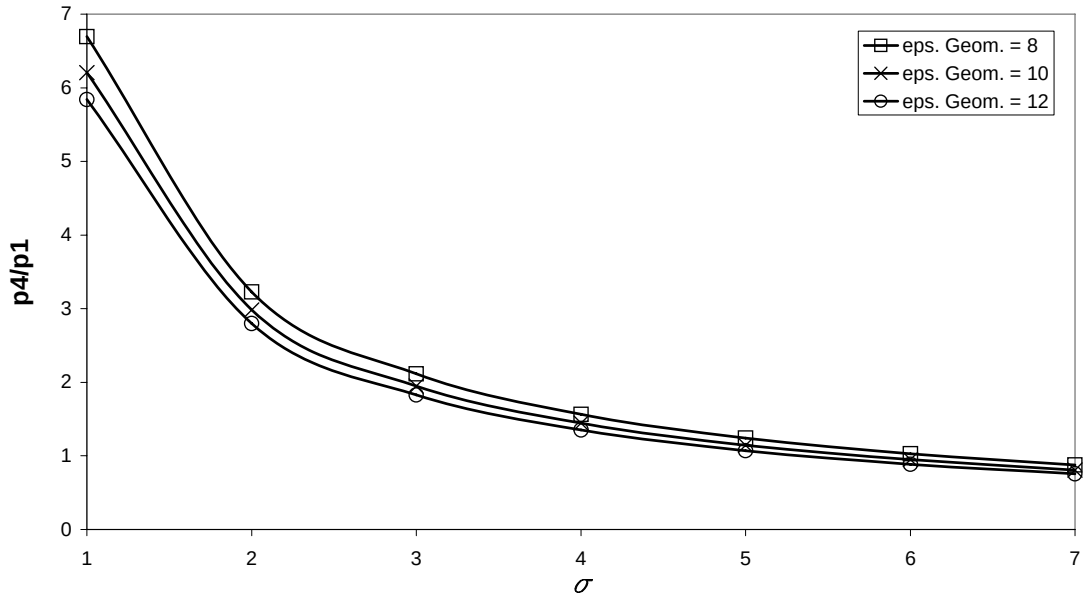

Figure 3-12 - Relation between p_4/p_1 and σ for different ε_g.

From Figure 3-12 it is possible to conclude that σ may be increased up to a value close to 6, in which the pressure value at the end of expansion is closer to the pressure at 1. It also is possible to conclude that the higher the ε_g the lower the ratio between p_4 and p_1, for the same values of σ.

To determine the value of optimal σ, it is necessary to differentiate expression (3.18) in relation to σ, and to make it equal to 0, so obtaining the values of the optimal value of σ function of ε_{tr}.

$$\frac{d\eta}{d\sigma}=0 \quad \Rightarrow \sigma_{opt}=\left[1+\frac{(\gamma-1)\cdot B}{\varepsilon_{tr}^{\gamma-1}}\right]^{\frac{1}{\gamma}} \tag{3.21}$$

Knowing that p_4 should be higher than p_1 (limit situation of the Miller cycle) it comes:

$$\frac{1}{\sigma^{\gamma}}\left[1+\frac{(\gamma-1)\cdot B}{\varepsilon_{tr}^{\gamma-1}}\right] \geq 1 \quad \Leftrightarrow \quad \sigma \leq \left[1+\frac{(\gamma-1)\cdot B}{\varepsilon_{tr}^{\gamma-1}}\right]^{\frac{1}{\gamma}} \tag{3.22}$$

Figure 3-13 represents the relation between the value of optimal σ and the value of trapped compression ratio.

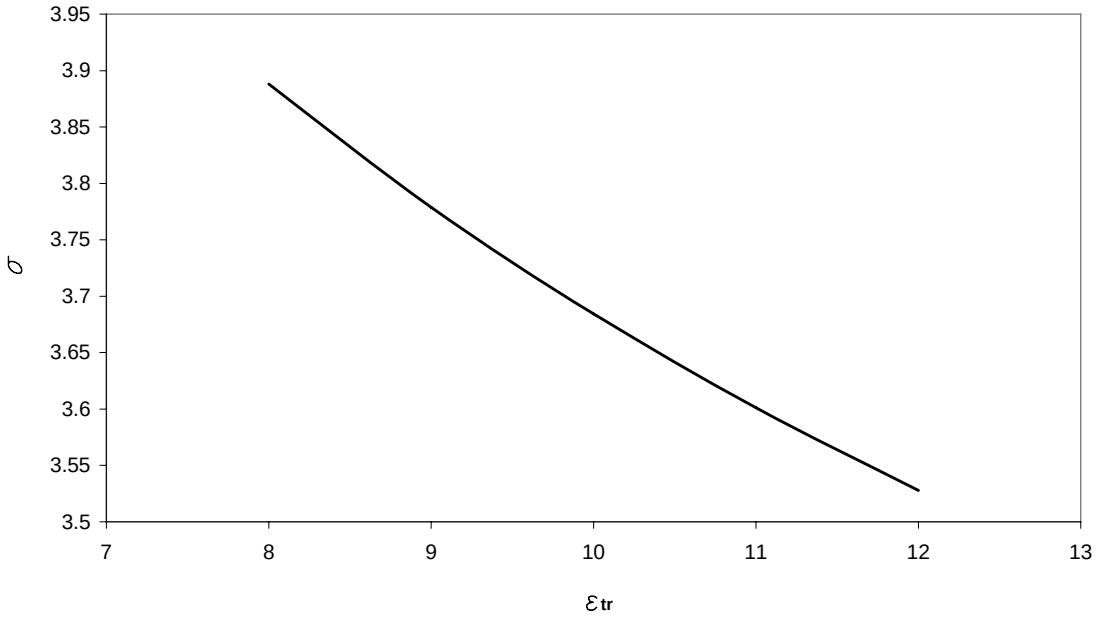

Figure 3-13 - Values for optimal σ for different values of trapped compression ratio.

It is possible to determine the maximum Miller cycle efficiency for different values of trapped compression ratio. The evolution of these values is represented in Figure 3-14. As said before the Miller cycle with full expansion to atmospheric pressure is also known as the Atkinson cycle.

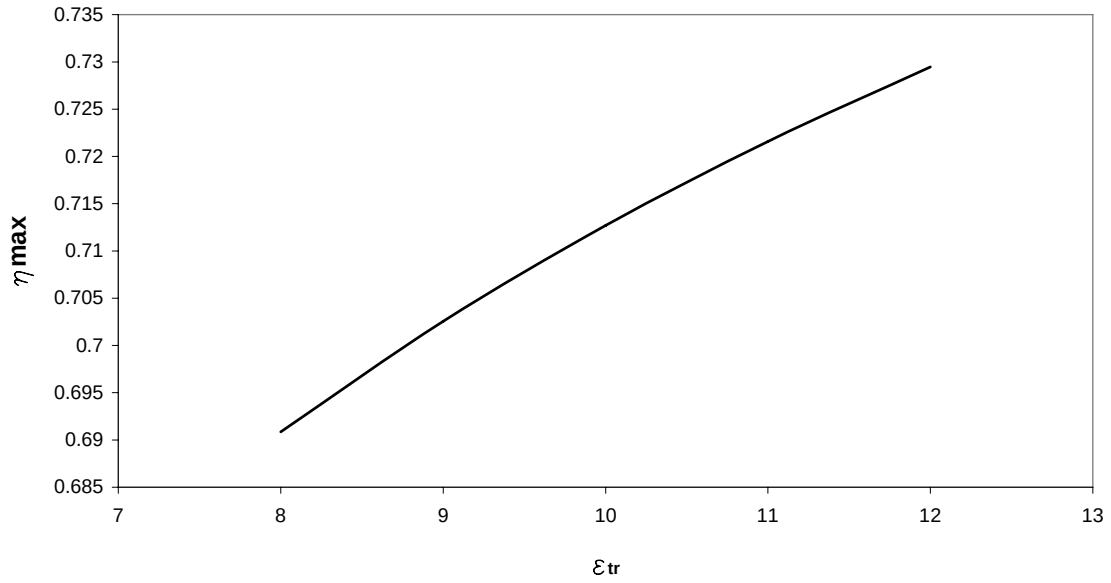

Figure 3-14 - Maximum efficiency vs. trapped compression ratio.

3.2.6 Diesel cycle at part load

In the Diesel cycle the load is controlled by the amount of fuel supplied during the injection. The amount of intake air is the same, as there is no restriction on the intake. So, the change in the cycle configuration due to a lower load (lean mixture) will be the reduction of the heat supplied during the isobaric heating. In the *p*-*V* diagram (Figure 3-15) it can be seen the difference between the full load cycle and the part load cycle, plotted by a dashed line.

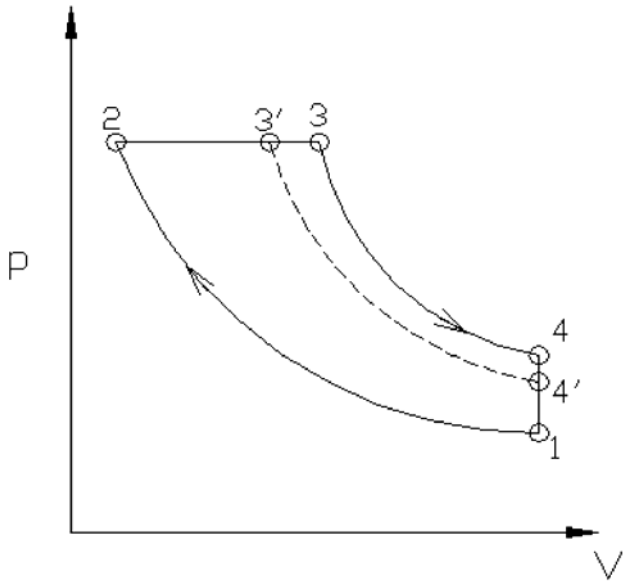

Figure 3-15 – *p*-*V* diagram of the Diesel cycle.

The efficiency of this cycle can be expressed (Annex A) by:

$$\eta_D = 1 - \frac{[A(\Phi)]^{\gamma} \cdot \left(\frac{1}{\varepsilon}\right)^{\gamma-1} - \left(\frac{1}{\varepsilon}\right)^{\gamma-1}}{\gamma \cdot [A(\Phi) - 1]} = 1 - \left(\frac{1}{\varepsilon}\right)^{\gamma-1} \cdot \frac{[A(\Phi)]^{\gamma} - 1}{\gamma \cdot [A(\Phi) - 1]} \tag{3.23}$$

The values for the efficiency of this cycle are plotted in Figure 3-16, using this expression.

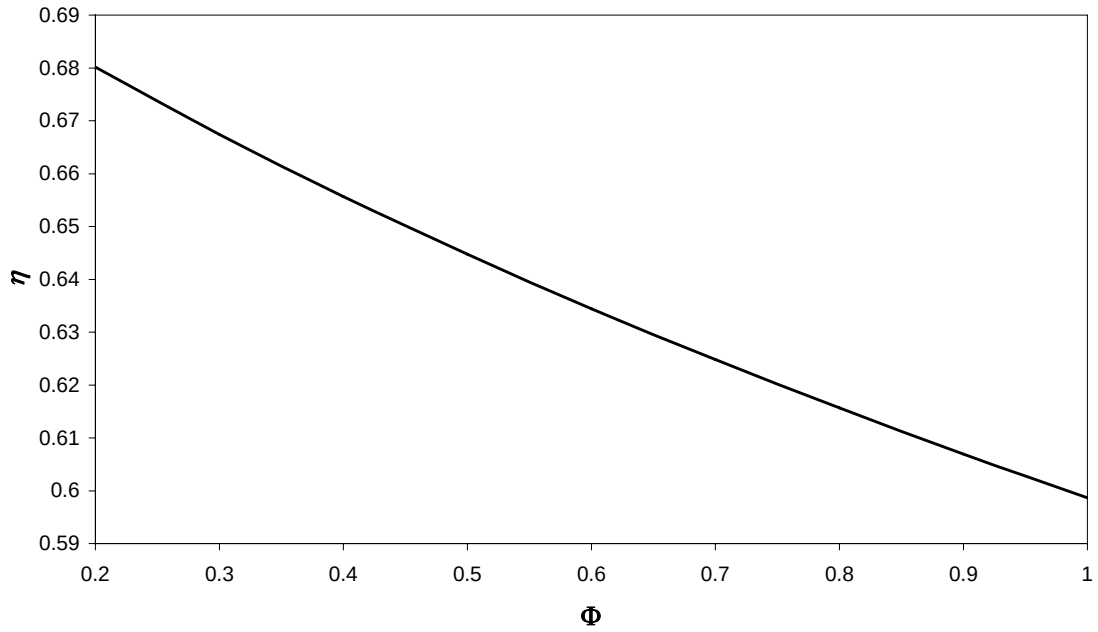

Figure 3-16 - Thermal efficiency as a function Φ for the Diesel cycle.

As it can be seen, the efficiency increases as the mixture becomes leaner. Then, the heat supplied during the combustion is lower, which will cause the pressure at final of expansion to be also lower, therefore with less losses when the exhaust valve opens. In the extreme case, (no heat supplied) the expansion leads to the initial point (but no work is done, also).

3.2.7 Dual cycle at part load

In the dual cycle the heat is supplied at the TDC, at constant volume (isochoric) and during the descent of the piston, at constant pressure (isobaric). Load reduction is made

via the reduction of heat supplied during the isobaric part of the combustion (3-4' in Figure 3-17). The heat supplied at constant volume in TDC is considered constant and independent of the load. This heat can be considered as the fuel supplied during the pre-injections used in the modern Diesel engines, (which is roughly constant with load) and at the first part of the main injection. In this work the fuel supplied at constant volume is considered to be 1/10 of the stoichiometric fuelling.

In the *p-V* diagram of the dual cycle (Figure 3-17) it is possible to see, (dashed line) the expansion stroke of the dual cycle at part load, under the line for the full load expansion.

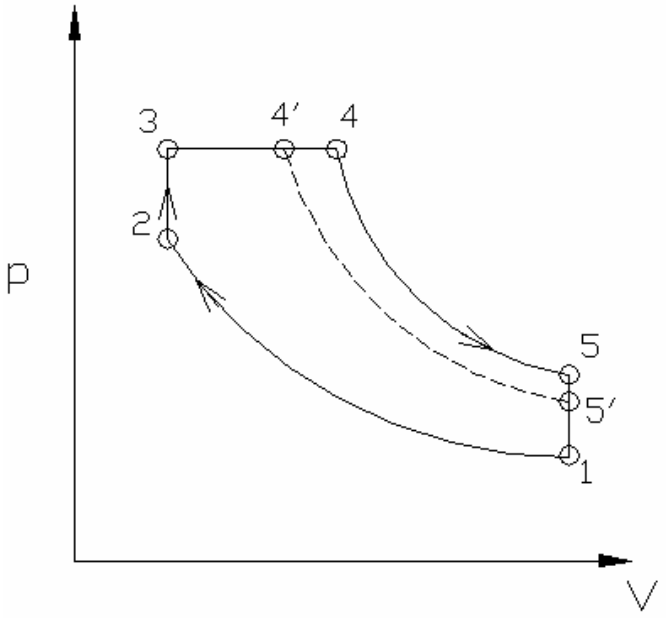

Figure 3-17 - *p-V* diagram of the dual cycle.

For the dual cycle, the thermal efficiency may be written as (Annex A):

$$\eta_d = 1 - \left(\frac{1}{\varepsilon}\right)^{\gamma-1} \cdot \frac{C(\Phi,\Psi)^{\gamma-1} \cdot \frac{1 + B(\Phi,\Psi) + (\gamma-1)\cdot A(\Psi)}{\gamma} - 1}{B(\Phi,\Psi)} \tag{3.24}$$

Where:

$$B(\Phi,\Psi)=1+\frac{(\gamma-1)\cdot Q_{LHV}}{R\cdot T_1\cdot\varepsilon^{\gamma-1}}\cdot\frac{1}{1+\frac{\left(A/F\right)_S}{\Phi}} \tag{3.25}$$

$$A(\Psi)=1+\frac{(\gamma-1)\cdot\Psi\cdot Q_{LHV}}{R\cdot T_1\cdot\varepsilon^{\gamma-1}}\cdot\frac{1}{1+\left(A/F\right)_S} \tag{3.26}$$

$$C(\Phi,\Psi)=1+\frac{\left(1-\frac{\Psi}{\Phi}\right)\cdot Q_{LHV}}{\frac{\gamma}{\gamma-1}\cdot R\cdot A(\Psi)\cdot T_1\cdot\varepsilon^{\gamma-1}}\cdot\frac{1}{1+\frac{\left(A/F\right)_S}{\Phi}} \tag{3.27}$$

Considering:

$$\Phi=\frac{Q_T{}'}{Q_T}\quad \Psi=\frac{Q_V}{Q_T}\quad \Psi'=\frac{Q_V}{Q'_T} \tag{3.28 a,b,c}$$

It results:

$$\Psi'=\frac{\Psi}{\Phi} \tag{3.29}$$

In fact, Φ can be considered as the load factor, as it represents the relation between the heat supplied at part load and the heat supplied at full load.

Figure 3-18 presents the values of the thermal efficiency of the cycle for a compression ratio of 18, closer to compression ratios used in compression ignition engines. As expected the efficiency decreases with the increase of load (richness of the mixture).

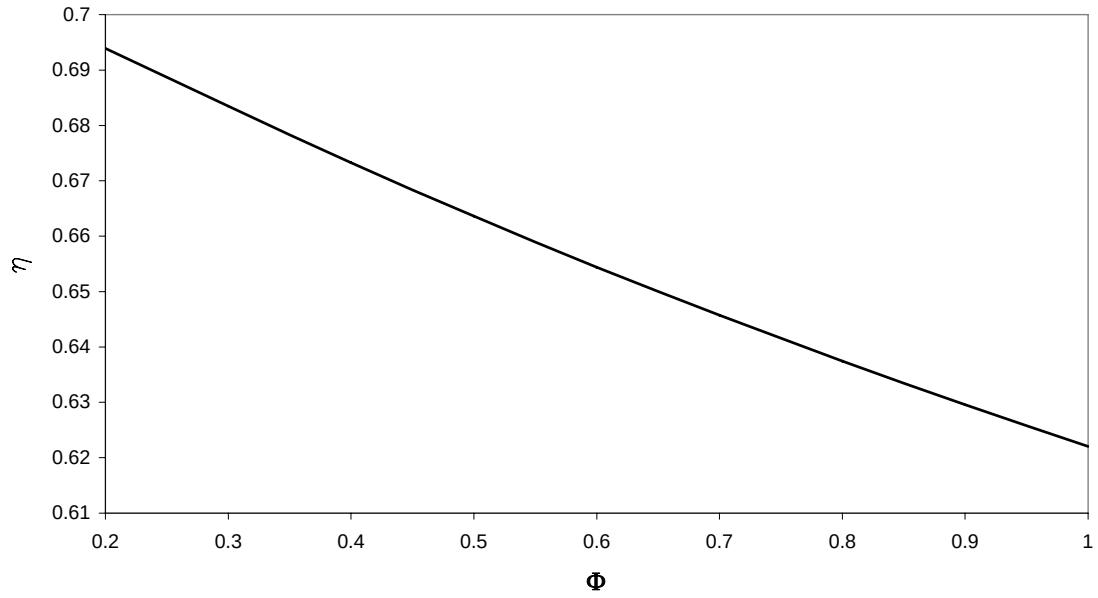

Figure 3-18 – Thermal efficiency of the dual cycle as a function of Φ for ε=18:1.

3.2.8 Natural Aspirated Cycles Comparison

The comparison of all the discussed cycles is done as a function of the load of the engine in Figure 3-19. For the Otto cycle the load is represented by the ratio W/W_{max} as mentioned above (3.20). For the Otto cycle with direct injection, the Diesel cycle and the dual cycle the load is represented by Φ (the fuel/air equivalent ratio), and in the Miller cycle (with fixed ε_{tr} and fixed ε_g) the load is represented by the inverse of the expansion ratio (σ = 2 is the same as ½ load). A compression ratio of 12 was considered for the Miller and Otto cycles, 20 for the dual cycle at part load and 22 for the Diesel cycle.

As it can be seen in the graph for the several efficiency curves as functions of the load (Figure 3-19), two behaviours may be distinguished. The Diesel and dual cycles have an efficiency that increases as the load decreases, while, on the other hand, the Otto cycle and the Miller (geometric) cycle have efficiencies that increase as the load also increases.

As the load gets closer to 1, the Otto part load cycle, Otto direct injection cycle and Miller cycle tend to the same value, 63 %, which corresponds to the Otto cycle at full load (WOT). As can be seen, the Otto direct injection cycle keeps its efficiency independent of the load factor.

When comparing the five spark ignition engines, Miller trapped, Miller geometric, Otto part load, Otto Variable Compression Ratio and Otto direct injection, it is clear that for engines mainly operated at partial loads the use of the Miller VCR cycle is always the best, because the engine is always running near its limiting (by knock) conditions. The use of the Variable Compression Ratio technology in SI engines is also beneficial for engines operated at part load (although at a lower level), with the advantage of only one engine modification relatively to the conventional engine mechanical configuration, i.e. introducing VCR technology only instead of the VCR + VVT of the Miller VCR cycled engine. This proves (at least theoretically) that both VVT and VCR technologies, improve the efficiency of SI engines.

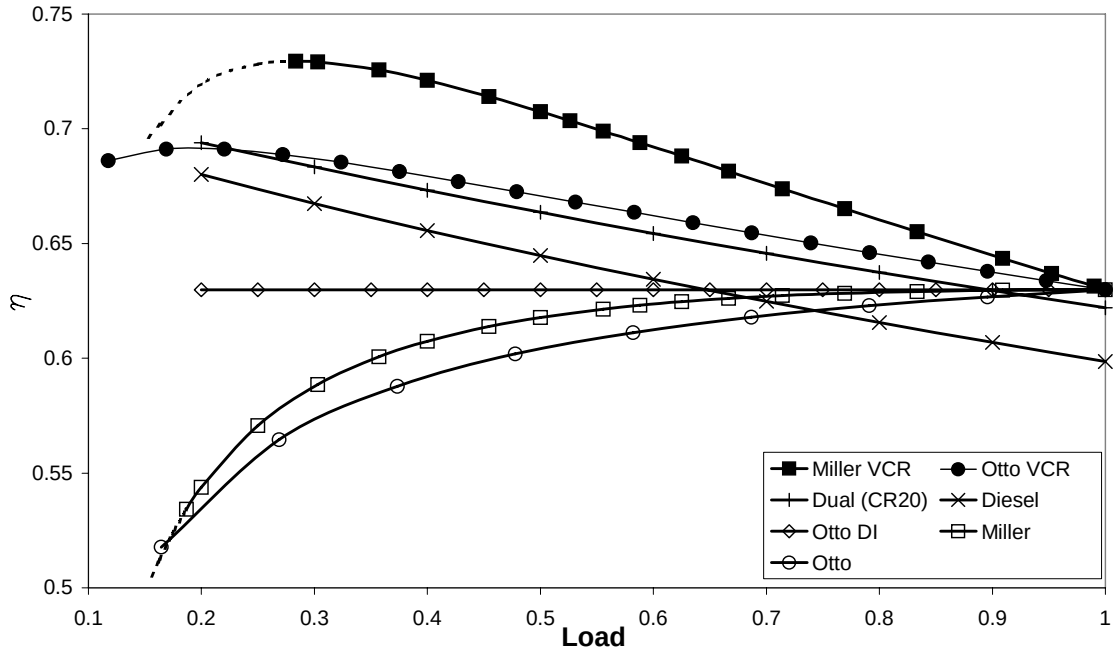

Figure 3-19 - Comparison of the thermal efficiency of the several cycles at part load.

In Figure 3-19 the plotted dual cycle has a compression ratio of 20, this being the closest to the Miller VCR. A more detailed comparison was made between these two cycles, plotting the efficiency of the dual cycle for higher compression ratios of 22 and 25. The values of the efficiency for these cycles are plotted in Figure 3-20.

As it can be seen from Figure 3-20, the Miller VCR cycle still is more efficient than the dual cycle at a compression ratio of 25, (which can be considered excessive), for a load factor of less than 0.7.

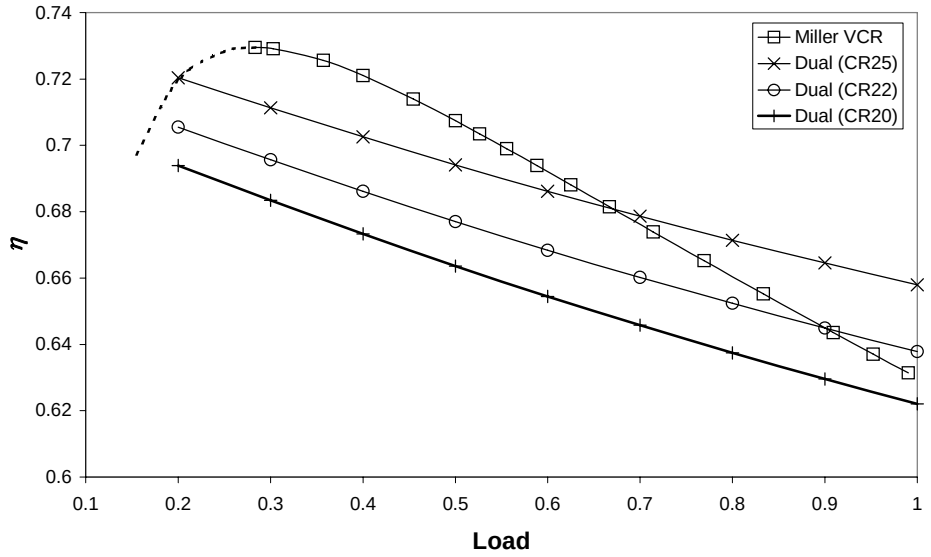

Figure 3-20 - Comparison of the Miller cycle and the dual cycle thermal efficiencies at different compression ratios.

3.3 Supercharged engine cycles [3]

The power produced by an engine is limited by the amount of fuel that the engine is able to burn. This amount of fuel is dependent on the amount of air present in the cylinder, as a function of its volume. Supercharging is a method used to compress the inducted air before entry into the cylinder in order to increase its density and so to increase the mass of inducted air in each cycle, allowing for the presence and burning of a larger amount of fuel.

To perform this function the following methods can be used [4]:

Mechanical supercharging: A pump, blower or compressor, usually driven by power taken from the engine, provides the compressed air;

Turbocharging: A turbocharger – a compressor and turbine on a single shaft – is used to boost the inlet air (or mixture) pressure. The energy available in the engine's exhaust stream is used to drive the turbocharger turbine, which drives the turbocharger compressor;

Pressure wave supercharging: Wave action in the intake and exhaust systems is used to compress the intake mixture.

In the following analysis only turbocharging will be considered. The objective is to determine the potential of power increase per unit displacement volume due to the use of the energy of the exhaust gases.

In a theoretical *p*-*V* diagram of a dual air cycle (Figure 3-21) it is possible to see the potentially available energy. This energy is represented by the enthalpy of the exhaust gases present in the cylinder at the opening of the exhaust valve.

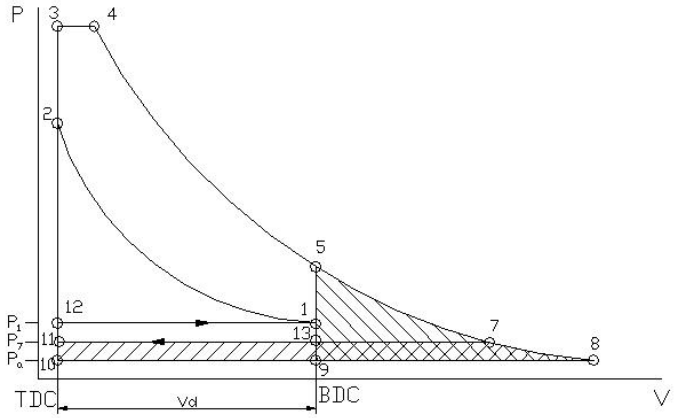

Figure 3-21 - Ideal turbocharged limited pressure cycle.

This work, also called 'blow-down' energy [5], can be recovered using a turbocharger turbine, placed in the exhaust manifold, which will use the 'blow-down' of the exhaust gases from the pressure at exhaust valve opening (EVO) to the atmospheric pressure. The blow-down energy is represented in a p-V diagram as the area 5-8-9-5.

The exhaust manifold pressure (p_7) is above ambient pressure (p_a). The exhaust process is represented by 5-13-11. The 5-13 period is the blow-down at EVO, which is followed by the movement of the piston from BDC to TDC making the exhaust of the remainder gases to the exhaust manifold. These gases are also at a pressure above the ambient pressure and so they have potential to perform work during its expansion to the ambient pressure. This work is represented by the area 13-9-10-11-13.

The total energy that could be used to drive the turbine is the sum of the areas 5-8-9-5 and 13-9-10-11-13. However, it is not possible to recover all this energy. To do so, it would be necessary that the turbine inlet pressure would rise instantaneously to p_5 followed by an expansion to the ambient pressure. After this and during the piston

displacement the pressure in the exhaust manifold should be held at p_7. This sequence of processes is impractical [5].

For this reason, two turbocharging systems may be considered [5]:

Constant pressure turbocharging: The manifold chamber is sufficiently large to damp down pulsations in exhaust gas flow. In this case the turbine would work as a flow restrictor keeping the pressure at a constant value. The energy available would be represented by area 7-8-10-11-7.

Pulse turbocharging: The turbine wheel is placed directly downstream of the engine, very close to the exhaust valve. The gas would expand through the turbine along the line 5-7-8. If the turbine is sufficiently large, the pressure in the cylinder and in the turbine inlet would drop equally close to the ambient pressure, before the piston has moved significantly from BDC. Thus the pumping work of the piston would be zero during its displacement. The energy available would be represented by area 5-8-9-5.

In automotive applications usually the pulse turbocharging system is used due to its good turbocharger acceleration, good performance at low speed and load and because the available energy is higher.

Supercharging applied to the Miller cycle has been studied and applied before [6, 7], with good results in terms of bmep and establishing a comparison between the Miller supercharged cycle thermal efficiency with the DI Diesel engine thermal efficiency. Turbocharging was also studied [8] in combination with other available fuel economy technologies such Variable Valve Actuation (VVA) and variable compression ratio (VCR) in order to evaluate the fuel economy consequences.

The theoretical analysis of turbocharged Otto and Miller cycle was made previously [9] but the comparison is based in different effective compression ratios which lead to no efficiency advantage of the Miller cycle when turbocharged.

Three turbocharged cycles will be analysed, the Otto, the dual (to simulate a Diesel engine) and the Miller. It will be considered that all cycles work using the pulse turbocharging system.

3.3.1 Otto Supercharged Cycle

Analysing the naturally aspirated Otto cycle, the following assumptions were made (Figure 3-1 where $p_1 = p_0$):

a) Temperature and pressure at 1 are atmospheric;
b) Temperature and pressure at 2 and 3 are fixed and are determined by the knock conditions, taken as a result of a compression ratio of 12:1 on a naturally aspirated engine;
c) Stoichiometric mixture;
d) Q_{LHV} is 44 MJ/kg.

These assumptions lead to a situation where all the cycle is perfectly defined and it shall be considered as the maximum efficiency conditions for the conventional Otto ideal cycle. Under these conditions the cycle efficiency is 63 % as seen above.

If an Otto supercharged cycle is considered (Figure 3-22), the same knock limit (points 2 and 3 as in Figure 3-1 with $p_1 = p_0$) is imposed. Although there are different ways for accessing the onset of knock, it is assumed here that the important parameter is the maximum pressure (and temperature) achieved in the cycle (point 3). However, as the intake mixture is considered always stoichiometric, point 2 and 3 in the supercharged cycle are the same as in the naturally aspirated cycle, as it can be seen in Figure 3-22. In order to achieve these conditions the displacement of the engine is smaller and point 4 and 1 have less volume than the old points (4' and 5'). This is what is known as "engine downsizing".

Point 5' is at atmospheric conditions (p_{atm}, T_{atm}) and the air in the compressor (of the turbo-charger) passes from 5´ to 1 by an isentropic process. Therefore, while on the baseline Otto cycle the compression by the piston was 5'-2, on the Otto turbocharged the piston does only the work to compress from 1 to 2.

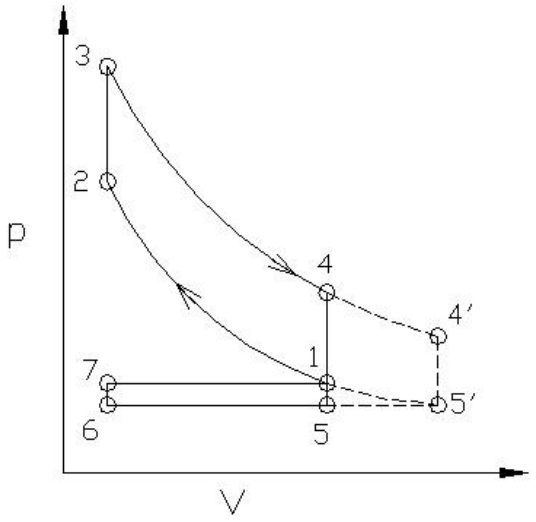

Figure 3-22 – *p* – *V* diagram of a supercharged Otto cycle.

The efficiency of this cycle can then be written as (Annex A):

$$\eta = 1 - \frac{1}{\varepsilon^{\gamma-1}} + \frac{(\beta-1)(\varepsilon-1)}{B \cdot \varepsilon \cdot \beta^{\frac{1}{\gamma}}} \tag{3.30}$$

where:

$$B = \frac{Q_{LHV}}{R \cdot T_0} \cdot \frac{1}{1 + A/F} \tag{3.31}$$

$$\beta = \frac{p_1}{p_0} \tag{3.32}$$

$$\varepsilon = \frac{V_1}{V_2} \tag{3.33}$$

Considering the knock limitations mentioned above (3.11) about the limiting compression ratio for a given supercharge ratio, the efficiency equation (3.30) may then be written as:

$$\eta = 1 - \frac{\beta^{\frac{\gamma-1}{\gamma}}}{\varepsilon_{lim}^{\gamma-1}} + \frac{(\beta-1)\left(\frac{\varepsilon_{lim}}{\beta^{\frac{1}{\gamma}}} - 1\right)}{\varepsilon_{lim}} \tag{3.34}$$

Plotting equation (3.34) as function of the supercharge ratio (β) (Figure 3-23), it can be seen that as the supercharging is increased (up to a ratio of 5 in the example), the thermal efficiency of the engine falls continuously. This is a result of the higher enthalpy losses by the exhaust gases. The higher the value of β, the higher the pressure and temperature at point 4. However, if the intake pressure is lowered bellow the atmospheric value (part load operation), then the thermal efficiency increases up to a value of 69% with a supercharge ratio of 0.2. Further decreasing of the intake pressure leads to the thermal efficiency decreasing abruptly when approaching zero as the intake pressure approaches the vacuum.

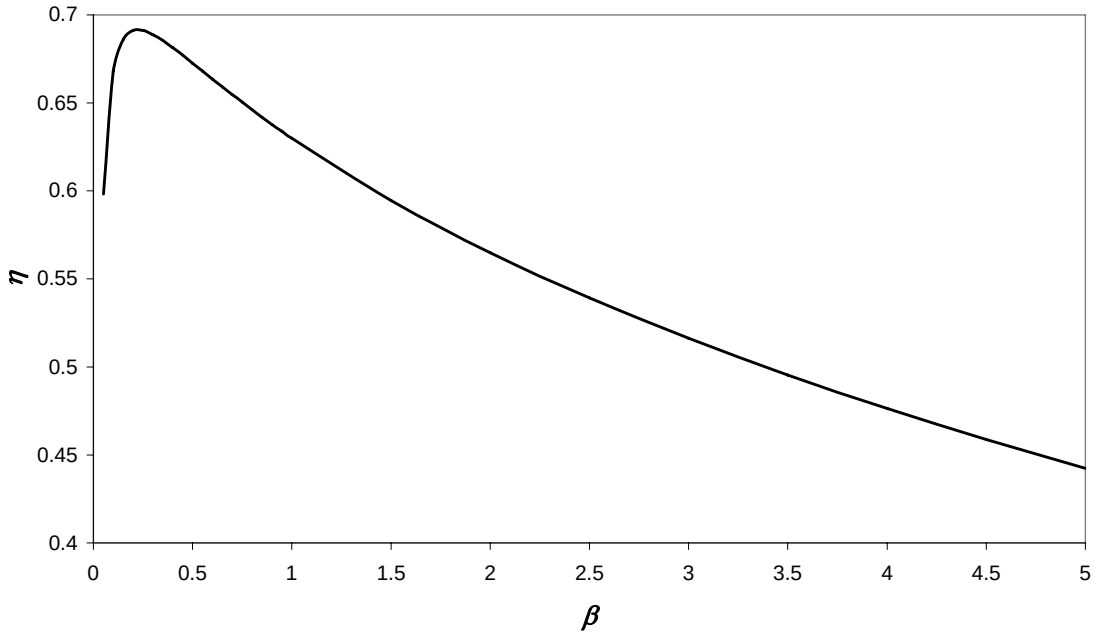

Figure 3-23 – Thermal efficiency of a supercharged engine as function of the supercharge ratio.

3.3.2 Supercharged Miller cycle

The supercharged Miller cycle (Figure 3-24) has been theoretically studied [7,8], but the Miller cycle engine thermal efficiency is not presented as a function of the load.

In this cycle, the load is changed by control of the intake valve closure timing. Considering always a stoichiometric mixture, the load will be defined as a function of the amount of air or mixture trapped inside the cylinder (at the time of the closure of the intake valve).

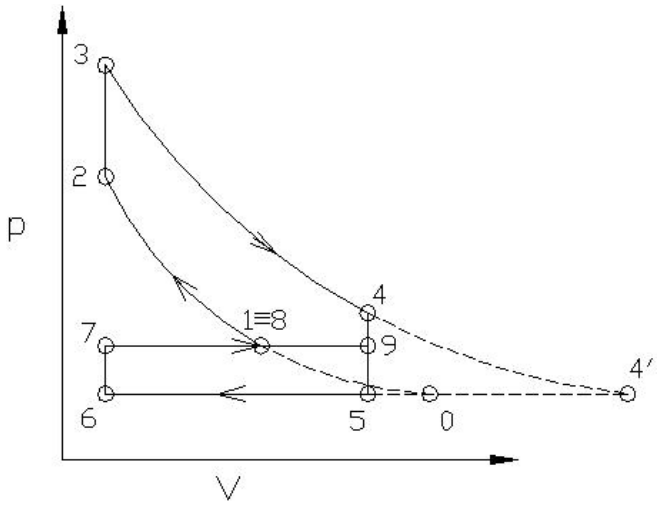

Figure 3-24 - p-V diagram of the Miller cycle with supercharging.

An expression for the efficiency of this cycle can be determined following the same approach as described above for the supercharged Otto cycle. Again the efficiency is defined as the relation between the work performed and the heat supplied during combustion.

From Annex A the thermal efficiency of the Miller supercharged cycle is expressed as:

$$\eta_{MSc} = 1 - \frac{1}{\varepsilon_{tr}^{\gamma-1}} \frac{1}{\sigma^{\gamma-1}} - \frac{\sigma^{1-\gamma} - \gamma}{\frac{B(\gamma-1)}{\beta^{\frac{\gamma-1}{\gamma}}}} - \frac{\sigma + \frac{\beta-1}{\varepsilon_{tr}}}{B\beta^{\frac{1}{\gamma}}} \tag{3.35}$$

where:

$$B = \frac{Q_{LHV}}{R \cdot T_0} \cdot \frac{1}{1 + A/F} \tag{3.36}$$

This expression is plotted in a graphic shown in Figure 3-25.

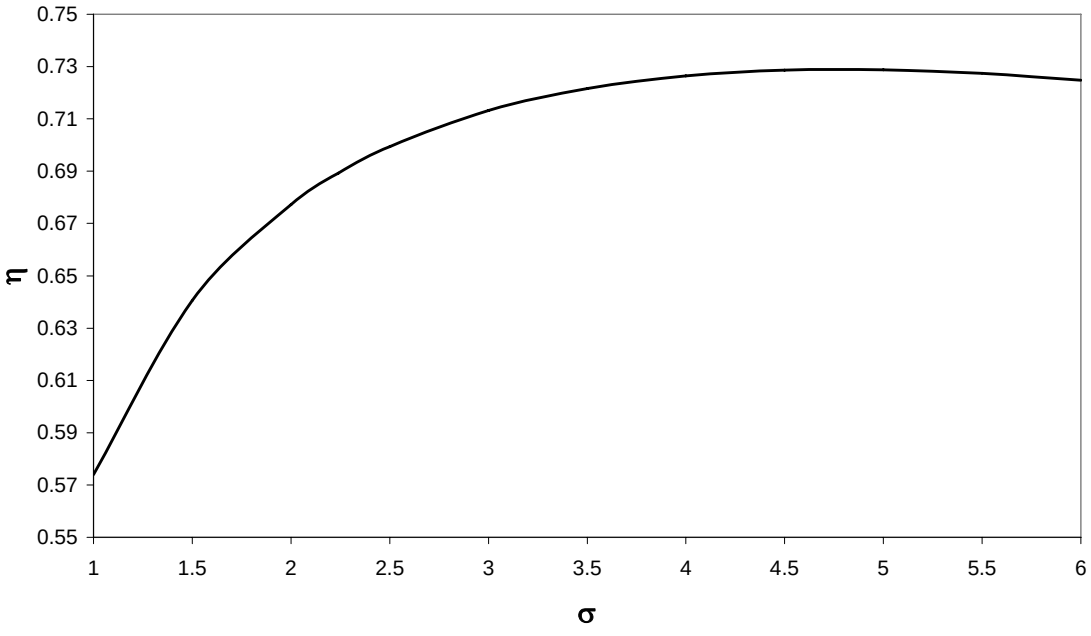

Figure 3-25 - Efficiency of the Miller supercharged cycle as function of σ (β=1.5; ε_{tr}=8).

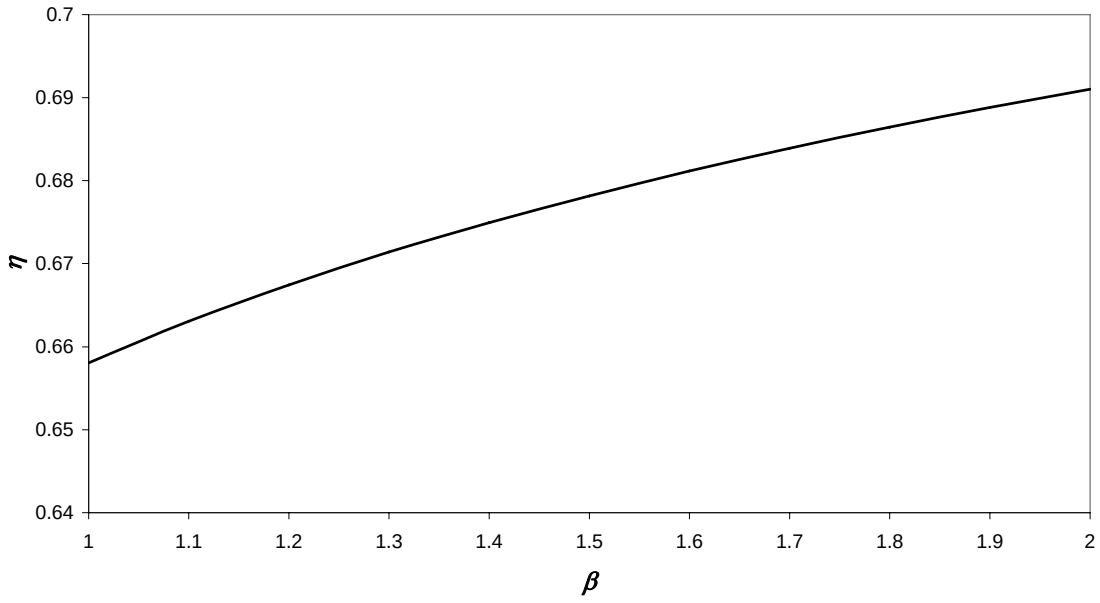

Figure 3-26 - Efficiency of the Miller supercharged cycle as function of β (σ=2; ε_{tr}=8).

In Figure 3-25 the evolution of the curve is for a constant β not regarding the turbocharger efficiency. A turning point may be identified which corresponds to the point of full expansion (pressure in the cylinder at the exhaust valve opening equals the atmospheric pressure) using a β= 1.5. For higher values of σ, the cycle efficiency decreases. The maximum efficiency point at these conditions corresponds to a value of σ= 4.84. In Figure 3-26 efficiency of the engine cycle is plotted against the supercharge ratio for a constant ε_{tr} and expansion. As it can be seen the efficiency value is always increasing. It must be noted that as the intake pressure rises with the supercharge ratio and all the geometric conditions of the engine are kept constant the pressure during the combustion has higher values that may lead to the onset of knock. This fact makes that the line plotted in Figure 3-26 must be cut at the knock onset point and shall not rise indefinitely.

When using the Miller cycle on an engine with no variable valve timing the lost admission mass of air can be compensated by increasing the inlet pressure. This is what happens in existing Miller engines [10].

The knock point has to be respected and if the mixture is again considered as stoichiometric, points 2 and 3 (Figure 3-24) and the compression line shall be the same that have been considered in the previous cycles. The compression includes starting

from point 0, i.e. atmospheric conditions, followed by 0-1, given by the supercharger. The engine compression ratio gives the increase 1-2.

In (3.35), if the value of the effective compression ratio is adjusted for each working conditions (supercharge ratio) in order to obtain always the maximum compression ratio for a given fuel, the variable ε_{tr} may be replaced by a relation determined from (3.11), and then (3.35) could be written as:

$$\eta_{MSc} = 1 - \varepsilon_{lim}^{1-\gamma}\sigma^{1-\gamma}\beta^{\frac{\gamma-1}{\gamma}} - \frac{\sigma^{1-\gamma}-\gamma}{\frac{B(\gamma-1)}{\beta^{\frac{\gamma-1}{\gamma}}}} - \frac{\sigma\frac{\varepsilon_{lim}}{\beta^{\frac{1}{\gamma}}}+\beta-1}{\varepsilon_{lim}\cdot B} \tag{3.37}$$

In Figure 3-27 and Figure 3-28 this expression is plotted for several conditions of supercharging and expansion.

Now considering the knock limit described above and the relation imposed between the effective compression ratio and the intake supercharge ratio, an efficiency limit for several values of the expansion ratio can be established. When the values so obtained are plotted the result shows the evolution seen on Figure 3-29. Note that in that figure, each line has the supercharged pressure changing, so the knock conditions are always obtained.

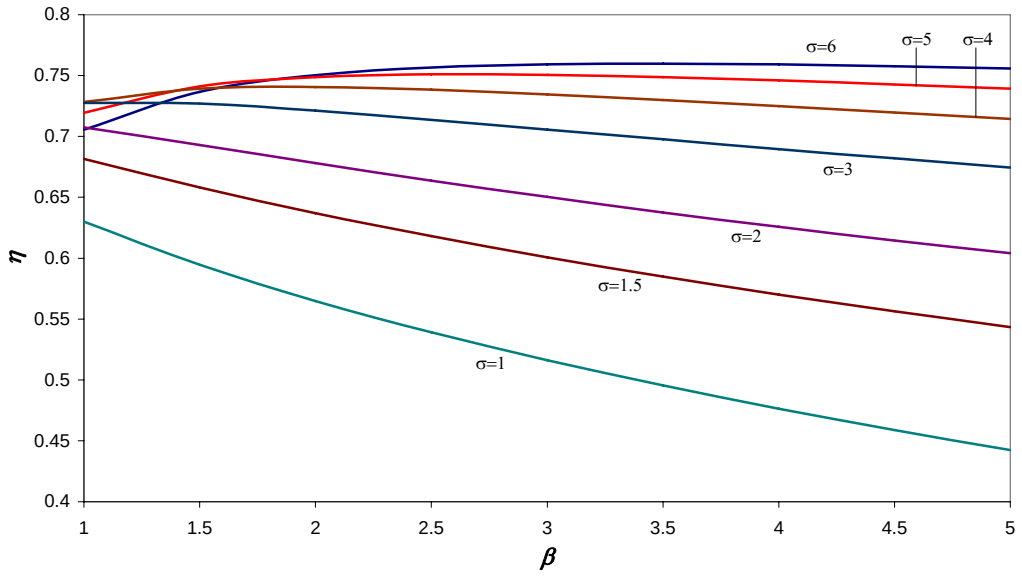

Figure 3-27 – Efficiency of the supercharged Miller cycle as function of the supercharge ratio and the expansion ratio.

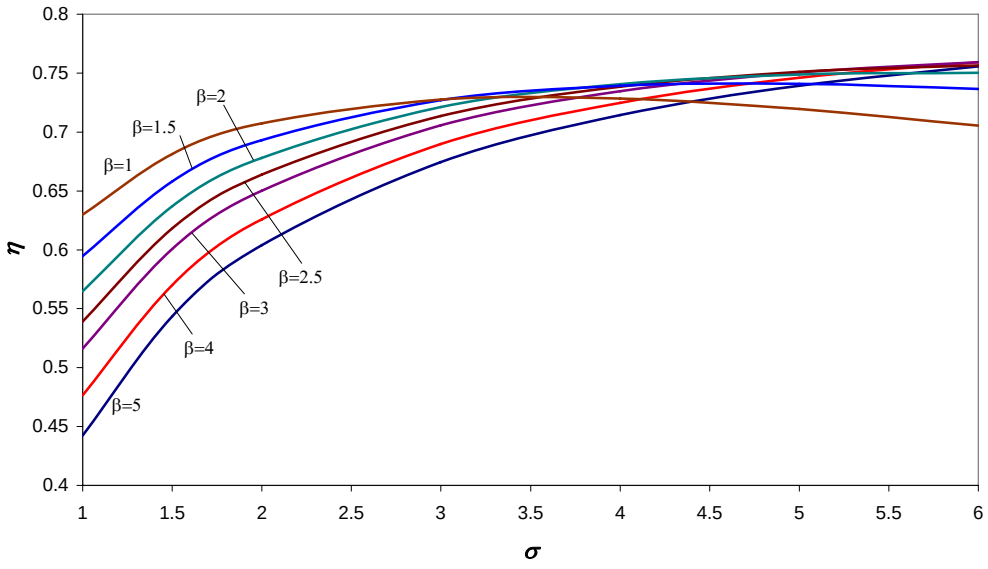

Figure 3-28 - Efficiency of the supercharged Miller cycle as function of the expansion ratio for several values of the supercharge ratio.

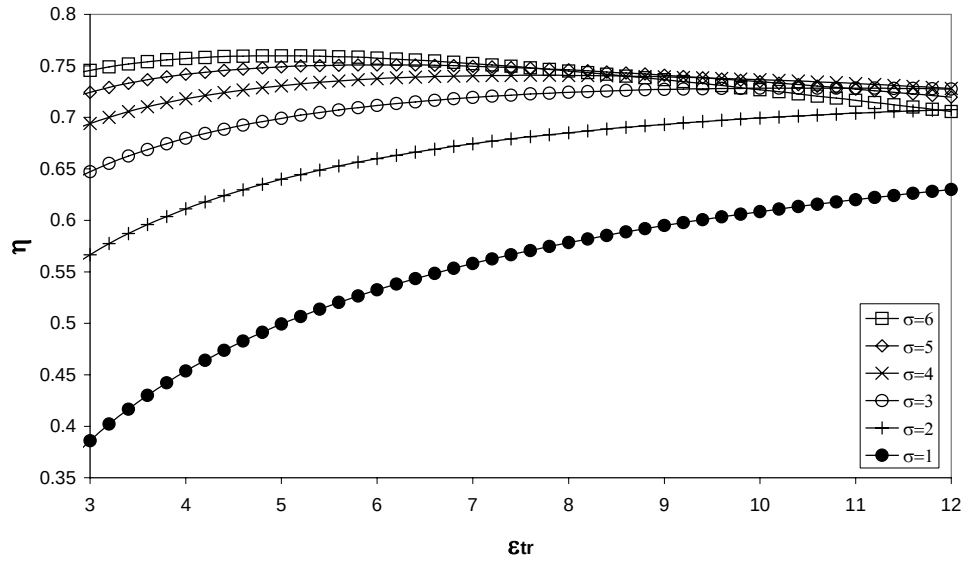

Figure 3-29 - Efficiency of the Miller cycle for several expansion ratios at the knock limit.

It can be seen that as the expansion ratio rises from 1 to 3 the efficiency raises for all values of compression ratio, but if the expansion ratio is increased above the value of 3, the efficiency will only increase if the compression ratio is below 7.5. If the expansion ratio is above 4, the maximum efficiency is obtained for compression ratios lower than 6.

For each expansion ratio line, the maximum efficiency corresponds to the point where the work delivered to the turbine by the exhaust gases equals the work done by the

compressor to raise the intake pressure from the atmospheric value to the supercharge value corresponding to the value of β. For an expansion ratio of 1 or 2, that point of maximum efficiency can be obtained for values of the compression ratio even higher than the 12. For expansion ratio of 3 and 4, the point of maximum efficiency exists for compression ratios of 10.6 and 7.6 approximately. And for the expansion ratios of 5 or higher the point of maximum efficiency is obtained for compression ratios lower than 6. The value for maximum expansion ratio will be obtained differentiating the efficiency equation (3.37) in relation to σ and setting it to 0. This leads to the relation between the expansion ratio and the supercharge ratio for the maximum efficiency conditions:

$$\sigma = \beta\left[1 + \frac{B(\gamma - 1)}{\varepsilon_{lim}^{\gamma-1}}\right]^{\frac{1}{\gamma}} \tag{3.38}$$

Which plotted, yields:

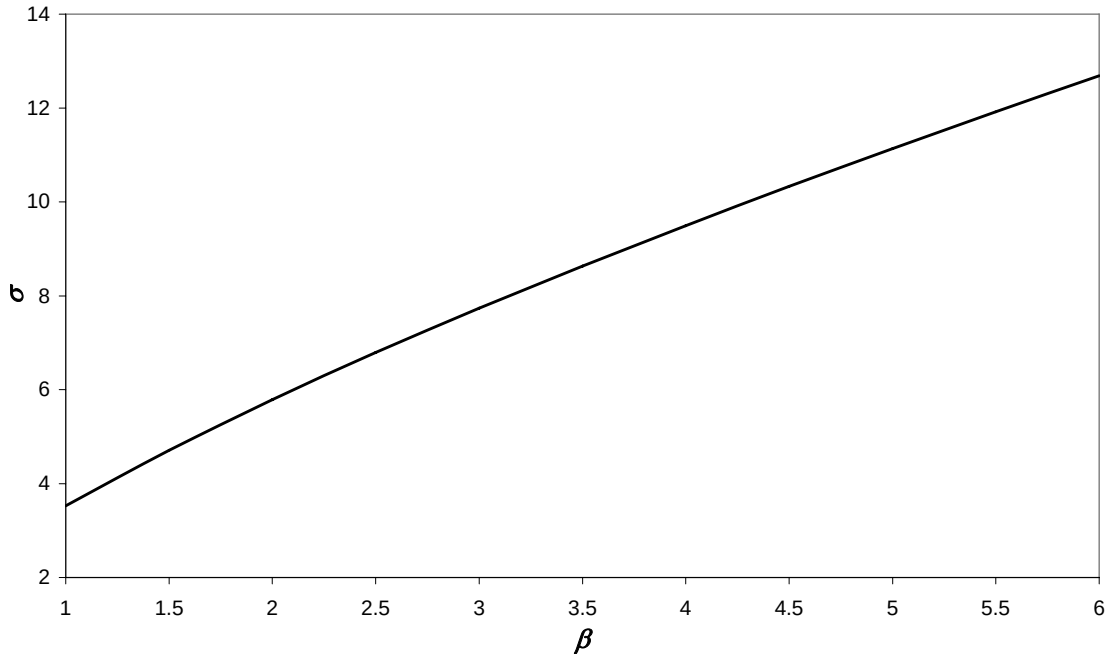

Figure 3-30 - Expansion values as a function of supercharge ratio for maximum cycle efficiency.

These values correspond to a 100% efficiency of the turbine and compressor. If a lower efficiency is considered for the turbine and compressor system, a relation may be

established between the work delivered to the turbine (W_T) and the work supplied by the compressor (W_C):

$$W_C \leq W_T \cdot \eta_{trbch} \tag{3.39}$$

Where η_{trbch} is the efficiency of the turbocharger.

The work performed by the compressor (W_C) to raise the pressure of a certain volume of air (V_0) from atmospheric pressure (p_0) to p_1 is given by:

$$W_C = \frac{p_1 V_1 - p_0 V_0}{\gamma - 1} = p_0 V_1 \frac{\beta^{\frac{1}{\gamma}} - \beta}{\gamma - 1} \tag{3.40}$$

The work that the exhaust gases can supply to the turbine is determined by the work from the expansion (isentropic) from 4 to 4', which corresponds to the area limited by 4-4'-5 of Figure 3-24. It can be expressed as:

$$W_T = W_{44'} + W_{4'5} = p_0 V_1 \left\{ \frac{\left[\beta \left(\frac{1}{\sigma} \right)^{\gamma-1} + \left(\frac{1}{\sigma} \right)^{\gamma-1} \frac{B(\gamma-1)}{\varepsilon_{tr}^{\gamma-1} \beta^{\frac{1}{\gamma}}} \right] - \left[1 + \frac{B(\gamma-1)}{\varepsilon_{tr}^{\gamma-1} \beta^{\frac{\gamma-1}{\gamma}}} \right]^{\frac{1}{\gamma}}}{\gamma - 1} + \sigma - \beta^{\frac{1}{\gamma}} \left[1 + \frac{B(\gamma-1)}{\varepsilon_{tr}^{\gamma-1} \beta^{\frac{\gamma-1}{\gamma}}} \right]^{\frac{1}{\gamma}} \right\} \tag{3.41}$$

Due to the efficiency of the turbine and the compressor, the work delivered to the turbine must be higher than the work supplied by the compressor.

From this point of maximum efficiency, the energy released by the exhaust gases at the exhaust valve opening is not enough to make the compressor to raise the intake pressure until a desired β. The limit for the expansion may be established for several values of the supercharge ratio and turbocharger efficiency, as it can be seen in Figure 3-31.

It is possible then to define the optimum working point for the Miller cycle using supercharging. This point will be defined using the above defined values for the maximum expansion ratio, supercharge ratio and turbocharger efficiency as shown in Figure 3-32.

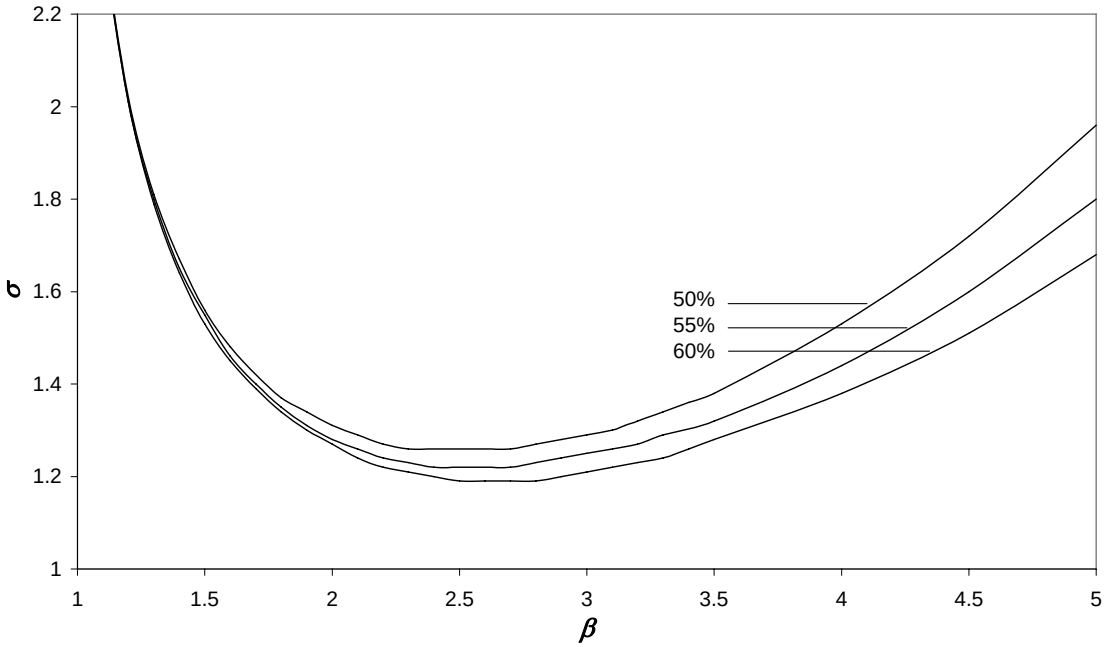

Figure 3-31 - Maximum expansion ratio function of the supercharge ratio and turbocharger efficiency.

As it can be seen on Figure 3-32 there is a maximum improvement limit line that corresponds to the point where the pressure at the exhaust opening event is just enough to make the compressor deliver the desired pressure for a given β. (considering a turbocharger efficiency of 60 %). So, for a certain β, the expansion may be increased until the interception between the efficiency line and the limit line. Surpassing that line, the pressure of the exhaust gases will make the compressor to deliver a pressure lower that the one desired and β will fall. This leads to lower pressures in the cycle and the knock point will not be reached. Thus a reduction in the cycle efficiency may be expected as the trapped compression ratio is kept constant and the expansion ratio is increased.

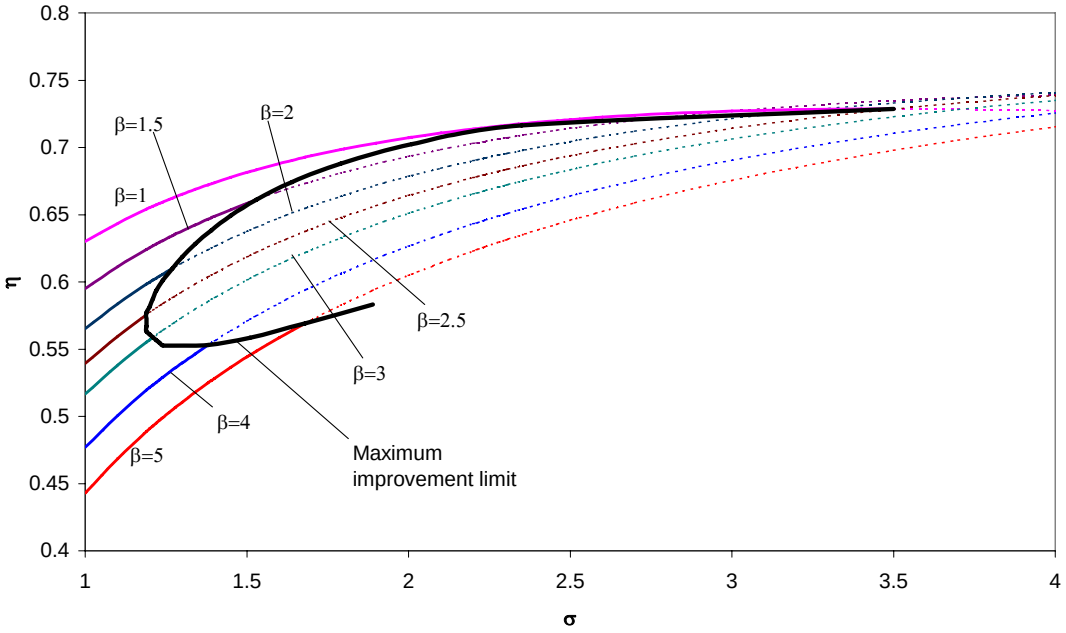

Figure 3-32 - The thermal efficiency as a function of supercharge ratio (β) and expansion ratio (σ) for a turbine and compressor efficiency of 60%.

The efficiency of the supercharged cycle is then limited by the efficiency of the turbocharger. The energy of the exhaust gas shall be enough to allow the compressor to supply a mixture with an established β. Fixing the engine working conditions, namely geometric compression ratio ($\varepsilon_g = \varepsilon_{tr}.\sigma$), it is possible to define an envelope where the energy carried by the exhaust gases is enough to keep these working conditions.

If the expansion ratio is increased over a certain value, the energy of the exhaust gases is lower because it was used in the piston expansion, and it is not enough to allow the compressor to supply an intake pressure, such that it accomplishes with the β value. This can be defined as a second working envelope, which will be limited by the point where the exhaust gas pressure is equal to the atmospheric pressure (Atkinson cycle), and then no energy is supplied to the turbocharger.

3.3.3 Supercharged dual cycle

In the dual cycle the fuel combustion is done in two steps. Firstly at constant volume (isochoric combustion) and secondly at constant pressure (isobaric combustion) as it can be seen in Figure 3-33. To simplify, in the case of a load change (change in the heat supplied), it is considered that the amount of fuel burned at a constant volume is kept

constant, and the change will be imposed at the isobaric combustion, which will be longer (3 – 4) or shorter (3 – 4'). The heat supplied at constant volume will be considered 10% of the maximum total heat supplied. Depending on the energy available at the exhaust (turbine), the intake pressure (p_k) may vary.

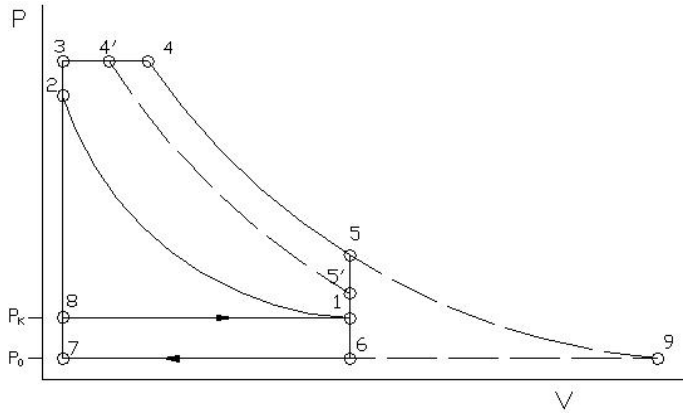

Figure 3-33 - *p-V* diagram of a dual supercharged cycle.

The heat supplied during the first part of the combustion process, the isochoric combustion, is considered independent of the load. This heat supplied at constant volume is compared to the pre-injections made in Diesel engines to improve the burnt of the total amount of injected fuel. The Ψ variable is defined as the ratio between the heat supplied during the isochoric combustion (Q_v) and the total heat supplied in the cycle for full load (Q_T).

$$\Psi = \frac{Q_V}{Q_T} \tag{3.42}$$

The efficiency of this cycle can be expressed (Annex A):

$$\eta_{dSc} = \frac{\dfrac{\beta \cdot \left(1-\varepsilon^{\gamma-1}\right)}{\gamma-1} + \beta \cdot A(\Psi) \cdot \varepsilon^{\gamma-1} \cdot \left[C(\Psi,\Phi)-1\right] + \dfrac{\beta \cdot A(\Psi)}{\gamma-1} \cdot \left[\varepsilon^{\gamma-1} \cdot C(\Psi,\Phi) - C(\Psi,\Phi)^{\gamma}\right] + (\beta-1) \cdot \dfrac{\varepsilon-1}{\varepsilon}}{\dfrac{\beta}{\gamma-1} \cdot \varepsilon^{\gamma-1} \cdot \left\{A(\Psi)-1+\gamma \cdot A(\Psi) \cdot \left[C(\Psi,\Phi)-1\right]\right\}} \tag{3.43}$$

where:

$$\beta = \frac{p_1}{p_0} > 1 \tag{3.44}$$

$$A(\Psi) = 1 + \frac{(\gamma - 1) \cdot \Psi \cdot Q_{LHV}}{R \cdot T_1 \cdot \varepsilon^{\gamma - 1}} \cdot \frac{1}{1 + \left(A/F\right)_S} \tag{3.45}$$

$$C(\Psi, \Phi) = \frac{V_{4'}}{V_3} \tag{3.46}$$

with:

$$\Phi = \frac{Q_{T'}}{Q_T} \tag{3.47}$$

Fixing the value of Ψ = 0.1, the values of the thermal efficiency, are plotted as a function of Φ, in Figure 3-34, calculated in the following conditions:

Intake temperature (T_1): 340 K

R: 287 J/kgK

γ: 1.4

Q_{LHV}: 44 MJ/kg

Air/Fuel: 15

As it can be seen from Figure 3-34, the thermal efficiency decreases as the charge increases. As more heat is introduced in the cylinder (Φ rising), the pressure at the end of expansion is higher which means that more energy is available at the exhaust valve opening time. As the value of the supercharge ratio is kept constant (work delivered by the compressor is constant) there is more energy (heat and pressure) being lost by the exhaust system of the engine.

This is why the efficiency curve for the supercharged dual cycle decreases with the increment of the load. In fact as the charge increases, the pressure (and temperature) of the exhaust gases also increases. This means that more energy is available to make the turbocharger work. But at the same time the quantity of exhaust gases enthalpy is not used in the turbine, being lost to the exhaust, making the efficiency of the cycle to decrease. At the limit, the heat will be supplied during all the piston descent from TDC to BDC and there will be no expansion, which will make the exhaust gases pressure to be the maximum of the cycle at the exhaust valve open.

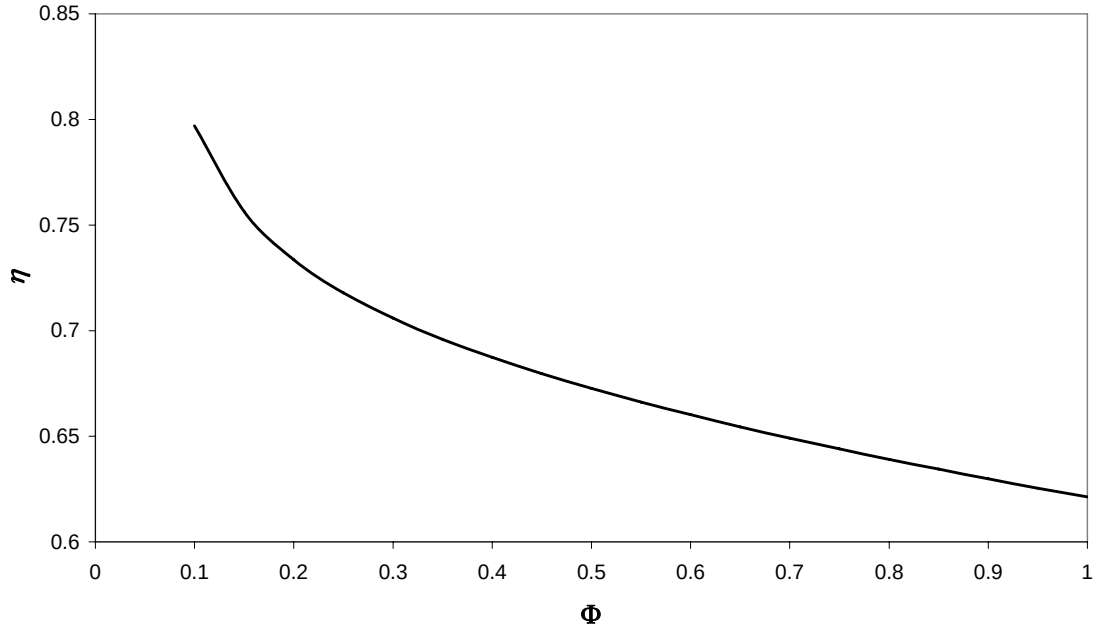

Figure 3-34 - Thermal efficiency of the dual cycle as function of Φ (β=1.5; ε=18).

As determined in the Miller cycle, it is necessary to study the efficiency of the supercharged dual cycle taking into account the turbocharger efficiency. Using the same relations used for the Miller cycle:

$$W_C \leq W_T \cdot \eta_{trbch} \tag{3.48}$$

The work supplied to the turbine as exhaust gas enthalpy corresponds to the area 5-9-6-5 (Figure 3-33). This work can be determined as:

$$W_T = W_{59} + W_{96} = p_0 V_1 \left\{ \frac{\beta \cdot A(\Psi) \cdot C^{\gamma}(\Psi,\Phi) - \left[\beta \cdot A(\Psi) \cdot C^{\gamma}(\Psi,\Phi)\right]^{\frac{1}{\gamma}}}{\gamma - 1} + \left[1 - \left[\beta \cdot A(\Psi) \cdot C^{\gamma}(\Psi,\Phi)\right]^{\frac{1}{\gamma}} \right] \right\} \tag{3.49}$$

And the work supplied by the compressor to the intake gas is the same as defined for the Miller cycle, defined in (3.40).

With equation (3.49) it is possible to establish limits for the load as a function of the supercharge ratio, under which it is not possible to have a desired supercharge ratio because the enthalpy from the exhaust gases is not enough to supply the compressor with work to compress up to a desired supercharge pressure. This limit (for a

turbocharger efficiency of 60%) is plotted in Figure 3-35, with several supercharge ratios efficiency curves.

In case of load values lower than the limit, the exhaust gases enthalpy at the exhaust valve opening will be lower, and the turbocharger will not be able to raise the intake mixture to the needed pressure.

In the case of the dual cycle (compression ignition engine) the limit for the supercharge ratio is not imposed by fuel knock onset conditions.

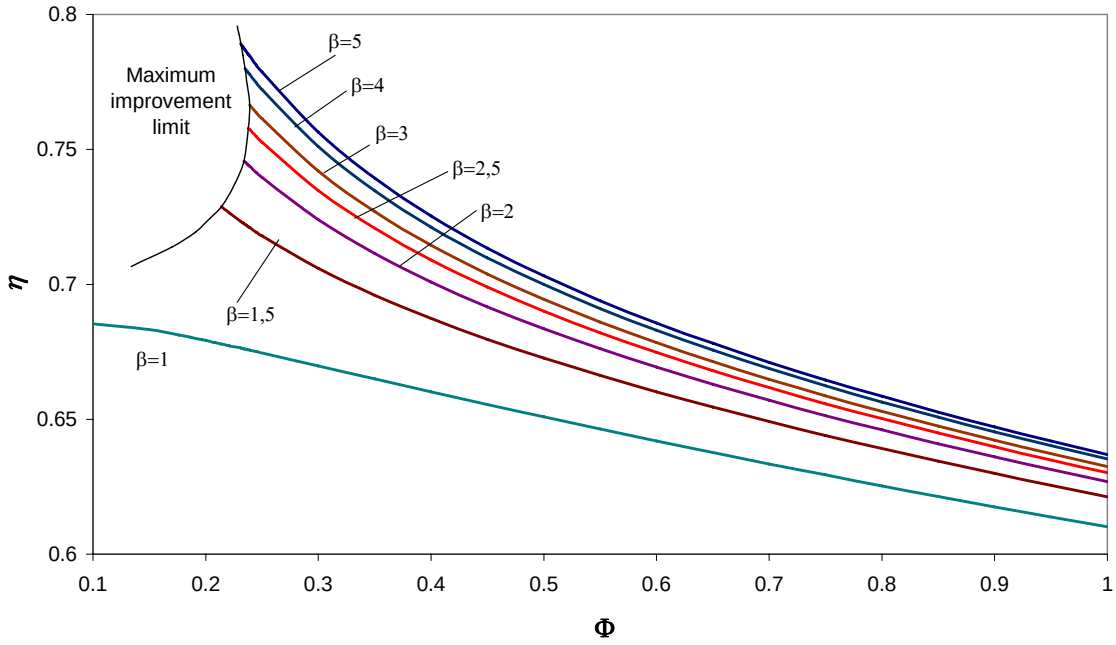

Figure 3-35 - Efficiency of the dual cycle for several supercharge ratios.

3.3.4 Supercharge Cycles Comparison

Figure 3-36 presents the efficiency curves of the three cycles considered. As it can be seen, the dual cycle has the best performance, followed by the Miller and the Otto. The efficiency curves plotted on Figure 3-36 represent the maximum improvement limit curves also plotted in Figure 3-32 and in Figure 3-35. They represent the maximum efficiency obtained on each supercharged cycle.

There is an opposite tendency in the dual and Miller cycle. The first has an increasing efficiency as the supercharge increases and Miller has a decreasing efficiency. The reason for this difference is due to the fact that the only limitation imposed to the dual cycle is that the enthalpy of the exhaust gases must be enough to generate a certain

supercharge at the turbine. In the Miller cycle, besides this condition, a knock limit is established, fixing the maximum value for the peak pressure in the cycle. As the supercharge ratio increases, the compression made by the piston is smaller and increases the compression made by the compressor. But as this presents efficiencies lower than 100%, there are energy losses in the recovery of the enthalpy from the exhaust gases, leading the efficiency of the cycle to decrease.

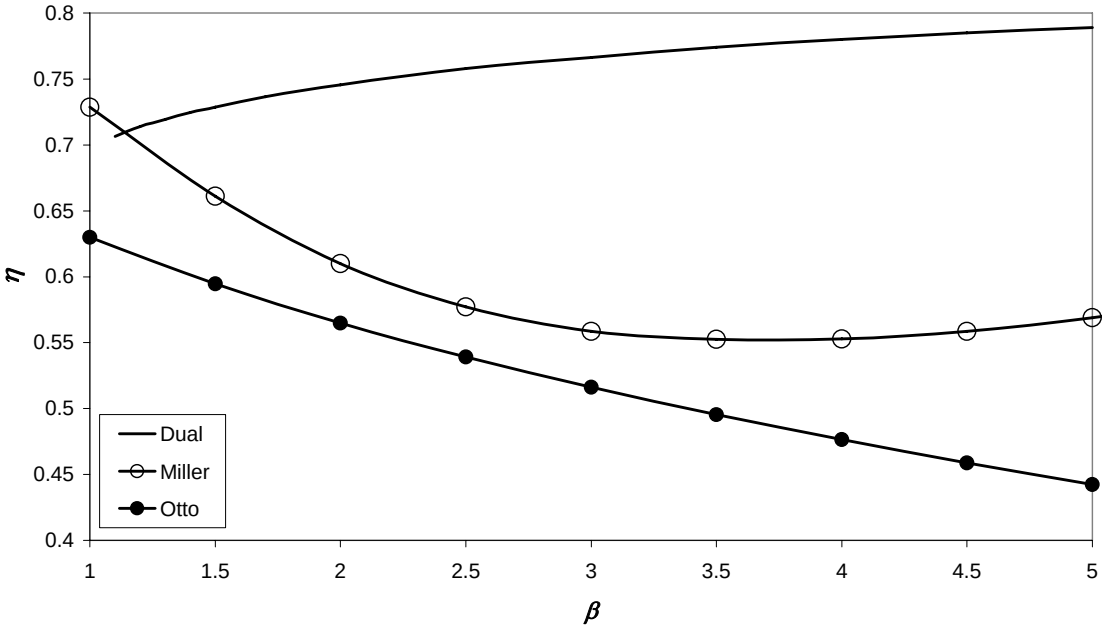

Figure 3-36 - Thermal efficiency of the three cycles.

The Otto cycle has a thermal efficiency smaller then the Miller cycle, because it does not use over-expansion. And due to the same knock limitation, it has a decreasing tendency when the supercharge increases.

3.4 Summary

Both, naturally aspirated and supercharged cycles were analysed. For spark ignition engines the use of over-expansion and the combination with VCR are the most promising techniques for engines improvement. The results obtained are theoretical and do not account with other parameters that affect engine performance. More accurate results can be obtained if the referred engines improvement technologies are analysed using other methodologies like numerical simulation.

3.5 References

1 Drangel, H., Bergsten, L., *The new Saab SVC engine – An Interaction of Variable Compression Ratio, High Pressure Supercharging and Donwsizing for Considerably Reduced Fuel Consumption*, 9. Aachener Kolloquium Fahrzeug und Motorentechnik, October 4-6, 2000.

2 Martins, J., Uzuneanu, K., Ribeiro, B., Jasansky, O., *Thermodynamic Analysis of an Over-Expanded Engine*, SAE 2004-01-0617, 2004.

3 Ribeiro, B., Martins, J., Uzuneanu, K., *Theoretical Comparison of Otto and Miller Cycles with Turbocharging*, Galati, Romania, 2005.

4 Heywood, John B., *Internal Combustion Engine Fundamentals*, McGraw-Hill, 1988.

5 Challen, Bernard; Baranescu, Rodica, *Diesel Engine Reference Book*, Butterworth-Heinemann, second edition, 1999.

6 Hitomi, M, et al. *Mechanism of improving fuel efficiency by Miller cycle and its future prospect*, SAE 950974.

7 Hatamura, K., et al. *A study of the improvement effect of Miller cycle on mean effective pressure limit for high pressure supercharged gasoline engines*, JSAE Review 18 (1997) 101-106.

8 Wirth, M., et al. *Turbocharging the DI Gasoline Engine*, SAE 2000-01-0251.

9 Wu, C., Puzinauskas, P. V., Tsai, J. S., *Performance analysis and optimisation of a supercharged Miller cycle Otto engine*, Applied Thermal Engineering 23 (2003), 511-521.

10 Hitomi, M., Sasaki, J., Hatamura, K., Yano, Y., *Mechanism of Improving Fuel Efficiency by Miller Cycle and Its Future Prospect*, SAE 950974, 1995.

4 – Engine Modelling

4 ENGINE MODELLING

4.1 Introduction

Engine modelling allows for engine research and design to be less expensive as experimental work can be previously assessed and some set-up conditions to the experiment so defined, thus saving time and resources during the test phase of a project.
Internal combustion engine models can be of single or multiple zone (in the first, all the mass inside the engine is considered to have a uniform pressure, temperature and chemical constitution). In these models, the combustion chamber geometry is not taken into consideration as well as differences in temperature and composition distribution. Fluid flow effects are not considered as depending on space but rather described by coefficients. These types of models are used to predict pressure variation in the cylinder, considering a certain correlation for combustion rate, and evaluate the engine performance, using several parameters.
Multiple zone models consider not only differences in the cylinder charge composition but also different distribution of temperature, allowing for a more accurate analysis to be achieved if combustion chamber geometry or emissions formation are studied.
The work being developed aims the evaluation of engine performance (through specific fuel consumption and power) avoiding large investments in computational resources, programming and running time, hence a single zone model was adopted, this being considered as sufficient to reach the intended objectives.
A thermodynamic engine model was developed and implemented in Simulink, a toolbox from Matlab. It is a model of a single cylinder four-stroke engine, and includes instantaneous volume, pressure and temperature calculation, chemical species characteristics, mass exchange, combustion, heat transfer, and friction.
In a second stage, the model was extended to perform an analysis based on the second law of thermodynamics. The model is able to calculate the entropy generation during the engine cycle. This parameter can be used later as an extra engine parameter for performance evaluation.
A detailed description of the model using the diagram blocks from the Simulink environment is presented in Annex B.

4.2 Engine model

4.2.1 Engine motion

The engine moving parts are the first to be modelled. Included among these are the crankshaft (speed and position), piston (speed and position) and valve (lift and open area). The position of these engine components also allow for the calculation of the area for heat transfer and compression ratio (geometric and effective) to be made. Figure 4-1 shows the diagrammatic geometry taken in this analysis.

4.2.1.1 Crankshaft

Crankshaft movement/rotation is considered constant and is one of the model variables (engine speed in rpm). All other engine or cycle data are referred to a time variable directly connected to the engine speed. The first of these variables is the crankshaft position, usually named as crank angle (assuming values from 0º up to 720º for a 4 stroke engine). The relation between time and crankshaft angle is expressed as the rate:

$$\frac{d\theta}{dt} = \frac{2\pi N}{60} \tag{4.1}$$

where θ is crank angle, t is time and N is engine speed in rpm. The crank angle value at each time step is used to determine the cycle position and to start and finish other processes in the model, such as valve opening or closure, combustion start or performance calculations based in complete cycle results, as thermal efficiency or power.

4.2.1.2 Cylinder

The piston position and speed are used to determine the cylinder volume, rate of change of the cylinder volume and the cylinder surface area.
The cylinder volume at any crank angle θ is [1]:

$$V = V_c + \frac{\pi B^2}{4}\left\{ l + a - \left[a\cos\theta + (l^2 - a^2\,sin^2\,\theta)^{1/2} \right] \right\} \tag{4.2}$$

or in the rate form:

$$\frac{dV}{dt} = V_c + \frac{\pi B^2}{4}\left\{ l + a - \left[a\cos\frac{d\theta}{dt} + \left(l^2 - a^2\,sin^2\,\frac{d\theta}{dt} \right)^{1/2} \right] \right\} \tag{4.3}$$

Where V_c is the combustion chamber volume, B is the cylinder bore, l is the connecting rod length and a is the crank radius (Figure 4-1).

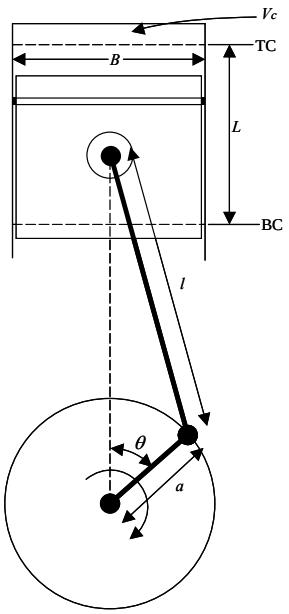

Figure 4-1 – Engine geometry.

The combustion chamber volume was defined for a cylindrical combustion chamber and for a defined geometrical compression ratio (maximum cylinder volume / minimum cylinder volume). The height of the combustion chamber may be changed to get different compression ratios for an engine with almost the same configuration.

The cylinder surface area A at any crank position θ is given by:

$$A = A_c + A_p + \pi B\left\{ l + a - \left[a\cos\theta + \left(l^2 - a^2\,sin^2\,\theta \right)^{1/2} \right] \right\} \tag{4.4}$$

Where A_c is the combustion chamber surface area, which corresponds to a top flat surface with a diameter of B and a cylinder wall with a diameter of B and length equal to the combustion chamber height. The A_p is the piston crown surface area, which is considered as a flat surface with a diameter of B and the area is defined by $A_p=\pi B^2/4$. As the combustion chamber and piston surface areas remain constant for the complete cycle, the area change rate is expressed as:

$$\frac{dA}{dt} = A_{ch} + A_p + \pi B\left\{ l + a - \left[a\cos\frac{d\theta}{dt} + \left(l^2 - a^2 \sin^2 \frac{d\theta}{dt} \right)^{1/2} \right] \right\} \tag{4.5}$$

The piston speed is given by:

$$\frac{S_p}{\overline{S}_p} = \frac{\pi}{2}\sin\theta\left[1 + \frac{\cos\theta}{\left(R^2 - \sin^2\theta\right)^{1/2}} \right] \tag{4.6}$$

Where R is the ratio of connecting rod length to crank radius ($R = l/a$) and $\overline{S}_p$ is the mean piston speed:

$$\overline{S}_p = 4aN \tag{4.7}$$

4.2.2 Analysis based on the First Law of Thermodynamics

Single zone models are based on the First Law of Thermodynamics, which is expressed as:

$$dU = dQ - dW + h_{in}dm_{in} - h_{out}dm_{out} \tag{4.8}$$

where:

$$dU = udm + mdu \tag{4.9}$$

where *dm* is the mass differential of the cylinder content. For a perfect gas, the internal energy depends only on the temperature and is defined as:

$$du = c_v(T)dT \tag{4.10}$$

As temperature changes with time and considering (4.10), expression (4.9) may be written in terms of rate as:

$$\frac{dU}{dt} = c_v(T)T\frac{dm}{dt} + mc_v(T)\frac{dT}{dt} + mT\frac{dc_v(T)}{dt} \tag{4.11}$$

The work differential (*dW*) is written as:

$$dW = -pdV \tag{4.12}$$

being *p* the pressure inside the cylinder and *dV* the cylinder volume differential. When expression (4.12) is written in terms of time rates comes:

$$\frac{dW}{dt} = -p\frac{dV}{dt} \tag{4.13}$$

For perfect gases, enthalpy is assumed to be only temperature dependent [2] and so may be defined as:

$$dh = c_p(T)dT \tag{4.14}$$

and in time rate form comes:

$$\frac{dh}{dt} = c_p(T)\frac{dT}{dt} + T\frac{dc_p(T)}{dt} \tag{4.15}$$

Temperature is calculated in a differential form deduced from the first law of thermodynamics applied to closed and open systems and considering the mass

conservation principle. During compression, combustion and expansion, the cylinder is considered as a closed system and that there is no mass exchange. Temperature is then calculated through:

$$m_{cyl}c_v(T)\frac{dT}{dt} + m_{cyl}T\frac{dc_v(T)}{dt} = \frac{dQ}{dt} - p\frac{dV}{dt} \tag{4.16}$$

During the period of open valves, the system is considered open and the same equation will come as:

$$m_{cyl}c_v(T)\frac{dT}{dt} + m_{cyl}T\frac{dc_v(T)}{dt} + Tc_v(T)\frac{dm_{cyl}}{dt} = \frac{dQ}{dt} - p\frac{dV}{dt} + \sum T_n c_p(T)_n \frac{dm_n}{dt} \tag{4.17}$$

Where m_{cyl} is the mass of working fluid contained in the cylinder, $\frac{dm_n}{d\theta}$ is the flow rate through each one of the valves. T_n and $c_p(T)_n$ are the temperature and c_p of the flow through each valve. For the exhaust flows these conditions are the same as the internal mass contained in the cylinder. In the case of mass flows coming into the cylinder, the characteristics of the flow are fixed as:

Table 4-1 - Mass inflow pressure and temperature.

		Pressure (Pa)	**Temperature (K)**
Intake valve	Mixture (air + fuel)	101325	293
Exhaust valve	Burned gases	101325	800

To calculate the pressure the ideal gas equation is used in the differential form, as:

$$pV = \sum_i m_i R_i T \tag{4.18}$$

and

$$\frac{dp}{dt}V + p\frac{dV}{dt} = T\sum_i R_i \frac{dm_i}{dt} + \sum_i R_i m_i \frac{dT}{dt} \Leftrightarrow$$
$$\Leftrightarrow \frac{dp}{dt} = \frac{T\sum_i R_i \frac{dm_i}{dt} + \sum_i R_i m_i \frac{dT}{dt} - p\frac{dV}{dt}}{V} \quad (4.19)$$

where m_i is the mass amount of each of the chemical zones in the model (air and fuel mixture or exhaust gases) and where R_i is the gas constant of the chemical constituents of each one of the chemical zones. Using continuous integration, the value of the internal pressure of the cylinder is calculated.

4.2.3 Combustion

During combustion, the mass of fresh mixture is converted into burned gases by subtracting the same mass quantity at a defined conversion rate from the fresh mixture and adding it to the exhaust gas.
The model considers that the mixture is always stoichiometric, thus it can be written [3]:

$$C_x H_y + a(O_2 + 3.76N_2) \rightarrow xCO_2 + \left(y/2\right)H_2O + 3.76aN_2 \quad (4.20)$$

Where $a = x + \frac{y}{4}$

The total heat released by the fuel during the combustion process does not correspond to the total heating value but some combustion inefficiency is considered. The heat released is given by:

$$Q_R = \eta_c m_f Q_{LHV} \quad (4.21)$$

Where m_f is the fuel mass trapped in the cylinder in each cycle, Q_{LHV} is the lower heating value of the fuel and η_c is the combustion efficiency and is defined as [4]:

$$\eta_c = \eta_{c\,max}\left(-1.6082 + 4.6509\lambda - 2.0764\lambda^2\right) \qquad 0.75 < \lambda < 1.2 \quad (4.22)$$

Considering that η_{cmax} equals 0.9 for a spark ignition engine.

The heat released by the fuel is not delivered at once but during a certain interval of time defined in terms of crank angle. The combustion start time is another variable defined in terms of crank angle before TDC. The burned gas fraction will then be given by the Wiebe function:

$$x_b = 1 - exp\left[-a\left(\frac{\theta - \theta_0}{\Delta\theta} \right)^{m+1} \right] \tag{4.23}$$

With a = 5 and m = 2, θ_0 is the spark time at the beginning of combustion in crank angle and $\Delta\theta$ is the burning interval in crank angle. The heat released rate will then be given by:

$$\frac{dQ}{dt} = Q_R \frac{dx_b}{dt} \tag{4.24}$$

4.2.4 Gas properties

The specific heat, gas constant and specific heat ratio of the gases passing through valves and of the gases inside the cylinder are calculated considering two kinds of gas mixtures. A stoichiometric mixture of air and fuel, being the air fuel ratio calculated for each fuel type, and the burn gases mixture of CO_2, H_2O and N_2. These characteristics are calculated as function of temperature (instantaneous temperature inside the cylinder or the assumed temperature for the mass inflow as shown in Table 4-1). The expression for c_p calculation of each chemical specie is written as [2]:

$$c_p(T)_n = \frac{a + bT + cT^2 + dT^3}{M_n} \tag{4.25}$$

with T in K, M_n the molar mass of the substance in kg/kmol, c_p in kJ/(kg·K) and the coefficients a to d are given in Table 4-2 [2]:

Table 4-2 – Coefficients for c_p calculation (eq. 4.25).

Substance		*A*	*b*	*c*	*D*
Air	-	28.11	0.1967×10^{-2}	0.4802×10^{-5}	-1.966×10^{-9}
Nitrogen	N_2	28.90	-0.1571×10^{-2}	0.8081×10^{-5}	-2.873×10^{-9}
Carbon dioxide	CO_2	22.26	5.981×10^{-2}	-3.501×10^{-5}	7.469×10^{-9}
Water steam	H_2O	32.24	0.1923×10^{-2}	1.055×10^{-5}	-3.595×10^{-9}

For fuel the specific heat is given by [5]:

$$\frac{c_p}{R_f} = a_0 + b_0 T + c_0 T^2 \tag{4.26}$$

where T is in K and R is the fuel gas constant in J/kg K. The coefficients are:

$a_0 = 4.0652$

$b_0 = 6.0977$ E-02

$c_0 = -1.8801$ E-05

The total value of c_p and R of the mixture of the referred gases are calculated considering the amount of mass of each chemical species present at each moment in the mixture:

$$c_{p,mix} = \sum_{i=1}^{j} \frac{m_i c_{p,i}}{m_{total}} \tag{4.27}$$

where j is the total amount of chemical species present at each moment.

4.2.5 Gas exchange processes

During a complete cycle of an internal combustion engine two main gas exchange processes exist. Intake, where a mixture of air and fuel is inducted into the engine cylinder through the intake valve, and exhaust, when gases resulting from the combustion process are expelled out of the engine cylinder.

The model considers three volumes of different working fluids. The exhaust manifold contains exhaust gas with a chemical composition resulting from a complete

combustion of a stoichiometric mixture. The intake manifold contains a stoichiometric mixture of air and fuel at atmospheric pressure and temperature, plus a quantity of exhaust gas, which was exhausted to the intake manifold during the upward movement of the piston. This exhausted gas is the first to be inducted during intake process. Finally, inside the cylinder and before combustion a certain amount of fresh mixture of air and fuel are present, and a certain quantity of burned gas resulting from the dead volume of the combustion chamber and from the recirculation of exhaust gas. After combustion only burned gas is present inside the cylinder.

To calculate the mass flow through the valve two situations shall be considered depending of the flow regime (i.e. relation between the pressures up and downstream of the valve). The flow rate through the valve is then given by [1]:

$$\frac{dm}{dt} = \dot{m} = \frac{C_D A_R p_0}{(RT_0)^{1/2}} \left(\frac{p_T}{p_0}\right)^{\frac{1}{\gamma}} \left\{ \frac{2\gamma}{\gamma - 1} \left[1 - \left(\frac{p_T}{p_0}\right)^{\frac{\gamma-1}{\gamma}} \right] \right\}^{1/2} \tag{4.28}$$

When the flow is choked, i.e. the flow speed equals the sound speed:

$$\frac{p_T}{p_0} \leq \left(\frac{2}{\gamma + 1}\right)^{\frac{\gamma}{\gamma-1}} \tag{4.29}$$

the flow rate is given by:

$$\frac{dm}{dt} = \dot{m} = \frac{C_D A_R p_0}{(RT_0)^{1/2}} \gamma^{1/2} \left(\frac{2}{\gamma + 1}\right)^{(\gamma+1)/2(\gamma-1)} \tag{4.30}$$

Where C_D is the discharge coefficient, p_0 and T_0 are the upstream pressure and temperature respectively, p_T is the downstream pressure and R is the gas constant.

The exhaust process may be divided into two phases, the blow-down phase (just after the opening of the exhaust valve until the pressure inside the cylinder equals the pressure of the exhaust manifold) and the exhaust phase, where cylinder content is expelled out. These phenomena were simulated using only the mass flow rate equations presented above, (4.28) and (4.30).

4.2.6 Heat transfer

The heat transfer was separated in three components corresponding to the three surfaces that limit the cylinder (cylinder liner, piston crown and combustion chamber surface). The Annand heat transfer coefficient was used, which is said to be more accurate when applied to spark ignition engines [6]. Annand separates the convection and radiation terms. The convection heat transfer coefficient is related to the Nusselt number by [6]:

$$\alpha_{conv} = \frac{C_k Nu}{B} \tag{4.31}$$

Where:

$$C_k = 6.1944 \times 10^{-3} + 7.3814 \times 10^{-5} T - 1.2491 \times 10^{-8} T^2 \tag{4.32}$$

C_k is the thermal conductivity of the air, B is the cylinder bore and Nu is the Nusselt number, which relates the Reynolds number and a specific constant for four-stroke engines as:

$$Nu = 0.49\, Re^{0.7} \tag{4.33}$$

where Re is the Reynolds number calculated as:

$$Re = \frac{B \cdot S_p \cdot \rho}{\mu} \tag{4.34}$$

Where S_p is the mean piston speed and μ is the viscosity of the mixture inside the cylinder, calculated by [6]:

$$\mu = 7.457 \times 10^{-6} + 4.1547 \times 10^{-8} T - 7.4793 \times 10^{-12} T^2 \tag{4.35}$$

And ρ is the density of the mixture inside the cylinder calculated by the ideal gas equation.

The radiation heat transfer coefficient is given by [6]:

$$\alpha_{rad} = 4.25 \times 10^{-9} \frac{T_{cyl}^4 - T_{cw}^4}{T_{cyl} - T_{cw}} \tag{4.36}$$

Where T_{cyl} is the in cylinder gas temperature and T_{cw} is the wall (cylinder, piston or engine head) temperature, assumed as constant during all engine cycle. For each heat transfer surface, the expression for the rate of heat exchange is:

$$\frac{dQ}{dt} = \left(\alpha_{conv} + \alpha_{rad}\right)\left(T_{cyl} - T_{cw}\right)A_{tr} \tag{4.37}$$

Where A_{tr} is the heat transfer area that is fixed for the engine head and piston and variable for the cylinder walls.

4.2.7 Valve motion

When modelling the valve motion, the two important variables are the open area at each valve position and the valve lift profile. The valve motion itself is divided into 5 phases [6]. A rise ramp period, a principal rise period, a dwell period, a principal falling period and a final falling ramp period. The ramp periods correspond to the clearance of the valve train. During this short period the valve does not move but the rise in the cam shape allows every component of the valve train to fit perfectly. After this first rise period the valve starts to open.

For the simulation of the valve motion, the lift profile geometry is defined by the opening time (in terms of crank angle) of the valve and the total opening duration angle (θ_v). The dwell angle (θ_{dw}) is also defined and the ramp period angles (θ_{ur} and θ_{dr}) which are considered equal, meaning that the valve lift profile is symmetrical. In terms of lifting the total lift high (L_v) and the lift during the ramp period (L_{ur} and L_{dr}) are defined. All other variables are calculated as function of this data.

For the successive periods of the valve motion a set of equations is established to describe the lifting of the valve (during this analysis the θ means the camshaft angle and not the crank angle).

In the model, the inputs are the came profile, which is defined by a polynomial curve and the dwell angle, other inputs in the model being the valve train size and configuration. With this last input it is possible to convert the rise of the cam in rise of the valve. In a secondary stage, this relation between the valve movement and the cam profile allows for the design of cams, which comply better with the working specification of the engine.

In the case of the implemented valve train, the push rods configuration (Figure 4-2) was selected, because that is the configuration of the engine under study. The variables to be defined in this configuration are the length of each component and its position, so that a cinematic model may be built.

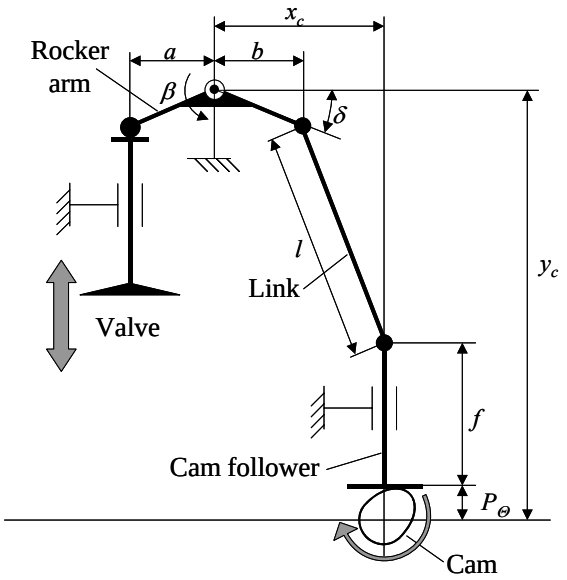

Figure 4-2 – Valve train configuration.

The valve lift is given by:

$$L(\beta) = a\ sin(\beta) \tag{4.38}$$

where β is the rotation angle of the rocker arm. This rotation angle is directly dependent of the lift of the came as a function of the came angle (θ_c). That relation is obtained by the relative movement of the elements of the valve train, since the cam until the rocker arm:

$$\begin{cases} x_c = l_x + b \cdot cos(\delta - \beta) \\ y_c = l_y + b \cdot sin(\delta - \beta) + P_\theta + f \end{cases} \tag{4.39}$$

Once $l^2 = l_x^2 + l_y^2$ equation (4.38) can be written as:

$$\left[y_c - P_\theta - f - b \cdot sin(\delta - \beta)\right]^2 = l^2 - \left[x_c - b \cdot cos(\delta - \beta)\right]^2 \tag{4.40}$$

Let $K_\theta = y_c - P_\theta - f$ and (4.40) after arrangement yields:

$$\frac{K_\theta^2 - l^2 + x_c^2 + b^2}{2b\sqrt{K_\theta^2 + x_c^2}} = \frac{K_\theta \, sin(\delta - \beta) + x_c \, cos(\delta - \beta)}{\sqrt{K_\theta^2 + x_c^2}} \tag{4.41}$$

Let φ be defined as:

$$\begin{cases} cos(\varphi) = \dfrac{K_\theta}{\sqrt{K_\theta^2 + x_c^2}} \\ sin(\varphi) = \dfrac{x_c}{\sqrt{K_\theta^2 + x_c^2}} \end{cases} \tag{4.42}$$

Hence:

$$\frac{K_\theta^2 - l^2 + x_c^2 + b^2}{2b\sqrt{K_\theta^2 + x_c^2}} = cos(\varphi)sin(\delta - \beta) + sin(\varphi)cos(\delta - \beta) = sin(\varphi + \delta - \beta) \tag{4.43}$$

The relation between the rocker arm rotation angle and the cam angle is established as:

$$\beta = \varphi + \delta - arcsin(C_\theta) \quad with \quad C_\theta = \frac{K_\theta^2 - l^2 + x_c^2 + b^2}{2b\sqrt{K_\theta^2 + x_c^2}} \tag{4.44}$$

The real lift of the valve is calculated using (4.37) and (4.44):

$$L_\theta = a \, sin\left[\varphi + \delta - arcsin(C_\theta)\right] \tag{4.45}$$

The value of the real lift (L_θ) is used to calculate the restriction flow section opened by the valve. This flow section may correspond to the surface area of a frustum of a cone or the area of the duct depending of the area opened by the valve. If the valve lift is lower

than a certain limit, the restriction area is the surface area of the frustum of a cone opened by the valve. If the lift is higher than the referred limit, the restriction area is the section of the duct upstream of the valve. The value of the limit lift is given by [6]:

$$L_{lim} = \frac{d_{os} - d_{is}}{sin\,2\phi} \tag{4.46}$$

Where d_{os} and d_{is} are the head diameter and the inner seat diameter respectively. The ϕ angle is the seat angle of the valve as shown in Figure 4-3. For the two situations mentioned above the value of the flow area comes:

$$L \le L_{lim} \Rightarrow A_t = \pi L \cos\phi \left(d_{is} + L \sin\phi \cos\phi\right) \tag{4.47}$$

or

$$L > L_{lim} \Rightarrow A_t = \pi \left(\frac{d_{os} + d_{is}}{2}\right) \sqrt{\left(L - \frac{d_{os} - d_{is}}{2} tg\phi\right)^2 + \left(\frac{d_{os} - d_{is}}{2}\right)^2} \tag{4.48}$$

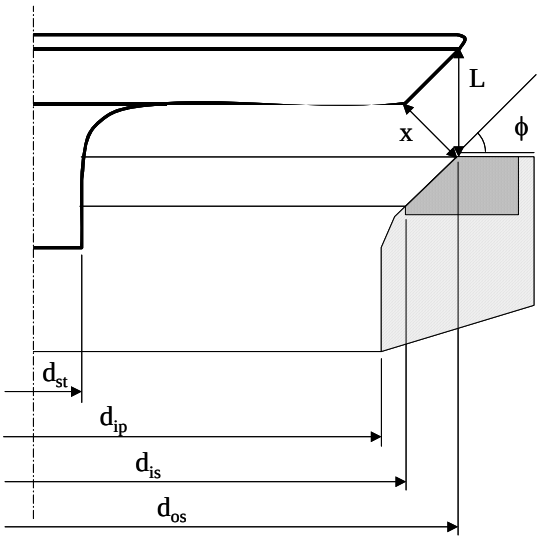

Figure 4-3 – Valve and seat geometry.

The value of A_t will be multiplied by the number of inlet or exhaust valves to calculate the total flow area. This value of total flow area will also be affected by a discharge coefficient due to all obstacles and pipe geometry. If A_p is considered the flow area of the pipe before the valve, the restricted area (A_r) to be considered in flow calculations shall be:

$A_r = A_t$ if $A_t < A_p$

$A_r = A_p$ if $A_t \geq A_p$

4.2.8 Friction

An expression for total *fmep* was presented [7] and lately improved [8]. This friction model includes the friction of the crankshaft bearings, connecting rod bearings, piston and piston rings and all valve train, lubricant viscosity also being taken into account. The resulting expression for friction calculation is written as:

$$fmep = 1.22\times10^{5}\left(\frac{D_b}{B^2 Sn_c}\right) + 3.03\times10^{-4}\sqrt{\frac{\mu}{\mu_0}}\left(\frac{ND_b^3 L_b n_b}{B^2 Sn_c}\right) + 1.35\times10^{-10}\left(\frac{D_b^2 N^2 n_b}{n_c}\right) +$$
$$+ 2.94\times10^{2}\sqrt{\frac{\mu}{\mu_0}}\left(\frac{S_p}{B}\right) + 4.06\times10^{4}\left(\frac{F_t}{F_{t0}}C_r\right)\left(1+\frac{500}{N}\right)\frac{1}{B^2} + 3.03\times10^{-4}\sqrt{\frac{\mu}{\mu_0}}\left(\frac{ND_b^3 L_b n_b}{B^2 Sn_c}\right) +$$
$$+ \frac{p_i}{p_a}\left[\sqrt{\frac{\mu}{\mu_0}}0.088r_c + 0.182\left(\frac{F_t}{F_{t0}}\right)r_c^{(1.33-KS_p)}\right] + 244\sqrt{\frac{\mu}{\mu_0}}\frac{Nn_b}{B^2 Sn_c} + C_{ff}\left(1+\frac{500}{N}\right)\frac{n_v}{Sn_c} +$$
$$+ C_{oh}\sqrt{\frac{\mu}{\mu_0}}\left(\frac{L_v^{1.5}N^{o.5}n_v}{BSn_c}\right) + C_{om}\left(1+\frac{500}{N}\right)\frac{L_v n_v}{Sn_c} + 8.3155 + 1.86\times10^{-3}N + 7.45\times10^{-7}N^2 \quad (4.49)$$

Where:

Db: bearing diameter (mm)

B: Bore (mm)

S: Stroke (mm)

nc: Number of cylinders

N: Engine speed (rpm)

Lb: Bearing length (mm)

nb: Number of bearings

Sp: Mean Piston Speed (m/s)

F_t/F_{t0}: Piston Ring Tension Ratio

C_r: Piston Roughness constant

pi: Intake pressure (kPa)

pa: Atmospheric pressure (kPa)

rc: Compression ratio

K: Constant of Bishop (2.38 ´ 10-2 s/m)

Cff: Constant for Flat Followers

nv: Number of Valves

Coh: Constant for Oscillating Hydrodynamic

Lv: Maximum Valve Lift (mm)

Com: Constant for Oscillating Mixed

The factor:

$$\sqrt{\frac{\mu}{\mu_0}} \tag{4.50}$$

represents a scaling factor for the hydrodynamic friction, where μ is the viscosity of the oil in the engine for which friction predictions are being made, and μ_0 is the reference viscosity for the oil used in the engines that provided the data used to calibrate the model when it was developed.

4.2.9 Engine performance parameters

To understand the changes in engine performance due to cycle or engine modifications, several performance parameters are calculated. It is possible to compare the performance of various engines or cycles by using these parameters.
In the model the implemented engine performance parameters are work per cycle, power, thermal efficiency or specific fuel consumption and mean effective pressure.
The indicated output work (W_i) from the engine in each cycle is obtained by integrating the pressure curve in relation to the volume change rate during the cycle:

$$W_i = \oint p \frac{dV}{dt} \tag{4.51}$$

It is then possible to calculate the engine indicated power output per cylinder from the indicated work per cycle:

$$P_i = \frac{W_i N}{120} \tag{4.52}$$

The thermal efficiency (η_i) or indicated specific fuel consumption (*isfc*) uses again the indicated work per cycle and the total amount of fuel supplied in the same cycle (m_f), and is expressed as:

$$\eta_i = \frac{W_i}{m_f Q_{LHV}}$$
$$isfc = \frac{m_f}{W_i} = \frac{1}{\eta_i Q_{LHV}} \qquad (4.53\ a,b)$$

Mean effective pressure (*mep*) represent the work delivered to the piston (W_c) over the volume displaced (V_d) during one cycle:

$$mep = \frac{W_c}{V_d} \qquad (4.54)$$

This parameter can be divided into several parts in order to simplify the analysis. The brake mean effective pressure (*bmep*) can be divided as follows:

$$bmep = imep + pmep - fmep \qquad (4.55)$$

where *imep* is the indicated mean effective pressure, *pmep* is the pumping mean effective pressure and *fmep* is the friction mean effective pressure as defined above [8]. The value of *imep* is calculated as stated above (4.54) using the indicated work (W_i) per cycle. The *pmep* represents the work delivered by the piston to the cylinder charge during the intake and exhaust strokes and can be calculated through:

$$pmep = \frac{W_{i,int+exh}}{V_d} \qquad (4.56)$$

Pumping losses will be discussed bellow.

4.2.10 Cam profiles

In order to have simulation results as close as possible to the real engine performance (as tested in chapter 6), the real engine cam profiles were used in the simulation. After measuring the cam profiles a 18 degree polynomial curve was fitted for the rise and fall of the cam profile. To enlarge the scope of the simulations, the two kinds of cams for performing VVT were simulated (LIVC and EIVC). In the case of LIVC, the change of

valve timing was made just by modifying the value of the dwell angle at which the cam keeps its maximum lift (Figure 4-4). In this way, the returning side of the cam was shifted by an angle equal to the increase of the dwell angle. In the case of the original cam, the dwell angle is 8º CA. For the LIVC cams dwell angles from 20º CA up to 120º CA were considered. Due to the problem of ignition before intake valve closure, the maximum dwell angle of 130º could not be surpassed. For the simulation of the EIVC strategy, three new cams were generated. In this case the cam design followed another method. Cam geometry had to be changed so to respect the continuity conditions for velocity, acceleration and jerk [9], and for the movement transmitted from the cam to the follower to be smooth and without vibrations. The third derivative of the cam profile equation gives the jerk function and the continuity of this function was the criterion used for the new cam design. Throughout the third derivative function of the cam rise profile, points with 0 value were identified. The last part of the profile from the last 0 third derivative point until the end of the rise profile was considered constant. This segment corresponds to the last 5º of the rise profile. As the beginning of this segment has a 0 value on the third derivative, it was connected with other points in the profile with 0 derivative value. At each substitution, the profile was removed after the point of connection and substituted by the 5º segment referred above. The resulting junction has assured the continuity of the third derivative. With these new cam profile described by the discrete points of the first and last profile segments, new polynomial curves were fitted to the cam profile, so that they could be introduced in the simulation model of the engine. The falling profile is symmetrical to the rising profile.

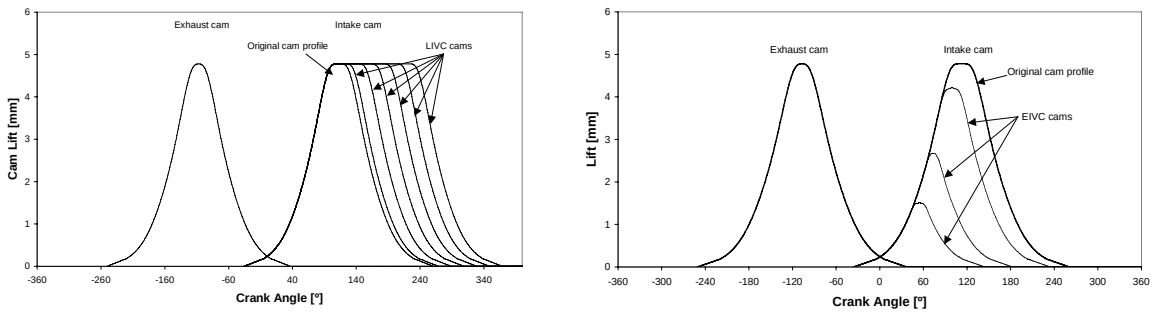

Figure 4-4 - Different cam profiles used in the simulations (left: LIVC; right: EIVC).

4.3 Engines comparison

Four engine cycles were analysed, the Otto cycle, the Miller cycle (which is an over-expanded engine cycle), a Miller cycle (by late intake valve closure - LIVC) with compression ratio adjustment and a Miller cycle (by early intake valve closure – EIVC) also with compression ratio adjustment. In the Otto engine cycle, load is controlled by the intake manifold pressure, which decreases from the atmospheric pressure down to a pressure level, which results in zero brake work. In all Miller cycles load is controlled by the intake valve closure time, whether by late intake valve closure (leading to a back-flow from the cylinder to the intake manifold) or by early intake valve closure (in which after valve closure a depression is created in the cylinder before compression starts). For the last two engine cycles, variable compression ratio is used to compensate the decrease of effective compression resulting from the change of the intake valve closure timing. To make the change of the compression ratio for the Miller VCR engine, the combustion chamber (considered of a cylindrical shape) has variable height, maintaining the combustion chamber shape. The engines specifications are described in Table 4-3.

Table 4-3 – Engine model specifications.

	1	2	3	4
	Otto	Miller	Miller VCR LIVC	Miller VCR EIVC
Bore	80 mm			
Displacement	211 cm^3			
Speed	2500 rpm			
IVO	20º BTDC			
IVC (*)	32º A	32º A- 162º A		32º A – 80º B
EVO	40º BBDC			
EVC	12º ATDC			
Intake Valve Diameter	30 mm			
Exhaust Valve Diameter	25 mm			
Intake Valve Lift	7.2 mm			
Exhaust Valve Lift	7.2 mm			
Ignition timing	20º BTDC			

(*) Angles referred to Bottom Dead Centre. A - After; B - Before

For the Otto cycle at WOT the maximum temperature of the cycle is 2082 K and peak pressure is 75 bar. This temperature and pressure were used as a reference for the compression ratio adjustment when intake valve closure time was changed. Due to the fact that temperature and pressure are uniform for the entire cylinder content, peak

pressure becomes the main variable in defining the compression ratio. Once the peak temperature value does not reduce significantly with compression ratio decrease.

As presented in [10] if only the intake valve closing time changed, an increase in the efficiency is expected in relation to the Otto cycle, but the efficiency still decreases with load reduction. If compression ratio is adjusted then an improvement is possible in terms of thermal efficiency and power decreasing load, which is the main aim of this work.

Figure 4-5 shows the efficiency versus engine load for the several engine versions: Otto, Miller and Miller VCR. It can be seen that there is an improvement just by using a variable valve train to control the load via late intake valve closure (LIVC). When compression ratio adjustment is used, the benefit in terms of thermal efficiency becomes much more important. It is relevant to refer that with the Miller VCR engine the thermal efficiency increases from 32.8% up to 34.3% as the load is reduced from full throttle down to approximately 7 bar bmep.

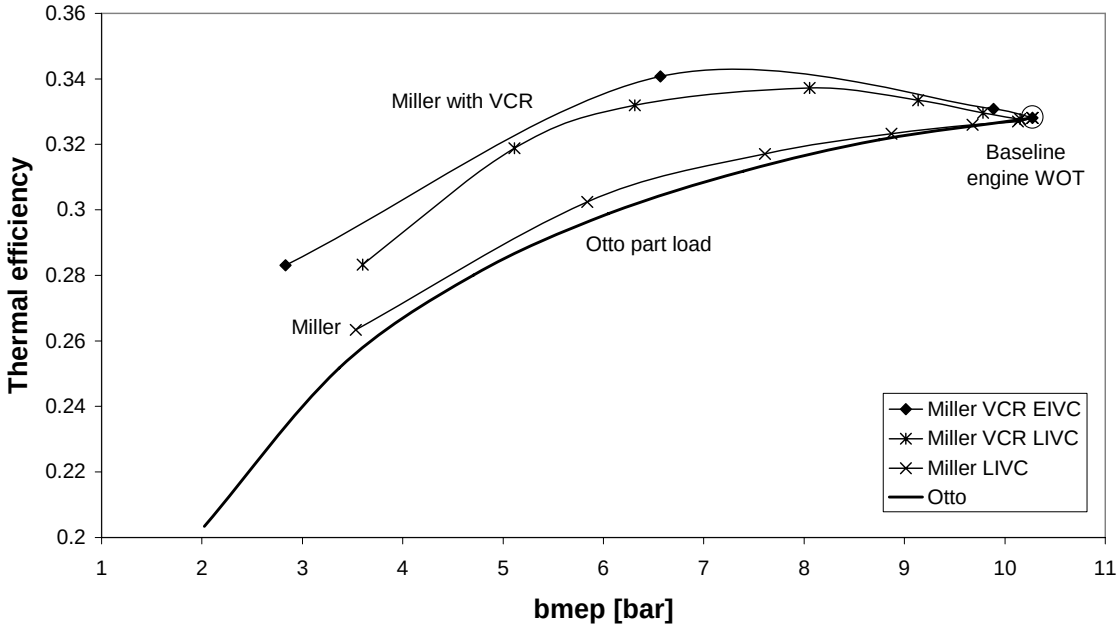

Figure 4-5 - Thermal efficiency as a function of load for 2500 rpm simulations.

At very low loads or at idle, the compression ratio required to keep the Miller VCR engine strategy working might be so high that it becomes physically impossible to realize, because there is no space between piston and poppet valves. In the case of idle the use of the throttle valve may be required when the LIVC strategy is used, as the

delay required to the intake valve to close is so high that the ignition would occur with the intake valve still open [11].

In the case of LIVC the minimum load presented in Figure 4-5 is close to the minimum possible due to the referred problem of ignition during open intake valve. If early intake valve closure (EIVC) is used for load control much lower loads can be achieved.

The engine, either working as simple Miller or as Miller with VCR has better efficiency if EIVC is used instead of LIVC. This is mainly caused by reduced pumping losses. In the case of LIVC the air/fuel mixture is inducted into the cylinder and after the BDC it is blown-back again to the intake manifold. This effect is more intense as longer IVC delays are used.

From the simulations it can be noticed that in terms of enthalpy (as pressure and temperature) lost to the environment after the opening of the exhaust valve, some gain is achieved with the use of the Miller VCR engine. As seen in Figure 4-6 temperature and pressure fall with decreasing loads for all engine cycles. For the Miller VCR engine cycle, both with LIVC or EIVC, the decrease of these parameters reduces more than for the Otto or Miller engine cycles. This allows a significant gain in terms of thermal efficiency from the Miller VCR engine.

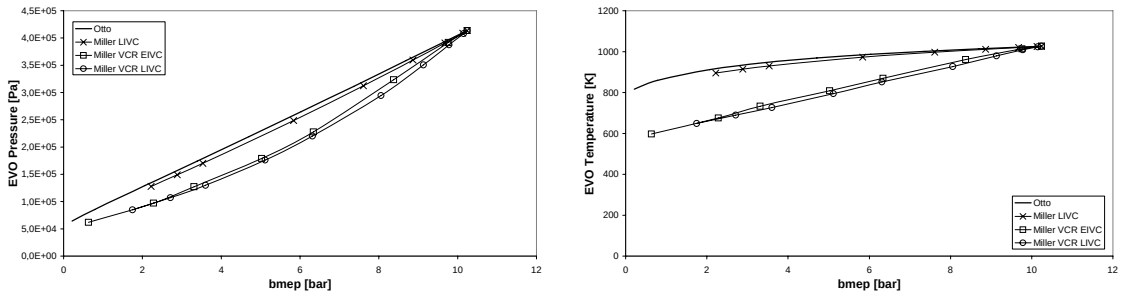

Figure 4-6 – EVO pressure and temperature (2500 rpm).

As for the ignition timing and considering the same parameters, it can be seen that the Miller VCR engine cycle has a higher pressure (Figure 4-7), caused by the compression ratio increase with the load decrease. As for the temperature, it can be seen that the blow-back phenomenon happening significantly in the LIVC engine cycles causes a decrease of the temperature at this instant due to the fact that while the air is inducted and blown-back to the intake manifold it cools down the engine cylinder content. The

combination of both effects leads to an increase of the work produced per cycle with a consequently increase of the engine thermal efficiency.

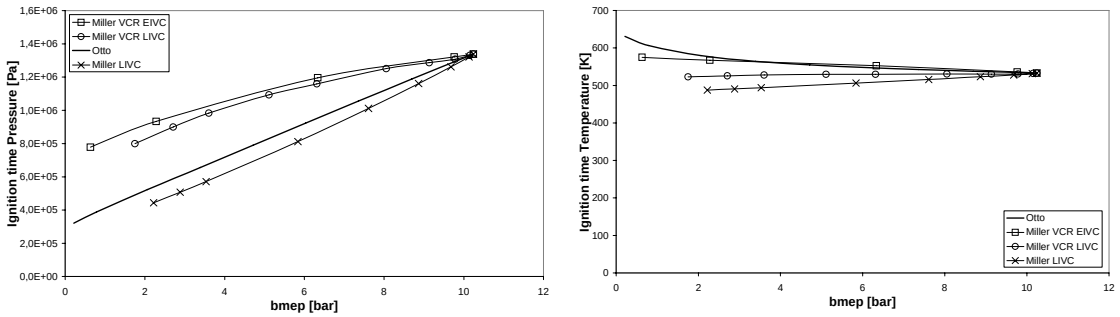

Figure 4-7 – Ignition time pressure and temperature (2500 rpm).

4.3.1 Friction losses

The friction model used for friction calculations [7,8] considers the geometrical dimensions of the engine parts where friction happens and a series of other parameters that somehow influence the engine internal friction. These parameters are engine speed (and piston speed), intake pressure and compression ratio. Friction between moving parts increases when their speed increases. The compression ratio and the intake pressure dictate the cycle maximum pressure, which influences the friction between the piston and piston rings and the cylinder liner, once more pressure acts on the rear surface of the piston rings thus increasing the force that these make over the cylinder liner surface.

Figure 4-8 presents values of the friction mean effective pressure for the several cycles under analysis. It can be noticed that in the case of the Otto cycle (which is the only changing variable with the load decrease), the friction has a general reduction tendency with load decrease due to the decrease of the intake pressure. In this case the maximum values of the pressure in the cycle are reduced and consequently friction is also reduced. In the case of the Miller cycle, the only changing parameter for load variation is the intake valve closure timing. All the other working parameters stay constant, thus engine internal friction results constant. In the case of the Miller VCR engine cycles, either EIVC or LIVC, a significant increase in the engine internal friction is noticed. In these two engine cycles, the compression variation is the only variable that influences the

change in the engine friction. In fact as the load is reduced the compression ratio is increased which in turn changes the friction value.

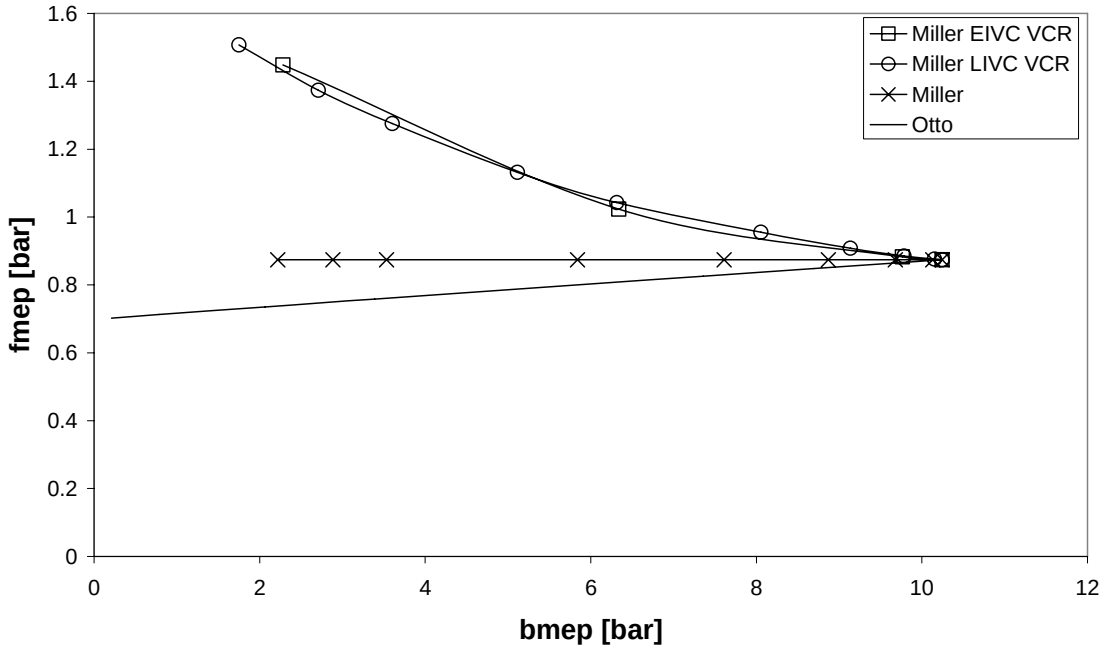

Figure 4-8 – Friction mean effective pressure.

4.3.2 Pumping losses

The definition of pumping losses was considered to be made by two methods [12,13]:

1) 360º Integration

With this method, pumping work is defined as the integral of cylinder pressure with respect to cylinder volume calculated from the BDC of the exhaust stroke to BDC of the intake stroke (area B and area C from Figure 4-9). The indicated work is defined as the integral of cylinder pressure with respect to cylinder volume from BDC of compression stroke to BDC of the expansion stroke (area A and area C). Clearly, when VVT is used to reduce pumping work or to perform load control, the use of this method largely inaccurate for not considering some pumping work spend during both compression and expansion strokes.

2) Area B Calculation

This method includes the area B only and not area C in the calculation of the pumping work (Figure 4-9). This is because area C occurs as negative work during the gas exchange period of the cycle and as positive work during the compression/expansion portion of the cycle, therefore the net effect of area C on the work of the full 720º engine cycle is zero. This method still does not include the full exhaust period, and factors affecting the first part of the exhaust event do not impact on area B pumping work.

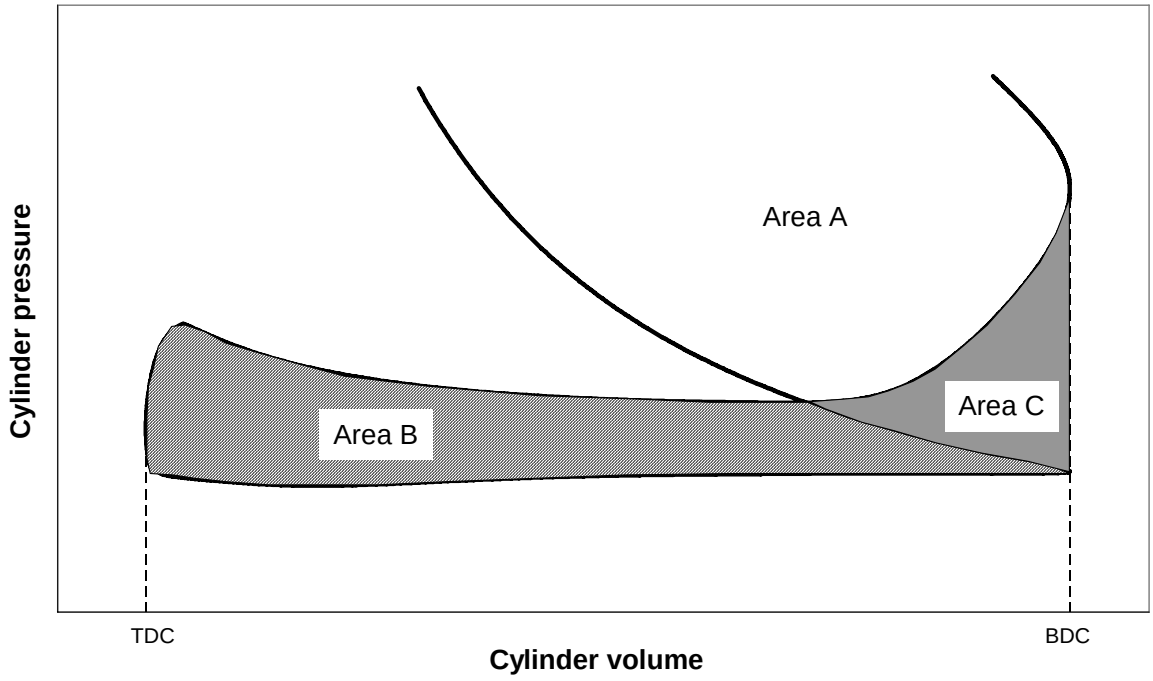

Figure 4-9 – Pumping work and indicated work.

A more accurate methodology for pumping losses measurement/calculation was recently proposed [13]. With this method the valve timing is accounted for pumping losses effects, leading to more realistic values.

Corrected pumping calculation

The total value of the pumping work is calculated from three components: the $PMEP_{360}$; the EVO expansion loss and the incremental compression work. The first component is the pumping work as calculated in the first method described above. The EVO

expansion loss corresponds to the work loss from the exhaust valve opening down to BDC, which may be expressed in terms of *mep* as:

$$EVO_{loss}mep = \frac{1}{V_d}\int_{EVO}^{BDC}\left(p_{extrapolated} - p_{measured}\right)dV \tag{4.57}$$

where $P_{extrapolated}$ is the pressure value extrapolated from EVO to BDC using a curve fitted to PV^{γ}, γ being based on the measured expansion stroke data prior to EVO. $P_{measured}$ is the cylinder effective pressure measured.

The incremental compression work corresponds to the work spent mainly in LIVC engines to perform the blow-back of mixture from the cylinder to the intake manifold. It can be expressed in terms of *mep* as:

$$ICWmep = \frac{1}{V_d}\int_{BDC}^{IVC}\left(p_{measured} - p_{extrapolated}\right)dV \tag{4.58}$$

In this case the extrapolation is made from the compression data after IVC down to BDC.

The total value of the pumping work can be expressed as:

$$PMEP = PMEP_{360} + ICWmep + EVO_{loss}mep \tag{4.59}$$

These methods were used to evaluate and compare the expected pumping losses in engines working under the Miller cycle whether by EIVC or LIVC. From the results of the simulations performed, the pumping losses were calculated using method 1 first (360º integration) and secondly the corrected method described above [13]. Figure 4-10 presents the pumping loops of the three cycles (Otto, Miller LIVC and Miller EIVC) for an approximately constant load of 6.3 bar bmep. Looking at these p-V diagrams and using the convention of the 360º integration it can be seen that the Miller LIVC cycle presents less pumping losses. Figure 4-11 shows pumping losses calculation using the 360º integration. In the Otto cycle engine, pumping losses increase with the decrease of load, as expected, due to the use of the throttle valve, which reduces the pressure in the intake manifold. In the case of the Miller engine two situations may occur depending on

the load control strategy used. When LIVC is used, the pumping losses calculated by the first method decrease with the load. That is understandable as the pressure at BDC after the opening of the exhaust valve becomes significantly lower. When the EIVC load control strategy is used, two phenomena must be considered. First there is a reduction of the pressure at BDC after the exhaust valve opening leading to a reduction of the pumping losses. On the other hand the intake valve open area is reduced with load decrease, leading to higher pumping losses. These two phenomena reduce pumping losses up to 7 bar bmep and increase it as load reduces onwards that point.

In the case of the engine simulated here especially due to the large delays of IVC used, the effect of the blow-back after BDC have to be considered in the pumping losses calculations. Using the corrected method proposed above [13], the pumping losses become significantly different for the case of the LIVC strategy. Figure 4-12 presents the pumping losses calculated using the referred corrected method. In this case there is a slight increase in the values of the pumping losses for the Otto cycle engine and for the Miller EIVC engine, due to the addition of the losses from EVO until BDC and from BDC until IVC (only in the Otto cycle). When LIVC strategy is evaluated by the corrected method, the pumping losses due to the blow-back phenomenon increase significantly with the load decrease. In fact blow-back increases with the load decrease. Figure 4-13 shows the increase of the *ICWmep* component for the Miller LIVC engine cycle.

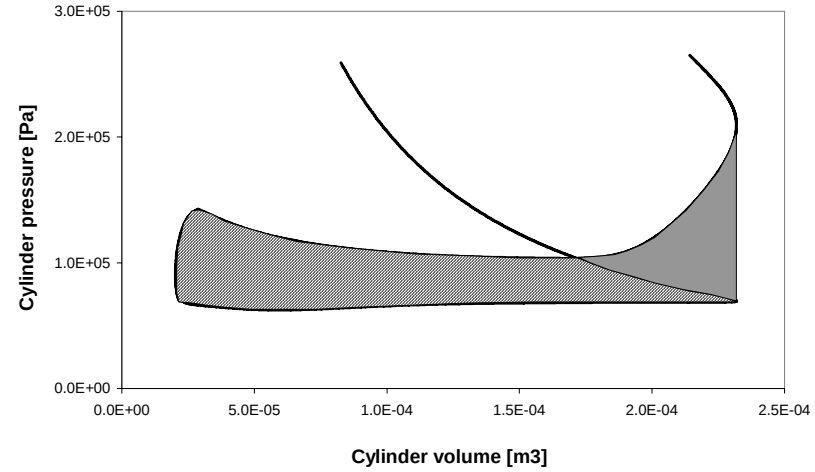

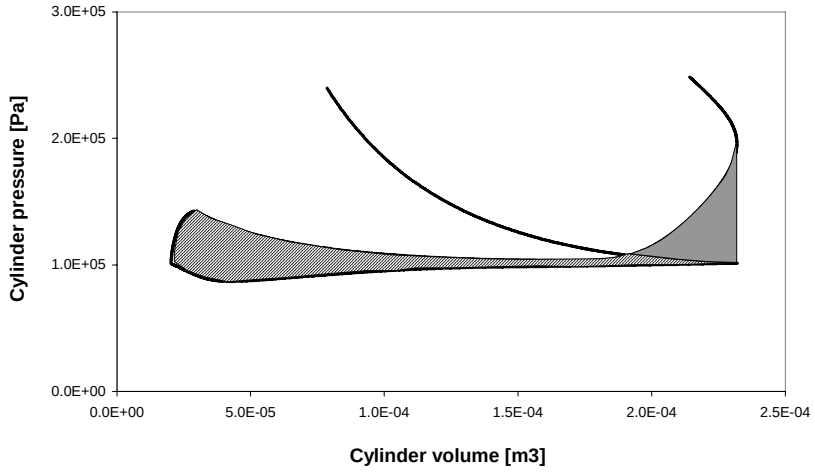

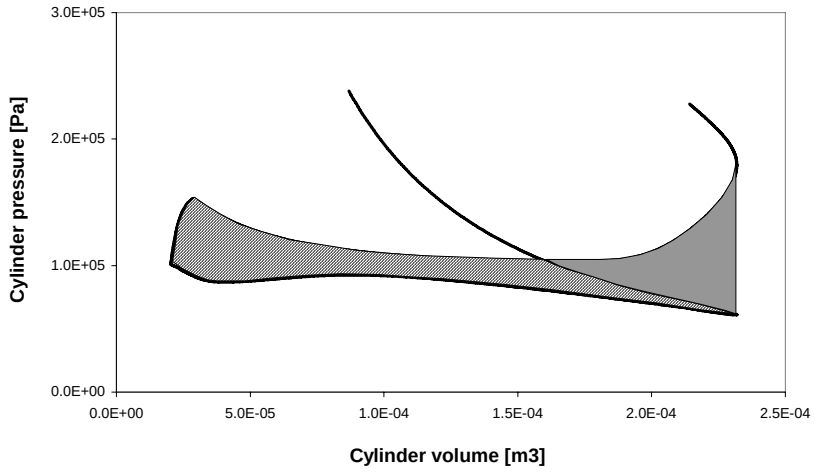

Figure 4-10 – Pumping loops for the Otto, Miller LIVC and Miller EIVC cycles.

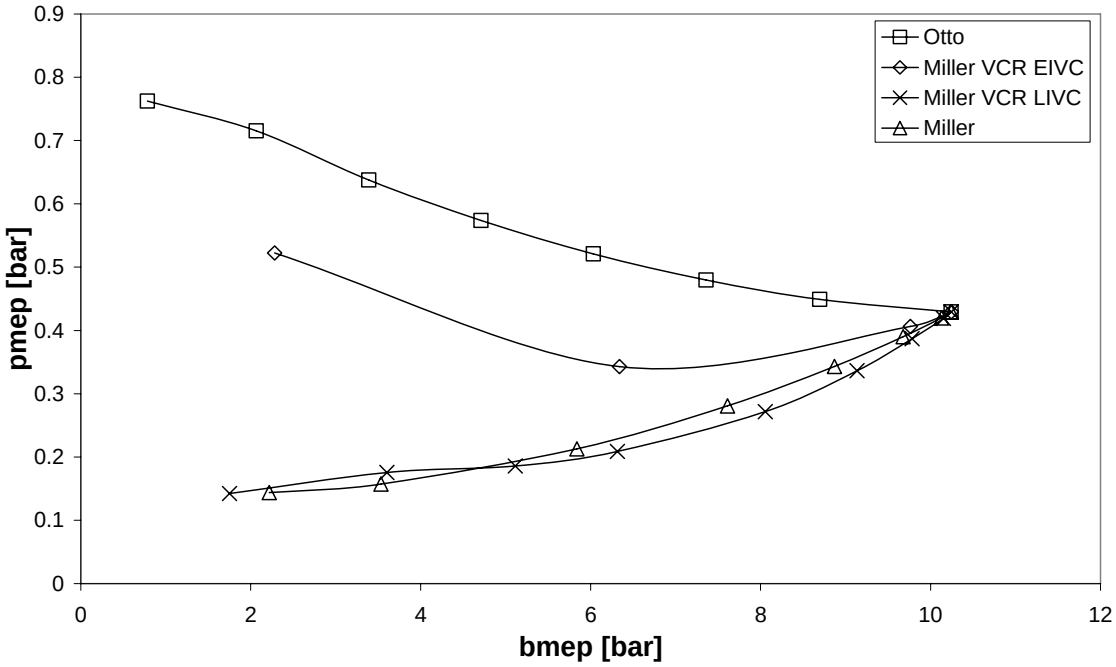

Figure 4-11 – Pumping losses calculated by the 360º integration.

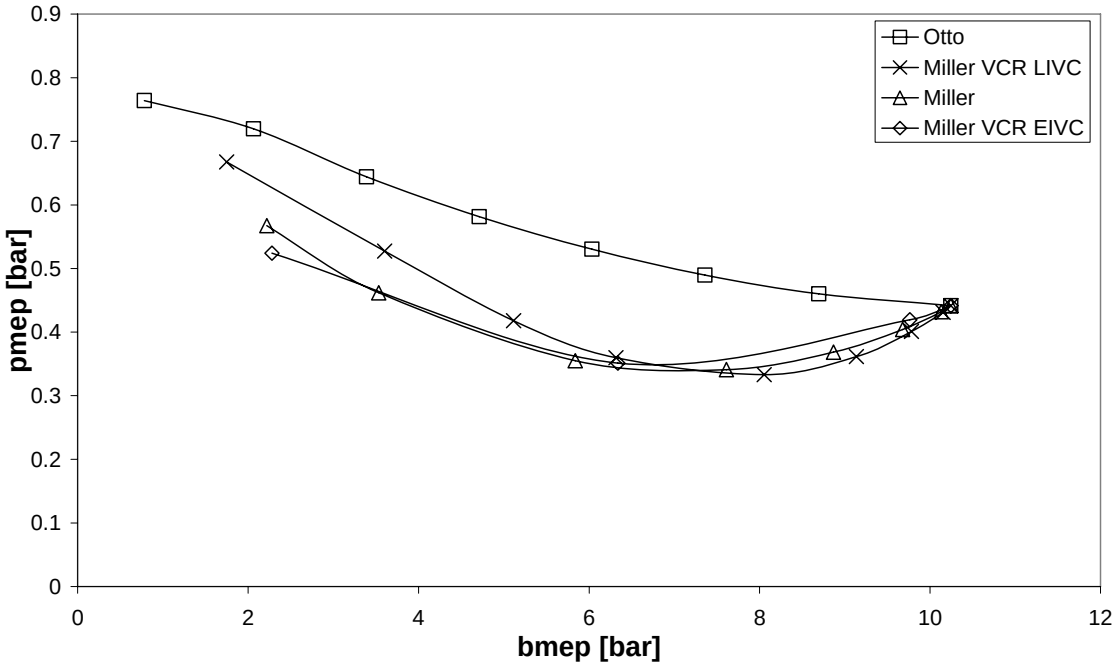

Figure 4-12 – Pumping losses calculated with the corrected method.

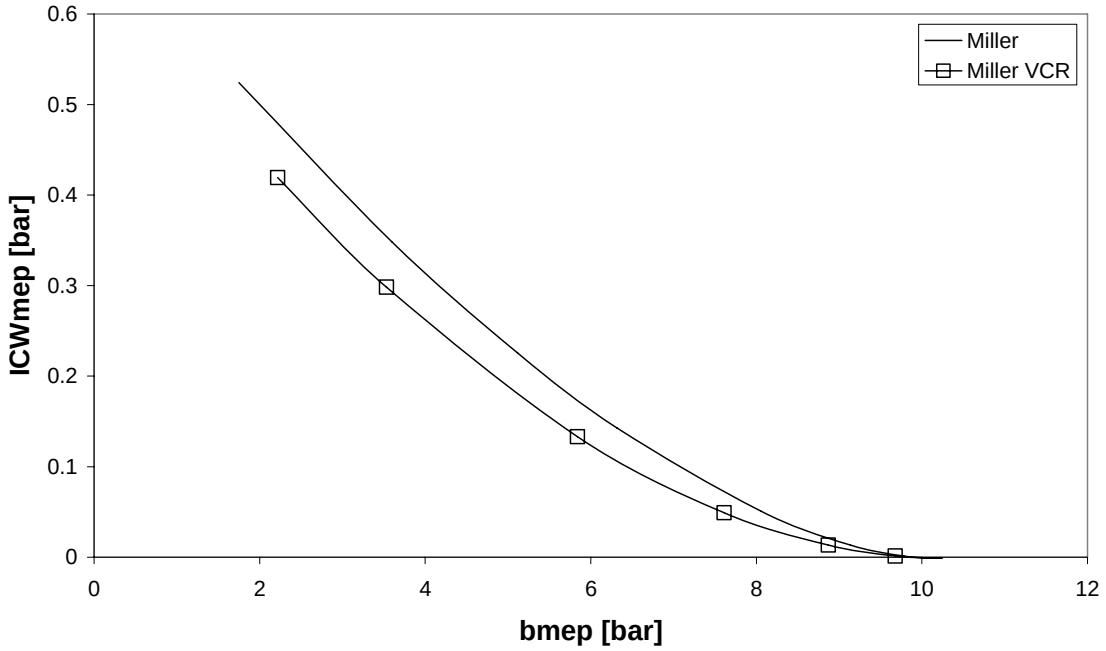

Figure 4-13 – Pumping losses during the period from BDC to IVC in the Miller cycle engine, using LIVC.

4.4 Automotive Application [14]

A four cylinder 1.4L engine was simulated in order to get its performance when used in an automotive application. The engine configuration is described in Table 4-4. This engine size was chosen as a typical engine for a small city car. In the Otto cycle the load variation was obtained by the reduction of the intake manifold pressure from the atmospheric pressure (101 kPa) down to 30 kPa, which corresponds to a 10 % of the full load torque. The tests were performed for an engine speed ranging from 1500 to 3750 rpm. The simulation speed range was limited by these values since the speed demanded by the chosen driving cycle has a maximum value of 3250 rpm, as described bellow.

The results of the Otto cycle engine simulations are presented in Figure 4-14 as a specific fuel consumption map.

The Miller cycle was simulated with the same engine, but the load variation was not made by varying the intake manifold pressure (or throttle valve position). In this case the load was set by reducing the effective opening of the inlet valve, changing with it the IVC timing.

Table 4-4 – Otto cycle gasoline engine configuration.

Bore [mm]	75
Crank Radius [mm]	40
Connecting rod length [mm]	119
Combustion chamber height [mm]	7.3
Intake Valve Diameter [mm]	30
Exhaust Valve Diameter [mm]	25
IVO [CA]	20 BTDC
IVC [CA]	32 ABDC
EVO [CA]	40 BBDC
EVC [CA]	12 ATDC

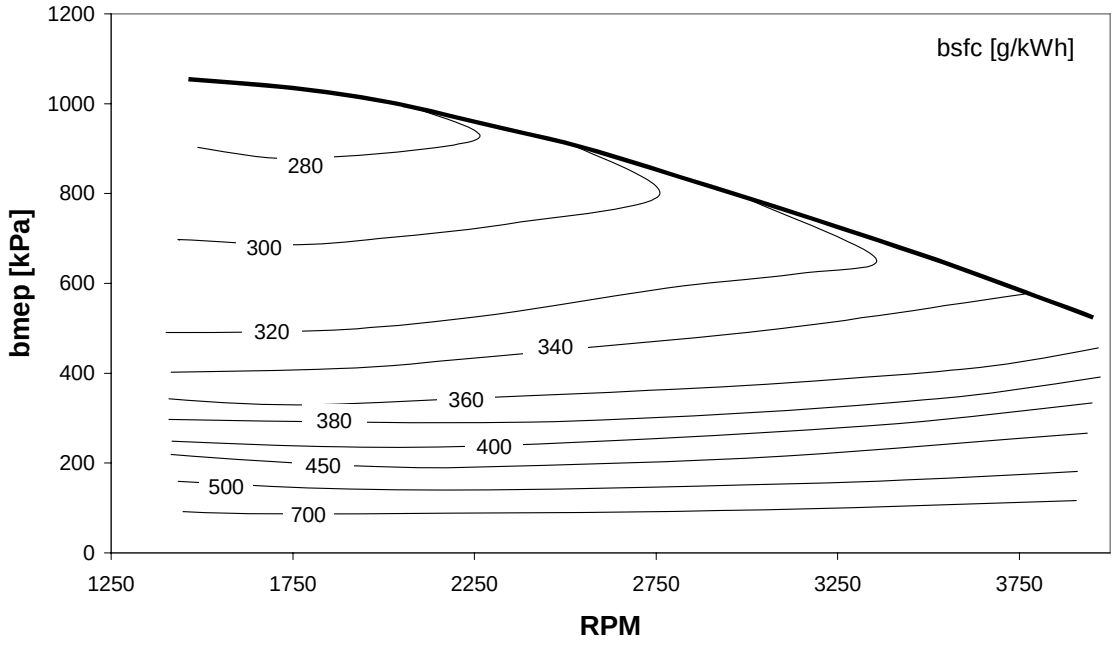

Figure 4-14 – Break Specific fuel consumption map of the Otto cycle.

At each engine load simulation the combustion chamber height was changed in order to always get the same maximum pressure and temperature. This modelled the VCR effect. The value for the maximum pressure was set by the maximum pressure obtained with the Otto cycle simulations, which was 67 kPa.

The results of the Miller cycle engine simulations are presented in Figure 4-15 as a brake specific fuel consumption map.

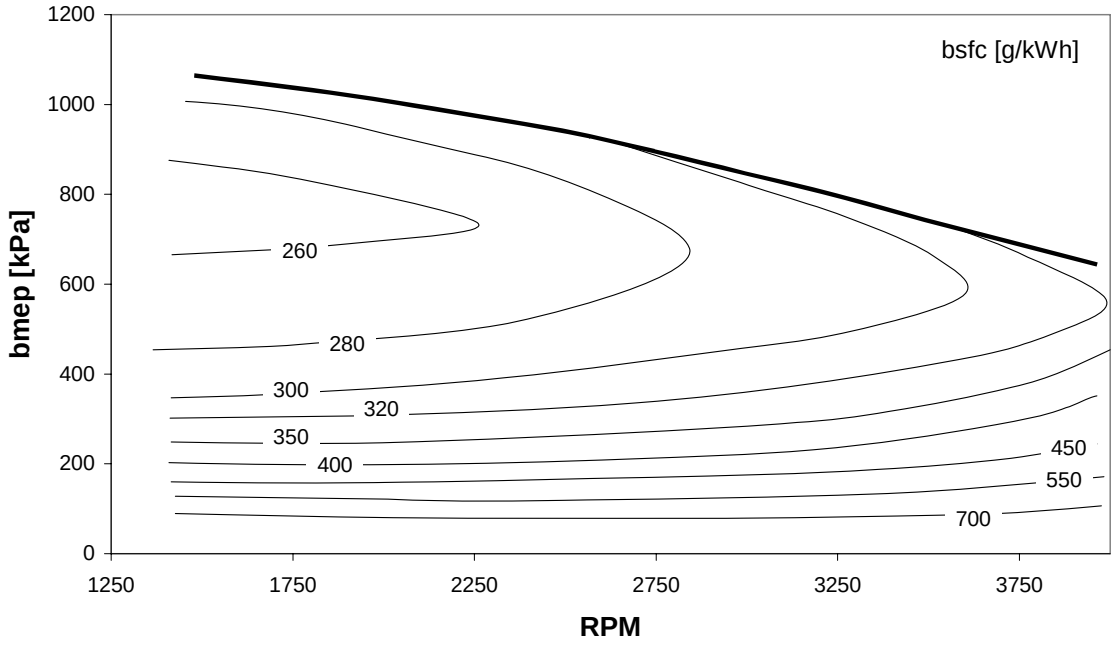

Figure 4-15 – Break specific fuel consumption map of the Miller engine.

When comparing both engines (Figure 4-14 and Figure 4-15) it can be seen that, as expected, the thermodynamical performance of the Miller cycle engine is better than that of the Otto cycle one. The difference in terms of break specific fuel consumption (bsfc) between the two engines is presented in Figure 4-16. At part load operation the difference (Otto – Miller) increases showing the better performance of the Miller engine in relation to the Otto cycle engine at these conditions.

The data resulting from the computer model previously described were used to simulate a car performing a defined driving cycle and thus to compare the benefits when using this new engine arrangement. Driving cycles are generally defined by the vehicle speed and the gear selection. Together with actual tire dimension and gear ratios it is possible to define the required engine speed. The load will depend on vehicle inertia and running resistance (mainly defined by the rolling resistance), air drag and weight of the vehicle. It is important to remember that this load is related to the amount of power at the wheels and not at the flywheel of the engine. If the load is to be related to the engine, then the actual transmission losses must be added. Figure 4-17 shows the New European Driving Cycle (NEDC), which was chosen to calculate the required power at the wheels.

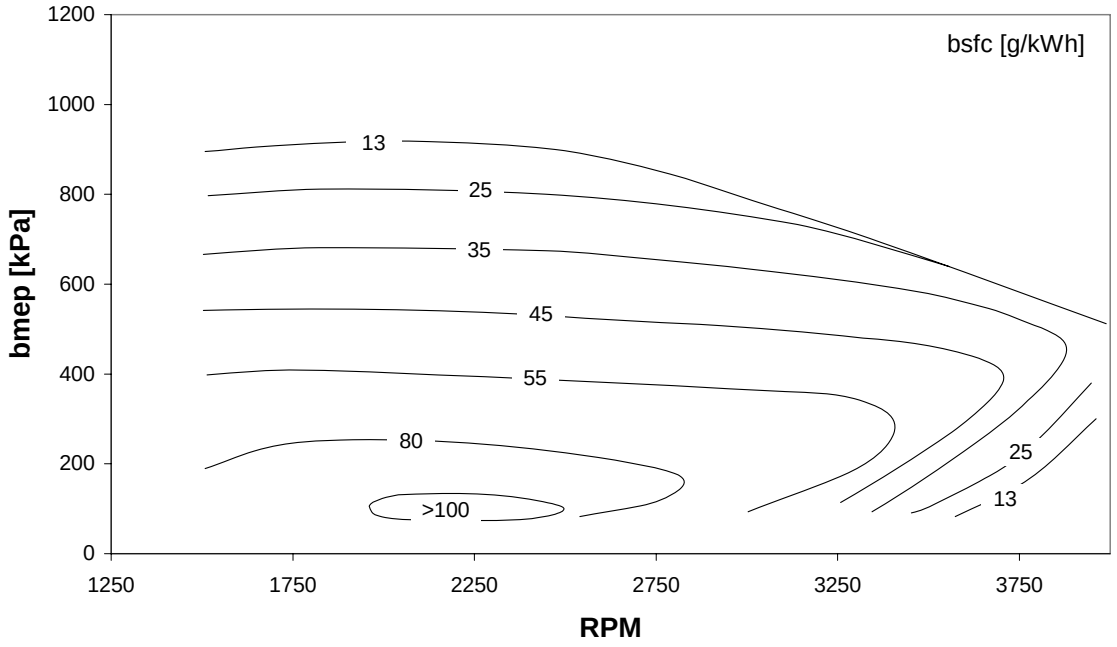

Figure 4-16 – Break Specific fuel consumption difference (g/kWh).

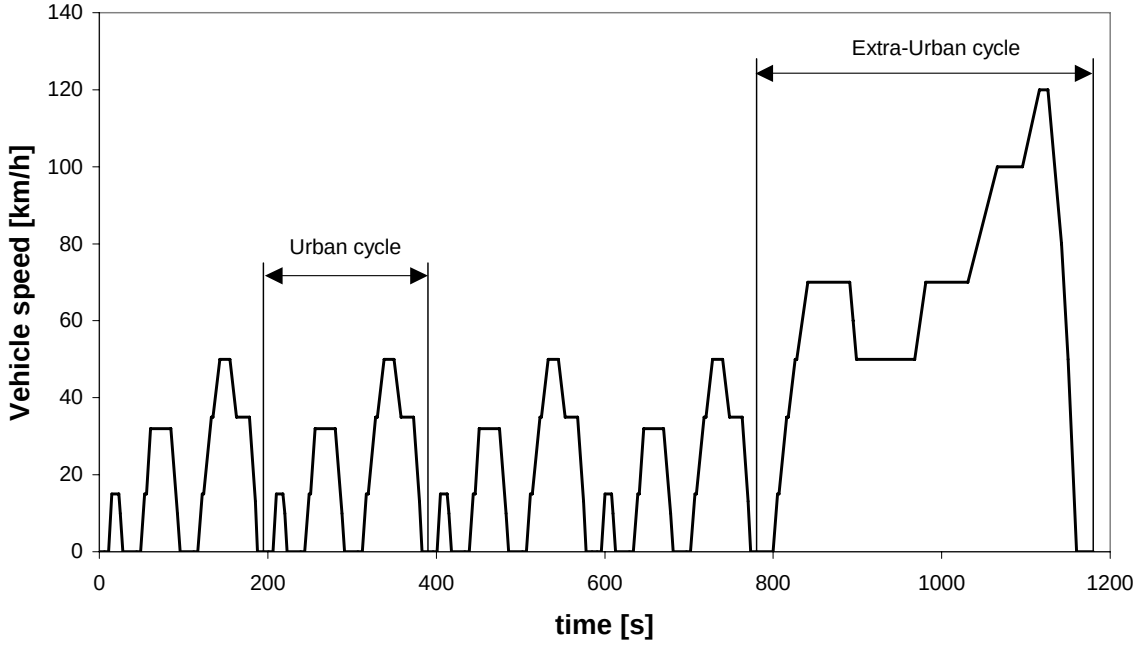

Figure 4-17 – New European Driving Cycle.

Newton's first law is applied to obtain the engine torque during the driving cycle as described below.

$$F = C_{tre}\frac{T(N)\cdot G\cdot g_k}{r} - C_{rr}\cdot m\cdot g - \frac{C_d\cdot A\cdot \rho\cdot v^2}{2} \tag{4.60}$$

and

$$F = m \cdot a \tag{4.61}$$

where:

F : net force acting on the car
C_{tre} : transmission efficiency coefficient
$T(N)$: engine torque as function of engine speed
G : final drive ratio
g_k : k-th gear ratio
r : radius of tire
C_{rr} : rolling resistance coefficient
m : mass of the car
g : gravity acceleration (9.8 ms^{-2})
C_d : drag (air resistance) coefficient
A : frontal area of the car
ρ : air density
v : car velocity

Engine speed at every instant of the driving cycle, as shown in Figure 4-18, is calculated using the relationship:

$$N = \frac{v \cdot G \cdot g_k}{r} \tag{4.62}$$

Table 4-5 describes the values of the variables used to calculate the power demand during the driving cycle simulation. These values correspond to an advanced city car characteristics with a five speed gear box.

Combining (4.60) and (4.61) it is possible to obtain the required engine torque $T(N)$ at every instant of the driving cycle. Engine speed at every instant of the driving cycle can be obtained from relation (4.62). With this torque and engine speed, it is possible to calculate the fuel consumption for each engine using their respective performance map.

From the vehicle speed, gear ratio and acceleration at each instant, the engine speed and the corresponding engine torque can be calculated, hence engine power can also be calculated by the expression:

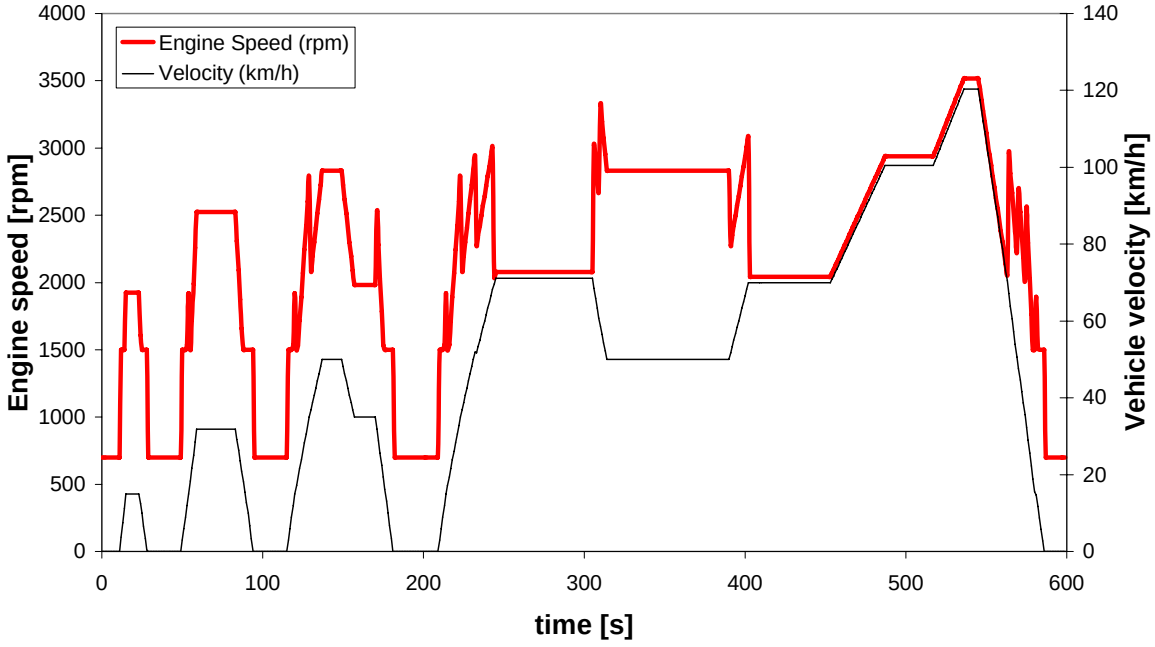

Figure 4-18 – Engine speed and vehicle speed during the NEDC.

$$\dot{W} = T \cdot N \tag{4.63}$$

Table 4-5 – Car characteristics.

Mass	1050 kg
Drag coefficient (C_d)	0.2
Frontal Area	2.1 m^2
Tire Radius	0.3 m
Rolling resist. coef. (C_{rr})	0.015
1st gear ratio	3.827
2nd gear ratio	2.36
3rd gear ratio	1.685
4th gear ratio	1.312
5th gear ratio	0.9
Final drive ratio	3.8
Transmission efficiency coef. (C_{tre})	0.9
Idle engine speed	700 rpm

Power was calculated for each driving instant of the NEDC. These values are plotted in Figure 4-19 and, as can be seen, the maximum required power is 27 kW when the speed is high and the car is still accelerating.

The engine speed may also be calculated the same way. Figure 4-18 shows that the maximum engine speed has a value of 3520 rpm during the period of maximum vehicle speed.

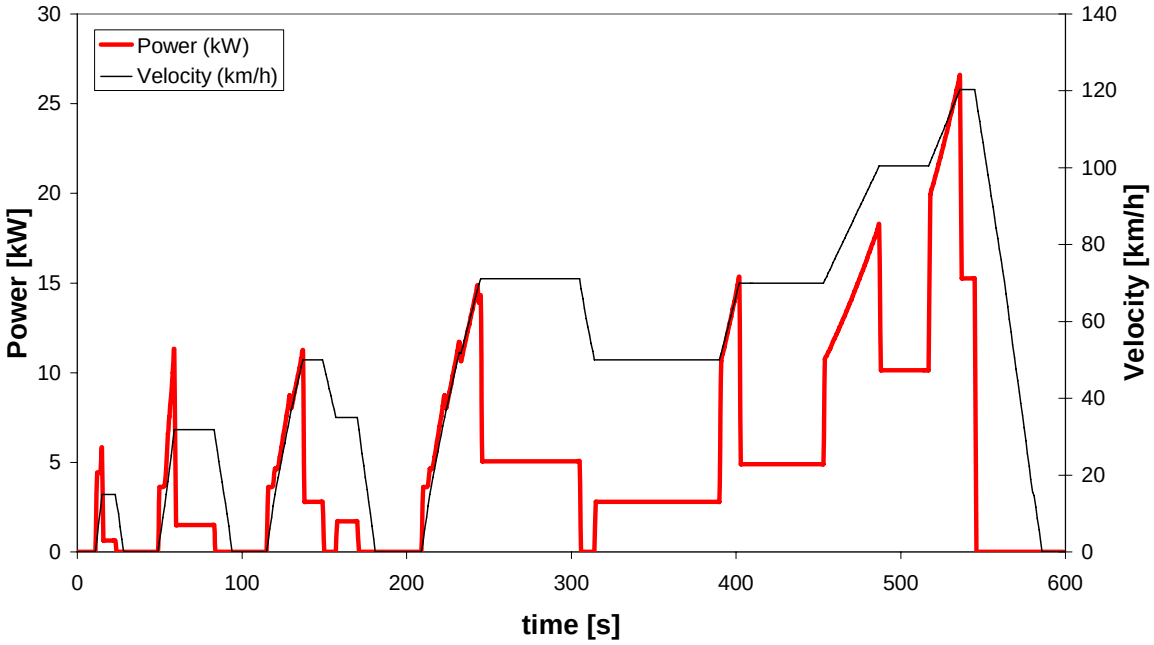

Figure 4-19 – Power demand and vehicle speed during the NEDC.

4.4.1 Comparison of the Two Engines With a Manual Gear Box

Simulations were made using the same car (including similar gear box) and the same driving cycle with the two engines described above (Otto and Miller).

4.4.1.1 Otto Cycle Engine

Figure 4-20 shows the results of the instantaneous fuel consumption. Integrating the values for the whole cycle it is possible to obtain the total fuel consumed during the cycle. Considering the total distance run, the mileage (fuel consumption) for this cycle engine is 17.8 km/L, or 5.6 L per 100 km.

4.4.1.2 Miller Cycle Engine

The use of the Miller cycle engine was tested in the same car and lead to the fuel consumption rate presented in Figure 4-21. Again integrating the values of the fuel

consumption rate for the overall driving cycle gave the total amount of fuel consumed. Considering the total distance run in the cycle, the mileage for this engine results in 19 km/L, or 5.3 L per 100 km.

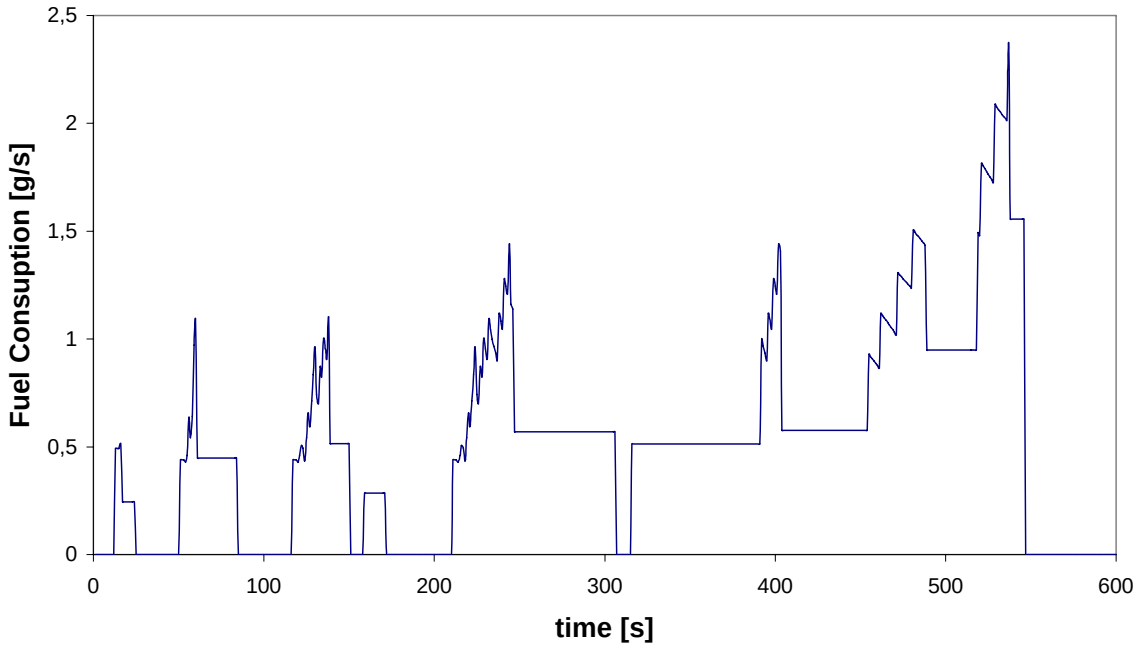

Figure 4-20 – Otto cycle engine fuel consumption rate.

When comparing the two engines using the same car and the same gear box, the improvement by the use of the Miller cycle is 0.3 km/L, which represents a 6% saving of fuel consumed.

If the operating points for the New European Driving Cycle, are plotted over the bsfc maps of both engines, using the described manual gear box (Figure 4-22 and Figure 4-23), it can be found that in the case of the Otto cycle most of the operating points lie below the 320 g/kWh line of bsfc. In the case of the Miller cycle a significant number of operating points lie between the 280 and 320 g/kWh lines of bsfc.

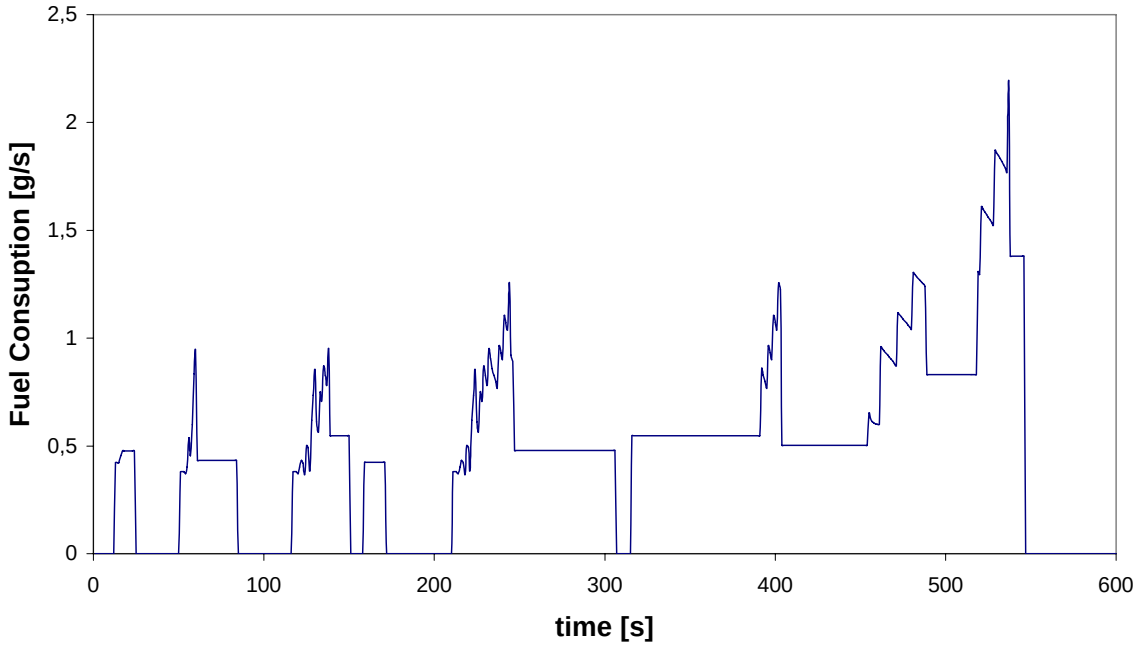

Figure 4-21 – Miller cycle engine fuel consumption rate with manual gear box.

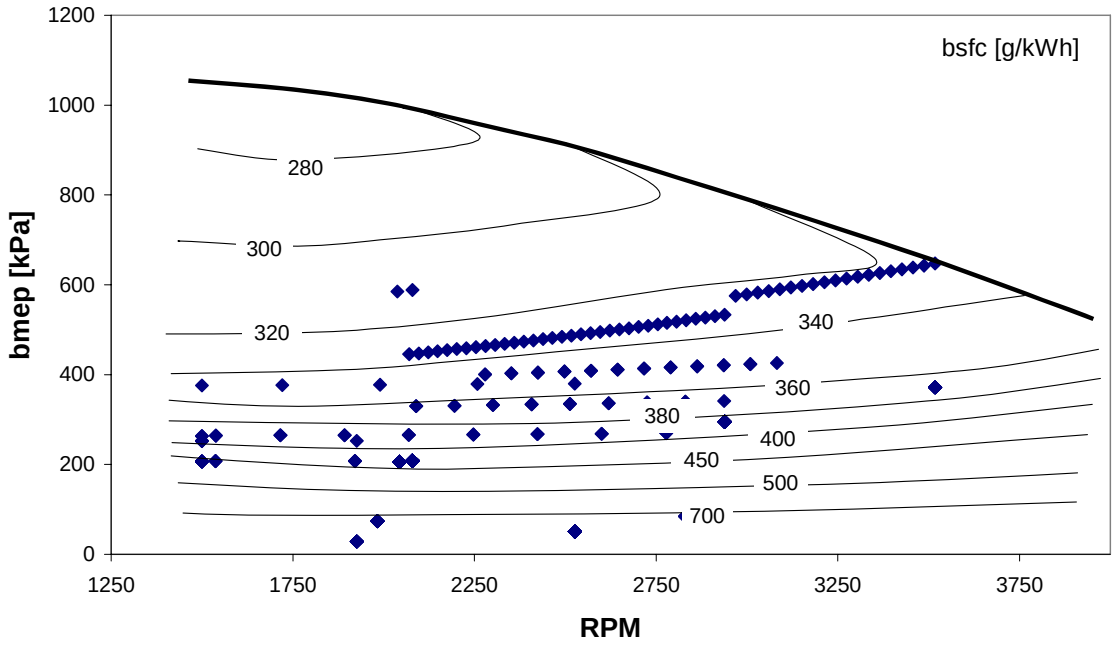

Figure 4-22 – Operating points of the Otto cycle engine with manual gear box.

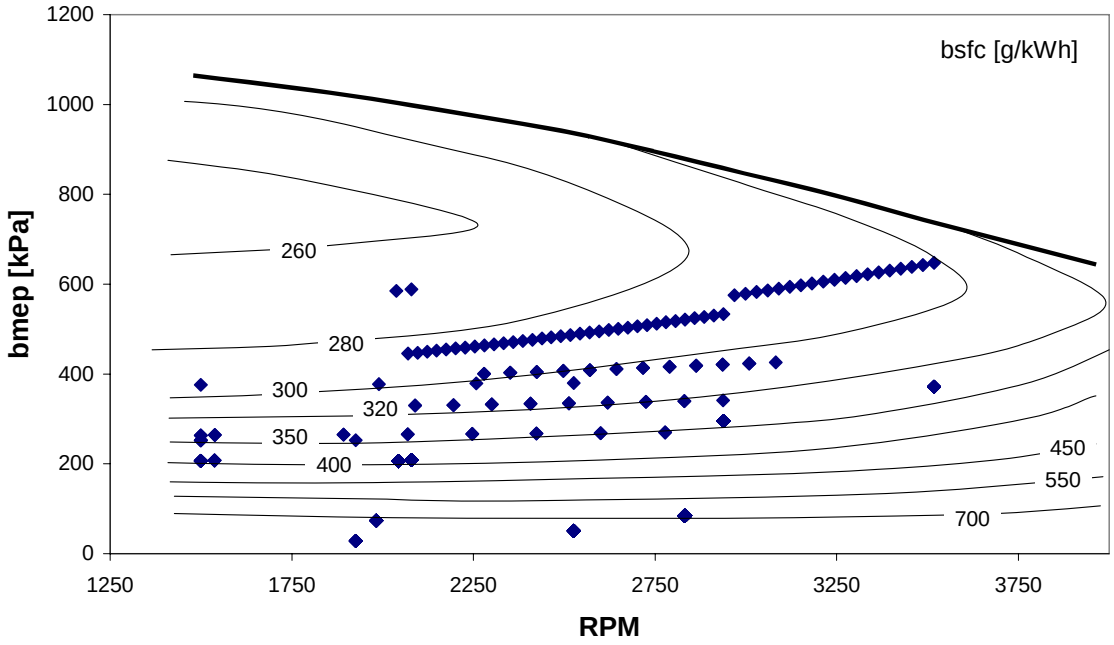

Figure 4-23 - Operating points of the Miller cycle engine with manual gear box.

4.4.2 Improving with CVT

An important improvement was reached by just changing the engine, but a second interesting improvement can be obtained if the gear box adapts itself to the engine lower consumption level as the car speed changes. That is the main benefit of continuous variable transmission (CVT). With this kind of transmission the ratio may be changed, or made to change, in order to always have the lowest bsfc conditions at any working point. In theory the amount of gears is infinite.

So, for a particular instant in the driving cycle the power required is known. This power can be transmitted at different engine speed and torque values. But with a continuous variable transmission the torque/speed coordinate with minimum fuel consumption can be chosen for optimal fuel consumption at each instant.

An algorithm was developed to determine the minimum fuel consumption for each point of the power curve. Since power is known, (4.62) was used to determine the best (T, N) point (which corresponds to minimum fuel consumption point) in the maps of Figure 4-14 and Figure 4-15.

4.4.2.1 Otto Engine

Using the same method described for the manual gear box, the fuel consumption rate for the Otto cycle engine working in a car with CVT and managed in a manner to have the lowest fuel consumption possible is represented in Figure 4-24. The mileage using the NEDC is of 19.8 km/L or 5.1 L per 100 km, which represents an improvement of 10% relatively to the same engine operated with a manual gear box.
Using the Otto engine cycle, the operating zone of the engine using CVT is shown in Figure 4-25. It is possible to figure out that the minimum fuel consumption points are mostly used during engine operation.

4.4.2.2 Miller Engine

Using the Miller cycle engine with the CVT technology, the mileage of this engine during the NEDC is 22.2 km/L or 4.5 L per 100 km, which represents an improvement of 14.5% relatively to the same Miller engine using the manual gear box. The value for the fuel consumption rate during the cycle is presented in Figure 4-26.

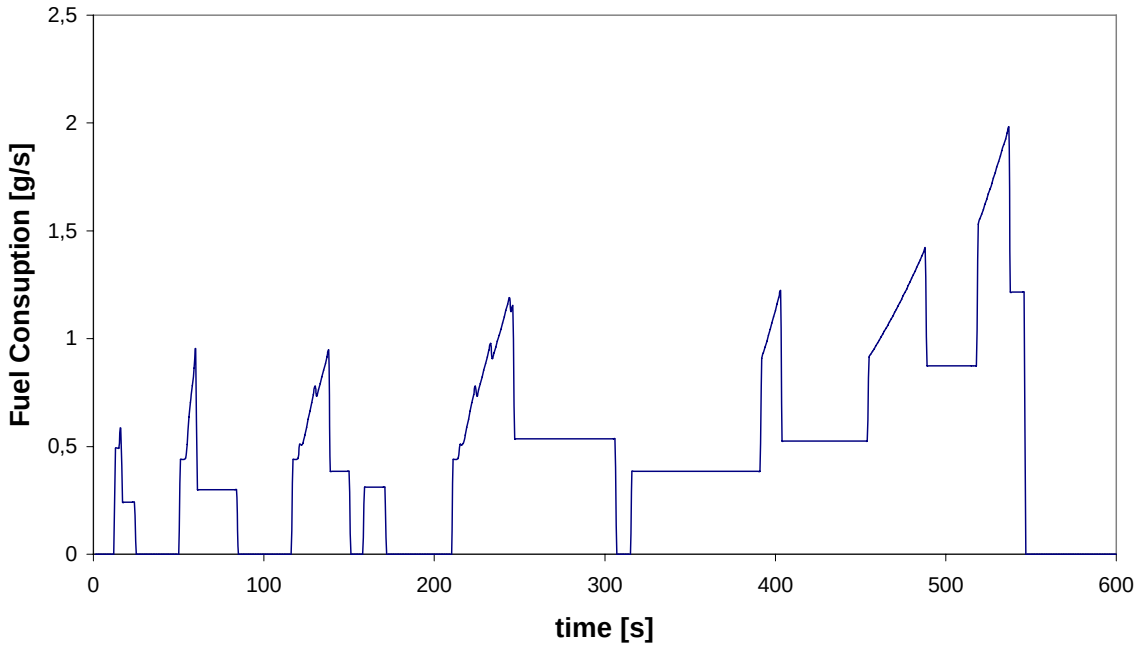

Figure 4-24 – Fuel consumption rate for the Otto cycle engine with CVT during the NEDC.

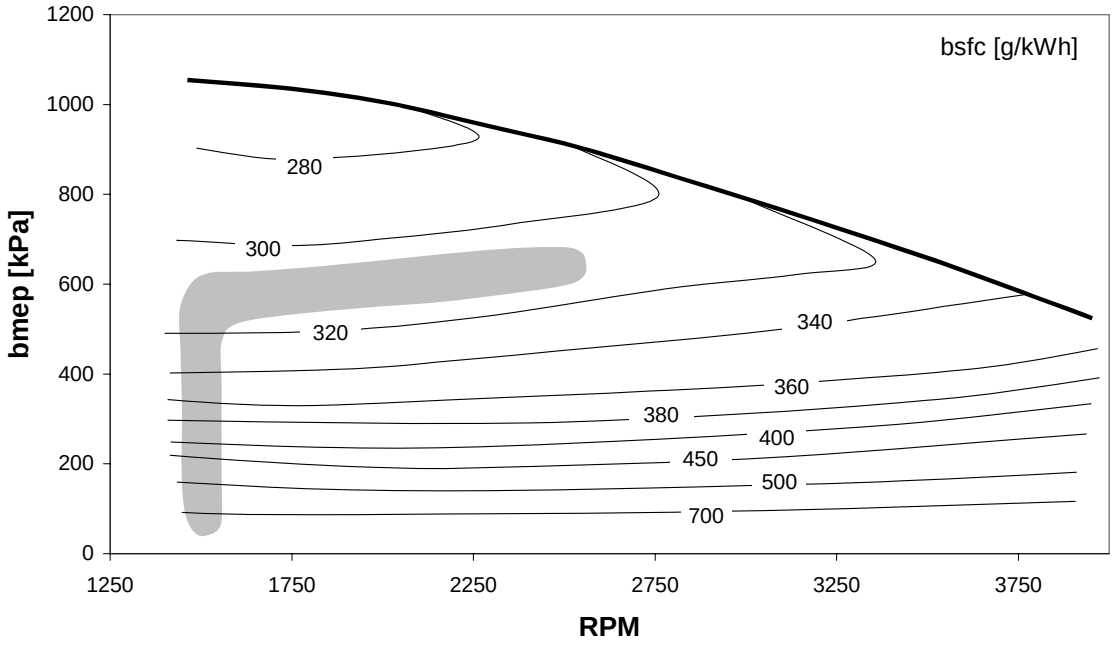

Figure 4-25 - Zone of engine operation for the Otto cycle engine using CVT.

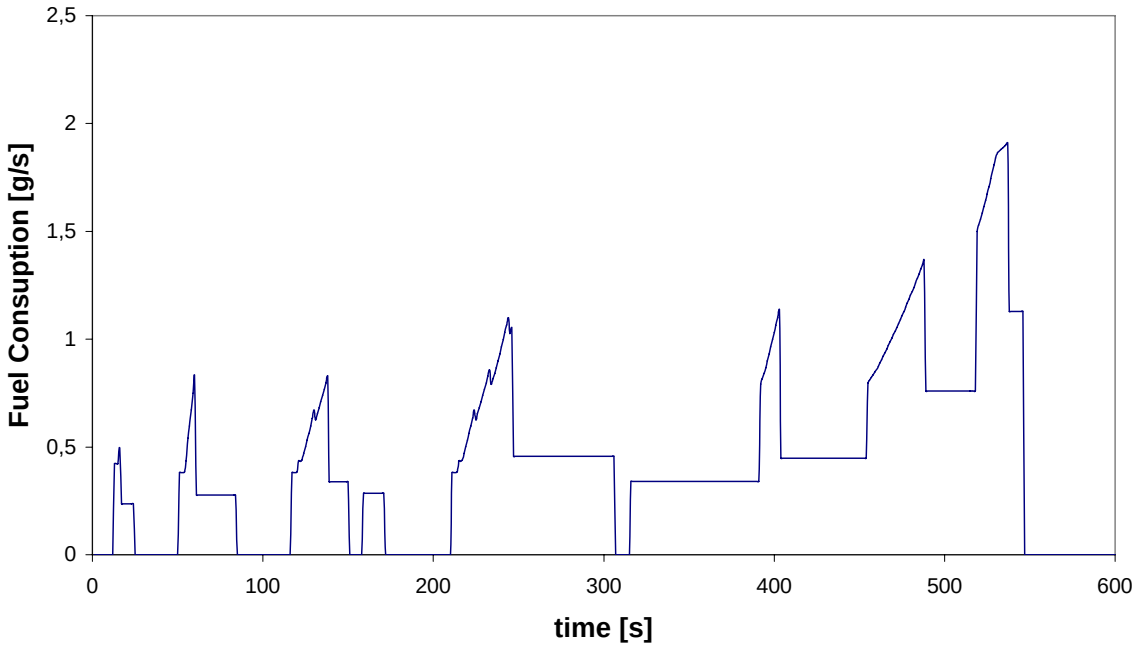

Figure 4-26 - Fuel consumption rate for the Miller cycle engine with CVT during the NEDC

In the case of the CVT, the mileage for Otto cycle engine comes out to be 19.8 km/L, and for the Miller cycle engine it comes out as 22.2 km/L, which represents a gain of 12%.

Using the Miller engine cycle, the operating zone of the engine using CVT is shown in Figure 4-27. This zone covers a significant area of lowest bsfc values.

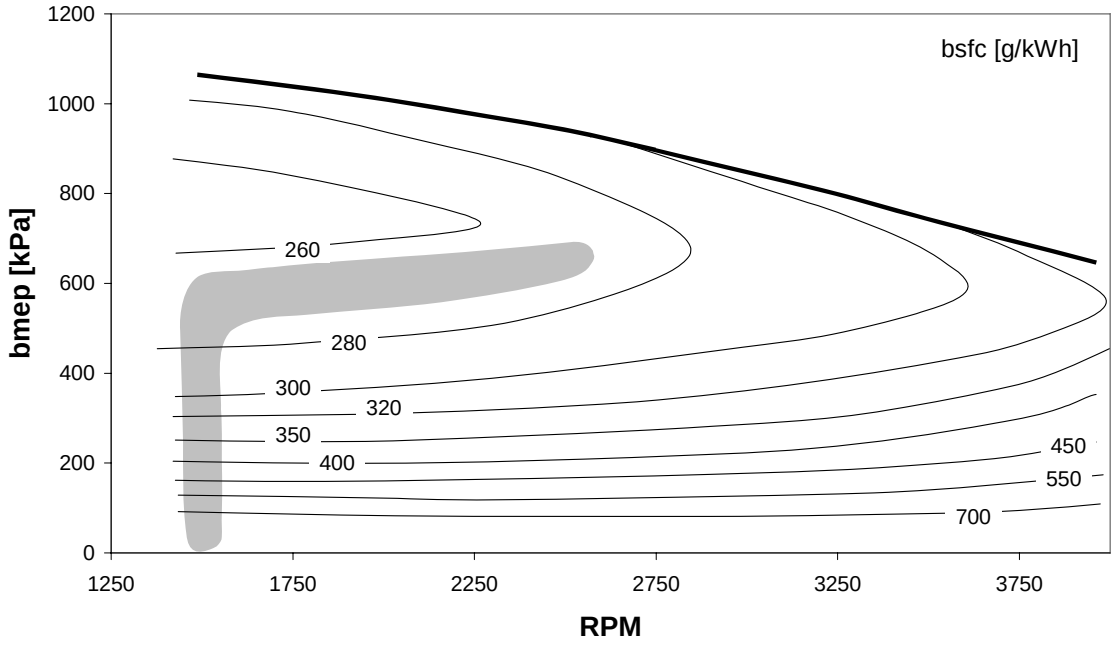

Figure 4-27 – Zone of engine operation for the Miller cycle engine using CVT.

The Otto cycle engine with CVT has 2.0 km/L more mileage than the Otto cycle engine with manual transmission. The Miller cycle engine with CVT has 3.2 km/L more mileage then Miller cycle engine with manual transmission. This highlights the greater number of low brake specific fuel consumption points in the Miller cycle performance map (Figure 4-27).

The continuous variable transmission obviously gives more mileage because of the large number of transmission ratios possible. However, usually this type of transmission is considered less efficient than a normal gear box, which should reduce the differences between both technologies, but in the simulations a constant value for the transmission efficiency is considered in both cases.

4.5 Model Calibration

After engine tests, a significant amount of information on the performance of the engine is available. This set of data can be used for comparison with the output from the computer model and to calculate the adequate coefficients, which are then introduced in the model so that its output is tuned to the real situation. After this engine calibration task, the resulting output from the model is similar to the real engine output results. The

model can then be used to simulate the engine in other working conditions and reliable results can be achieved.

4.5.1 Calibration strategy

The main variables obtained from the engine tests are: engine speed, torque, fuel consumption. With the value of these variables several performance parameters may be calculated as power, break mean effective pressure, specific fuel consumption and volumetric efficiency. In the model structure, torque, power and specific fuel consumption are calculated from break mean effective pressure results after friction mean effective pressure has been applied over the indicated data. Volumetric efficiency of the model is calculated using the amount of fuel mass trapped in each engine cycle. As this parameter depends only on the mass flow sub-model, the first coefficient (B1) to be introduced in the model corrects the amount of mass trapped in each engine cycle in order to obtain the same volumetric efficiency as the real engine. This correction is made via a reduction of the intake pressure (input to the mass flow rate calculation: equations (4.27) and (4.29)). The value of this first parameter was determined by trial and error until a difference of 2% or less was obtained when comparing the volumetric efficiency calculated from the model with the tests results.

A second coefficient (B2) was used to correct directly the value of the mean effective pressure. This coefficient introduces corrections related to the friction value, heat transfer and combustion models. It is multiplied by the calculated break mean effective pressure from the model and its value is determined by dividing the break mean effective pressure obtained from the engine tests by the break mean effective pressure obtained after the correction of the first coefficient mentioned above. The error of the resulting mean effective pressure in this case is negligible (always less than 1% on the break mean effective pressure).

Data resulting from friction measurements extend through a very narrow range and their use for model calibration is not possible. This is the reason for the correction for bmep to be made directly and no correction being made over friction mean effective pressure. The model results in terms of friction are the same with or without calibration.

For the Otto cycle the coefficients are a function of the engine speed and the throttle position. In the case of the Miller and Miller VCR engine, coefficients are function of engine speed and IVC timing (both EIVC and LIVC).

4.5.2 Calibration results

Calibration coefficients for all cycle models are presented in Annex C. The results from the calibrated model in terms of volumetric efficiency and in terms of bmep have an error of 2% or less for all the engine cycle models. In terms of thermal efficiency (or specific fuel consumption) the results have an error that is higher than the 2% limit. Figure 4-28 presents the error of the thermal efficiency calculation for the Otto cycle and Figure 4-29 presents the same parameter for the Miller cycle. As can be seen the calculations for speeds higher than 3000 rpm in the Otto cycle are not reliable, showing errors that can go higher than 20%. For the Miller cycle, the error never goes over 8% but again, at the highest speed, the error is the largest.

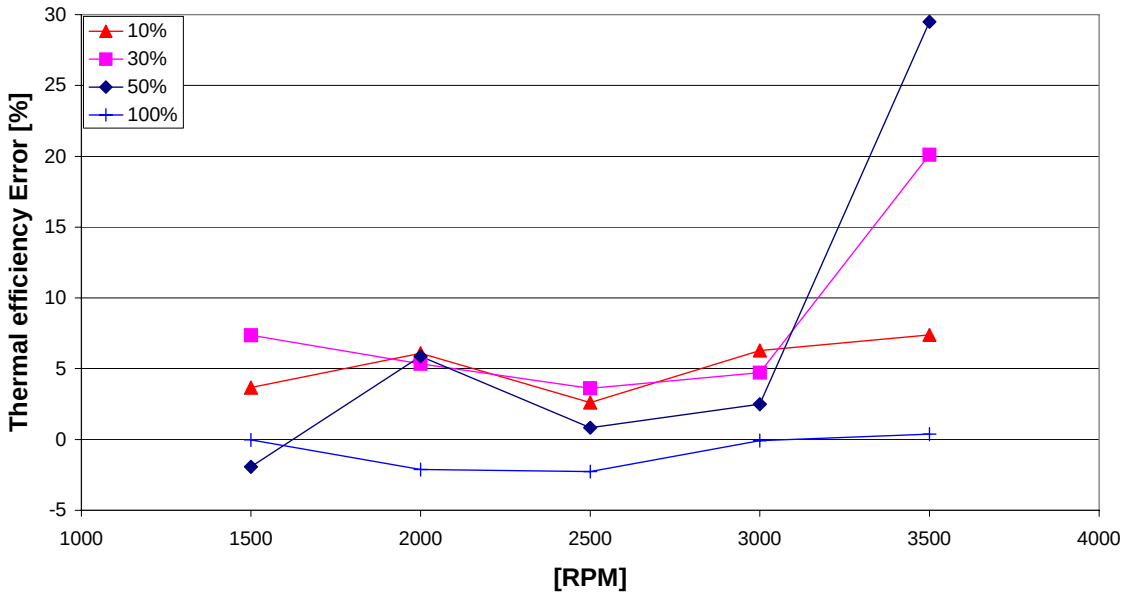

Figure 4-28 – Thermal efficiency error of the calibrated Otto cycle engine model, for several throttle positions.

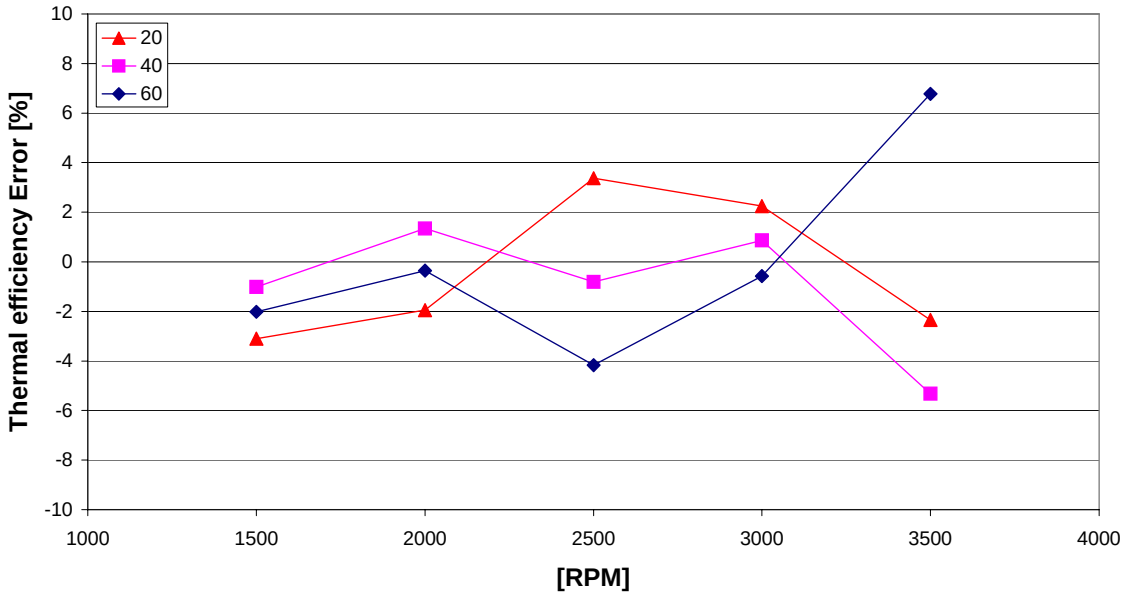

Figure 4-29 - Thermal efficiency error of the calibrated Miller cycle engine model.

4.6 Second Law Analysis

Thermodynamic optimisation of thermal engines or systems has begun to be applied to low temperature refrigeration as a method of design and optimisation [15]. It can be performed under the equivalent titles of entropy generation minimization (EGM), finite-time, and endoreversible thermodynamics. Thermal engines have been analysed using finite time thermodynamics [16,17,18], however this analysis tends to be abandoned due to fundamental flaws, over-reliance on highly simplified models and lack of engagement with real-world considerations [19].

The optimisation of endoreversible engines has being made through four main paths: power output, thermal efficiency, entropy production and an ecological benefit. The latter represents a good compromise between high power output and low entropy production. This ecological optimisation criterion consists of the maximization of a function E that represents a good compromise between high power output and low entropy production. This function is given by [20]:

$$E = P - T_2 \cdot S_{gen} \tag{4.64}$$

Where P is the power output of the cycle, S_{gen} the total entropy production (system plus surroundings) per cycle, and T_2 is the temperature of the cold reservoir. When (4.64) is maximized the cycle efficiency is given by [20]:

$$\eta_E \approx \frac{1}{2}\left(\eta_C + \eta_{CA}\right) \tag{4.65}$$

Where η_C is the Carnot efficiency and η_{CA} is the Curzon-Alhborn efficiency [21].
Endoreversible engines are modelled locating all the entropy sources at the links between the working fluid and the environment. However, this method leads to engine models which are very sensitive to heat transfer laws. Hence, expression (4.65) was demonstrated [20] to be independent of the heat transfer law using a function that links power output with entropy production (also being independent of the heat transfer law). A corollary of (4.64) was presented stating that the power output at the maximum ecological regime is 75% of the cycle's maximum power and the entropy produced at the same regime is only 25% of the entropy produced at the maximum power. These proves lead to some discussion on the subject [22,23].
Later a similar general property was proved to be applicable for non-endoreversible thermal engines [24]. This is just the extension of the general property already used for endoreversible engines. It is expressed as:

$$\eta^*_{ME} = \frac{1}{2}\left(\eta'_C + \eta^*_{MP}\right) \tag{4.66}$$

where η^*_{ME} is the efficiency at the maximum ecological regime, η^*_{MP} is the maximum power efficiency for the non-endoreversible engine and η'_C is similar to the Carnot efficiency but affected of the non-endoreversible parameter (R):

$$\eta'_C = 1 - \frac{1}{R}\frac{T_2}{T_1} \tag{4.67}$$

The irreversibility parameter R is defined as the ratio of the entropy entering the cycle to the entropy leaving the cycle [25]. This parameter may assume values from 0 to 1.

On the specific field of the internal combustion engines, several works have been presented lately [26,27,28,29,30,31,32,33,34,35]. Almost all refer to a Second Law analysis, but all consider just an exergy analysis or evaluation of the exergy destruction. All these works use computer models for engine simulation and are more elaborate than the models used for the finite time thermodynamics analysis.

Like mass and energy, entropy can be stored within systems and transferred across system boundaries. However, unlike mass and energy, entropy is not conserved, but generated (or produced) by irreversibilities within systems. The Entropy Generation Minimization (EGM) method widely used by Bejan [36,37,38,39] can be applied to power plants and used for optimisation of systems and processes, leading to entropy minimization as well as to power maximization. It covers heat transfer, mass exchange and thermodynamics. To apply such a method to internal combustion engines it is necessary to identify the various entropy generation mechanisms in an engine throughout the above referred entropy generation branches. In the case of internal combustion engines, entropy generation is evaluated for the overall cycle rather than for a closed system. The interest of using EGM is mainly the identification of the design variables that lead to entropy generation in the working cycle, which in turn will enable its reduction for design modifications and alterations of the working parameters.

Herein a new model is implemented in order to simulate a spark ignition internal combustion engine cycle entropy generation based on a first law model presented above. Apart from the entropy generation sources referred by Bejan (heat transfer, fluid flow, free expansion) [36-39], the entropy generation due to combustion and friction will also be considered.

As referred above, the theoretical treatment of this problem has been widely explored but there are no examples or application cases of the EGM method to internal combustion engines. This application to spark-ignition engines aims at the development of a tool for thermodynamic improvement of internal combustion engines.

4.7 Entropy generation model

The basic theoretical internal combustion engine cycle (Otto cycle), is composed of an adiabatic compression, followed by a combustion process where heat is considered to be supplied to the engine charge at constant volume. After combustion there is an adiabatic

expansion and a cooling process back to the initial point of the cycle. The entropy variation within the cycle is shown in a T-s diagram in Figure 4-30.

The theoretical diagram shown in Figure 4-30 does not represent the real indicated diagram of an internal combustion engine, once it is not considered mass transfer from and into the engine cylinder. However for the processes between points 1 and 4 (compression, combustion and expansion) the entropy variation of the theoretical and real cycles are somehow similar. The cooling process between 4 and 1 can not be compared with that of the indicated diagram because these are modelled as open systems, where mass enters and leaves the system, which leads to a T-s diagram quite different from the theoretical of Figure 4-30.

For an open system, the entropy variation may be expressed as:

$$\underbrace{\frac{dS}{dt}}_{\substack{\text{change of entropy}\\ \text{inside the control}\\ \text{volume}}} = \underbrace{\sum_i \frac{\dot{Q}_i}{T_i}}_{\substack{\text{entropy}\\ \text{transferred}\\ \text{with heat}}} - \underbrace{\sum_{out} \dot{m}s - \sum_{in} \dot{m}s}_{\substack{\text{entropy flow rate corresponding}\\ \text{to mass flowing in and out}\\ \text{of the control volume}}} + \underbrace{\dot{S}_{gen}}_{\substack{\text{Rate of entropy}\\ \text{generated}}} \tag{4.68}$$

The entropy variation of a system/control volume is equal to the sum of three components: the entropy transferred to the surroundings through heat, the entropy transferred with mass exchange and the entropy generated due to irreversibilities of the various thermodynamic processes happening during the engine cycle. Figure 4-31 shows the difference between a theoretical and a real process. In both situations a variation in the entropy of the system is expected. However, the final entropy is not the same at point 2 and 2'. This is due to a certain amount of excess entropy generated during the transformation between 1 and 2.

The total entropy generated is calculated by adding the entropy generated due to each particular irreversibility mechanism. This approach enables observing the direct interaction between various design concepts and the irreversibilities [40].

In the internal combustion engine, the entropy generation occurs due to the heat transferred into and from the cylinder charge, gas flow through intake and exhaust valves, during the free expansion at intake and exhaust, internal friction, and combustion (due to a chemical irreversible reaction and heat transfer between hot and cold gases).

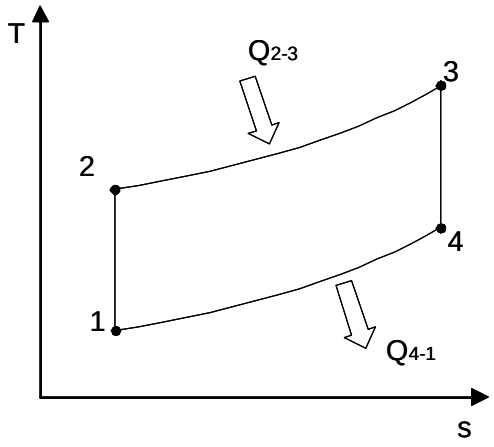

Figure 4-30 – T-s diagram for a theoretical engine cycle.

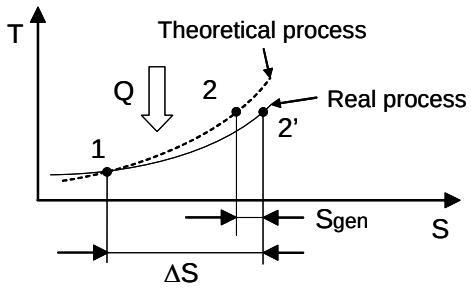

Figure 4-31 – Comparison of a theoretical and a real heating process.

4.7.1 Heat Transfer

As seen previously, in a conventional SI engine there is always heat transferred between the cylinder charge and the cylinder walls (cylinder liner, engine head and piston head). This heat is transferred due to a finite temperature difference between the wall temperature and the temperature of the gas contacting that wall. The temperature variation inside the cylinder makes the heat flux sense to be inverted for part of the engine cycle. Namely during the intake stroke, due to the inlet of fresh air, the temperature of the cylinder content lowers to a level bellow the wall temperature and the heat flux is from the wall to the gas, heating it. As a consequence of the heat released during combustion, the heat transferred from the gas to the wall over the entire cycle is significantly superior to the heat transferred from the walls to the gas during the intake stroke.

Meanwhile, at the outside of the engine, heat is transferred from the walls to the surrounding environment. At this point, the temperature difference between the wall and the atmosphere always makes the heat to flow from the wall to the surroundings. Considering the surrounding environment as a heat sink, the temperature of the atmosphere can be considered as constant. The outside engine wall temperature, which warms up from engine start until it reaches an equilibrium value, can also be considered constant over an entire engine cycle, once the thermal inertia of the walls and the cycle time do not allow significant temperature variations.

Figure 4-32 illustrates the heat transfer phenomena in an internal combustion engine,

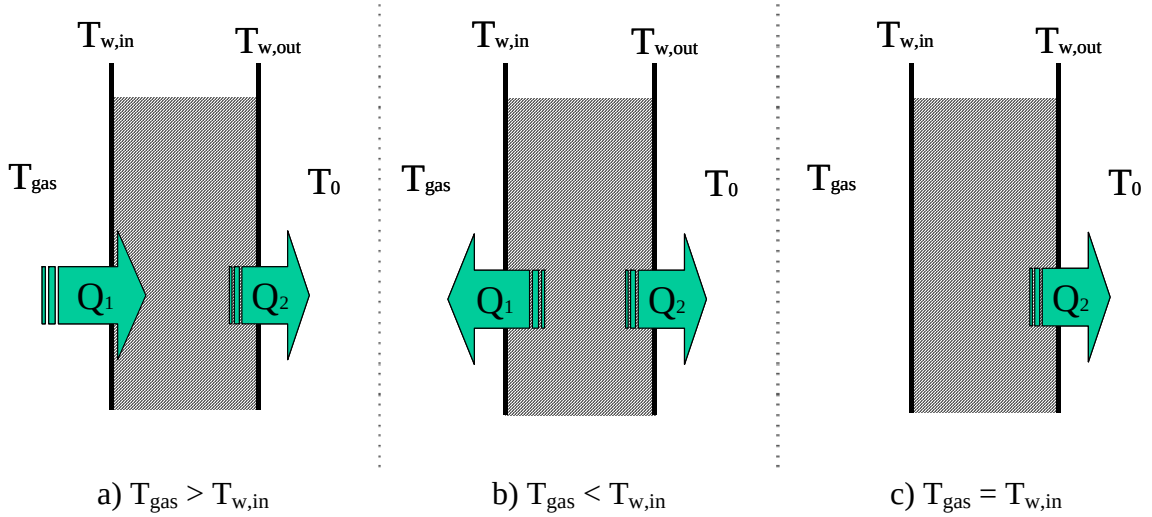

Figure 4-32 – Heat transfer situations during the internal combustion engine cycle.

where $T_{w,in}$ is the temperature of the engine wall in contact with the cylinder charge and $T_{w,out}$ is the temperature of the engine wall in contact with the surrounding environment.

During this analysis the cylinder content may be considered as one system and the engine wall as another system. In reality the gas inside the cylinder contacts the wall of the cylinder, but for analysis purposes, it is considered that they do not contact each other and between exists a third system usually referred as the "temperature gap" [38]. The same method is used on the interface between the outside wall and the environment. The heat transferred enters and leaves the intermediate system undiminished.

Applying the second law of thermodynamics to the temperature gap system, the entropy generation in this system is:

$$S_{gen} = \frac{Q}{T_L} - \frac{Q}{T_H} = \frac{Q(T_H - T_L)}{T_L T_H} \tag{4.69}$$

where Q is the heat transferred, T_H is the highest temperature and T_L is lowest temperature of the temperature gap.

In the case of the internal combustion engine, this analysis must be applied to the "temperature gap" between the gas and the inner wall, between the outer wall and the environment and between the inner wall and the outer wall (considering the engine wall as another temperature gap), coming:

$$S_{gen} = Q_1\left(\frac{1}{T_{w,in}} - \frac{1}{T_{gas}}\right) + Q_2\left(\frac{1}{T_{w,out}} - \frac{1}{T_{w,in}}\right) + Q_2\left(\frac{1}{T_0} - \frac{1}{T_{w,out}}\right) \quad (4.70)$$

where T_{gas} is the in-cylinder gas temperature, $T_{w,in}$ is the temperature of the inner wall, $T_{w,out}$ is the temperature of the outer wall, T_0 is the environment temperature. Q_1 is the heat that crosses the first temperature gap, which may assume different senses depending on the temperature difference on the first gap, and Q_2 is the heat transferred through the second and third temperature gaps. For this analysis the following assumptions shall be made:

1) The heat balance of the entire wall (considered as a system) over the entire cycle is zero;
2) The heat crosses the wall at a constant rate over the entire cycle. Both (inner and outer) wall temperatures and the environment temperature are considered constant. So the heat flux that crosses the second and third temperature gap is considered constant in sign and value;
3) The heat lost or gained by the cylinder gases crosses the first temperature gap only. This means that between the first and second gap the heat may be stored during the cycle but according to assumption 1), the balance is zero over the entire cycle.

Considering assumption 2), equation (4.70) can be written as:

$$S_{gen} = Q_1\left(\frac{1}{T_{w,in}} - \frac{1}{T_{gas}}\right) + Q_2\left(\frac{1}{T_0} - \frac{1}{T_{w,in}}\right) \quad (4.71)$$

and considering assumptions 1) and 3), the amount of entropy generated for a complete engine cycle can be expressed by rewriting equation (4.71), which brings:

$$S_{gen} = Q_1\left(\frac{1}{T_0} - \frac{1}{T_{gas}}\right) \quad (4.72)$$

Which in rate terms may be written as:

$$\dot{S}_{gen,heat} = \frac{\dot{Q}\left(T_{gas} - T_0\right)}{T_0 T_{gas}} \tag{4.73}$$

where T_0 is the environment temperature and considering the absolute value of the heat transfer rate ($\dot{Q}$). The heat transfer rate is calculated by the expression [41]:

$$\dot{Q} = \left(\alpha_{conv} + \alpha_{rad}\right)\left(T_{gas} - T_w\right)A \tag{4.74}$$

Where A is the heat transfer area, α_{conv} is the heat transfer coefficient due to convection and α_{rad} is the heat transfer coefficient due to radiation, calculated following the method presented by Annand [6], considered as the most applicable to spark ignition engines.
The entropy generated in an internal combustion engine due to heat transfer from the cylinder charge to the surroundings is independent of the wall temperature and only dependant on the temperature differential between the gas and the environment. Now, this is independent on the heat flux sense over the cycle, so entropy is generated by the existence of heat transfer independently if the heat is transferred from or into the engine. The wall temperature and transfer conditions (coefficient and area) influence only the absolute value of the heat flux.

4.7.2 Combustion

Combustion processes are known to be a major form of irreversibility but few literature reports deal with the particular aspects of the combustion process. The primary causes for irreversibility in combustion processes have been identified [42] and are presented as:

1) Reactant diffusion
2) Reaction (fuel oxidation)
3) Internal thermal energy exchange (i.e. heat transfer between gas constituents within the reactor)
4) Product mixing

Some models have been presented for the comprehension of the combustion process from a Second Law of Thermodynamics point of view. Two of such models were presented in [33, 43]. The first one [43] is more general and a second model contemplates a more specific application to internal combustion spark ignition engines [33].

For thermal engines with continuous combustion a basic model was created [43] that allows the division of the exergy destructions in sections and processes. This model is to be applicable to combustion processes in furnaces, gas turbines, and other such devices. The combustion process is then divided in the following sequence. As the air and fuel enter the reactor the oxygen and fuel molecules mix with each other through a diffusion process that consumes useful power, used to separate them from the reactant gas stream. The second step consists in the reaction of the oxygen with the fuel molecules, forming product molecules. From this process come net changes of energy in the forms of 1) internal chemical energy – energy associated with intramolecular forces, 2) radiation energy, and 3) internal thermochemical energy – associated with particle motions and intermolecular forces between system constituents. Having stabilized (reacted) these interactions between the participating species have added entropy to the system.

The combustion zone is divided in a sequence of serial and parallel sub-chambers where the combustion proceeds in an incremental fashion. Each increment is divided in three steps (Figure 4-33). In the first secondary step (step 2.1) three zones do exist 1) a zone of fuel, 2) a zone of oxygen, and 3) a zone of stoichiometric mixture of fuel and oxygen that is transferred from the previously referred zones and where fuel reacts adiabatically into combustion products. In the second secondary step (step 2.2) the system continues divided in three zones. At this stage, heat transfer is allowed between the zones but not with the ambient surroundings and no mixing of chemical species is allowed. The exit from the second step is assumed to be at thermal equilibrium conditions i.e., temperature of all zones is equal. At the third step (step 2.3) the products from the reaction are mixed with the unreacted air at adiabatic conditions.

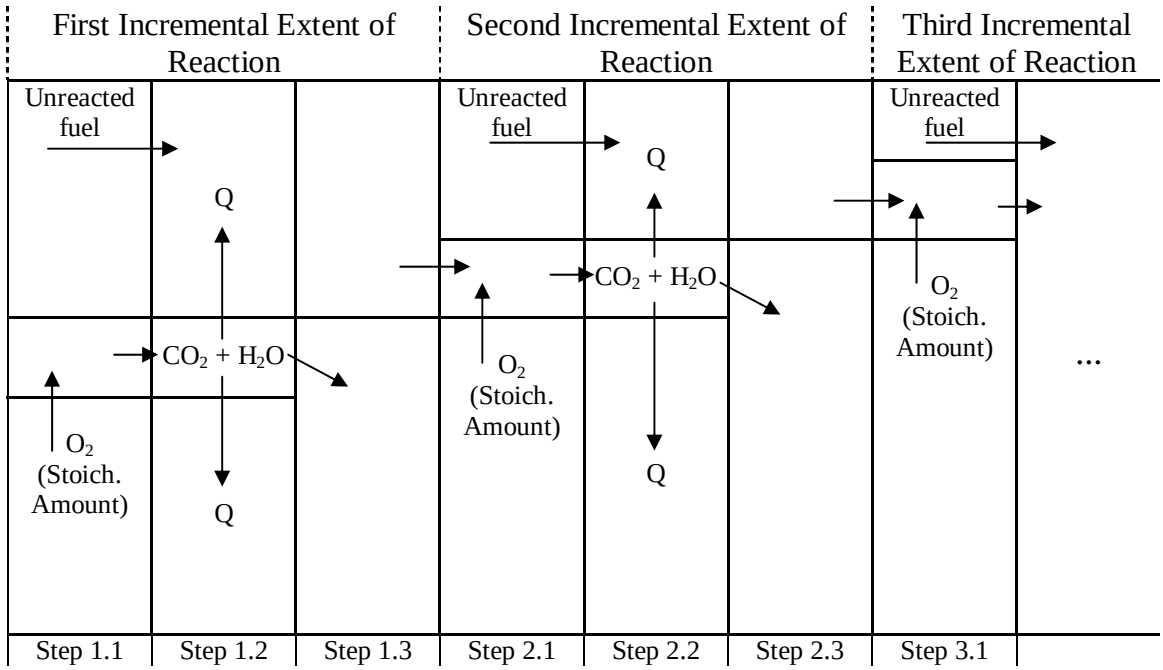

Step	Process
1.1	Difusion/Reaction [$C_nH_m + (n+m/4)O_2 \rightarrow nCO_2 + (m/2)H_2O$]
1.2	Internal Thermal Energy Exchange
1.3	Mix (Products/Depleted Air)
2.1	Difusion/Reaction [$C_nH_m + (n+m/4)O_2 \rightarrow nCO_2 + (m/2)H_2O$]
2.2	Internal Thermal Energy Exchange
2.3	Mix (Products/Depleted Air)
3.1	Difusion/Reaction [$C_nH_m + (n+m/4)O_2 \rightarrow nCO_2 + (m/2)H_2O$]

Figure 4-33 – Hypothetical combustion chamber [43].

The second model was created especially for internal combustion engines application [33]. It was presented for the study of destruction of availability, but it can be used for entropy generation studies. The system is considered closed, with constant volume and adiabatic combustion chamber (Figure 4-34), so that any change in availability can be attributed to the combustion process. Since the system is adiabatic, no entropy can be transferred due to heat transfer and as the volume is closed, no entropy is transferred due to mass transfer. Since the volume is constant, no boundary work is possible (and no other form of work is allowed). Therefore any change in the entropy of the system may be attributed solely to the combustion process inefficiencies.

In this model the thermodynamic system is the chamber contents; the combustion chamber contents are assumed to be spatially homogeneous and to occupy one zone; the fuel is fully vaporized and mixed with the reactant air; thermodynamic properties (pressure, temperature, etc.) are spatially uniform and are calculated from established

formulations; chemical species are assumed to obey the ideal gas equation of state; composition of the combustion products is assumed to be that for complete combustion and for equilibrium conditions; the combustion efficiency is considered to be 100%, i.e. no unburned fuel is left at the end of the combustion process.

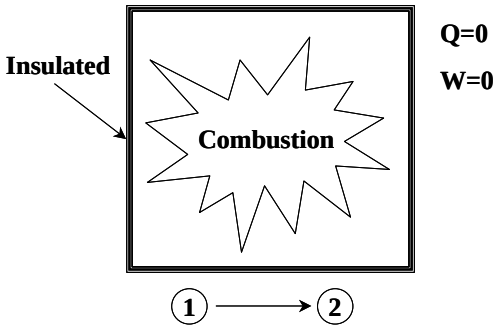

Figure 4-34 – Adiabatic, constant volume system. [33]

Using the model presented in Figure 4-34, First and Second Law of Thermodynamics are reduced to the following forms:

$$U_1 = U_2 \tag{4.75}$$

$$S_2 - S_1 = S_{gen} \tag{4.76}$$

where U_1 and U_2 are the internal energy of the system at the start and finish of the process respectively, S_1 and S_2 are the entropy of the system at the start and finish of the process respectively, and S_{gen} is the amount of entropy generated due to any internal irreversibility. From equation (4.76) it can be proved that the entropy generated in an internal combustion engine corresponds to the difference of the entropy of the system before and after the combustion has occurred.

For the combustion process, the entropy generation rate is calculated through:

$$\dot{S}_{gen,comb} = \sum_{i=1}^{n} \dot{N}_{pi} \bar{s}_{pi} - \sum_{i=1}^{m} \dot{N}_{ri} \bar{s}_{ri} = \sum_{i=1}^{n} \dot{m}_{pi} s_{pi} - \sum_{i=1}^{n} \dot{m}_{ri} s_{ri} \tag{4.77}$$

where:

$$\sum_{i=1}^{n} \dot{m}_{ri} s_{ri} = \dot{m}_a s_a(T_2, p_2) + \dot{m}_f s_f(T_2, p_2)$$
$$\sum_{i=1}^{n} \dot{m}_{pi} s_{pi} = \sum_{k} \dot{m}_k s_k(T_3, p_3) \qquad (4.78\ a, b)$$

The specific entropy of each chemical species of the reactants (s_{ri}) is calculated at the instantaneous temperature inside the cylinder. The specific entropy of the products (s_{pi}) is calculated using the adiabatic flame temperature calculated at each time step.

The entropy of the several chemical species present in the system is calculated by the following expressions [5]:

- (air entropy)

$$s_a(T,p) = s^0(T,p_0) - R_{air}\, ln\frac{p_{air}}{p_0} = \frac{N_{O_2}\bar{s}(T)_{O_2} + N_{N_2}\bar{s}(T)_{N_2}}{N_{O_2} + N_{N_2}} - R_{air}\, ln\frac{p_{air}}{p_0} \qquad (4.79)$$

- (fuel entropy)

$$s_f(T,p) = s_f^0(T,p_0) - R_f\, ln\frac{p_f}{p_0}$$
$$= R_f\left(4.0652 \ln T + 6.0977 \cdot 10^{-2} T - \frac{1.8801 \cdot 10^{-5}}{2} T^2 + 15.45\right) - R_f\, ln\frac{p_f}{p_0} \qquad (4.80)$$

Where R_f and R_{air} are the gas constant for the fuel being used (considering the fuel as a gas) and air respectively, p_f and p_{air} are the partial pressure of the fuel and air respectively, in the air/fuel mixture.

The exhaust gases specific entropy is calculated by:

$$s_k(T, x_k p) = s_k'(T, p_0) - R_k\, ln\left(\frac{x_k p}{p_0}\right) \qquad (4.81)$$

Where k=CO_2, N_2, H_2O

$$s_k'(T, p_0) = \frac{R_u}{M_k}\left(a_1 \ln T + a_2 T + \frac{a_3}{2} T^2 + \frac{a_4}{3} T^3 + \frac{a_5}{4} T^4 + a_7\right) \qquad (4.82)$$

Where T is the adiabatic flame temperature within a range of 1000 – 5000 K. The a_1 to a_7 coefficients are presented in Table 4-6 [44].

Table 4-6 – Coefficients for the calculation of the specific entropy of exhaust gases [44].

k	***a1***	***a2***	***a3***	***a4***	***a5***	***a7***
CO_2	4.453623	0.03140168E-01	-0.12784105E-05	0.02393996E-08	-0.16690333E-13	-0.9553959
H_2O	2.672145	0.03056293E-01	-0.08730260E-05	0.12009964E-09	-0.06391618E-13	6.862817
N_2	2.926640	0.14879768E-02	-0.05684760E-05	0.10097038E-09	-0.06753351E-13	5.980528

4.7.3 Flow Through Valves

The gases passing through valves suffer a pressure drop due to the valve and duct geometry. Some of the work produced by the engine is used to overcome this resistance to fluid flow. The entropy generated in this process may then be seen as the work lost to perform the intake or the exhaust process. Considering a quasi-steady gas flow through the valve, the entropy generation rate can be calculated from the state properties:

$$\begin{aligned}
\dot{S}_{gen,valve} &= \dot{m}\int_u^d ds = \dot{m}\left[c_p\, ln\left(\frac{T_u}{T_d}\right) - R\, ln\left(\frac{p_u}{p_d}\right)\right] = \\
&= \dot{m}\left[c_p\, ln\left(1 - \frac{k-1}{2} M^2\right) + c_p \frac{k-1}{k} ln\left(\frac{p_u}{p_d}\right)\right] = \\
&= \dot{m} c_p\, ln\left[\left(1 - \frac{k-1}{2} M^2\right)\left(\frac{p_u}{p_d}\right)^{\frac{k-1}{k}}\right]
\end{aligned} \tag{4.83}$$

where:

p_u; p_d – gases pressure upstream and downstream of valve respectively;

T_u; T_d - gases temperature upstream and downstream of valve respectively;

k – specific heat ratio: $k = \frac{c_p}{c_v}$

M – Mach number of gases at valve inlet: $M = \frac{u}{c}$;

u – gases velocity in pipe;

c – sound velocity in gases: $c = \sqrt{kRT_c}$.

This calculation method is applied also to the throttle valve of the engine.

4.7.4 Free Expansion During Exhaust and Intake

An important entropy generating process in an internal combustion engine is the release of the exhaust gases during the exhaust stroke, especially during the blow-down phase, where high temperature and pressure gases are freely released to the atmosphere without producing any work. As stated by the Gouy-Stodola theorem [38], the entropy generated is equal to the work lost divided by the environment temperature.

$$W_{lost} = T_0 \cdot S_{gen} \tag{4.84}$$

In this case the work lost is represented by the enthalpy of the gases that flow out of the engine at a different state than the environmental. The entropy generation rate is calculated by [37]:

$$\dot{S}_{gen,enthalpy} = \sum_{in} \frac{\dot{m}}{T_0}(h - h_0) - \sum_{out} \frac{\dot{m}}{T_0}(h - h_0) \tag{4.85}$$

Where h is the enthalpy of each chemical species prior to passing the exhaust valve and h_0 is the enthalpy of each chemical species at T_0 and p_0.

4.7.5 Friction

In the engine, several components have relative movement and contact with each other, generating friction. Again the Gouy-Stodola theorem (4.84) is applicable to this case and the lost work is considered to be the difference between the indicated and the break work developed by the engine. It comes:

$$\dot{S}_{gen,friction} = \frac{\dot{W}_{lost,friction}}{T_0} \tag{4.86}$$

The work lost as a result of friction is calculated using a friction model [8], which calculates the friction mean effective pressure.

4.7.6 Entropy Generation Results

The same engines presented in Table 4-3, were used for entropy generation calculations.

4.7.6.1 Combustion

The entropy generated in the combustion is due to the chemical reactions that take place in this process. Before combustion, there is a certain amount of mixture of air and fuel at a certain temperature and pressure, inside the engine cylinder. As the combustion takes place there is a conversion of chemical species and also an increase of pressure and temperature, due to heat release. It will be assured that all the mixture of air and fuel react entirely, generating burned gas species, such as H_2O, CO_2 and N_2. As a consequence of the temperature raise, the specific heats of air, fuel, and burned gas species increase significantly, increasing the values of the specific entropy of each chemical component. As shown above (eq. (4.80) - eq. (4.82)), the entropy depends also on the logarithm of the ratio between the pressure inside the engine (which increases significantly) and the environment pressure. The reduction of the entropy generated during this process may be achieved by combustion at higher temperatures (and pressures), for example by compression ratio increase. The constant reduction of the entropy generated in all cycles, as seen in Figure 4-35, is caused just by the reduction of the amount of mass (air and fuel) involved in the reaction as load decreases.
Figure 4-35 shows the entropy generated by the combustion process in each cycle. The Otto and Miller cycles have a reduction of maximum pressure and temperature as the load is reduced. On the other hand, the Miller VCR cycles have a constant maximum pressure and temperature, higher than the previous, leading to a reduction on the entropy generated due to the combustion process.

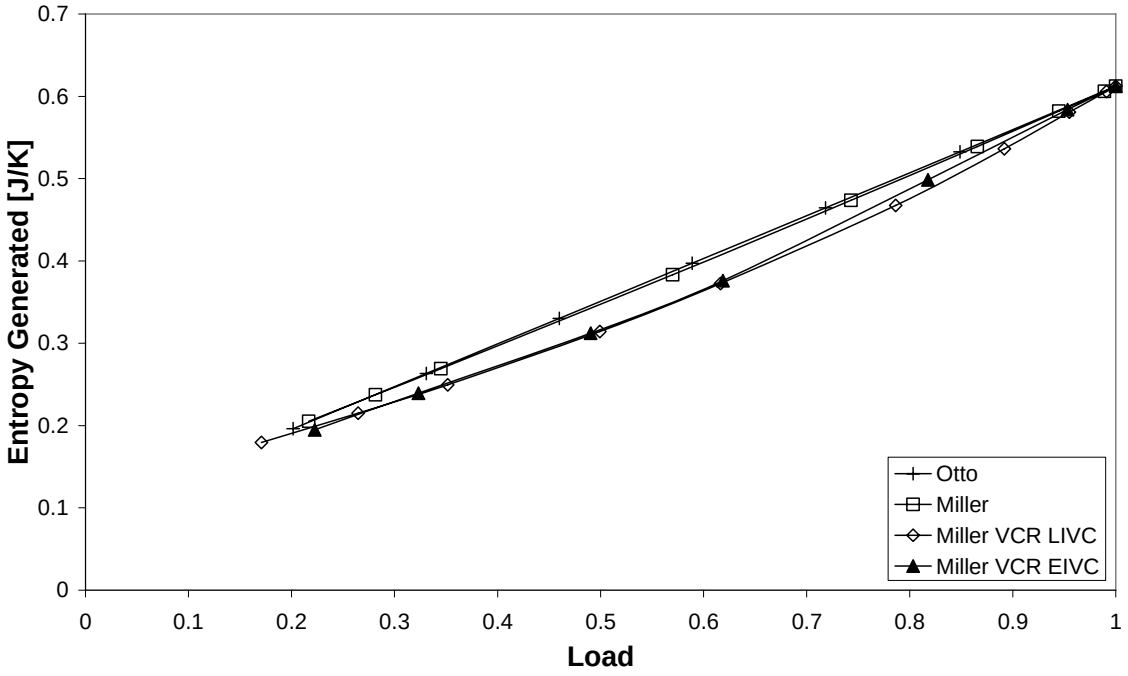

Figure 4-35 – Entropy generated due to combustion.

4.7.6.2 Free Expansion

After the expansion stroke, when the exhaust valve opens, the burned gases contained within the cylinder are still at high temperature and pressure. Some of its enthalpy could be converted into work if left expanding down to the atmospheric pressure and temperature.

The main contribution of this entropy generating process is made during the blow-down, where real high enthalpy gases are released to the environment. In the computer model presented here the intake mixture is considered always to be at atmospheric pressure and temperature.

Figure 4-36 shows the entropy generated due to the free expansion after the opening of the exhaust valve (blow-down) and the free expansion during the intake process. In all cycles the entropy generated reduces with load, as a consequence of the lower pressure and temperature obtained at the exhaust valve opening instant. The Miller cycle (Miller and Miller VCR in Figure 4-36) is simulated with late intake valve closure (LIVC), meaning that during the intake stroke some amount of the mixture of air and fuel is blown-back to the intake manifold. It can be seen that for very low loads, the decrease tendency is smaller. This means that the free expansion losses became more significant

because there is a free expansion of the mixture when coming into the cylinder and when some of the mixture is blown-back, which increases with the reduction of load. Another attempt for performing the Miller VCR cycle is made with early intake valve closure (EIVC). In this case all the mixture is inducted into the cylinder and it remains there. The free expansion caused by blow-back is saved, but the valve lift is smaller and the opening duration is shorter, thus increasing the free expansion losses at induction. The depression produced inside the cylinder to make the mixture inlet is higher (due to the smaller area opened by the valve) causing a greater pressure difference across the valve.

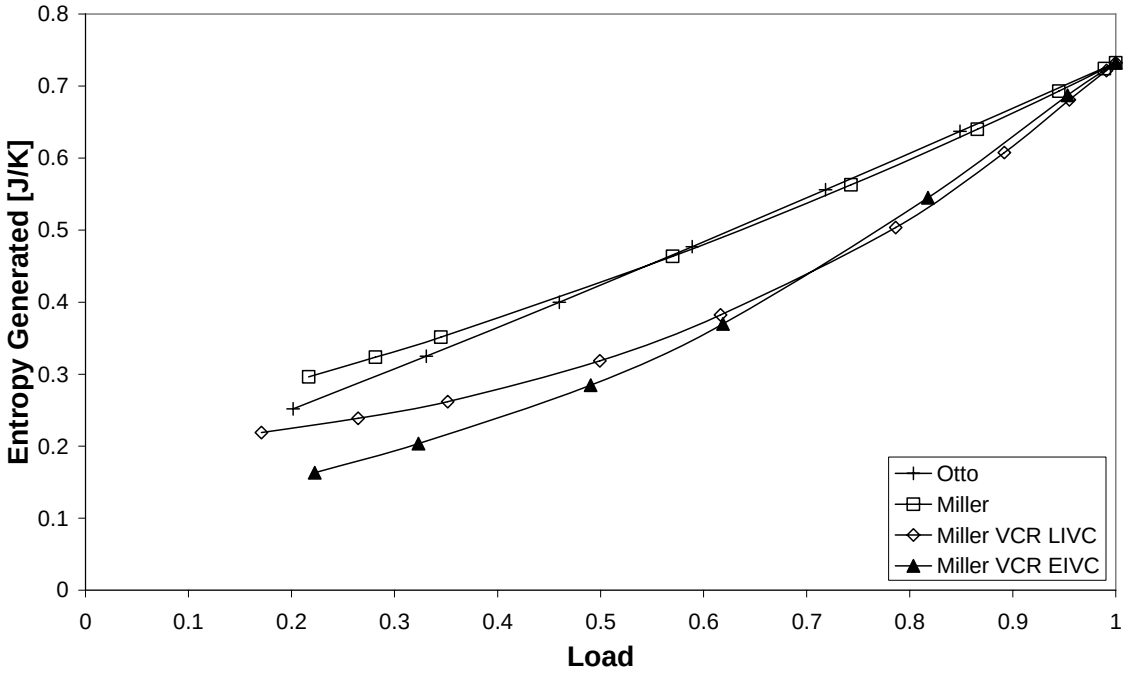

Figure 4-36 – Entropy generated due to free expansion.

When comparing the Miller cycle with LIVC and with EIVC, the advantage is evident at the lower loads. The blow-back work increases significantly for loads below 60%. This makes the EIVC strategy more adequate for load control at very low loads. The two engine versions LIVC and EIVC were compared for a load of 3 bar bmep (corresponding approximately to 36% of load) and the entropy generated due to the intake process was found to be reduced by 39%.

The Miller cycle without compression ratio adjustment has more entropy generation than the Otto cycle as load reduces for values lower than 50%. The cause of this is the

increase in the entropy generated due to the free expansion during the blow-back period that surpasses the benefit achieved in the blow-down period. For the same reason the Miller VCR by LIVC cycle also has a tendency for inverting the decrease of the entropy generated as load decreases.

4.7.6.3 Heat Transfer

The heat gain or lost by the engine charge is transferred to and from the cylinder walls, piston head and engine head. All these components have different surface temperatures, which are considered constant during all the cycle (mean wall temperature for each surface) and the same temperatures are considered to all engine cycles. These surface temperatures are used to calculate the heat flux into or out of the engine walls. The atmospheric temperature and the enclosed gases temperature are used to calculate the entropy generated.

Figure 4-37 shows the entropy generated by heat transfer between the engine cylinder gases and the surroundings considered at standard atmospheric conditions. For all engine cycles the entropy generated by this mechanism does not change significantly. A reduction of peak temperature occurs from the Otto to the Miller cycle thus reducing the absolute amount of heat transferred and thus the amount of entropy generated. On the case of the Miller VCR cycle, the compactness of the combustion chamber and an increase of the cooling rate during expansion makes that the amount of heat transferred to be reduced, thus reducing the amount of entropy generated, despite the higher peak temperatures in the cycle.

Some measures may be proposed to minimize the entropy generated. These focus on reducing the amount of heat transferred, whether by reducing the gases temperature inside the cylinder (which is not a good solution because, at the combustion period, as lower temperatures increase entropy generation), or reducing the heat transfer area (with a more compact combustion chamber configuration), or by increasing the combustion chamber walls temperature (always avoiding the knock occurrence).

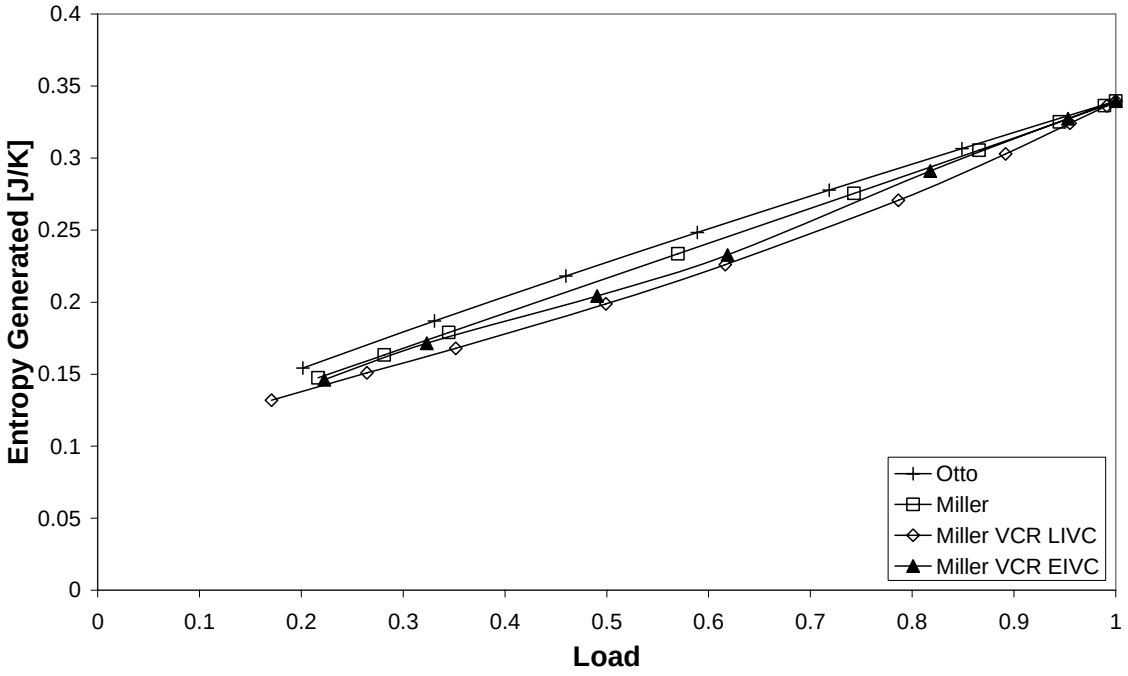

Figure 4-37 – Entropy generated due to heat transfer between the engine cylinder and surroundings.

4.7.6.4 Flow Through Valves

Figure 4-38 shows the amount of entropy generated due to the gas flow across the intake and exhaust valves of the engine and across the throttle valve in the case of the Otto cycle engine. It should be noted that the entropy axis is one order of magnitude smaller than for the previous cases. As can be seen, all the Miller cycle versions have significantly lower amount of entropy generated than the Otto cycle at part load operation. This is mainly due to the lack of throttle valve for load control. In the case of the Miller cycles, for loads higher than 70%, the Miller with LIVC has the lower amount of entropy generated because the valve is fully opened and the blow-back is low. For lower loads the blow-back is significant and the entropy generated increases.
Again in this case, the reduction of pressure and temperature of the exhaust gases is an important mean of reducing the entropy generation rate and the total entropy generated.

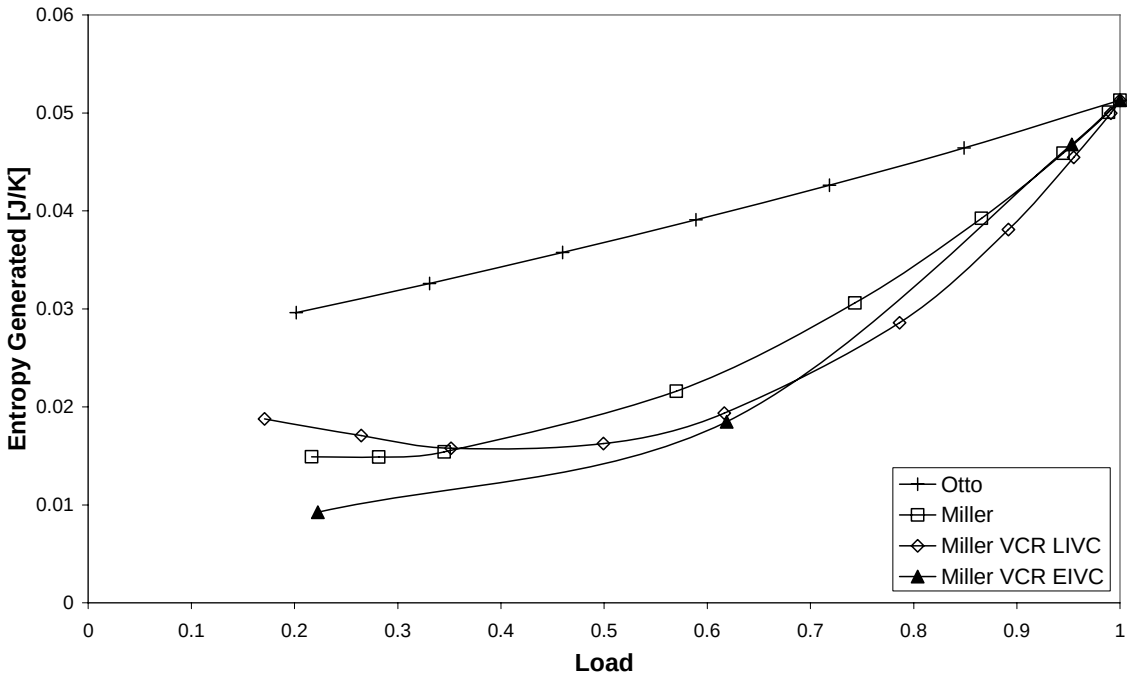

Figure 4-38 – Entropy generated due to gas flow through valves.

4.7.6.5 Friction

In the case of the single cylinder used in these simulations, the changes happen only when parameters such as intake pressure (in the case of the Otto cycle) and compression ratio (in the case of the Miller VCR cycles) change. Figure 4-39 shows the entropy generated due to internal friction in the engine.

For the Otto cycle, the entropy generation has a tendency to decrease with the reduction of the load. This is a result of the intake pressure reduction to create lower loads. For the Miller cycle, as the intake pressure and the compression ratio are constant, the friction losses result constant for all load conditions. As the Miller VCR cycles have higher compression ratios as the load decreases, the friction losses increase and so does the entropy generated.

When comparing these cycles, the difference between them is relevant only for light loads.

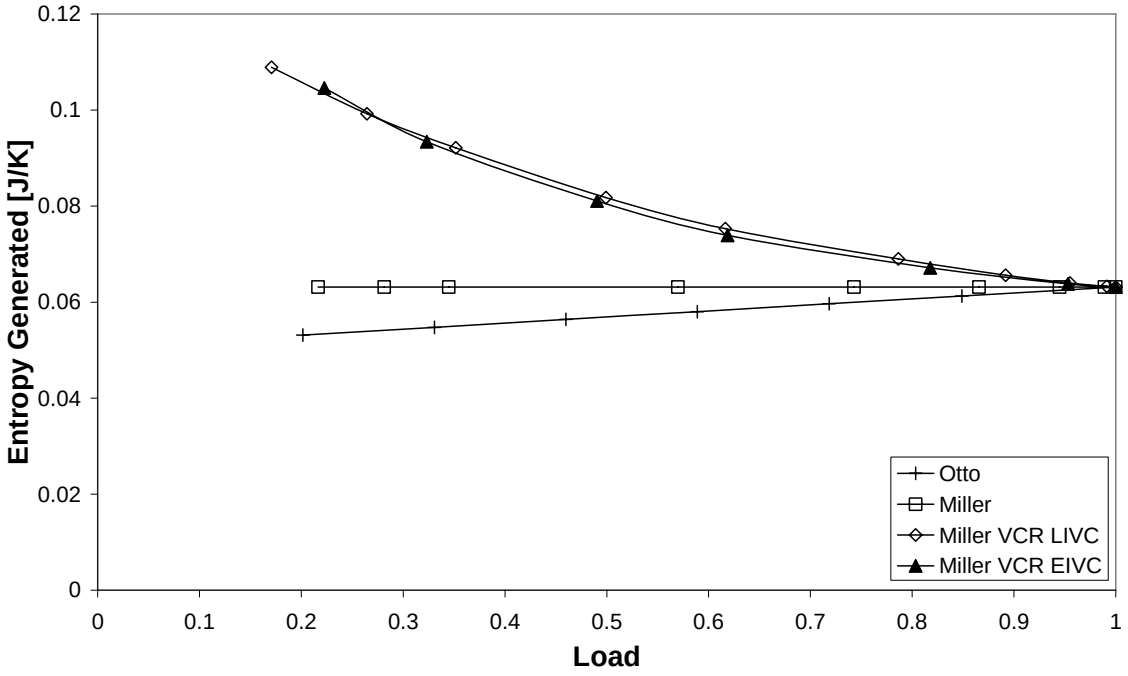

Figure 4-39 – Entropy generated due to friction.

4.7.6.6 Over-All Entropy Generation

Calculating the overall entropy generated in each cycle and at different load conditions, it is possible to compare the working cycles and conclude about the one with the best thermodynamic performance for part load operation. Comparing all cycles for different load, the Otto cycle has the highest amount of entropy generated and the Miller VCR cycle by EIVC is the most thermodynamic efficient, as shown in Figure 4-40. However for loads higher than 65% the Miller VCR cycle by LIVC has a small advantage on the total entropy generated, when compared to the EIVC cycle. For all cycles, the entropy generated in each cycle decreases as the load decreases.

Specific entropy generated (entropy generated per work unit produced) can be used for cycle comparisons and again the Miller VCR engine cycle is the one with the lowest specific entropy generated (Figure 4-41). For loads higher than approximately 70% the use of LIVC is more thermodynamic efficient, while for loads lower than 65% the use of EIVC is shown to be the most efficient of all analysed cycles. For lower loads the specific entropy generated increases for all the four cycles.

The optimum working point, the one with the lowest specific entropy generated is found to be between the 60% - 80% of load, as it can be seen in Figure 4-41. This is where the

transition from LIVC to EIVC is required for lower specific entropy generated. These are the working conditions that should be used when looking for the best efficiency (lower consumption and lower environment degradation). Only if maximum torque or power is desired should the Otto cycle be chosen. At maximum load all four cycles are similar.

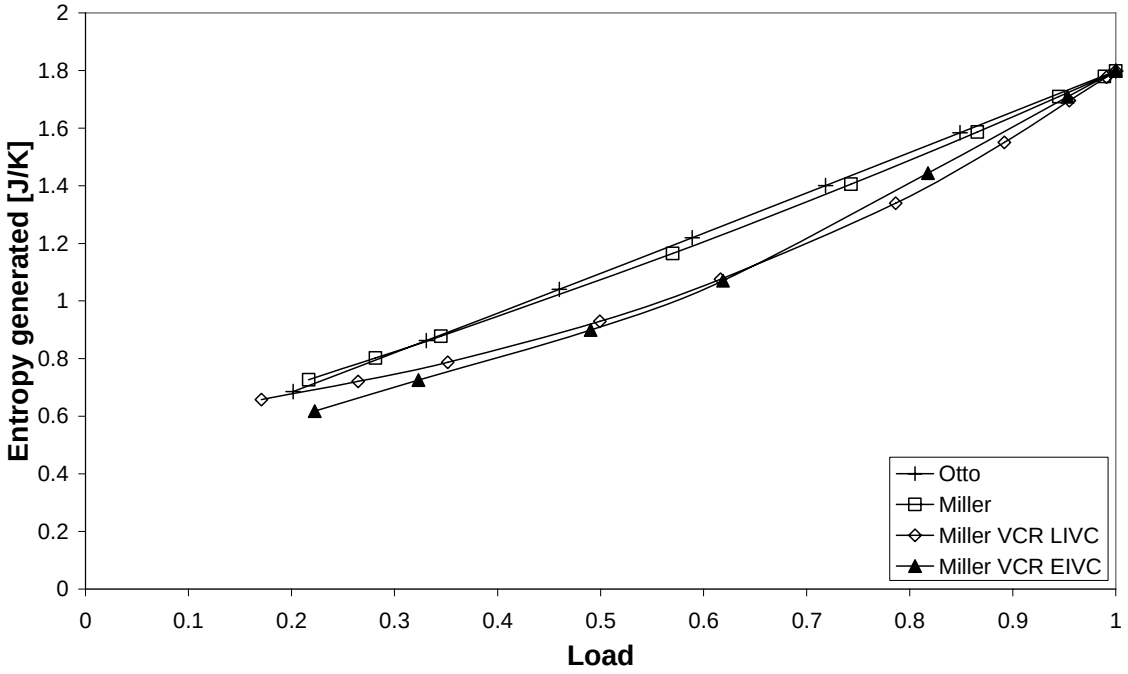

Figure 4-40 – Entropy generated with load variation.

Figure 4-42 represents the entropy generated by the different inefficiency sources for the four cycles at 60% of load. The component of free expansion and combustion are the dominant of the overall entropy generated, contributing for approximately 70% of the total entropy generated. It can be seen that changing from Otto to Miller, there is a reduction in the entropy generated by the flow through the valves resulting from the absence of throttle valve. When comparing the Miller cycle with the Miller VCR cycles a reduction in the free expansion component is evident, explained by the lower temperatures and pressures at EVO.

Due to the importance of the free expansion in the over-all entropy generated, the elimination or reduction of the entropy generated due to this process is the most efficient mean for thermodynamic improvement of spark ignition engines at part load conditions.

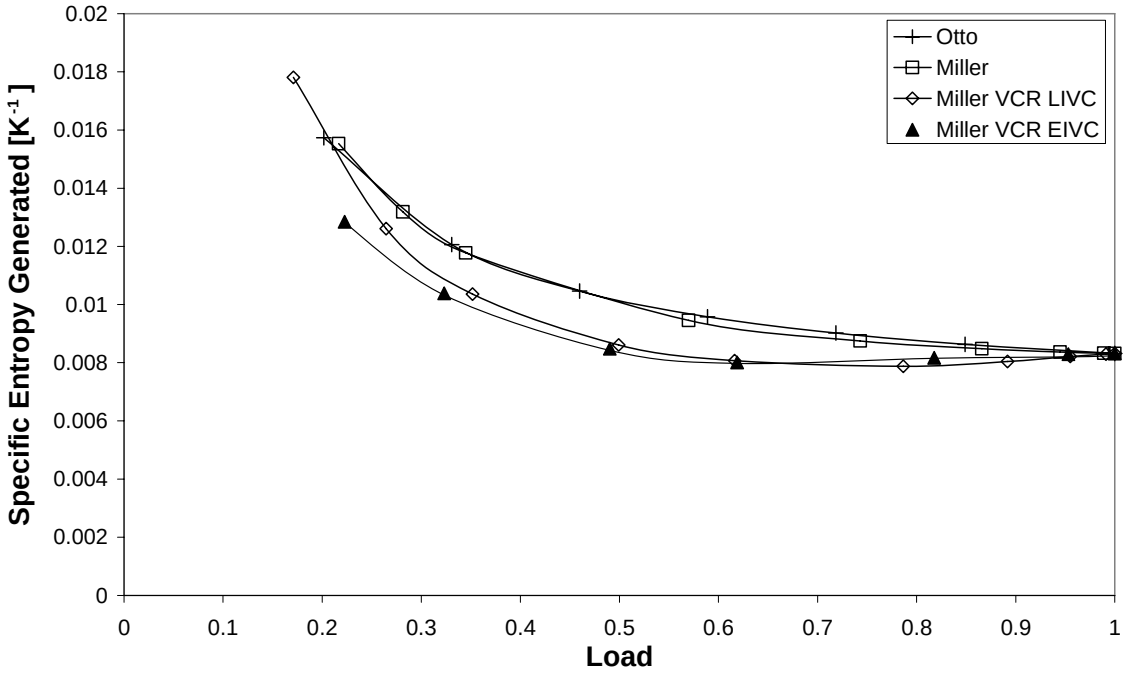

Figure 4-41 – Specific entropy generated with load variation.

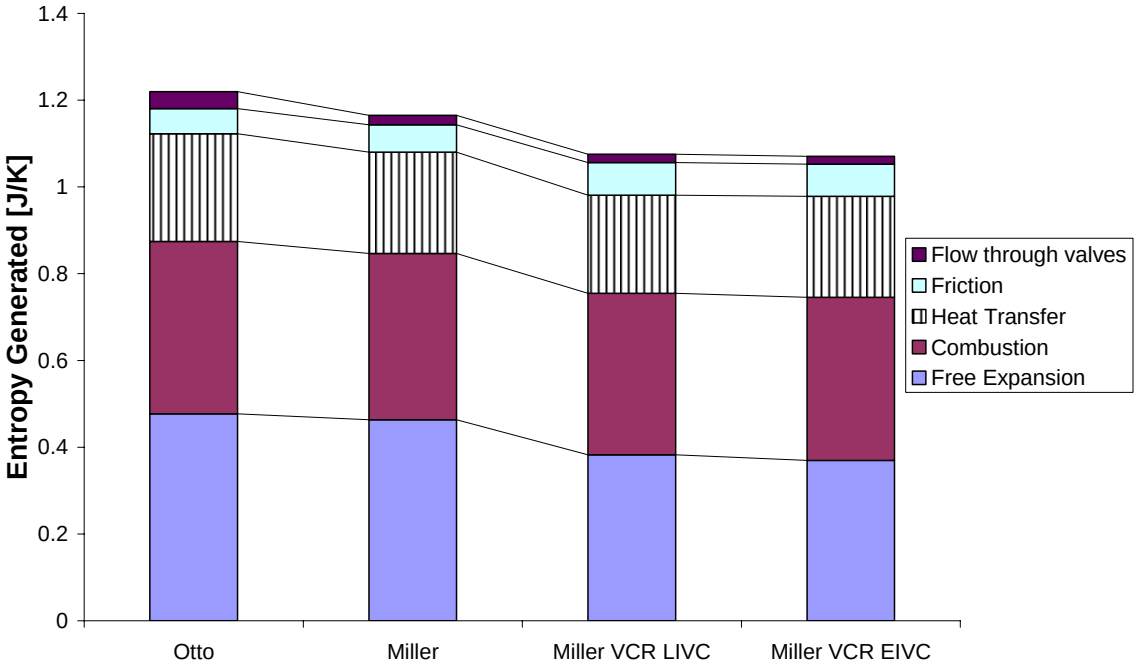

Figure 4-42 – Entropy generated by the several mechanisms at 60% load.

4.8 Summary

Using computer simulation is possible to obtain engine performance results close to the reality. From the refined results presented in this chapter an improvement prediction of the Miller VCR engine was achieved, relatively to the Otto and Miller engine. Validation of these results is made through real engine bench tests.

4.9 References

1 Heywood, J. B., *Internal Combustion Engines Fundamentals*, McGraw-Hill, 1988.

2 Çengel, Y. A., Boles, M. A., *Thermodynamics An Engineering Approach* Third edition, McGraw-Hill, 1998.

3 Turns, Stephen R. *An Introduction to Combustion Concepts and Applications*, McGrawHill, 2000.

4 Abd Alla, G. H. *Computer simulation of a four stroke spark ignition engine*, En. Convers. Mng. 43 (2002), 1043-1061.

5 Ferguson, Colin R., *Internal Combustion Engines Applied Thermodynamics*, J. Wiley & Sons, 1986.

6 Blair, G. P. *Design and Simulation of Four-Stroke Engines*, SAE, 1999.

7 Patton, K. J., et al. *Development and Evaluation of a Friction Model for Spark-Ignition Engines*, SAE 890836, 1989.

8 Sandoval, D., Heywood, J., *An Improved Friction Model for Spark-Ignition Engines*, SAE 2003-01-0725, 2003.

9 Rego, R., *Cam Profile Modelation for Use in Airflow Engine Simulation*, MSc. Thesis, University of Central England, Birmingham, 1999.

10 Martins, J., Uzuneanu, K., Ribeiro, B., Jasansky, O., *Thermodynamic Analysis of an Over-Expanded Engine*, SAE 2004-01-0617, 2004.

11 Ahmad, T., Theobald, M. A., *A Survey of Variable-Valve-Actuation Technology*, SAE 891674, 1989.

12 Kerley, R. V., Thurston, K. W., *The Indicated Performance of Otto-Cycle Engines*, SAE 620508, 1962.

13 Shelby, M., Stein, R., Warren, C., *A New Analysis Method for Accurate Accounting of IC Engine Pumping Work and Indicated Work*, SAE 2004-01-1262, 2004.

14 Ribeiro, B., Martins, J., Kothari, N., *Otto and VCR Miller Engine Performance during the European Driving Cycle*, SAE 2006-01-0440, 2006.

15 Bejan, A., Mamut, E. (eds.), *Thermodynamic Optimization of Complex Energy Systems*, 45 – 60, 1999, Kluwer Academic Publishers.

16 Angulo-Brown, F. et. al., *Compression ratio of an optimized air standard Otto-cycle model*, Eur. J. Phys. 15 (1994) 38-42.

17 Calvo Hernandez, A. et. al., *On an irreversible air standard Otto-cycle model*, Eur. J. Phys. 16 (1995) 73-75.

18 Calvo Hernandez, A. et. al., *An irreversible and optimized four stroke cycle model for automotive engines*, Eur. J. Phys. 17 (1996) 11–18.

19 Moran, M.J., *On Second-Law Analysis and the Failed Promise of Finite-time Thermodynamics*, Energy Int. J., 23, 517-519 (1998).

20 Arias-Hernández, L. A., Angulo-Brown, F. *A general property of endoreversible thermal engines*, J. Appl. Phys. 81 (1997) 2973.

21 Curzon, F. L., Ahlborn, B. *Efficiency of a Carnot Engine at Maximum Power Output*, Am. J. Phys. 43, 22 (1975).

22 Yan, Zijun, *Comment on "A general property of endoreversible thermal engines" [J. Appl. Phys. 81 (1997) 2973]*, J. Appl. Phys. 89 (2001) 1518.

23 Arias-Hernández, L. A., Angulo-Brown, F. *Reply to "Comment on 'A general property of endoreversible thermal engines'" [J. Appl. Phys. 89 (2001) 1518]*, J. Appl. Phys. 89 (2001) 1520.

24 Angulo-Brown, F., Arias-Hernández, L. A., Páez-Hernández, R., A general property of non-endoreversible thermal cycles, J. Phys. D: Appl. Phys. 32 (1999) 1415-1420.

25 Ozkaynak, S., Goktun, S., Yavuz, H., *Finite-time thermodynamics analysis of a radiative heat engine with internal irreversibility*, J. Phys. D: Appl. Phys. 27 (1994) 1139-1143.

26 Shapiro, H. N., Gerpen, J. V., *Two Zone Combustion Models for Second Law Analysis of Internal Combustion Engines*, SAE 890823, 1989.

27 Bozza, Fabio, et. al., *Second Law Analysis of Turbocharged Engine Operation*, SAE 910418, 1991.

28 Caton, Jerald A., *A Cycle Simulation Including the Second Law of Thermodynamics for a Spark-Ignition Engine: Implications of the Use of Multiple-Zones for Combustion*, SAE 2002-01-0007, 2002.

29 Caton, Jerald A., *A Review of Investigations Using the Second Law of Thermodynamics to Study Internal Combustion Engines*, SAE 2000-01-1081, 2000.

30 Lipkea, William H., DeJoode, Arnold D., *A Comparison of the Performance of Two Direct Injection Diesel Engines From a Second Law Perspective*, SAE 890824, 1889.

31 Anderson, Michael K., et. al., *First and Second Law Analyses of a Naturally-Aspirated, Miller Cycle, SI Engine with Late Intake Valve Closure*, SAE 980889, 1998.

32 Caton, J., *Operating Characteristics of a Spark Ignition Engine Using the Second Law of Thermodynamics: Effects of Speed and Load*, SAE 2000-01-0952, 2000.

33 Caton, J., *On the destruction of availability (exergy) due to combustion processes – with specific application to internal-combustion engines*, Energy 25 (2000), 1097-1117.

34 Caton, J., *Use of a Cycle Simulation Incorporating the Second Law of Thermodynamics: Results for Spark-Ignition Engines Using Oxygen Enriched Combustion Air*, SAE 2005-01-1130, 2005.

35 Farrell J. T., Stevens, J. G., Weissman, W., *A Second Law Analysis of High Efficiency Low Emission Gasoline Engine Concepts*, SAE 2006-01-0491, 2006.

36 Bejan, A., *Fundamentals of exergy analysis, entropy generation minimization, and the generation of flow architecture*, Int. J. Energy Res. 2002; 26:545-565.

37 Bejan, A., *Advanced Engineering Thermodynamics,* Second Edition, John Wiley & Sons, New York, 1997.

38 Bejan, A., *Entropy generation through heat and fluid flow,* John Wiley& Sons, New York, 1994.

39 Bejan, A., *Entropy Generation Minimization*, CRC Press, Boca Raton, 1996.

40 Nakonieczny, N., *Entropy generation in a diesel engine turbocharging system*, Energy 27 (2002), 1027-1056.

41 Martins, Jorge, Motores de Combustão Interna, Publindústria, Porto, 2005. (in portuguese)

42 Dunbar, W. R., Lior, N., *Sources of Combustion Irreversibility*, Combustion Sci. and Tech., 103, pp. 41-61.

43 Lior, N., *Irreversibility in Combustion*, ECOS'01, Istanbul, July 2001.

44 Turns, Stephen, R., An Introduction to Combustion: concepts and applications, 2nd ed., McGraw-Hill, 2000.

5 – Experimental Apparatus

5 EXPERIMENTAL APPARATUS

5.1 Introduction

The engine tests described in chapter 6 were performed at the internal combustion engines laboratory of the Mechanical Engineering Department of Universidade do Minho. Some equipment was acquired specifically for the present work while other basic apparatus were already part of the laboratory equipment.
In this chapter all the equipment used in the tests of this research project is described.

5.2 Engine

The objective of the work was to evaluate and compare the engine performance with different configuration solutions for part load operation, in relation to the Otto cycle engine and the Diesel engine configurations.
The requirements established for engine selection were then:

a) To work as Diesel engine
b) To work as gasoline engine
c) Possibility of inlet valve opening variation
d) Possibility of compression ratio variation

To fulfil all the established requirements the adopted solution was to use a Diesel engine at first and use several different camshafts and several different pistons. After measuring the performance of the baseline Diesel engine, it was converted into a spark ignition engine. Amongst other modifications, compression ratio should be reduced and that was made by modifying the Diesel pistons to create combustion chambers with larger volumes. The piston used to perform the Otto cycle was the one with lowest compression ratio. Other compression ratio pistons were manufactured with values between the Otto cycle piston and the Diesel cycle piston.

5.2.1 Engine description

The original Yanmar engine was a single-cylinder, 4-cycle air cooled DI Diesel (Figure 5-3 and Figure 5-4), whose main specifications are presented in Table 5-1.

Table 5-1 – YANMAR L48AE engine specifications.

Number of Cylinders		1
Bore – Stroke (mm)		70 x 55
Displacement (dm^3)		0.211
Compression Ratio		19.9:1
Cooling System		Forced air cooling by flywheel fan
Combustion System		Direct Injection System
Starting System		Starting motor
Maximum Output (kW)		3.5
Speed at no-load, max/min (rpm)		3800 ± 15 / 1200
Fuel	Injection Pump	Bosch Type, YANMAR PFE M-type
	Injection Timing (BTDC)	14 ± 1
	Injection Nozzle	Hole nozzle, YANMAR YDLLA-P type
	Injection Pressure (MPa)	19.6
Lubricating Oil	Type of Lubrication	Forced lubrication via trochoid pump; splash lubrication for valve rocker arm chamber
	Lubricating Oil Selection	SAE 10W30, API grade CC or higher

5.2.2 Engine modifications

To convert a Diesel engine into a spark ignition several modifications had to be implemented. Basically these were:

1. To decrease the compression ratio
2. To install a spark ignition system
3. To install a fuel (petrol) supply system
4. To install a load control system (throttle valve)

5.2.3 Decreasing the compression ratio

The original configuration of the engine, as a Diesel had a compression ratio of 19.9. The piston had a deep toroidal bowl combustion chamber. With this kind of design it is possible to enlarge the combustion chamber in the piston to a cylindrical bowl chamber (Figure 5-1 and Figure 5-2). Several pistons were used with different size bowl

combustion chambers to reach different compression ratios in the engine. As the original design of the piston has a deep bowl, the height of the bowl was kept constant on the modified pistons and only the bowl diameter was changed. The pistons specifications are presented in Table 5-2. Piston 1 was used to perform the Otto cycle. Pistons 2 up to 7 were used with the Miller cycle.

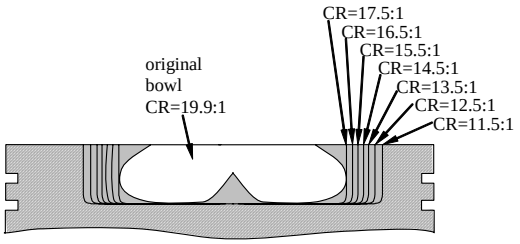

Figure 5-1 - Original and modified combustion chambers.

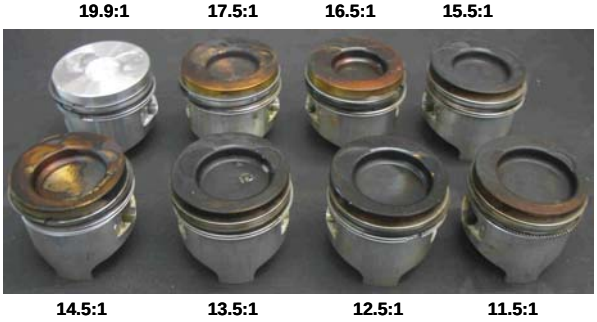

Figure 5-2 - Pistons used in tests.

Table 5-2 – Pistons specifications.

Piston	**Original**	**1**	**2**	**3**	**4**	**5**	**6**	**7**
Death Volume [cm3]	2.5	2.5	2.5	2.5	2.5	2.5	2.5	2.5
Piston Bowl Volume [cm3]		17.5	15.8	14.3	13.1	12	11.1	10.3
Displacement [cm3]	211	211	211	211	211	211	211	211
Compression Ratio	**19.9**	**11.6**	**12.5**	**13.6**	**14.6**	**15.6**	**16.6**	**17.6**
Bowl Depth [mm]		9.5	9.5	9.5	9.5	9.5	9.5	9.5
Bowl Diameter [mm]		48.4	46.0	43.8	41.8	40.1	38.5	37.1

5.2.4 Installing a spark ignition system

In the original engine, the fuel was injected directly into the combustion chamber (piston bowl chamber) at an angle relatively to the cylinder axis. The location of the fuel injector was assumed to be adequate for the placement of a spark plug. The hole, where the injector was located, was modified for the placement of the spark plug (Figure 5-5). Other equipment needed to be added to the engine, to allow the operation of the ignition system. This was the ignition coil and the ignition module. At high speeds the magnetic field generated by the ignition coil interfered with the temperature acquisition board so the ignition coil was then enclosed into a grounded Faraday cage, which solve the problem.

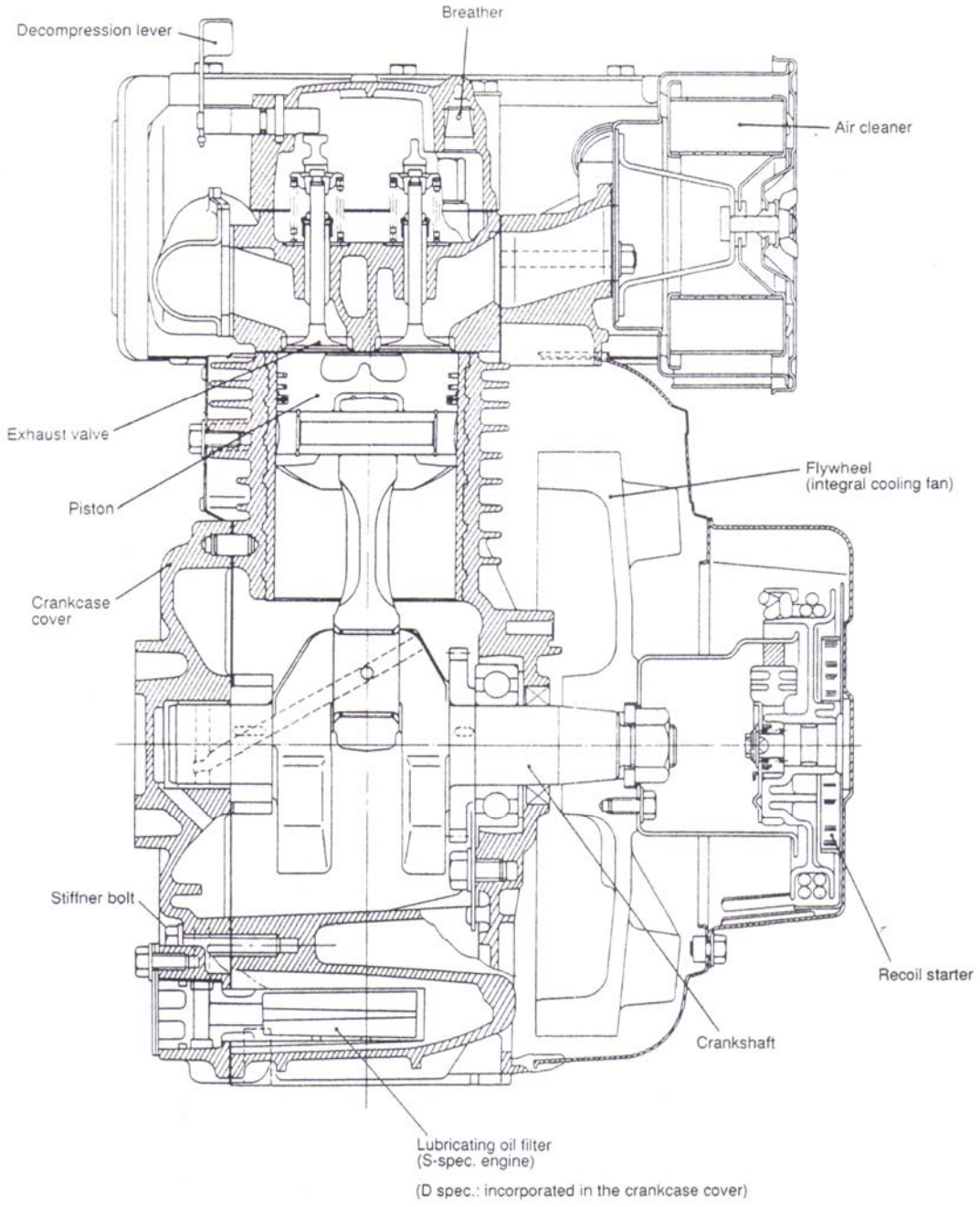

Figure 5-3 – Side view of the Yanmar Diesel engine.

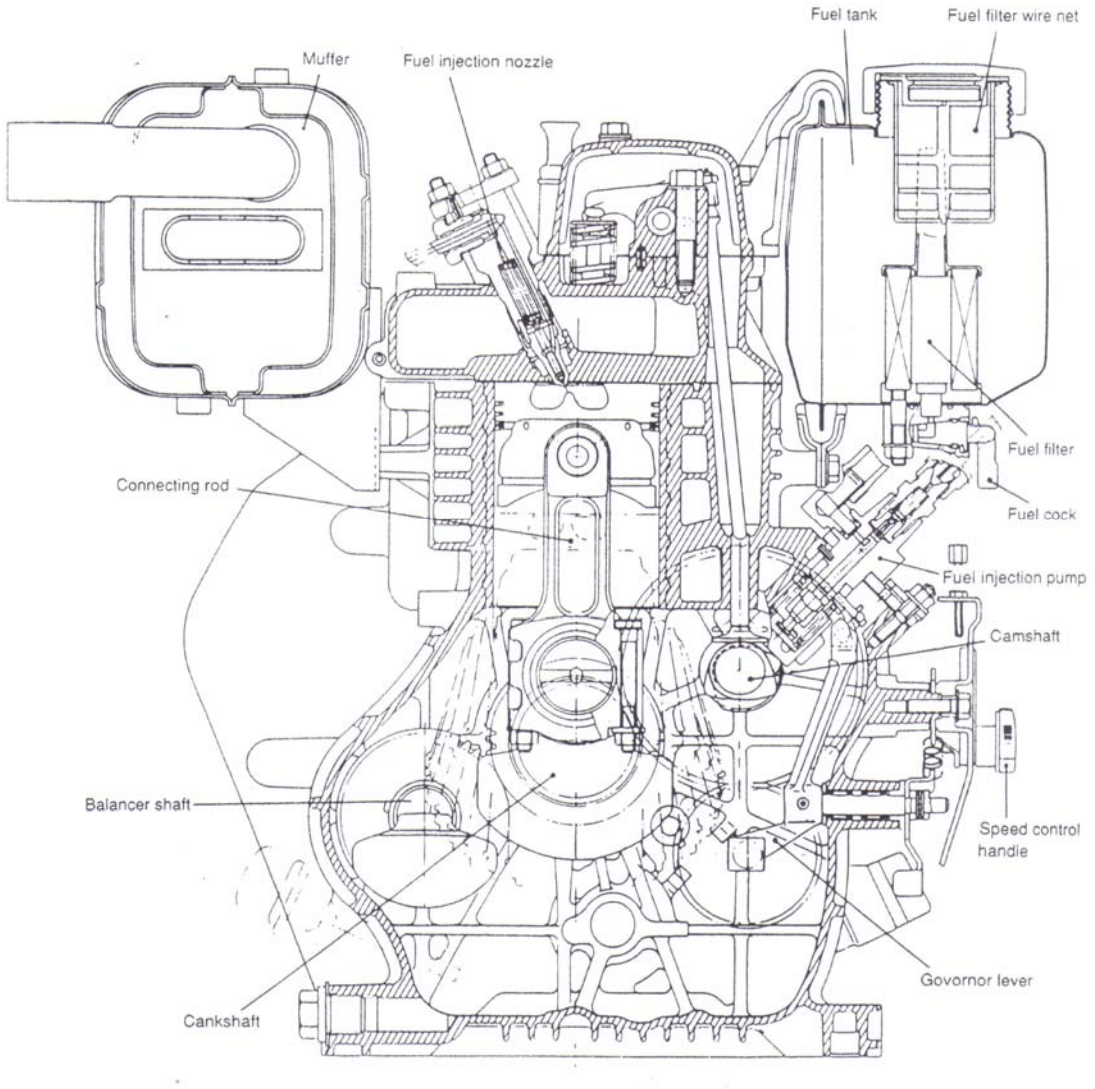

Figure 5-4 – Front view of the Yanmar Diesel engine.

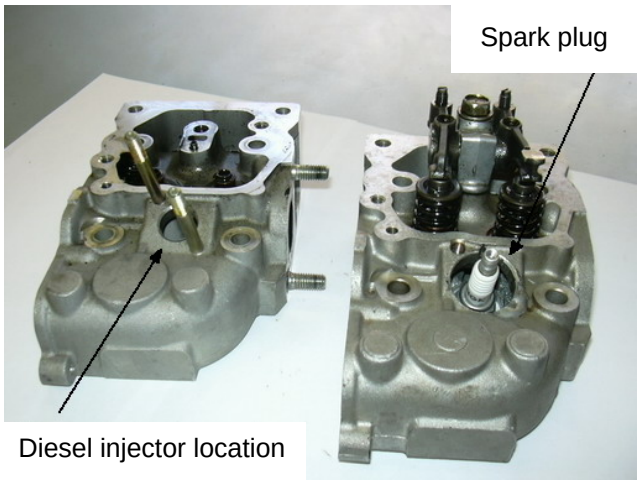

Figure 5-5 – Original and modified engine head.

Figure 5-6 – Ignition coil and the Faraday cage.

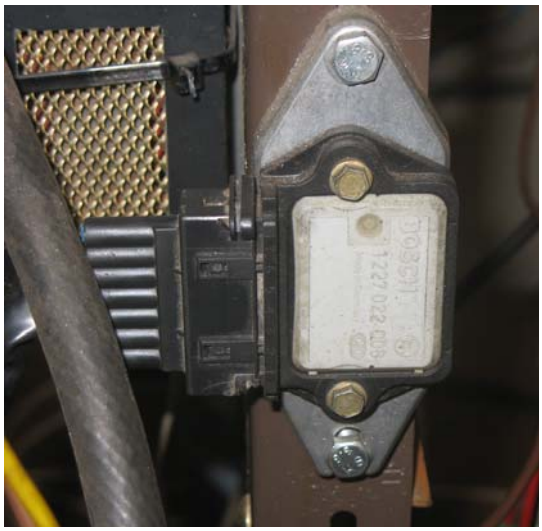

Figure 5-7 – Ignition module.

5.2.5 Installation of the fuel supply system

A new intake manifold was designed and manufactured (Figure 5-8), which includes a seat for the fuel injector and this was fixed pointing to the intake valve (port fuel injection) and a suitable volume (pipe) upstream of the fuel injector position. The volume of this pipe was sufficiently large to prevent the mixture loss when working with the highest late intake valve closure timing, where a great amount of mixture is blown-back from the cylinder to the intake manifold.

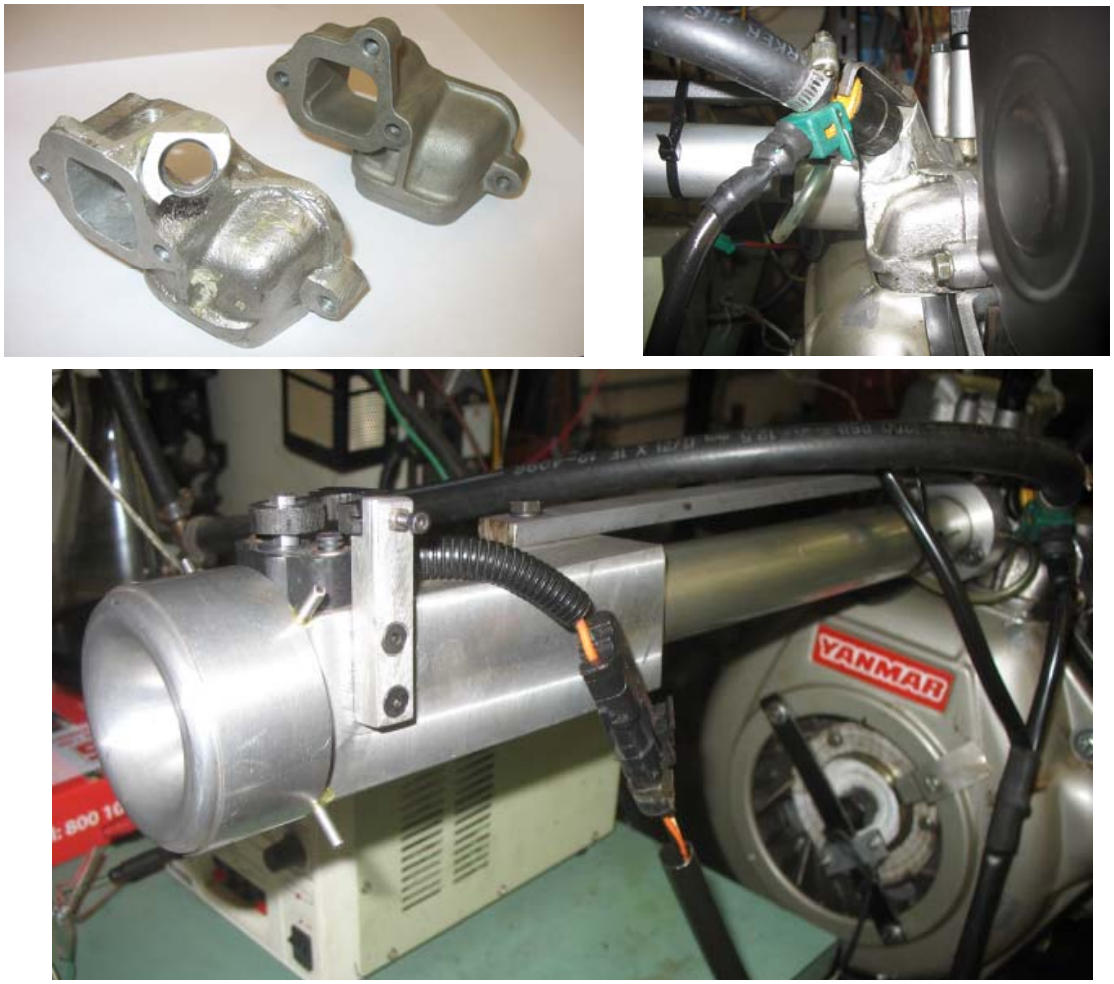

Figure 5-8 – New designed intake duct and placement of the fuel injector.

The engine head was measured so that the angle for the position of the injector could be determined. The position of the injector was selected pointing towards the intake valve. A new intake entrance was casted and drilled to allow for the placement of the fuel injector (Figure 5-8).

In the original Diesel version of the engine, the fuel was supplied from the fuel tank using a fuel pump/injection pump. After its removal, an external fuel pump was installed to supply the fuel to the engine. The fuel is pumped continuously from the glass fuel tank to the fuel circuit at 2.8 bar. A limiting pressure valve regulates the circuit pressure and recirculates the excess of fuel back into the fuel tank.

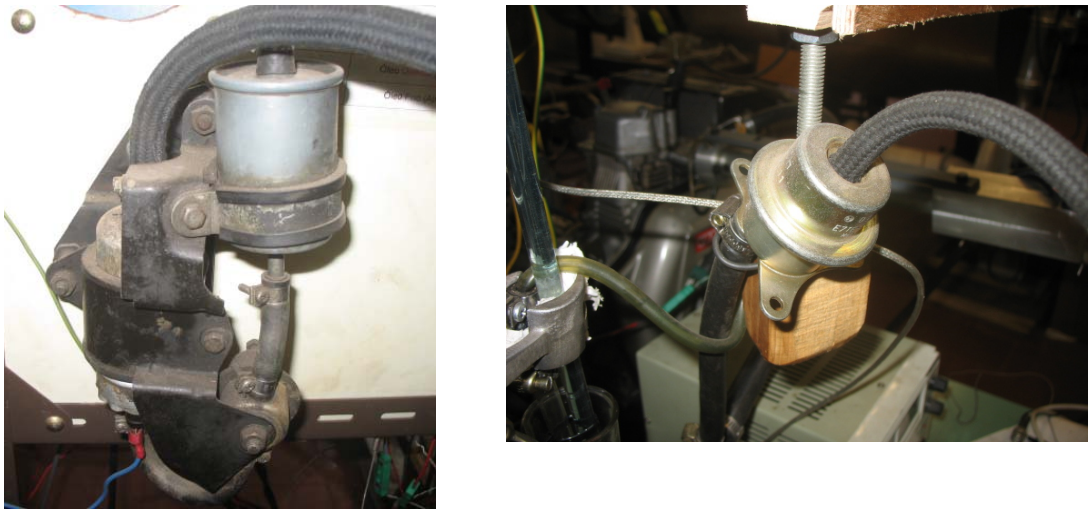

Figure 5-9 – Fuel pump and limiting pressure valve.

5.2.6 Installation of the load control system

To perform the load control function, a throttle valve was installed in a newly designed intake manifold. Several methods may be applied to the design of the throttle body and air entrance [1,2]. In order to reduce pressure losses, an elliptical contour nozzle was used upstream of the throttle position. Figure 5-10 shows the drawing and the throttle body.

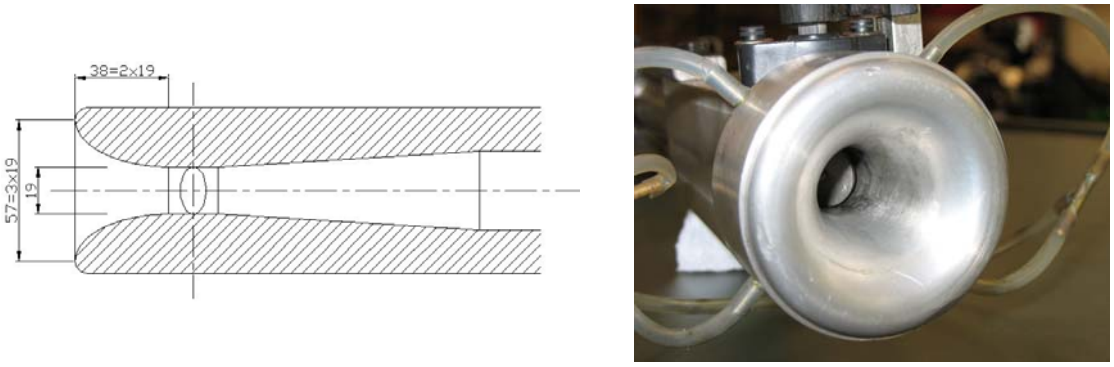

Figure 5-10 – Throttle body.

Design calculations of the throttle valve were based on the standard orifice equations for compressible fluid flow [2]. On a throttle valve, whose opening area is A_{th}, the mass flow rate equation is:

$$\frac{dm}{dt} = \dot{m} = \frac{C_D A_{th} p_0}{(RT_0)^{1/2}} \left(\frac{p_T}{p_0}\right)^{\frac{1}{\gamma}} \left\{ \frac{2\gamma}{\gamma - 1} \left[1 - \left(\frac{p_T}{p_0}\right)^{\frac{\gamma-1}{\gamma}} \right] \right\}^{1/2} \tag{5.1}$$

When the flow is choked, i.e. the flow speed equals the sound speed:

$$\frac{p_T}{p_0} \leq \left(\frac{2}{\gamma + 1}\right)^{\frac{\gamma}{\gamma-1}} \tag{5.2}$$

Then the flow rate is given by:

$$\frac{dm}{dt} = \dot{m} = \frac{C_D A_{th} p_0}{(RT_0)^{1/2}} \gamma^{1/2} \left(\frac{2}{\gamma + 1}\right)^{(\gamma+1)/2(\gamma-1)} \tag{5.3}$$

Where C_D is the discharge coefficient, p_0 and T_0 are the upstream pressure and temperature respectively, p_T is the downstream pressure and R is the gas constant.
This allows for the relationship between air flow rate, throttle angle, intake manifold pressure and engine speed and for the definition of the most favourable diameter for the throttle valve to be possible. After several iterations using the above mentioned relationship, as depicted in Figure 5-11, a diameter of 19 mm was chosen.

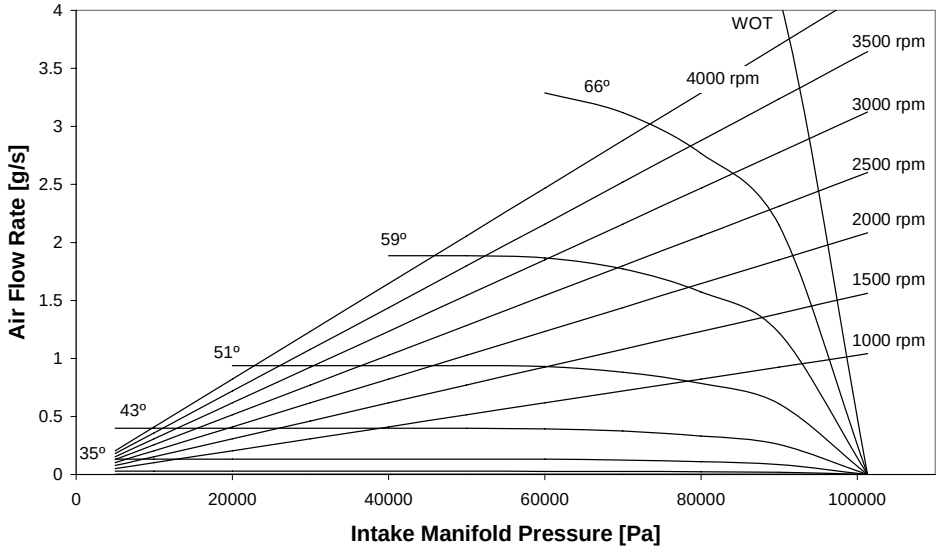

Figure 5-11 – Variation in air flow rate past a throttle, with inlet manifold pressure, throttle angle and engine speed.

The pressure drop across the throttle valve was measured for several throttle positions. These results are presented in Figure 5-12 and in Annex D. It can be seen that the effect of the throttle valve is not significant at very high loads (small difference between 100% and 82% opening curves), while for lower loads the throttle valve effect is more accurate. The elliptical profile mouth produces a small pressure drop in the intake as shows Figure 5-13 (values are presented in Annex D). The sum of the two components of the pressure drop represents the overall pressure drop at the intake manifold.

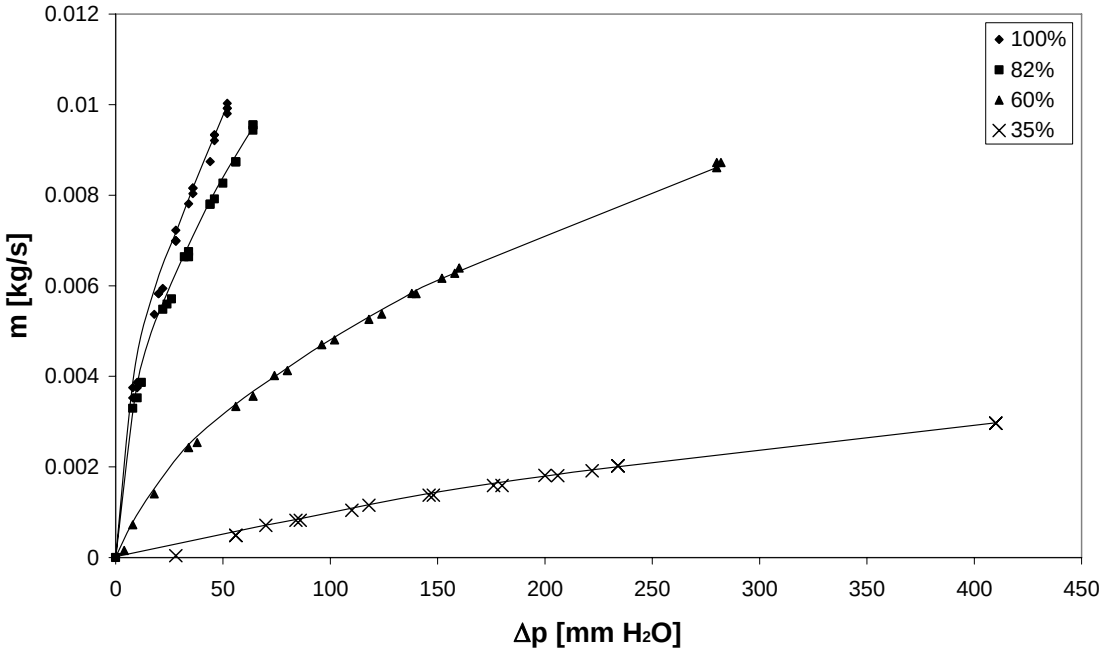

Figure 5-12 – Pressure drop across the throttle valve.

The values for the pressure drop presented above were obtained for continuous flow in the throttle valve and air intake duct. When the engine is running, the air flow through the throttle valve is pulsating, and in some working conditions, like with late intake valve closure, reversed. This leads to a quite complex pressure fluctuation set-up in the intake manifold and intake mouth, which does not allow for these calibration values to be used for air intake calculations.

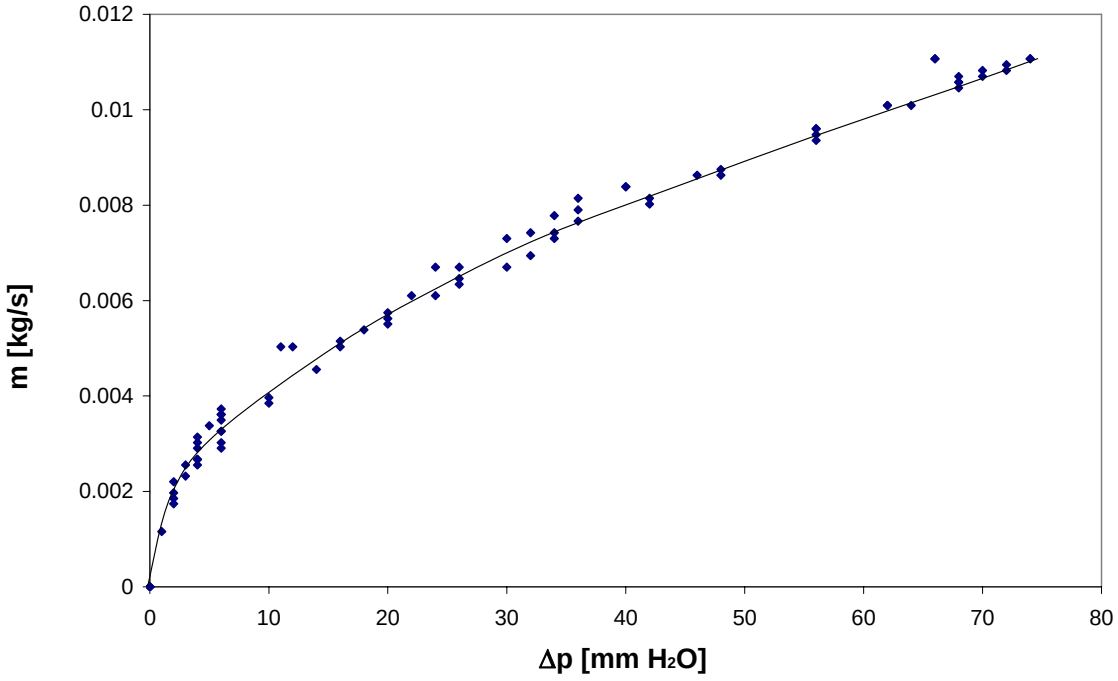

Figure 5-13 – Pressure drop upstream of the throttle valve.

5.2.7 Electronic control unit

The injection and ignition are controlled by a Haltech E6A electronic control unit (ECU). This uses a special-purpose programmable microcomputer suited for engine management. The E6A system includes the ECU (Figure 5-14), engine sensors and a special wiring connecting harness. The engine speed and crank position are measured by a Hall Effect sensor placed in the engine crankshaft (Figure 5-15). The throttle has a position sensor that measures the load applied to the engine. The system controls the injection by setting an injection time in the injection map for each engine working conditions (load and speed). The injection duration may be adjusted by other system inputs like atmospheric pressure and temperature, since these variables produce changes in the air density hence in the volumetric efficiency of the engine. The signal from the hall sensor triggers the system to inject. The same happens to the ignition timing. The trigger signal establishes the reference point and the ignition happens by adding the advance to be used to that reference point. The advance and injection duration to be used at each working conditions are stored in a table, dependant on the engine speed and load conditions. [3]

Figure 5-14 – Electronic Control Unit.

Figure 5-15 – Hall effect sensor placed in the crankshaft.

5.3 Swirl

Swirl is defined as an "organized rotation of the charge about the cylinder axis" [2]. The swirl is created during the intake process where the air mass flowing into the cylinder is inducted with an angular momentum. Swirl is used in CI engines to promote a more rapid mixing between the inducted air charge and the injected fuel. It can also be used in SI engines to speed up the mixture formation and the combustion process.

Swirl generation can be done either by forcing the air to rotate about the axis of the intake valve, or making the air induction tangentially to the cylinder wall, where it is deflected sideways and downward creating a swirling motion. Another alternative is to mask or shroud part of the peripheral inlet open area. Also, an alternative method of swirl generation is to use helical ports. With this solution the discharge coefficient is increased resulting on higher volumetric efficiency.

The original engine head from the Diesel engine had a swirl induction channel around the valve guide and a deflector at the end of that channel (Figure 5-17). The same head with the same intake port was used in the engine working as a spark ignition engine.

The result of a stoichiometric combustion of an hydrocarbon is N_2, CO_2 and H_2O. In real combustion processes and specifically in internal combustion engines, the combustion products are divided in a greater number of chemical species. Besides the ones referred above, CO, O_2, NO_x may be present, as well as unburned HC and many other species in less relevant quantities. The presence of O_2 in the combustion products results mainly from incomplete combustion, misfire or air mass in crevices, depending on the amount of O_2 present in the burned gases.

During the first tests, combustion problems were noticed by an excess of oxygen in the exhaust gas composition and a significant amount of HC. After disassembling it was noticeable that the mixture did not burn in a uniform way. The spark plug was clean in one side and "dirty" on the other side (Figure 5-16). This corresponded to the zone where flame did exist (carbon deposits) and the zone where it did not propagate (clean zone).

The improvement (reduction) of the swirl effect in the combustion chamber was achieved by a modification in the induction duct.

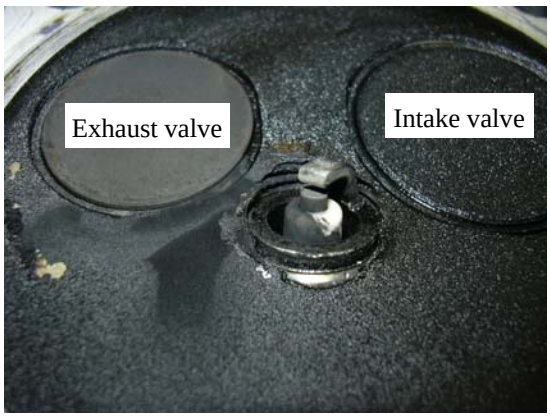

Figure 5-16 – Spark plug in the SI engine head after very first tests.

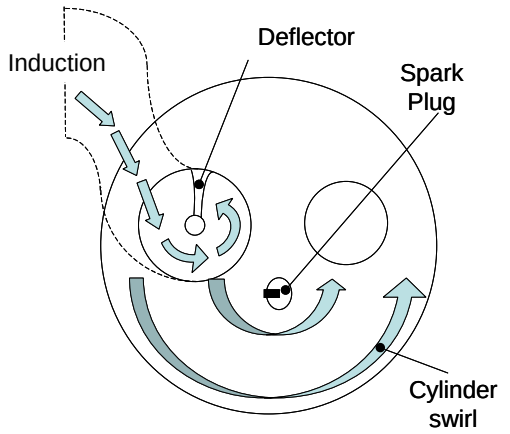

Figure 5-17 – Induction in the original engine head (top view).

5.3.1 Swirl measurement

Several criteria have been presented to quantify the swirl inside the engine cylinder. Firstly, even before the engine is put to work, swirl can be measured using a paddle wheel anemometer and a swirl torquemeter [4]. Due to laboratory equipment availability, swirl measurements were made through the use of the paddle wheel

anemometer. In this case, five different definitions of swirl parameters (C_{sp}) can be used:

Annand and Roe [5]

$$C_{sp1} = \frac{\Omega_p B^3}{V} \tag{5.4}$$

Where: Ω_p: paddle angular velocity (rad/s)

B: Bore (m)

V: volume flow rate (m^3/s)

Eisele [6]

$$C_{sp2} = \frac{paddle\ tip\ speed}{air\ axial\ velocity} = \frac{\Omega_p / B/2}{V/\left(\pi B^2/4\right)} = \frac{\pi\Omega_p B^3}{8V} \tag{5.5}$$

$$\text{hence, } C_{sp2} = C_{sp1}\frac{\pi}{8} \tag{5.6}$$

Heywood [7]

$$C_{sp3} = \frac{\Omega_p B}{v_0} \tag{5.7}$$

Where v_0 is the flow velocity (m/s) through the valve if this is frictionless. v_0 can be calculated from the compressible or incompressible flow equation, used as:

$$v_0 = \sqrt{\frac{2\left(p_0 - p_c\right)}{\rho}} \tag{5.8}$$

Since $V = A_c\, C_d\, v_0$ then:

$$C_{sp3} = \frac{A_c C_d \Omega_p B}{V} = C_{sp1} \frac{A_c C_d}{B^2} \tag{5.9}$$

Where p_0 and p_c are the pressures in the port and in the cylinder (N/m^2) respectively, ρ is the air density (kg/m^3), A_c is the valve curtain area (m^2), C_d is the valve discharge coefficient.

Etminan [8]

Assuming that the air trapped in the cylinder entered at a constant flow rate during the induction stroke, the ratio of the paddle wheel angular velocity to the equivalent engine angular velocity (Ω_e) is:

$$C_{sp4} = \frac{\Omega_p}{\Omega_e} = \frac{\Omega_p B^3}{V} \times \frac{V}{\Omega_e B^3} \tag{5.10}$$

Noting that:

$$V = V_s \eta v \Omega_e / \pi \text{ and } V_s = \frac{\pi B^2 S}{4} \tag{5.11}$$

$$V = B^2 S \eta_v \Omega_e / 4 \tag{5.12}$$

Substituting from equations (5.12) and (5.4) into (5.10) gives:

$$C_{sp4} = C_{sp1} \frac{S \eta_v}{4B} \tag{5.13}$$

Thien [9]

Considering a 100% volumetric efficiency, the swirl parameter can be written as:

$$C_{sp5} = \frac{B^2 S \Omega_p}{4V} \tag{5.14}$$

5.3.2 Swirl test bench

The swirl/discharge coefficient test bench was build in the Aerodynamic laboratory at the Universidade do Minho with the configuration shown in Figure 5-18.

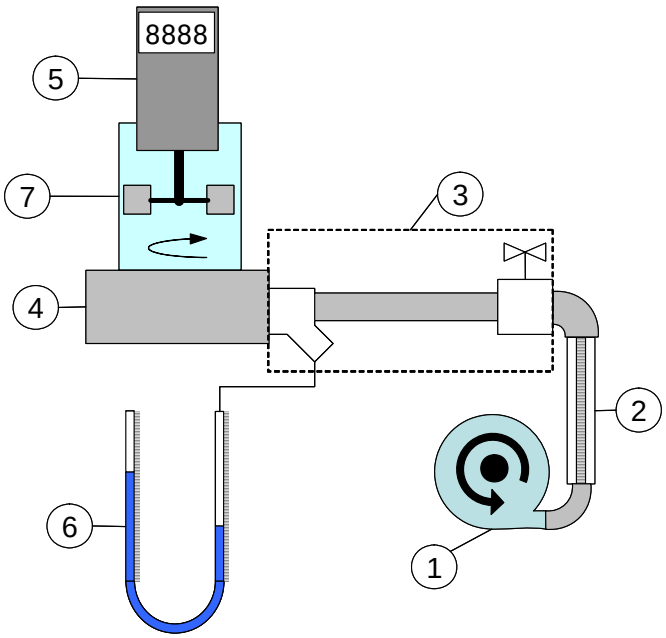

1	Air fan
2	Flow meter
3	Intake manifold
4	Engine head
5	Paddle wheel and rpm meter
6	Differential manometer
7	Glass cylinder

Figure 5-18 – Swirl and pressure drop test bench scheme.

The engine head was tested with both valves mounted, the exhaust valve completely closed and the intake valve open at its maximum lift. The spark plug was also in place. The complete intake manifold was also used at full throttle position. The flow meter was chosen with a working range suited for the amount of air flow inducted during the opening of the inlet valve of the running engine. At the entrance of the intake port of the engine head a pressure line was installed in order to measure the discharge coefficient that the configuration changes made to the intake port. The swirl was measured using the first method mentioned above. A paddle wheel was manufactured and mounted on a tachometer. Tachometer specifications are presented in Table 5-3.

Table 5-3 – Tachometer specifications.

Graham & White Instruments	
Measurement	0.5 to 19,999 rpm
Resolution	0.1 rpm (0.5 to 999.9 rpm) 1 rpm (over 1000 rpm)
Accuracy	± (0.05% + 1 digit)
Sampling time	1sec. over 6 rpm

5.3.3 Flow meter calibration

Considering the engine bore, stroke and a maximum speed, an approximate maximum flow inducted by the engine can be calculated. For the engine under study, with a displacement of 211 cm^3 and a maximum speed of 4000 rpm an approximate maximum flow of 25 m^3/h was calculated. The flow meter used was previously calibrated for the working conditions and pipe geometry. A pitot tube was installed at the end of a straight pipe so that fully developed flow was established. The pressure difference between the total and the static pressures, the temperature and environment pressure were used to calculate the equivalence between the percent scale of the flow meter and the actual air flow in the circuit. The results from that calibration are presented in Figure 5-19 where the polynomial equation for the tendency line is also shown (values are presented in Annex D).

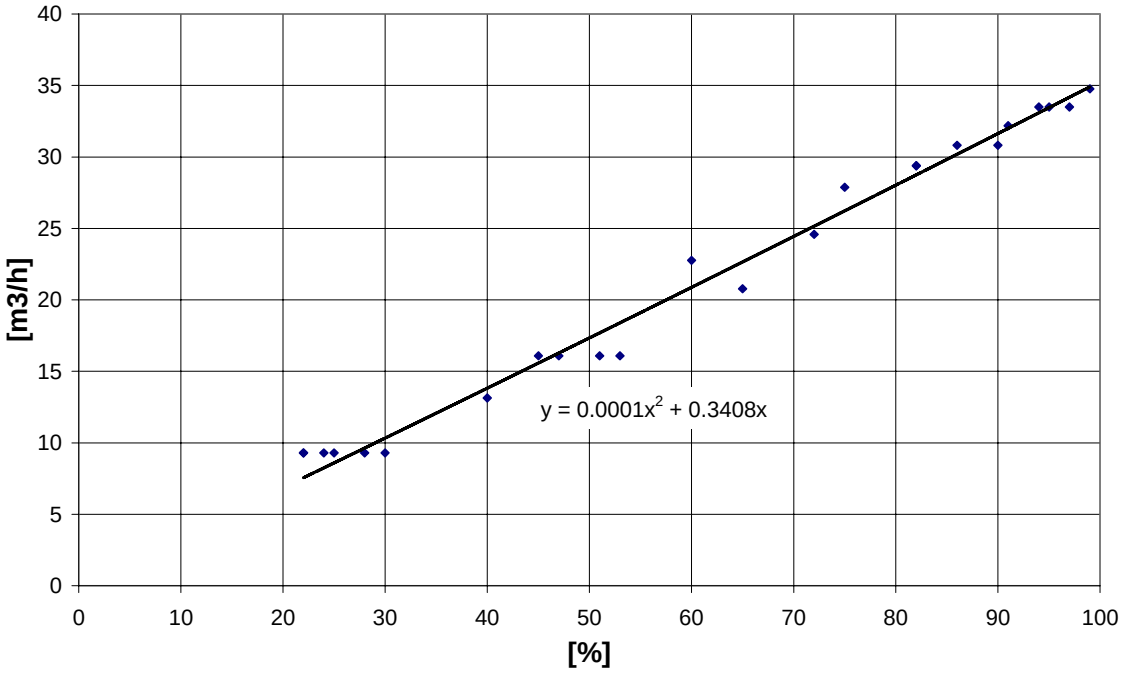

Figure 5-19 – Flow meter scale calibration.

5.3.4 Modifications to the intake port

As a result from the observations of the combustion problems, already mentioned in section 5.3, a first modification was made to the intake port so to create a deflector in the opposite side of the existing one (Figure 5-20). This was eliminated and the deflector added was built in such a way that it interrupted the air flow at the entrance of the swirl induct channel. This channel was also filled up in order to eliminate even more the swirl pattern of the induced air. The swirl was measured at several distances from the engine head and the results are presented in Figure 5-21 (experimental values are included in Annex D). The reduction of the swirl, as a function of the distance taken from the inlet valve includes, varies from 60% up to 80%.

Figure 5-20 – (Left) Original intake duct; (Right) Modified intake duct.

Hence the discharge coefficient of the induction port changed and a modification of the intake port was made in order to minimize the increase of the pressure drop in that passage. After that, the discharge coefficient increased slightly but the difference is acceptable for the case of an intake port. Figure 5-22 shows the discharge coefficient with and without the modification and its evolution as a function of the air mass flow (experimental values are presented in Annex D).

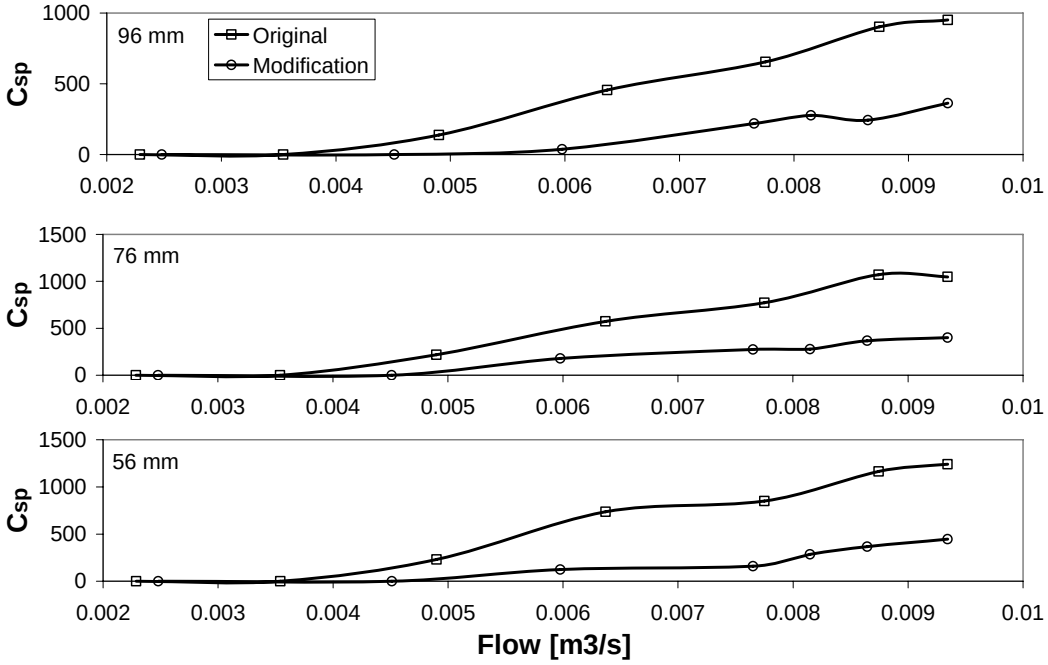

Figure 5-21 – Swirl coefficient measurements.

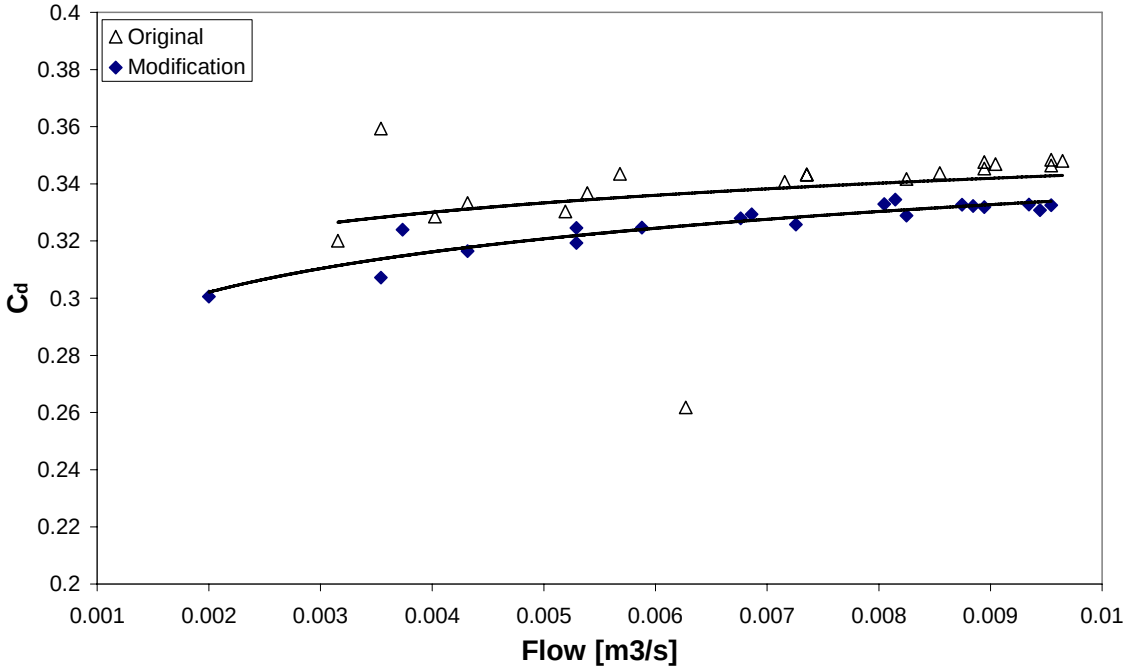

Figure 5-22 – Discharge coefficient of the original and modified intake port.

5.3.5 Results in the combustion

The combustion on the original engine was very unstable with high levels of emissions. The stoichiometric conditions were unattainable, the O_2 percentage in the exhaust gases reaching 18% meaning that a very poor, or almost no combustion was taking place, a value of 3000 ppm of HC being recorded. After the above modification in the inflow swirl, values of CO_2 of 14% and stoichiometric burning conditions were obtained.

5.4 Hydraulic Dynamometer

A Go-Power Systems Dynamometer D-100 was used to brake the engine and measure its torque output. This is a hydraulic dynamometer (Figure 5-23) fitted with a strain gage load cell (Figure 5-24) and a working range up to 14 000 rpm and 100 hp as shown in Figure 5-25. [10]

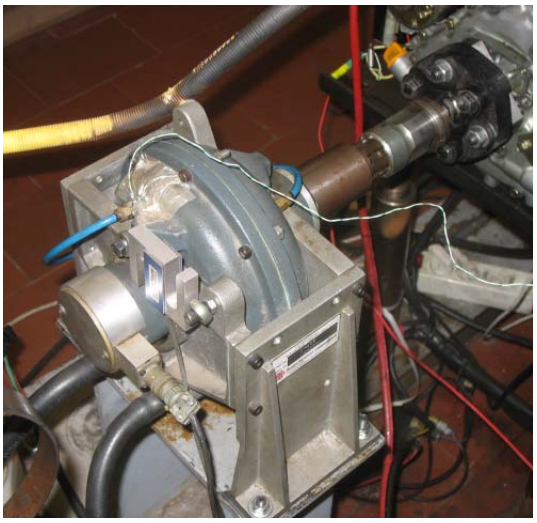

Figure 5-23 – Hydraulic dynamometer.

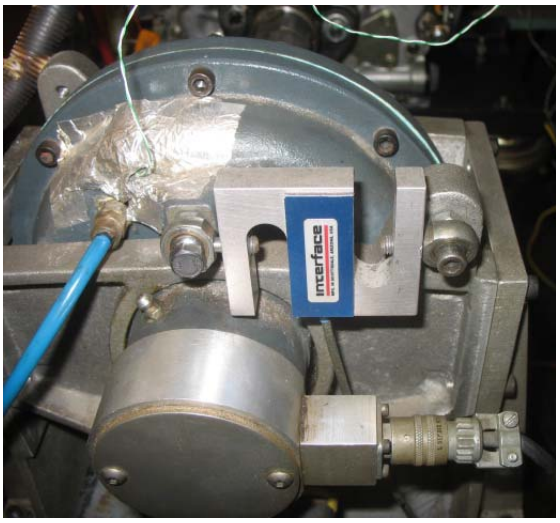

Figure 5-24 – Load cell.

5.4.1 Installation circuit

The working envelope of the hydraulic dynamometer is presented in Figure 5-25. From preliminary engine tests it was clear that its torque output was very low when compared to the working range of the hydraulic brake. To control the engine speed, only the fine adjustment valve of the brake water circuit was used and even then a constant water pressure was required to ensure that no braking torque oscillations existed. For this a

modification on the water circuit had to be made. The pressure in the feed line had to be constant at all times, thus the water pump was connected to a limiting pressure valve. Figure 5-26 shows the final hydraulic dynamometer installation circuit.

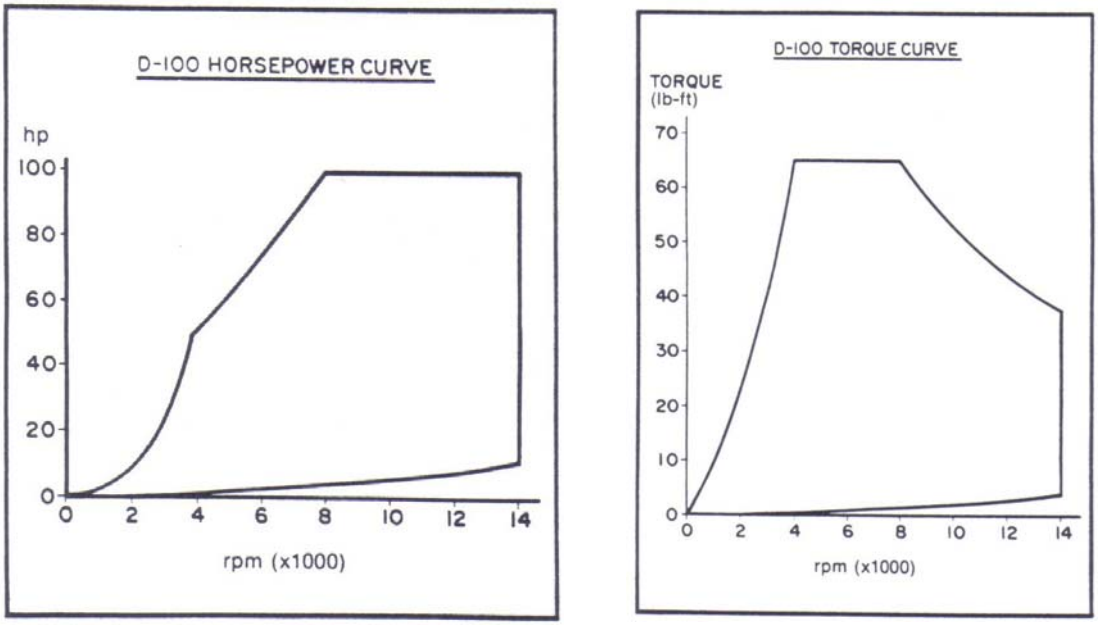

Figure 5-25 – Hydraulic dynamometer working envelope.

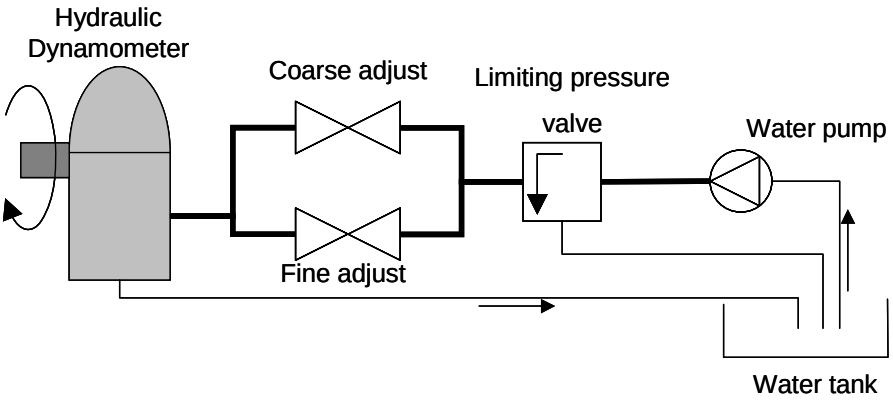

Figure 5-26 – Installation circuit of the brake dynamometer.

5.4.2 Load cell calibration

The load cell calibration was made following the procedure referred in the dynamometer operating manual. A 0.5 m length bar was attached to the brake and different weights were applied to produce different torque values. The DC voltage

output signal was read with a voltage meter. During engine tests the output signal from the load cell was directly acquired by an acquisition board (NI 4350 High precision temperature and voltage meter) as a DC voltage signal, which was then converted in torque values using the calibration curve shown in Figure 5-27 (experimental values are presented in Annex D).

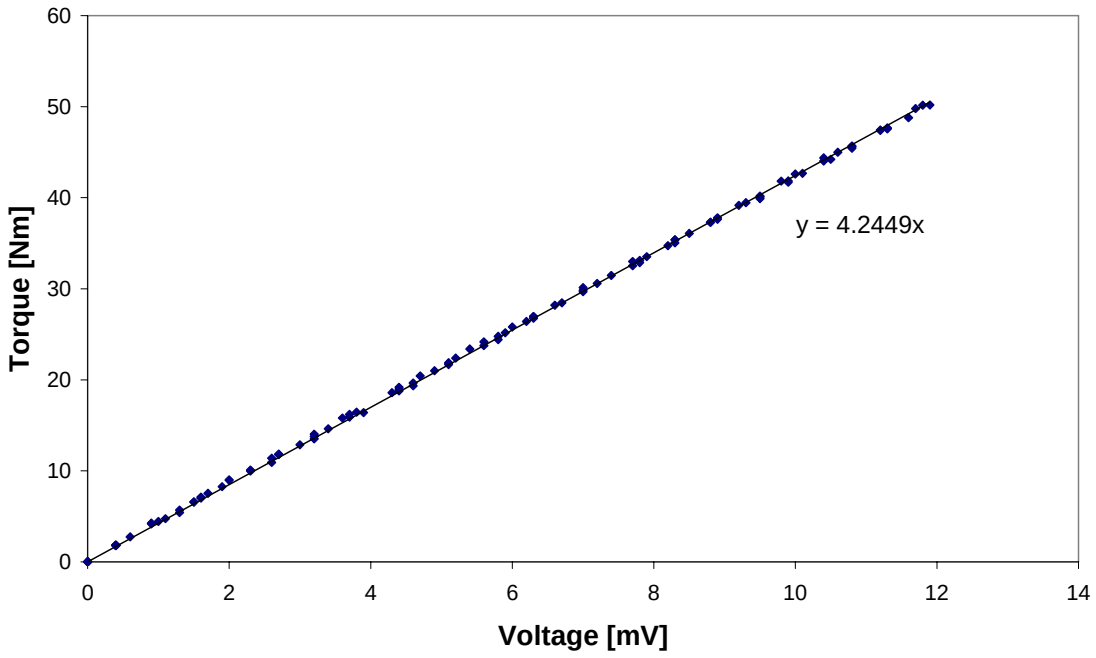

Figure 5-27 – Calibration curve for the load cell.

5.5 Fuel measurement

The fuel tank is placed over an AND EK-1200G electronic balance (Figure 5-28) for fuel consumption measuring [11]. Maximum measuring weight of the balance is 1200 g with a resolution of 0.1 g.

With this arrangement the fuel mass was measured at fixed time intervals and a fuel flow rate was then be calculated. The specific fuel consumption is derived from only three measured quantities: the mass of fuel consumed, the engine speed and the mean torque [12].

Figure 5-28 – Fuel measuring equipment.

5.6 Temperature measurement

Several thermocouples (all K type) were placed at various locations of the engine for temperature measurements (Figure 5-29):

a) Exhaust temperature: The thermocouple was located downstream of the exhaust valve, on the first section of the exhaust pipe.
b) Intake temperature: The thermocouple was located at the end of the intake manifold pipe, just upstream of the fuel injector.
c) Oil temperature: The oil temperature thermocouple was located in the oil sump.
d) Cooling air temperature: The cooling air of the engine has three possible exits, and thermocouples were placed at each of these exists, thus measuring the air temperatures just at these exits.

All the thermocouples were connected to an acquisition board (NI 4350 high precision temperature and voltage meter) for data recording.

a) Exhaust

b) Intake

c) Oil

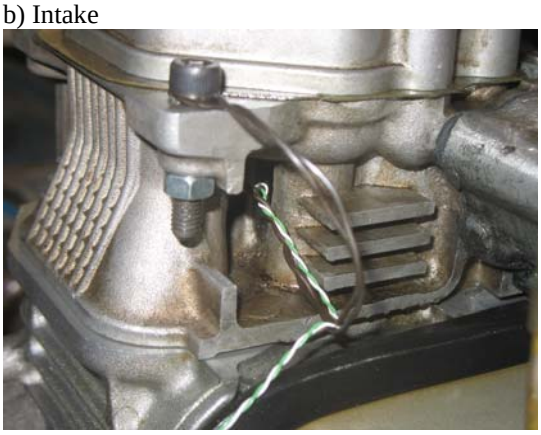

d) Cooling air in front

e) Cooling air at engine back

Figure 5-29 – Thermocouples position on the engine.

5.7 Pressure Sensor

The pressure inside the cylinder allowed for the measurement and analysis of the pumping work to be made and the indicated work in each engine cycle to be worked out. This was made by integrating the pressure curve in the p-V diagram of the cycle, using the expression:

$$W = \int pdV \tag{5.15}$$

For this calculation the pressure profile along the cycle in relation to time or crank angle had to be known.

An Optrand AutoPSI pressure sensor specially conceived for in cylinder pressure measuring was used. This pressure sensor in assembled in a spark plug modified for that effect. A channel exists along the spark plug thread, which is opened to the combustion chamber from one side and connects to the pressure sensor at the other. The sensing element is coupled via an optical fibre to the electronic unit, which was then connected to the power source and data acquisition system. The dynamic pressure sensor specifications are presented in Table 5-4.

Table 5-4 – Pressure sensor specifications.

Pressure Measuring Range	0 – 1500 psi (0 – 103 bar)
Frequency Range	0.1 Hz to 25 kHz
Pressure Output signal	Analog, 0.5 – 5V
Non-Linearity and Hysteresis	±0.5% FS under non-combustion conditions, under constant pressure ±1% FS under combustion conditions, i.e., varying temperature within one combustion cycle

The pressure sensor output is a voltage signal, which was calibrated using a known static pressure. The calibration of the Optrand AutoPSI pressure sensor was made following the procedures presented in the users manual [13]. All the installation was assembled and two potentiometers were installed between the diagnostic wire and the ground. A 10 kΩ potentiometer for coarse adjustment of the resistance and a 1 kΩ for fine adjustment were used. An oil pump capable of supplying oil at a maximum pressure of 80 bar was used. For voltage output reading a voltmeter was used and the oil pressure was read in the manometer installed in the oil circuit.

After the system was turned on, the output voltage is 0V. The potentiometers were then regulated until an output voltage of 0.6 V was reached. The system was let to stabilize for 20 minutes, after which the calibration procedures were started. Two series of measurements were performed, one by raising the pressure and other by lowering it. These results are presented in Figure 5-30 and in Annex D.

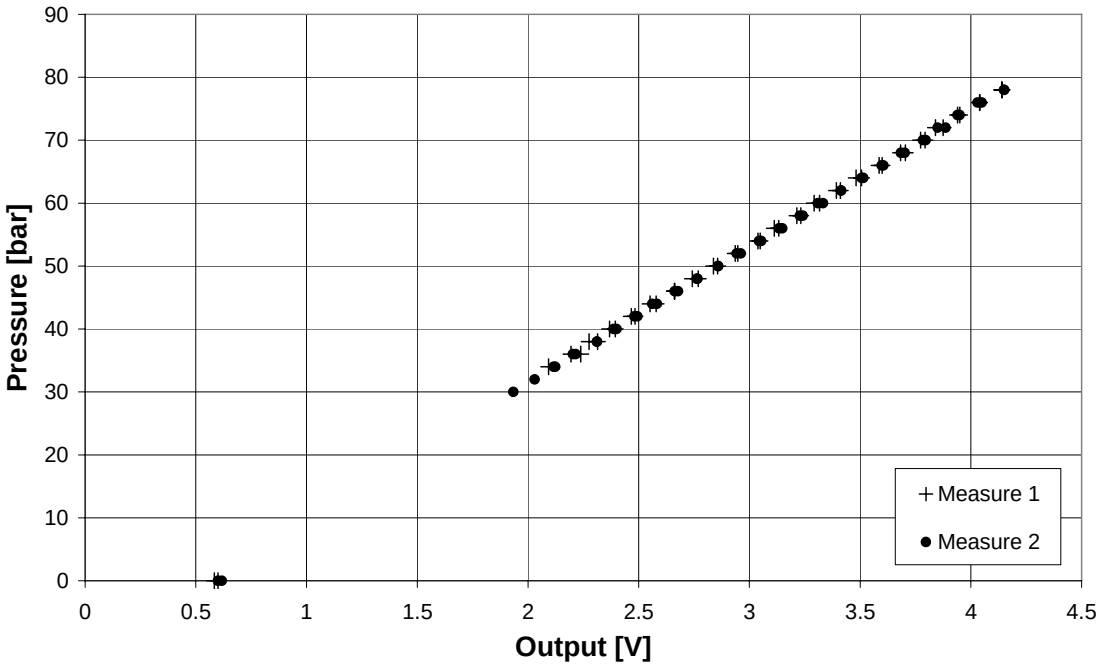

Figure 5-30 – Measuring results in the hydraulic bench.

An almost linear tendency was recorded as seen in Figure 5-30. A best fit was adjusted to these data and compared with the calibration factor supplied by the sensor manufacturer. The calibration factor supplied by the manufacturer, i.e. the line slope is 2.99 mV/psi. After unit conversion both lines are plotted in the graph of Figure 5-31.
A difference of 5% less exists between the calibration factor supplied by the manufacturer and the calibration values. The new calibration factor was used for pressure measurements during the engine tests.

Data acquisition

Data supplied by the pressure sensor unit was read by using an oscilloscope as the data output frequency is typically in between 6 kHz and 24 kHz, which corresponds to an acquisition rate of 360 readings per engine revolution for an engine speed range of 1000 rpm up to 4000 rpm.
For appropriate construction of p-V diagrams, two signals were used: the pressure signal from the pressure sensor, and the crankshaft position signal from the hall sensor in the engine. This signal was used to trigger the oscilloscope signal. At the same

instant, the hall sensor signal marks a certain crank position for data acquisition, thus enabling the correct phasing of the pressure curve relatively to the cylinder volume.

The oscilloscope used in these tests was a YOKOGAWA DL 1540L with four input channels. In the range of 5V/div the accuracy is ± 2.5 %.

The data read in the digital oscilloscope was saved as an image format and in numerical file format, which can be used latter to build the p-V diagrams of the working conditions of the engine.

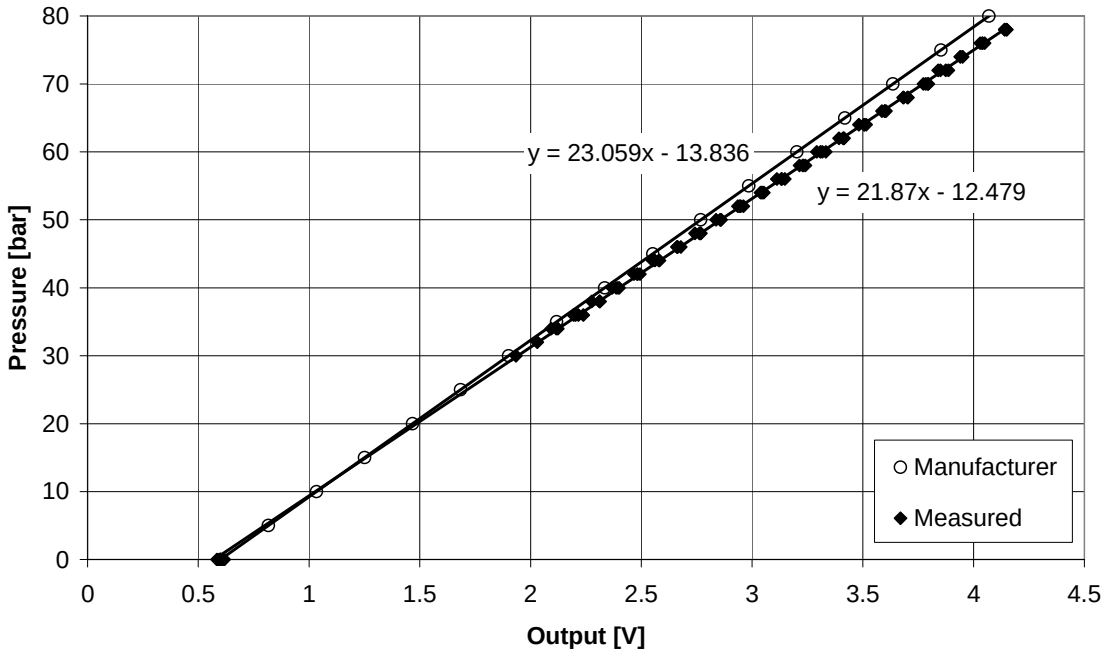

Figure 5-31 – Calibration factors comparison.

5.8 Air-Fuel Ratio Meter

A Motec wide range air-fuel ratio meter was installed in the exhaust duct. The information supplied by this device was used in setting the injection time for the engine to run at constant stoichiometric conditions ($\lambda = 1$). The lambda sensor is connected to a digital display, which shows the air-fuel ratio value. The sensor is placed in the exhaust pipe in a position and location recommended by the user manual [14].

The air-fuel sensor is a Bosch LSU 4 Lambda Sensor. The sensor and meter specifications are described in Table 5-5.

Table 5-5 – Motec Air-Fuel Ratio Meter specifications.

Measurement range	0.7 to 32.0
Accuracy	± 1.5%
A/F Ratio	Fuel Dependant
Maximum Exhaust Temperature	850 ºC
Normal Temperature Range	150 – 800 ºC

5.9 Exhaust Gas Analyser

5.9.1 Multigas Analyser

The Signal 9000 MGA gas analyser utilises two well-established measurement techniques to enable measurements of three separate sample gases (CO, CO_2 and O_2).
To measure the O_2, a dumb-bell paramagnetic sensor is used, which is sensitive and presents a linear response. The sensor is heated to prevent condensation and to minimise drift.
To measure the concentration of the other two gases, the analyser applies an infra-red gas filter correlation technique using gas-filled optical filters for maximum selectivity. A single beam optical path increases tolerance to contamination [15].
This gas analyser model is capable of measuring gases in the ranges presented in Table 5-6.

Table 5-6 – Signal 9000 MGA analyser reading ranges.

CO [ppm]	**CO_2 [%]**	**O_2 [%]**
1000 / 5000 / 10000	5 / 10 / 20	5 / 10 / 25

For calibration of the gas analyser different dilutions of span gases in nitrogen are used. The dilution values of the span gases are presented in Table 5-7.

Table 5-7 – Dilution values of span gases.

Gas	**Dilution**	**Unit.**
CO	5000	ppm
CO_2	10	%
O_2	20	%

5.9.2 NO_x Analyser

For the analysis of the concentration of NO_x components in the exhaust gases a Signal 4000VM Heated Vacuum NO_x Analyser was used. This works under the chemiluminescent principle, using ozone. On a reading range up to 10000 ppm the analyser uses a heated line for the sample transport from the exhaust pipe to the analyser, preventing condensations. The heated line is set at 140 ºC. The analyser has a sample oven nominally set to 190 ºC. [16]

Figure 5-32 depicts the complete gas analyser installation scheme and Figure 5-33 shows the gas analysis unit in the internal combustion engines laboratory of the Mechanical Engineering Department of Universidade do Minho.

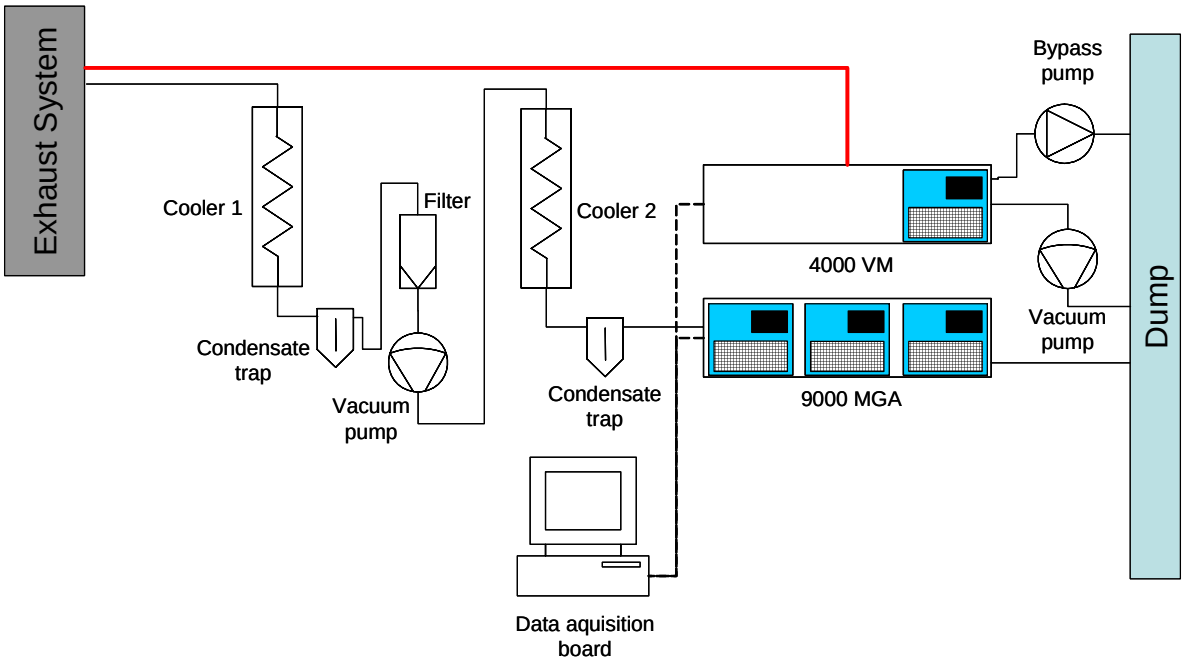

Figure 5-32 – Scheme of the gas analysis unit.

Figure 5-33 – Gas analysis unit.

5.10 Summary

An engine and modification to make it able to perform the Miller and the Miller VCR cycle were described. Also, testing equipment was described. With the engine and equipment mentioned, tests and measurements can be performed to assess the real thermodynamic improvement obtained with the proposed engine modifications.

5.11 References

1 Pignone, G. A., Vercelli, U. R., *Motori Ad Alta Potenza Specifica*, Giorgio Nada Editore, Italy, 1995.

2 Heywood, J., *Internal Combustion Engines Fundamentals*, 1988, McGraw-Hill.

3 *E6A Engine Management System, Instruction Manual*, Haltech, Australia, 1996.

4 Stone, C. R., Ladommatos, N., *The measurement and Analysis of Swirl in Steady Flow*, SAE 921642, 1992.

5 Annand, W.J.D., Roe, G.E., *Gas Flow in the Internal Combustion Engine*, 1974, Foulis, Yeovil.

6 Powling, L.J., *The measurement and Analysis of Axial Swirl and Tumble Within Automotive Engine Cylinders*, Final Year Project Report, Department of Manufacturing and Engineering Systems, Brunel University, 1990.

7 Heywood, J. B., *Internal Combustion Engine Fundamentals*, 1986, McGraw Hill, London.

8 Etminan, Y., Induction Tuning of a Single Cylinder Diesel Engine, MPhil Thesis, 1989, Brunel University.

9 Thien, G., 'Entwicklungsarbeiten an Ventilkanalen von Viertakt – Dieschmotoren' (Development work on Valve Ports of Four-cycle Diesel Engines), Osterreichische Ingenieur Zeitschrift. Jahrgang 8, Heft. 9.1965.

10 *D-100 Series Portable Dynamometer Installation, Operating and Service Manual*, Go-Power Systems, USA.

11 Martins, Jorge, *Motores de Combustão Interna*, (in Portuguese), Publindústria, Porto, 2005.

12 Plint, M.A., Martyr, Anthony, *Engine Testing: Theory and Practice*, Butherworth-Heinemann, 1995.

13 *AutoPSI-S Pressure Sensor Operating Instructions*, Optrand Incorporated, OD-002D (02/16/05), 2005, USA.

14 *Professional Lambda Meter, User Manual*, MOTEC Pty Ltd, 2005.

15 *9000 MGA Multi Gas Analyser Operating Manual*, Signal Group Limited, England, 2003.

16 *4000VM Heated Vacuum NOx Analyser*, Signal Group Limited, England, 2003.

6 – Engine Tests Results

6 ENGINE TESTS RESULTS

6.1 Introduction

Testing a baseline engine and a modified engine and comparing the results of each other gives the real improvement achieved with an engine modification. The improvement tendency found in test results can be used to improve other engines.

In the previous chapters a comparison of several spark ignition engine cycles both theoretically and using computer simulation was made. The engine tests described in the following sections aims the assessment of the real potential of the Miller VCR engine cycle, in terms of thermodynamic improvement, as an alternative to the conventional Otto cycle and the Miller cycle engine for part load applications. In chapter 3 a comparison between several spark ignition and compression ignition engine cycles was made. In the tests described herein the same engine operated as spark ignition and as compression ignition was tested, allowing a direct comparison of both engine versions. The original version of the engine was a compression ignition. It was tested in that version and after that converted to spark ignition. It was tested as an Otto cycle engine and then with different camshafts it was tested as a Miller engine and to finish this sequence it was tested as a Miller VCR engine, with different camshafts and different pistons (with different compression ratios).

6.2 Engine Friction

The relative movement of the engine parts generates mechanical losses due to friction between the contact surfaces of the moving components. In the case of the engine used in the tests, the sources of friction, thus mechanical losses are:

1. Crankshaft bearings and sealing ring;
2. Gear engagement between crankshaft gear and the balance shaft gear;
3. Balance shaft bearings;
4. Gear engagement between crankshaft gear and the camshaft gear;
5. Camshaft bearings;

6. Gear engagement between crankshaft gear and the oil pump gear;
7. Oil pump;
8. Cam followers contact;
9. Valve train (valves, rocker arms);
10. Connection between the connecting rod and crankshaft;
11. Connection between the connecting rod and the piston pin;
12. Piston skirt and rings contact with the cylinder liner.

6.2.1 Friction measurement

The existing methods for measuring the mechanical losses that may be applied to the case of a single cylinder spark ignition engine are mainly [1]:

6.2.1.1 Mechanical losses from indicator diagram and measured power output

This method relates the power measured by a dynamometer with the indicated mean effective pressure (*imep*) taken from the indicated diagram of the engine at constant working conditions. The friction mean effective pressure (*fmep*) for a four-stroke engine is then calculated as:

$$fmep = imep - bmep \tag{6.1}$$

where

$$imep = \frac{\int_{-180}^{180} pdV}{V_s} \tag{6.2}$$

$$bmep = \frac{P60 \cdot 2}{V_s N} \tag{6.3}$$

Where:

p: measured cylinder pressure [Pa]

V: Cylinder volume [m^3]

P: measured power of the engine [W]

V_s: swept volume [m^3]

N: engine speed [rpm]

However, this method has some disadvantages such as:

- There is a problem in obtaining an accurate recording of the cylinder pressure.
- Exact determination of true TDC is difficult, and small errors in this may lead to significant differences in the *imep* (e.g. 1º CA of the TDC may lead to a 5% difference in the *imep* value).

6.2.1.2 Motoring test

This method is implemented using a 4-quadrant dynamometer. The ignition and fuel injection are cut and the power necessary to motor the engine at the same speed is measured as quickest as possible. However, this method has some disadvantages like:

- Under non-firing conditions the cylinder pressure is greatly reduced, with a consequent reduction in friction losses between piston rings, piston skirt and cylinder liner and in the running gear.
- The cylinder wall temperature falls very rapidly as soon as combustion ceases, with a consequent increase in viscous drag that may lead to some extent compensate for the above effect.
- Pumping losses are generally much changed in the absence of combustion.

6.2.2 Friction results

In the case of the present study a method similar to the motoring tests described above for friction measurement was used. However, instead of running the engine on firing conditions and then cut ignition and injection, the engine was run with an auxiliary electric motor, and the required torque for turning the engine at that particular speed was measured. These friction tests were made under several conditions, such as with and without spark plug to reduce both the pumping work and the compression work. The complete engine was also tested with several throttle valve positions, thus gathering some results of pumping work as well.

From the test results the torque difference required to turn the engine when the spark plug is removed could be worked out. In this case, there is no compression within the cylinder but there always is flow through the spark hole, which induces some pumping losses, although considerably smaller than in the case of compression.

Friction in internal combustion engines takes into account several components, which some of which are proportional to the engine speed (friction) others being proportional to the speed squared (hydrodynamic lubrication) and other still being proportional to the cube of engine speed (turbulence, pumping, fluid flow through narrow valves). The most significant of all these components are expected to be those proportional to square of the speed. The friction curve for the engine is then expected to be a second-degree polynomial approximately [2]. Such curve was adjusted to the experimental results of the friction tests, which is plotted in Figure 6-1. In this figure, results for two part-load throttle positions (60% and 7%) are depicted.

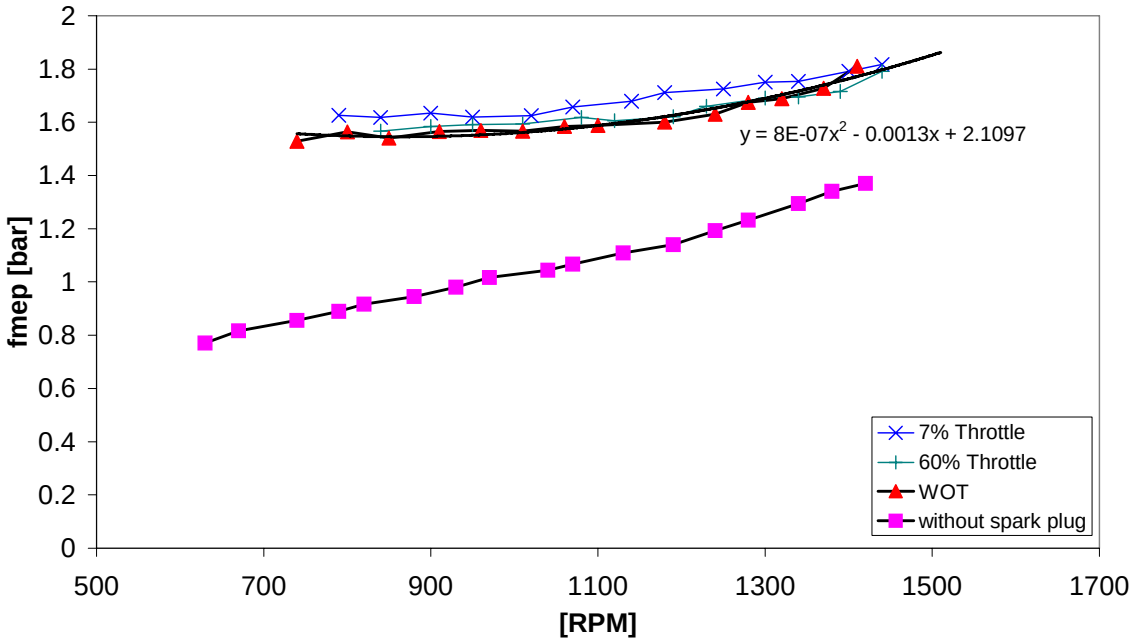

Figure 6-1 – Friction results from the engine.

6.3 Variable Valve Timing

For valve timing variation several systems do exist which were described in chapter 2. Most of these systems are not commercially available and require a significant

investment for their application and use with an engine such as this. In the case of the present work, an alterative was created to substitute a VVT system. Several camshafts with different cam profiles were used to create different valve events. With this method, valve timing variation is achieved by substitution of the camshaft.

In order to save on design effort and reduce the number of variables, the baseline cam profile considered was the one from the original Yanmar Diesel engine.

The design of the intake cam profiles followed the method described in 4.2.10. The different cams that were used in the engine had either LIVC with different maximum lift dwell angles or EIVC with different opening periods. The LIVC cams had dwell angles of 20, 40, 60 CA. Two EIVC cams were tested to evaluate and compare the ability of each load control strategy to reduce the engine load, as shown in Figure 6-2.

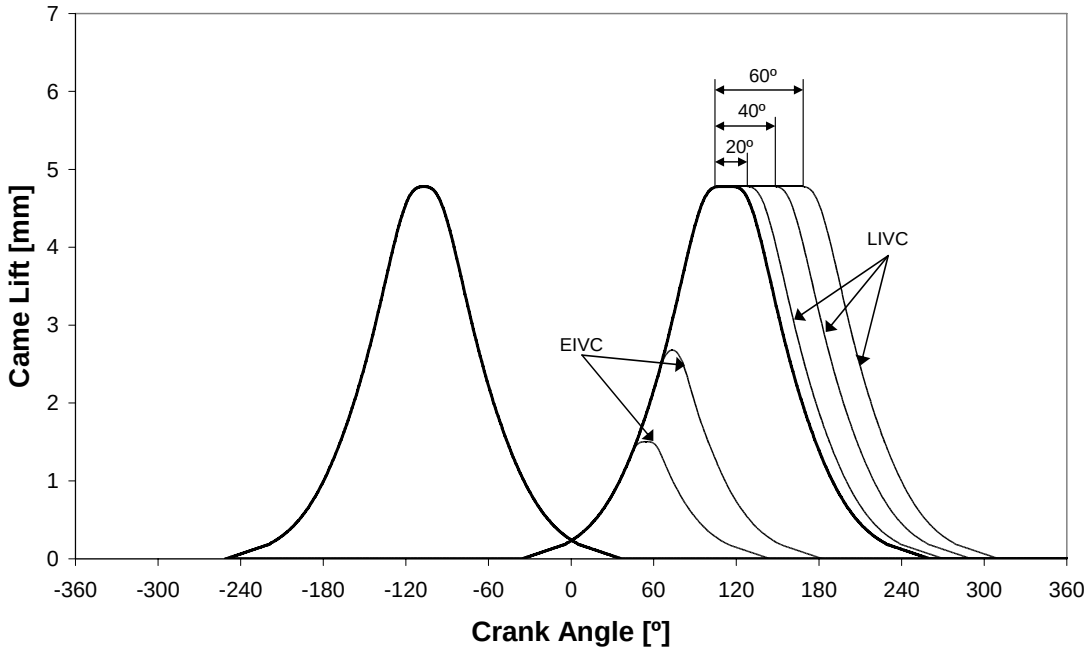

Figure 6-2 – Different cam profiles tested.

The exhaust timing and the intake valve opening position were kept always constant. Figure 6-2 shows the lift of the cam during the cycle completion for the different camshafts used to achieve different loads. Figure 6-3 presents the volumetric efficiency associated with each of these camshafts, calculated from the test results performed at stoichiometric conditions. With the designed EIVC camshafts lower volumetric efficiency cams were obtained, which corresponded to lower loads than the LIVC camshafts.

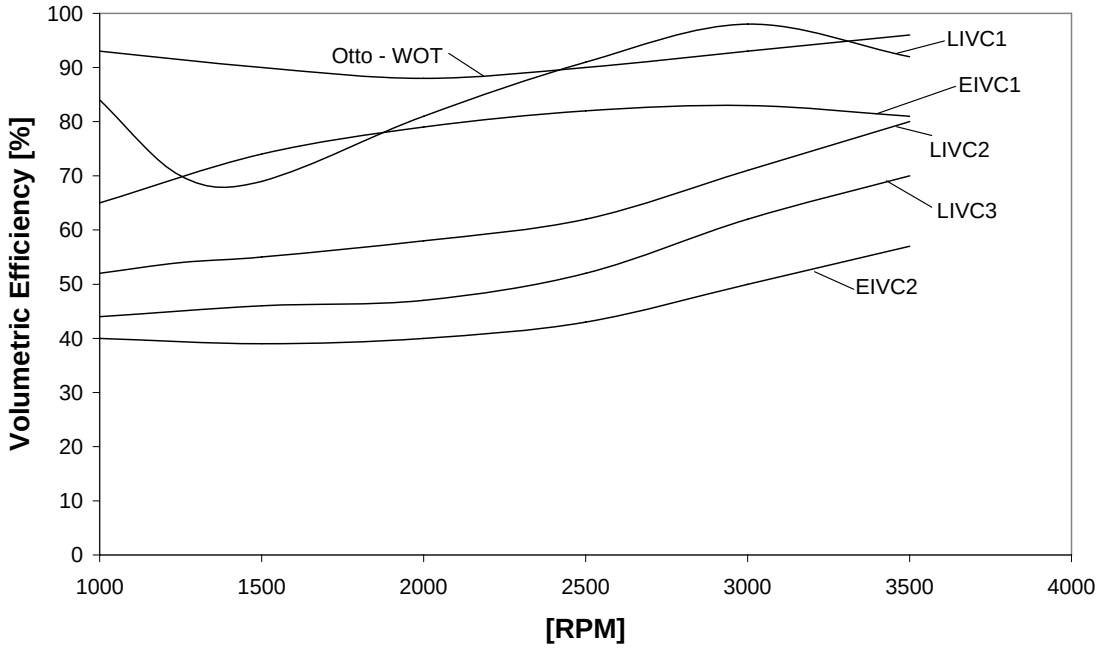

Figure 6-3 - Volumetric efficiency of each camshaft.

6.4 Variable Compression Ratio

To achieve the variation of the compression ratio, different pistons were used. As the original engine was a DI Diesel engine, original pistons were used, and the piston bowls of standard Diesel pistons are enlarged to create different combustion chamber volume, therefore different compression ratios are obtained. Table 6-1 reports the pistons size and compression ratios, including the original Diesel engine piston. This combustion chamber shape is not the ideal for SI engines, but this was the possible chamber to be manufactured from the original combustion chamber (Diesel) of the engine.

Table 6-1 - Pistons specifications.

Piston	Combustion chamber diameter [mm]	Compression Ratio
1	48.4	11.5:1
2	46.0	12.5:1
3	43.8	13.5:1
4	41.8	14.5:1
5	40.1	15.5:1
6	38.5	16.5:1
7	37.1	17.5:1
Diesel	-	19.9:1

6.5 Test procedures

6.5.1 Warm-up

After the engine start-up it was run for the required time until the warm up was considered complete. In most engine versions the warm-up limit temperature was considered to be the lubricant oil temperature higher than 80 ºC. In the Miller cycle engines with the lower loads (camshafts LIVC3 and EIVC2) this temperature was never reached even at the highest speed and in these cases the warm up limit temperature was considered to be 70ºC.

6.5.2 Engine mapping

The electronic control unit applied to the engine has injection and ignition maps in steps of 500 rpm. Thus, the engine was stabilized using the hydraulic brake at a constant speed, starting from 1000 rpm and increasing with 500 rpm steps until the maximum 3500 rpm. At these working conditions the injection duration was timed until stoichiometric mixture was reached. The λ value was considered acceptable within the range of 0.98 to 1.02 (the accuracy of the air/fuel ratio meter is ± 1.5%). In some working conditions the stabilization of the stoichiomteric mixture was quite difficult due to engine speed variations.

The setting of the optimum ignition time was made also at a stabilized engine speed. The ignition was then increased in steps of 5 CA degrees. Usually as ignition advance is increased the engine torque increases and as a consequence, increases the engine speed. With the use of the hydraulic brake the engine was reset at the initial engine speed and a new increase of the ignition time was attempted. When near the maximum brake torque (MBT) conditions the engine speed variation was not so perceptible and the step increase of the ignition time was reduced to 1 CA degree, then the value of the output torque was checked until a maximum was reached, or until a speed decrease was detected. All this procedure was interrupted when audible knock was detected. In this situation the MBT conditions were not the criterion for ignition setting but the knock onset.

6.5.3 Testing

Tests were only performed after the engine was completely mapped. Before tests effectively begun, data acquisition systems were initiated in the logging mode. These systems recorded data from temperature sensors, torque load cell and gas analysers. These data acquisition systems were running in different computers so the computer clocks were synchronized so that the recorded data from different systems could be related.

The engine was stabilized at speed values near 1500, 2000, 2500, 3000 and 3500 rpm. An engine speed variation of ± 50 rpm was considered acceptable. The engine was maintained at the set speed for periods of 3 minutes. During this period 6 readings were made of both the fuel weight in the fuel tank and engine speed. Using these values 5 differences were calculated for fuel consumption in periods of 30 seconds. These were the basis for engine efficiency and volumetric efficiency calculations.

During tests the value of the air/fuel ratio was continuously monitorised so that it could be maintained within the range defined above. Corrections were made when necessary.

6.5.4 Data analysis

Resulting points were calculated from the data records. The calculation of the several performance parameters of the engine was made as follows:

Torque (T)

$$T = \frac{\sum_{t-30}^{t} T_r}{r} \tag{6.4}$$

where:

t – time of the reading [s]

T_r – Value of the torque recorded at each instant [Nm]

r – number of recordings

Power (P)

$$P = T\frac{N}{60}2\pi \tag{6.5}$$

where:
N – Engine speed [rpm]

The output power given by an engine changes with the atmospheric conditions (pressure, temperature and moisture content). The values read from the engine test were therefore corrected [1] with reference to atmospheric standard conditions, taken as for Europe:

Pressure: 1.01325 bar
Temperature: 20 ºC (293 K)
Corresponding density: ρ_s = 1.205 kg/m^3

The air density under non-standard conditions, p_a and T_a is given by:

$$\frac{\rho_s}{\rho} = \frac{1.01325}{p_a}\frac{T_a}{293} \tag{6.6}$$

Assuming that the power of the engine varies directly with air density, hence with the mass of the air charge into the engine, equation (6.6) would also define the correction factor for the power output.
However, the volumetric efficiency of an engine is also a function of the flow conditions in the inlet manifold and past the valves. These velocities are generally quite high and compressibility effects come into play. These are a function of the Mach number of the flow, the higher the Mach number the greater the tendency for the flow to be ‘choked’ or limited.
For a given velocity Mach number varies inversely with the square root of the absolute temperature. Hence it is reasonable to write:

Power correction factor = density factor x Mach number factor

$$\frac{P_s}{P} = \frac{1.01325}{p_a}\frac{T_a}{293}\sqrt{\frac{293}{T_a}} \tag{6.7}$$

$$P_s = P\frac{1.01325}{p_a}\sqrt{\frac{T_a}{293}} \tag{6.8}$$

where P is the measured power and P_s is the corrected power at standard conditions. This relationship is accepted but has no absolute validity: it does not necessarily mean that a real engine performance will change with atmospheric conditions variation the same way as the correction factor.

The effect of humidity on performance is very small and may indeed affect power in either direction. In European practice it is generally ignored, though [3], which gives extremely complicated expressions for standardizing power output, specifies a relative humidity of 60% as standard.

Fuel Mass Flow Rate ($\dot{m}_f$)

$$\dot{m}_f = \frac{f_{t-30} - f_t}{30} \tag{6.9}$$

where:

f – mass of fuel in the tank

t – time of the reading

Specific Fuel Consumption (*sfc*)

$$sfc = \frac{\dot{m}_f \cdot 3600}{P} \tag{6.10}$$

Thermal Efficiency (η_t)

$$\eta_t = \frac{P}{\dot{m}_f \cdot Q_{LHV}} 100 \tag{6.11}$$

where:

Q_{LHV} – Lower heating value of the fuel, considered 44 MJ/kg

Volumetric Efficiency (η_{vol})

$$\eta_{vol} = \frac{2\dot{m}_{air}}{N \cdot V_d \cdot \rho_{a,s}} \tag{6.12}$$

where:

V_d – Engine displacement

$\rho_{a,s}$ – Standard air density

$\dot{m}_{air}$ - Air mass flow rate, calculated as:

$$\dot{m}_{air} = \dot{m}_f \cdot \lambda \cdot (A/F)_{stoich} \tag{6.13}$$

where:

λ – Air fuel ratio used, considered 1 (stoichiometry) in the present tests

$(A/F)_{stoich}$ – Air/Fuel ratio at stoichiometry of the used fuel, considered here as 14.5

Points resulting from these calculations were plotted and a tendency line was then fitted to these results in order to have workable data for comparison between engine versions and working conditions.

6.6 Engine Tests

6.6.1 Diesel engine

The original version (commercial) of the Diesel engine was set to work at full load condition. Figure 6-4 presents the manufacturers engine performance specification. As can be seen from this graph, the fuel cut-off is made above 3600 rpm.

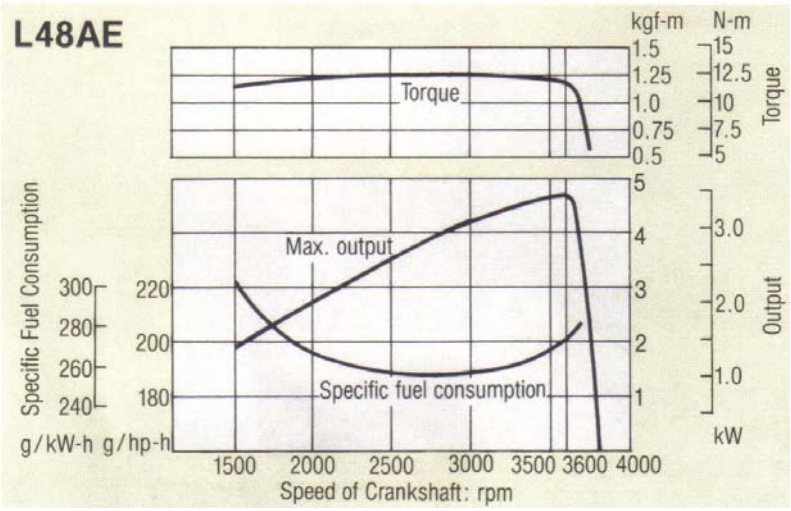

Figure 6-4 – Engine manufacturer performance specification.

Initial tests were made with the engine in its commercial (standard) Diesel version, so that the results could be used as a baseline for comparison and evaluation of improvements. In the Diesel engine, load variation was achieved through a direct actuation on the injection pump. Several load conditions were tested at different engine speeds (Figure 6-5). Values of the Diesel engine tests results are presented in Annex E. As can be seen in that figure, the original torque curve supplied by the engine manufacturer is quite close to the results obtained during the Diesel engine tests. The rest of the loads have their fuel cut-off limit reduced in terms of speed and for engine speed lower than that limit the torque curve is no longer flat as it can be seen to fall when reducing speed.

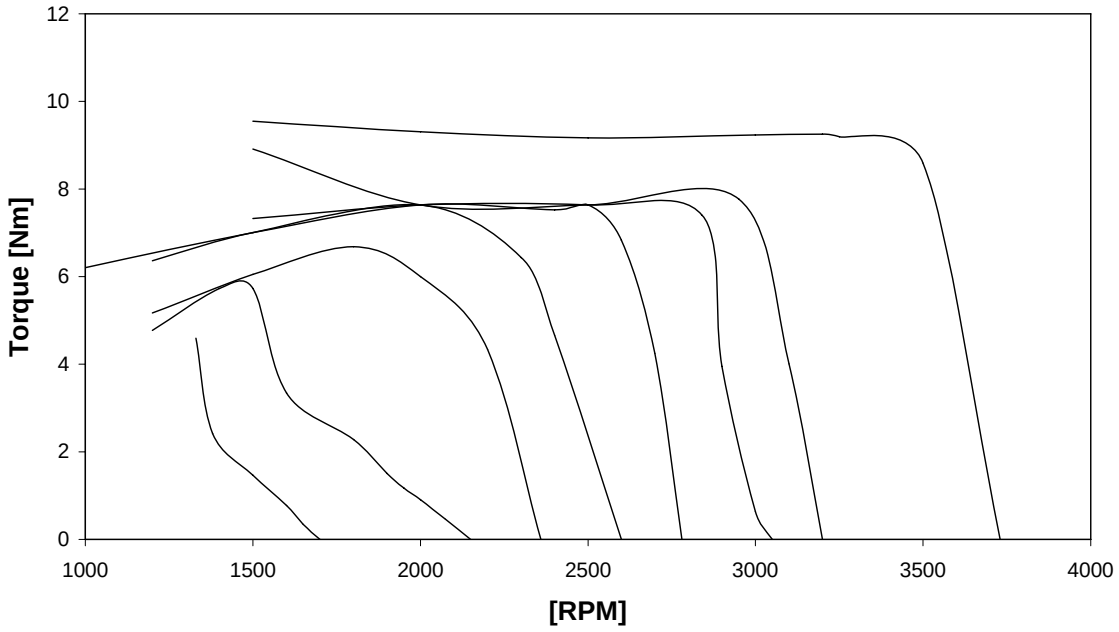

Figure 6-5 – Torque results for the different Diesel engine load conditions.

The measured Diesel engine specific fuel consumption map is shown in Figure 6-6.

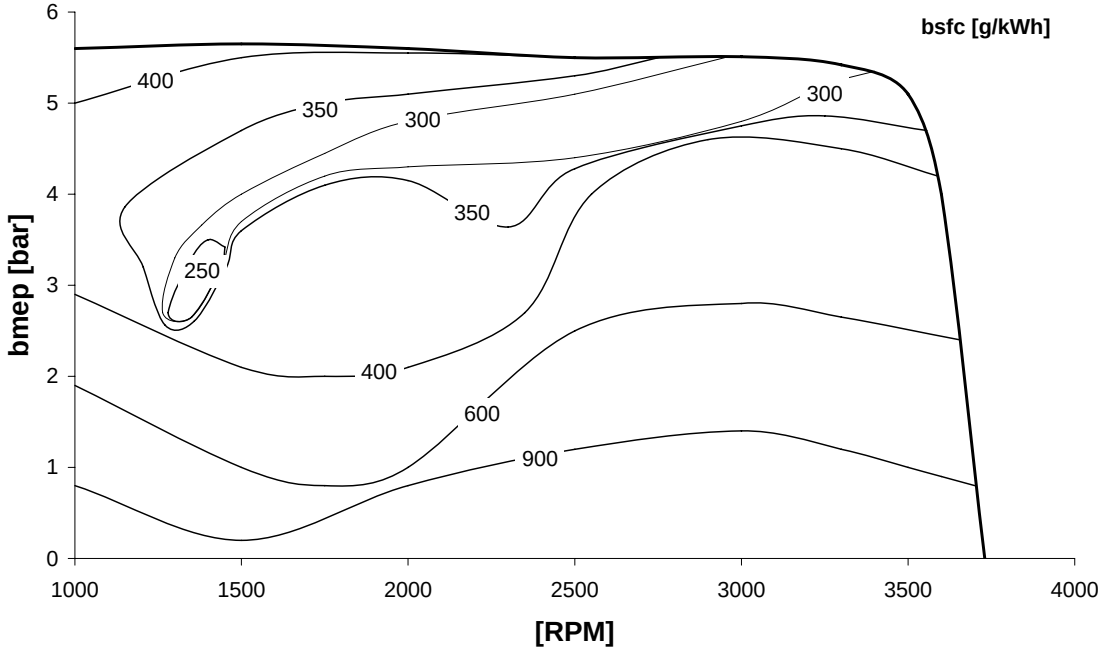

Figure 6-6 - Diesel engine specific consumption map.

The most favourable working conditions in terms of fuel consumption correspond in Figure 6-6 to a strip from the full load at 3000 rpm to 3500 rpm down to 3 bar bmep at 1500 rpm. Out of this strip the engine specific fuel consumption starts to rise.

6.6.2 Otto engine

After the engine conversion to SI and some preliminary tests, the Otto engine version was completely mapped from 10% of throttle up to WOT. In this Otto engine the same camshaft was used as in the Diesel engine, taking it as a baseline for all the SI engine tests made. As expected, the engine modification from Diesel to SI lead to a maximum torque and maximum power improvement of 41 % (Figure 6-7) and 49 %, respectively. The maximum speed of the engine was set similar for Diesel and SI versions, i.e. 3500 rpm. Experimental results of the Otto engine tests are presented in Annex E.

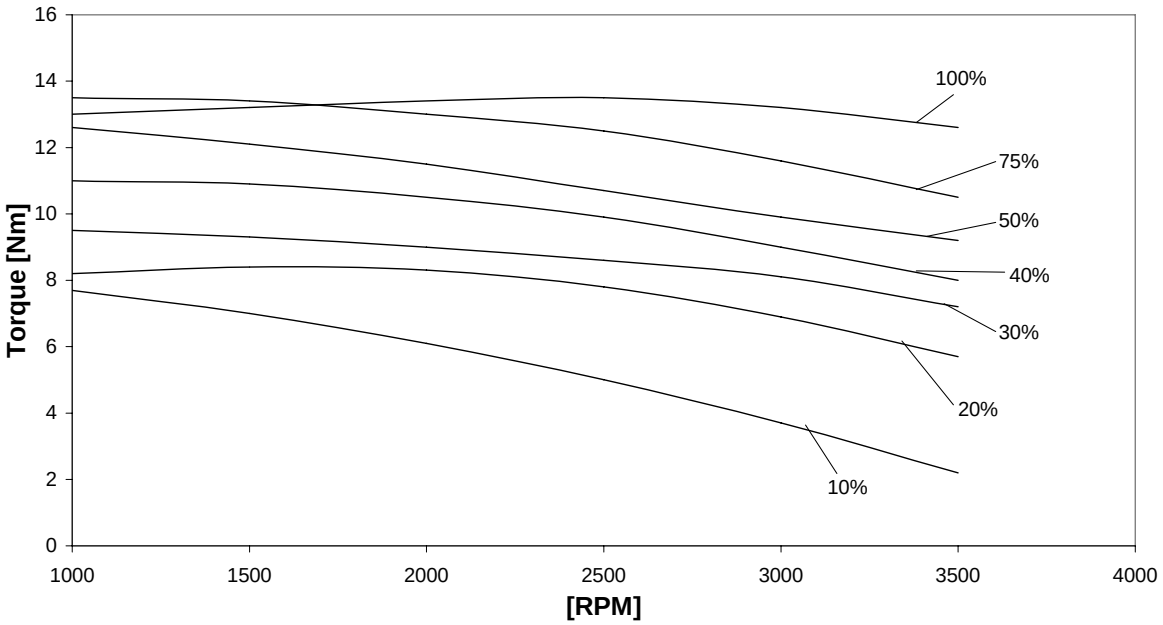

Figure 6-7 – Torque output of the Otto engine at several throttle positions.

As shown in Figure 6-7, torque values for the Otto engine have a general tendency to decrease with engine speed increase.

The resulting specific fuel consumption map is presented in Figure 6-8. Where the highest engine efficiency can be seen to occur at almost every engine speed within the range of 75 to 78% of the engine load. The specific fuel consumption rises as the load is reduced from that point, until reaching a minimum load. For engine speeds higher than

3500 rpm the minimum specific fuel consumption is achieved for 100% of load, but it must be taken into account that for engine speeds of 3500 rpm and higher only few measurements were taken and so the results for those engine speeds cannot be taken as representative.

The speed range from 1500 rpm to 2500 rpm is the most favourable one in terms of specific fuel consumption. A peak of efficiency can be seen at approximately 2000 rpm and 6 bar bmep.

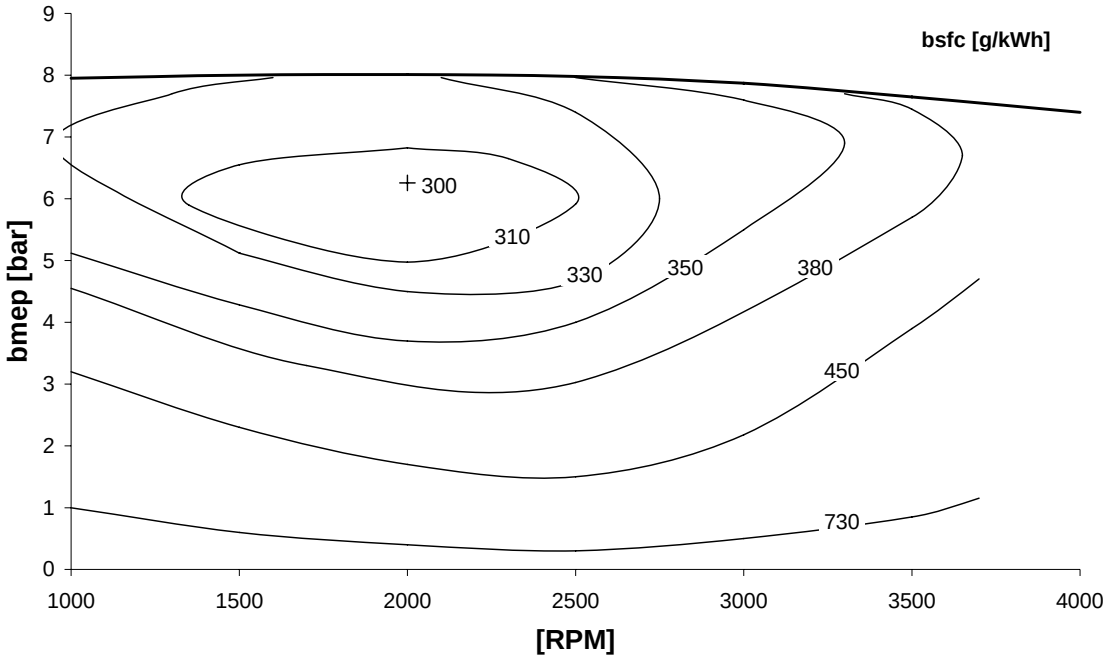

Figure 6-8 - Otto engine specific fuel consumption map.

6.6.3 Miller engine

The engine was also tested using a 11.5:1 compression ratio piston with all the different camshafts at WOT conditions (Miller engine). This set of tests intended to evaluate the ability of the intake valve timing to substitute the throttle valve as an engine load control strategy. Experimental data of the Miller engine tests are presented in Annex E.

A specific fuel consumption map was build based on the data from both the LIVC and EIVC camshafts, which is presented in Figure 6-9. This engine map depicts the performance of the Miller engine with constant compression ratio. Where the points of minimum specific fuel consumption are mostly between the 68 to 74% of load. When compared to the Otto cycle referred above, it may be concluded that just by following this load control strategy, the fuel consumption at part load operation reduces. This

reduction is made in relative terms of load, the minimum fuel consumption point being obtained at lower load, but at the same time, the absolute value of the specific fuel consumption at that point is reduced by 7%.

Comparing the Miller engine with the Otto engine an improvement in terms of torque and bmep can be seen from 2000 up to 3500 rpm. This improvement is due to the performance of the first LIVC camshaft, which has better volumetric efficiency at these speeds (Figure 6-3).

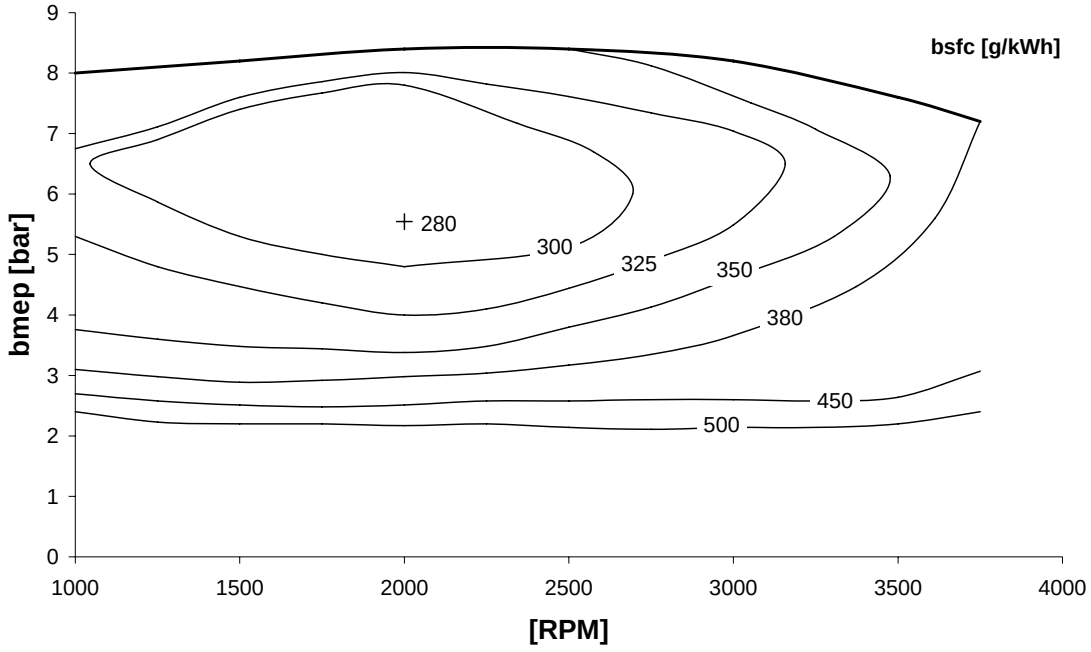

Figure 6-9 - Miller engine specific fuel consumption map.

Superposing the maps of the Otto engine and the Miller engine (Figure 6-10), it can be seen that from full down to 30% of load there always is improvement when using the Miller cycle. Bellow 30% of load, the improvement is only achievable at certain engine speeds. This load region, in the case of the Miller engine, was achieved with the EIVC camshaft with less overture when the engine run particularly “rough” and lacked stability of running. Probably, the cause is the reduction of swirl resulting from the earlier intake valve closure event leading to combustion instability.

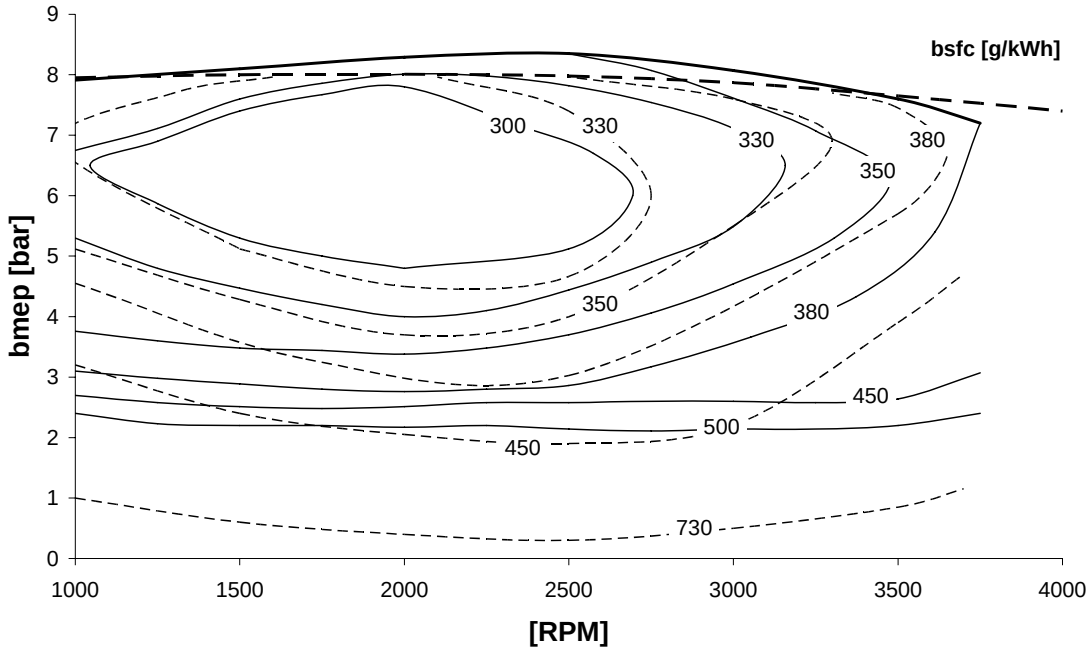

Figure 6-10 - Comparison of the Otto and Miller engine. Continuous line for Miller engine; Dashed line for Otto engine.

6.6.4 Miller VCR

The last set of experimental tests was conducted with the various camshafts and the different pistons. For each camshaft the compression ratio was sequentially increased until audible knock was detected. Table 6-2 shows the performed tests for each camshaft and compression ratio (grey squares). The best conditions for specific fuel consumption are represented by the dark squares. For the camshafts producing the lower loads (LIVC3 and EIVC2) the compression ratio was increased, without reaching audible knock with rare exceptions. The tests were stopped at a compression ratio of 17.5:1, because with both camshafts the torque decreased and the specific fuel consumption of the engine increased.

Figure 6-11 shows the torque and the specific fuel consumption for the EIVC2 camshaft with different compression ratios for 2500 rpm. Torque decrease after this point may be explained by an increase of the engine internal friction as a result of the higher compression ratio.

Table 6-2 - Performed tests for the Miller VCR engine.

Cam	Compression ratio						
	11.5	12.5	13.5	14.5	15.5	16.5	17.5
LIVC1							
LIVC2							
LIVC3							
EIVC1							
EIVC2							

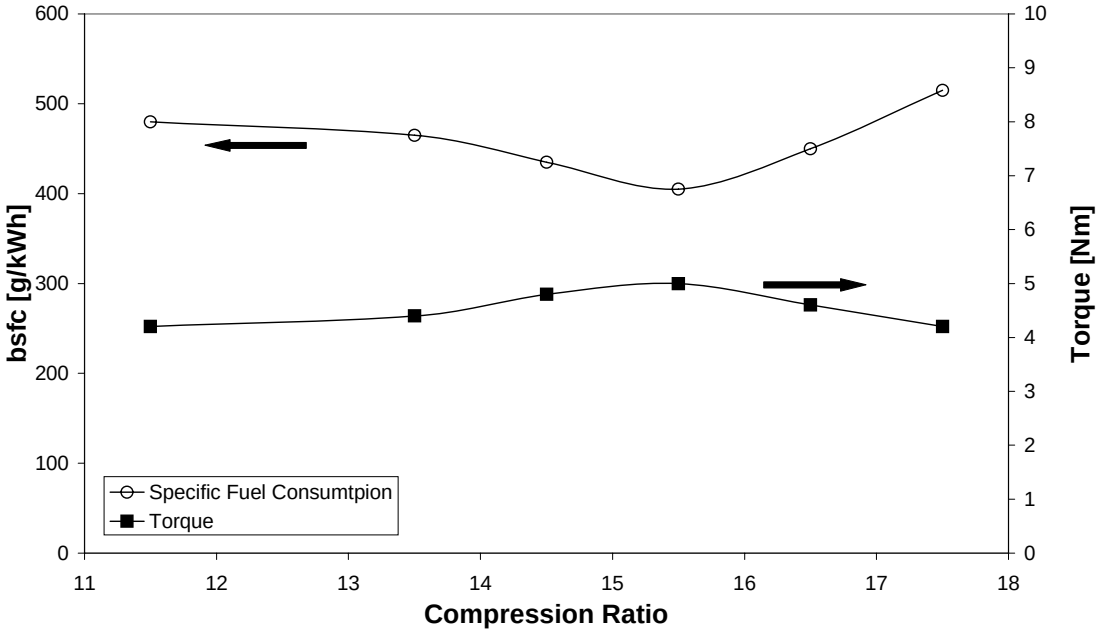

Figure 6-11 - Torque and specific fuel consumption as a function of compression ratio (2500 rpm; cam 2EIVC).

Figure 6-12 presents the fuel consumption map for the Miller VCR engine. For this map the values of the Miller VCR engine using the best efficient camshaft/piston were selected. These optimum points are shown in Table 6-2 with dark squares. Experimental results of the Miller VCR engine tests are presented in Annex E.

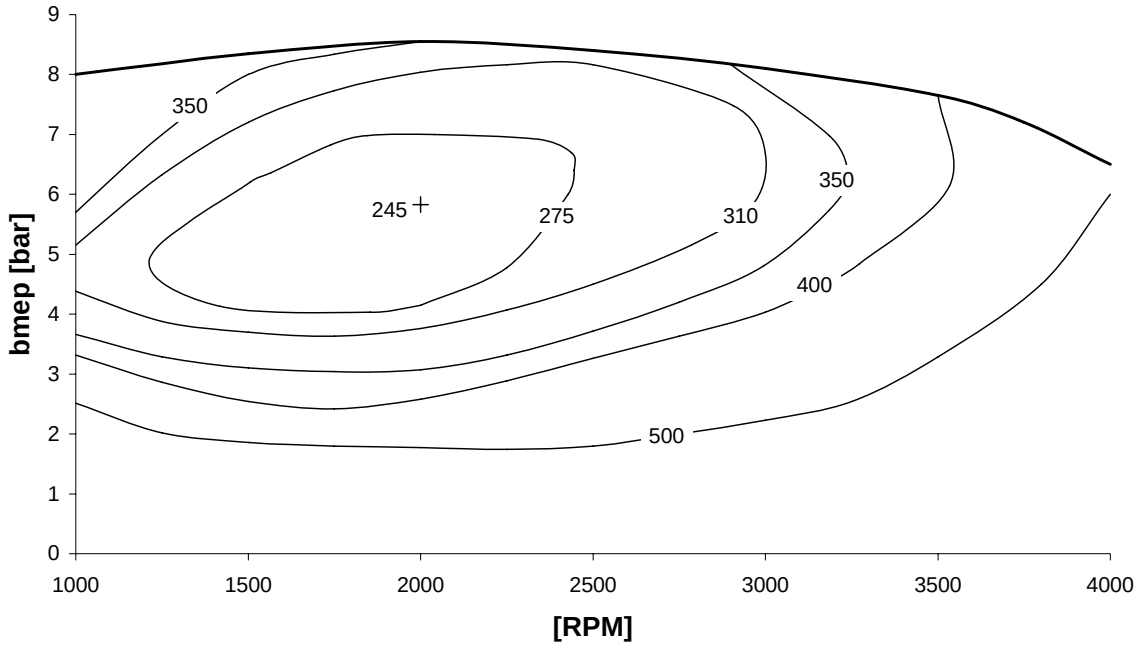

Figure 6-12 - Miller VCR engine specific fuel consumption map.

In the Miller VCR cycle engine fuel consumption map (Figure 6-12) can be seen that the best efficiency points are at speeds within the range of 1500 to 2500 rpm and for loads from 5 to 6 bar bmep. The minimum specific fuel consumption is obtained for 64 to 73% of load. The improvement of the Miller VCR cycle engine can be evaluated by making the comparison between that engine and the Otto engine. Figure 6-13 presents this difference in terms of specific fuel consumption. In relative terms (Figure 6-14) the comparison of the fuel consumption of the Miller VCR cycle engine and the Otto cycle engine shows that within the speed range of 1300 to 2300 rpm, the specific fuel consumption improvement is always higher than 15 %, corresponding to loads from 65% up to 75%. Within that range the maximum improvement of 26% is reached at 1300 rpm and 5.45 bar bmep. At high speeds the Miller VCR engine loses efficiency when compared with the Otto engine. At this speed range, the dynamic effects of air intake can lead to different working conditions that may require other intake valve timing strategy and compression ration variation.

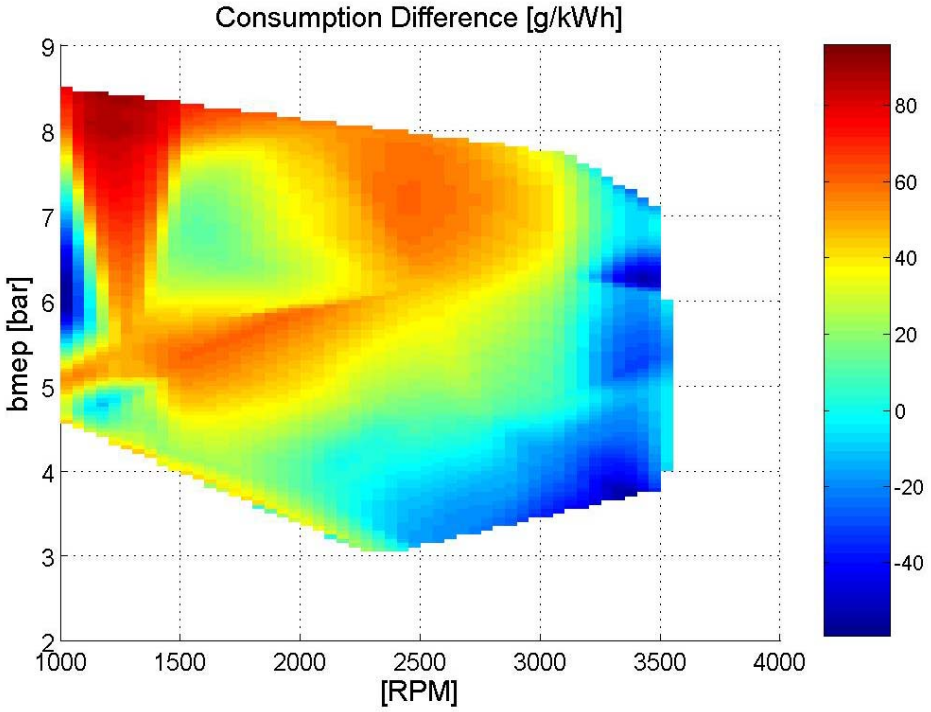

Figure 6-13 - Comparison of the Otto and Miller VCR engine.

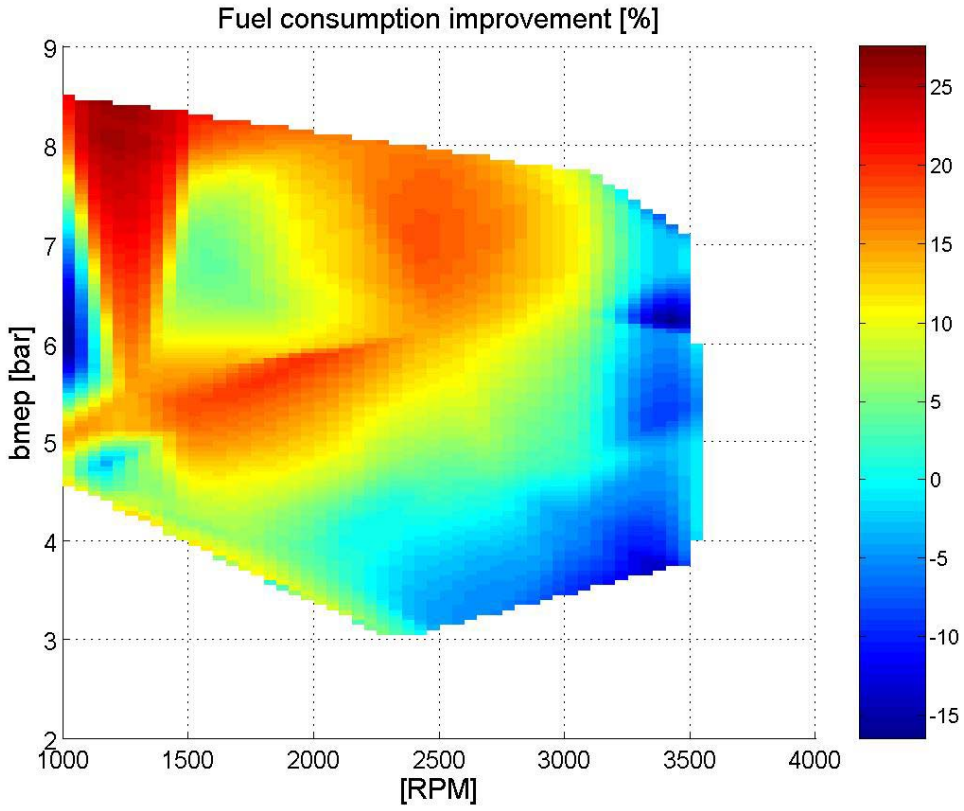

Figure 6-14 – Relative improvement of the Miller VCR cycle engine in comparison to the Otto cycle engine.

As noticed for the Miller engine (Figure 6-9), the Miller VCR shows an increase of torque in the 1000 to 3500 rpm engine speed range. This can be explained by the torque increase due to the increase of the compression ratio and at the same time an improved volumetric efficiency achieved with the modified intake cam, LIVC1. This cam is also the cause for the decrease of efficiency at the high speed and high load region.

Figure 6-15 presents the specific fuel consumption curves for three different speeds. It can be seen that the Miller VCR engine is always more efficient than the Otto engine. However at high speed and very low load the Otto cycle engine can have a slightly better performance in terms of specific fuel consumption. The minimum consumption for the Miller VCR engine happens between the 63% and 80% of the engine load, while on the Otto engine is always around 75% or higher load. Focusing on the mid load range, the maximum improvement is achieved at 2000 rpm and 5.8 bar bmep. In this particular case, the fuel consumption savings reaches its maximum of 19 %.

Figure 6-16 presents the relative improvement from the Diesel engine to the Miller VCR engine. The maximum improvement happens for the maximum loads of the Diesel engine, 4 to 6 bar of bmep and for engine speed ranging from 1500 rpm to 2500 rpm. At these conditions the improvement can go over 60%. This is the region where the Miller VCR engine performs better (Figure 6-12) and complementarily, the Diesel engine runs very unstable. For higher speeds the Miller VCR engine loses efficiency when compared to the Diesel.

To reduce the number of optimising variables, it was decided to use stoichiometric conditions for all SI engines tests. Therefore it would be possible to further improve these engines (Miller) in terms of thermal efficiency by the use of lean and extra-lean mixtures. This way the improvement comparing to the Diesel engine would be further extended.

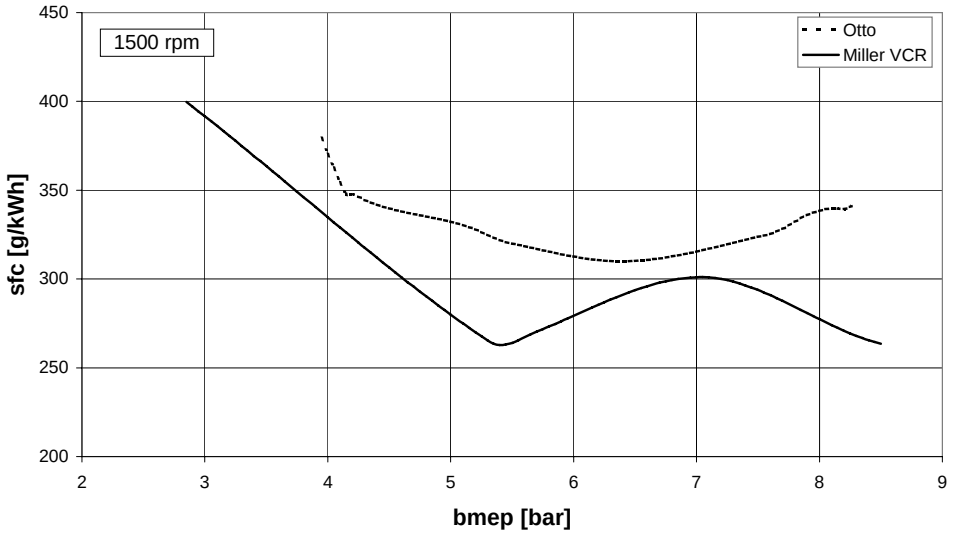

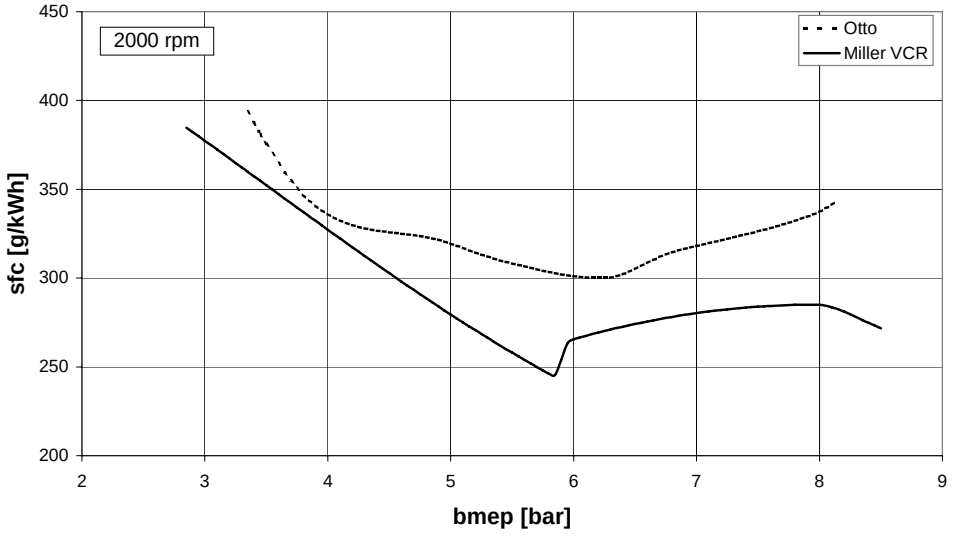

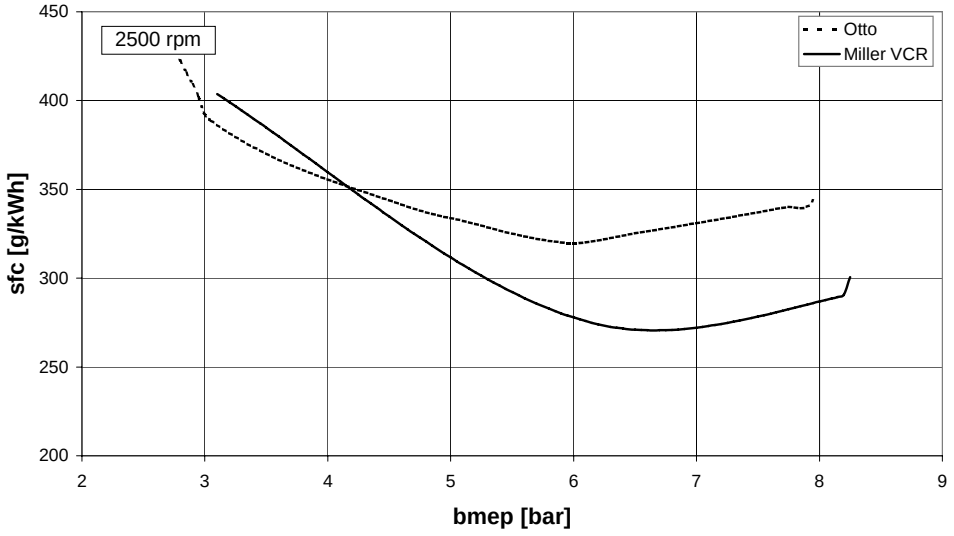

Figure 6-15 – Specific fuel consumption for 1500, 2000 and 2500 rpm.

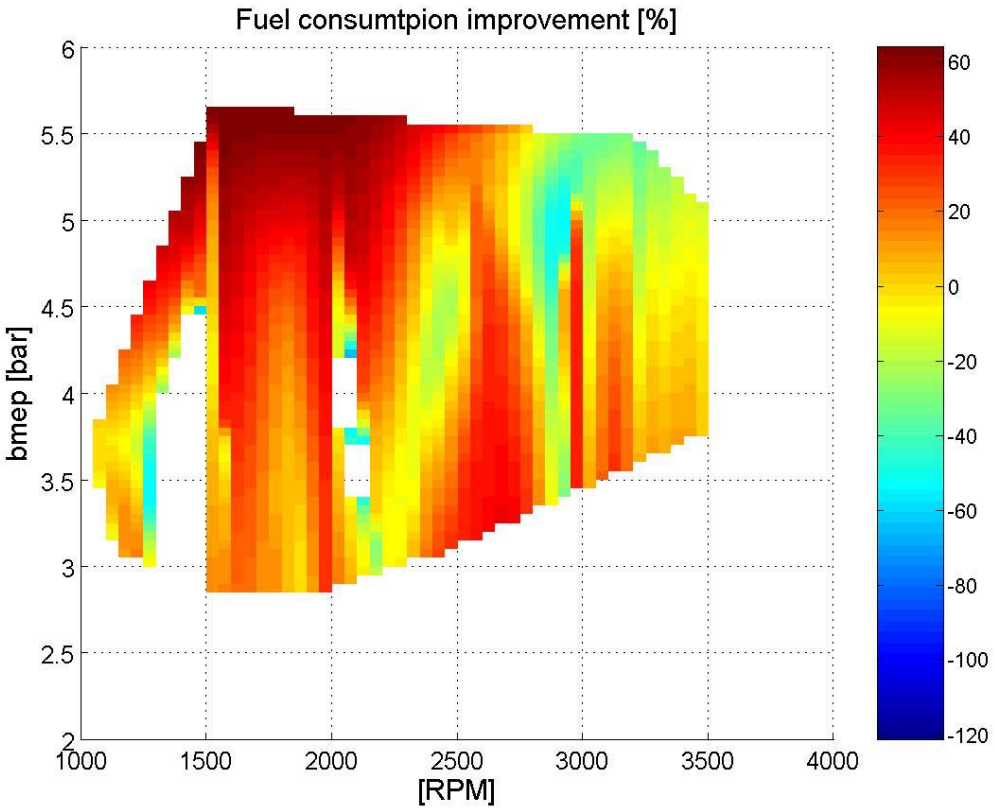

Figure 6-16 - Improvement from the Diesel engine to the Miller VCR engine.

6.6.5 Heat transfer

Part of the improvement shown above may be explained by heat transfer improvement, i.e. reduction. Comparing the Otto engine and the Miller VCR cycle engine at 2500 rpm, it can be seen that heat loss is reduced (Figure 6-17). Cooling air temperature was measured in both exits in the front side of the engine and on the back side. Oil temperature was also measured and compared. As it can be seen from Figure 6-17, for all load conditions there is a reduction of the temperature when changing from the Otto engine to the Miller VCR. The oil temperature difference increases with load and reached a maximum reduction of 14%. The cooling air exiting from the front side had a temperature reduction between 11% and 16%, increasing the temperature difference as load increases. The cooling air exiting from the back side of the engine had a temperature reduction between 23% and 26%, increasing the temperature difference as load increases.

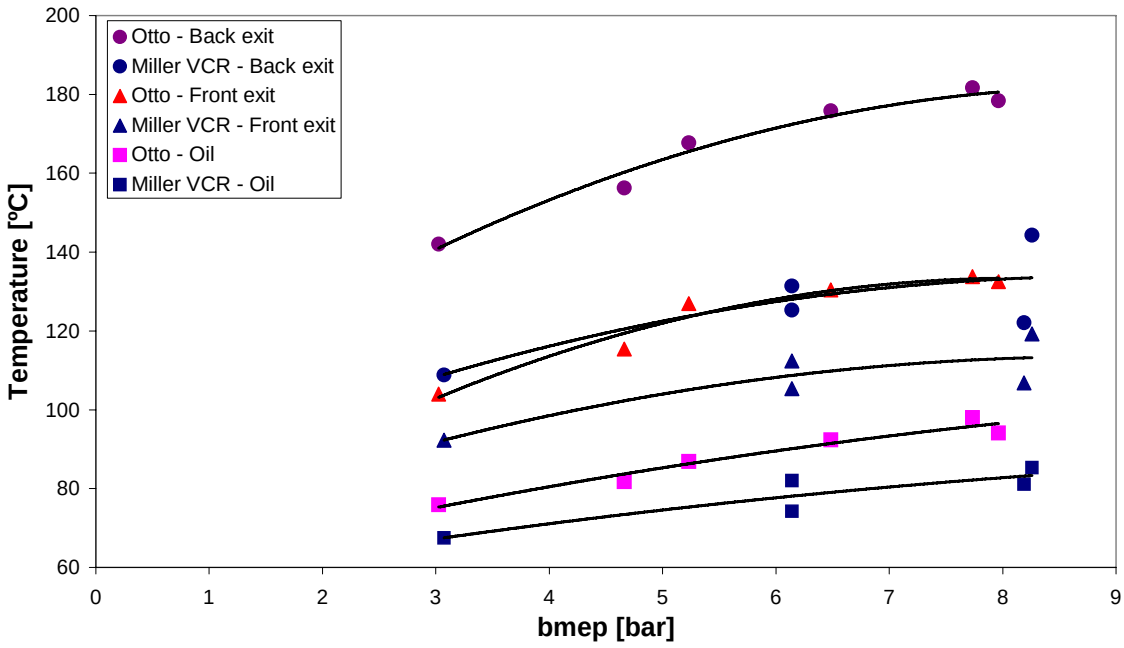

Figure 6-17 – Temperature values of cooling air and oil for Otto and Miller VCR (2500 rpm).

6.7 Summary

The results from the experimental tests performed allow for the conclusion of the improvement obtained with the use of over-expansion and VCR as technologies for fuel consumption improvement of spark ignition engines at part-load operating conditions. The improvement can also be assessed relatively to the compression ignition cycle engines, again at part-load conditions.

6.8 References

1 Plint, M.A., Martyr, Anthony, *Engine Testing: Theory and Practice*, Butherworth-Heinemann, 1995.

2 Martins, Jorge, *Motores de Combustão Interna*, Publindústria, 2005. (in Portuguese)

3 ISO 3046/111 Reciprocating Internal Combustion Engines: Performance.

7 – Conclusions and Future Work

7 CONCLUSIONS AND FUTURE WORK

7.1 Conclusions

A new configuration for a spark ignition engine for use in part load conditions is proposed. This new configuration gives the engine the same performance of the conventional spark ignition engine at full load and better specific fuel consumption at part load. It is based on two principles:

a) Over-expansion: Effective compression stroke is shorter than the expansion stroke. The latter remains constant at all working conditions. The compression stroke depends on the intake valve closure timing. The effective amount of air and fuel mixture trapped in the cylinder is reduced with the use of different intake valve closure timings. The intake valve may close earlier than BDC or after BDC. When closing earlier a depression is produced within the cylinder until the piston reaches BDC, starting the compression from that point. When closing after BDC, a certain amount of inducted air and fuel mixture is blown-back to the intake manifold. This mass is inducted in the subsequent cycle. The higher the difference from intake valve closure to BDC, the lower the mass that is trapped in the cylinder and thus less load is applied to the engine.
b) Compression ratio variation: Compression ratio of the engine is adjusted to the mass of intake mixture so that maximum allowable pressure and temperature are reached in combustion. When different intake valve closure timings are used, effective compression is reduced and the pressure and temperature during combustion reduces, decreasing the work produced in the cycle. The use of a compression ratio adequate to the valve timing allows further optimisation of the engine.

Several engine cycles were analysed using classical thermodynamics. Otto, Otto DI, Otto VCR, Miller, Miller VCR, Diesel and dual cycles were analysed. A comparison between these engine cycles was made on the load basis. The Miller engine brings some improvement relatively to the Otto cycle for the lower loads, but it also has a decreasing efficiency with the load. The use of VCR with the Otto cycle and with the Miller cycle changes this tendency, and efficiency improves with the decrease of the load. In the case of the Miller VCR, its thermal efficiency is even better than that of the compression ignition cycles (Diesel and dual). Supercharged cycles were also analysed. Spark

ignition engines Otto and Miller VCR do not show any improvement with the use of supercharging. On the other hand, the dual cycle shows improved efficiency when supercharge is used.

A computer model for spark ignition internal combustion engines was developed. This is a one zone model and includes sub models, which allow for temperature and pressure calculations, mass induction and exhaust, combustion, heat transfer, friction and gas properties calculations.

The model was calibrated using experimental results from engine tests. From the calibrated model results for speeds higher than 3000 rpm, calculated thermal efficiency differs significantly from the measurements in the engine tests. This fact can be attributed to not including air flow dynamics in the model, which become very important at speeds higher than that level.

The model was used to evaluate pumping losses of the several configurations of spark ignition engines. The Otto cycle and the Miller cycle (with early and late intake valve closure) were evaluated using the classical definition of pumping losses, i.e. calculating the area of the p-V diagram between BDC at exhaust valve opening until BDC of intake valve closure. With this method the Miller cycle with late intake valve closure is the one with lower pumping losses. Considering the blow-back work spend on this cycle, the real pumping losses increase and in fact the cycle with the lower pumping losses is the Miller cycle with early intake valve closure.

Another set of simulations was made to evaluate the optimisation of the use of the Miller VCR cycle in automotive applications. The New European Driving Cycle was used as a basis for comparison between the three engine configurations: Otto, Miller and Miller VCR. A 1400 cc engine and a typical configuration car were used. Results reveal that from the Otto engine to the Miller VCR engine, the benefits can rise from 17.8 km/L up to 19 km/L. The simulations were extended with the use of continuous variable transmission (CVT) and with this technology the improvement from Otto to Miller VCR goes from 19.8 km/L up to 22.2 km/L. Hence, for automotive applications the use of the Miller VCR engine associated with CVT can lead to an improvement in car consumption of about 25% relatively to the actual Otto engine with manual transmission.

Through an analysis using the entropy generation criterion, the thermodynamic performance of the engine was evaluated. Five entropy generating processes were identified: free expansion at exhaust and intake, combustion, heat transfer, fluid flow

through valves and friction. Apart from friction, the use of the Miller VCR cycle is beneficial regarding all other entropy generating processes, particularly with early intake valve closure. Using this, the benefit reduces during the free expansion and in fluid flow through valves processes, as expected, due to the blow-back phenomenon.

The specific entropy generated criterion evaluates each engine performance considering the entropy generated and the work produced per cycle. The Miller VCR cycle with is always the one with less specific entropy generated. The use of early intake valve closure is found to be beneficial for loads lower than 70%, while for higher loads the use of late intake valve is the best option. The optimum working point is found to be in the 60% up to 80% of the engine load.

A Diesel engine was tested at several load conditions to be used as a baseline for comparison of the potential improvement of the proposed new engine configuration. The same engine was modified to work as a spark ignition. Different camshafts and pistons were manufactured so that different valve timings and compression ratios could be studied. The spark ignition engine was tested in several configurations, namely Otto, Miller and Miller VCR, either with early intake valve closure or late intake valve closure. From the engine tests, it can be concluded that:

a) The minimum consumption for the Miller VCR engine happens between the 63% and 80% of the engine load range and for engine speed between 1000 rpm and 2500 rpm. This is the same load range forecast by the computer simulations for minimum specific entropy generated. Thermal efficiency improvement with the use of the Miller VCR in relation to the Otto cycle engine can go up to a maximum of 26%.
b) At higher loads (> 70%), knock is the limiting condition for compression ratio increase. For loads lower than that limit, compression ratio is limited by maximum break torque. For compression ratios higher than that, specific fuel consumption rises. This may be caused by an increase in the engine internal friction.
c) With the adoption of the Miller VCR strategy for load control, the heat lost by the engine is reduced through the whole load range. The reduction of heat loss was evaluated in relative terms to be from 11% up to a maximum of 26%.

7.2 Future work

The research work performed up to date allowed some conclusions to be reached as described in the previous section. More work should be done in order to obtain more detailed conclusions and to study other phenomena related to the performance of the engine. Suggestions for future work include:

1. To enhance the heat transfer model in the computer model in order to include:
   a) Latent heat of the fuel
   b) Heat transfer to the income mixture at the passage to the intake duct and intake valve
   c) Swirl effect on the heat transfer coefficient (variation of the Reynolds number)
2. To test the engine with different camshafts producing lower levels of load than that obtained in this work and comparing the results with the Otto engine.
3. To assess engine performance through the whole load range, using the two load control strategies: late intake valve closure and early intake valve closure.
4. To test the engine using the original camshaft and different pistons to assess the potential of the VCR technology when used in a conventional Otto cycle engine with load variation by a throttle valve.
5. To test lean mixtures to evaluate the potential of this method to further improve engine thermal efficiency.
6. To improve engine combustion chamber so that better combustion conditions may be achieved. At the same time, turbulence inside the engine should be improved and probably make it dependent on the intake valve closure timing, in the case of the Miller and Miller VCR engine. With these new configuration characteristics the engine should be tested and emissions should be evaluated (in terms of NOx and CO).
7. To test a Miller VCR engine under transient conditions in order to evaluate the potential improvement on thermal efficiency at those closer to reality conditions and to understand their requirements and constraints for engine design.
8. To install a direct injection system in the engine in order to take advantage of the charge cooling, so to increase even more the compression ratio and attain more gains in terms of fuel economy. Lean mixtures should also be tested to assess its possibility for further improvement.

9. To try and implement a Miller VCR cycle in a two-stroke engine and to evaluate its benefits at part load operation.
10. To test the combination of Miller VCR engine cycle with supercharging using a four-stroke engine.

Annex A – Theoretical Analysis of Engine Cycles

A THEORETICAL ANALYSIS OF ENGINE CYCLES

A.1 Otto Cycle at part load

Analyzing the work involved in this cycle:

$$W = W_{1'2} + W_{34} + W_{51'} + W_{1'6} + W_{71} + W_{11'} \tag{A.1}$$

The first term, which corresponds to the compression work from the atmospheric pressure until p_2 is considered an isentropic process:

$$W_{1'2} = \frac{p_{1'} \cdot V_{1'} - p_2 \cdot V_2}{\gamma - 1} \tag{A.2}$$

Considering:

$$p_{1'} = p_0 \quad V_{1'} = V_1 \left(\frac{p_1}{p_0} \right)^{\frac{1}{\gamma}} \quad p_2 = p_1 \cdot \varepsilon^{\gamma} \quad \varepsilon = \frac{V_1}{V_2} \tag{A.3 a, b, c, d}$$

where ε is the compression ratio of the engine.
Expression (A.2) can then be written as:

$$W_{1'2} = \frac{p_0 \cdot V_1 \left(\frac{p_1}{p_0} \right)^{\frac{1}{\gamma}} - p_1 \cdot V_1 \cdot \varepsilon^{\gamma - 1}}{\gamma - 1} \tag{A.4}$$

For the expansion stroke, also considered an isentropic process, its work corresponds to:

$$W_{34} = \frac{p_3 \cdot V_3 - p_4 V_4}{\gamma - 1} \tag{A.5}$$

Considering:

$$\tau = \frac{p_3}{p_2} = \frac{T_3}{T_2} \quad p_3 = \tau \cdot p_1 \cdot \varepsilon^{\gamma} \quad V_3 = \frac{V_1}{\varepsilon} \tag{A.6}$$

The increase of temperature/pressure in combustion is caused by the heat supplied to the system (engine) by the combustion of the fuel.

$$Q_{2-3} = m \cdot c_v \cdot (T_3 - T_2) = m_f \cdot Q_{LHV} \tag{A.7}$$

Leading to a combustion temperature ratio:

$$\tau = \frac{T_3}{T_2} = 1 + \frac{(\gamma - 1) \cdot \dfrac{m}{1 + A/F} \cdot Q_{LHV}}{\varepsilon^{\gamma - 1} \cdot p_1 \cdot \Delta V} = 1 + \frac{(\gamma - 1) \cdot B}{\varepsilon^{\gamma - 1}} \tag{A.8}$$

where: $B = \dfrac{\dfrac{1}{1 + A/F} \cdot Q_{LHV}}{R \cdot T_1}$ is a constant (the mixture is always stoichiometric)

$$p_3 \cdot V_3^{\gamma} = p_4 \cdot V_4^{\gamma} \qquad p_4 = p_3 \cdot \left(\frac{V_3}{V_4}\right)^{\gamma} = \tau \cdot p_1 \tag{A.9 a, b}$$

And the work involved in the expansion process (A.5) may be written as:

$$W_{34} = \frac{\tau \cdot p_1 \cdot \varepsilon^{\gamma} \cdot \dfrac{V_1}{\varepsilon} - \tau \cdot p_1 \cdot V_1}{\gamma - 1} = \frac{\tau \cdot p_1 \cdot V_1}{\gamma - 1}\left(\varepsilon^{\gamma - 1} - 1\right) \tag{A.10}$$

The exhaust process is considered an isobaric process. To simplify the analysis this work was divided in two parts, from 5 to 1' and from 1' to 6. Thus the work can be determined as:

$$W_{51'} = p_0 \cdot (V_{1'} - V_5) = p_0 \cdot V_1 \left[\left(\frac{p_1}{p_0} \right)^{\frac{1}{\gamma}} - 1 \right] \tag{A.11}$$

And

$$W_{1'6} = p_0 (V_6 - V_{1'}) = p_0 \left[\frac{V_1}{\varepsilon} - V_1 \cdot \left(\frac{p_1}{p_0} \right)^{\frac{1}{\gamma}} \right] = p_0 \cdot V_1 \left[\frac{1}{\varepsilon} - \left(\frac{p_1}{p_0} \right)^{\frac{1}{\gamma}} \right] \tag{A.12}$$

The pumping work from the intake stroke can be described as an isobaric process and it becomes:

$$W_{71} = p_1 \cdot (V_1 - V_7) = p_1 \cdot \left(V_1 - \frac{V_1}{\varepsilon} \right) = p_1 \cdot V_1 \left(1 - \frac{1}{\varepsilon} \right) \tag{A.13}$$

The first part of the compression from p_1 up to the atmospheric pressure, p_0, is described as an isentropic process.

$$W_{11'} = \frac{p_1 \cdot V_1 - p_{1'} \cdot V_{1'}}{\gamma - 1} = \frac{p_1 \cdot V_1 - p_0 \cdot V_1 \cdot \left(\frac{p_1}{p_0} \right)^{\frac{1}{\gamma}}}{\gamma - 1} \tag{A.14}$$

Considering equations (A.4), (A.10), (A.11), (A.12), (A.13) and (A.14), the work (A.1) of this cycle can be determined as:

$$\begin{aligned} W &= \frac{p_1 \cdot V_1}{\gamma - 1} (\tau - 1) \cdot \left(\varepsilon^{\gamma - 1} - 1 \right) - V_1 \cdot (p_0 - p_1) \frac{\varepsilon - 1}{\varepsilon} = \\ &= p_1 \cdot V_1 \cdot \frac{B}{\varepsilon^{\gamma - 1}} \left(\varepsilon^{\gamma - 1} - 1 \right) - V_1 \cdot (p_0 - p_1) \frac{\varepsilon - 1}{\varepsilon} \end{aligned} \tag{A.15}$$

The thermal efficiency is calculated as:

$$\eta_O = \frac{W}{Q_H} = \frac{p_1 \cdot V_1 \cdot \frac{B}{\varepsilon^{\gamma-1}}\left(\varepsilon^{\gamma-1} - 1\right) - p_1 \cdot V_1 \cdot \left(\frac{1}{\beta} - 1\right)\frac{\varepsilon - 1}{\varepsilon}}{\frac{m}{1 + A/F} \cdot Q_{LHV}} \tag{A.16}$$

A.2 Otto cycle with direct injection (STRATIFIED CHARGE) at part load

The efficiency of this cycle can be written as:

$$\eta_{OD} = 1 - \frac{\frac{T_{4'}}{T_2} - \frac{T_1}{T_2}}{\frac{T_{3'}}{T_2} - 1} \tag{A.17}$$

Considering:

$$\frac{T_1}{T_2} = \frac{1}{\varepsilon^{\gamma-1}} \tag{A.18}$$

$$\frac{T_{3'}}{T_2} = 1 + \frac{(\gamma - 1) \cdot Q_{LHV}}{R \cdot T_1 \cdot \varepsilon^{\gamma-1}} \cdot \frac{1}{1 + \frac{\left(A/F\right)_S}{\Phi}} = 1 + \frac{(\gamma - 1) \cdot C}{\varepsilon^{\gamma-1}} \cdot \frac{1}{1 + \frac{\left(A/F\right)_S}{\Phi}} \tag{A.19}$$

where : $C = \frac{Q_{LHV}}{R \cdot T_1}$ is a constant.

Φ is the fuel/air equivalent ratio and defined as the relation of the stoichiometric mixture and the effective intake mixture:

$$\Phi = \frac{\left(A/F\right)_S}{A/F} = \frac{F/A}{\left(F/A\right)_S} \tag{A.20}$$

This Φ represents the load. In fact, when the mixture is stoichimetric, Φ will assume the value of 1 and less of 1 for lean mixtures.

$$\frac{T_{4'}}{T_2} = \frac{T_{4'}}{T_{3'}} \cdot \frac{T_{3'}}{T_2} \tag{A.21}$$

$$\frac{T_{4'}}{T_{3'}} = \left(\frac{V_{3'}}{V_{4'}}\right)^{\gamma-1} = \left(\frac{1}{\varepsilon}\right)^{\gamma-1} \tag{A.22}$$

Comes then:

$$\frac{T_{4'}}{T_2} = \frac{1}{\varepsilon^{\gamma-1}} \cdot \left[1 + \frac{(\gamma-1)\cdot C}{\varepsilon^{\gamma-1}} \cdot \frac{1}{1 + \frac{\left(A/F\right)_S}{\Phi}}\right] \tag{A.23}$$

It comes then that the efficiency of this cycle will be:

$$\eta_{OD} = 1 - \frac{\frac{1}{\varepsilon^{\gamma-1}} \cdot \left[1 + \frac{(\gamma-1)\cdot C}{\varepsilon^{\gamma-1}} \cdot \frac{1}{1 + \frac{\left(A/F\right)_S}{\Phi}}\right] - \frac{1}{\varepsilon^{\gamma-1}}}{\frac{(\gamma-1)\cdot C}{\varepsilon^{\gamma-1}} \cdot \frac{1}{1 + \frac{\left(A/F\right)_S}{\Phi}}} = 1 - \frac{1}{\varepsilon^{\gamma-1}} \tag{A.24}$$

A.3 Miller Cycle

Values for point 1 are considered the standard atmospheric pressure and temperature, p_1, T_1.

Point 2 corresponds to the end of compression (assumed as isentropic) initiated at 1, so the calculation of T_2 is made applying the conditions of isentropic transformations for ideal gases:

$$T_2 = T_1\left(\frac{V_1}{V_2}\right)^{\gamma-1} = T_1\varepsilon_{tr}{}^{\gamma-1} = T_1\left(\frac{\varepsilon_g}{\sigma}\right)^{\gamma-1} \tag{A.25}$$

The evolution from 2 to 3 corresponds to the internal combustion of the air-fuel mixture. The process is isochoric and can be described as the pressure and temperature increase, as a result of the combustion of the fuel presented in the cylinder. The generated heat during this reaction may be expressed as:

$$m \cdot c_v \cdot (T_3 - T_2) = m_f \cdot Q_{L\,HV} \tag{A.26}$$

Where m is the mass of the mixture inside the cylinder, c_v is the specific heat at constant volume, m_f is the mass of fuel contained in the mixture and Q_{LHV} is the lower heating value of the fuel.
From (A.26) comes:

$$\frac{T_3}{T_2} = 1 + \frac{m_f \cdot Q_L}{m \cdot c_v \cdot T_1 \cdot \varepsilon^{\gamma-1}} = 1 + \frac{(\gamma-1)\cdot\dfrac{m}{\dfrac{A}{F}+1}\cdot Q_{LHV}}{\varepsilon_{tr}^{\gamma-1}\cdot p_1 \cdot \Delta V} \tag{A.27}$$

Considering:

$$B = \frac{m \cdot Q_{LHV}}{p_1 \cdot \Delta V \cdot \left(1 + A/F\right)} \tag{A.28}$$

This, and substituting T_2 by (A.25) will allow (A.27) to be written as:

$$\frac{T_3}{T_1} = \left(\frac{\varepsilon_g}{\sigma}\right)^{\gamma-1} + (\gamma-1)\cdot B \tag{A.29}$$

Expansion of the burned gases resulting from combustion is made from point 3 to 4. The expansion is made through the entire piston stroke and is considered as an isentropic process. Applying the perfect gas law to an isentropic process, comes:

$$\frac{T_4}{T_3} = \left(\frac{1}{\varepsilon_g} \right)^{\gamma-1} \tag{A.30}$$

Substituting T_3 by (A.29) comes:

$$\frac{T_4}{T_1} = \frac{1}{\sigma^{\gamma-1}} + \frac{(\gamma-1)\cdot B}{\varepsilon_g^{\gamma-1}} \tag{A.31}$$

Or

$$\frac{T_4}{T_1} = \frac{1}{\sigma^{\gamma-1}} + \frac{(\gamma-1)\cdot B}{\sigma^{\gamma-1}\varepsilon_{tr}^{\gamma-1}} \tag{A.32}$$

At point 5 it is considered that the pressure is equal to the pressure at point 1, which allows the deduction using the perfect gas law:

$$\frac{T_5}{T_1} = \sigma \tag{A.33}$$

To calculate the thermal efficiency and using the second law corollaries, the expression used to calculate the thermal efficiency of the Miller cycle is that keeps constant the geometric compression ratio (G refers to geometric compression ratio):

$$\eta_{MG} = 1 - \frac{Q_{4-5} + Q_{5-1}}{Q_{2-3}} = 1 - \frac{T_4 - T_5 + \gamma(T_5 - T_1)}{T_3 - T_2} \tag{A.34}$$

Substituting T_2, T_3, T_4 e T_5 by (A.25), (A.29), (A.32) e (A.33) respectively, (A.34) can be written as:

$$\eta_{MG} = 1 - \frac{1}{\varepsilon_g^{\gamma-1}} - \frac{\sigma^{\gamma}(\gamma-1) - \gamma\cdot\sigma^{\gamma-1} + 1}{(\gamma-1)\cdot\sigma^{\gamma-1}\cdot B} \tag{A.35}$$

A.4 Diesel cycle at part load

The efficiency of this cycle can be calculated by:

$$\eta_D = 1 - \frac{T_{4'} - T_1}{\gamma \cdot (T_{3'} - T_2)} = 1 - \frac{\frac{T_{4'}}{T_2} - \frac{T_1}{T_2}}{\gamma \cdot \left(\frac{T_{3'}}{T_2} - 1 \right)} \tag{A.36}$$

The first process of the cycle is the isentropic compression process during the entire compression stroke from 1 to 2:

$$p_2 = p_1 \cdot \varepsilon^{\gamma} \quad T_2 = T_1 \cdot \varepsilon^{\gamma - 1} \quad V_2 = \frac{V_1}{\varepsilon} \tag{A.37}$$

Combustion is represented as an isobaric heating from 2 to 3.

$$Q_{2-3} = m \cdot c_p \cdot (T_{3'} - T_2) = m_f \cdot Q_{LHV} \tag{A.38}$$

$$\frac{T_{3'}}{T_2} = 1 + \frac{m_f \cdot Q_{LHV}}{m \cdot c_p \cdot T_2} = 1 + \frac{(\gamma - 1) \cdot Q_{LHV}}{\gamma \cdot R \cdot T_1 \cdot \varepsilon^{\gamma - 1}} \cdot \frac{1}{1 + \frac{\left(A/F \right)_S}{\Phi}} = A(\Phi) \tag{A.39}$$

With Φ defined as (A.20).

After the end of combustion the rest of the expansion stroke is considered an isentropic expansion from 3 to 4.

$$T_{3'} \cdot {V_{3'}}^{\gamma - 1} = T_{4'} \cdot {V_{4'}}^{\gamma - 1} \Leftrightarrow T_{4'} = T_{3'} \cdot \left(\frac{V_{3'}}{V_{4'}} \right)^{\gamma - 1} \tag{A.40}$$

$$\frac{T_{4'}}{T_2} = \frac{T_{3'}}{T_2} \cdot \left(\frac{V_{3'}}{V_{4'}} \right)^{\gamma - 1} = A(\Phi) \cdot \left(\frac{V_{3'}}{V_{4'}} \right)^{\gamma - 1} \tag{A.41}$$

With (A.37) and (A.39):

$$\frac{T_{3'}}{T_2} = \frac{V_{3'}}{V_2} \qquad V_{3'} = \frac{V_1}{\varepsilon} \cdot A(\Phi) \tag{A.42}$$

Comes:

$$\frac{T_{4'}}{T_2} = \left[A(\Phi)\right]^{\gamma} \cdot \left(\frac{1}{\varepsilon}\right)^{\gamma-1} \tag{A.43}$$

The expression (A.36) for the efficiency of this cycle can be written as:

$$\eta_D = 1 - \frac{\left[A(\Phi)\right]^{\gamma} \cdot \left(\frac{1}{\varepsilon}\right)^{\gamma-1} - \left(\frac{1}{\varepsilon}\right)^{\gamma-1}}{\gamma \cdot \left[A(\Phi) - 1\right]} = 1 - \left(\frac{1}{\varepsilon}\right)^{\gamma-1} \cdot \frac{\left[A(\Phi)\right]^{\gamma} - 1}{\gamma \cdot \left[A(\Phi) - 1\right]} \tag{A.44}$$

A.5 Dual cycle at part load

For the dual cycle, the thermal efficiency may be determined by:

$$\eta_d = 1 - \frac{T_{5'} - T_1}{T_3 - T_2 + \gamma \cdot (T_{4'} - T_3)} = 1 - \frac{\frac{T_{5'}}{T_2} - \frac{T_1}{T_2}}{\frac{T_3}{T_2} - 1 + \gamma \cdot \left(\frac{T_{4'}}{T_2} - \frac{T_3}{T_2}\right)} \tag{A.45}$$

The heat supplied during the combustion, at constant volume and at constant pressure may be represented as:

$$Q_{2-3} + Q_{3-4} = m \cdot c_v \cdot \left[(T_3 - T_2) + \gamma \cdot (T_4 - T_3)\right] = m_f \cdot Q_{LHV} \tag{A.46}$$

Comes then:

$$\frac{T_3}{T_2}+\gamma\cdot\left(\frac{T_{4'}}{T_2}-\frac{T_3}{T_2}\right)=1+\frac{(\gamma-1)\cdot Q_{LHV}}{R\cdot T_1\cdot\varepsilon^{\gamma-1}}\cdot\frac{1}{1+\frac{\left(A/F\right)_S}{\Phi}}=1+B(\Phi,\Psi) \tag{A.47}$$

$$\frac{T_{4'}}{T_2}=\frac{1+B(\Phi,\Psi)+\frac{T_3}{T_2}\cdot(\gamma-1)}{\gamma} \tag{A.48}$$

Where:

$$B(\Phi,\Psi)=1+\frac{(\gamma-1)\cdot Q_{LHV}}{R\cdot T_1\cdot\varepsilon^{\gamma-1}}\cdot\frac{1}{1+\frac{\left(A/F\right)_S}{\Phi}} \tag{A.49}$$

Considering:

$$\Phi=\frac{Q_T{}'}{Q_T}\quad \Psi=\frac{Q_V}{Q_T}\quad \Psi'=\frac{Q_V}{Q'_T} \tag{A.50 a,b,c}$$

It results:

$$\Psi'=\frac{\Psi}{\Phi} \tag{A.51}$$

In fact, Φ can be considered the load factor. In equation (A.20) Φ is defined as the fuel/air equivalent ratio, representing the relation between the effective intake fuel and the stoichiometric fuel quantity. The same relation can be obtained (considering that the heat supplied at constant volume is always constant) when the relation is established between the heat supplied at constant pressure for a determined amount of fuel and the heat supplied at constant pressure when considering a stoichiometric mixture.
The heat supplied during the constant volume combustion is represented as:

$$Q_{2-3}=m\cdot c_v\cdot(T_3-T_2)=\Psi\cdot m_f\cdot Q_{LHV}\qquad with\quad \Psi<1 \tag{A.52}$$

Comes then:

$$\frac{T_3}{T_2} = 1 + \frac{(\gamma - 1)\cdot \Psi \cdot Q_{LHV}}{R \cdot T_1 \cdot \varepsilon^{\gamma-1}} \cdot \frac{1}{1 + \left(A/F\right)_S} = A(\Psi) \tag{A.53}$$

$$T_3 = A(\Psi)\cdot T_2 = A(\Psi)\cdot T_1 \cdot \varepsilon^{\gamma-1} \tag{A.54}$$

(A.48) can be written as:

$$\frac{T_{4'}}{T_2} = \frac{1 + B(\Phi,\Psi) + (\gamma-1)\cdot\left[1 + \frac{(\gamma-1)\cdot\Psi\cdot Q_{LHV}}{R\cdot T_1\cdot\varepsilon^{\gamma-1}}\cdot\frac{1}{1+\left(A/F\right)_S}\right]}{\gamma} = \frac{1 + B(\Phi,\Psi) + (\gamma-1)\cdot A(\Psi)}{\gamma} \tag{A.55}$$

The expansion, considered as an isentropic process can be represented as:

$$\frac{T_{5'}}{T_{4'}} = \left(\frac{V_{4'}}{V_{5'}}\right)^{\gamma-1} = \left(\frac{V_{4'}}{V_1}\right)^{\gamma-1} \tag{A.56}$$

Considering:

$$Q_{3-4'} = m\cdot c_p\cdot\left(T_{4'} - T_3\right) = \left(1 - \Psi'\right)\cdot m_f\cdot Q_{LHV} \tag{A.57}$$

$$\frac{T_{4'}}{T_3} = C(\Phi,\Psi) = 1 + \frac{\left(1 - \frac{\Psi}{\Phi}\right)\cdot Q_{LHV}}{\frac{\gamma}{\gamma-1}\cdot R\cdot A(\Psi)\cdot T_1\cdot\varepsilon^{\gamma-1}}\cdot\frac{1}{1+\frac{\left(A/F\right)_S}{\Phi}} = C(\Phi,\Psi) \tag{A.58}$$

$$\frac{T_{4'}}{T_3} = \frac{V_{4'}}{\frac{V_1}{\varepsilon}} \tag{A.59}$$

(A.56) can be written as :

$$\frac{T_{5'}}{T_{4'}} = \left[\frac{C(\Phi,\Psi)}{\varepsilon}\right]^{\gamma-1} \tag{A.60}$$

From (A.60) and (A.55):

$$\frac{T_{5'}}{T_2} = \frac{T_{5'}}{T_{4'}} \cdot \frac{T_{4'}}{T_2} = \left(\frac{1}{\varepsilon}\right)^{\gamma-1} \cdot C(\Phi,\Psi)^{\gamma-1} \cdot \frac{1 + B(\Phi,\Psi) + (\gamma-1)\cdot A(\Psi)}{\gamma} \tag{A.61}$$

From (A.47), (A.55) and (A.61), the efficiency (A.45) can be written as:

$$\eta_d = 1 - \left(\frac{1}{\varepsilon}\right)^{\gamma-1} \cdot \frac{C(\Phi,\Psi)^{\gamma-1} \cdot \frac{1 + B(\Phi,\Psi) + (\gamma-1)\cdot A(\Psi)}{\gamma} - 1}{B(\Phi,\Psi)} \tag{A.62}$$

A.6 Otto Supercharged Cycle

Dividing the total work performed in several terms, we get different processes that are part of the cycle:

$$W = W_{12} + W_{34} + W_{56} + W_{71} \tag{A.63}$$

The compression stroke from 1 to 2 is considered an isentropic process, so that the corresponding work is defined as:

$$W_{12} = \frac{p_1 \cdot V_1 - p_2 \cdot V_2}{\gamma - 1} \tag{A.64}$$

Using the definition of β:

$$p_1 = \beta \cdot p_0 \tag{A.65}$$

$$V_2 = \frac{V_1}{\varepsilon} \tag{A.66}$$

And p_2 can be defined as:

$$p_2 = \beta \cdot p_0 \cdot \varepsilon^{\gamma} \tag{A.67}$$

Considering the compression process in the turbocharger as an isentropic process, T_1 can be determined through:

$$T_1 = T_0 \cdot \left(\frac{p_1}{p_0} \right)^{\frac{\gamma-1}{\gamma}} = T_0 \cdot \beta^{\frac{\gamma-1}{\gamma}} \tag{A.68}$$

Considering (A.65), (A.67) and the definition of compression ratio (A.66), (A.64) can be written as:

$$W_{12} = \frac{\beta \cdot p_0 \cdot V_1}{\gamma - 1} \cdot \left(1 - \varepsilon^{\gamma-1}\right) \tag{A.69}$$

The combustion is considered isochoric, so the heat supplied is:

$$Q_{in} = m \cdot c_v \cdot \left(T_3 - T_2\right) = m_f \cdot Q_{LHV} \tag{A.70}$$

The following relation can be established:

$$\frac{T_3}{T_2} = 1 + \frac{(\gamma-1) \cdot Q_{LHV}}{R \cdot T_1 \cdot \varepsilon^{\gamma-1}} \cdot \frac{1}{1 + A/F} = 1 + \frac{(\gamma-1) \cdot Q_{LHV}}{R \cdot T_0 \cdot \beta^{\frac{\gamma-1}{\gamma}} \cdot \varepsilon^{\gamma-1}} \cdot \frac{1}{1 + A/F} = 1 + \frac{B \cdot (\gamma-1)}{\varepsilon^{\gamma-1} \cdot \beta^{\frac{\gamma-1}{\gamma}}} \tag{A.71}$$

Where:

$$B = \frac{Q_{LHV}}{R \cdot T_0} \cdot \frac{1}{1 + A/F} \tag{A.72}$$

And *A/F* is the air fuel ratio of the mixture used.

p_3 can be defined as (using (A.68) and (A.71)):

$$p_3 = \beta \cdot p_0 \cdot \varepsilon^{\gamma} \cdot \left(1 + \frac{B(\gamma - 1)}{\varepsilon^{\gamma - 1} \cdot \beta^{\frac{\gamma - 1}{\gamma}}} \right) \tag{A.73}$$

Considering the expansion stroke an isentropic process and (A.73), p_4 can be defined as:

$$p_4 = p_3 \cdot \left(\frac{V_3}{V_4} \right)^{\gamma} = \beta \cdot p_0 \cdot \left(1 + \frac{B(\gamma - 1)}{\varepsilon^{\gamma - 1} \cdot \beta^{\frac{\gamma - 1}{\gamma}}} \right) \tag{A.74}$$

The work performed during the expansion, considered isentropic, is calculated through (using (A.73), (A.74) and the definition of ε):

$$W_{34} = \frac{p_3 \cdot V_3 - p_4 \cdot V_4}{\gamma - 1} = \frac{\beta \cdot p_0 \cdot V_1 \cdot \left(1 + \frac{B(\gamma - 1)}{\varepsilon^{\gamma - 1} \cdot \beta^{\frac{\gamma - 1}{\gamma}}} \right)}{(\gamma - 1)} \cdot \left(\varepsilon^{\gamma - 1} - 1 \right) \tag{A.75}$$

The work related to the exhaust and intake strokes is defined as:

$$W_{56} = p_0 \cdot (V_6 - V_5) = p_0 \cdot V_1 \cdot \left(\frac{1}{\varepsilon} - 1 \right) \tag{A.76}$$

$$W_{71} = p_1 \cdot (V_1 - V_7) = \beta \cdot p_0 \cdot V_1 \cdot \left(1 - \frac{1}{\varepsilon} \right) \tag{A.77}$$

From (A.69), (A.75), (A.76), (A.77), it is possible to write the total cycle work expression as:

$$W = \frac{\beta \cdot p_0 \cdot V_1}{\gamma - 1} \cdot \left(1 - \varepsilon^{\gamma-1}\right) + \frac{\beta \cdot p_0 \cdot V_1 \cdot \left(1 + \dfrac{B(\gamma-1)}{\varepsilon^{\gamma-1} \cdot \beta^{\frac{\gamma-1}{\gamma}}}\right)}{(\gamma-1)} \cdot \left(\varepsilon^{\gamma-1} - 1\right) + p_0 \cdot V_1 \cdot \left(\frac{1}{\varepsilon} - 1\right) + \beta \cdot p_0 \cdot V_1 \cdot \left(1 - \frac{1}{\varepsilon}\right) \quad \text{(A.78)}$$

And the total amount of heat supplied to the mixture as (considering (A.71), (A.67) and the definition of ε):

$$Q_{in} = m \cdot c_v \cdot \left(T_3 - T_2\right) = \beta \cdot p_0 \cdot V_1 \cdot \left(\frac{B}{\beta^{\frac{\gamma-1}{\gamma}}}\right) \quad \text{(A.79)}$$

The efficiency of this cycle can then be written as:

$$\eta = 1 - \frac{1}{\varepsilon^{\gamma-1}} + \frac{(\beta-1)(\varepsilon-1)}{B \cdot \varepsilon \cdot \beta^{\frac{1}{\gamma}}} \quad \text{(A.80)}$$

A.7 Supercharged Miller cycle

The compression stroke from 1 to 2 is considered an isentropic process, so that the corresponding work is defined as:

$$W_{12} = \frac{p_1 \cdot V_1 - p_2 \cdot V_2}{\gamma - 1} \quad \text{(A.81)}$$

Considering β as the relation between the intake pressure and the atmospheric pressure (A.65), ε_{tr} as the effective compression ratio (3.14) and σ is the expansion ratio (3.16), p_2 can be written as:

$$p_2 = \beta \cdot p_0 \cdot \varepsilon_{tr}^{\ \gamma} \quad \text{(A.82)}$$

Considering (A.65), (A.82) and the definition of ε_{tr}, (A.81) can be written as:

$$W_{12} = \frac{\beta \cdot p_0 \cdot V_1}{\gamma - 1} \cdot \left(1 - \varepsilon_{tr}^{\gamma-1}\right) \tag{A.83}$$

The combustion is considered isochoric, so the heat supplied is:

$$Q_{in} = m \cdot c_v \cdot \left(T_3 - T_2\right) = m_f \cdot Q_{LHV} \tag{A.84}$$

Considering the compression process in the turbocharger as an isentropic process, T_1 can be determined through:

$$T_1 = T_0 \cdot \left(\frac{p_1}{p_0}\right)^{\frac{\gamma-1}{\gamma}} = T_0 \cdot \beta^{\frac{\gamma-1}{\gamma}} \tag{A.85}$$

The following relation can then be established:

$$\frac{T_3}{T_2} = 1 + \frac{(\gamma-1)\cdot Q_{LHV}}{R \cdot T_1 \cdot \varepsilon_{tr}^{\gamma-1}} \cdot \frac{1}{1 + A/F} = 1 + \frac{(\gamma-1)\cdot Q_{LHV}}{R \cdot T_0 \cdot \beta^{\frac{\gamma-1}{\gamma}} \cdot \varepsilon_{tr}^{\gamma-1}} \cdot \frac{1}{1 + A/F} = 1 + \frac{B \cdot (\gamma-1)}{\varepsilon_{tr}^{\gamma-1} \cdot \beta^{\frac{\gamma-1}{\gamma}}} \tag{A.86}$$

Where:

$$B = \frac{Q_{LHV}}{R \cdot T_0} \cdot \frac{1}{1 + A/F} \tag{A.87}$$

And p_3 can be defined as (using (A.82), (A.86) and the ideal gas equation):

$$p_3 = \beta \cdot p_0 \cdot \varepsilon_{tr}^{\gamma} \cdot \left(1 + \frac{B(\gamma-1)}{\varepsilon_{tr}^{\gamma-1} \cdot \beta^{\frac{\gamma-1}{\gamma}}}\right) \tag{A.88}$$

Considering the expansion stroke an isentropic process, p_4 can be defined as:

$$p_4 = p_3 \cdot \left(\frac{V_3}{V_4}\right)^{\gamma} = \beta \cdot p_0 \cdot \left(\frac{1}{\sigma}\right)^{\gamma} \cdot \left(1 + \frac{B(\gamma - 1)}{\varepsilon_{tr}^{\gamma-1} \cdot \beta^{\frac{\gamma-1}{\gamma}}}\right) \tag{A.89}$$

The work performed during the expansion, considered isentropic, is calculated through (using (A.88), (A.89) and the definition of σ and ε_{tr}):

$$W_{34} = \frac{p_3 \cdot V_3 - p_4 \cdot V_4}{\gamma - 1} = \frac{\beta \cdot p_0 \cdot V_1 \cdot \left(1 + \frac{B(\gamma - 1)}{\varepsilon_{tr}^{\gamma-1} \cdot \beta^{\frac{\gamma-1}{\gamma}}}\right)}{\gamma - 1} \cdot \left(\varepsilon_{tr}{}^{\gamma-1} - \frac{1}{\sigma^{\gamma-1}}\right) \tag{A.90}$$

The work related to the exhaust and intake stroke is defined as:

$$W_{56} = p_0 \cdot (V_6 - V_5) = p_0 \cdot V_1 \cdot \left(\frac{1}{\varepsilon_{tr}} - \sigma\right) \tag{A.91}$$

$$W_{71} = p_k \cdot (V_1 - V_7) = \beta \cdot p_0 \cdot V_1 \cdot \left(1 - \frac{1}{\varepsilon_{tr}}\right) \tag{A.92}$$

From (A83), (A.90), (A.91) and (A.92) it is possible to write the total cycle work expression as:

$$W = \frac{\beta \cdot p_0 \cdot V_1}{\gamma - 1} \cdot \left(1 - \varepsilon_{tr}^{\gamma-1}\right) + \frac{\beta \cdot p_0 \cdot V_1 \cdot \left(1 + \frac{B(\gamma - 1)}{\varepsilon_{tr}^{\gamma-1} \cdot \beta^{\frac{\gamma-1}{\gamma}}}\right)}{\gamma - 1} \cdot \left(\varepsilon_{tr}^{\gamma-1} - \frac{1}{\sigma^{\gamma-1}}\right) +$$

$$+ p_0 \cdot V_1 \cdot \left(\frac{1}{\varepsilon_{tr}} - \sigma\right) + \beta \cdot p_0 \cdot V_1 \cdot \left(1 - \frac{1}{\varepsilon_{tr}}\right) \tag{A.93}$$

And the total amount of heat supplied to the mixture as (considering (A.82), (A.86) and the definition of ε_{tr}):

$$Q_{in} = m \cdot c_v \cdot (T_3 - T_2) = \beta \cdot p_0 \cdot V_1 \cdot \left(\frac{B}{\beta^{\frac{\gamma-1}{\gamma}}} \right) \tag{A.94}$$

The efficiency of this cycle can then be written as:

$$\eta_{MSc} = 1 - \frac{1}{\varepsilon_{tr}^{\gamma-1}} \frac{1}{\sigma^{\gamma-1}} - \frac{\dfrac{\sigma^{1-\gamma} - \gamma}{B(\gamma-1)}}{\beta^{\frac{\gamma-1}{\gamma}}} - \frac{\sigma + \dfrac{\beta-1}{\varepsilon_{tr}}}{B\beta^{\frac{1}{\gamma}}} \tag{A.95}$$

A.8 Supercharged dual cycle

The work produced by this cycle can be expressed as:

$$W = W_{12} + W_{34'} + W_{4'5'} + W_{1678} \tag{A.96}$$

And the heat supplied during the combustion process, Q_{in} is written as:

$$Q_{in} = Q_v + Q_p = m \cdot c_v \cdot (T_3 - T_2) + m \cdot c_p \cdot (T_{4'} - T_3) \tag{A.97}$$

The starting conditions (at point 1) are considered as:

$$p_1 = \beta \cdot p_0 \quad defined\ as \quad \beta = \frac{p_1}{p_0} > 1 \tag{A.98}$$

T_1 is the temperature after the air compression in the turbocharger, so it can be defined as:

$$T_1 = T_k = T_0 \cdot \left(\frac{p_k}{p_0} \right)^{\frac{\gamma-1}{\gamma}} = T_0 \cdot \beta^{\frac{\gamma-1}{\gamma}} \qquad \text{(A.99)}$$

The compression work, considered as an isentropic process, is described as:

$$W_{12} = \frac{p_1 \cdot V_1 - p_2 \cdot V_2}{\gamma - 1} = \frac{\beta \cdot p_0 \cdot V_1 \cdot \left(1 - \varepsilon^{\gamma-1}\right)}{\gamma - 1} \qquad \text{(A.100)}$$

The heat supplied during the first part of the combustion process, the isochoric combustion, is defined as:

$$Q_V = m \cdot c_v \cdot \left(T_3 - T_2\right) = \Psi \cdot m_f \cdot Q_{LHV} \qquad \text{(A.101)}$$

where Ψ is defined as:

$$\Psi = \frac{Q_V}{Q_T} \qquad \text{(A.102)}$$

From now on it will be considered Ψ = 0.1 and constant for the several values of load. Knowing that:

$$m_f = \frac{m}{\frac{A}{F} + 1} \qquad T_2 = T_1 \cdot \varepsilon^{\gamma-1} \qquad C_V = \frac{R}{\gamma - 1} \qquad \text{(A.103, A.104, A.105)}$$

It can be established that:

$$\frac{T_3}{T_2} = 1 + \frac{\left(\gamma - 1\right) \cdot \Psi \cdot Q_{LHV}}{R \cdot T_1 \cdot \varepsilon^{\gamma-1}} \cdot \frac{1}{1 + \left(A/F\right)_S} = A\left(\Psi\right) \qquad \text{(A.106)}$$

where $(A/F)_S$ is the stoichiometric air to fuel ratio of the mixture used. The value of $A(\Psi)$ is also constant with load as it only depends on Ψ.

As the combustion process is considered isochoric, the following relation may be established:

$$\frac{p_3}{p_2} = A(\Psi) \tag{A.107}$$

From (A.107) and (A.106), p_3 and T_3 can also be written as:

$$p_3 = \beta \cdot p_0 \cdot \varepsilon^{\gamma} \cdot A(\Psi) \tag{A.108}$$

$$T_3 = T_1 \cdot \varepsilon^{\gamma-1} \cdot A(\Psi) \tag{A.109}$$

During the second part of the combustion, isobaric combustion, the heat supplied is:

$$Q_p = m \cdot c_p \cdot (T_{4'} - T_3) = \left(1 - \frac{\Psi}{\Phi}\right) \cdot m_f \cdot Q_{LHV} \tag{A.110}$$

Considering the load factor:

$$\Phi = \frac{Q_{T'}}{Q_T} \tag{A.111}$$

Where Q_T is the total amount of heat supplied during the combustion at full load (until 4) and $Q_{T'}$ is the total amount of heat supplied during the combustion until 4' (part load). The ratio Ψ/Φ represents the amount of heat supplied at constant volume in relation to the total amount of heat supplied when the combustion goes until 4'. Based on (A.109), the following relation can then be established:

$$\frac{T_{4'}}{T_3} = 1 + \frac{\left(1 - \frac{\Psi}{\Phi}\right) \cdot Q_{LHV}}{\frac{\gamma}{\gamma - 1} \cdot R \cdot T_1 \cdot \varepsilon^{\gamma-1} \cdot A(\Psi)} \cdot \frac{1}{1 + \frac{\left(A/F\right)_S}{\Phi}} = C(\Psi, \Phi) \tag{A.112}$$

As the combustion process is isobaric the following relation may be written:

$$\frac{V_{4'}}{V_3} = C(\Psi,\Phi) \tag{A.113}$$

The work performed by an isobaric process is defined as (considering (A.108), (A.113) and the definition of ε):

$$W_{34'} = p_3 \cdot (V_{4'} - V_3) = p_3 \cdot V_3 \cdot \left(\frac{V_{4'}}{V_3} - 1\right) = \beta \cdot p_0 \cdot V_1 \cdot A(\Psi) \cdot \varepsilon^{\gamma-1} \cdot [C(\Psi,\Phi) - 1] \tag{A.114}$$

The expansion process is analyzed as an isentropic process. The work performed during this process is defined as:

$$W_{4'5'} = \frac{p_{4'} \cdot V_{4'} - p_{5'} V_{5'}}{\gamma - 1} \tag{A.115}$$

Knowing that $p_{4'} = p_3$, comes:

$$p_{4'} = \beta \cdot p_0 \cdot \varepsilon^{\gamma} \cdot A(\Psi) \tag{A.116}$$

From (A.113), and knowing that $V_5 = V_1$, comes:

$$V_{4'} = \frac{V_1}{\varepsilon} \cdot C(\Psi,\Phi) \tag{A.117}$$

As the expansion stroke can be considered an isentropic process, it can be written:

$$p_{5'} = p_{4'} \cdot \left[\frac{C(\Psi,\Phi)}{\varepsilon}\right]^{\gamma} \tag{A.118}$$

(A.115) can then be written as:

$$W_{4'5'} = \frac{\beta \cdot p_0 \cdot V_1 \cdot A(\Psi)}{\gamma - 1} \cdot \left\{ \varepsilon^{\gamma-1} \cdot C(\Psi,\Phi) - \left[C(\Psi,\Phi) \right]^{\gamma} \right\} \quad \text{(A.119)}$$

During the exhaust and intake strokes, the work performed, can be written as:

$$W_{1678} = (p_k - p_0) \cdot V_d = (\beta - 1) \cdot p_0 \cdot V_1 \cdot \frac{\varepsilon - 1}{\varepsilon} \quad \text{(A.120)}$$

To determine the total heat supplied to the mixture present in the cylinder, it will be considered that:

$$T_3 - T_2 = T_1 \cdot \varepsilon^{\gamma-1} \cdot [A(\Psi) - 1] \quad \text{(A.121)}$$

$$T_{4'} - T_3 = T_1 \cdot \varepsilon^{\gamma-1} \cdot A(\Psi) \cdot [C(\Psi,\Phi) - 1] \quad \text{(A.122)}$$

And the total heat supplied (A.97) can be written as:

$$Q_{in} = \frac{\beta \cdot p_0 \cdot V_1}{\gamma - 1} \cdot \varepsilon^{\gamma-1} \cdot \{A(\Psi) - 1 + \gamma \cdot A(\Psi) \cdot [C(\Psi,\Phi) - 1]\} \quad \text{(A.123)}$$

Considering all the work terms (A.100), (A.114), (A.119) and (A.120) and the total heat expression (A.123), it is possible to determine the thermal efficiency of this cycle:

$$\eta_{dSc} = \frac{\frac{\beta \cdot (1 - \varepsilon^{\gamma-1})}{\gamma - 1} + \beta \cdot A(\Psi) \cdot \varepsilon^{\gamma-1} \cdot [C(\Psi,\Phi) - 1] + \frac{\beta \cdot A(\Psi)}{\gamma - 1} \cdot \left[\varepsilon^{\gamma-1} \cdot C(\Psi,\Phi) - C(\Psi,\Phi)^{\gamma} \right] + (\beta - 1) \cdot \frac{\varepsilon - 1}{\varepsilon}}{\frac{\beta}{\gamma - 1} \cdot \varepsilon^{\gamma-1} \cdot \{A(\Psi) - 1 + \gamma \cdot A(\Psi) \cdot [C(\Psi,\Phi) - 1]\}}$$

(A.124)

Annex B - Computer Model Architecture

B COMPUTER MODEL ARCHITECTURE

B.1 First Law model global structure

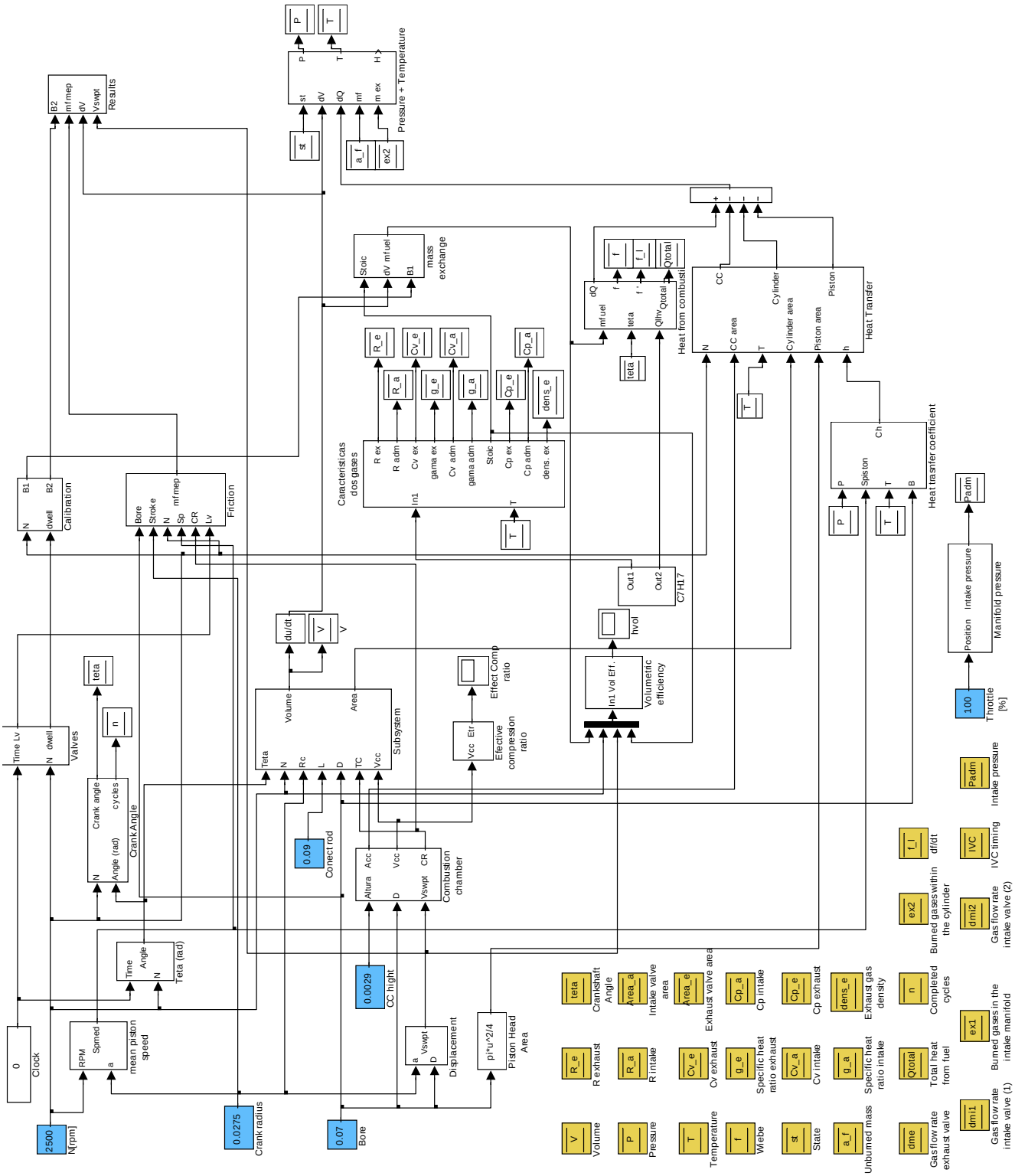

The model comprehends several subsystems and a set of variables (yellow blocks). Each of the subsystems will be described bellow.

B.1.1 Mean piston speed

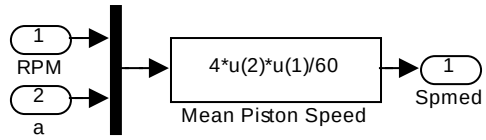

Calculates the mean piston speed considering the crank speed (rpm) and the crank radius (a) and using equation (4.7).

B.1.2 Rotation angle (rad)

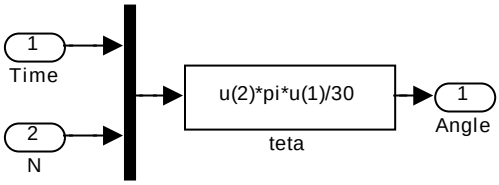

Calculates the amount of crank angle rotated from the simulation beginning, considering the simulation time and the crank speed (N). The resulting angle unit is radians.

B.1.3 Crank Angle

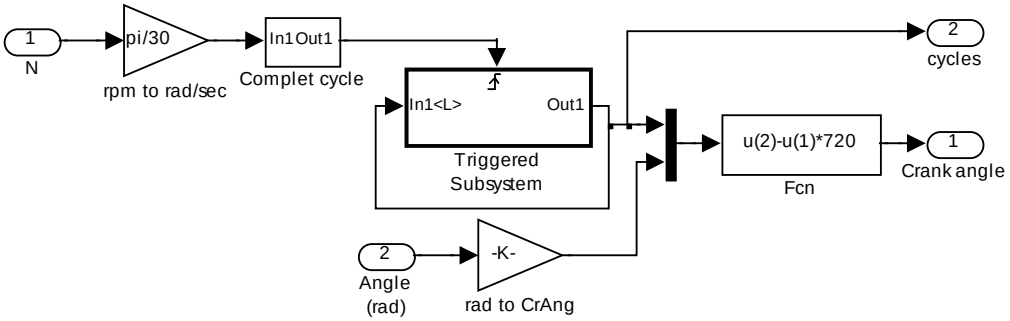

Calculates de value of the crank angle and the number of completed cycles since the simulation start. The **Complet cycle** subsystem outputs a signal everytime a cycle is finished (i.e. when CA is equal to 720º). The signal from the **Triggered Subsystem** gives the number of completed cycles, which is used to calculate the actual crank angle

(0 – 720º CA) in the **Fcn** block, using the full crank angle rotated from the simulation start.

B.1.3.1 Triggered Subsystem

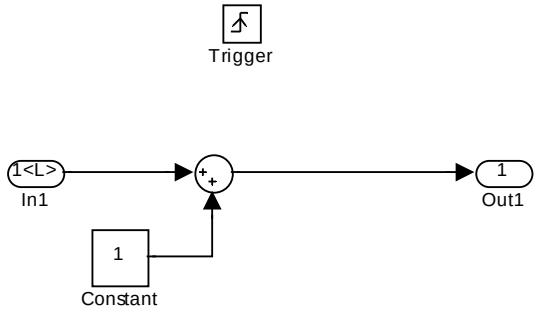

Every time there is a trigger signal (the cycle completes its four strokes), the input is added of a quantity of 1. The output is then the number of cycles already completed.

B.1.4 Displacement

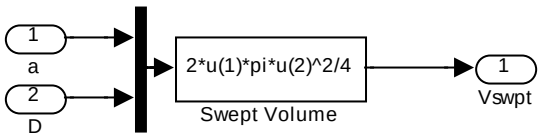

Calculates the engine displacement using the crank radius (**a**) and the cylinder bore (**D**). The swept volume is constant during all the simulation time.

B.1.5 Combustion Chamber (CC)

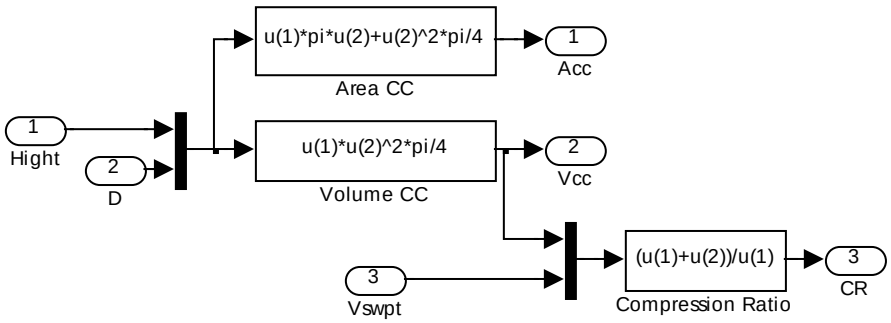

At this subsystem is calculated the exposure area of the combustion chamber, considered as a cylinder (roof and cylinder wall), and the combustion chamber volume. This volume is used to calculate the geometric compression ratio.

B.1.6 Volume + Area

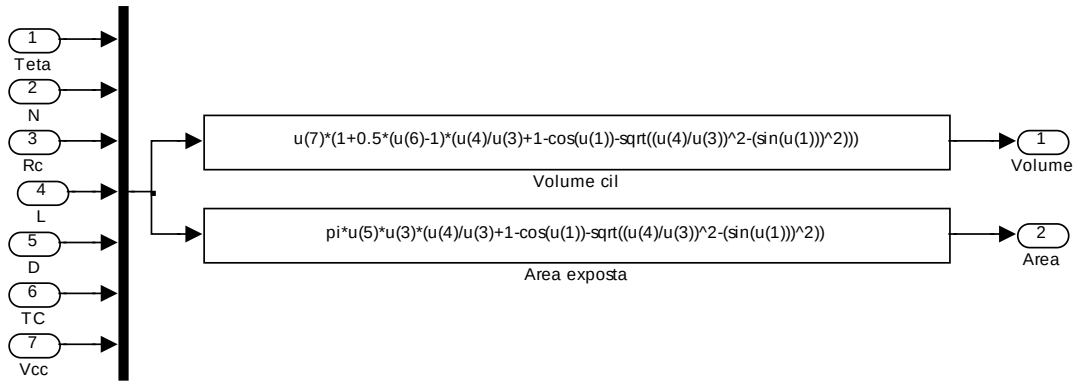

Calculates the volume of the cylinder (including the combustion chamber volume) and the exposed cylinder side wall, at each simulation time step.

B.1.7 Effective compression ratio

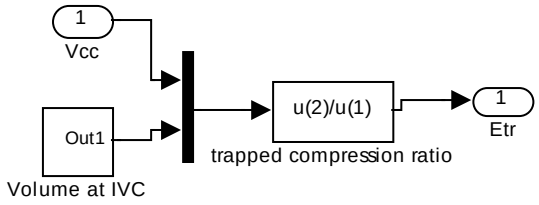

Calculates the effective compression ratio considering the combustion chamber volume and the volume at intake valve closure time (as calculated in B.1.7.1). As the effective compression ratio is continuously calculated, the result at IVC time is the real effective compression ratio. This value is kept constant during the cycle period when both valves are closed.

B.1.7.1 Volume at IVC

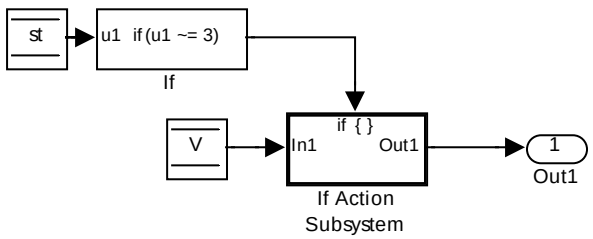

The value of the cylinder volume passes only when any of the valves is open (st ~= 3). When the intake valve closes, the output value is the value at IVC and remains constant until EVO.

B.1.8 Volumetric efficiency

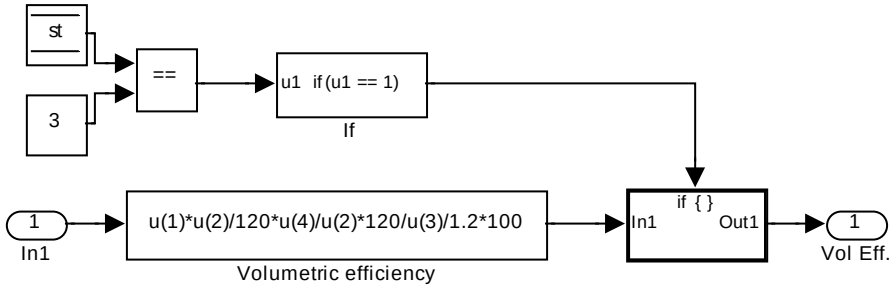

Calculates the volumetric efficiency at each time step, but the output is only changed when the intake valve closes and the fuel mass amount becomes constant.

B.1.9 Manifold pressure

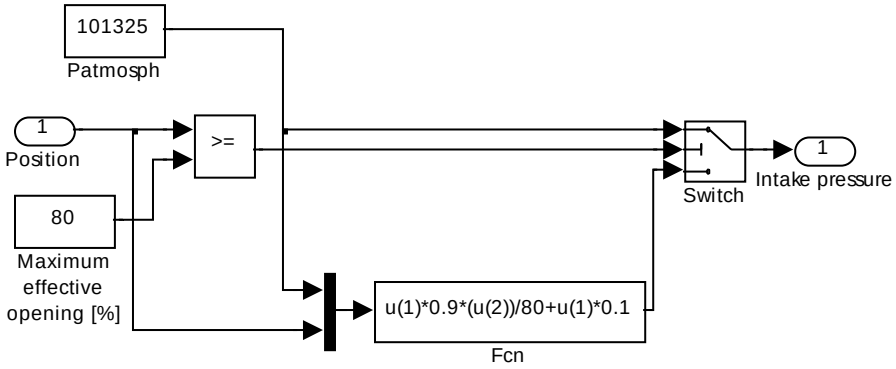

Calculates the intake manifold pressure considering that the effective open area remains constant for throttle open higher than 80%, and assuming that when the throttle is fully closed the intake manifold pressure is 10% of the absolute atmospheric pressure.

B.1.10 Valves

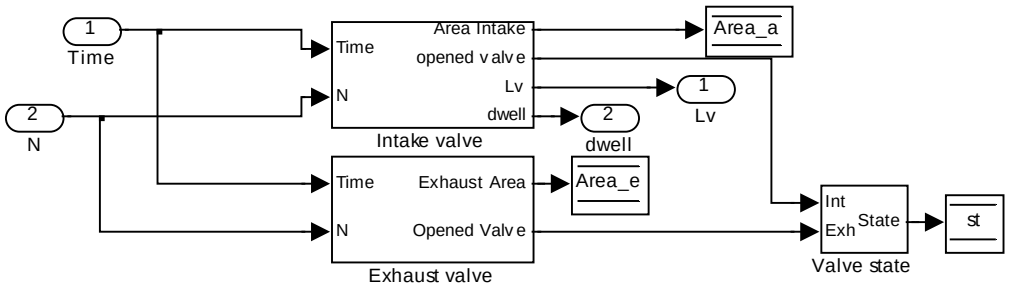

At this subsystem is calculated the valves opening areas and is defined the value of the **st** variable, which is 1 for overlap period, 2 for intake valve open period, 3 for the closed cylinder period and 4 for the exhaust valve open period (B.1.10.2).

B.1.10.1 Intake valve (exhaust valve)

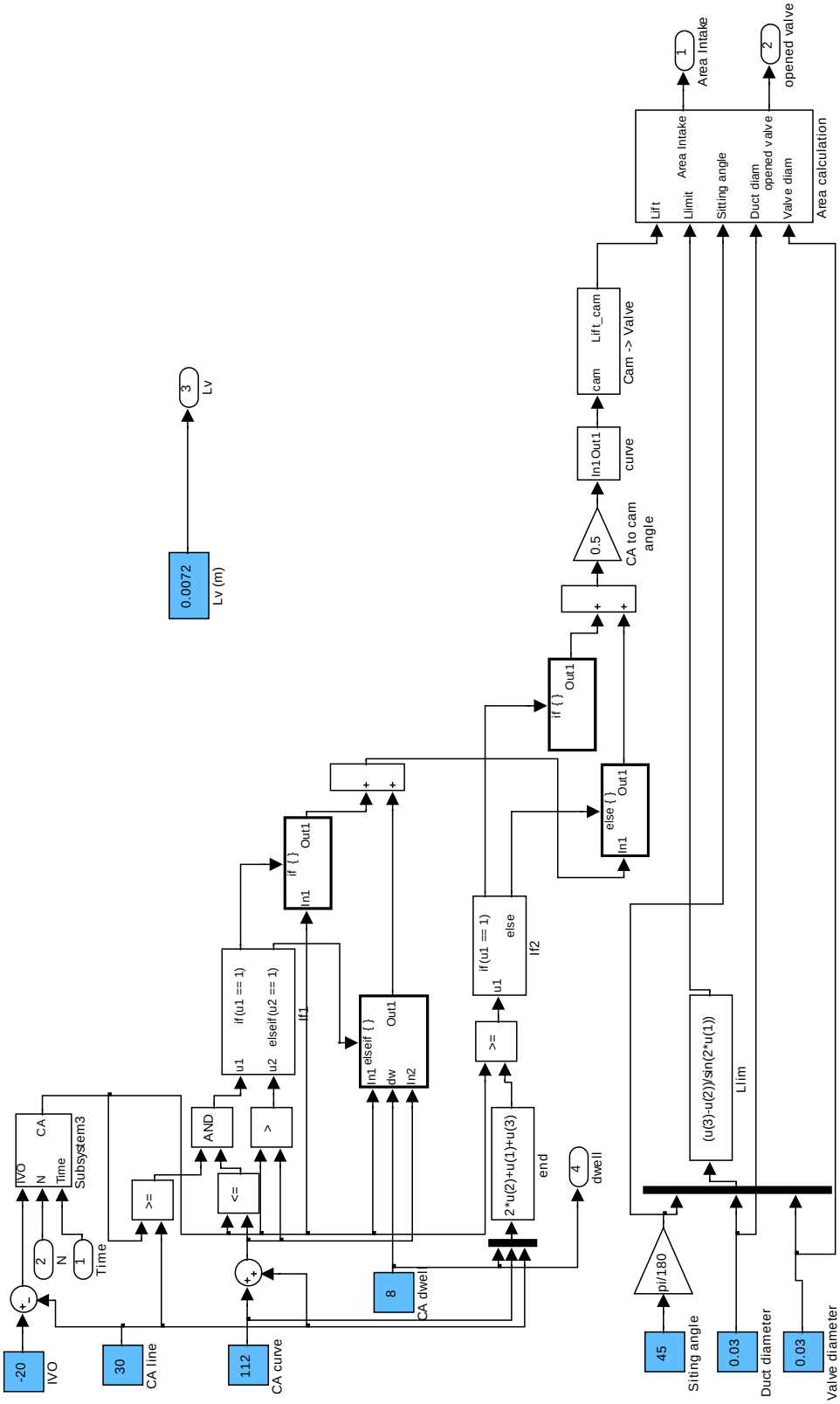

At this subsystem (that is structurally equal for intake and for exhaust) is calculated the opening area of the valve.

Subsystem3

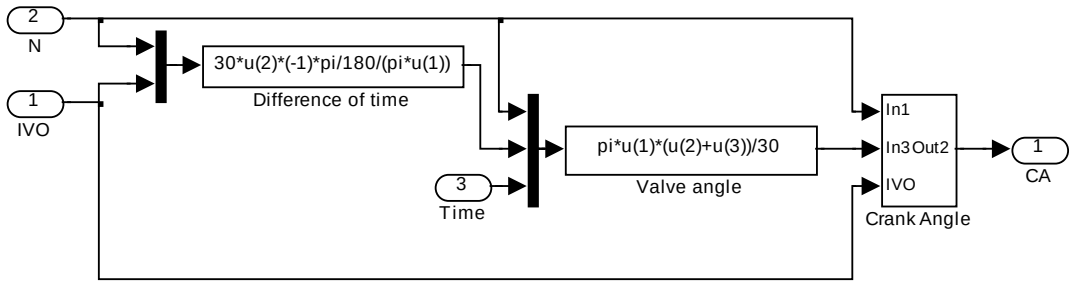

Calculates the time difference between the TDC time of the Crankshaft and the IVO time. This time difference is used to calculate the valve angle (which is similar to the Crank Angle but 0 is at valve opening time. A phase difference exists between Crank Angle and Valve Angle, and this phase difference is equal to **Difference of time**).

Crank Angle

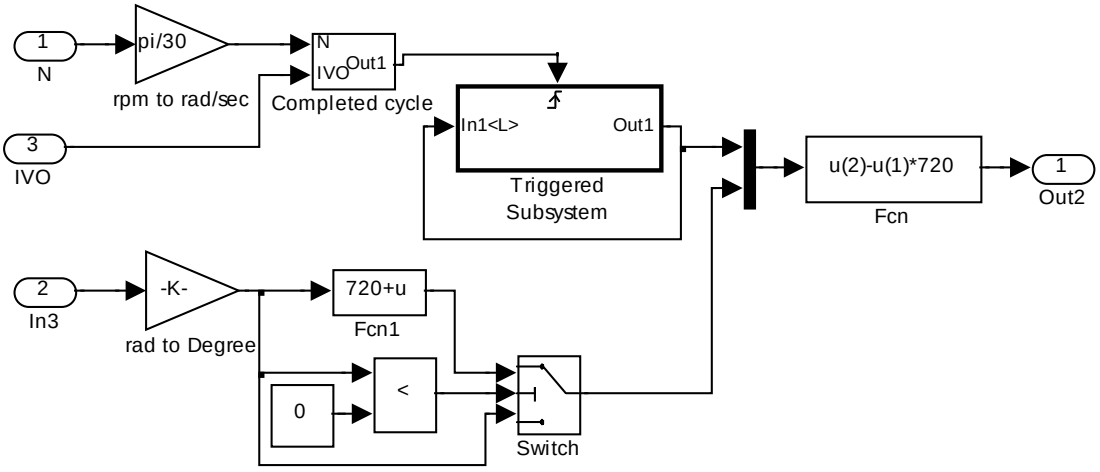

Calculates the value of valve angle (0 – 720º). The **Completed cycle** subsystem:

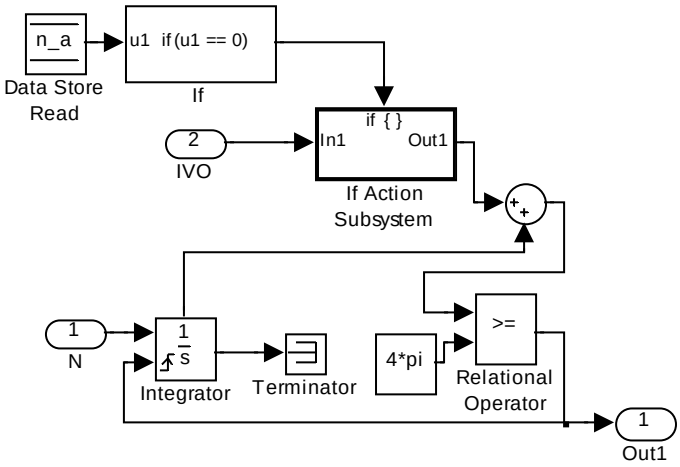

Outputs a trigger signal every time the intake valve opens. This is the moment when the valve cycle is completed.

At the intake valve subsystem, when the valve angle is more than **CA line** (silent ramp length on the valve profile) and less than **CA curve** (valve rise curve length on the cam profile) + **CA line**, **If1** block allows the valve angle to pass, else if the valve angle is more than **CA curve** + **CA line**:

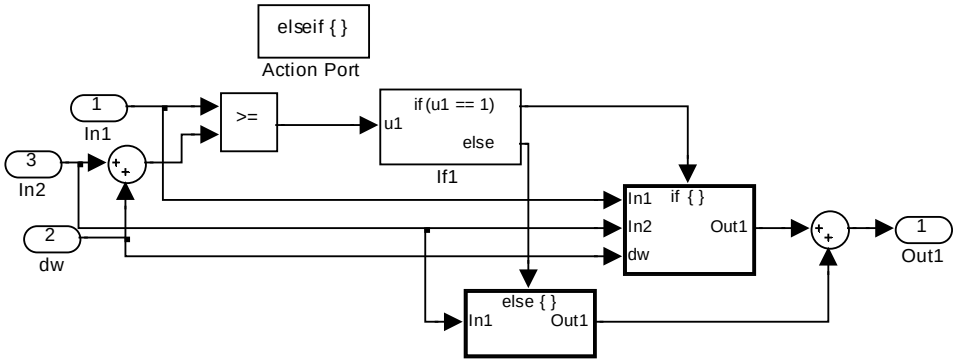

If **CA curve** + **CA line** + **dwell** is less than valve angle, the valve angle value passes (**Else** block), if that value is more than the valve angle (beginning of the descent ramp):

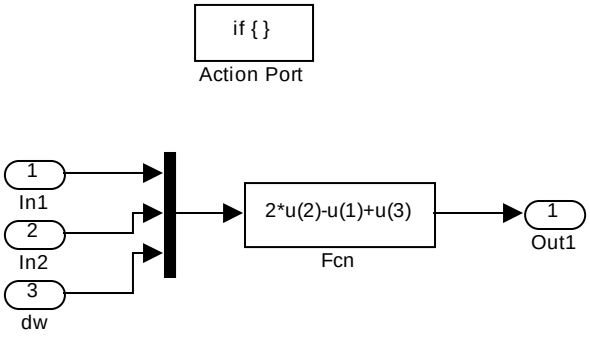

Passes the value of the descent ramp angle (calculated in the **Fcn** block).

At the **Curve** subsystem:

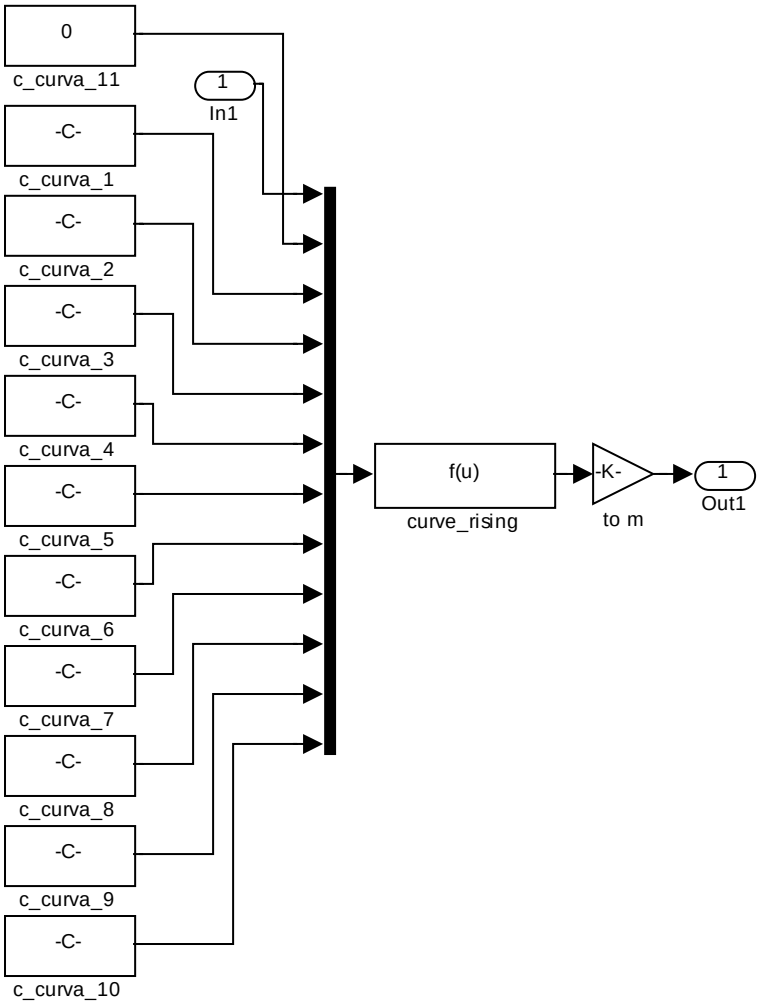

Using the polynomial coefficients from **c_curva_1** to **c_curva_11** calculates the rising of the cam (in mm), which is than converted to meters.

At the **Cam -> Valve** subsystem the value of the lift of the cam is converted to lift of the valve (using the conversion method presented in 4.2.7):

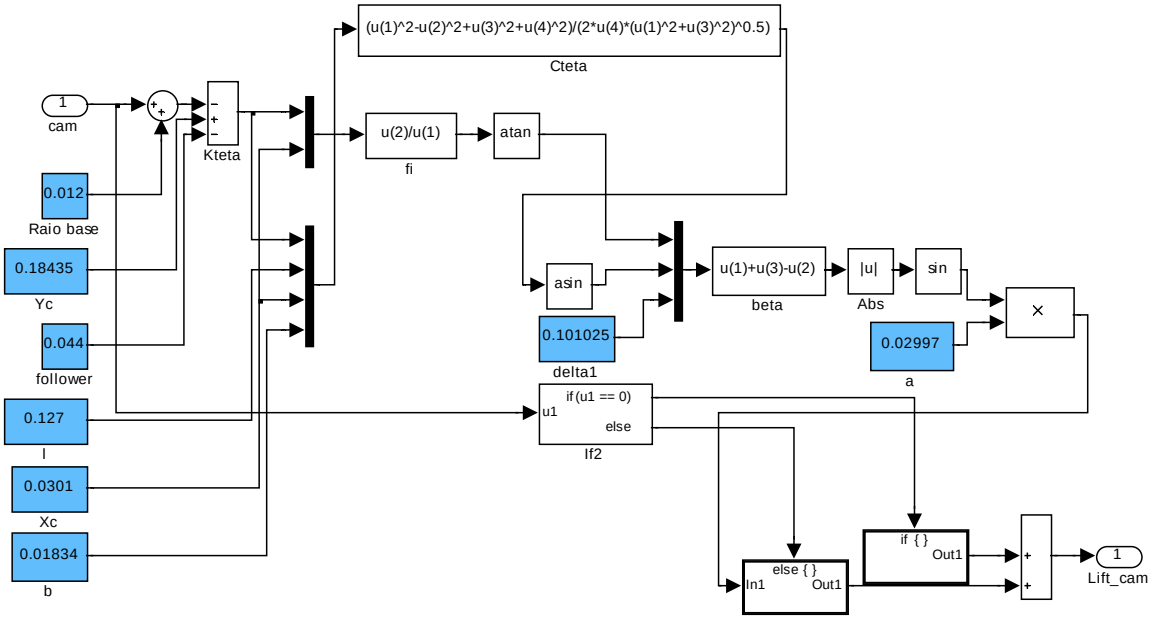

The **Area calculation** subsystem, calculates the effective opening area of the valve, using equations (4.47 and 4.48) considering the port geometry and the lift limit (**Llimit** input port block) defined in equation (4.46):

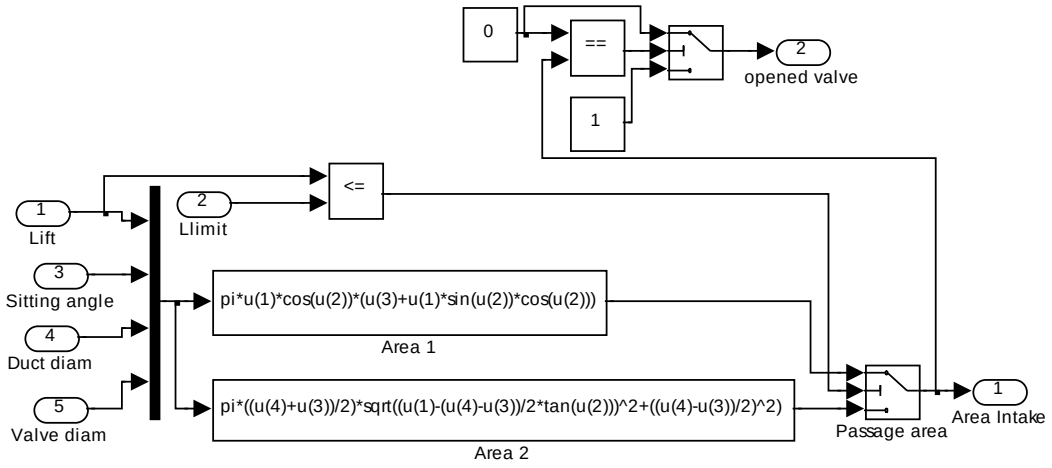

B.1.10.2 Valve state

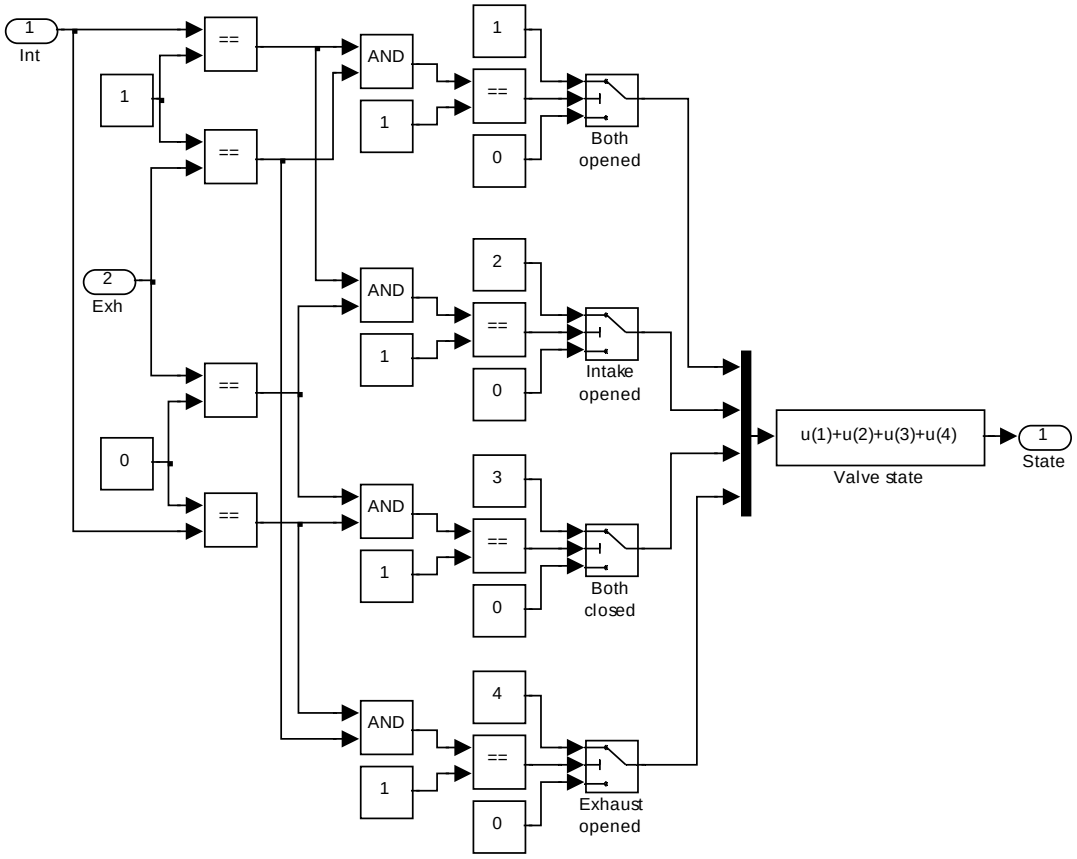

Calculates the value of the **st** variable, depending on the valve state.

B.1.11 Fuel

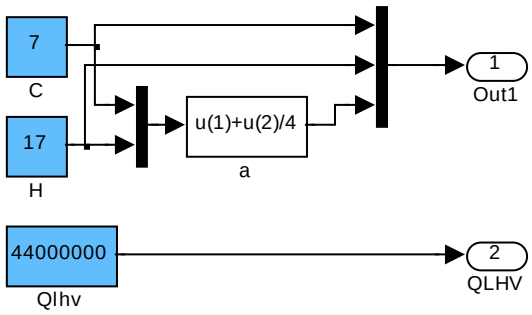

At this subsystem is defined the chemical structure of the fuel and its lower heating value.

B.1.12 Gas characteristics

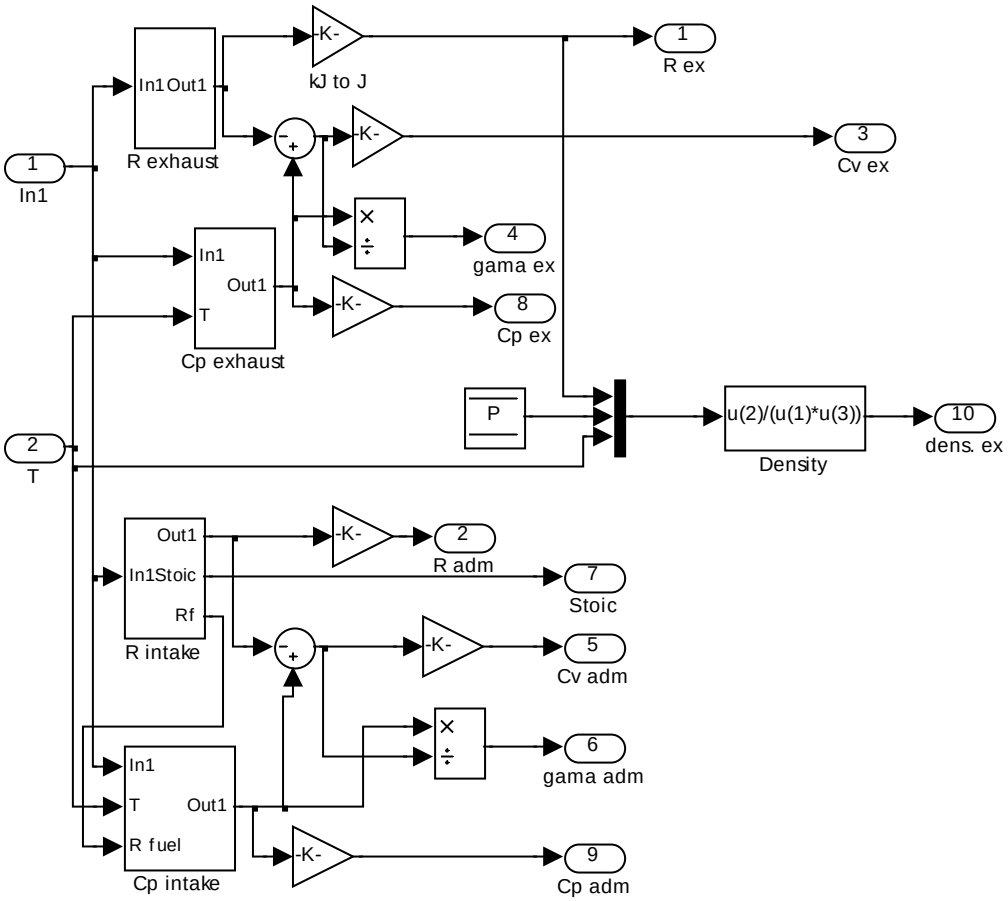

Calculates all the gas characteristics of air+fuel mixture and burned gases.

B.1.12.1 R exhaust

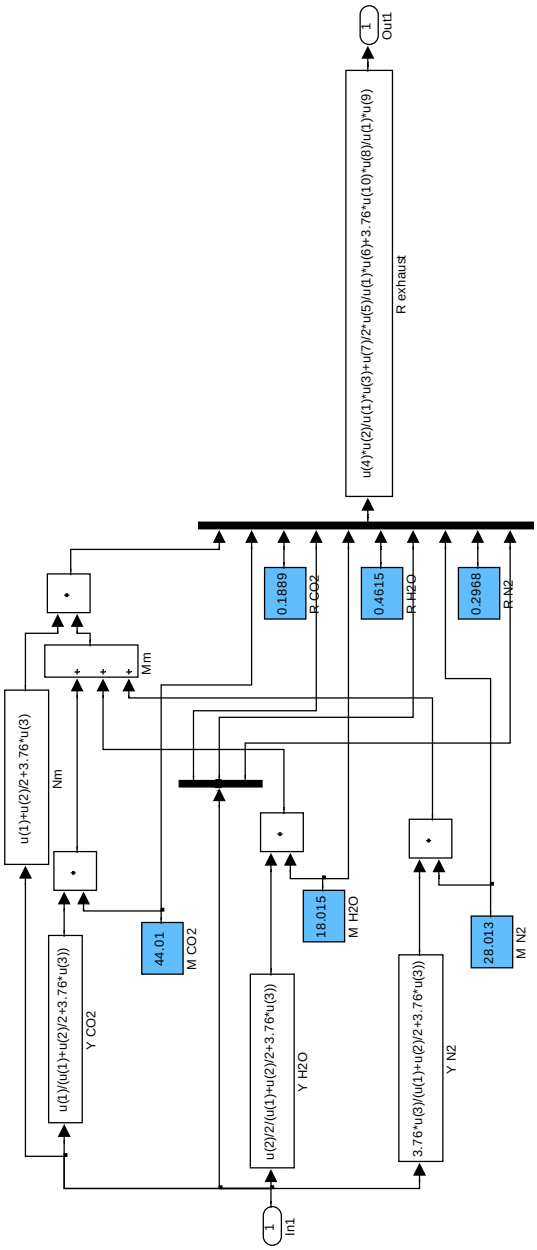

Calculates the value of the gas constant of the burned gases within the cylinder, considering the instantaneous temperature of the gases and the burned gases mixture composition.

B.1.12.2 Cp exhaust

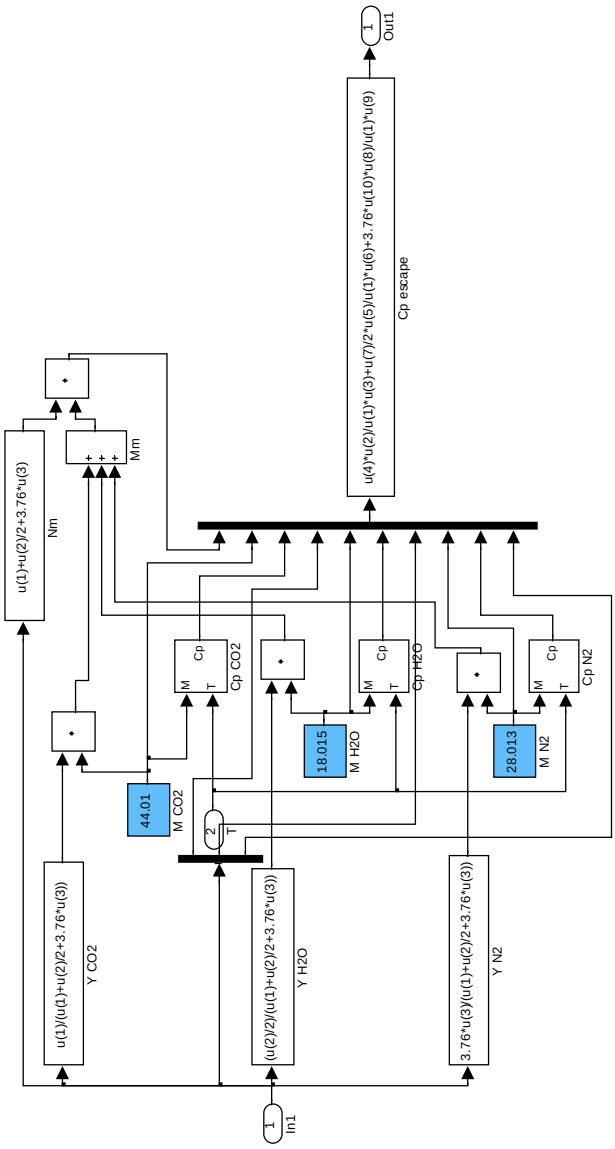

Calculates the specific heat of the burned gases considering its composition and using equation (4.27).

B.1.12.3 R intake

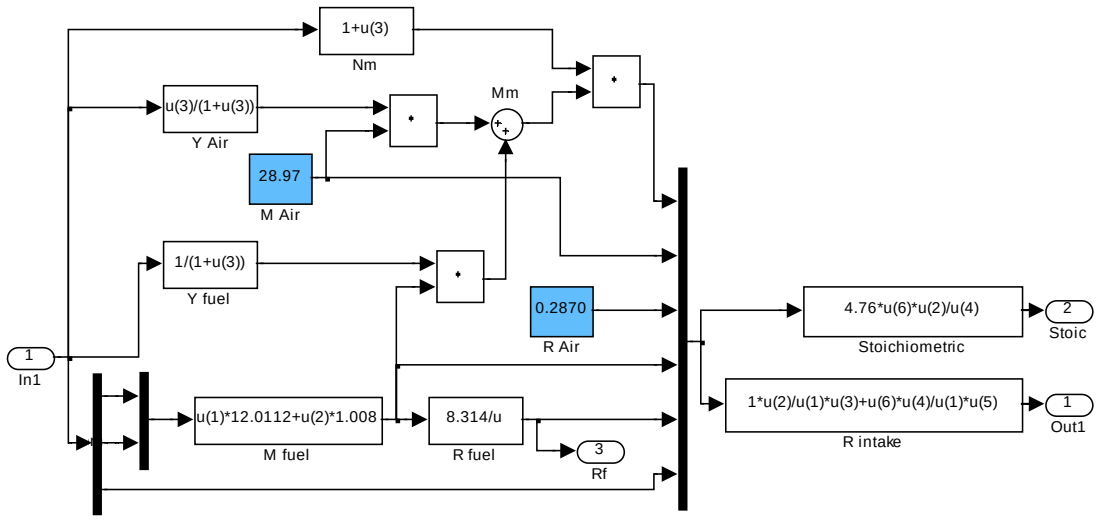

Calculates the value of the gas constant of the air+fuel mixture within the cylinder, considering the instantaneous temperature of the gases and the air+fuel mixture composition. It also calculates the air/fuel ratio for stoichiometric conditions.

B.1.12.4 Cp intake

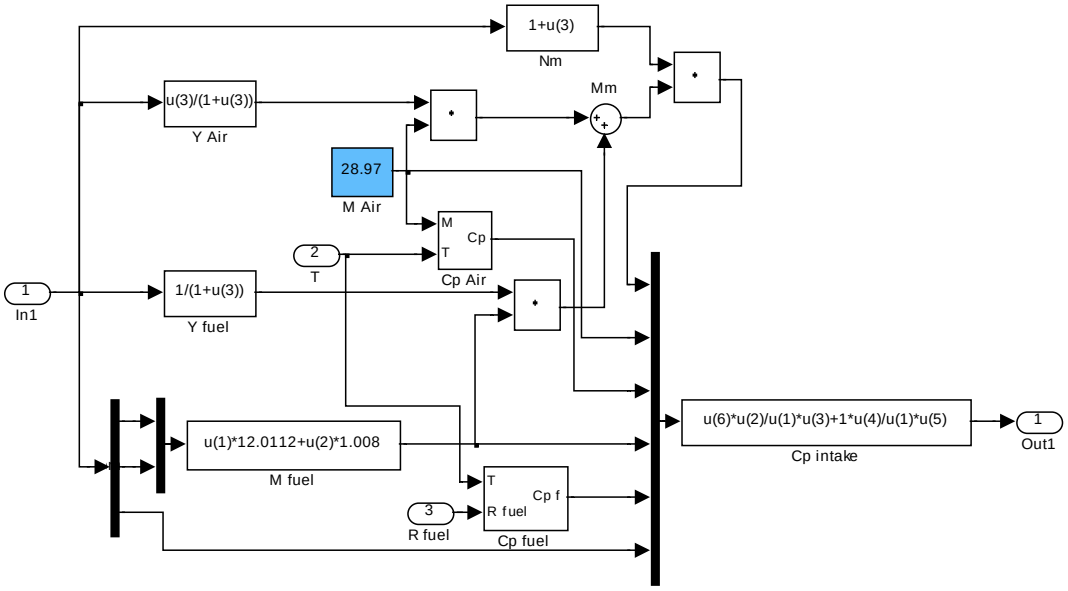

Calculates the specific heat of the air+fuel mixture considering its composition and using equation (4.27).

B.1.13 Heat from combustion

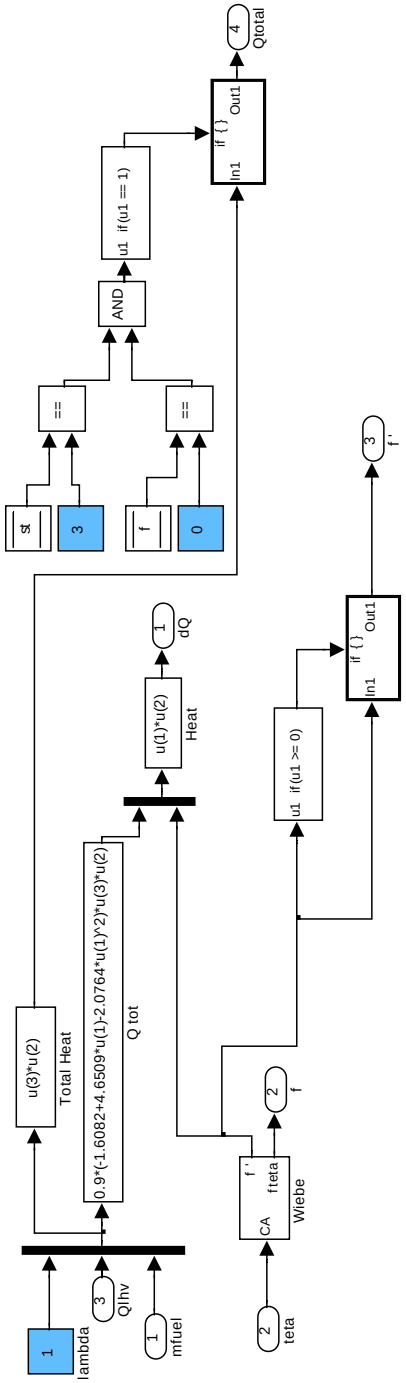

Calculates the total amount of heat supplied to the system with the fuel, the total amount of heat resulting from the combustion using a certain degree of inefficiency as described in equation (4.22), and the heat supply rate from the combustion process.

B.1.13.1 Wiebe

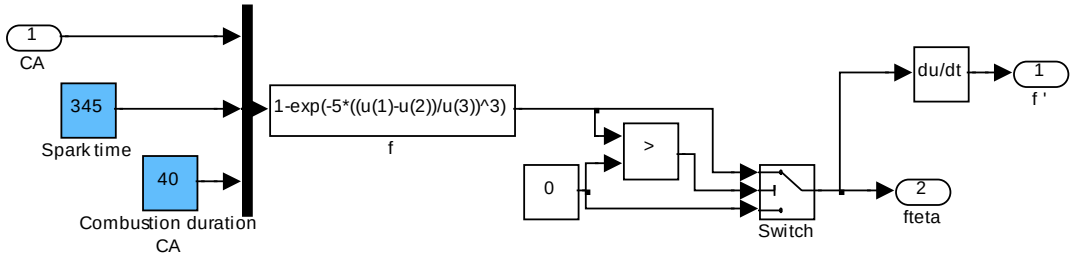

Calculates the ratio of fuel mass burned and rate of heat released during the combustion. These results are calculated from the Wiebe function defined by equation (4.23)

B.1.14 Heat transfer coefficient

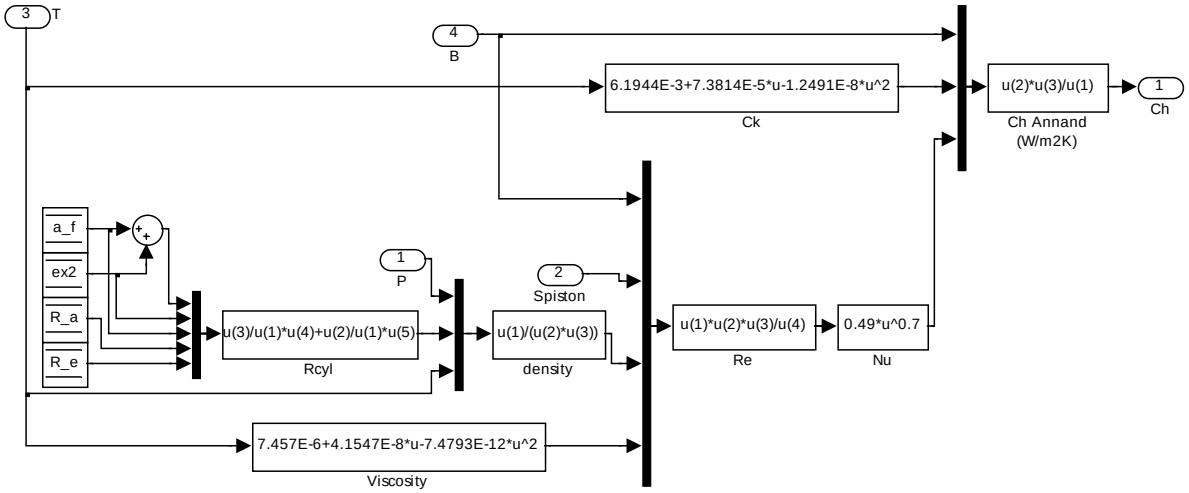

This subsystem calculates the Annand heat transfer coefficient as described in 4.2.6.

B.1.15 Heat transfer

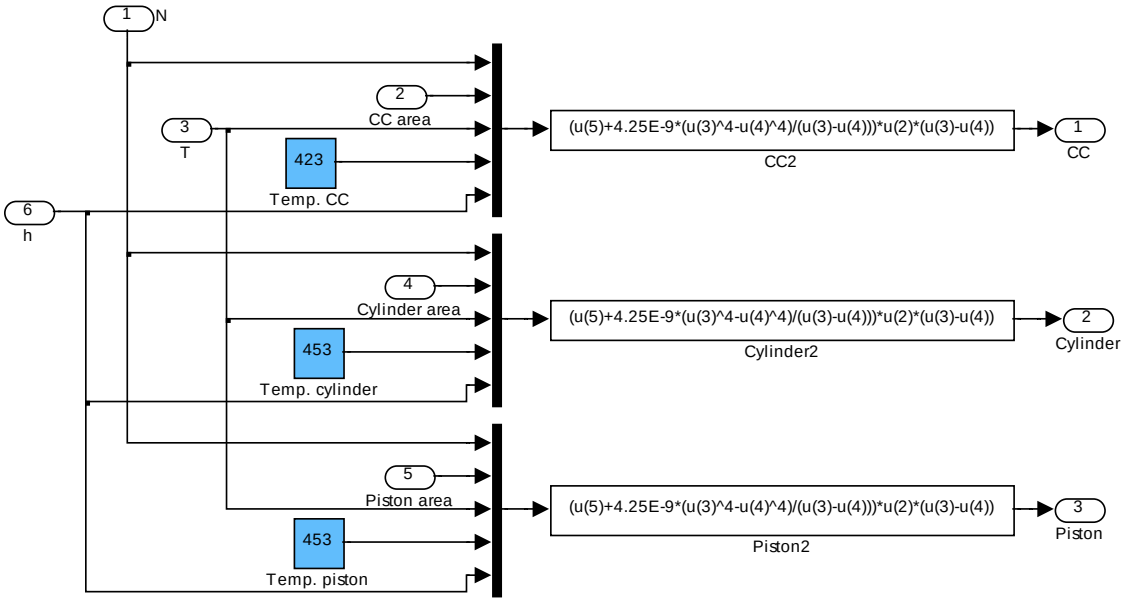

Calculates the heat transfer ratio through the engine head, cylinder walls and piston crown using equation (4.37). It considers constant surface temperatures. Uses the as input the Annand heat transfer coefficient and the areas of each of the heat transfer surfaces.

B.1.16 Pressure + Temperature

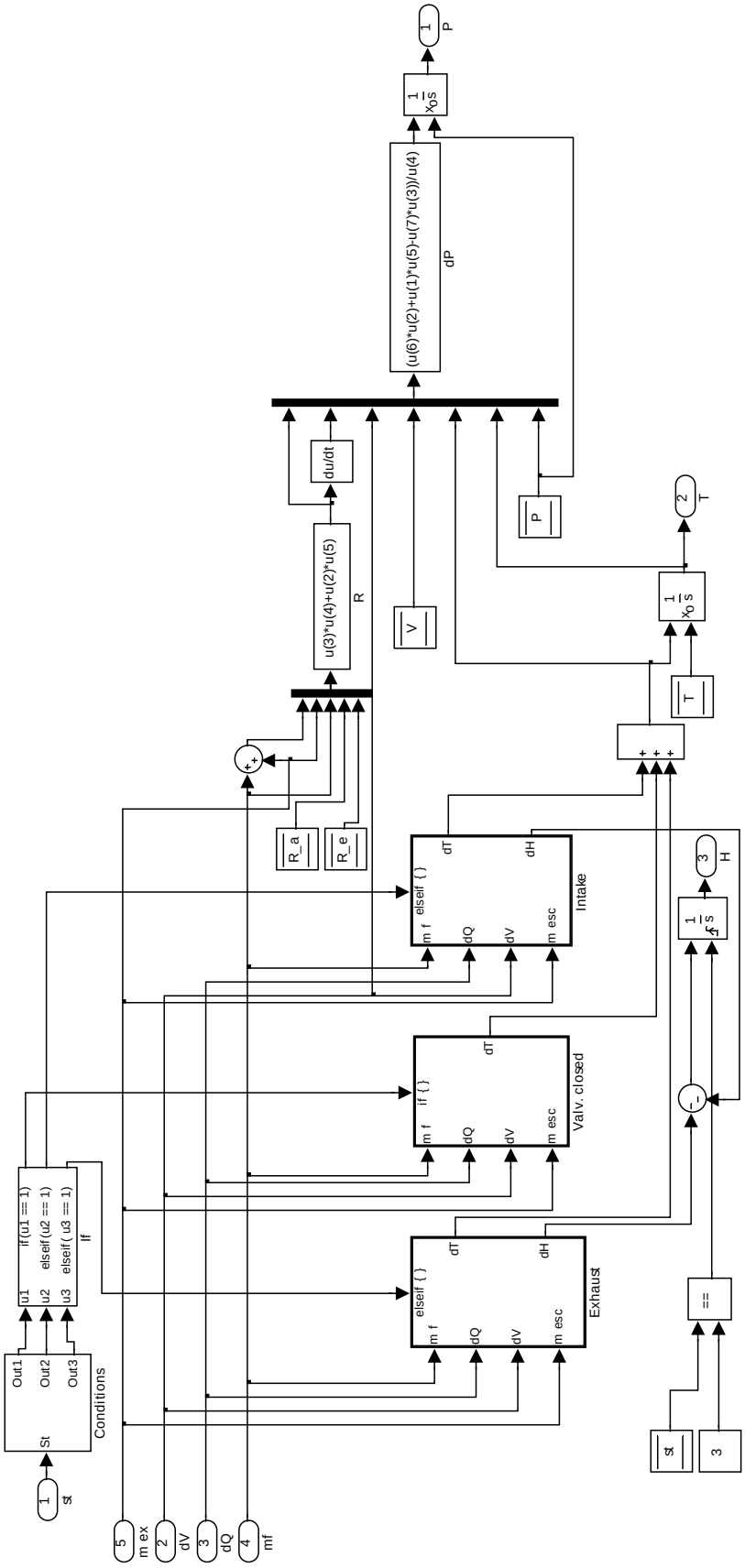

Calculates the temperature and pressure of the inner cylinder gases. It also calculates the enthalpy of exhaust and intake gases.

B.1.16.1 Conditions

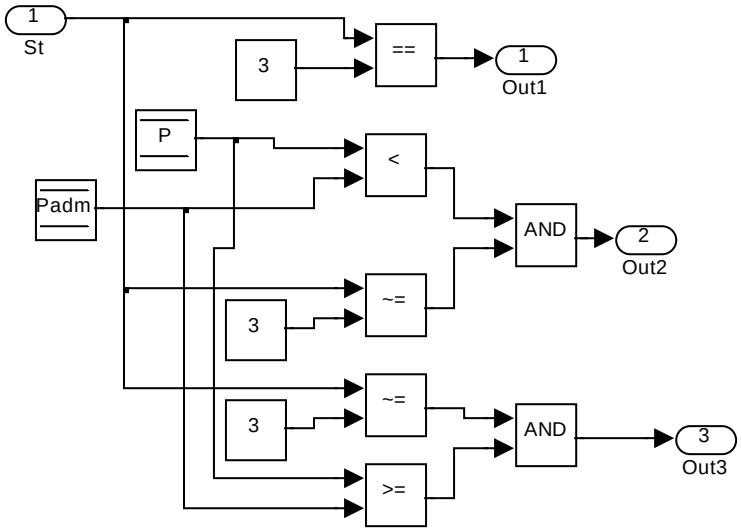

Establishes which of the subsystems from the **Pressure + Temperature** system shall make the output, depending on the cycle time. **Out1** when valves are closed, **Out2** when engine is intaking and **Out3** when engine is exhausting.

B.1.16.2 Exhaust

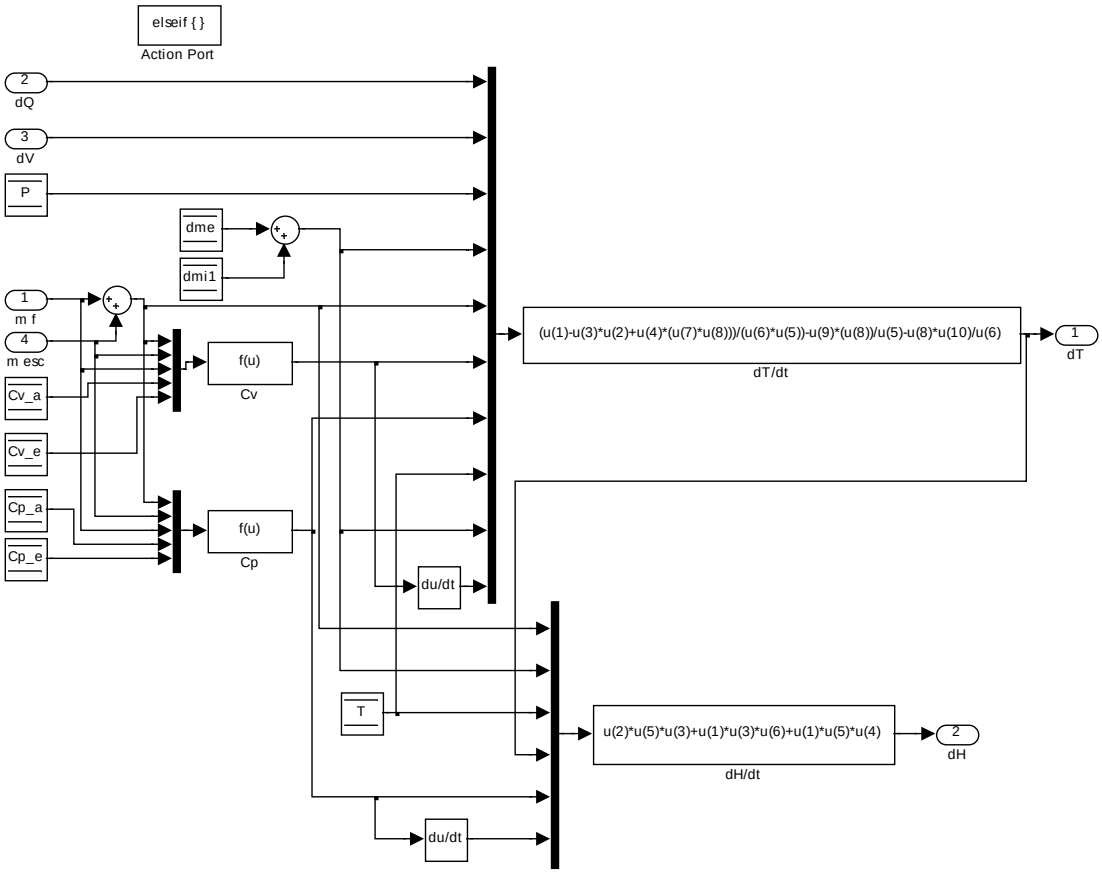

Calculates the temperature change rate (using equation (4.17)) and the enthalpy change rate (using equation (4.15)), during the exhaust or blow-back period.

B.1.16.3 Valves closed

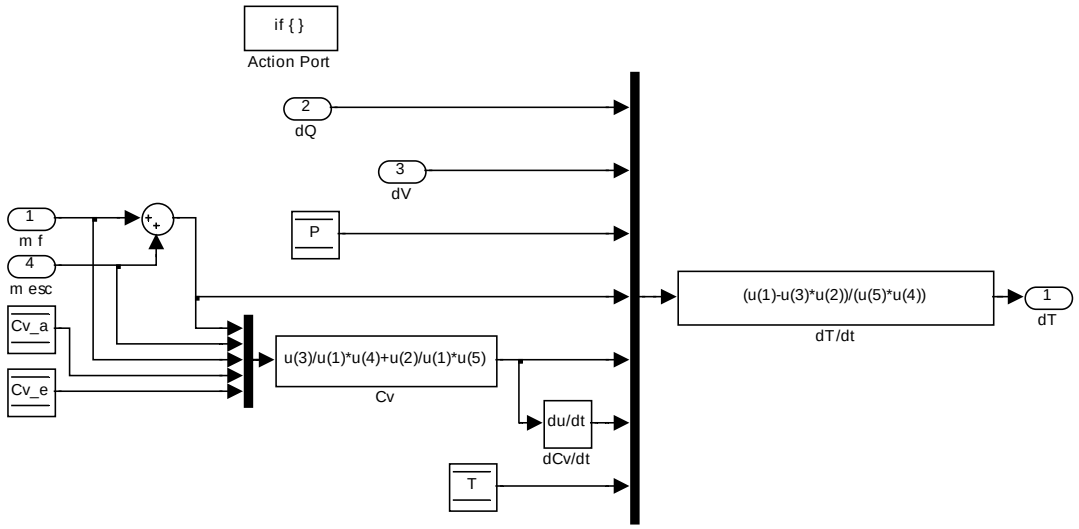

Calculates the temperature change rate during the closed cylinder period (using equation (4.16).

B.1.16.4 Intake

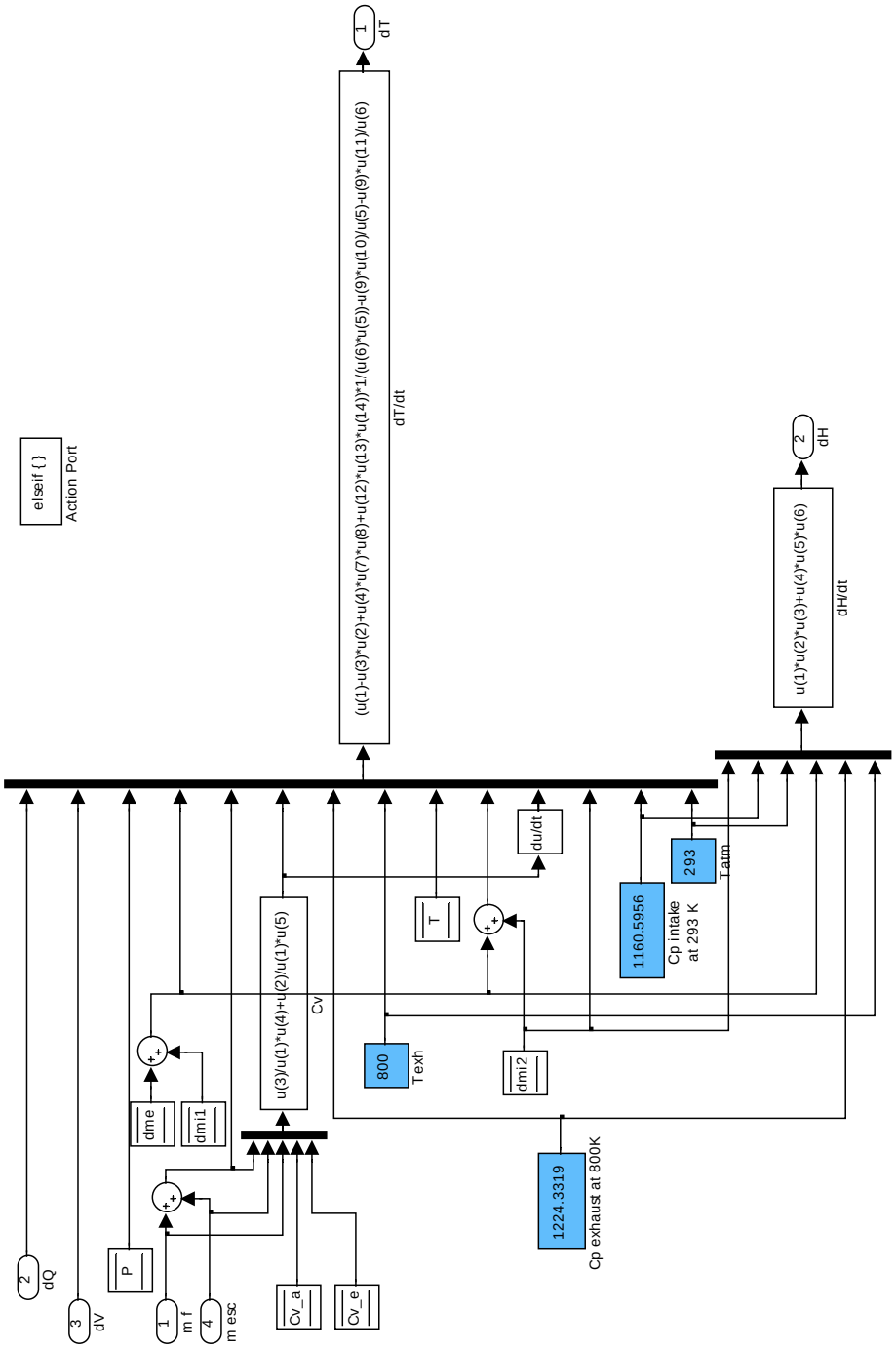

Calculates the temperature change rate (using equation (4.17)) and the enthalpy change rate (using equation (4.15)), during the intake period.

B.1.17 Mass Exchange

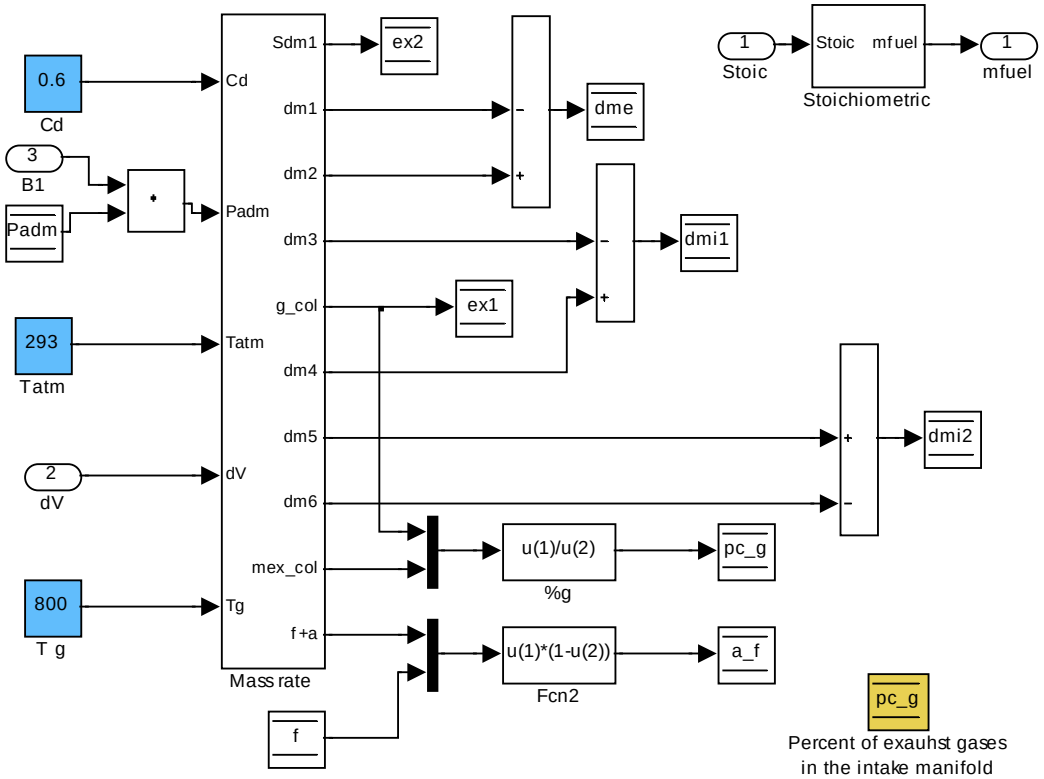

Outputs the mass flow rates types through the several valves and calculates the fuel mass amount in the cylinder.

B.1.17.1 Stoichiometric

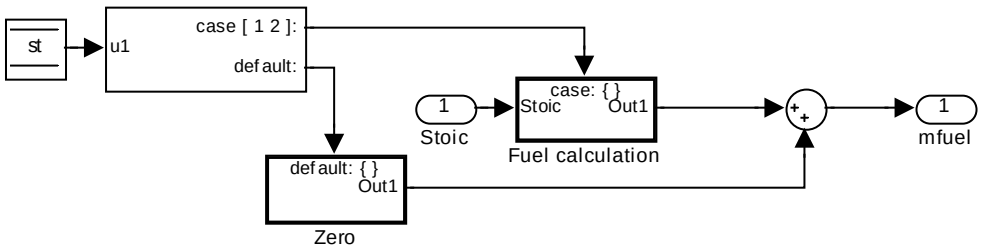

Calculates the amount of fuel mass inside the cylinder considering the air fuel ratio for the stoichiometric conditions and the amount of air+fuel mixture inside the cylinder :

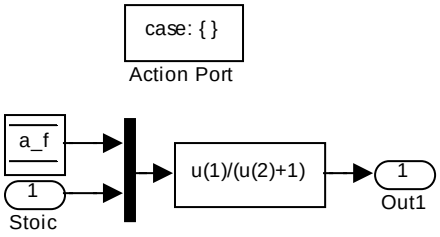

When air+fuel mixture are not being inducted into the cylinder, the amount of fuel mass is considered constant until a reset signal resets the air+fuel mass variable.

B.1.17.2 Mass rate

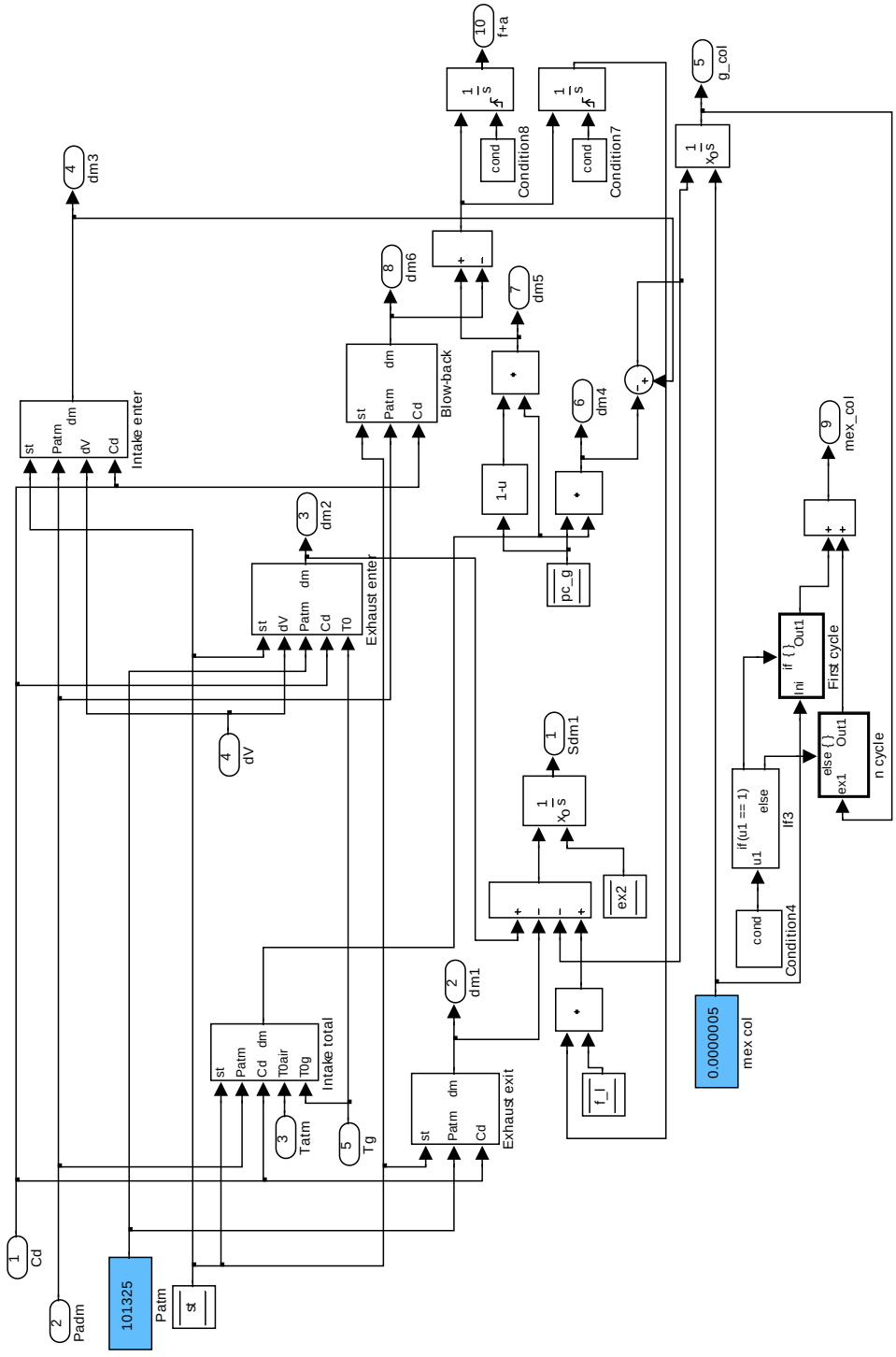

The **Mass rate** subsystem calculates the mass flow rate of every gas mixture flowing into or out of the cylinder, depending on several conditions.

Exhaust exit

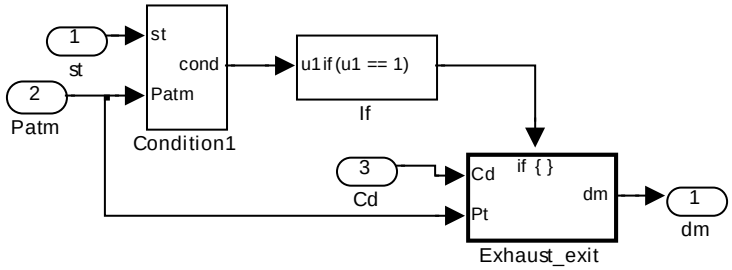

Exhaust gases exit the cylinder when **Condition1**:

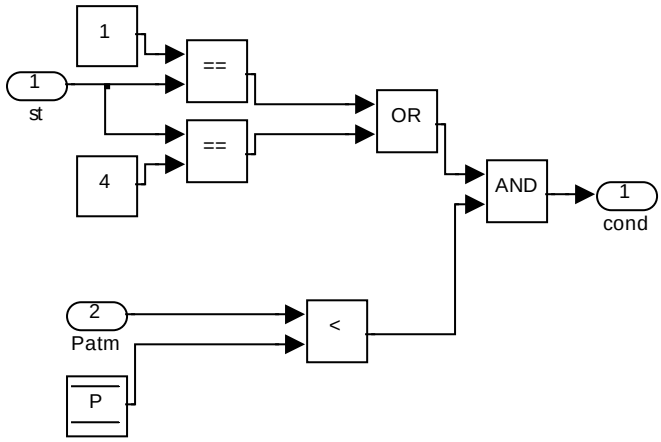

Exhaust exit subsystem uses equations (4.28) and (4.30) to calculate the amount of exhaust mass flowing out of the cylinder:

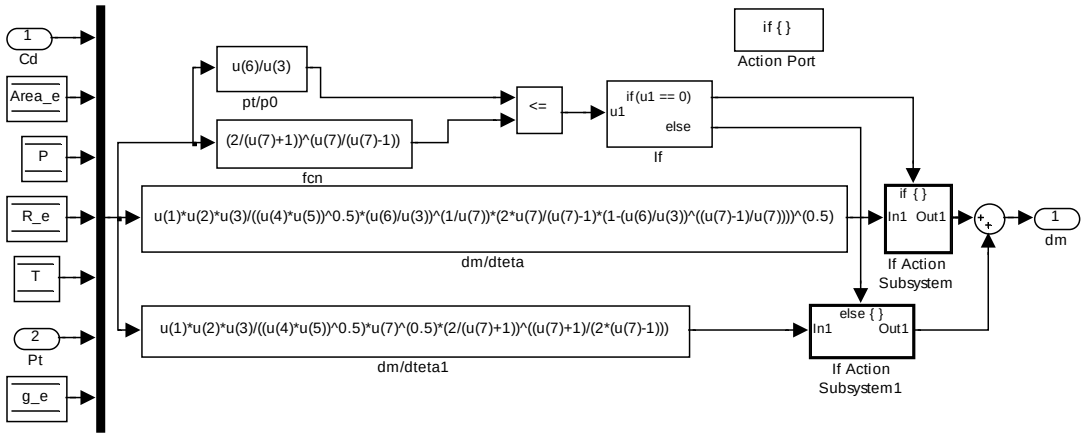

Exhaust enter

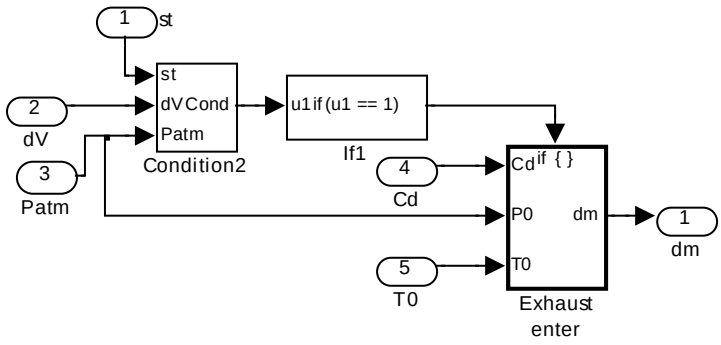

Exhaust gases enter the cylinder when **Condition2**:

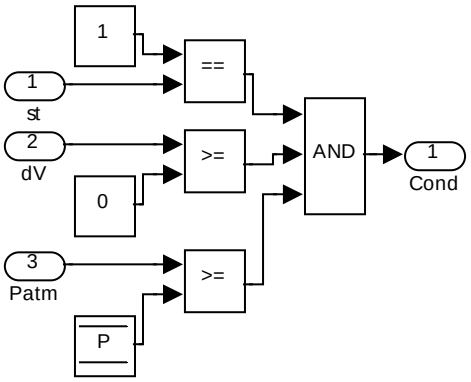

Exhaust enter subsystem uses equations (4.28) and (4.30) to calculate the amount of exhaust mass flowing into of the cylinder:

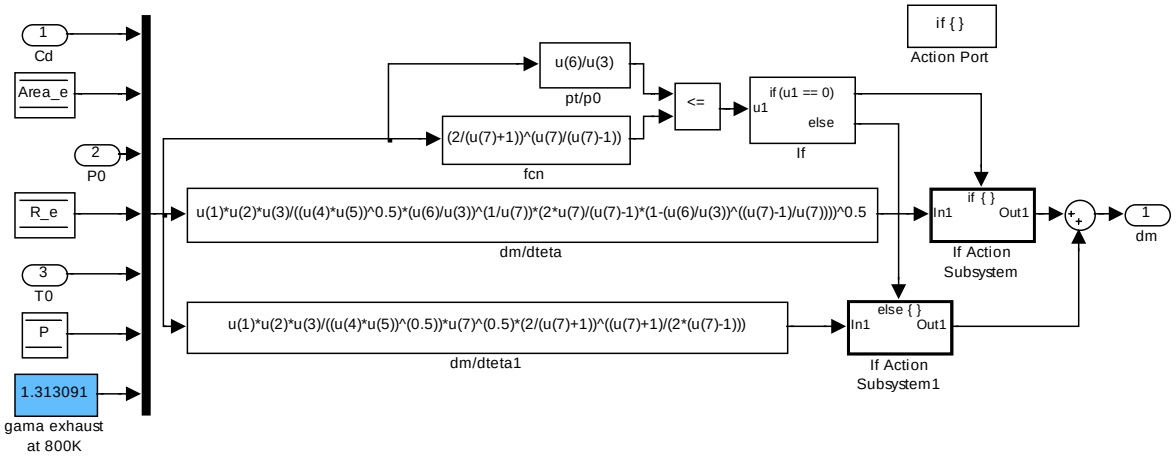

Air intake

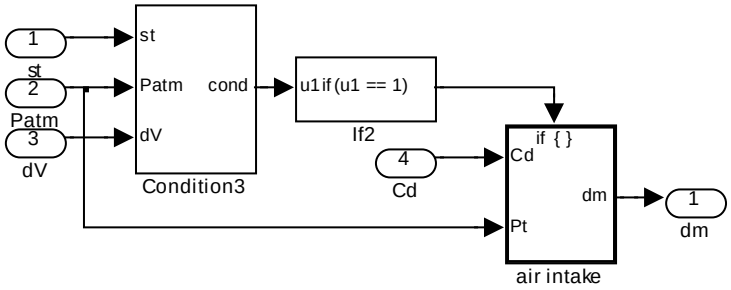

Air+fuel mixture enter the cylinder when **Condition3**:

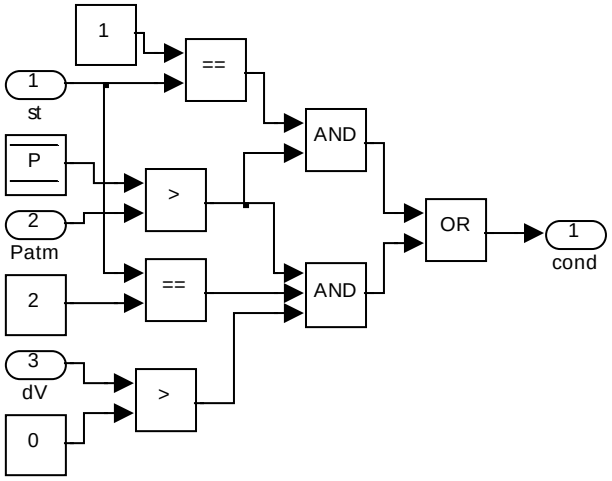

Air intake subsystem uses equations (4.28) and (4.30) to calculate the amount of air+fuel mixture flowing into of the cylinder:

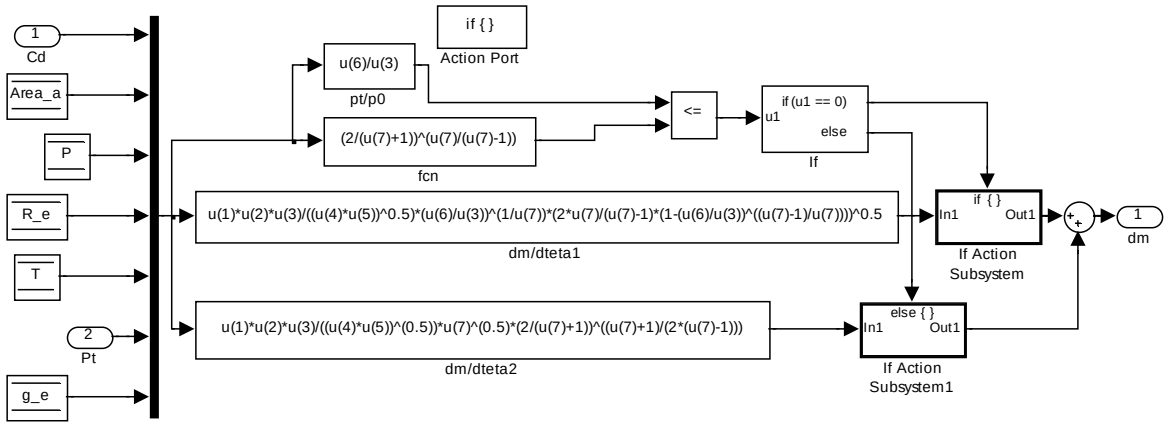

Intake total

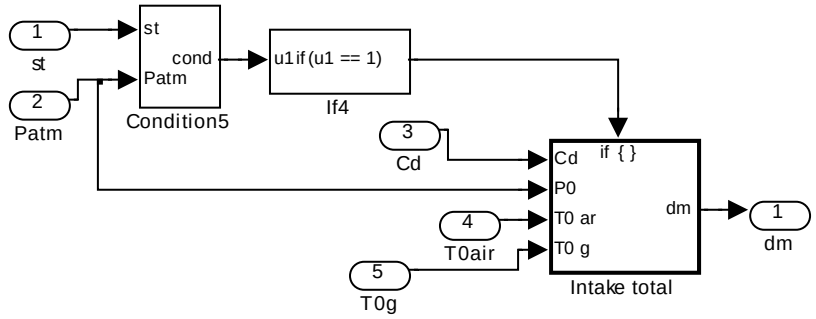

Air+fuel mixture mixed with exhaust gases at the intake manifold enter the cylinder when **Condition5**:

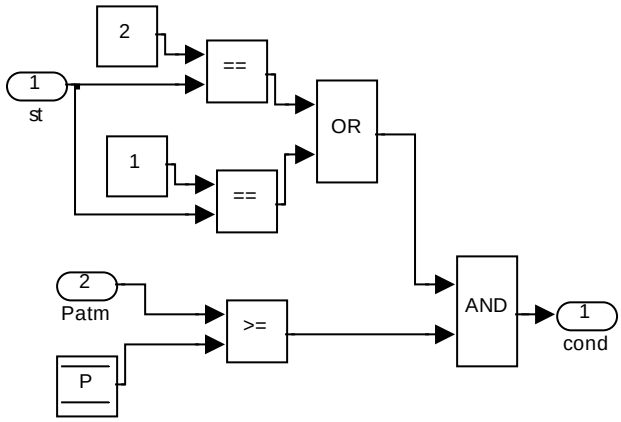

Intake total subsystem uses equations (4.28) and (4.30) to calculate the amount of air+fuel mixture and exhaust mass flowing into of the cylinder:

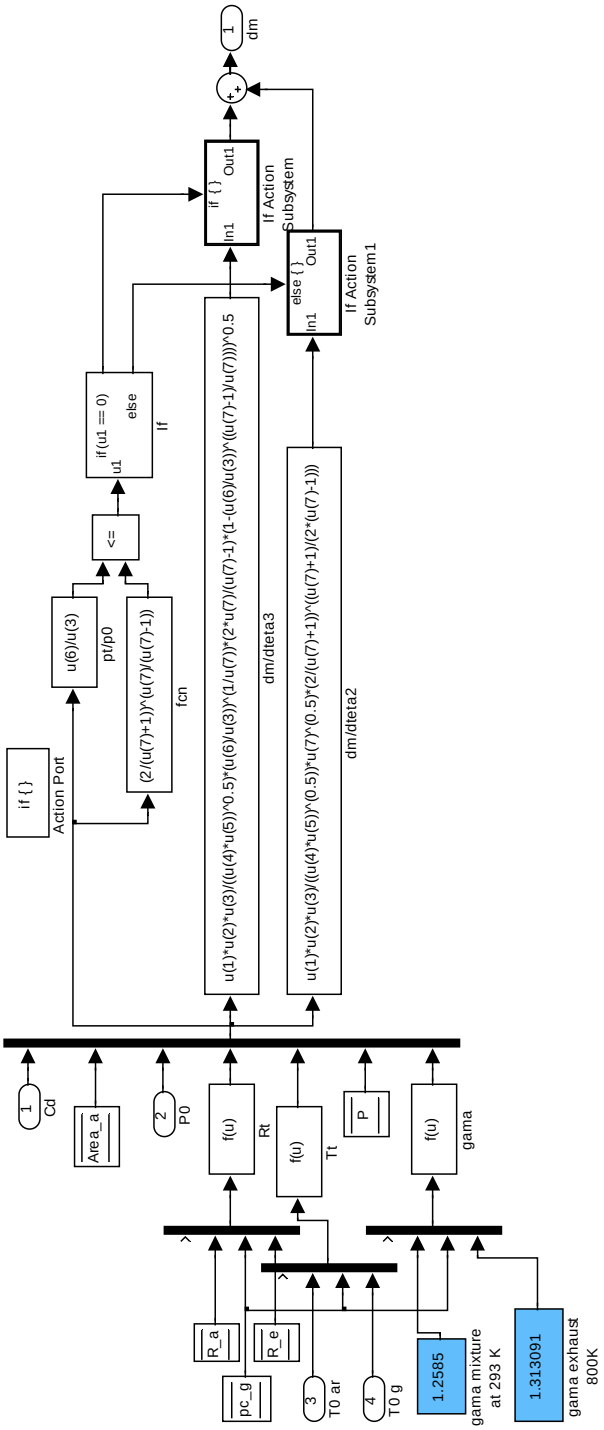
1
dm
if { }
In1
Out1
If Action Subsystem
else { }
If Action Subsystem1
if(u1 == 0)
u1
else
If
<=
u(6)/u(3)
pt/p0
(2/(u(7)+1))^(u(7)/(u(7)-1))
fcn
if { }
Action Port
u(1)*u(2)*u(3)/((u(4)*u(5))^0.5)*(u(6)/u(3))^(1/u(7))*(2*u(7)/(u(7)-1)*(1-(u(6)/u(3))^((u(7)-1)/u(7))))^0.5
dm/dteta3
u(1)*u(2)*u(3)/((u(4)*u(5))^0.5)*u(7)^(0.5)*(2/(u(7)+1))^((u(7)+1)/(2*(u(7)-1)))
dm/dteta2
1
Cd
Area_a
2
P0
f(u)
Rt
f(u)
Tt
P
f(u)
gama
R_a
R_e
pc_g
3
T0 ar
4
T0 g
1.2585
gama mixture at 293 K
1.313091
gama exhaust 800K

Blow-back

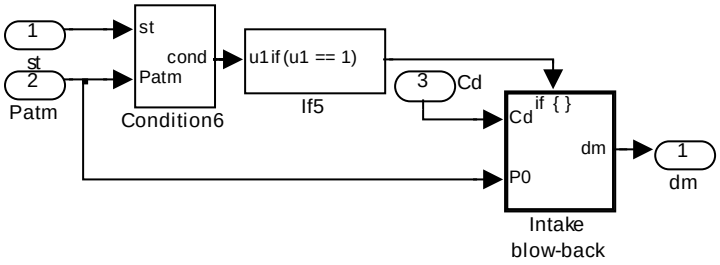

Blow-back of air+fuel mixture when **Condition6**:

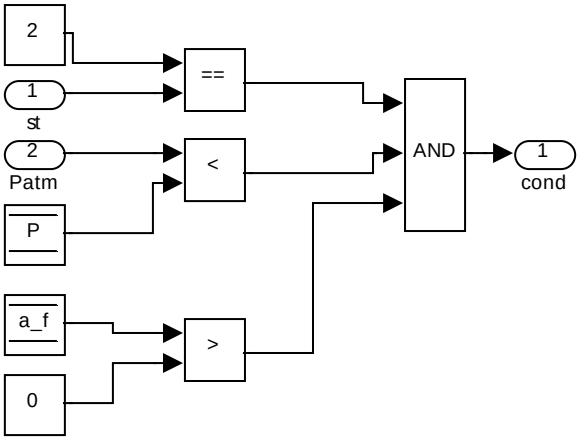

Intake blow-back subsystem uses equations (4.28) and (4.30) to calculate the amount of air+fuel mixture that is blown-back out of the cylinder:

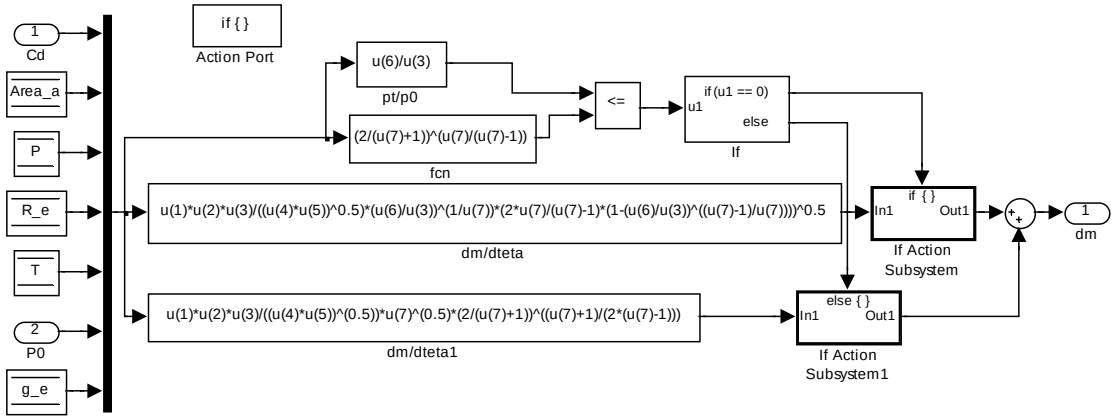

Condition4

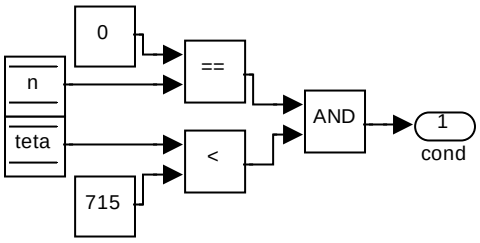

For the first cycle of the simulation is considered a reduced amount of burned gases inside the intake manifold (**mex col**). For the subsequent cycles that amount of mass is calculated through the integration of the exhaust mass flow rate to the intake manifold. **Condition4** defines the time for the total amount of exhaust gases in the intake manifold to be considered **mex col** or the resulting from the blow-back of exhaust gases to the intake manifold during the overlap period. At the **Mass Exchange** subsystem, **mex col** is used as the maximum value of exhaust mass amount at the intake manifold to calculate the exhaust mass percent still in the exhaust manifold.

Condition7

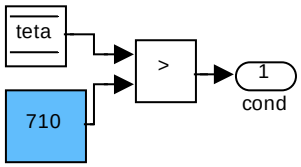

Resets the air+fuel mass integrator that is used to calculate the amount of air+fuel mass converted to burned gases during the combustion process.

Condition8

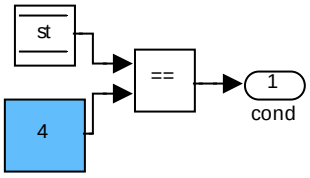

Makes the reset of the air+fuel mixture flow rate integration. When exhaust valve opens (**st**=4) the value of the integrator of air+fuel in the cylinder is reset. The integration starts from 0 as soon as air+fuel flows into the cylinder.

B.1.18 Results

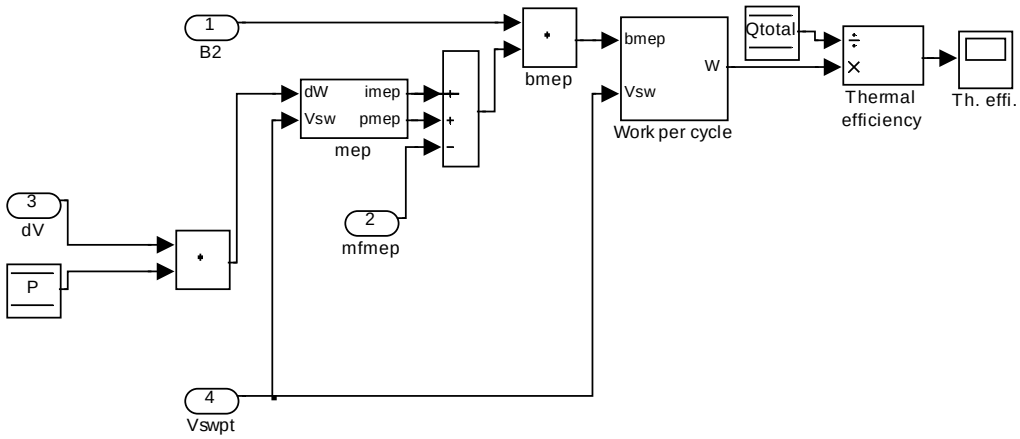

At this system are calculated the imep, pmep, bmep, work per cycle and thermal efficiency of each cycle.

B.1.18.1 mep

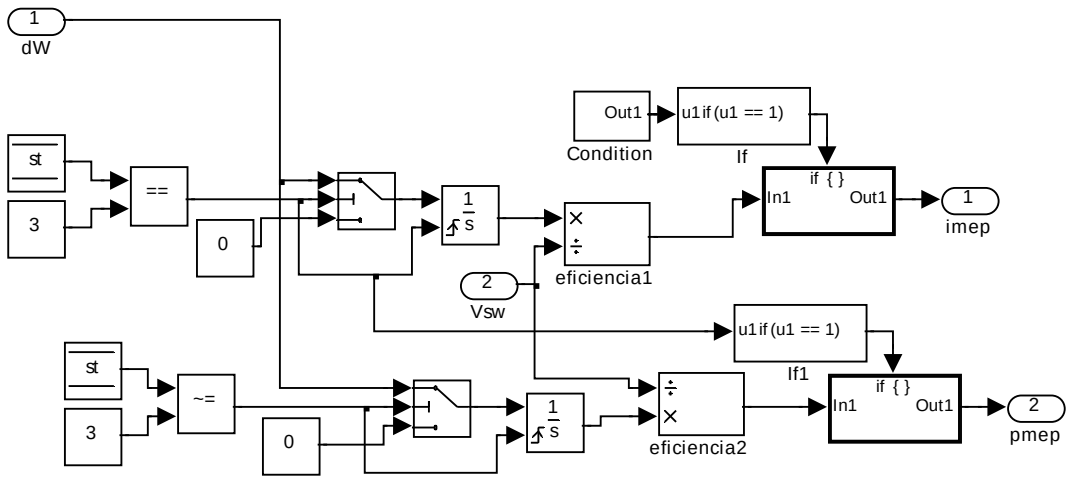

Calculates imep as an integration of the cycle power (during the close period of the cycle) divided by the engine swept volume. Pmep is calculated as an integration of the cycle power (during the period of the cycle when any of the valves is opened) divided by the engine swept volume.

B.1.18.2 Work per cycle

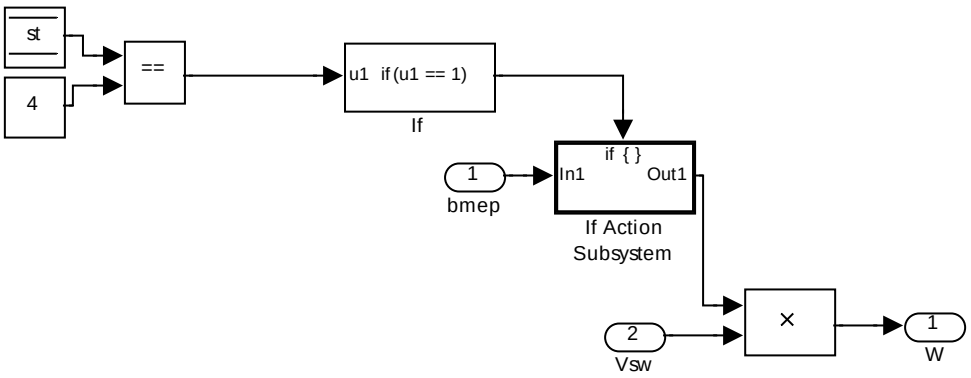

Considering the bmep value at the end of the cycle, i.e. when exhaust valve opens, and multiplying by the engine swept volume results the break work performed by the engine at each cycle.

B.1.19 Friction

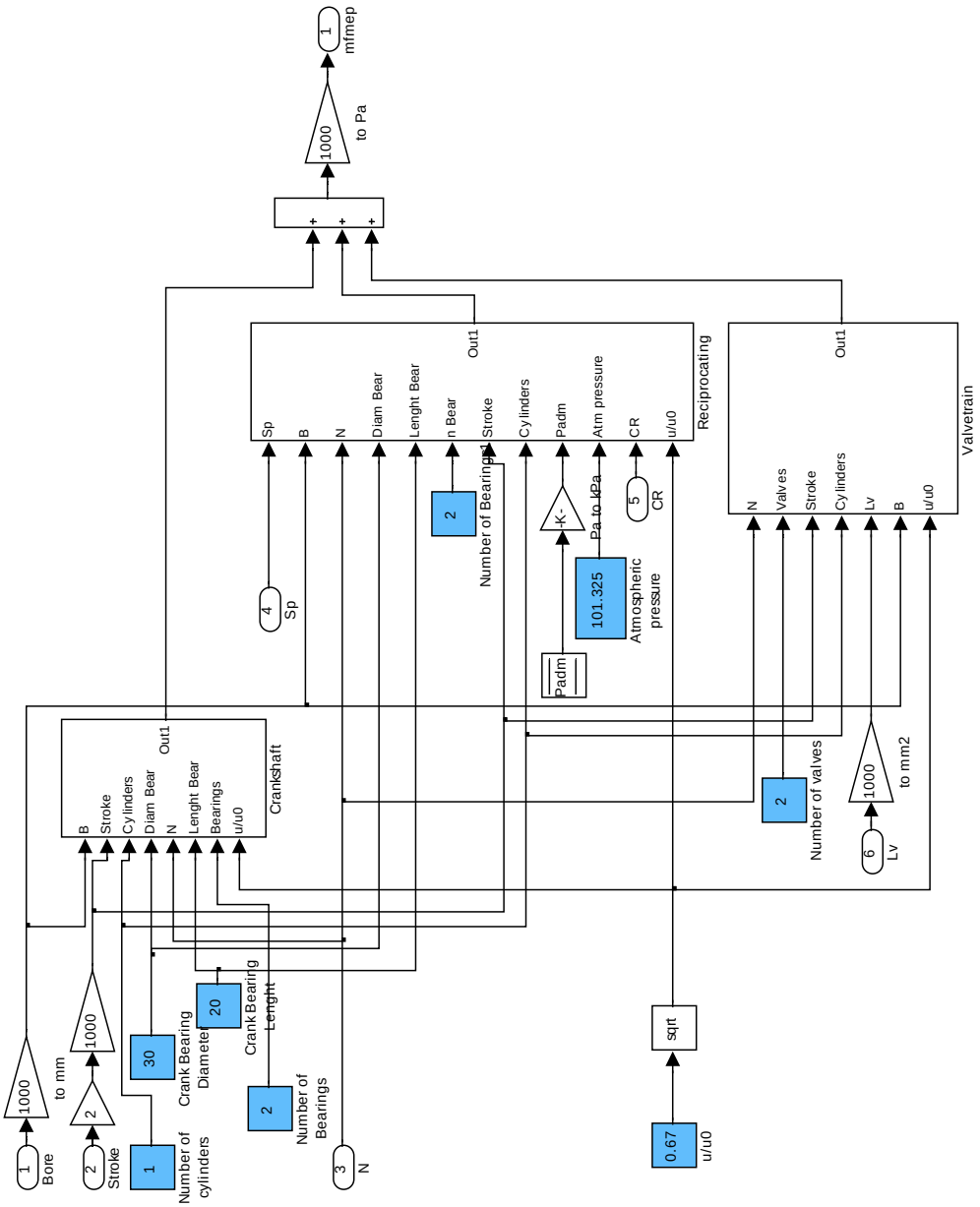

Friction mean effective pressure is calculated using the expression presented in 4.2.8. The following subsystems model each of the friction components:

B.1.19.1 Crankshaft

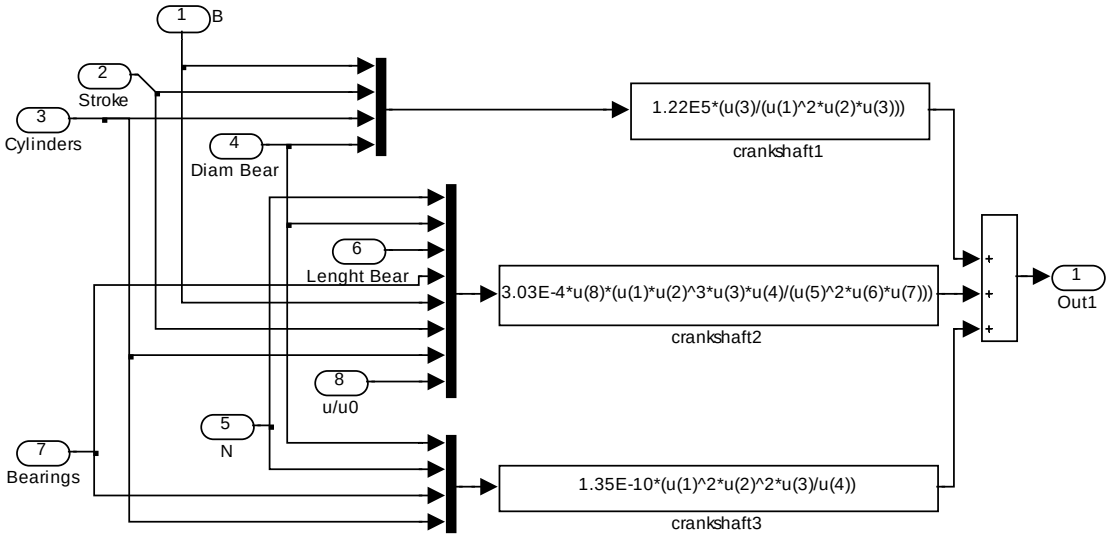

B.1.19.2 Reciprocating

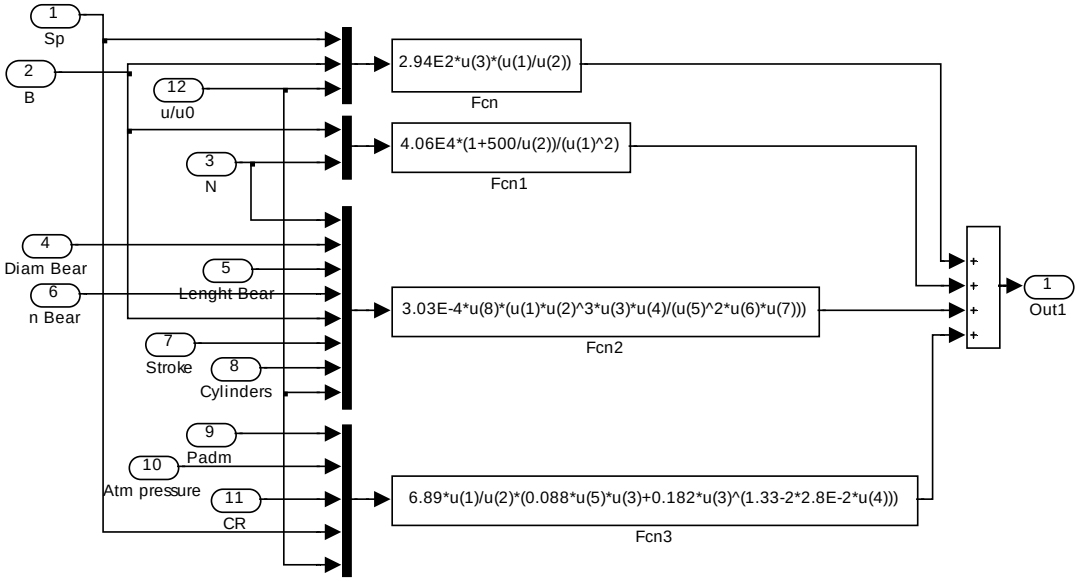

B.1.19.3 Valve train

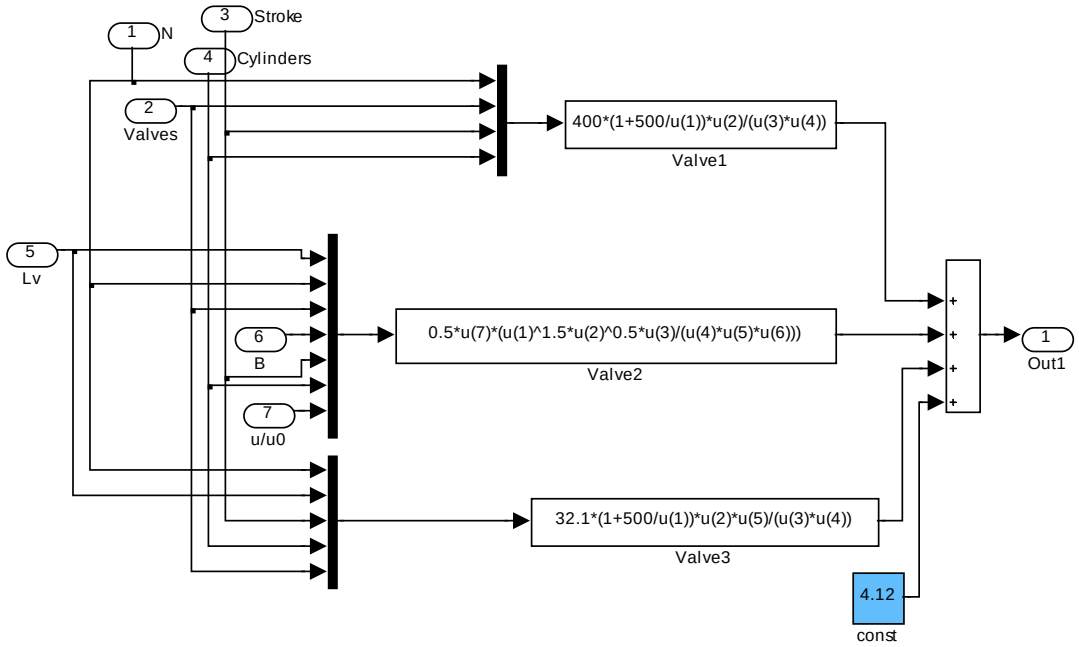

B.1.20 Calibration

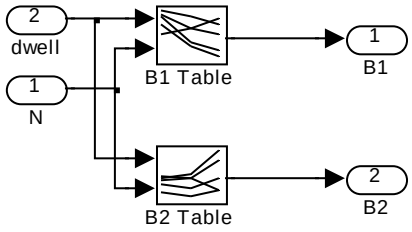

At **B1 Table** and **B2 Table** are the calibration factors for the model. B1 is used to calibrate the air+fuel mass amount within the cylinder at each cycle and B2 is used to calibrate the value of the bmep and all other performance parameters calculated from that result.

B.2 Entropy generation model

Total amount of entropy generated on each cycle is made by the cycle integration of the sum of the entropy generation change rates calculated for each entropy generating mechanism. Each of these mechanisms is presented below.

B.2.1 Friction

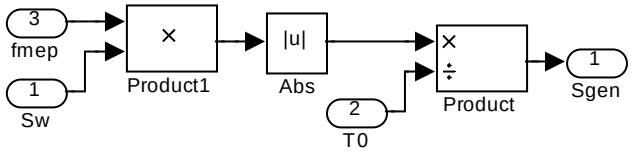

The friction component of entropy generated is calculated for all the cycle. Considering the fmep and the swept volume of the engine and using equation (4.86).

B.2.2 Heat transfer

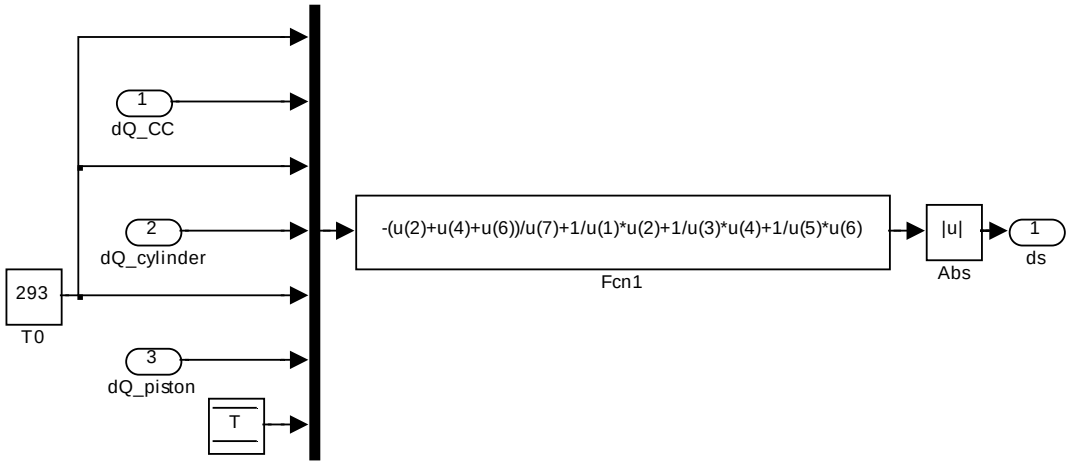

Heat transfer entropy generation is calculated using equation (4.73). Heat transfer rates for the three surfaces is considered and $\mathbf{T_0}$ = 293 K.

B.2.3 Free expansion

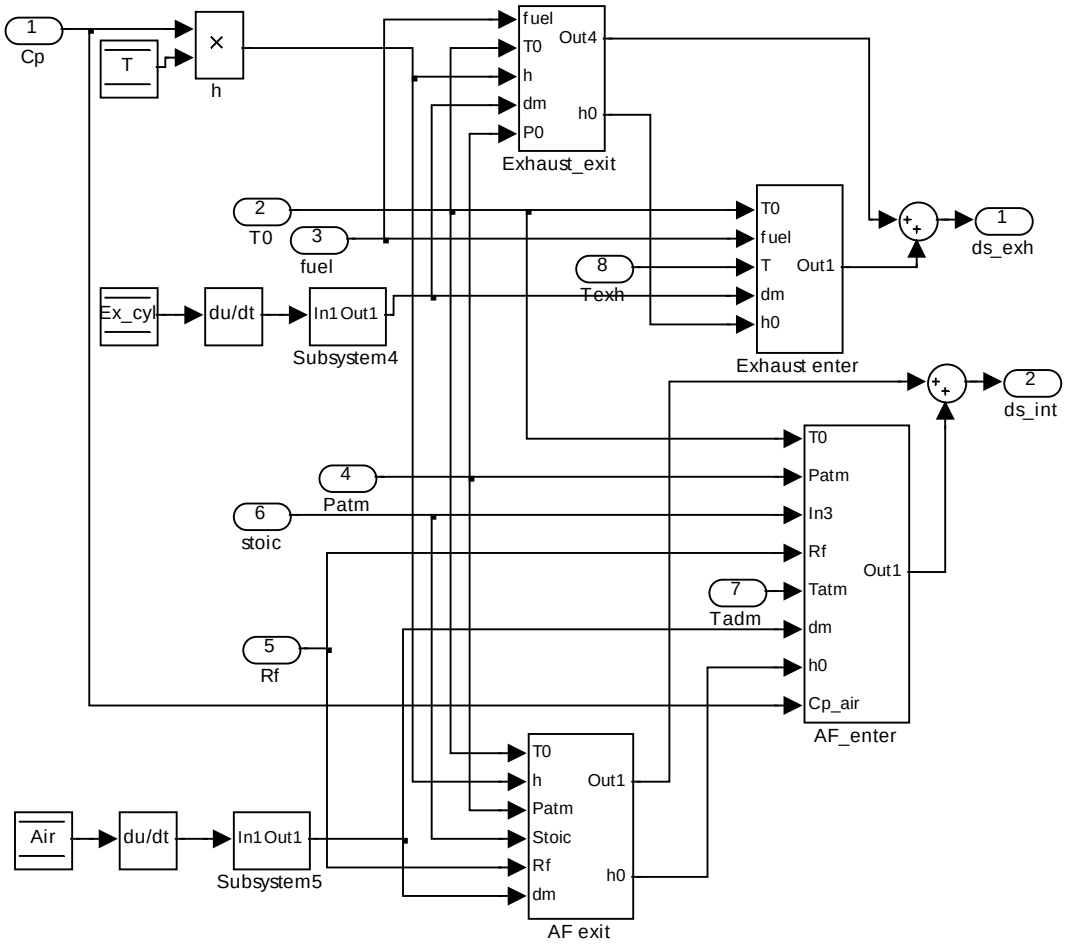

Entropy generated due to free expansion is calculated separately for each of the valves and for each of the flow directions. At **Subsystems 4** and **5**, mass flow rate is filtered and only passes positive values of mass flow rate:

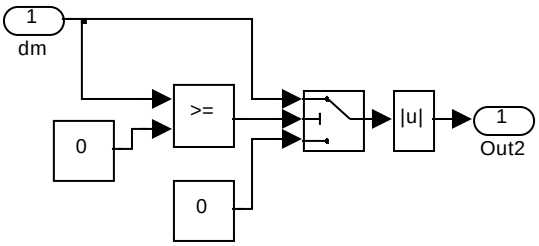

Exhaust exit

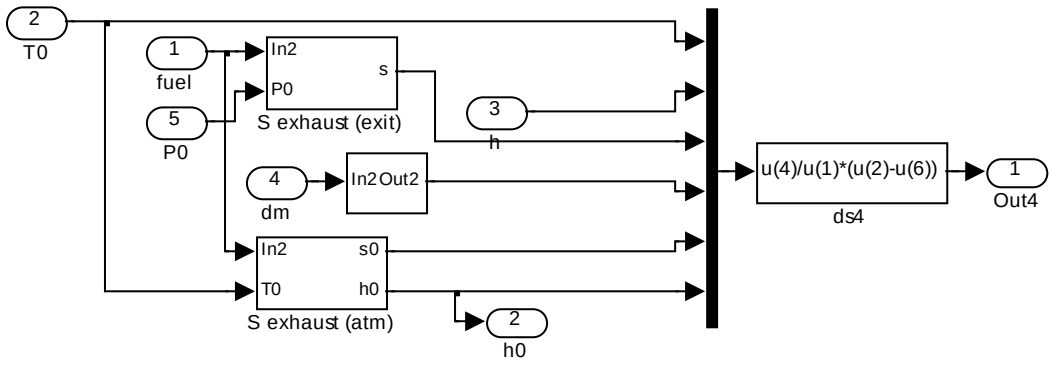

Calculates the entropy generation rate at the exhaust valve when mass flows out of the cylinder. The calculation is made using equation (4.85). Enthalpy at environment conditions is calculated at **S exhaust (atm)**:

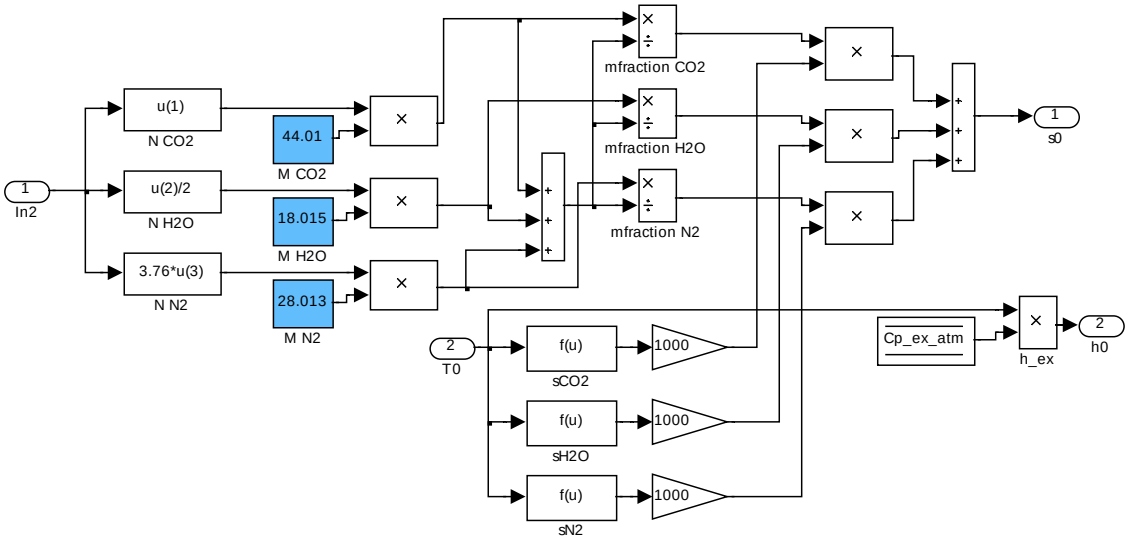

Exhaust enter

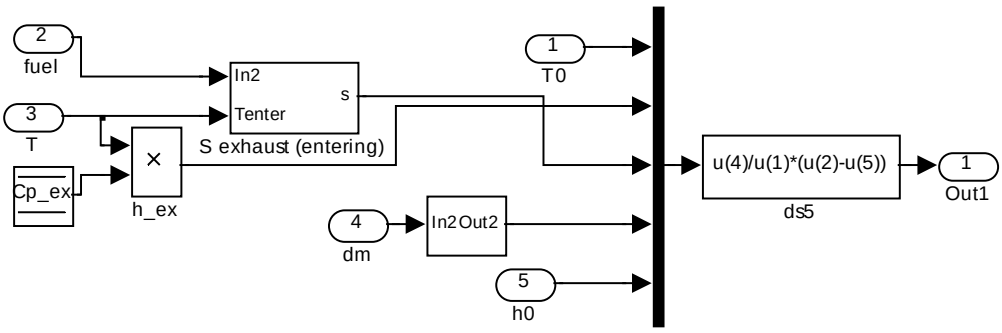

Calculates the entropy generation rate at the exhaust valve when mass flows into the cylinder. The calculation is made using equation (4.85).

Intake enter

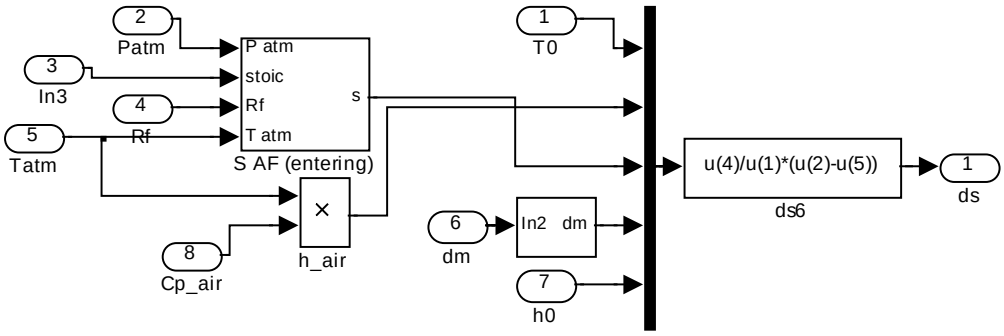

Calculates the entropy generation rate at the intake valve when mass flows into the cylinder. The calculation is made using equation (4.85).

Intake exit

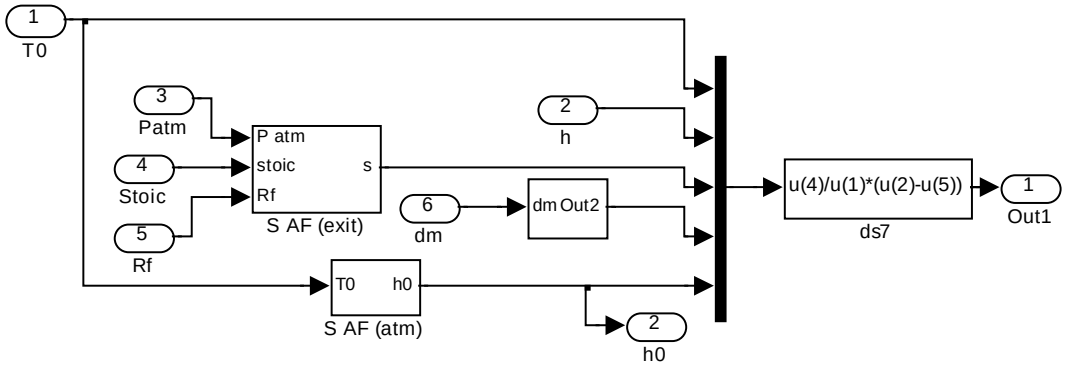

Calculates the entropy generation rate at the intake valve when mass flows out of the cylinder. The calculation is made using equation (4.85). Enthalpy at environment conditions is calculated at **S AF (atm)**:

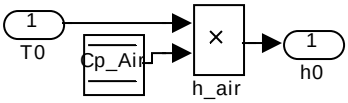

B.2.4 Adiabatic flame temperature

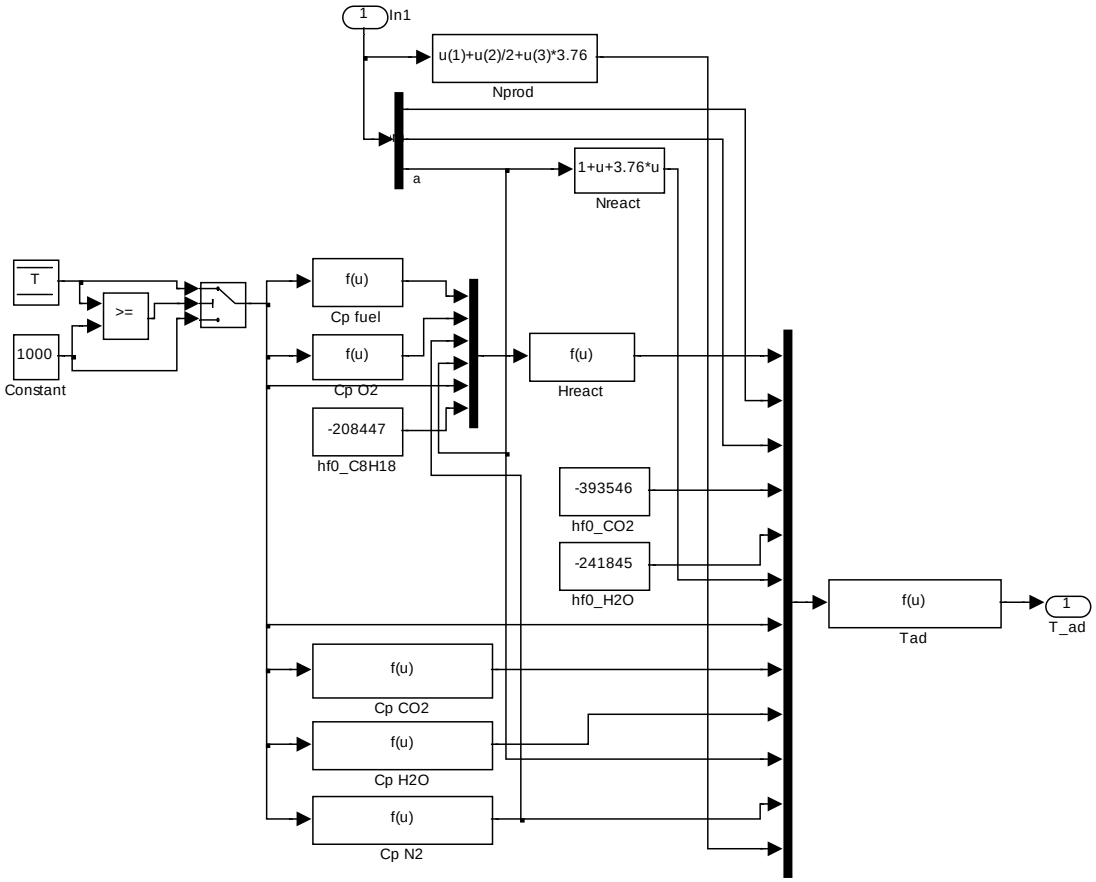

Calculates the instantaneous adiabatic flame temperature. During combustion, cylinder gas temperature is always higher than 1000 K and Cp of the several chemical species is calculated using the cylinder temperature. When the temperature falls below the 1000 K, this value is assumed as constant for that purpose.

B.2.5 Combustion

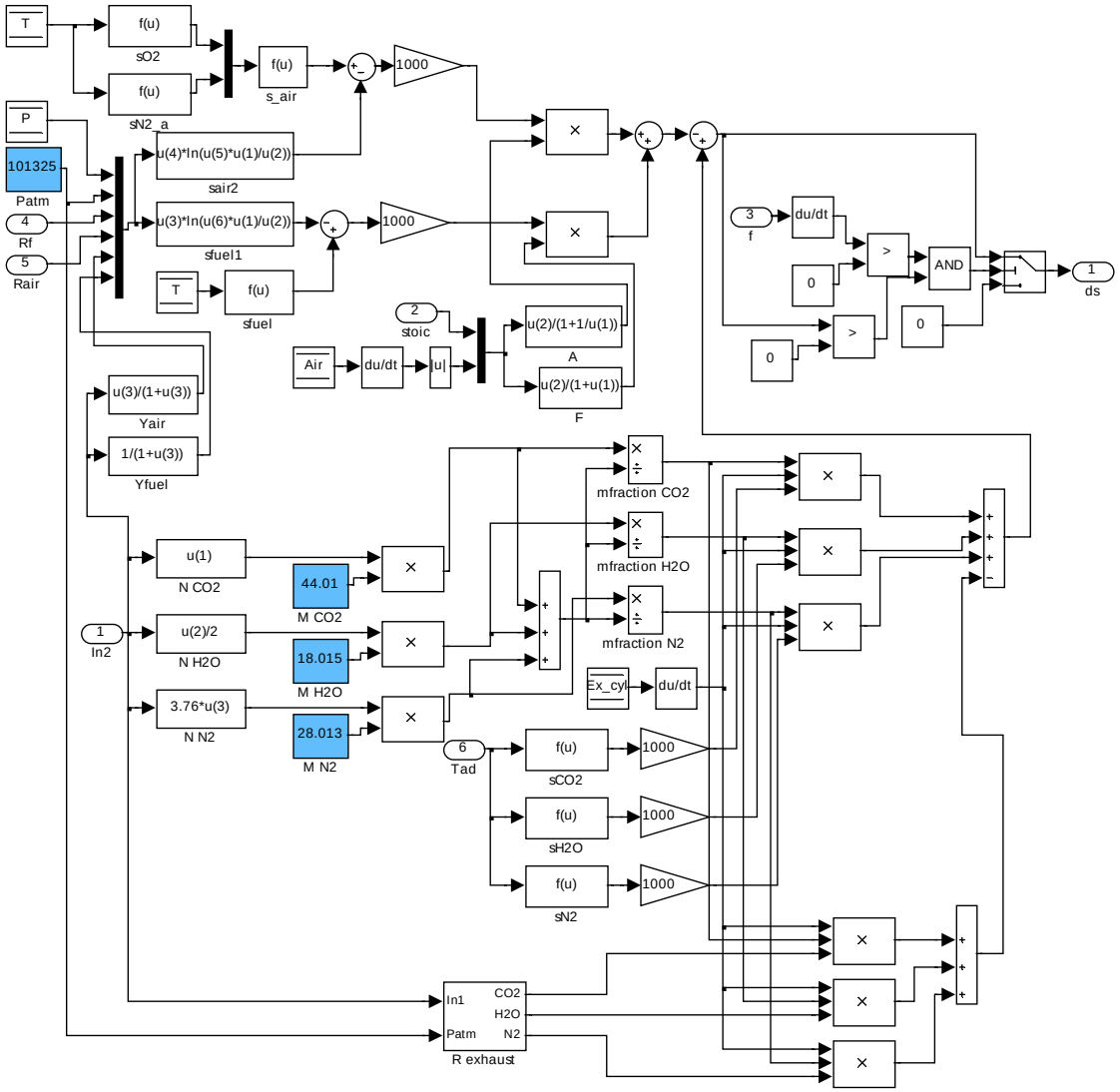

Calculates the entropy generated on the combustion process, using equation (4.77). Values for the entropy of each of the chemical species is made using equations (4.79) to (4.82).

B.2.6 Flow through valves

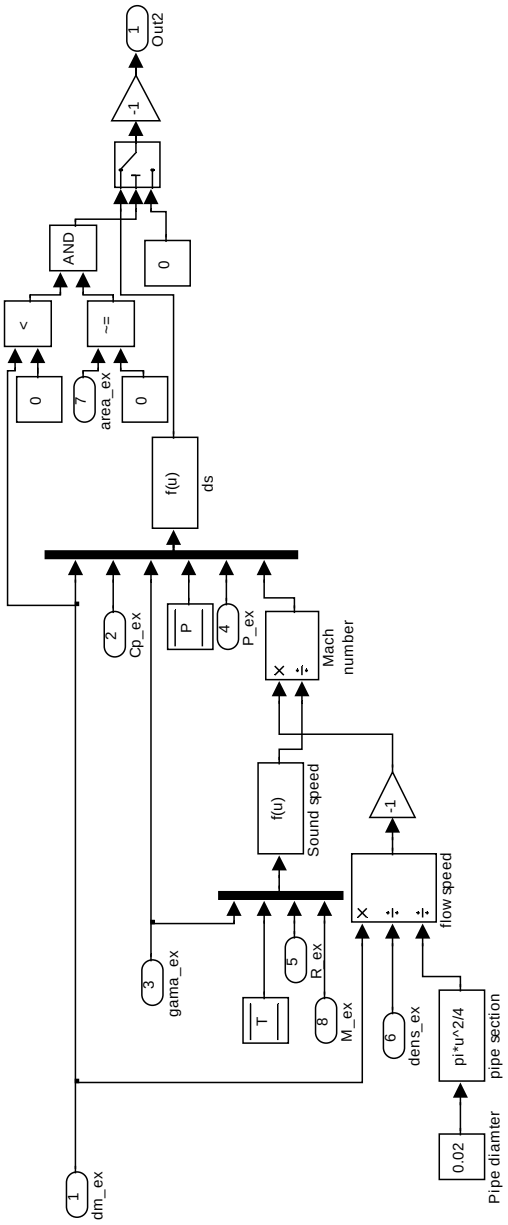

Calculates the entropy generated due to flow of the gases through the valves (including the throttle valve). The entropy generated is calculated at the exhaust valve in the two flow directions of exhaust gases, at the intake valve in the two flow directions and for exhaust gases and air+fuel mixture and at the throttle valve.

Annex C – Model Calibration Coefficients

C MODEL CALIBRATION COEFFICIENTS

C.1 Otto cycle model

		Throttle Position [%]						
	B1	10	20	30	40	50	75	100
Engine Speed [rpm]	1500	2.380	1.700	1.410	1.190	1.175	0.920	0.875
	2000	2.130	1.600	1.310	1.120	1.100	0.895	0.860
	2500	1.850	1.590	1.310	1.140	1.040	0.870	0.880
	3000	1.750	1.580	1.400	1.250	1.070	0.860	0.910
	3500	1.550	1.620	1.560	1.400	1.250	0.870	0.960

	B2	10	20	30	40	50	75	100
Engine Speed [rpm]	1500	0.978	1.032	0.953	1.035	0.967	0.882	0.872
	2000	0.980	1.077	1.034	1.077	0.943	0.908	0.886
	2500	1.020	1.024	0.996	1.000	0.932	0.925	0.865
	3000	0.846	0.949	0.852	0.839	0.855	0.895	0.826
	3500	0.746	0.781	0.620	0.664	0.668	0.802	0.785

C.2 Miller LIVC

		Dwell Angle [CA]		
	B1	20	40	60
Engine Speed [rpm]	1500	0.750	0.640	0.640
	2000	0.830	0.650	0.630
	2500	0.930	0.680	0.650
	3000	0.960	0.730	0.730
	3500	0.900	0.750	0.840

	B2	20	40	60
Engine Speed [rpm]	1500	1.067	1.150	1.201
	2000	0.974	1.118	1.204
	2500	0.846	1.071	1.183
	3000	0.796	0.979	0.988
	3500	0.815	0.943	0.795

C.3 Miller VCR LIVC

		Dwell Angle [CA]		
	B1	20	40	60
Engine Speed [rpm]	1500	0.710	0.749	0.820
	2000	0.780	0.630	0.563
	2500	0.826	0.660	0.605
	3000	0.840	0.745	0.710
	3500	0.870	0.830	0.780

	B2	20	40	60
Engine Speed [rpm]	1500	1.030	0.989	0.830
	2000	0.993	1.056	1.389
	2500	0.950	0.995	1.248
	3000	0.908	0.851	0.981
	3500	0.798	0.735	0.829

C.4 Miller EIVC

		Cams EIVC			
		Miller		Miller VCR	
	B1	1EIVC	2EIVC	1EIVC	2EIVC
Engine Speed [rpm]	1500	0.950	0.950	0.980	0.960
	2000	1.070	0.970	1.110	1.020
	2500	1.130	1.030	1.220	1.150
	3000	1.200	1.240	1.330	1.500
	3500	1.280	1.600	1.400	1.960

	B2	1EIVC	2EIVC	1EIVC	2EIVC
Engine Speed [rpm]	1500	1.055	0.851	1.162	0.834
	2000	0.985	0.938	1.040	0.845
	2500	0.987	0.959	0.963	0.863
	3000	0.939	0.798	0.892	0.717
	3500	0.892	0.627	0.832	0.621

Annex D - EQUIPMENT CALIBRATION AND MEASURING DATA

D EQUIPMENT CALIBRATION AND MEASURING DATA

D.1 Pressure drop at the throttle valve

Throt. Pos	Q		$\dot{m}$	Q correct	h/2	h	p
[%]	[%]	[m^3/s]	[kg/s]	[kg/s]	[mmH_2O]	[mmH_2O]	[Pa]
100	0	0	0		0	0	0
100	87	30.550	36.100	33.003	26	52	509.959
100	81	28.385	33.608	30.511	23	46	451.118
100	71	24.796	29.378	26.280	18	36	353.049
100	63	21.942	26.008	22.911	14	28	274.593
100	52	18.043	21.384	18.287	11	22	215.752
100	33	11.376	13.507	10.410	5	10	98.069
100	86	30.189	35.698	32.600	26	52	509.959
100	81	28.385	33.585	30.488	23	46	451.118
100	71	24.796	29.358	26.260	18	36	353.049
100	61	21.231	25.148	22.051	14	28	274.593
100	51	17.690	20.970	17.873	10	20	196.138
100	33	11.376	13.506	10.408	4	8	78.455
100	86	30.189	35.710	32.613	26	52	509.959
100	80	28.025	33.148	30.051	23	46	451.118
100	70	24.439	28.934	25.837	18	36	353.049
100	61	21.231	25.182	22.085	14	28	274.593
100	51	17.690	20.977	17.880	10	20	196.138
100	34	11.725	13.922	10.824	5	10	98.069
100	31	10.679	12.687	9.590	4	8	78.455
100	47	16.280	19.329	16.232	9	18	176.524
100	61	21.231	25.182	22.085	14	28	274.593
100	68	23.724	28.113	25.016	17	34	333.435
100	76	26.588	31.475	28.378	22	44	431.504
100	85	29.827	35.283	32.185	26	52	509.959
82	0	0.000	0.000		0	0	0.000
82	82	28.745	33.951	30.854	32	64	627.642
82	76	26.588	31.438	28.341	28	56	549.187
82	69	24.081	28.503	25.405	23	46	451.118
82	59	20.521	24.317	21.220	17	34	333.435
82	50	17.337	20.561	17.463	13	26	254.980
82	34	11.725	13.919	10.822	6	12	117.683
82	83	29.106	34.388	31.291	32	64	627.642
82	76	26.588	31.438	28.341	28	56	549.187
82	68	23.724	28.066	24.969	22	44	431.504
82	58	20.166	23.894	20.796	16	32	313.821
82	49	16.985	20.140	17.042	12	24	235.366
82	31	10.679	12.684	9.587	5	10	98.069
82	29	9.983	11.864	8.767	4	8	78.455
82	48	16.632	19.732	16.635	11	22	215.752
82	58	20.166	23.897	20.800	17	34	333.435
82	68	23.724	28.086	24.988	22	44	431.504

82	72	25.154	29.751	26.653	25	50	490.346
82	83	29.106	34.377	31.279	32	64	627.642
60	85	29.827	34.495	31.398	141	282	2765.549
60	84	29.467	34.085	30.988	140	280	2745.935
60	63	21.942	25.702	22.605	79	158	1549.492
60	59	20.521	24.072	20.975	70	140	1372.967
60	55	19.104	22.438	19.340	62	124	1216.057
60	50	17.337	20.400	17.303	51	102	1000.305
60	44	15.225	17.967	14.869	40	80	784.553
60	39	13.472	15.923	12.825	32	64	627.642
60	30	10.331	12.241	9.144	19	38	372.663
60	20	6.864	8.149	5.051	9	18	176.524
60	9	3.077	3.658	0.561	2	4	39.228
60	14	4.794	5.698	2.601	4	8	78.455
60	29	9.983	11.834	8.737	17	34	333.435
60	37	12.772	15.113	12.015	28	56	549.187
60	43	14.874	17.563	14.465	37	74	725.711
60	49	16.985	20.011	16.914	48	96	941.463
60	54	18.750	22.035	18.938	59	118	1157.215
60	59	20.521	24.077	20.980	69	138	1353.354
60	62	21.587	25.292	22.195	76	152	1490.650
60	64	22.298	26.105	23.008	80	160	1569.106
60	85	29.827	34.502	31.405	140	280	2745.935
35	35	12.074	13.774	10.676	205	410	4020.833
35	26	8.941	10.390	7.293	117	234	2294.817
35	24	8.248	9.611	6.514	103	206	2020.224
35	22	7.555	8.828	5.730	88	176	1726.016
35	20	6.864	8.049	4.952	73	146	1431.809
35	18	6.173	7.257	4.160	59	118	1157.215
35	15	5.139	6.060	2.963	43	86	843.394
35	12	4.107	4.856	1.759	28	56	549.187
35	8	2.734	3.244	0.147	14	28	274.593
35	12	4.107	4.858	1.760	28	56	549.187
35	14	4.794	5.663	2.566	35	70	686.484
35	15	5.139	6.061	2.964	42	84	823.780
35	17	5.828	6.854	3.757	55	110	1078.760
35	20	6.864	8.045	4.948	74	148	1451.423
35	22	7.555	8.827	5.730	90	180	1765.244
35	24	8.248	9.614	6.517	100	200	1961.382
35	25	8.594	9.996	6.899	111	222	2177.134
35	26	8.941	10.390	7.293	117	234	2294.817
35	35	12.074	13.778	10.681	205	410	4020.833

D.2 Pressure drop upstream of the throttle valve

Q		$\dot{m}$	Q correct	h/2	h	p
[%]	[m^3/h]	[kg/s]	[kg/s]	[mmH_2O]	[mmH_2O]	[Pa]
0	0.000	0.0000		0	0	0.000
90	31.636	0.0107	0.0098	34	68	666.870
80	28.025	0.0095	0.0086	28	56	549.187
74	25.871	0.0087	0.0078	24	48	470.732
68	23.724	0.0080	0.0071	21	42	411.890
57	19.812	0.0067	0.0058	15	30	294.207
47	16.280	0.0055	0.0046	10	20	196.138
26	8.941	0.0030	0.0021	3	6	58.841
25	8.594	0.0029	0.0020	3	6	58.841
43	14.874	0.0050	0.0041	8	16	156.911
55	19.104	0.0065	0.0055	13	26	254.980
59	20.521	0.0069	0.0060	16	32	313.821
65	22.655	0.0077	0.0067	18	36	353.049
73	25.512	0.0086	0.0077	24	48	470.732
81	28.385	0.0096	0.0087	28	56	549.187
85	29.827	0.0101	0.0092	31	62	608.028
88	30.912	0.0105	0.0095	34	68	666.870
90	31.636	0.0107	0.0098	35	70	686.484
93	32.723	0.0111	0.0101	37	74	725.711
91	31.998	0.0108	0.0099	36	72	706.098
89	31.273	0.0106	0.0097	34	68	666.870
85	29.827	0.0101	0.0092	32	64	627.642
79	27.666	0.0094	0.0084	28	56	549.187
73	25.512	0.0086	0.0077	23	46	451.118
63	21.942	0.0074	0.0065	17	34	333.435
52	18.043	0.0061	0.0052	12	24	235.366
33	11.376	0.0038	0.0029	5	10	98.069
22	7.555	0.0026	0.0016	2	4	39.228
48	16.632	0.0056	0.0047	10	20	196.138
54	18.750	0.0063	0.0054	13	26	254.980
62	21.587	0.0073	0.0064	17	34	333.435
69	24.081	0.0081	0.0072	21	42	411.890
81	28.385	0.0096	0.0087	28	56	549.187
85	29.827	0.0101	0.0092	31	62	608.028
89	31.273	0.0106	0.0097	34	68	666.870
91	31.998	0.0108	0.0099	35	70	686.484
92	32.360	0.0109	0.0100	36	72	706.098
93	32.723	0.0111	0.0101	37	74	725.711
93	32.723	0.0111	0.0101	33	66	647.256
71	24.796	0.0084	0.0075	20	40	392.276
67	23.368	0.0079	0.0070	18	36	353.049
63	21.942	0.0074	0.0065	16	32	313.821
57	19.812	0.0067	0.0058	13	26	254.980
52	18.043	0.0061	0.0052	11	22	215.752
46	15.928	0.0054	0.0045	9	18	176.524
39	13.472	0.0046	0.0036	7	14	137.297
23	7.901	0.0027	0.0017	2	4	39.228
16	5.483	0.0019	0.0009	1	2	19.614

28	9.636	0.0033	0.0023	3	6	58.841
34	11.725	0.0040	0.0030	5	10	98.069
44	15.225	0.0051	0.0042	8	16	156.911
49	16.985	0.0057	0.0048	10	20	196.138
57	19.812	0.0067	0.0058	12	24	235.366
62	21.587	0.0073	0.0064	15	30	294.207
66	23.011	0.0078	0.0069	17	34	333.435
69	24.081	0.0081	0.0072	18	36	353.049
71	24.796	0.0084	0.0075	20	40	392.276
93	32.723	0.0111	0.0101	33	66	647.256
43	14.874	0.0050	0.0041	6	12	117.683
31	10.679	0.0036	0.0027	3	6	58.841
30	10.331	0.0035	0.0026	3	6	58.841
28	9.636	0.0033	0.0023	3	6	58.841
26	8.941	0.0030	0.0021	2	4	39.228
23	7.901	0.0027	0.0017	2	4	39.228
20	6.864	0.0023	0.0014	1.5	3	29.421
17	5.828	0.0020	0.0010	1	2	19.614
10	3.420	0.0012	0.0002	0.5	1	9.807
15	5.139	0.0017	0.0008	1	2	19.614
19	6.518	0.0022	0.0013	1	2	19.614
22	7.555	0.0026	0.0016	1.5	3	29.421
25	8.594	0.0029	0.0020	2	4	39.228
27	9.288	0.0031	0.0022	2	4	39.228
29	9.983	0.0034	0.0025	2.5	5	49.035
31	10.679	0.0036	0.0027	3	6	58.841
32	11.027	0.0037	0.0028	3	6	58.841
43	14.874	0.0050	0.0041	5.5	11	107.876

D.3 Flow meter calibration data

Q	Δp	V	Q		Re
[%]	Pa	m/s	m3/s	m3/h	[10^3]
75	9	3.860	0.0077	27.874	1.426
82	10	4.069	0.0082	29.381	1.504
91	12	4.457	0.0089	32.186	1.647
95	13	4.639	0.0093	33.500	1.714
53	3	2.229	0.0045	16.093	0.824
25	1	1.287	0.0026	9.291	0.475
22	1	1.287	0.0026	9.291	0.475
28	1	1.287	0.0026	9.291	0.475
40	2	1.820	0.0036	13.140	0.672
65	5	2.877	0.0058	20.776	1.063
82	10	4.069	0.0082	29.381	1.504
90	11	4.268	0.0086	30.816	1.577
97	13	4.639	0.0093	33.500	1.714
60	6	3.152	0.0063	22.759	1.165
30	1	1.287	0.0026	9.291	0.475
22	1	1.287	0.0026	9.291	0.475
45	3	2.229	0.0045	16.093	0.824
47	3	2.229	0.0045	16.093	0.824
99	14	4.815	0.0097	34.765	1.779
94	13	4.639	0.0093	33.500	1.714
86	11	4.268	0.0086	30.816	1.577
72	7	3.404	0.0068	24.582	1.258
51	3	2.229	0.0045	16.093	0.824
24	1	1.287	0.0026	9.291	0.475

D.4 Swirl modifications data

D.4.1 Swirl coefficients form the original and modified intake port

Q	Measuring position			Q	Measuring position		
[%]	56	76	96	[m3/s]	56	76	96
24	0	0	0	0.0023	0	0	0
37	0	0	0	0.0035	0	0	0
51	35	33	21	0.0049	923.581	870.805	554.149
66	145	113	90	0.0064	2943.893	2294.206	1827.244
80	204	185	157	0.0078	3403.231	3086.264	2619.153
90	315	290	244	0.0087	4657.748	4288.085	3607.906
96	359	303	275	0.0093	4968.060	4193.098	3805.617
Q	Measuring position			Q	Measuring position		
[%]	56	76	96	[m3/s]	56	76	96
26	0	0	0	0.0025	0	0	0
47	0	0	0	0.0045	0	0	0
62	23	33	7	0.0060	497.662	714.037	151.462
79	38	65	52	0.0077	642.144	1098.404	878.723
84	72	70	70	0.0081	1142.633	1110.893	1110.893
89	98	98	65	0.0086	1465.778	1465.778	972.200
96	129	116	105	0.0093	1785.180	1605.279	1453.054

D.4.2 Discharge coefficient on the original port

Q			Qtheor	CD
[%]	[m3/s]	[m3/h]	[m3/h]	
42	0.004025	14.49	44.09959	0.328574
56	0.005388	19.3984	57.59823	0.336788
76	0.007355	26.4784	77.12795	0.343305
85	0.008247	29.6905	86.89246	0.341692
92	0.008944	32.2	92.62768	0.347628
98	0.009544	34.3588	98.60969	0.348432
33	0.003154	11.3553	35.4737	0.320105
54	0.005193	18.6948	56.59645	0.330318
74	0.007157	25.7668	75.63018	0.340695
65	0.006271	22.5745	86.23167	0.261789
93	0.009044	32.5593	93.85459	0.346912
99	0.009644	34.7193	99.76306	0.348018
37	0.003541	12.7465	35.4737	0.359323
45	0.004316	15.5385	46.62157	0.33329
59	0.005682	20.4553	59.55126	0.343491
76	0.007355	26.4784	77.12795	0.343305
88	0.008546	30.7648	89.48684	0.343791
92	0.008944	32.2	93.24315	0.345334
98	0.009544	34.3588	99.18805	0.346401

D.4.3 Discharge coefficient on the modified port

Q			Qtheor	CD
[%]	[m3/s]	[m3/h]	[m3/h]	
39	0.003734	13.4433	41.49596	0.323966
55	0.005291	19.0465	58.68415	0.32456
71	0.006861	24.7009	74.99948	0.329348
83	0.008049	28.9753	87.04267	0.332886
92	0.008944	32.2	97.02131	0.331886
97	0.009444	33.9985	102.7671	0.330831
21	0.002	7.2009	23.95771	0.300567
45	0.004316	15.5385	49.09869	0.316475
61	0.005878	21.1609	65.172	0.324693
75	0.007256	26.1225	80.17782	0.325807
85	0.008247	29.6905	90.27955	0.328873
90	0.008745	31.482	94.62535	0.332702
96	0.009344	33.6384	101.0777	0.332798
37	0.003541	12.7465	41.49596	0.307174
55	0.005291	19.0465	59.65421	0.319282
70	0.006763	24.346	74.23024	0.32798
84	0.008148	29.3328	87.6996	0.334469
91	0.008845	31.8409	95.83082	0.332262
98	0.009544	34.3588	103.3241	0.332534

D.5 Load cell calibration data

Voltage	Torque		Voltage	Torque		Voltage	Torque
mV	Nm		mV	Nm		mV	Nm
0	0.000		0	0.000		0	0.000
0.4	1.779		0.4	1.829		0.4	1.819
0.9	4.180		1.1	4.737		0.6	2.748
1.5	6.581		1.6	7.121		1	4.437
2	8.982		2	8.987		1.3	5.688
2.6	11.383		2.7	11.780		1.7	7.530
3.2	13.784		3.4	14.621		2.3	9.982
3.7	16.185		3.7	15.901		2.7	11.838
4.3	18.586		4.4	18.790		3.2	14.017
4.9	20.987		4.6	19.638		3.8	16.430
5.4	23.388		5.1	21.869		4.4	19.175
6	25.789		5.6	23.750		4.7	20.421
6.6	28.190		5.9	25.174		5.2	22.393
7.2	30.591		6.3	26.939		5.6	24.163
7.7	32.992		7	29.828		6.2	26.409
8.3	35.393		7.7	32.520		6.7	28.467
8.9	37.794		8.2	34.727		7.4	31.456
9.5	40.195		8.8	37.309		7.9	33.529
10	42.596		9.3	39.458		8.3	35.376
10.6	44.997		9.9	41.848		8.9	37.631
11.2	47.398		10.5	44.218		9.5	40.092
11.7	49.799		10.8	45.685		9.9	41.699
0	0.000		11.3	47.599		10.4	44.031
0.4	1.841		11.6	48.798		10.8	45.609
0.9	4.242		0	0.000		11.3	47.590
1.6	7.001					11.9	50.191
2.3	10.082					11.3	47.681
3	12.851					10.8	45.441
3.6	15.802					10.1	42.677
4.4	18.970					9.5	39.903
5.1	21.791					8.8	37.283
5.8	24.772					8.3	35.047
6.3	26.945					7.8	32.864
7	30.141					7	29.678
7.8	33.112					6.3	26.755
8.5	36.092					5.8	24.409
9.2	39.178					5.1	21.669
9.8	41.817					4.6	19.342
10.4	44.389					3.9	16.391
11.2	47.436					3.2	13.521
11.8	50.166					2.6	10.915
0	0.000					1.9	8.252
						1.5	6.564
						1.3	5.423
						0.4	1.804
						0.4	1.824
						0	0.000

D.6 Pressure sensor calibration data

Measure 1			Measure 2	
Pressure	Output Voltage		Pressure	Output Voltage
[bar]	[V]		[bar]	[V]
0	0.6		0	0.6
36	2.238		34	2.123
38	2.314		36	2.216
40	2.394		38	2.311
42	2.483		40	2.4
44	2.579		42	2.494
46	2.663		44	2.582
48	2.769		46	2.678
50	2.856		48	2.766
52	2.948		50	2.858
54	3.048		52	2.961
56	3.132		54	3.053
58	3.232		56	3.148
60	3.317		58	3.241
62	3.411		60	3.333
64	3.506		62	3.415
66	3.599		64	3.515
68	3.704		66	3.605
70	3.793		68	3.702
72	3.875		70	3.796
74	3.94		72	3.886
76	4.04		74	3.95
78	4.14		76	4.05
78	4.14		78	4.15
76	4.04		78	4.15
74	3.95		76	4.03
72	3.84		74	3.94
70	3.773		72	3.85
68	3.682		70	3.784
66	3.586		68	3.684
64	3.482		66	3.598
62	3.393		64	3.506
60	3.292		62	3.413
58	3.214		60	3.309
56	3.112		58	3.228
54	3.038		56	3.134
52	2.936		54	3.043
50	2.838		52	2.943
48	2.742		50	2.86
46	2.661		48	2.762
44	2.551		46	2.663
42	2.466		44	2.561
40	2.368		42	2.481
38	2.276		40	2.387
36	2.194		38	2.312

34	2.093		36	2.203
0	0.584		34	2.116
			32	2.03
			30	1.934
			0	0.617

Annex E - Engine Tests Results

E ENGINE TESTS RESULTS

E.1 Diesel cycle engine

E.1.1 Load 1

N(RPM)	Fuel (g)	Fuel difference (kg)	Average torque (Nm)	Power (kW)	Fuel flow rate (g/s)	SFC (g/kW-h)	Thermal Effic. (%)
3710	1088	0.0038	0.527	0.206	0.127	2210.625	3.701
3710	1086.2	0.0018	0.081	0.032	0.060	6803.517	1.203
3740	1081.8	0.0044	0.168	0.066	0.147	7980.374	1.025
3730	1078.6	0.0032	0.104	0.041	0.107	9347.826	0.875
3730	1075.5	0.0031	0.235	0.092	0.103	4032.157	2.029
3590	1055.7	0.0062	5.470	2.070	0.207	359.387	22.766
3590	1049.8	0.0059	5.736	2.171	0.197	326.133	25.087
3590	1043.6	0.0062	5.821	2.203	0.207	337.700	24.228
3590	1037.8	0.0058	5.996	2.269	0.193	306.692	26.678
3600	1030.8	0.007	6.114	2.321	0.233	361.983	22.603
3530	947.1	0.0089	8.649	3.219	0.297	331.778	24.661
3520	938.7	0.0084	8.399	3.117	0.280	323.371	25.302
3530	930	0.0087	8.340	3.104	0.290	336.356	24.325
3520	921.9	0.0081	8.361	3.103	0.270	313.263	26.118
3530	913.1	0.0088	8.417	3.133	0.293	337.090	24.272
3140	809.8	0.0044	9.075	3.004	0.293	351.508	23.276
3100	806.7	0.0031	9.019	2.948	0.207	252.402	32.416
3280	802.8	0.0039	9.093	3.144	0.260	297.675	27.486
3170	799.1	0.0037	9.020	3.015	0.247	294.568	27.776
3280	795.3	0.0038	9.003	3.113	0.253	292.920	27.932
3330	790.9	0.0044	8.987	3.155	0.293	334.682	24.447
3260	784.8	0.0061	9.044	3.109	0.407	470.954	17.373
3210	778.9	0.0041	9.088	3.076	0.273	319.940	25.573
3200	775.6	0.0033	8.876	2.994	0.220	264.493	30.934
3250	771	0.0046	8.969	3.073	0.307	359.214	22.777
3270	767.6	0.0034	9.004	3.104	0.227	262.878	31.124
3250	763.7	0.0039	9.053	3.102	0.260	301.747	27.115
3240	759.9	0.0038	9.115	3.114	0.253	292.890	27.935
3220	755.8	0.0041	9.048	3.072	0.273	320.360	25.539
3270	752.3	0.0035	8.931	3.079	0.233	272.814	29.990
3250	748.2	0.0041	8.933	3.061	0.273	321.483	25.450
3320	744.3	0.0039	9.108	3.188	0.260	293.585	27.869
3360	740.1	0.0042	8.905	3.155	0.280	319.535	25.605
3300	736.5	0.0036	9.036	3.144	0.240	274.839	29.769
2770	1104.8	0.0027	8.208	2.397	0.180	270.338	30.265
2770	1101.2	0.0036	8.195	2.393	0.240	361.019	22.663
2770	1096.1	0.0036	8.128	2.374	0.240	363.983	22.479
2780	1093.1	0.003	8.285	2.428	0.200	296.504	27.594
2750	1090.7	0.0024	8.162	2.367	0.160	243.397	33.615
2290	1087.2	0.0035	8.151	1.968	0.233	426.848	19.168
2810	1084.7	0.0025	8.259	2.447	0.167	245.218	33.365
2780	1081.6	0.0031	8.303	2.434	0.207	305.708	26.763
2800	1078.7	0.0029	8.145	2.404	0.193	289.465	28.265

2770	1075.8	0.0029	8.232	2.404	0.193	289.493	28.263
2710	1072.9	0.0029	8.124	2.321	0.193	299.864	27.285
2780	1070	0.0029	8.246	2.417	0.193	287.991	28.410
2790	1067.3	0.0027	8.260	2.430	0.180	266.705	30.677
2810	1064.2	0.0031	8.195	2.428	0.207	306.427	26.701
2750	1061.5	0.0027	8.021	2.326	0.180	278.635	29.364
2780	1058.5	0.003	8.217	2.408	0.200	298.952	27.368
2760	1055.5	0.003	8.261	2.404	0.200	299.536	27.315
2720	1052.8	0.0027	8.130	2.331	0.180	277.937	29.438
2760	1049.9	0.0029	8.072	2.349	0.193	296.301	27.613
2630	1022.2	0.0032	8.934	2.477	0.213	310.012	26.392
2630	1019.2	0.003	8.559	2.373	0.200	303.367	26.970
2630	1016	0.0032	8.930	2.476	0.213	310.171	26.378
2620	1013.7	0.0023	8.841	2.442	0.153	226.042	36.196
2620	1009.7	0.004	8.714	2.407	0.267	398.826	20.515
2620	1006.7	0.003	9.129	2.522	0.200	285.514	28.656
2630	1003.6	0.0031	9.163	2.541	0.207	292.812	27.942
2620	1000.4	0.0032	9.122	2.520	0.213	304.782	26.845
2620	997.2	0.0032	8.737	2.413	0.213	318.236	25.710
2620	994.1	0.0031	8.487	2.344	0.207	317.364	25.781
2620	991.2	0.0029	8.630	2.384	0.193	291.980	28.022
2620	988.4	0.0028	9.003	2.487	0.187	270.217	30.279
2630	985.1	0.0033	9.112	2.527	0.220	313.449	26.103
2420	883.2	0.0045	10.100	2.577	0.300	419.083	19.523
2420	878.8	0.0044	10.043	2.562	0.293	412.120	19.853
2390	874.5	0.0043	10.073	2.538	0.287	406.591	20.123
2340	870	0.0045	9.796	2.417	0.300	446.861	18.310
2310	865.4	0.0046	9.723	2.368	0.307	466.237	17.549
2280	860.7	0.0047	9.670	2.325	0.313	485.265	16.861
2280	855.4	0.0053	9.833	2.364	0.353	538.143	15.204
2270	850.7	0.0047	9.698	2.321	0.313	486.011	16.835
2270	846.4	0.0043	9.662	2.312	0.287	446.310	18.332
2270	841.1	0.0053	9.719	2.326	0.353	546.854	14.962
2280	836	0.0051	9.720	2.337	0.340	523.847	15.619
2300	831.3	0.0047	9.721	2.357	0.313	478.522	17.098
2290	826.5	0.0048	9.731	2.349	0.320	490.354	16.686
2300	821.7	0.0048	9.760	2.367	0.320	486.767	16.808
2300	816.6	0.0051	9.700	2.352	0.340	520.362	15.723
2300	811.6	0.005	9.710	2.355	0.333	509.655	16.054
2040	1102.4	0.0058	9.337	2.008	0.387	693.159	11.804
2020	1096.8	0.0056	9.544	2.033	0.373	661.198	12.374
2000	1091.3	0.0055	9.597	2.024	0.367	652.311	12.543
2010	1085.8	0.0055	9.600	2.034	0.367	648.869	12.609
2010	1075.7	0.0101	9.587	2.032	0.673	1193.092	6.858
2000	1073.9	0.0018	9.586	2.021	0.120	213.719	38.283
1980	1068.2	0.0057	9.644	2.013	0.380	679.538	12.040
1970	1062.3	0.0059	9.486	1.970	0.393	718.671	11.385
1960	1056.7	0.0056	9.452	1.953	0.373	688.099	11.890
1950	1051	0.0057	9.509	1.955	0.380	699.783	11.692
1920	1044.8	0.0062	9.577	1.939	0.413	767.538	10.660
1970	1039.6	0.0052	9.345	1.941	0.347	642.996	12.725
1950	1034.1	0.0055	9.382	1.929	0.367	684.370	11.955
1990	1028.2	0.0059	9.470	1.987	0.393	712.656	11.481

2010	1022.3	0.0059	9.401	1.992	0.393	710.781	11.511
2000	1016.5	0.0058	9.406	1.983	0.387	701.836	11.658
1840	907.3	0.0058	9.502	1.843	0.387	755.171	10.834
1830	901.6	0.0057	9.639	1.860	0.380	735.558	11.123
1840	895.6	0.006	9.820	1.905	0.400	755.868	10.824
1860	890.3	0.0053	9.750	1.912	0.353	665.275	12.298
1860	878.8	0.0115	9.741	1.910	0.383	722.430	11.325
1870	873	0.0058	9.688	1.910	0.387	728.784	11.227
1860	867	0.006	9.766	1.915	0.400	751.888	10.882
1870	861.4	0.0056	9.712	1.915	0.373	701.902	11.657
1830	855.7	0.0057	9.615	1.855	0.380	737.443	11.095
1740	850.2	0.0055	9.373	1.720	0.367	767.644	10.658
1680	844.7	0.0055	9.353	1.657	0.367	796.828	10.268
1640	839.6	0.0051	9.160	1.584	0.340	772.797	10.587
1650	834.3	0.0053	9.092	1.582	0.353	804.184	10.174
1710	829	0.0053	9.275	1.672	0.353	760.712	10.755
1740	823.8	0.0052	9.537	1.750	0.347	713.346	11.470
1750	818.3	0.0055	9.576	1.767	0.367	747.075	10.952
1750	812.7	0.0056	9.375	1.730	0.373	777.000	10.530
1730	807.3	0.0054	9.578	1.747	0.360	741.868	11.029
1730	801.4	0.0059	9.532	1.739	0.393	814.443	10.046
1800	852.3	0.0107	9.505	1.804	0.357	711.811	11.494
1860	840.4	0.0119	9.793	1.920	0.397	743.573	11.003
1760	829.7	0.0107	9.781	1.815	0.357	707.455	11.565
1740	823.8	0.0059	9.838	1.805	0.393	784.562	10.429
1680	818.5	0.0053	9.484	1.680	0.353	757.219	10.805
1660	813.3	0.0052	9.572	1.675	0.347	744.938	10.983
1630	808.7	0.0046	9.670	1.662	0.307	664.362	12.315
1600	803.2	0.0055	9.827	1.658	0.367	796.277	10.275
1580	797.8	0.0054	9.740	1.622	0.360	798.774	10.243
1560	793.4	0.0044	9.645	1.586	0.293	665.673	12.291
1540	788.5	0.0049	9.972	1.619	0.327	726.369	11.264
1530	784.1	0.0044	9.493	1.531	0.293	689.581	11.865
1500	779.8	0.0043	9.574	1.514	0.287	681.583	12.004
1600	765.5	0.005	9.395	1.585	0.333	757.154	10.806
1630	760.8	0.0047	9.777	1.680	0.313	671.331	12.187
1670	755.8	0.005	9.544	1.680	0.333	714.123	11.457
1690	750.4	0.0054	9.605	1.711	0.360	757.305	10.804
1700	745.7	0.0047	9.513	1.705	0.313	661.602	12.367
3450	892.4	0.0184	9.173	3.361	0.307	328.429	24.912
3410	876.2	0.0162	9.332	3.380	0.270	287.575	28.451
3400	860	0.0162	9.395	3.393	0.270	286.492	28.559
3420	843.4	0.0166	9.447	3.432	0.277	290.231	28.191
3430	825.4	0.018	9.444	3.441	0.300	313.903	26.065
2300	764.5	0.0119	9.726	2.376	0.198	300.504	27.227
2300	753	0.0115	9.694	2.368	0.192	291.366	28.081
2290	740.9	0.0121	9.657	2.349	0.202	309.072	26.472
2300	728.9	0.012	9.680	2.365	0.200	304.470	26.872
2300	717.1	0.0118	9.644	2.356	0.197	300.505	27.227
2280	693.3	0.0115	9.631	2.332	0.192	295.826	27.658
2280	681.3	0.012	9.595	2.324	0.200	309.867	26.404
2240	668.2	0.0131	9.529	2.267	0.218	346.689	23.600
2290	656.5	0.0117	9.490	2.308	0.195	304.106	26.905

2280	644.3	0.0122	9.475	2.295	0.203	319.016	25.647
2260	1061.1	0.0129	9.272	2.226	0.215	347.736	23.529
2200	1048.2	0.0129	9.240	2.159	0.215	358.460	22.825
2210	1035	0.0132	9.293	2.181	0.220	363.074	22.535
2200	1021.8	0.0132	9.255	2.163	0.220	366.202	22.342
2170	1009	0.0128	9.176	2.115	0.213	363.111	22.533
1930	829.4	0.0137	9.135	1.873	0.228	438.941	18.640
1930	817.2	0.0122	9.269	1.900	0.203	385.238	21.238
1970	805.2	0.012	9.162	1.917	0.200	375.573	21.785
1980	792.4	0.0128	9.283	1.952	0.213	393.396	20.798
1970	779.3	0.0131	9.221	1.929	0.218	407.368	20.085

E.1.2 Load 2

N(RPM)	Fuel (g)	Fuel difference (kg)	Average torque (Nm)	Power (kW)	Fuel flow rate (g/s)	SFC (g/kW-h)	Thermal Effic. (%)
3200	1017.4	0.0013	0.058	0.020	0.087	15971.95	0.512
3200	1016.3	0.0011	0.012	0.004	0.073	65321.20	0.125
3200	1009	0.0024	0.052	0.017	0.160	32941.78	0.248
3200	1004.2	0.0024	0.108	0.036	0.160	15847.67	0.516
3190	1001.7	0.0025	0.090	0.030	0.167	19803.54	0.413
3200	999.3	0.0024	0.089	0.030	0.160	19153.27	0.427
3030	976.6	0.0044	5.007	1.597	0.293	661.313	12.372
3030	971.9	0.0047	5.078	1.620	0.313	696.509	11.747
3030	967.3	0.0046	5.190	1.655	0.307	667.002	12.267
3040	962.8	0.0045	5.122	1.639	0.300	658.983	12.416
3030	958.3	0.0045	5.191	1.655	0.300	652.449	12.540
2660	920.9	0.0051	7.885	2.207	0.340	554.480	14.756
2560	915.5	0.0054	7.722	2.081	0.360	622.881	13.135
2600	912.9	0.0026	7.614	2.084	0.173	299.485	27.320
2630	910.7	0.0022	7.785	2.155	0.147	245.030	33.391
2640	907.4	0.0033	7.875	2.188	0.220	361.941	22.605
2590	904.8	0.0026	7.603	2.072	0.173	301.086	27.174
2600	902.2	0.0026	7.816	2.139	0.173	291.736	28.045
2600	899.2	0.003	7.713	2.111	0.200	341.117	23.985
2620	897.3	0.0019	7.830	2.159	0.127	211.191	38.741
2610	894.7	0.0026	7.822	2.149	0.173	290.398	28.174
2610	891.9	0.0028	7.971	2.190	0.187	306.913	26.658
2600	889.4	0.0025	7.933	2.171	0.167	276.401	29.601
2590	886.2	0.0032	7.732	2.108	0.213	364.385	22.454
2600	884.2	0.002	7.753	2.122	0.133	226.243	36.164
2660	881.5	0.0027	8.021	2.246	0.180	288.552	28.355
2630	878.8	0.0027	7.949	2.200	0.180	294.499	27.782
2620	876.1	0.0027	7.914	2.182	0.180	296.940	27.554
2610	873.8	0.0023	7.996	2.196	0.153	251.316	32.556
2980	849.5	0.0061	8.113	2.545	0.407	575.317	14.221
2980	843.2	0.0063	7.987	2.505	0.420	603.596	13.555
2980	836.9	0.0063	8.061	2.528	0.420	598.031	13.681
2980	830.7	0.0062	7.918	2.483	0.413	599.170	13.655
2980	824.8	0.0059	7.915	2.483	0.393	570.388	14.344
2410	802.3	0.0022	7.487	1.899	0.147	278.048	29.426
2430	799.5	0.0028	7.559	1.933	0.187	347.608	23.537
2440	797.4	0.0021	7.432	1.909	0.140	264.080	30.982

2440	794.4	0.003	7.638	1.962	0.200	367.051	22.291
2480	792.6	0.0018	7.711	2.013	0.120	214.641	38.119
2440	787.6	0.0037	7.702	1.978	0.247	448.929	18.225
2440	785.5	0.0021	7.628	1.959	0.140	257.300	31.799
2430	783.3	0.0022	7.571	1.936	0.147	272.688	30.004
2450	780.8	0.0025	7.794	2.010	0.167	298.527	27.407
2440	771.3	0.0021	7.690	1.975	0.140	255.206	32.060
2400	769.1	0.0022	7.675	1.939	0.147	272.367	30.040
2430	766.2	0.0029	7.601	1.944	0.193	358.037	22.852
2460	764.1	0.0021	7.741	2.004	0.140	251.464	32.537
2420	761.8	0.0023	7.700	1.961	0.153	281.452	29.070
2480	759	0.0028	7.688	2.007	0.187	334.877	24.432
2480	756.8	0.0022	7.924	2.068	0.147	255.292	32.049
2240	726.1	0.0024	7.943	1.873	0.160	307.580	26.601
2180	723.8	0.0023	7.901	1.813	0.153	304.503	26.869
2120	721.9	0.0019	7.688	1.715	0.127	265.843	30.777
2070	719.7	0.0022	7.625	1.661	0.147	317.841	25.742
2140	717.7	0.002	7.745	1.744	0.133	275.161	29.735
2090	715.6	0.0021	7.832	1.723	0.140	292.533	27.969
2080	713.7	0.0019	7.592	1.662	0.127	274.355	29.822
2120	707.5	0.0019	7.654	1.708	0.127	267.018	30.641
2130	705.2	0.0023	7.982	1.789	0.153	308.472	26.524
2130	703.2	0.002	7.569	1.697	0.133	282.900	28.921
2180	701.3	0.0019	7.775	1.784	0.127	255.606	32.010
2130	699.2	0.0021	7.849	1.760	0.140	286.445	28.563
2150	697.1	0.0021	7.661	1.734	0.140	290.738	28.142
2140	695.1	0.002	7.758	1.747	0.133	274.694	29.785
2150	692.9	0.0022	7.777	1.760	0.147	300.048	27.268
2160	691	0.0019	7.814	1.776	0.127	256.693	31.874
2150	688.8	0.0022	7.669	1.735	0.147	304.255	26.891
2140	686.7	0.0021	7.780	1.752	0.140	287.629	28.446
2140	684.7	0.002	7.805	1.758	0.133	273.064	29.963
2160	682.6	0.0021	7.773	1.767	0.140	285.198	28.688
1820	1111.9	0.002	7.804	1.495	0.133	321.082	25.482
1820	1110.2	0.0017	7.726	1.480	0.113	275.698	29.677
1810	1108.6	0.0016	7.906	1.506	0.107	254.960	32.091
1810	1106.6	0.002	7.919	1.509	0.133	318.171	25.715
1810	1104.9	0.0017	7.946	1.514	0.113	269.537	30.355
1820	1102.9	0.002	7.915	1.516	0.133	316.596	25.843
1820	1101.3	0.0016	7.939	1.521	0.107	252.503	32.403
1810	1099.3	0.002	7.977	1.520	0.133	315.864	25.903
1810	1097.6	0.0017	7.962	1.517	0.113	268.979	30.418
1810	1095.8	0.0018	7.946	1.514	0.120	285.396	28.668
1810	1094	0.0018	7.915	1.508	0.120	286.504	28.557
1810	1092.2	0.0018	8.012	1.526	0.120	283.047	28.906
1800	1090.3	0.0019	8.033	1.522	0.127	299.656	27.304
1810	1088.5	0.0018	7.979	1.520	0.120	284.204	28.789
1800	1086.4	0.0021	7.967	1.509	0.140	333.904	24.503
1800	1084.8	0.0016	8.005	1.517	0.107	253.209	32.313
1800	1083	0.0018	7.940	1.504	0.120	287.201	28.488
1800	1081	0.002	8.015	1.518	0.133	316.129	25.881
1800	1079.4	0.0016	7.938	1.504	0.107	255.359	32.040
1790	1077.5	0.0019	8.043	1.515	0.127	300.934	27.188

1600	1055.1	0.0023	8.638	1.455	0.153	379.482	21.560
1610	1053	0.0021	9.009	1.527	0.140	330.157	24.782
1580	1051.1	0.0019	9.043	1.504	0.127	303.222	26.983
1580	1048.9	0.0022	8.973	1.492	0.147	353.838	23.123
1570	1046.4	0.0025	9.032	1.492	0.167	402.021	20.352
1560	1044.6	0.0018	9.079	1.491	0.120	289.811	28.232
1560	1042.2	0.0024	9.114	1.496	0.160	384.941	21.255
1570	1040	0.0022	8.912	1.473	0.147	358.563	22.818
1560	1037.8	0.0022	8.973	1.473	0.147	358.404	22.828
1550	1035.9	0.0019	9.212	1.503	0.127	303.431	26.964
1550	1033.7	0.0022	9.152	1.493	0.147	353.642	23.136
1550	1031.5	0.0022	8.691	1.418	0.147	372.420	21.969
1550	1029.4	0.0021	8.858	1.445	0.140	348.774	23.459
1540	1027.3	0.0021	8.996	1.458	0.140	345.638	23.672
1530	1025	0.0023	8.750	1.409	0.153	391.761	20.885
1570	1023	0.002	9.049	1.495	0.133	321.007	25.488
1600	1020.8	0.0022	8.828	1.487	0.147	355.171	23.036
1610	1018.7	0.0021	8.781	1.488	0.140	338.734	24.154
1600	1016.6	0.0021	8.785	1.479	0.140	340.680	24.016
1610	1014.7	0.0019	8.970	1.520	0.127	300.007	27.272

E.1.3 Load 3

N(RPM)	Fuel (g)	Fuel difference (kg)	Average torque (Nm)	Power (kW)	Fuel flow rate (g/s)	SFC (g/kW-h)	Thermal Effic. (%)
3060	999.5	0.0065	0.138	0.044	0.433	35121.08	0.233
3060	998.5	0.001	0.064	0.021	0.067	11574.15	0.707
3060	997.3	0.0012	0.036	0.012	0.080	24782.54	0.330
3060	996.4	0.0009	0.051	0.016	0.060	13107.70	0.624
3060	995.3	0.0011	0.082	0.026	0.073	9986.399	0.819
3050	993.3	0.001	0.066	0.021	0.067	11356.57	0.720
3050	992.2	0.0011	0.021	0.007	0.073	39633.95	0.206
3050	991.1	0.0011	0.047	0.015	0.073	17344.21	0.472
3050	990.1	0.001	0.045	0.014	0.067	16583.52	0.493
3050	989	0.0011	0.070	0.023	0.073	11697.22	0.699
3050	988	0.001	0.076	0.025	0.067	9794.417	0.835
3050	986.8	0.0012	0.019	0.006	0.080	47219.40	0.173
2930	985.6	0.0012	1.755	0.541	0.080	532.043	15.378
2910	983.7	0.0019	3.739	1.145	0.127	398.179	20.548
2880	981.8	0.0019	5.182	1.571	0.127	290.283	28.186
2860	979.6	0.0022	5.956	1.793	0.147	294.490	27.783
2850	976.8	0.0028	6.822	2.046	0.187	328.397	24.914
2860	974.5	0.0023	7.379	2.221	0.153	248.515	32.923
2850	971.4	0.0031	7.437	2.231	0.207	333.516	24.532
2850	968.6	0.0028	7.386	2.216	0.187	303.317	26.974
2850	966.1	0.0025	7.360	2.208	0.167	271.778	30.105
2840	963.5	0.0026	7.286	2.178	0.173	286.542	28.554
2850	960.9	0.0026	7.321	2.196	0.173	284.149	28.794
2850	958	0.0029	7.128	2.138	0.193	325.509	25.135
2850	955.8	0.0022	7.163	2.149	0.147	245.737	33.295
2850	952.7	0.0031	7.335	2.200	0.207	338.146	24.196
2850	950.3	0.0024	7.303	2.191	0.160	262.950	31.116
2850	947.3	0.003	7.269	2.180	0.200	330.227	24.776

2850	944.7	0.0026	7.303	2.190	0.173	284.872	28.721
2850	942.2	0.0025	7.262	2.178	0.167	275.456	29.703
2850	939.7	0.0025	7.322	2.196	0.167	273.198	29.948
2850	936.6	0.0031	7.226	2.167	0.207	343.259	23.836
2850	934	0.0026	7.217	2.165	0.173	288.240	28.385
2850	931.5	0.0025	7.266	2.180	0.167	275.284	29.721
2850	928.9	0.0026	7.290	2.187	0.173	285.366	28.671
2580	901.8	0.0021	7.601	2.064	0.140	244.197	33.505
2600	898.9	0.0029	7.820	2.140	0.193	325.245	25.156
2650	896.1	0.0028	7.784	2.171	0.187	309.533	26.433
2610	893.5	0.0026	7.916	2.174	0.173	286.965	28.512
2570	891.2	0.0023	7.655	2.071	0.153	266.583	30.691
2550	888.5	0.0027	7.623	2.046	0.180	316.748	25.831
2600	886	0.0025	7.684	2.103	0.167	285.355	28.672
2650	883.3	0.0027	7.857	2.191	0.180	295.717	27.668
2660	880.9	0.0024	7.919	2.217	0.160	259.794	31.493
2660	878.1	0.0028	7.900	2.212	0.187	303.825	26.929
2600	875.3	0.0028	7.906	2.163	0.187	310.620	26.340
2660	872.8	0.0025	7.772	2.176	0.167	275.752	29.671
2680	870.1	0.0027	8.011	2.260	0.180	286.779	28.530
2650	867.5	0.0026	7.954	2.218	0.173	281.271	29.089
2640	864.8	0.0027	7.937	2.205	0.180	293.827	27.846
2660	862.1	0.0027	7.955	2.227	0.180	290.955	28.121
2690	859.5	0.0026	8.066	2.284	0.173	273.261	29.941
2680	856	0.0035	7.987	2.253	0.233	372.849	21.944
2670	853.7	0.0023	7.954	2.235	0.153	246.953	33.131
2320	843	0.002	7.687	1.877	0.133	255.736	31.993
2310	840.6	0.0024	7.526	1.830	0.160	314.791	25.991
2300	838.3	0.0023	7.629	1.847	0.153	298.896	27.373
2320	836.1	0.0022	7.592	1.854	0.147	284.833	28.725
2320	833.9	0.0022	7.747	1.892	0.147	279.137	29.311
2320	831.8	0.0021	7.590	1.853	0.140	271.962	30.084
2300	829.4	0.0024	7.544	1.826	0.160	315.430	25.939
2300	827.3	0.0021	7.581	1.835	0.140	274.654	29.790
2310	825	0.0023	7.699	1.872	0.153	294.912	27.743
2300	823	0.002	7.587	1.837	0.133	261.337	31.308
2280	820.7	0.0023	7.629	1.831	0.153	301.538	27.134
2300	818.4	0.0023	7.512	1.818	0.153	303.575	26.952
2300	816.4	0.002	7.566	1.832	0.133	262.068	31.220
2290	814.1	0.0023	7.509	1.810	0.153	305.009	26.825
2300	812.1	0.002	7.565	1.831	0.133	262.098	31.217
2310	809.7	0.0024	7.534	1.832	0.160	314.482	26.017
2280	807.7	0.002	7.541	1.810	0.133	265.246	30.846
2280	805.4	0.0023	7.568	1.816	0.153	303.935	26.920
2280	803.3	0.0021	7.522	1.805	0.140	279.231	29.301
2280	801.1	0.0022	7.554	1.813	0.147	291.285	28.089
1940	783.7	0.0019	7.853	1.603	0.127	284.393	28.769
1940	782	0.0017	7.747	1.582	0.113	257.922	31.722
1940	780	0.002	7.721	1.576	0.133	304.485	26.871
1950	778.1	0.0019	7.681	1.576	0.127	289.251	28.286
1940	776.2	0.0019	7.706	1.573	0.127	289.818	28.231
1950	774.4	0.0018	7.466	1.532	0.120	281.948	29.019
1950	772.4	0.002	7.783	1.597	0.133	300.510	27.226

1960	770.7	0.0017	7.857	1.621	0.113	251.742	32.501
1960	768.6	0.0021	7.726	1.594	0.140	316.218	25.874
1970	766.8	0.0018	7.821	1.622	0.120	266.404	30.712
1960	764.8	0.002	7.713	1.591	0.133	301.691	27.120
1970	762.9	0.0019	7.751	1.607	0.127	283.750	28.835
1980	760.9	0.002	7.749	1.615	0.133	297.259	27.524
1980	759	0.0019	7.841	1.634	0.127	279.074	29.318
1990	757.1	0.0019	7.849	1.644	0.127	277.371	29.498
2000	755.2	0.0019	7.662	1.613	0.127	282.744	28.937
2000	753.3	0.0019	7.699	1.621	0.127	281.364	29.079
2000	751.3	0.002	7.770	1.636	0.133	293.466	27.880
2000	749.3	0.002	7.672	1.615	0.133	297.221	27.528
2030	747.1	0.0022	7.754	1.657	0.147	318.726	25.670
1550	1129.6	0.0015	8.017	1.308	0.100	275.269	29.723
1560	1128.1	0.0015	7.200	1.182	0.100	304.545	26.866
1570	1126.6	0.0015	7.551	1.248	0.100	288.510	28.359
1580	1125.1	0.0015	7.283	1.211	0.100	297.246	27.525
1570	1123.6	0.0015	7.306	1.207	0.100	298.215	27.436
1560	1122.1	0.0015	7.596	1.247	0.100	288.639	28.346
1540	1120.6	0.0015	7.104	1.151	0.100	312.666	26.168
1540	1119	0.0016	7.143	1.158	0.107	331.689	24.667
1540	1117.5	0.0015	7.547	1.223	0.100	294.286	27.802
1550	1116.1	0.0014	7.945	1.296	0.093	259.231	31.562
1570	1114.5	0.0016	7.209	1.191	0.107	322.376	25.380
1590	1113.1	0.0014	7.386	1.236	0.093	271.850	30.097
1620	1111.5	0.0016	7.071	1.206	0.107	318.490	25.689
1670	1110	0.0015	7.150	1.257	0.100	286.462	28.562
1670	1108.4	0.0016	7.362	1.294	0.107	296.743	27.572
1630	1106.8	0.0016	7.416	1.272	0.107	301.828	27.108
1590	1105.3	0.0015	7.254	1.214	0.100	296.554	27.590
1580	1103.8	0.0015	7.447	1.238	0.100	290.694	28.146
1540	1102.4	0.0014	7.237	1.173	0.093	286.445	28.563
1550	1100.8	0.0016	6.960	1.135	0.107	338.186	24.193

E.1.4 Load 4

N(RPM)	Fuel (g)	Fuel difference (kg)	Average torque (Nm)	Power (kW)	Fuel flow rate (g/s)	SFC (g/kW-h)	Thermal Effic. (%)
2780	1082.3	0.0019	0.044	0.013	0.127	35758.64	0.229
2780	1080.7	0.0016	0.080	0.023	0.107	16430.73	0.498
2780	1078.6	0.0021	0.170	0.050	0.140	10132.54	0.807
2780	1076.8	0.0018	0.127	0.037	0.120	11587.62	0.706
2780	1075	0.0018	0.125	0.036	0.120	11851.15	0.690
2590	1060.7	0.0046	6.831	1.862	0.307	592.851	13.801
2590	1056.6	0.0041	6.853	1.868	0.273	526.768	15.532
2590	1052	0.0046	6.850	1.867	0.307	591.199	13.839
2590	1048	0.004	6.827	1.861	0.267	515.868	15.860
2600	1043.1	0.0049	6.813	1.864	0.327	630.823	12.970
2370	999.4	0.0024	7.454	1.859	0.160	309.810	26.409
2370	997.2	0.0022	7.553	1.884	0.147	280.239	29.196
2380	994.9	0.0023	7.479	1.873	0.153	294.662	27.767
2400	992.7	0.0022	7.549	1.907	0.147	276.895	29.548
2410	990.5	0.0022	7.412	1.880	0.147	280.855	29.132

2390	988.2	0.0023	7.550	1.899	0.153	290.654	28.150
2380	985.8	0.0024	7.422	1.859	0.160	309.811	26.409
2400	983.4	0.0024	7.544	1.905	0.160	302.287	27.066
2400	981.4	0.002	7.544	1.905	0.133	251.906	32.480
2400	978.8	0.0026	7.500	1.894	0.173	329.388	24.839
2400	976.7	0.0021	7.473	1.888	0.140	266.991	30.645
2390	974.1	0.0026	7.497	1.886	0.173	330.884	24.727
2400	972	0.0021	7.469	1.887	0.140	267.149	30.626
2400	969.6	0.0024	7.468	1.886	0.160	305.364	26.794
2410	967.5	0.0021	7.525	1.909	0.140	264.060	30.985
2420	965.3	0.0022	7.473	1.903	0.147	277.402	29.494
2410	962.9	0.0024	7.577	1.922	0.160	299.692	27.301
2410	960.8	0.0021	7.521	1.908	0.140	264.195	30.969
2400	958.4	0.0024	7.504	1.895	0.160	303.882	26.924
2390	955.9	0.0025	7.418	1.866	0.167	321.571	25.443
2230	928.1	0.002	7.464	1.752	0.133	274.009	29.860
2250	925.7	0.0024	7.611	1.802	0.160	319.580	25.602
2230	923.5	0.0022	7.490	1.758	0.147	300.344	27.241
2250	921.6	0.0019	7.577	1.794	0.127	254.133	32.195
2260	919.2	0.0024	7.679	1.827	0.160	315.355	25.945
2260	917.4	0.0018	7.643	1.818	0.120	237.631	34.431
2230	914.8	0.0026	7.551	1.772	0.173	352.116	23.236
2260	912.9	0.0019	7.691	1.829	0.127	249.275	32.822
2240	911	0.0019	7.661	1.806	0.127	252.461	32.408
2270	908.4	0.0026	7.603	1.816	0.173	343.534	23.817
2230	906.6	0.0018	7.595	1.783	0.120	242.337	33.762
2260	904.4	0.0022	7.473	1.778	0.147	297.031	27.545
2210	902.3	0.0021	7.643	1.778	0.140	283.514	28.859
2240	900.1	0.0022	7.568	1.784	0.147	295.928	27.648
2230	898	0.0021	7.653	1.796	0.140	280.598	29.158
2250	896	0.002	7.513	1.779	0.133	269.806	30.325
2250	893.8	0.0022	7.612	1.803	0.147	292.897	27.934
2250	891.4	0.0024	7.623	1.805	0.160	319.087	25.641
2270	889.2	0.0022	7.474	1.786	0.147	295.673	27.672
2240	887.2	0.002	7.569	1.784	0.133	269.001	30.416
1920	869.8	0.0017	7.607	1.537	0.113	265.416	30.826
1980	867.8	0.002	7.739	1.613	0.133	297.640	27.489
1970	866	0.0018	7.553	1.566	0.120	275.863	29.659
1960	863.9	0.0021	7.676	1.583	0.140	318.292	25.705
1950	862.2	0.0017	7.521	1.544	0.113	264.309	30.955
1930	860.2	0.002	7.522	1.528	0.133	314.164	26.043
1930	858.4	0.0018	7.614	1.547	0.120	279.300	29.294
1940	856.4	0.002	7.779	1.588	0.133	302.199	27.074
1950	854.8	0.0016	7.792	1.599	0.107	240.136	34.072
1940	852.8	0.002	7.650	1.562	0.133	307.285	26.626
1950	851	0.0018	7.684	1.577	0.120	273.926	29.869
1960	849	0.002	7.654	1.579	0.133	304.010	26.913
1960	847	0.002	7.563	1.560	0.133	307.651	26.594
1960	845.2	0.0018	7.681	1.585	0.120	272.626	30.011
1970	843.3	0.0019	7.644	1.585	0.127	287.697	28.439
1980	841.2	0.0021	7.568	1.577	0.140	319.559	25.603
2020	839.4	0.0018	7.578	1.611	0.120	268.156	30.511
2040	837.4	0.002	7.740	1.662	0.133	288.836	28.327

2050	835.3	0.0021	7.411	1.599	0.140	315.203	25.957
2070	833.6	0.0017	7.319	1.594	0.113	255.888	31.974
1390	801	0.0013	7.074	1.035	0.087	301.461	27.141
1310	799.8	0.0012	6.535	0.901	0.080	319.661	25.595
1250	798.5	0.0013	6.720	0.884	0.087	352.900	23.185
1100	797.7	0.0008	6.323	0.732	0.053	262.295	31.193
1110	796.3	0.0014	6.261	0.731	0.093	459.330	17.812
1100	795.2	0.0011	6.204	0.718	0.073	367.545	22.261
1060	794.1	0.0011	6.484	0.723	0.073	364.929	22.420
1100	793	0.0011	6.295	0.729	0.073	362.231	22.587
1100	792	0.001	6.247	0.723	0.067	331.831	24.657
1120	790.8	0.0012	6.564	0.774	0.080	372.195	21.983
1200	789.7	0.0011	6.303	0.796	0.073	331.654	24.670
1330	788.5	0.0012	6.545	0.916	0.080	314.373	26.026
1410	787.3	0.0012	6.693	0.993	0.080	289.964	28.217
1490	786	0.0013	7.350	1.153	0.087	270.669	30.228
1590	784.6	0.0014	7.408	1.240	0.093	271.039	30.187
1620	783.1	0.0015	7.224	1.232	0.100	292.281	27.993
1680	781.5	0.0016	7.130	1.261	0.107	304.578	26.863
1770	780	0.0015	7.404	1.379	0.100	260.996	31.348
1740	778.3	0.0017	7.445	1.363	0.113	299.235	27.342
1680	776.8	0.0015	7.327	1.295	0.100	277.890	29.443
1630	775.1	0.0017	7.442	1.277	0.113	319.558	25.604
1550	773.6	0.0015	7.134	1.164	0.100	309.339	26.449
1510	772.1	0.0015	7.793	1.238	0.100	290.675	28.148
1440	770.7	0.0014	6.528	0.989	0.093	339.595	24.093
1390	769.4	0.0013	6.974	1.020	0.087	305.788	26.757
1370	768.2	0.0012	6.840	0.986	0.080	292.017	28.018
1360	767	0.0012	6.449	0.923	0.080	311.979	26.226
1370	765.8	0.0012	6.585	0.950	0.080	303.302	26.976
1380	764.5	0.0013	6.729	0.977	0.087	319.240	25.629
1400	763.2	0.0013	6.682	0.985	0.087	316.905	25.818
1460	761.9	0.0013	6.666	1.024	0.087	304.599	26.861
1530	760.6	0.0013	7.144	1.150	0.087	271.196	30.169
1530	759.2	0.0014	7.207	1.161	0.093	289.514	28.261
1520	757.8	0.0014	6.948	1.112	0.093	302.272	27.068
1480	756.3	0.0015	7.053	1.099	0.100	327.671	24.970
1450	754.7	0.0016	7.445	1.136	0.107	337.990	24.207
1470	753.7	0.001	6.581	1.018	0.067	235.719	34.710
1460	752.3	0.0014	7.183	1.104	0.093	304.433	26.876
1490	751	0.0013	6.817	1.069	0.087	291.859	28.034
1500	749.6	0.0014	6.889	1.088	0.093	308.932	26.484

E.1.5 Load 5

N(RPM)	Fuel (g)	Fuel difference (kg)	Average torque (Nm)	Power (kW)	Fuel flow rate (g/s)	SFC (g/kW-h)	Thermal Effic. (%)
2600	1153.9	0.0017	0.221	0.061	0.113	6741.376	1.214
2590	1152.2	0.0017	0.258	0.070	0.113	5797.512	1.411
2590	1150.6	0.0016	0.281	0.077	0.107	5013.102	1.632
2590	1149	0.0016	0.273	0.074	0.107	5157.645	1.586
2590	1147.2	0.0018	0.253	0.069	0.120	6257.717	1.307
2590	1145.6	0.0016	0.208	0.057	0.107	6772.508	1.208

2420	1135	0.0015	3.994	1.017	0.100	353.928	23.117
2410	1133.5	0.0015	4.074	1.033	0.100	348.353	23.487
2410	1132	0.0015	4.216	1.069	0.100	336.665	24.303
2410	1130.6	0.0014	4.274	1.084	0.093	309.934	26.399
2410	1129.1	0.0015	4.409	1.118	0.100	321.898	25.417
2410	1127.6	0.0015	4.420	1.121	0.100	321.115	25.479
2400	1126	0.0016	4.490	1.134	0.107	338.613	24.163
2400	1124.4	0.0016	4.548	1.149	0.107	334.233	24.479
2400	1122.7	0.0017	4.529	1.144	0.113	356.658	22.940
2400	1121.1	0.0016	4.614	1.165	0.107	329.476	24.833
2400	1119.2	0.0019	4.642	1.172	0.127	388.914	21.038
2400	1118.1	0.0011	4.733	1.195	0.073	220.834	37.050
2400	1114.8	0.0033	4.701	1.188	0.220	666.903	12.268
2400	1111.5	0.0033	4.848	1.225	0.220	646.700	12.652
2140	1084.1	0.0022	7.267	1.637	0.147	322.597	25.362
2140	1082	0.0021	7.269	1.637	0.140	307.842	26.578
2140	1080.2	0.0018	7.164	1.614	0.120	267.735	30.559
2130	1077.8	0.0024	7.333	1.644	0.160	350.407	23.350
2150	1076	0.0018	7.160	1.620	0.120	266.651	30.684
2130	1073.9	0.0021	7.257	1.627	0.140	309.796	26.410
2160	1071.8	0.0021	7.081	1.610	0.140	313.079	26.133
2150	1069.8	0.002	7.124	1.612	0.133	297.738	27.480
2130	1067.7	0.0021	7.195	1.613	0.140	312.469	26.184
2150	1065.5	0.0022	7.420	1.679	0.147	314.456	26.019
2140	1063.6	0.0019	7.239	1.630	0.127	279.694	29.253
2140	1061.5	0.0021	7.065	1.591	0.140	316.709	25.834
2130	1059.6	0.0019	7.383	1.655	0.127	275.517	29.696
2150	1057.3	0.0023	7.298	1.651	0.153	334.278	24.476
2140	1055.3	0.002	7.001	1.577	0.133	304.399	26.879
2120	1053.4	0.0019	7.316	1.632	0.127	279.358	29.288
2130	1051.4	0.002	7.021	1.574	0.133	304.954	26.830
2140	1049.2	0.0022	6.653	1.499	0.147	352.336	23.222
2140	1047	0.0022	6.915	1.558	0.147	338.989	24.136
2140	1045	0.002	7.239	1.630	0.133	294.405	27.791
1820	1028	0.0018	7.372	1.412	0.120	305.934	26.744
1840	1026.3	0.0017	7.419	1.437	0.113	283.977	28.812
1840	1024.5	0.0018	7.319	1.417	0.120	304.776	26.845
1850	1022.8	0.0017	7.336	1.428	0.113	285.638	28.644
1850	1020.9	0.0019	7.492	1.459	0.127	312.584	26.175
1870	1019.1	0.0018	7.615	1.499	0.120	288.246	28.385
1870	1017.4	0.0017	7.687	1.513	0.113	269.671	30.340
1880	1015.4	0.002	7.668	1.517	0.133	316.361	25.862
1870	1013.5	0.0019	7.659	1.507	0.127	302.518	27.046
1890	1011.8	0.0017	7.745	1.541	0.113	264.809	30.897
1900	1010.1	0.0017	7.686	1.537	0.113	265.441	30.823
1880	1008.2	0.0019	7.676	1.519	0.127	300.217	27.253
1870	1006.5	0.0017	7.647	1.505	0.113	271.099	30.180
1880	1004.6	0.0019	7.708	1.525	0.127	298.996	27.364
1870	1002.8	0.0018	7.657	1.507	0.120	286.662	28.542
1840	1001	0.0018	7.642	1.480	0.120	291.891	28.030
1840	999.3	0.0017	7.824	1.515	0.113	269.286	30.383
1840	997.4	0.0019	7.605	1.473	0.127	309.627	26.425
1840	995.7	0.0017	7.851	1.520	0.113	268.361	30.488

1840	993.9	0.0018	7.698	1.491	0.120	289.768	28.236
1550	976.2	0.0014	6.954	1.134	0.093	296.175	27.625
1580	974.7	0.0015	7.354	1.223	0.100	294.367	27.795
1590	973.2	0.0015	7.429	1.243	0.100	289.572	28.255
1520	971.8	0.0014	7.197	1.151	0.093	291.810	28.038
1360	970.4	0.0014	6.900	0.988	0.093	340.211	24.049
1330	969.2	0.0012	6.834	0.957	0.080	301.049	27.178
1340	967.9	0.0013	6.793	0.958	0.087	325.672	25.123
1360	966.7	0.0012	6.758	0.967	0.080	297.711	27.482
1340	965.5	0.0012	6.575	0.927	0.080	310.576	26.344
1370	964.2	0.0013	6.727	0.970	0.087	321.642	25.438
1440	962.8	0.0014	6.834	1.036	0.093	324.402	25.221
1540	961.6	0.0012	6.859	1.112	0.080	259.065	31.582
1610	960.2	0.0014	7.725	1.309	0.093	256.677	31.876
1570	958.7	0.0015	7.264	1.200	0.100	299.932	27.279
1520	957.1	0.0016	7.086	1.134	0.107	338.730	24.154
1460	955.8	0.0013	6.959	1.069	0.087	291.771	28.042
1410	954.4	0.0014	6.872	1.020	0.093	329.472	24.833
1360	953.2	0.0012	6.835	0.978	0.080	294.361	27.795
1360	951.9	0.0013	7.093	1.015	0.087	307.296	26.625
1370	950.7	0.0012	6.833	0.985	0.080	292.309	27.990
1360	949.5	0.0012	7.138	1.022	0.080	281.883	29.026
1350	948.2	0.0013	6.174	0.877	0.087	355.680	23.003
1350	947	0.0012	6.014	0.855	0.080	337.013	24.277
1350	945.7	0.0013	7.176	1.020	0.087	305.979	26.740
1350	944.6	0.0011	6.937	0.986	0.073	267.856	30.546
1350	943.3	0.0013	6.543	0.930	0.087	335.607	24.379
1340	942	0.0013	6.619	0.933	0.087	334.238	24.479
1340	940.8	0.0012	6.613	0.933	0.080	308.795	26.496
1350	939.6	0.0012	6.144	0.873	0.080	329.932	24.799
1380	938.4	0.0012	6.570	0.954	0.080	301.811	27.109
1370	937.1	0.0013	6.461	0.932	0.087	334.909	24.430
1650	935.7	0.0014	7.312	1.270	0.093	264.625	30.919
1660	934.1	0.0016	7.105	1.241	0.107	309.333	26.450
1660	932.5	0.0016	7.269	1.270	0.107	302.364	27.060
1300	928.3	0.0013	7.002	0.958	0.087	325.676	25.123
1260	927.1	0.0012	6.683	0.886	0.080	324.945	25.179
1310	926	0.0011	6.769	0.933	0.073	282.861	28.925
1370	924.7	0.0013	6.812	0.982	0.087	317.652	25.757
1450	923.4	0.0013	7.002	1.069	0.087	291.961	28.024
1490	922.1	0.0013	7.404	1.161	0.087	268.712	30.448
1490	920.7	0.0014	7.187	1.127	0.093	298.114	27.445
1510	919.3	0.0014	7.149	1.136	0.093	295.746	27.665

E.1.6 Load 6

N(RPM)	Fuel (g)	Fuel difference (kg)	Average torque (Nm)	Power (kW)	Fuel flow rate (g/s)	SFC (g/kW-h)	Thermal Effic. (%)
2360	1092.5	0.0007	0.208	0.051	0.047	3293.462	2.484
2360	1091.6	0.0009	0.218	0.053	0.060	4041.755	2.024
2370	1090.8	0.0008	0.242	0.060	0.053	3218.416	2.542
2360	1090.1	0.0007	0.227	0.056	0.047	3022.235	2.707
2370	1089.3	0.0008	0.209	0.051	0.053	3736.100	2.190

2370	1088.5	0.0008	0.215	0.053	0.053	3628.857	2.255
2370	1087.7	0.0008	0.253	0.062	0.053	3084.469	2.653
2370	1086.9	0.0008	0.229	0.056	0.053	3403.126	2.404
2370	1086.2	0.0007	0.214	0.053	0.047	3187.615	2.567
2360	1085.4	0.0008	0.204	0.050	0.053	3842.468	2.129
2360	1084.6	0.0008	0.247	0.061	0.053	3167.510	2.583
2360	1083.9	0.0007	0.236	0.058	0.047	2901.766	2.820
2210	1079	0.0013	3.073	0.706	0.087	442.074	18.508
2210	1077.7	0.0013	3.760	0.863	0.087	361.353	22.642
2200	1076.1	0.0016	4.158	0.951	0.107	403.972	20.253
2190	1074.6	0.0015	4.550	1.035	0.100	347.681	23.533
2190	1073	0.0016	4.810	1.095	0.107	350.801	23.323
2160	1071.3	0.0017	5.158	1.158	0.113	352.429	23.215
2150	1069.7	0.0016	5.373	1.200	0.107	319.915	25.575
2140	1068	0.0017	5.369	1.194	0.113	341.705	23.944
2140	1066	0.002	5.447	1.211	0.133	396.268	20.647
2160	1064.6	0.0014	5.529	1.241	0.093	270.743	30.220
2160	1062.8	0.0018	5.334	1.197	0.120	360.858	22.673
2160	1061.3	0.0015	5.249	1.178	0.100	305.585	26.774
2030	1039	0.0017	5.982	1.262	0.113	323.336	25.304
2020	1037	0.002	6.002	1.260	0.133	381.021	21.473
2020	1035.4	0.0016	5.969	1.253	0.107	306.468	26.697
2010	1033.6	0.0018	5.962	1.245	0.120	346.932	23.583
2010	1032	0.0016	5.978	1.249	0.107	307.533	26.605
2020	1030.1	0.0019	5.921	1.243	0.127	366.912	22.299
2010	1028.5	0.0016	5.945	1.242	0.107	309.227	26.459
2010	1026.7	0.0018	5.917	1.236	0.120	349.546	23.407
2010	1025	0.0017	5.930	1.239	0.113	329.417	24.837
2010	1023.3	0.0017	5.870	1.226	0.113	332.785	24.586
2000	1021.6	0.0017	5.876	1.221	0.113	334.097	24.489
2020	1019.7	0.0019	5.837	1.225	0.127	372.176	21.984
1850	993.6	0.002	6.651	1.279	0.133	375.430	21.793
1840	991.8	0.0018	6.784	1.297	0.120	333.034	24.568
1850	989.9	0.0019	6.663	1.281	0.127	355.971	22.984
1840	988.3	0.0016	6.330	1.210	0.107	317.270	25.788
1840	986.3	0.002	6.655	1.273	0.133	377.200	21.691
1850	984.6	0.0017	6.584	1.266	0.113	322.342	25.382
1840	982.8	0.0018	6.448	1.233	0.120	350.378	23.351
1840	980.8	0.002	6.485	1.240	0.133	387.090	21.137
1840	979	0.0018	6.853	1.310	0.120	329.701	24.816
1850	977.2	0.0018	6.840	1.315	0.120	328.554	24.903
1840	975.5	0.0017	6.415	1.227	0.113	332.615	24.598
1840	973.6	0.0019	6.619	1.266	0.127	360.330	22.706
1630	953.8	0.0016	6.094	1.032	0.107	372.014	21.993
1600	952.2	0.0016	5.890	0.979	0.107	392.127	20.865
1570	950.7	0.0015	6.120	0.999	0.100	360.534	22.694
1640	949.2	0.0015	6.110	1.041	0.100	345.716	23.666
1680	947.7	0.0015	6.346	1.108	0.100	324.959	25.178
1670	946.1	0.0016	6.168	1.070	0.107	358.762	22.806
1680	944.5	0.0016	6.212	1.084	0.107	354.082	23.107
1660	942.9	0.0016	6.051	1.044	0.107	367.907	22.239
1610	941.3	0.0016	5.662	0.947	0.107	405.349	20.185

1560	939.8	0.0015	6.191	1.004	0.100	358.689	22.810
1550	938.3	0.0015	6.240	1.005	0.100	358.169	22.843
1540	936.9	0.0014	6.037	0.966	0.093	347.818	23.523
1530	935.4	0.0015	6.011	0.956	0.100	376.675	21.721
1510	934	0.0014	6.062	0.951	0.093	353.236	23.162
1480	932.6	0.0014	5.996	0.922	0.093	364.389	22.454
1460	931.2	0.0014	6.222	0.944	0.093	355.953	22.986
1490	929.9	0.0013	5.851	0.906	0.087	344.424	23.755
1520	928.4	0.0015	5.970	0.943	0.100	381.771	21.431
1560	927	0.0014	6.050	0.981	0.093	342.621	23.880
1560	925.5	0.0015	6.160	0.999	0.100	360.489	22.696
1550	924	0.0015	5.895	0.950	0.100	379.145	21.580
1530	922.6	0.0014	6.144	0.977	0.093	343.979	23.786
1540	921.2	0.0014	5.946	0.952	0.093	353.097	23.172
1540	919.7	0.0015	5.972	0.956	0.100	376.666	21.722
1490	918.3	0.0014	6.194	0.959	0.093	350.325	23.355
1420	916.8	0.0015	5.594	0.826	0.100	436.092	18.762
1350	915.7	0.0011	5.363	0.752	0.073	350.920	23.315
1330	914.5	0.0012	5.513	0.762	0.080	377.982	21.646
1340	913.2	0.0013	5.378	0.749	0.087	416.640	19.638
1350	912	0.0012	5.453	0.765	0.080	376.468	21.733
1440	910.7	0.0013	5.198	0.778	0.087	401.150	20.396
1480	909.4	0.0013	5.963	0.917	0.087	340.210	24.049
1500	908	0.0014	5.948	0.927	0.093	362.411	22.576
1460	906.6	0.0014	6.052	0.918	0.093	365.947	22.358
1390	905.2	0.0014	5.933	0.857	0.093	392.064	20.869
1360	904.1	0.0011	5.375	0.760	0.073	347.567	23.540
1370	902.8	0.0013	5.091	0.725	0.087	430.519	19.005
1440	901.6	0.0012	5.315	0.795	0.080	362.142	22.593
1460	900.3	0.0013	6.016	0.913	0.087	341.808	23.937
1490	898.8	0.0015	6.137	0.950	0.100	378.846	21.597
1520	897.6	0.0012	6.095	0.963	0.080	299.153	27.350
1520	896.1	0.0015	6.114	0.966	0.100	372.764	21.949
1470	894.7	0.0014	6.318	0.965	0.093	348.127	23.502
1460	893.3	0.0014	5.819	0.883	0.093	380.568	21.499

E.1.7 Load 7

N(RPM)	Fuel (g)	Fuel difference (kg)	Average torque (Nm)	Power (kW)	Fuel flow rate (g/s)	SFC (g/kW-h)	Thermal Effic. (%)
2010	1057.7	0.0006	0.784	0.164	0.040	879.365	9.304
2010	1057.1	0.0006	0.837	0.175	0.040	823.354	9.937
2010	1056.5	0.0006	0.852	0.178	0.040	809.108	10.112
2010	1055.9	0.0006	0.857	0.179	0.040	804.303	10.173
2010	1055.3	0.0006	0.861	0.180	0.040	800.877	10.216
2010	1054.7	0.0006	0.870	0.182	0.040	792.439	10.325
2010	1054.1	0.0006	0.929	0.194	0.040	742.511	11.019
2010	1053.3	0.0008	0.948	0.198	0.053	970.077	8.434
2010	1052.8	0.0005	0.922	0.193	0.033	623.122	13.130
2020	1052.2	0.0006	0.915	0.192	0.040	749.532	10.916
2010	1051.6	0.0006	0.911	0.190	0.040	757.190	10.805
2010	1051	0.0006	0.910	0.190	0.040	757.799	10.797
1890	1047.2	0.0009	1.306	0.257	0.060	841.839	9.719

1870	1046.4	0.0008	1.428	0.277	0.053	691.951	11.824
1880	1045.5	0.0009	1.490	0.291	0.060	742.291	11.022
1890	1044.6	0.0009	1.434	0.282	0.060	766.762	10.671
1880	1043.7	0.0009	1.439	0.281	0.060	768.135	10.652
1880	1042.8	0.0009	1.423	0.278	0.060	776.843	10.532
1890	1042.2	0.0006	1.400	0.275	0.040	523.835	15.619
1890	1041.1	0.0011	1.394	0.274	0.073	964.096	8.487
1880	1040.2	0.0009	1.395	0.273	0.060	792.338	10.326
1890	1039.4	0.0008	1.391	0.273	0.053	702.967	11.639
1880	1038.5	0.0009	1.411	0.276	0.060	783.403	10.444
1890	1037.6	0.0009	1.405	0.276	0.060	782.538	10.455
1730	1028.7	0.001	2.769	0.498	0.067	482.054	16.973
1720	1027.6	0.0011	2.985	0.533	0.073	494.892	16.533
1680	1026.4	0.0012	3.121	0.545	0.080	528.525	15.480
1720	1025.2	0.0012	3.064	0.548	0.080	525.889	15.558
1720	1024.1	0.0011	3.123	0.558	0.073	472.945	17.300
1730	1023	0.0011	2.988	0.537	0.073	491.524	16.646
1740	1022.1	0.0009	2.935	0.531	0.060	407.042	20.101
1750	1020.9	0.0012	2.904	0.528	0.080	545.289	15.005
1750	1019.8	0.0011	2.899	0.527	0.073	500.797	16.338
1770	1018.7	0.0011	2.605	0.479	0.073	551.040	14.848
1770	1017.6	0.0011	2.750	0.506	0.073	521.967	15.675
1780	1016.6	0.001	2.584	0.478	0.067	502.131	16.294
1790	1015.5	0.0011	2.565	0.477	0.073	553.363	14.786
1790	1014.5	0.001	2.463	0.458	0.067	523.928	15.616
1800	1013.4	0.0011	2.378	0.445	0.073	593.649	13.782
1790	1012.4	0.001	2.388	0.444	0.067	540.272	15.144
1590	1002.3	0.0012	3.816	0.631	0.080	456.759	17.913
1590	1001	0.0013	3.518	0.581	0.087	536.722	15.244
1590	999.8	0.0012	3.445	0.569	0.080	506.019	16.169
1590	998.6	0.0012	3.373	0.557	0.080	516.758	15.833
1600	997.3	0.0013	3.529	0.587	0.087	531.780	15.386
1600	996.1	0.0012	3.166	0.526	0.080	547.160	14.953
1600	994.9	0.0012	3.420	0.569	0.080	506.483	16.154
1600	993.7	0.0012	3.321	0.552	0.080	521.569	15.687
1600	992.4	0.0013	3.643	0.606	0.087	515.091	15.884
1600	991.2	0.0012	3.408	0.567	0.080	508.242	16.098
1590	990	0.0012	3.306	0.546	0.080	527.283	15.517
1600	988.7	0.0013	3.812	0.634	0.087	492.234	16.622
1590	987.5	0.0012	3.206	0.530	0.080	543.745	15.047
1590	986.3	0.0012	3.533	0.584	0.080	493.391	16.583
1600	985.1	0.0012	3.386	0.563	0.080	511.556	15.994
1580	983.8	0.0013	3.568	0.586	0.087	532.565	15.363
1580	982.6	0.0012	3.578	0.588	0.080	490.189	16.691
1560	981.4	0.0012	3.712	0.602	0.080	478.553	17.097
1570	980.2	0.0012	3.708	0.605	0.080	476.125	17.184
1560	978.9	0.0013	4.004	0.649	0.087	480.728	17.020
1550	977.5	0.0014	4.557	0.734	0.093	457.753	17.874
1550	976.2	0.0013	5.218	0.840	0.087	371.219	22.040
1540	974.8	0.0014	4.437	0.710	0.093	473.212	17.290
1550	972.7	0.0021	3.654	0.589	0.140	856.384	9.554
1560	969.7	0.0013	3.754	0.609	0.087	512.644	15.960

1560	968.4	0.0013	3.754	0.609	0.087	512.701	15.958
1560	967.2	0.0012	3.831	0.621	0.080	463.760	17.642
1550	965.9	0.0013	4.017	0.647	0.087	482.224	16.967
1550	964.6	0.0013	4.403	0.709	0.087	439.923	18.598
1550	963.3	0.0013	3.894	0.627	0.087	497.435	16.448
1550	962	0.0013	4.531	0.730	0.087	427.519	19.138
1550	960.7	0.0013	4.414	0.711	0.087	438.874	18.643
1530	959.3	0.0014	4.684	0.745	0.093	451.140	18.136
1530	957.9	0.0014	4.798	0.763	0.093	440.429	18.577
1510	956.6	0.0013	4.721	0.741	0.087	421.219	19.424
1520	955.2	0.0014	4.874	0.770	0.093	436.444	18.747
1520	953.8	0.0014	4.929	0.779	0.093	431.538	18.960
1530	952.5	0.0013	4.937	0.785	0.087	397.450	20.586
1510	951	0.0015	5.227	0.820	0.100	438.947	18.640
1510	949.6	0.0014	5.185	0.814	0.093	412.996	19.811
1510	948.3	0.0013	5.709	0.896	0.087	348.314	23.490
1510	946.9	0.0014	5.860	0.919	0.093	365.418	22.390
1490	945.6	0.0013	6.281	0.972	0.087	320.839	25.501
1500	944.1	0.0015	5.836	0.910	0.100	395.716	20.676
1500	942.6	0.0015	5.842	0.911	0.100	395.343	20.695
1460	941.2	0.0014	5.993	0.909	0.093	369.555	22.140
1420	938.9	0.0023	5.828	0.860	0.153	641.837	12.747
1460	935.9	0.0024	5.943	0.902	0.160	638.851	12.807
1420	934.4	0.0015	5.803	0.856	0.100	420.435	19.460
1380	932.2	0.0022	5.754	0.825	0.147	639.841	12.787
1380	930.6	0.0013	5.621	0.806	0.087	387.039	21.140
1360	929.4	0.0012	5.381	0.760	0.080	378.712	21.604
1350	928.1	0.0013	5.486	0.770	0.087	405.437	20.180
1310	926.9	0.0012	5.662	0.771	0.080	373.643	21.897
1320	925.7	0.0012	5.803	0.796	0.080	361.813	22.613
1380	924.4	0.0013	5.547	0.796	0.087	392.204	20.861
1470	923.1	0.0013	5.683	0.868	0.087	359.432	22.763
1450	921.8	0.0013	5.965	0.899	0.087	347.127	23.570
1330	920.4	0.0014	5.094	0.704	0.093	477.259	17.143

E.1.8 Load 8

N(RPM)	Fuel (g)	Fuel difference (kg)	Average torque (Nm)	Power (kW)	Fuel flow rate (g/s)	SFC (g/kW-h)	Thermal Effic. (%)
1750	1122.6	0.0005	0.775	0.141	0.033	851.910	9.604
1760	1122.1	0.0005	0.733	0.134	0.033	894.921	9.143
1760	1121.5	0.0006	0.830	0.152	0.040	948.711	8.624
1760	1120.9	0.0006	0.856	0.157	0.040	919.892	8.894
1760	1120.5	0.0004	0.854	0.156	0.027	614.472	13.315
1760	1120	0.0005	0.878	0.161	0.033	747.367	10.948
1760	1119.4	0.0006	0.845	0.154	0.040	932.052	8.778
1760	1118.9	0.0005	0.934	0.171	0.033	702.302	11.650
1760	1118.4	0.0005	0.857	0.157	0.033	765.459	10.689
1760	1117.8	0.0006	0.939	0.172	0.040	838.946	9.752
1760	1117.3	0.0005	0.916	0.168	0.033	715.969	11.428
1760	1116.8	0.0005	0.864	0.158	0.033	759.478	10.773
1560	1111	0.0006	0.856	0.139	0.040	1038.232	7.881
1550	1110.3	0.0007	0.918	0.148	0.047	1136.300	7.200

1540	1109.5	0.0008	1.732	0.277	0.053	692.543	11.814
1540	1108.8	0.0007	0.838	0.134	0.047	1252.497	6.532
1530	1108.1	0.0007	1.023	0.163	0.047	1032.570	7.924
1530	1107.3	0.0008	0.919	0.146	0.053	1313.696	6.228
1530	1106.6	0.0007	1.225	0.195	0.047	862.465	9.487
1530	1105.9	0.0007	1.152	0.183	0.047	917.441	8.918
1520	1102.3	0.0007	1.329	0.210	0.047	800.563	10.220
1520	1101.5	0.0008	1.122	0.177	0.053	1083.145	7.554
1510	1100.8	0.0007	1.263	0.198	0.047	847.990	9.648
1510	1100	0.0008	1.452	0.228	0.053	842.755	9.708
1510	1099.3	0.0007	1.381	0.217	0.047	775.278	10.553
1510	1098.5	0.0008	1.346	0.211	0.053	909.175	8.999
1520	1097.8	0.0007	1.338	0.211	0.047	795.176	10.289
1520	1097	0.0008	1.429	0.226	0.053	850.736	9.617
1510	1096.2	0.0008	1.269	0.199	0.053	964.548	8.483
1510	1095.5	0.0007	1.395	0.219	0.047	767.360	10.662
1520	1094.7	0.0008	1.582	0.250	0.053	768.531	10.646
1510	1094	0.0007	1.443	0.226	0.047	741.967	11.027
1520	1093.2	0.0008	1.397	0.221	0.053	870.121	9.403
1510	1092.4	0.0008	1.261	0.198	0.053	970.156	8.434
1510	1091.7	0.0007	1.409	0.221	0.047	759.871	10.767
1510	1090.9	0.0008	1.457	0.229	0.053	839.670	9.744
1600	1086.5	0.0007	1.251	0.208	0.047	807.701	10.130
1380	1063.7	0.0008	2.370	0.340	0.053	565.007	14.481
1380	1062.8	0.0009	2.433	0.349	0.060	619.171	13.214
1370	1061.9	0.0009	2.477	0.353	0.060	612.631	13.355
1380	1061	0.0009	2.368	0.340	0.060	635.968	12.865
1390	1060	0.001	2.426	0.350	0.067	684.943	11.945
1370	1059.1	0.0009	2.338	0.333	0.060	648.944	12.608
1370	1058.2	0.0009	2.454	0.349	0.060	618.353	13.232
1370	1057.2	0.001	2.318	0.330	0.067	727.415	11.248
1370	1056.3	0.0009	2.291	0.326	0.060	662.185	12.356
1370	1055.4	0.0009	2.274	0.324	0.060	667.257	12.262
1380	1054.5	0.0009	2.435	0.349	0.060	618.557	13.227
1380	1053.5	0.001	2.420	0.347	0.067	691.617	11.830
1370	1052.6	0.0009	2.666	0.380	0.060	569.051	14.378
1360	1051.6	0.001	2.891	0.409	0.067	587.429	13.928
1360	1050.6	0.001	3.729	0.527	0.067	455.375	17.967
1360	1049.6	0.001	3.907	0.552	0.067	434.676	18.823
1350	1048.5	0.0011	3.209	0.450	0.073	586.518	13.950
1340	1047.5	0.001	3.368	0.469	0.067	511.770	15.987
1350	1046.5	0.001	3.426	0.481	0.067	499.306	16.386
1330	1038.1	0.0011	4.377	0.605	0.073	436.418	18.748
1330	1037	0.0011	4.357	0.602	0.073	438.367	18.664
1350	1036	0.001	4.575	0.642	0.067	373.949	21.879
1340	1034.9	0.0011	4.541	0.632	0.073	417.479	19.598
1340	1033.8	0.0011	4.551	0.634	0.073	416.630	19.638
1330	1032.7	0.0011	4.545	0.628	0.073	420.263	19.468
1330	1031.7	0.001	4.688	0.648	0.067	370.404	22.089
1320	1030.6	0.0011	4.649	0.638	0.073	413.997	19.763
1320	1029.5	0.0011	4.755	0.652	0.073	404.803	20.212
1330	1027.5	0.0014	4.617	0.638	0.093	526.520	15.539

1330	1026.2	0.0013	4.622	0.639	0.087	488.459	16.750
1330	1025	0.0012	4.708	0.651	0.080	442.604	18.486
1330	1024	0.001	4.688	0.648	0.067	370.397	22.089
1330	1022.8	0.0012	4.617	0.638	0.080	451.352	18.127

E.2 Otto cycle engine

E.2.1 Throttle: 10%

N(RPM)	Fuel (g)	Fuel difference (kg)	Average torque (Nm)	Power (kW)	Fuel flow rate (g/s)	SFC (g/kW-h)	Thermal Effic. (%)	Air flow rate (g/s)	Vol. Effic. (%)
1460	855.7								
1460	852.6	0.0031	7.328	1.120	0.103	332.040	24.641	1.498	48.638
1460	849.4	0.0032	7.311	1.118	0.107	343.533	23.817	1.547	50.207
1460	846.3	0.0031	7.229	1.105	0.103	336.578	24.309	1.498	48.638
1470	843.2	0.0031	7.216	1.111	0.103	334.867	24.433	1.498	48.307
1480	840.1	0.0031	7.160	1.110	0.103	335.215	24.408	1.498	47.980
1490	836.9	0.0032	7.121	1.111	0.107	345.624	23.673	1.547	49.196
2010	819.5								
2000	815.7	0.0038	6.057	1.269	0.127	359.434	22.763	1.837	43.523
2000	811.9	0.0038	6.089	1.275	0.127	357.586	22.881	1.837	43.523
2010	808.2	0.0037	6.095	1.283	0.123	346.069	23.642	1.788	42.167
2020	804.2	0.004	6.070	1.284	0.133	373.825	21.887	1.933	45.360
2050	800.3	0.0039	6.136	1.317	0.130	355.262	23.030	1.885	43.579
2480	750.5								
2450	746.1	0.0044	5.091	1.306	0.147	404.252	20.239	2.127	41.139
2450	742.1	0.004	5.187	1.331	0.133	360.705	22.683	1.933	37.399
2460	738.4	0.0037	5.184	1.335	0.123	332.485	24.608	1.788	34.453
2480	734.2	0.0042	5.095	1.323	0.140	380.933	21.478	2.030	38.794
2540	729.9	0.0043	4.993	1.328	0.143	388.564	21.057	2.078	38.779
2900	669.1								
2970	664.5	0.0046	3.772	1.173	0.153	470.540	17.388	2.223	35.479
3010	660	0.0045	3.638	1.147	0.150	470.944	17.373	2.175	34.246
2910	655.1	0.0049	3.747	1.142	0.163	515.009	15.887	2.368	38.572
2870	650.9	0.0042	3.977	1.195	0.140	421.688	19.403	2.030	33.522
2870	646.3	0.0046	4.037	1.213	0.153	455.011	17.982	2.223	36.715
2880	641.7	0.0046	4.050	1.222	0.153	451.886	18.106	2.223	36.587
2900	637.1	0.0046	3.948	1.199	0.153	460.425	17.770	2.223	36.335
2920	632.6	0.0045	3.868	1.183	0.150	456.531	17.922	2.175	35.302
2940	627.9	0.0047	3.788	1.166	0.157	483.600	16.919	2.272	36.620
2930	623.1	0.0048	3.779	1.159	0.160	496.778	16.470	2.320	37.526
3010	618.4	0.0047	3.670	1.157	0.157	487.563	16.781	2.272	35.768
3550	904.6								
3540	899.9	0.0047	2.315	0.858	0.157	657.086	12.452	2.272	30.413
3580	895.3	0.0046	2.203	0.826	0.153	668.415	12.241	2.223	29.433
3610	890.9	0.0044	2.126	0.804	0.147	656.925	12.455	2.127	27.920
3650	886.4	0.0045	2.084	0.797	0.150	677.957	12.068	2.175	28.241
3650	881.9	0.0045	2.038	0.779	0.150	693.079	11.805	2.175	28.241
3650	877.5	0.0044	1.976	0.755	0.147	699.156	11.702	2.127	27.614
3650	872.8	0.0047	2.017	0.771	0.157	731.725	11.182	2.272	29.496
3650	868.2	0.0046	2.036	0.778	0.153	709.354	11.534	2.223	28.869
3650	863.7	0.0045	2.053	0.785	0.150	688.312	11.887	2.175	28.241

E.2.2 Throttle: 20%

N(RPM)	Fuel (g)	Fuel difference (kg)	Average torque (Nm)	Power (kW)	Fuel flow rate (g/s)	SFC (g/kW-h)	Thermal Effic. (%)	Air flow rate (g/s)	Vol. Effic. (%)
1560	854.6								
1540	850.8	0.0038	8.542	1.378	0.127	331.008	24.718	1.837	56.523
1510	846.9	0.0039	8.419	1.331	0.130	351.561	23.273	1.885	59.163
1510	843.1	0.0038	8.335	1.318	0.127	345.992	23.647	1.837	57.646
1520	839.5	0.0036	8.236	1.311	0.120	329.534	24.828	1.740	54.253
1520	835.9	0.0036	8.394	1.336	0.120	323.335	25.304	1.740	54.253
1560	832	0.0039	8.476	1.385	0.130	337.982	24.208	1.885	57.267
1340	815.7								
1370	812.3	0.0034	8.083	1.160	0.113	351.825	23.255	1.643	56.849
1360	809.1	0.0032	8.156	1.161	0.107	330.608	24.748	1.547	53.898
1360	805.7	0.0034	8.240	1.174	0.113	347.668	23.533	1.643	57.267
1360	802.6	0.0031	8.235	1.173	0.103	317.185	25.795	1.498	52.214
1360	799.3	0.0033	8.208	1.169	0.110	338.766	24.152	1.595	55.583
2100	770.2								
2160	765.2	0.005	8.139	1.841	0.167	325.911	25.104	2.417	53.025
2060	760.5	0.0047	8.056	1.738	0.157	324.538	25.211	2.272	52.263
2020	755.8	0.0047	8.071	1.707	0.157	330.368	24.766	2.272	53.298
2090	751.1	0.0047	8.054	1.763	0.157	319.973	25.570	2.272	51.513
2090	746.5	0.0046	7.889	1.727	0.153	319.687	25.593	2.223	50.417
2100	741.7	0.0048	7.897	1.737	0.160	331.687	24.667	2.320	52.358
2100	737.3	0.0044	8.120	1.786	0.147	295.679	27.671	2.127	47.995
2530	697.6								
2600	691.7	0.0059	7.927	2.158	0.197	328.056	24.940	2.852	51.981
2550	685.4	0.0063	7.909	2.112	0.210	357.976	22.856	3.045	56.593
2530	679.4	0.006	7.649	2.026	0.200	355.306	23.028	2.900	54.324
2610	673.6	0.0058	7.694	2.103	0.193	330.989	24.719	2.803	50.904
2620	667.5	0.0061	7.888	2.164	0.203	338.230	24.190	2.948	53.333
2540	661.3	0.0062	7.713	2.052	0.207	362.637	22.562	2.997	55.914
2600	655.3	0.006	7.873	2.144	0.200	335.873	24.360	2.900	52.862
2990	617.3								
2990	610.6	0.0067	6.962	2.180	0.223	368.817	22.184	3.238	51.330
2990	603.8	0.0068	6.955	2.178	0.227	374.735	21.834	3.287	52.096
2990	596.7	0.0071	6.918	2.166	0.237	393.309	20.803	3.432	54.394
2960	590	0.0067	6.942	2.152	0.223	373.626	21.898	3.238	51.850
2990	583	0.007	6.881	2.154	0.233	389.898	20.985	3.383	53.628
2990	576	0.007	6.879	2.154	0.233	389.962	20.981	3.383	53.628
3490	968.1								
3550	961	0.0071	5.600	2.082	0.237	409.286	19.990	3.432	45.814
3630	953.3	0.0077	5.844	2.221	0.257	415.970	19.669	3.722	48.590
3460	946.2	0.0071	5.855	2.121	0.237	401.609	20.373	3.432	47.005
3480	938.8	0.0074	5.773	2.104	0.247	422.072	19.385	3.577	48.710
3480	931.6	0.0072	5.665	2.065	0.240	418.488	19.551	3.480	47.393
3480	924.4	0.0072	5.612	2.045	0.240	422.457	19.367	3.480	47.393
3480	917	0.0074	5.494	2.002	0.247	443.554	18.446	3.577	48.710
3480	909.6	0.0074	5.748	2.095	0.247	423.946	19.299	3.577	48.710

E.2.3 Throttle: 30%

N(RPM)	Fuel (g)	Fuel difference (kg)	Average torque (Nm)	Power (kW)	Fuel flow rate (g/s)	SFC (g/kW-h)	Thermal Effic. (%)	Air flow rate (g/s)	Vol. Effic. (%)
1870	663.6								
1880	658.7	0.0049	9.106	1.793	0.163	328.001	24.944	2.368	59.704
1890	654.2	0.0045	9.084	1.798	0.150	300.348	27.241	2.175	54.540
1880	649.7	0.0045	9.141	1.800	0.150	300.068	27.267	2.175	54.830
1870	645.2	0.0045	9.204	1.802	0.150	299.604	27.309	2.175	55.123
1870	640.5	0.0047	9.234	1.808	0.157	311.903	26.232	2.272	57.573
1440	627.7								
1460	623.9	0.0038	9.340	1.428	0.127	319.341	25.621	1.837	59.620
1460	620	0.0039	9.352	1.430	0.130	327.301	24.998	1.885	61.189
1460	616.3	0.0037	9.258	1.415	0.123	313.682	26.083	1.788	58.051
1460	612.4	0.0039	9.219	1.409	0.130	332.045	24.641	1.885	61.189
1460	604.4	0.008	9.182	1.404	0.133	341.905	23.930	1.933	62.758
2310	872.6								
2330	866.7	0.0059	8.942	2.182	0.197	324.509	25.213	2.852	58.004
2330	861	0.0057	8.831	2.155	0.190	317.454	25.773	2.755	56.038
2330	855.1	0.0059	8.767	2.139	0.197	330.964	24.721	2.852	58.004
2340	849.5	0.0056	8.660	2.122	0.187	316.668	25.837	2.707	54.820
2330	843.8	0.0057	8.626	2.105	0.190	324.996	25.175	2.755	56.038
2330	837.9	0.0059	8.615	2.102	0.197	336.809	24.292	2.852	58.004
2790	738.7								
2800	731.3	0.0074	8.541	2.504	0.247	354.599	23.073	3.577	60.539
2850	723.8	0.0075	8.519	2.543	0.250	353.961	23.115	3.625	60.281
2760	716	0.0078	8.608	2.488	0.260	376.225	21.747	3.770	64.737
2820	708.4	0.0076	8.555	2.526	0.253	360.992	22.665	3.673	61.735
2760	700.4	0.008	8.568	2.476	0.267	387.672	21.105	3.867	66.397
3120	584.2								
3120	576.1	0.0081	7.651	2.500	0.270	388.852	21.041	3.915	59.470
3020	568	0.0081	7.835	2.478	0.270	392.292	20.856	3.915	61.439
3190	560.2	0.0078	7.763	2.593	0.260	360.917	22.670	3.770	56.010
3010	552	0.0082	7.607	2.398	0.273	410.368	19.938	3.963	62.404
3070	543.7	0.0083	7.674	2.467	0.277	403.709	20.267	4.012	61.930
3030	535.7	0.008	7.738	2.455	0.267	391.015	20.925	3.867	60.480

E.2.4 Throttle: 40%

N(RPM)	Fuel (g)	Fuel difference (kg)	Average torque (Nm)	Power (kW)	Fuel flow rate (g/s)	SFC (g/kW-h)	Thermal Effic. (%)	Air flow rate (g/s)	Vol. Effic. (%)
1730	899.6								
1740	893.2	0.0064	10.830	1.973	0.213	389.167	21.024	3.093	84.255
1780	888.2	0.005	10.821	2.017	0.167	297.469	27.505	2.417	64.345
1770	883	0.0052	10.877	2.016	0.173	309.503	26.435	2.513	67.297
1740	877.4	0.0056	10.871	1.981	0.187	339.253	24.117	2.707	73.723
1720	872.7	0.0047	10.738	1.934	0.157	291.616	28.057	2.272	62.594
2100	802.9								
2090	796.8	0.0061	10.168	2.225	0.203	328.929	24.874	2.948	66.857
2100	791.3	0.0055	10.062	2.213	0.183	298.259	27.432	2.658	59.994
2110	785.7	0.0056	9.998	2.209	0.187	304.204	26.896	2.707	60.795

2100	779.9	0.0058	9.883	2.173	0.193	320.235	25.549	2.803	63.266
2100	774.2	0.0057	9.759	2.146	0.190	318.700	25.672	2.755	62.176
2110	768.5	0.0057	9.658	2.134	0.190	320.531	25.526	2.755	61.881
2570	918.1								
2590	910.3	0.0078	9.958	2.701	0.260	346.562	23.609	3.770	68.986
2510	888.3								
2530	881.4	0.0069	10.110	2.678	0.230	309.133	26.467	3.335	62.473
2550	874.3	0.0071	10.069	2.689	0.237	316.858	25.822	3.432	63.780
2550	867.2	0.0071	10.073	2.690	0.237	316.754	25.830	3.432	63.780
2550	853.1	0.0141	10.057	2.686	0.235	315.019	25.972	3.408	63.331
2530	846.2	0.0069	10.071	2.668	0.230	310.307	26.367	3.335	62.473
2530	839	0.0072	10.073	2.669	0.240	323.732	25.273	3.480	65.189
2530	831.9	0.0071	10.075	2.669	0.237	319.182	25.634	3.432	64.284
3080	768.7								
3010	759.8	0.0089	8.725	2.750	0.297	388.319	21.070	4.302	67.731
2970	886.7								
2990	877.8	0.0089	9.468	2.965	0.297	360.243	22.712	4.302	68.184
2990	868.9	0.0089	9.436	2.954	0.297	361.489	22.634	4.302	68.184
2970	860.1	0.0088	9.418	2.929	0.293	360.507	22.695	4.253	67.872
2980	851.2	0.0089	9.401	2.934	0.297	364.059	22.474	4.302	68.413
2950	842.4	0.0088	9.371	2.895	0.293	364.761	22.431	4.253	68.332
2990	833.8	0.0086	9.365	2.932	0.287	351.946	23.247	4.157	65.886
2990	825	0.0088	9.351	2.928	0.293	360.683	22.684	4.253	67.418

E.2.5 Throttle: 50%

N(RPM)	Fuel (g)	Fuel difference (kg)	Average torque (Nm)	Power (kW)	Fuel flow rate (g/s)	SFC (g/kW-h)	Thermal Effic. (%)	Air flow rate (g/s)	Vol. Effic. (%)
1910	918.5								
1900	912	0.0065	11.389	2.266	0.217	344.209	23.770	3.142	78.365
1910	906.1	0.0059	11.320	2.264	0.197	312.702	26.165	2.852	70.759
1910	899.6	0.0065	11.249	2.250	0.217	346.668	23.601	3.142	77.955
1950	893.5	0.0061	11.292	2.306	0.203	317.450	25.774	2.948	71.657
2590	856.8								
2620	848.7	0.0081	10.876	2.984	0.270	325.731	25.118	3.915	70.819
2620	840.5	0.0082	10.700	2.936	0.273	335.194	24.409	3.963	71.693
2620	832.2	0.0083	10.603	2.909	0.277	342.370	23.898	4.012	72.567
2620	824.2	0.008	10.499	2.881	0.267	333.253	24.551	3.867	69.944
2620	816	0.0082	10.416	2.858	0.273	344.316	23.763	3.963	71.693
2630	807.8	0.0082	10.270	2.828	0.273	347.889	23.518	3.963	71.420
2620	799.9	0.0079	10.229	2.806	0.263	337.803	24.221	3.818	69.070
2990	756.2								
2980	747.4	0.0088	10.193	3.181	0.293	331.984	24.645	4.253	67.644
2970	738.4	0.009	10.285	3.199	0.300	337.635	24.233	4.350	69.415
2990	719.9	0.0185	10.238	3.206	0.308	346.276	23.628	4.471	70.865
2990	710.3	0.0096	10.230	3.203	0.320	359.636	22.750	4.640	73.547
2990	701.1	0.0092	10.251	3.210	0.307	343.961	23.787	4.447	70.482
2990	691.8	0.0093	10.073	3.154	0.310	353.834	23.123	4.495	71.249
2990	682.3	0.0095	10.022	3.138	0.317	363.297	22.521	4.592	72.781
1520	913.6								
1520	908.2	0.0054	12.629	2.010	0.180	322.348	25.382	2.610	81.379
1520	902.6	0.0056	12.567	2.000	0.187	335.948	24.354	2.707	84.393

1530	892.2	0.0104	12.411	1.989	0.173	313.799	26.073	2.513	77.853
1530	881.6	0.0106	12.225	1.959	0.177	324.697	25.198	2.562	79.350
1530	876.4	0.0052	12.098	1.938	0.173	321.913	25.416	2.513	77.853
1530	871.3	0.0051	12.004	1.923	0.170	318.204	25.713	2.465	76.356
3440	824.9								
3500	815.1	0.0098	9.010	3.302	0.327	356.119	22.975	4.737	64.139
3340	805	0.0101	9.237	3.231	0.337	375.141	21.810	4.882	69.269
3360	794.9	0.0101	9.549	3.360	0.337	360.733	22.681	4.882	68.857
3140	785.2	0.0097	9.693	3.187	0.323	365.192	22.404	4.688	70.763

E.2.6 Throttle: 75%

N(RPM)	Fuel (g)	Fuel difference (kg)	Average torque (Nm)	Power (kW)	Fuel flow rate (g/s)	SFC (g/kW-h)	Thermal Effic. (%)	Air flow rate (g/s)	Vol. Effic. (%)
2590	918								
2610	907.8	0.0102	13.065	3.571	0.340	342.771	23.870	4.930	89.521
2600	897.8	0.01	12.946	3.525	0.333	340.452	24.032	4.833	88.103
2620	887.5	0.0103	12.910	3.542	0.343	348.949	23.447	4.978	90.053
2620	877.9	0.0096	12.786	3.508	0.320	328.376	24.916	4.640	83.933
2620	868.1	0.0098	12.624	3.464	0.327	339.539	24.097	4.737	85.682
2620	858.1	0.01	12.573	3.450	0.333	347.870	23.520	4.833	87.431
2620	848.6	0.0095	12.415	3.406	0.317	334.680	24.447	4.592	83.059
2620	838.4	0.0102	12.294	3.373	0.340	362.888	22.546	4.930	89.179
1870	915.2								
1880	907.9	0.0073	13.358	2.630	0.243	333.097	24.563	3.528	88.947
1910	900.9	0.007	13.224	2.645	0.233	317.586	25.763	3.383	83.952
1960	893.3	0.0076	13.150	2.699	0.253	337.905	24.213	3.673	88.822
2060	885.6	0.0077	13.174	2.842	0.257	325.132	25.165	3.722	85.622
2110	877.7	0.0079	12.993	2.871	0.263	330.199	24.778	3.818	85.765
2100									
2090	853.8	0.0239	12.677	2.774	0.266	344.571	23.745	3.851	87.316
2100	846.1	0.0077	12.453	2.739	0.257	337.398	24.250	3.722	83.992
2100	838.4	0.0077	12.253	2.695	0.257	342.913	23.860	3.722	83.992
2950	732.4								
3000	721.5	0.0109	11.190	3.516	0.363	372.066	21.990	5.268	83.228
3000	699.3	0.0222	11.241	3.532	0.370	377.175	21.692	5.365	84.755
3000	688.6	0.0107	11.114	3.491	0.357	367.758	22.248	5.172	81.701
3000	678	0.0106	11.152	3.504	0.353	363.060	22.536	5.123	80.937
3000	667.3	0.0107	11.315	3.555	0.357	361.199	22.652	5.172	81.701
3000	657.5	0.0098	11.294	3.548	0.327	331.444	24.685	4.737	74.829
3000	646.8	0.0107	11.174	3.510	0.357	365.780	22.368	5.172	81.701
1640	838.4								
1610	831.8	0.0066	13.546	2.284	0.220	346.794	23.593	3.190	93.904
1610	825.5	0.0063	13.447	2.267	0.210	333.452	24.537	3.045	89.635
1600	819.1	0.0064	13.485	2.259	0.213	339.920	24.070	3.093	91.627
1590	812.8	0.0063	13.513	2.250	0.210	336.000	24.351	3.045	90.763
1570	806.8	0.006	13.446	2.211	0.200	325.684	25.122	2.900	87.542
1560	800.7	0.0061	13.356	2.182	0.203	335.493	24.387	2.948	89.571
1550	794.6	0.0061	13.417	2.178	0.203	336.125	24.342	2.948	90.149
1550	788.6	0.006	13.442	2.182	0.200	329.986	24.794	2.900	88.671
1560	782.5	0.0061	13.379	2.186	0.203	334.920	24.429	2.948	89.571
1570	770.4	0.0121	13.411	2.205	0.202	329.263	24.849	2.924	88.271

3480	1026.3								
3020	1013.8	0.0125	11.434	3.616	0.417	414.826	19.723	6.042	94.813
3440	1002.1	0.0117	11.509	4.146	0.390	338.642	24.161	5.655	77.910
3430	989.5	0.0126	11.216	4.029	0.420	375.313	21.800	6.090	84.147
3480	977.3	0.0122	10.995	4.007	0.407	365.390	22.392	5.897	80.305
3490	965.4	0.0119	10.516	3.843	0.397	371.541	22.021	5.752	78.106
3510	953.3	0.0121	10.307	3.789	0.403	383.249	21.349	5.848	78.966

E.2.7 Throttle: 100%

N(RPM)	Fuel (g)	Fuel difference (kg)	Average torque (Nm)	Power (kW)	Fuel flow rate (g/s)	SFC (g/kW-h)	Thermal Effic. (%)	Air flow rate (g/s)	Vol. Effic. (%)
3370	784.9								
3390	770.8	0.0141	12.887	4.575	0.470	369.856	22.122	6.815	95.276
3390	756.8	0.014	12.885	4.574	0.467	367.286	22.276	6.767	94.600
3370	743.4	0.0134	12.931	4.563	0.447	352.373	23.219	6.477	91.083
3380	728.9	0.0145	12.958	4.586	0.483	379.375	21.567	7.008	98.269
3420	714.7	0.0142	12.958	4.641	0.473	367.167	22.284	6.863	95.110
3300	700.6	0.0141	12.957	4.478	0.470	377.874	21.652	6.815	97.874
2990	653.2								
3000	640.8	0.0124	13.358	4.197	0.413	354.580	23.075	5.993	94.681
3000	616.2	0.0246	13.210	4.150	0.410	355.663	23.004	5.945	93.918
3000	604.1	0.0121	12.855	4.038	0.403	359.550	22.756	5.848	92.391
3000	591.8	0.0123	12.789	4.018	0.410	367.374	22.271	5.945	93.918
3000	580	0.0118	12.606	3.960	0.393	357.546	22.883	5.703	90.100
3000	568.1	0.0119	12.515	3.932	0.397	363.197	22.527	5.752	90.864
1630	944.1								
1610	937.6	0.0065	13.635	2.299	0.217	339.289	24.115	3.142	92.481
1610	931.5	0.0061	13.490	2.274	0.203	321.836	25.422	2.948	86.790
1570	925.4	0.0061	13.247	2.178	0.203	336.091	24.344	2.948	89.001
1560	919.1	0.0063	13.449	2.197	0.210	344.101	23.777	3.045	92.508
1560	913.1	0.006	13.533	2.211	0.200	325.679	25.122	2.900	88.103
1560	907.1	0.006	13.523	2.209	0.200	325.926	25.103	2.900	88.103
1560	901.1	0.006	13.521	2.209	0.200	325.968	25.100	2.900	88.103
1530	888.8	0.0123	13.365	2.141	0.205	344.637	23.740	2.973	92.076
1950	850.5								
1900	842.8	0.0077	12.836	2.554	0.257	361.781	22.615	3.722	92.833
2070	813.6								
2060	805.9	0.0077	13.051	2.815	0.257	328.199	24.929	3.722	85.622
2060	797.9	0.008	13.066	2.819	0.267	340.593	24.022	3.867	88.958
2060	790.2	0.0077	12.961	2.796	0.257	330.471	24.758	3.722	85.622
2060	782.3	0.0079	12.794	2.760	0.263	343.476	23.821	3.818	87.846
2060	774.4	0.0079	12.724	2.745	0.263	345.376	23.690	3.818	87.846
2060	766.6	0.0078	12.623	2.723	0.260	343.733	23.803	3.770	86.734
2560	930.4								
2590	919.9	0.0105	13.881	3.765	0.350	334.672	24.447	5.075	92.865
2600	909.3	0.0106	13.712	3.733	0.353	340.703	24.015	5.123	93.389
2610	898.3	0.011	13.600	3.717	0.367	355.101	23.041	5.317	96.542
2620	887.3	0.011	13.405	3.678	0.367	358.914	22.796	5.317	96.174
2620	876.8	0.0105	13.364	3.667	0.350	343.644	23.809	5.075	91.802
2620	866.2	0.0106	13.226	3.629	0.353	350.523	23.342	5.123	92.676
2620	855.3	0.0109	13.224	3.628	0.363	360.497	22.696	5.268	95.299

2620	845.1	0.0102	13.213	3.625	0.340	337.639	24.232	4.930	89.179
2620	834.2	0.0109	13.330	3.657	0.363	357.639	22.877	5.268	95.299

E.3 Miller cycle engine

E.3.1 Cam 1 LIVC

N(RPM)	Fuel (g)	Fuel difference (kg)	Average torque (Nm)	Power (kW)	Fuel flow rate (g/s)	SFC (g/kW-h)	Thermal Effic. (%)	Air flow rate (g/s)	Vol. Effic. (%)
1470	979								
1510	974.1	0.0049	12.649	2.000	0.163	293.976	27.832	2.368	74.333
1470	968.9	0.0052	12.593	1.938	0.173	321.899	25.417	2.513	81.031
1450	959.7	0.0092	12.561	1.907	0.153	289.412	28.270	2.223	72.670
1520	954.7	0.005	12.517	1.992	0.167	301.144	27.169	2.417	75.351
1530	950	0.0047	12.497	2.002	0.157	281.676	29.047	2.272	70.367
1030	916.2								
960	912.7	0.0035	10.981	1.104	0.117	380.460	21.505	1.692	83.514
1110	909.2	0.0035	10.925	1.270	0.117	330.724	24.739	1.692	72.229
1010	905.7	0.0035	10.833	1.146	0.117	366.560	22.321	1.692	79.380
990	902.1	0.0036	10.863	1.126	0.120	383.578	21.330	1.740	83.297
1000	895.3	0.0068	10.751	1.126	0.113	362.395	22.577	1.643	77.883
1300	880.6								
1310	876.9	0.0037	11.202	1.537	0.123	288.936	28.317	1.788	64.699
1320	873.1	0.0038	11.187	1.546	0.127	294.889	27.745	1.837	65.944
1200	869	0.0041	11.274	1.417	0.137	347.285	23.559	1.982	78.265
1300	865.4	0.0036	11.368	1.548	0.120	279.147	29.310	1.740	63.434
1330	861.6	0.0038	11.360	1.582	0.127	288.217	28.388	1.837	65.448
1320	857.7	0.0039	11.439	1.581	0.130	295.980	27.643	1.885	67.679
1730	982								
1760	975.4	0.0066	13.467	2.482	0.220	319.099	25.640	3.190	85.900
1740	968.8	0.0066	13.311	2.425	0.220	326.551	25.055	3.190	86.888
1730	962.2	0.0066	13.241	2.399	0.220	330.158	24.782	3.190	87.390
1750	949.3	0.0129	13.139	2.408	0.215	321.453	25.453	3.118	84.428
1750	943	0.0063	13.080	2.397	0.210	315.386	25.942	3.045	82.464
1750	936.4	0.0066	13.065	2.394	0.220	330.789	24.734	3.190	86.391
1990	907.7								
1990	900.6	0.0071	13.331	2.778	0.237	306.687	26.678	3.432	81.728
2000	893.3	0.0073	13.302	2.786	0.243	314.434	26.021	3.528	83.610
1980	886.2	0.0071	13.166	2.730	0.237	312.098	26.216	3.432	82.141
2000	878.8	0.0074	13.252	2.776	0.247	319.934	25.573	3.577	84.755
1990	872	0.0068	13.193	2.749	0.227	296.801	27.567	3.287	78.274
2270	847.1								
2270	838.8	0.0083	13.784	3.277	0.277	303.973	26.916	4.012	83.756
2250	830.8	0.008	13.760	3.242	0.267	296.099	27.632	3.867	81.446
2230	822.8	0.008	13.799	3.222	0.267	297.914	27.464	3.867	82.177
2260	814.3	0.0085	13.758	3.256	0.283	313.270	26.117	4.108	86.154
2240	806.3	0.008	13.710	3.216	0.267	298.518	27.408	3.867	81.810
2490	998.3								
2490	987.2	0.0111	14.739	3.843	0.370	346.594	23.606	5.365	102.115
2530	976.1	0.0111	14.741	3.906	0.370	341.056	23.990	5.365	100.500
2540	965.1	0.011	14.740	3.921	0.367	336.669	24.302	5.317	99.203
2520	954.3	0.0108	14.754	3.893	0.360	332.872	24.579	5.220	98.172

2510	943.8	0.0105	14.630	3.845	0.350	327.665	24.970	5.075	95.825
2490	923.3	0.0205	14.597	3.806	0.342	323.156	25.318	4.954	94.295
3010	827.8								
3010	815.6	0.0122	12.583	3.966	0.407	369.130	22.165	5.897	92.845
3010	803.3	0.0123	12.525	3.948	0.410	373.855	21.885	5.945	93.606
3000	779.1	0.0242	12.544	3.941	0.403	368.453	22.206	5.848	92.391
3000	767.3	0.0118	12.959	4.071	0.393	347.819	23.523	5.703	90.100
3260	871.6								
3240	857.4	0.0142	13.549	4.597	0.473	370.684	22.072	6.863	100.394
3250	843.9	0.0135	13.533	4.606	0.450	351.735	23.261	6.525	95.151
3200	830	0.0139	13.596	4.556	0.463	366.105	22.348	6.718	99.501
3260	816.3	0.0137	13.190	4.503	0.457	365.099	22.410	6.622	96.265
3210	803	0.0133	12.656	4.254	0.443	375.156	21.809	6.428	94.910
3240	786.8	0.0162	13.219	4.485	0.540	433.434	18.877	7.830	114.534
3490	761.9								
3480	748.5	0.0134	13.056	4.758	0.447	337.952	24.210	6.477	88.204
3490	734.6	0.0139	12.638	4.619	0.463	361.129	22.656	6.718	91.233
3500	720.8	0.0138	12.597	4.617	0.460	358.666	22.812	6.670	90.318
3500	707.3	0.0135	12.331	4.520	0.450	358.432	22.827	6.525	88.355
3360	693.6	0.0137	11.087	3.901	0.457	421.441	19.414	6.622	93.400
3667	820.7	0.0985	11.750	4.512	0.469	374.214	21.864	6.801	87.897

E.3.2 Cam 2LIVC

N(RPM)	Fuel (g)	Fuel difference (kg)	Average torque (Nm)	Power (kW)	Fuel flow rate (g/s)	SFC (g/kW-h)	Thermal Effic. (%)	Air flow rate (g/s)	Vol. Effic. (%)
1190	898.4								
1090	895.6	0.0028	8.661	0.989	0.093	339.886	24.072	1.353	58.843
1040	890.2	0.0054	8.478	0.923	0.090	350.893	23.317	1.305	59.470
1060	887.5	0.0027	8.523	0.946	0.090	342.474	23.890	1.305	58.347
1090	884.7	0.0028	8.522	0.973	0.093	345.419	23.687	1.353	58.843
1100	882	0.0027	8.527	0.982	0.090	329.873	24.803	1.305	56.226
1100	879.3	0.0027	8.477	0.977	0.090	331.797	24.659	1.305	56.226
1270	860.8								
1280	858.1	0.0027	9.027	1.210	0.090	267.764	30.556	1.305	48.319
1280	855	0.0031	8.953	1.200	0.103	309.995	26.393	1.498	55.477
1280	852.1	0.0029	8.941	1.198	0.097	290.369	28.177	1.402	51.898
1280	848.9	0.0032	8.906	1.194	0.107	321.664	25.436	1.547	57.267
1290	845.9	0.003	8.887	1.201	0.100	299.851	27.286	1.450	53.272
1540	835.3								
1520	831.2	0.0041	9.771	1.555	0.137	316.345	25.864	1.982	61.788
1510	827.7	0.0035	9.725	1.538	0.117	273.131	29.956	1.692	53.095
1510	823.9	0.0038	9.769	1.545	0.127	295.200	27.716	1.837	57.646
1500	820.5	0.0034	9.767	1.534	0.113	265.925	30.767	1.643	51.922
1510	816.5	0.004	9.723	1.538	0.133	312.195	26.207	1.933	60.680
1740	785.9								
1830	781.5	0.0044	10.134	1.942	0.147	271.868	30.095	2.127	55.076
1700	776.8	0.0047	10.124	1.802	0.157	312.918	26.147	2.272	63.331
1650	772.7	0.0041	9.998	1.728	0.137	284.788	28.730	1.982	56.920
1740	768.5	0.0042	10.046	1.831	0.140	275.320	29.717	2.030	55.292

1790	763.6	0.0049	10.185	1.909	0.163	307.987	26.565	2.368	62.706
1710	759.1	0.0045	10.081	1.805	0.150	299.129	27.352	2.175	60.281
1710	754.5	0.0046	10.063	1.802	0.153	306.315	26.710	2.223	61.621
1700	750.1	0.0044	10.107	1.799	0.147	293.446	27.882	2.127	59.288
2040	730								
2070	724.9	0.0051	10.154	2.201	0.170	278.051	29.426	2.465	56.437
1930	719.2	0.0057	10.163	2.054	0.190	332.995	24.570	2.755	67.652
1950	714.5	0.0047	10.039	2.050	0.157	275.125	29.738	2.272	55.211
2100	709.1	0.0054	10.183	2.239	0.180	289.364	28.275	2.610	58.903
2100	703.2	0.0059	10.155	2.233	0.197	317.044	25.807	2.852	64.357
2100	697.7	0.0055	10.053	2.211	0.183	298.540	27.406	2.658	59.994
2100	692	0.0057	9.958	2.190	0.190	312.360	26.194	2.755	62.176
2110	686.4	0.0056	9.916	2.191	0.187	306.701	26.677	2.707	60.795
2530	653.3								
2530	646.5	0.0068	10.543	2.793	0.227	292.138	28.007	3.287	61.568
2500	639.7	0.0068	10.632	2.783	0.227	293.167	27.908	3.287	62.306
2500	632.8	0.0069	10.597	2.774	0.230	298.456	27.414	3.335	63.223
2520	625.6	0.0072	10.626	2.804	0.240	308.122	26.554	3.480	65.448
2520	618.8	0.0068	10.598	2.797	0.227	291.775	28.042	3.287	61.812
3120	880								
3120	870.6	0.0094	10.597	3.462	0.313	325.799	25.113	4.543	69.014
3120	860.8	0.0098	10.612	3.467	0.327	339.192	24.121	4.737	71.951
3300	627.9								
3320	617.9	0.01	10.694	3.718	0.333	322.766	25.349	4.833	68.996
3310	607.4	0.0105	10.592	3.672	0.350	343.182	23.841	5.075	72.665
3340	597.1	0.0103	10.855	3.797	0.343	325.539	25.133	4.978	70.641

E.3.3 Cam 3 LIVC

N(RPM)	Fuel (g)	Fuel difference (kg)	Average torque (Nm)	Power (kW)	Fuel flow rate (g/s)	SFC (g/kW-h)	Thermal Effic. (%)	Air flow rate (g/s)	Vol. Effic. (%)
1410	835.2								
1370	832.2	0.003	8.361	1.199	0.100	300.135	27.260	1.450	50.161
1360	829	0.0032	8.458	1.205	0.107	318.776	25.666	1.547	53.898
1350	826.2	0.0028	8.423	1.191	0.093	282.182	28.995	1.353	47.510
1370	823.3	0.0029	8.435	1.210	0.097	287.555	28.453	1.402	48.489
1420	820.4	0.0029	8.384	1.247	0.097	279.147	29.310	1.402	46.781
1460	817.1	0.0033	8.471	1.295	0.110	305.761	26.759	1.595	51.776
1420	814	0.0031	8.489	1.262	0.103	294.678	27.765	1.498	50.008
2070	772.9								
2000	762.8	0.0101	9.146	1.915	0.168	316.369	25.862	2.441	57.840
2020	753.9	0.0089	9.142	1.934	0.148	276.124	29.631	2.151	50.463
2070	749.4	0.0045	9.238	2.002	0.150	269.670	30.340	2.175	49.797
2050	744.9	0.0045	9.346	2.006	0.150	269.152	30.399	2.175	50.283
1970	740.4	0.0045	9.306	1.920	0.150	281.280	29.088	2.175	52.325
1970	735.7	0.0047	9.335	1.926	0.157	292.857	27.938	2.272	54.651
2010	731.1	0.0046	9.450	1.989	0.153	277.517	29.482	2.223	52.424
1690	718.5								
1700	714.7	0.0038	9.273	1.651	0.127	276.240	29.618	1.837	51.203
1710	710.6	0.0041	9.367	1.677	0.137	293.328	27.893	1.982	54.923
1720	706.9	0.0037	9.397	1.693	0.123	262.333	31.189	1.788	49.276
1730	702.5	0.0044	9.451	1.712	0.147	308.383	26.531	2.127	58.260

1740	698.5	0.004	9.585	1.747	0.133	274.825	29.771	1.933	52.659
1750	694.6	0.0039	9.566	1.753	0.130	266.961	30.648	1.885	51.049
2190	653.3								
2210	648.5	0.0048	9.748	2.256	0.160	255.308	32.047	2.320	49.752
2270	643.5	0.005	9.804	2.330	0.167	257.462	31.779	2.417	50.455
2260	637.9	0.0056	9.853	2.332	0.187	288.187	28.391	2.707	56.760
2210	632.6	0.0053	9.708	2.247	0.177	283.064	28.904	2.562	54.935
2200	627.7	0.0049	9.662	2.226	0.163	264.153	30.974	2.368	51.020
2290	622.2	0.0055	9.779	2.345	0.183	281.426	29.073	2.658	55.016
2500	597.2								
2500	591.5	0.0057	10.192	2.668	0.190	256.351	31.916	2.755	52.227
2540	585.4	0.0061	10.265	2.730	0.203	268.093	30.519	2.948	55.012
2450	578.8	0.0066	10.176	2.611	0.220	303.360	26.971	3.190	61.708
2460	573.1	0.0057	10.166	2.619	0.190	261.187	31.326	2.755	53.077
2460	567.1	0.006	10.208	2.630	0.200	273.794	29.883	2.900	55.870
2460	560.8	0.0063	10.171	2.620	0.210	288.532	28.357	3.045	58.664
2430	554.4	0.0064	10.063	2.561	0.213	299.928	27.279	3.093	60.331
3000	835.7								
2990	827.1	0.0086	9.585	3.001	0.287	343.854	23.794	4.157	65.886
3040	818.6	0.0085	9.538	3.036	0.283	335.925	24.356	4.108	64.049
2990	810	0.0086	9.750	3.053	0.287	338.048	24.203	4.157	65.886
2980	801.3	0.0087	9.838	3.070	0.290	340.051	24.061	4.205	66.876
2980	792.7	0.0086	9.793	3.056	0.287	337.684	24.229	4.157	66.107
2980	783.8	0.0089	9.583	2.990	0.297	357.142	22.909	4.302	68.413
3110	775.9	0.0079	9.775	3.183	0.263	297.792	27.475	3.818	58.188

E.3.4 Cam 1 EIVC

N(RPM)	Fuel (g)	Fuel difference (kg)	Average torque (Nm)	Power (kW)	Fuel flow rate (g/s)	SFC (g/kW-h)	Thermal Effic. (%)	Air flow rate (g/s)	Vol. Effic. (%)
1780	814.4								
1750	808.3	0.0061	12.879	2.360	0.203	310.155	26.380	2.948	79.847
1750	802.9	0.0054	12.677	2.323	0.180	278.930	29.333	2.610	70.684
1750	796.7	0.0062	12.521	2.295	0.207	324.238	25.234	2.997	81.155
1750	790.7	0.006	12.360	2.265	0.200	317.875	25.739	2.900	78.538
1790	785.3	0.0054	12.315	2.308	0.180	280.705	29.147	2.610	69.104
1780	779.4	0.0059	12.632	2.355	0.197	300.689	27.210	2.852	75.927
2240	722.7								
2190	715.7	0.007	12.671	2.906	0.233	289.075	28.303	3.383	73.218
2220	707.8	0.0079	12.633	2.937	0.263	322.782	25.348	3.818	81.515
2230	700.9	0.0069	12.593	2.941	0.230	281.559	29.059	3.335	70.878
2250	693.1	0.0078	12.560	2.959	0.260	316.292	25.868	3.770	79.410
2210	685.9	0.0072	12.426	2.876	0.240	300.440	27.233	3.480	74.628
1470	661.9								
1480	657.4	0.0045	11.782	1.826	0.150	295.731	27.666	2.175	69.649
1490	648.9	0.0085	11.556	1.803	0.142	282.840	28.927	2.054	65.338
1500	644.4	0.0045	11.264	1.769	0.150	305.211	26.807	2.175	68.720
1490	639.9	0.0045	11.130	1.737	0.150	310.936	26.314	2.175	69.182
1560	635	0.0049	11.992	1.959	0.163	300.141	27.260	2.368	71.951
1560	630.4	0.0046	12.290	2.008	0.153	274.937	29.759	2.223	67.546
1550	625.6	0.0048	12.402	2.013	0.160	286.135	28.594	2.320	70.937
1550	620.9	0.0047	12.401	2.013	0.157	280.192	29.201	2.272	69.459
1540	616.2	0.0047	12.328	1.988	0.157	283.684	28.841	2.272	69.910

1490	611.4	0.0048	11.710	1.827	0.160	315.255	25.953	2.320	73.794
1950	809								
1930	802.8	0.0062	12.326	2.491	0.207	298.643	27.397	2.997	73.587
1970	796.4	0.0064	12.271	2.532	0.213	303.370	26.970	3.093	74.418
2000	789.9	0.0065	12.076	2.529	0.217	308.411	26.529	3.142	74.447
2020	783.8	0.0061	12.168	2.574	0.203	284.399	28.769	2.948	69.174
2000	776.4	0.0074	12.421	2.601	0.247	341.358	23.968	3.577	84.755
1970	770	0.0064	12.474	2.573	0.213	298.443	27.415	3.093	74.418
1950	763.8	0.0062	12.534	2.559	0.207	290.690	28.146	2.997	72.832
1960	757.2	0.0066	12.440	2.553	0.220	310.190	26.377	3.190	77.135
1960	752.3	0.0049	12.302	2.525	0.163	232.874	35.134	2.368	57.267
1980	745	0.0073	12.270	2.544	0.243	344.311	23.763	3.528	84.454
2540	922.8								
2560	914.6	0.0082	12.279	3.292	0.273	298.935	27.370	3.963	73.373
2580	906.1	0.0085	12.439	3.361	0.283	303.501	26.958	4.108	75.468
2500	897.6	0.0085	12.454	3.260	0.283	312.852	26.152	4.108	77.883
2450	889.9	0.0077	12.379	3.176	0.257	290.926	28.123	3.722	71.993
2450	881.7	0.0082	12.372	3.174	0.273	309.988	26.394	3.963	76.668
2500	873.3	0.0084	12.341	3.231	0.280	311.984	26.225	4.060	76.967
2550	865.3	0.008	12.281	3.279	0.267	292.731	27.950	3.867	71.864
2780	821.9								
2840	812.6	0.0093	11.884	3.534	0.310	315.753	25.912	4.495	75.012
2800	804	0.0086	11.936	3.500	0.287	294.867	27.747	4.157	70.357
2770	794	0.01	11.903	3.453	0.333	347.551	23.541	4.833	82.696
2760	785.3	0.0087	11.875	3.432	0.290	304.180	26.898	4.205	72.206
2780	776.6	0.0087	11.908	3.467	0.290	301.149	27.169	4.205	71.687
2780	767.5	0.0091	11.956	3.481	0.303	313.742	26.078	4.398	74.983
2790	758.6	0.0089	11.869	3.468	0.297	307.991	26.565	4.302	73.072
3130	699.2								
3130	689.3	0.0099	11.209	3.674	0.330	323.343	25.304	4.785	72.453
3140	678.7	0.0106	11.382	3.743	0.353	339.873	24.073	5.123	77.329
3120	668.7	0.01	11.248	3.675	0.333	326.539	25.056	4.833	73.419
3100	658.7	0.01	11.382	3.695	0.333	324.781	25.192	4.833	73.893
3120	648.9	0.0098	11.200	3.659	0.327	321.358	25.460	4.737	71.951
3100	638.6	0.0103	11.149	3.619	0.343	341.516	23.957	4.978	76.110

E.3.5 Cam 2 EIVC

N(RPM)	Fuel (g)	Fuel difference (kg)	Average torque (Nm)	Power (kW)	Fuel flow rate (g/s)	SFC (g/kW-h)	Thermal Effic. (%)	Air flow rate (g/s)	Vol. Effic. (%)
1290	946								
1290	943.8	0.0022	5.044	0.681	0.073	387.411	21.119	1.063	39.066
1290	941.7	0.0021	5.060	0.683	0.070	368.696	22.191	1.015	37.290
1290	939.4	0.0023	5.081	0.686	0.077	402.081	20.349	1.112	40.842
1280	937.3	0.0021	5.087	0.682	0.070	369.586	22.138	1.015	37.581
1290	935	0.0023	5.038	0.681	0.077	405.559	20.174	1.112	40.842
1530	913.3								
1580	910.7	0.0026	4.772	0.790	0.087	395.163	20.705	1.257	37.695
1520	905.6	0.0051	4.767	0.759	0.085	403.277	20.288	1.233	38.429
1470	903.3	0.0023	4.780	0.736	0.077	375.120	21.811	1.112	35.841
1470	900.9	0.0024	4.805	0.740	0.080	389.340	21.015	1.160	37.399
1470	898.5	0.0024	4.776	0.735	0.080	391.702	20.888	1.160	37.399
1480	896.1	0.0024	4.768	0.739	0.080	389.770	20.991	1.160	37.146
1480	893.7	0.0024	4.759	0.738	0.080	390.432	20.956	1.160	37.146

1490	891.2	0.0025	4.737	0.739	0.083	405.877	20.158	1.208	38.434
1740	863.5								
1750	860.6	0.0029	4.618	0.846	0.097	411.174	19.899	1.402	37.960
1750	857.8	0.0028	4.530	0.830	0.093	404.766	20.214	1.353	36.651
1740	1000.3								
1740	997.2	0.0031	4.319	0.787	0.103	472.660	17.310	1.498	40.811
1750	994.3	0.0029	4.260	0.781	0.097	445.790	18.354	1.402	37.960
1750	991.3	0.003	4.224	0.774	0.100	465.012	17.595	1.450	39.269
1750	988.3	0.003	4.235	0.776	0.100	463.811	17.640	1.450	39.269
1750	985.4	0.0029	4.179	0.766	0.097	454.424	18.005	1.402	37.960
2100	865.8								
2110	862.3	0.0035	3.883	0.858	0.117	489.522	16.714	1.692	37.997
2120	858.8	0.0035	3.673	0.815	0.117	515.039	15.886	1.692	37.818
2080	848.6								
2110	845.4	0.0032	4.434	0.980	0.107	391.973	20.873	1.547	34.740
2110	842	0.0034	3.660	0.809	0.113	504.501	16.218	1.643	36.911
2610	926								
2610	922	0.004	4.006	1.095	0.133	438.397	18.663	1.933	35.106
2610	917.8	0.0042	3.997	1.093	0.140	461.313	17.736	2.030	36.862
2610	913.5	0.0043	4.234	1.157	0.143	445.937	18.347	2.078	37.739
2610	909.7	0.0038	4.777	1.306	0.127	349.248	23.427	1.837	33.351
2610	905.5	0.0042	4.391	1.200	0.140	419.955	19.483	2.030	36.862
2980	827.5								
2980	816.8	0.0107	4.280	1.336	0.178	480.709	17.020	2.586	41.125
2980	811.5	0.0053	4.269	1.332	0.177	477.354	17.140	2.562	40.740
2990	806.3	0.0052	4.209	1.318	0.173	473.515	17.279	2.513	39.838
2990	800.9	0.0054	4.421	1.384	0.180	468.090	17.479	2.610	41.370
3050	795.6	0.0053	4.198	1.341	0.177	474.340	17.249	2.562	39.805

E.4 Miller VCR cycle engine

E.4.1 Cam 1 LIVC

N(RPM)	Fuel (g)	Fuel difference (kg)	Average torque (Nm)	Power (kW)	Fuel flow rate (g/s)	SFC (g/kW-h)	Thermal Effic. (%)	Air flow rate (g/s)	Vol. Effic. (%)
1150	955.8	0.0037	11.226	1.352	0.123	328.418	24.913	1.788	73.700
1190	952	0.0038	11.253	1.402	0.127	325.188	25.160	1.837	73.148
1090	944.4	0.0076	11.298	1.290	0.127	353.599	23.139	1.837	79.859
1000	940.8	0.0036	10.867	1.138	0.120	379.617	21.553	1.740	82.464
1000	937.4	0.0034	10.520	1.102	0.113	370.359	22.092	1.643	77.883
1120	933.7	0.0037	11.160	1.309	0.123	339.224	24.119	1.788	75.674
1250	922.3	0.0037	11.312	1.481	0.123	299.846	27.287	1.788	67.804
1270	918.3	0.004	11.217	1.492	0.133	321.753	25.429	1.933	72.147
1280	914.5	0.0038	11.406	1.529	0.127	298.270	27.431	1.837	68.005
1200	910.8	0.0037	11.272	1.416	0.123	313.449	26.103	1.788	70.629
1280	907.1	0.0037	11.272	1.511	0.123	293.855	27.843	1.788	66.215
2060	866.8	0.0067	12.108	2.612	0.223	307.805	26.581	3.238	74.503
1990	859.8	0.007	12.276	2.558	0.233	328.344	24.918	3.383	80.577
2010	853.1	0.0067	12.191	2.566	0.223	313.326	26.113	3.238	76.356
1950	846.2	0.0069	12.237	2.499	0.230	331.354	24.692	3.335	81.055
1910	839.4	0.0068	11.793	2.359	0.227	345.931	23.652	3.287	81.553
2070	832.9	0.0065	11.958	2.592	0.217	300.898	27.191	3.142	71.930
1990	825.8	0.0071	12.232	2.549	0.237	334.246	24.478	3.432	81.728
1950	819.4	0.0064	12.050	2.461	0.213	312.121	26.214	3.093	75.181
1590	801.2	0.0052	11.045	1.839	0.173	339.322	24.112	2.513	74.915
1720	757	0.0053	12.482	2.248	0.177	282.886	28.923	2.562	70.585
1730	751.2	0.0058	12.336	2.235	0.193	311.423	26.272	2.803	76.797
1760	745.1	0.0061	11.743	2.164	0.203	338.218	24.191	2.948	79.393
1820	739.2	0.0059	11.573	2.206	0.197	320.998	25.489	2.852	74.258
1550	713.5	0.0045	10.816	1.756	0.150	307.588	26.600	2.175	66.504
1610	708.8	0.0047	11.167	1.883	0.157	299.573	27.312	2.272	66.871
1580	703.5	0.0053	11.184	1.850	0.177	343.696	23.805	2.562	76.839
1510	699	0.0045	11.027	1.744	0.150	309.702	26.418	2.175	68.265
1470	694.7	0.0043	10.691	1.646	0.143	313.541	26.095	2.078	67.006
1470	690.2	0.0045	10.642	1.638	0.150	329.638	24.821	2.175	70.123
1490	686.1	0.0041	10.580	1.651	0.137	298.026	27.453	1.982	63.032
2200	816	0.0084	12.448	2.868	0.280	351.475	23.279	4.060	87.462
2160	808.3	0.0077	12.314	2.785	0.257	331.739	24.663	3.722	81.658
2280	800.4	0.0079	12.418	2.965	0.263	319.727	25.590	3.818	79.370
2370	791.7	0.0087	12.571	3.120	0.290	334.621	24.451	4.205	84.088
2250	767.3	0.0079	12.433	2.930	0.263	323.599	25.284	3.818	80.428
2300	759.6	0.0077	12.602	3.035	0.257	304.428	26.876	3.722	76.688
2280	751.2	0.0084	12.571	3.001	0.280	335.846	24.362	4.060	84.393
2240	743.2	0.008	12.574	2.950	0.267	325.465	25.139	3.867	81.810
2200	727.4	0.0158	12.378	2.852	0.263	332.443	24.611	3.818	82.256
2480	786.1	0.0106	13.487	3.503	0.353	363.150	22.530	5.123	97.908
2500	776	0.0101	13.498	3.534	0.337	342.967	23.856	4.882	92.543
2490	765.8	0.0102	13.560	3.536	0.340	346.161	23.636	4.930	93.835
2540	755.5	0.0103	13.606	3.619	0.343	341.531	23.956	4.978	92.890
2550	744.6	0.0109	13.520	3.610	0.363	362.288	22.584	5.268	97.915
2720	749.9	0.0119	13.773	3.923	0.397	364.008	22.477	5.752	100.217

2730	737.1	0.0128	13.904	3.975	0.427	386.427	21.173	6.187	107.402
2770	724.8	0.0123	13.784	3.998	0.410	369.159	22.163	5.945	101.716
2780	712.6	0.0122	13.780	4.012	0.407	364.925	22.421	5.897	100.526
2760	700.1	0.0125	13.804	3.990	0.417	375.973	21.762	6.042	103.745
2940	961.1	0.0131	13.917	4.285	0.437	366.882	22.301	6.332	102.068
3060	947.8	0.0133	13.920	4.461	0.443	357.798	22.867	6.428	99.562
3040	934.1	0.0137	13.968	4.447	0.457	369.701	22.131	6.622	103.231
3100	921	0.0131	13.780	4.474	0.437	351.401	23.283	6.332	96.800
3040	907.8	0.0132	13.680	4.355	0.440	363.710	22.495	6.380	99.464

E.4.2 Cam 2 LIVC

N(RPM)	Fuel (g)	Fuel difference (kg)	Average torque (Nm)	Power (kW)	Fuel flow rate (g/s)	SFC (g/kW-h)	Thermal Effic. (%)	Air flow rate (g/s)	Vol. Effic. (%)
3120	873.7								
3120	863.6	0.0101	10.398	3.397	0.337	356.763	22.933	4.882	74.153
3120	853.4	0.0102	10.401	3.398	0.340	360.194	22.715	4.930	74.888
3120	843.2	0.0102	10.302	3.366	0.340	363.659	22.499	4.930	74.888
3120	832.9	0.0103	10.349	3.381	0.343	365.538	22.383	4.978	75.622
3120	822.9	0.01	10.226	3.341	0.333	359.149	22.781	4.833	73.419
2500	749.1								
2500	741.8	0.0073	10.684	2.797	0.243	313.186	26.124	3.528	66.888
2480	735	0.0068	10.623	2.759	0.227	295.780	27.662	3.287	62.809
2520	728.6	0.0064	10.474	2.764	0.213	277.864	29.445	3.093	58.176
2480	721.5	0.0071	10.761	2.795	0.237	304.864	26.838	3.432	65.580
2480	714.2	0.0073	10.682	2.774	0.243	315.772	25.911	3.528	67.427
2490	707.3	0.0069	10.634	2.773	0.230	298.602	27.400	3.335	63.477
2500	700.2	0.0071	10.662	2.791	0.237	305.244	26.804	3.432	65.055
1960	668.2								
1960	662.9	0.0053	9.785	2.008	0.177	316.663	25.838	2.562	61.942
1960	658.1	0.0048	9.624	1.975	0.160	291.584	28.060	2.320	56.098
1960	653	0.0051	9.460	1.942	0.170	315.206	25.957	2.465	59.604
1960	643	0.01	9.337	1.916	0.167	313.085	26.133	2.417	58.436
1960	638.1	0.0049	9.246	1.898	0.163	309.840	26.407	2.368	57.267
1970	633.3	0.0048	9.169	1.892	0.160	304.510	26.869	2.320	55.814
1540	613.5								
1540	609.7	0.0038	9.804	1.581	0.127	288.413	28.368	1.837	56.523
1530	606.3	0.0034	9.856	1.579	0.113	258.360	31.668	1.643	50.904
1530	602.9	0.0034	9.802	1.570	0.113	259.803	31.492	1.643	50.904
1530	599	0.0039	9.822	1.574	0.130	297.386	27.512	1.885	58.390
1510	595.4	0.0036	9.680	1.531	0.120	282.233	28.990	1.740	54.612
1500	591.9	0.0035	9.392	1.475	0.117	284.693	28.739	1.692	53.449
1530	588.4	0.0035	9.451	1.514	0.117	277.367	29.498	1.692	52.401
3120	1018.2								
3120	1007.4	0.0108	9.097	2.972	0.360	436.038	18.764	5.220	79.293
3130	957.6								
3120	947.7	0.0099	9.598	3.136	0.330	378.824	21.598	4.785	72.685
3120	937.8	0.0099	9.584	3.131	0.330	379.407	21.565	4.785	72.685
3120	928	0.0098	9.535	3.115	0.327	377.473	21.675	4.737	71.951

2720	877.9								
2720	868.8	0.0091	9.291	2.647	0.303	412.612	19.829	4.398	76.637
2720	854	0.0148	9.319	2.654	0.247	334.535	24.457	3.577	62.320
2720	845.7	0.0083	9.633	2.744	0.277	362.986	22.540	4.012	69.899
2720	837.5	0.0082	9.580	2.729	0.273	360.618	22.688	3.963	69.057
2730	829.5	0.008	9.505	2.717	0.267	353.286	23.159	3.867	67.126
2730	821.4	0.0081	9.464	2.706	0.270	359.251	22.775	3.915	67.965
2740	813.5	0.0079	9.449	2.711	0.263	349.644	23.400	3.818	66.045
2730	805.2	0.0083	9.418	2.693	0.277	369.914	22.118	4.012	69.643
2230	749.7								
2220	744	0.0057	10.526	2.447	0.190	279.524	29.271	2.755	58.815
2210	738.7	0.0053	10.559	2.444	0.177	260.263	31.437	2.562	54.935
2220	733.3	0.0054	10.483	2.437	0.180	265.903	30.770	2.610	55.719
2240	728.2	0.0051	10.561	2.477	0.170	247.046	33.119	2.465	52.154
2250	722.4	0.0058	10.462	2.465	0.193	282.347	28.978	2.803	59.049
2190	716.8	0.0056	10.503	2.409	0.187	278.974	29.328	2.707	58.574
1610	700.2								
1610	696.4	0.0038	9.987	1.684	0.127	270.816	30.212	1.837	54.066
1600	692.6	0.0038	9.951	1.667	0.127	273.483	29.917	1.837	54.404
1600	688.8	0.0038	9.942	1.666	0.127	273.736	29.889	1.837	54.404
1610	684.7	0.0041	9.999	1.686	0.137	291.838	28.035	1.982	58.334
1620	680.7	0.004	10.058	1.706	0.133	281.323	29.083	1.933	56.560
1630	676.8	0.0039	10.097	1.723	0.130	271.547	30.130	1.885	54.808
1640	672.9	0.0039	10.165	1.746	0.130	268.078	30.520	1.885	54.473
1650	669	0.0039	10.176	1.758	0.130	266.159	30.740	1.885	54.143

E.4.3 Cam 3 LIVC

N(RPM)	Fuel (g)	Fuel difference (kg)	Average torque (Nm)	Power (kW)	Fuel flow rate (g/s)	SFC (g/kW-h)	Thermal Effic. (%)	Air flow rate (g/s)	Vol. Effic. (%)
2620	987.5								
2620	981	0.0065	9.887	2.713	0.217	287.535	28.455	3.142	56.830
2620	974.6	0.0064	10.019	2.749	0.213	279.397	29.284	3.093	55.956
2620	968.4	0.0062	10.177	2.792	0.207	266.444	30.707	2.997	54.207
2610	962.4	0.006	10.183	2.783	0.200	258.683	31.629	2.900	52.659
2620	956	0.0064	10.091	2.769	0.213	277.398	29.495	3.093	55.956
2100	920								
2090	915.6	0.0044	8.484	1.857	0.147	284.352	28.774	2.127	48.225
2100	911	0.0046	8.442	1.856	0.153	297.342	27.517	2.223	50.177
2100	906.9	0.0041	8.410	1.850	0.137	266.010	30.758	1.982	44.723
2100	902.1	0.0048	8.483	1.866	0.160	308.749	26.500	2.320	52.358
2100	897.5	0.0046	8.544	1.879	0.153	293.800	27.848	2.223	50.177
1540	844.7								
1540	841.6	0.0031	8.246	1.330	0.103	279.749	29.247	1.498	46.111
1560	838.4	0.0032	8.243	1.347	0.107	285.149	28.693	1.547	46.988
1550	835.4	0.003	8.393	1.362	0.100	264.260	30.961	1.450	44.336
1430	832.2	0.0032	8.183	1.225	0.107	313.365	26.110	1.547	51.260
1410	829.4	0.0028	8.040	1.187	0.093	283.016	28.909	1.353	45.489
1440	826.7	0.0027	8.014	1.209	0.090	268.095	30.518	1.305	42.950
1550	823.6	0.0031	8.390	1.362	0.103	273.175	29.951	1.498	45.814
1530	820.1	0.0035	8.353	1.338	0.117	313.821	26.072	1.692	52.401
1480	817.4	0.0027	8.270	1.282	0.090	252.780	32.367	1.305	41.789
3120	789.8								
3120	780.3	0.0095	10.649	3.479	0.317	327.640	24.972	4.592	69.748

3120	771	0.0093	10.609	3.466	0.310	321.963	25.412	4.495	68.280
3120	761.9	0.0091	10.354	3.383	0.303	322.806	25.346	4.398	66.811
3120	752.2	0.0097	9.822	3.209	0.323	362.704	22.558	4.688	71.217

E.4.4 Cam 1 EIVC

N (RPM)	Fuel (g)	Fuel difference (kg)	Average torque (Nm)	Power (kW)	Fuel flow rate (g/s)	SFC (g/kW-h)	Thermal Effic. (%)	Air flow rate (g/s)	Vol. Effic. (%)
2580	739.3								
2580	730.5	0.0088	13.595	3.673	0.293	287.503	28.458	4.253	78.132
2580	721.4	0.0091	13.568	3.666	0.303	297.886	27.466	4.398	80.795
2580	712.2	0.0092	14.008	3.785	0.307	291.710	28.048	4.447	81.683
2580	703.3	0.0089	14.499	3.917	0.297	272.634	30.010	4.302	79.020
2580	693.7	0.0096	14.154	3.824	0.320	301.247	27.160	4.640	85.235
2580	684.3	0.0094	13.465	3.638	0.313	310.062	26.388	4.543	83.459
2590	674.8	0.0095	13.621	3.694	0.317	308.584	26.514	4.592	84.021
2130	897.8								
2160	890.9	0.0069	13.374	3.025	0.230	273.702	29.893	3.335	73.174
2130	883.3	0.0076	13.493	3.010	0.253	303.022	27.001	3.673	81.733
2120	875.7	0.0076	13.769	3.057	0.253	298.361	27.423	3.673	82.119
2130	846.2								
2120	838.5	0.0077	14.849	3.297	0.257	280.295	29.190	3.722	83.199
2130	831.2	0.0073	14.262	3.181	0.243	275.368	29.712	3.528	78.507
2120	823.6	0.0076	13.827	3.070	0.253	297.097	27.539	3.673	82.119
2120	816.2	0.0074	13.768	3.056	0.247	290.531	28.162	3.577	79.958
2120	808.8	0.0074	13.998	3.108	0.247	285.744	28.633	3.577	79.958
3130	743.6								
3130	733	0.0106	12.461	4.084	0.353	311.427	26.272	5.123	77.576
3140	721.6	0.0114	12.585	4.138	0.380	330.585	24.750	5.510	83.165
3130	710.8	0.0108	12.611	4.134	0.360	313.532	26.096	5.220	79.039
3150	698.8	0.012	12.391	4.087	0.400	352.314	23.223	5.800	87.264
3130	686.8	0.012	12.747	4.178	0.400	344.653	23.739	5.800	87.822
3120	675	0.0118	12.573	4.108	0.393	344.689	23.737	5.703	86.635
1550	621.4								
1540	616.4	0.005	14.200	2.290	0.167	262.013	31.227	2.417	74.373
1540	611.2	0.0052	14.260	2.300	0.173	271.334	30.154	2.513	77.348
1540	606.2	0.005	14.276	2.302	0.167	260.617	31.394	2.417	74.373
1540	601.2	0.005	14.315	2.309	0.167	259.908	31.480	2.417	74.373
1540	596.2	0.005	14.328	2.311	0.167	259.675	31.508	2.417	74.373
1540	591	0.0052	14.320	2.309	0.173	270.205	30.280	2.513	77.348

E.4.5 Cam 2 EIVC

N (RPM)	Fuel (g)	Fuel difference (kg)	Average torque (Nm)	Power (kW)	Fuel flow rate (g/s)	SFC (g/kW-h)	Thermal Effic. (%)	Air flow rate (g/s)	Vol. Effic. (%)
2430	831.3								
2400	823	0.0083	4.551	1.144	0.138	435.425	18.790	2.006	39.610
2410	818.8	0.0042	4.950	1.249	0.140	403.435	20.280	2.030	39.921
2400	814.6	0.0042	4.970	1.249	0.140	403.455	20.279	2.030	40.087
2400	810.2	0.0044	5.025	1.263	0.147	418.105	19.569	2.127	41.996
2400	806	0.0042	5.024	1.263	0.140	399.160	20.498	2.030	40.087
2400	801.6	0.0044	5.005	1.258	0.147	419.754	19.492	2.127	41.996
1960	774.5								

1960	771.2	0.0033	4.671	0.959	0.110	413.049	19.808	1.595	38.568
1970	767.6	0.0036	4.688	0.967	0.120	446.650	18.318	1.740	41.860
1970	764.3	0.0033	4.635	0.956	0.110	414.099	19.758	1.595	38.372
1970	761	0.0033	4.619	0.953	0.110	415.535	19.690	1.595	38.372
1970	757.4	0.0036	4.590	0.947	0.120	456.208	17.934	1.740	41.860
3120	716.7								
3120	710	0.0067	4.629	1.513	0.223	531.546	15.392	3.238	49.191
3120	702.8	0.0072	4.630	1.513	0.240	571.198	14.324	3.480	52.862
3120	695.8	0.007	4.632	1.513	0.233	555.065	14.740	3.383	51.393
3120	688.8	0.007	4.600	1.503	0.233	558.960	14.638	3.383	51.393
3120	682	0.0068	4.585	1.498	0.227	544.655	15.022	3.287	49.925
3120	675.3	0.0067	4.588	1.499	0.223	536.314	15.256	3.238	49.191
3120	668.4	0.0069	4.539	1.483	0.230	558.331	14.654	3.335	50.659
1580	644.2								
1570	641.5	0.0027	5.049	0.830	0.090	390.285	20.964	1.305	39.394
1490	639	0.0025	5.065	0.790	0.083	379.597	21.554	1.208	38.434
1470	636.5	0.0025	4.984	0.767	0.083	390.984	20.926	1.208	38.957
1480	634.2	0.0023	4.969	0.770	0.077	358.409	22.828	1.112	35.598
1500	631.8	0.0024	4.948	0.777	0.080	370.547	22.080	1.160	36.651
1550	629.3	0.0025	5.042	0.818	0.083	366.585	22.319	1.208	36.946
1570	626.6	0.0027	5.073	0.834	0.090	388.440	21.063	1.305	39.394
1570	624	0.0026	5.124	0.842	0.087	370.386	22.090	1.257	37.935
1570	621.3	0.0027	5.118	0.841	0.090	385.086	21.247	1.305	39.394
1600	618.6	0.0027	5.315	0.891	0.090	363.835	22.488	1.305	38.655